Sat. Oct 28, 2023

Room D

Oral presentation in IAG'i

Regional Analysis #1

Chair: Mizuki Kawabata (Faculty of Economics, Keio University)
9:20 AM - 10:20 AM Room D (C-201 2nd floor of Bldg. C)

[D1-02] Can "Living Environment Score" forecast future population trends?
*Hisatoshi Ai[1] (1. Showa Women's University)
9:20 AM - 9:40 AM

[D1-03] Applicability of alternative data for the identification of urban activity centers (UAC)
*Vadim Boratinskii[1], Toshihiro Osaragi[1] (1. Tokyo Institute of Technology)
9:40 AM - 10:00 AM

[D1-04] A machine learning-based Improved soil moisture estimation: Synergistic use of satellite observations and land surface models over CONUS
*JAESE LEE[1], Jungho Im[1] (1. Ulsan National Institute of Science and Technology)
10:00 AM - 10:20 AM

Oral presentation in IAG'i

Regional Analysis #2

Chair: Hisatoshi Ai (Showa Women's University)
10:40 AM - 12:20 PM Room D (C-201 2nd floor of Bldg. C)

[D2-01] Estimating hourly $PM_{2.5}$ using top-of-atmosphere reflectance from Geostationary Ocean Color Imagers I and II
*Hyunyoung Choi[1], Seonyoung Park[2], Jungho Im[1] (1. Ulsan National Institute of Science &Technology (UNIST), 2. Seoul National University of Science and Technology)
10:40 AM - 11:00 AM

[D2-02] Mapping Emotional Geographical Trends and User Behaviors Based on Japanese Tweets: A Case Study of Urban Green Spaces in Tokyo 23 Wards
*Mingchen Liu[1], Yuya Shibuya[2], Yoshihide Sekimoto[2] (1. Department of Civil Engineering, The University of Tokyo, 2. Center for Spatial Information Science, The University of Tokyo)
11:00 AM - 11:20 AM

[D2-03] Revealing Access Equity: An Examination of Walking Course Distribution and Streetscape Quality for Residents
*Xinyu Tang[1], Mamoru Amemiya[1], Sunyong Eom[1] (1. University of Tsukuba)
11:20 AM - 11:40 AM

[D2-04] Population Aging and the Community-based Integrated Care System in Akita Prefecture
*Ketian Chen[1], Mizuki Kawabata[1] (1. Keio University)
11:40 AM - 12:00 PM

[D2-05] Route Search Method of Alternative Bus for Rail Line Adopting Ant Colony Optimization
*Kei Nagaoka[1], Kayoko Yamamoto[1] (1. Graduate School of Informatics and Engineering The University of Electro-Communications)
12:00 PM - 12:20 PM

Oral presentation in IAG'i

Disaster

Chair: Michinori Hatayama (Disaster Prevention Research Institute, Kyoto University)
3:20 PM - 4:40 PM Room D (C-201 2nd floor of Bldg. C)

[D4-02] A Comparison of Construction Sites for Temporary and Public Housing under Different Urban Reconstruction Policies - Based on Actual Cases in Japan and China
*Yang Zhou[1], Naoko Fujita[1], Suxueer Sun[1], Minghui Tang[1], Linda Gadhoum[1] (1. Art Program, Faculty of Comprehensive Human Sciences, University of Tsukuba)
3:20 PM - 3:40 PM

[D4-03] Assessing Urban Flood Susceptibility Maps Based on Machine Learning Models in Seoul, South Korea
*Julieber Toralde Bersabe[1], Byong-Woon Jun[1] (1. Kyungpook National University)
3:40 PM - 4:00 PM

[D4-04] Meteotsunamis in a Danshui River estuary, Taiwan
*Liching Lin[1], Wen-Cheng Liu[1], Chin H. Wu[2] (1. Department of Civil and Disaster Prevention Engineering, National United University, Taiwan, 2. Department of Civil and Environmental Engineering, University of Wisconsin-Madison, Madison, WI, USA)
4:00 PM - 4:20 PM

[D4-05] Comparison of the shorelines separately

detected from Sentinel-1 and 2 satellite imagery acquired on the east coast of Korea
*Yun-Jae Choung[1] (1. Geo C&I Co., Ltd.)
4:20 PM - 4:40 PM

Oral presentation in IAG'i

Data

Chair: Satoshi Kubota (Kansai University)
5:00 PM - 6:40 PM Room D (C-201 2nd floor of Bldg. C)

[D5-01] Enhancing large-scale footprint extraction evaluation: a two-level approach with proxy data and building-unit matching
*Shenglong Chen[1], Yoshiki Ogawa[1], Chenbo Zhao[1], Yoshihide Sekimoto[1] (1. University of Tokyo)
5:00 PM - 5:20 PM

[D5-02] Advancing Building Extraction in Thailand using the YOLOv8 Segment Model on Open-source Data across Diverse Land Use Types
*Bhanu Prasad CHINTAKINDI[1], Yoshiki OGAWA[1], Yoshihide SEKIMOTO[1] (1. The University of Tokyo)
5:20 PM - 5:40 PM

[D5-03] Marine Debris Monitoring and AI Application Optimization Plan by Geographic Characteristics and Research Devices
*BoRam Kim[1], Cholyoung Lee[1], Hynwoo Choi[1], TaeHoon Kim[1] (1. Korea Institute of Marine Science and Technology(KIOST))
5:40 PM - 6:00 PM

[D5-04] Another approach to terrain mapping method utilizing Unmanned Surface Vehicle and Light Detection and Ranging at shallow water area: A case study at Budai Port' s expansion sand filling project site.
*Amrico Hanafie[1], Kuan-Tsung Chang[2], Sheng-Yu Yu[3] (1. Master student, Dept. of Civil Eng. and Environmental Informatics, Minghsin Uni. of Science and Technology, 2. Corresponding author, Professor, Dept. of Civil Eng. and Environmental Informatics, Minghsin Uni. of Science and Technology, 3. Company, Manager, Strong Engineering Consulting Co.)
6:00 PM - 6:20 PM

[D5-05] The Public Sentiment During the Covid-19 Lockdowns in China: A Comparison of Wuhan and Shanghai
*Xuanda Pei[1], Yuzuru Isoda[1] (1. Tohoku university)
6:20 PM - 6:40 PM

Room E

Oral presentation in IAG'i

Landscape

Chair: Maki Kishimoto (Tokyo Institute of Technology)
9:00 AM - 10:20 AM Room E (C-301 3rd floor of Bldg. C)

[E1-01] Capturing Walking-related Perceptions and Willingness within Tokyo's Station Areas: Leveraging Crowd-sourced Methods and AI Approach
*LU HUANG[1], TAKUYA OKI[1], SACHIO MUTO[2], YOSHIKI OGAWA[2] (1. Tokyo Institute of Technology, 2. The University of Tokyo)
9:00 AM - 9:20 AM

[E1-02] The Generation Process and Data Characteristics of Volunteered Street View Imagery for Streetscape Monitoring: A Case Study in Tokyo
*Xinrui Zheng[1], Mamoru Amemiya[1] (1. University of Tsukuba)
9:20 AM - 9:40 AM

[E1-03] Analyzing the Authenticity and Integrity of Cultural Landscapes Using Geographic Data - A Case Study of Pickle-making in Sichuan Province, China.
*Suxueer Sun[1], Naoko Fujita[1], Hideki Kobayashi[2], Yang Zhou[1], Suzu Shimada[1], Zile Tian[1] (1. University of Tsukuba., 2. Kanazawa University)
9:40 AM - 10:00 AM

[E1-04] Geographic information analysis of the transmission of cultural landscape values through farmers' guesthouses in Aso
*Linda Gadhoum[1], Naoko Fujita[1], Yang Zhou[1], Suxueer Sun[1], Hideki Kobayashi[2] (1. University of Tsukuba, 2. Kanazawa University)
10:00 AM - 10:20 AM

Oral presentation in IAG'i

Environment

Chair: Tsutomu Suzuki (University of Tsukuba)
10:40 AM - 12:00 PM Room E (C-301 3rd floor of Bldg. C)

[E2-01] Seasonal ARIMA Prediction of Streamflow: Sobat River Tributary of the White Nile River
*MANZU GERALD SIMON KENYI[1], KAYOKO YAMAMOTO[1] (1. The University of Electro-Communications)

10:40 AM - 11:00 AM

[E2-02] Analysis of Thermal Environment of Greening Vacant Houses in Old Downtown Metropolitan Areas: A Case Study on Busan Metropolitan City*clear*

*YOKO KAMATA[1], Kwang Woo Nam[1] （1. Kyungsung University）

11:00 AM - 11:20 AM

[E2-03] An advanced tropical cyclone center estimation approach using geostationary satellite-based infrared channels

*Juhyun Lee[1], Jungho Im[1] （1. Ulsan National Institute of Science and Technology）

11:20 AM - 11:40 AM

[E2-04] COMPARATIVE ANALYSIS OF URBAN GREENING EVOLUTION AND IMPLICATIONS IN GLOBAL NORTH AND SOUTH CITIES OVER A 30-YEAR PERIOD

*Ahmed Derdouri[1], Yuji Murayama[1], Takehiro Morimoto[1] （1. Faculty of Life and Environmental Sciences, University of Tsukuba）

11:40 AM - 12:00 PM

Oral presentation in IAG'i

Mobility, Transportation and Navigation

Chair: Wataru Nakanishi (Kanazawa Univerisity)
3:00 PM - 4:40 PM Room E (C-301 3rd floor of Bldg. C)

[E4-01] Generating Human Daily Activity Sequences Using Neural Networks Models

*Weiying WANG[1], Toshihiro Osaragi[1] （1. Tokyo Institute of Technology）

3:00 PM - 3:20 PM

[E4-02] Towards Pseudo People Flow: Developing a Deep Generative Model based on Person Trip Survey Data to Reproduce Large-Scale Daily People Activity Profiles.

*Yurong Zhang[1], Yoshihide Sekimoto[1], Yanbo Pang[1], Kunyi Zhang[1] （1. The University of Tokyo）

3:20 PM - 3:40 PM

[E4-03] Location-Based Content Tourism Support System on Foot

*Nobuaki Nagano[1], Kayoko Yamamoto[1] （1. Graduate School of Informatics and Engineering, University of Electro-Communications）

3:40 PM - 4:00 PM

[E4-04] Development of Food Tourism Support System Adopting Location-Based AR

*Makoto Hirano[1], Kayoko Yamamoto[1] （1. Electro-Communications Univ.）

4:00 PM - 4:20 PM

[E4-05] Effect of Speed Control for Travel Time and Emission Reduction in Connected Vehicle Environment

*Yuheng Liu[1], Sunyong Eom[1], Tsutomu Suzuki[1] （1. University of Tsukuba）

4:20 PM - 4:40 PM

Oral presentation in IAG'i

Spatial Analysis

Chair: Takahiro Yoshida (Center for Spatial Information Science, The University of Tokyo)
5:00 PM - 6:20 PM Room E (C-301 3rd floor of Bldg. C)

[E5-01] Evaluating spatial design in office buildings through behaviors identified by Wi-Fi sensing and Bluetooth technology

*Xinting Gao[1,2], Toshihiro Osaragi[2], Weimin Zhuang[2] （1. Tsinghua University, 2. Tokyo Insitute of Technology）

5:00 PM - 5:20 PM

[E5-02] Exploring Separation Strategies for Car-Bicycle Integration

*Liling Liu[1], Sunyong Eom[1], Tsutomu Suzuki[1] （1. University of Tsukuba）

5:20 PM - 5:40 PM

[E5-03] Regional-Spatial Analysis and Comparison of Social Farming in Japan and the Netherlands by Using GIS

*Zile Tian[1], Naoko Fujita[2], Max Hanssen[1], Ding Ma[3], Suzu Shimada[1] （1. Doctoral Program in Arts, Graduate School of Comprehensive Human Sciences, University of Tsukuba, 2. Institute of Arts and Design, University of Tsukuba, 3. Master Program in Arts, Graduate School of Comprehensive Human Sciences, University of Tsukuba）

5:40 PM - 6:00 PM

[E5-04] Accessibility of Third Places around a University Campus: A Spatial Analysis on Travel Times and Usage Patterns

*Max Hanssen[1], Naoko Fujita[1], Ding Ma[1], Suzu Shimada[1], Zile Tian[1], Linda Gadhoum[1], Joris Zandbergen[2], André Jacob Lodewijks[2], SeungHee Lee[1] （1. University of Tsukuba, Graduate School of

Comprehensive Human Science, Art, 2. University of Technology Eindhoven, Industrial Design）

6:00 PM - 6:20 PM

Oral presentation in IAG'i

Regional Analysis #1

Chair: Mizuki Kawabata (Faculty of Economics, Keio University)

Sat. Oct 28, 2023 9:20 AM - 10:20 AM Room D (C-201 2nd floor of Bldg. C)

[D1-02] Can "Living Environment Score" forecast future population trends?

*Hisatoshi Ai[1] （1. Showa Women's University）

9:20 AM - 9:40 AM

[D1-03] Applicability of alternative data for the identification of urban activity centers (UAC)

*Vadim Boratinskii[1], Toshihiro Osaragi[1] （1. Tokyo Institute of Technology）

9:40 AM - 10:00 AM

[D1-04] A machine learning-based Improved soil moisture estimation: Synergistic use of satellite observations and land surface models over CONUS

*JAESE LEE[1], Jungho Im[1] （1. Ulsan National Institute of Science and Technology）

10:00 AM - 10:20 AM

Can "Living Environment Score" forecast future population trends?

Hisatoshi AI *

Owing to the significant change in the Japanese population trend from increasing to declining, the city planning system of Japan has changed its main issue from growth control to compact city planning. In compact city planning, it is important to identify areas that attract residents to their living environments. The living environment score (LES) is a comprehensive evaluation score derived from 13 living environment indices with the point of view of whether the area attracts residents. This study visualizes the LES levels and population trends. Our main focus was on census grids where population was overestimated and showing population decline with a high LES. However, we could not find any clear spatial pattern of those grids; hence, we must further discuss the characteristics of these grids in future work.
Keywords: Compact City, Living Environment, Population Trends

1. Introduction

The city planning system of Japan is now facing a big challenge because it simultaneously faces population decline and rapidly aging issues. The current city planning system of Japan is originally designed as a growth control system in the era of economic growth and population increase; however, the keywords have changed to “compact city” and “smart shrinking” today. Since it is difficult to force people to reallocate where they live under the Japanese social system, the realistic choice to make cities compact for planners, mainly municipalities, is to designate areas with a high potential to attract residents and to design an attractive urban core considering the potential of the area. In practice, a location normalization plan [1)] was introduced in 2014. For decision-making in the above planning, a quantitative and comprehensive evaluation method for the area regarding its attractiveness from the residents’ perspective is required.

2. Living Environment Score

2.1. Basic Concept of the Living Environment Score

The living environment score (Ai, 2014), hereafter referred to as the LES, was derived by analyzing population trends and living environment indices. These indices were obtained mainly from census statistics and spatial data. The LES is a type of deviation score with an average of 50 and a standard deviation of 10, which represents the comprehensive attractiveness of an area. Ai (2014) proposed calculating the LES for each local district, a spatial subdivision smaller than municipalities, in the Greater Tokyo Metropolitan Area, followed by Ai (2016), who subdivided the population data into two generations: the young generation (aged 0–17) and productive-age generation (aged 18–59). Ai (2020) applied the LES method to maintain the generation subdivision; however, it changed its spatial unit from local districts to 500-meter census grids. In Japan, several statistics are aggregated in a uniform census grid system with unique code numbers, designated as the Japanese Industrial Standard. In this study, we employ the so-called “1/2 region mesh” which has the width of 22.5 seconds longitude and the height of 15 seconds latitude; in the case of Japan, both width and height will be approximately 500 meters.

Thirteen living environment indices were considered for the LES calculation (Table 1). The target area of this analysis is the Greater Tokyo Metropolitan Area, which consists of Tokyo, Saitama, Chiba, and Kanagawa Prefectures. Census grids with zero population and grids designated as confidential because of their small population were omitted from the analysis, leaving 22,863 grids for the young generation and 27,904 grids for the productive-age generation.

* 正会員 (GISA member) 昭和女子大学 人間社会学部 (Showa Women’s University) **hisaai@swu.ac.jp**

Table 1. Living environment indices and the data source

Index	Data source
Distance to railway station	DNLI, Railway time-series data
Distance to hospital	DNLI, Public facility data (2006); hospitals, medical centers
Distance to police	DNLI, Public facility data (2006); police stations, police boxes
Distance to firefighting services	DNLI, Public facility data (2006); fire departments, fire houses
Presence or absence of parks	DNLI, Urban park data (2011)
Number of stores	Establishment and Enterprise Census (2006); stores, restaurants
Number of businesses	Establishment and Enterprise Census (2006); establishments, offices
Slopes	DNLI, Elevation and slope data / 5th level census grid (2011)
Population density	National Census (2000)
Aging rate	National Census (2000)
Average number of household members	National Census (2000)
Vacant lot rate	DNLI, Detailed land use data / 5th level census grid (2011)
Detached house rate	National Census (2000)

* DNLI: digital national land information
Translated into English based on Table 2 appears in Ai (2020)

2.2. Calculation of the Living Environment Score

The calculation of the LES is roughly divided into three parts.

In the first part, we categorize the 500-meter census grids into population trends groups of "increase" and "non-increase" based on the population data of National Census conducted in 2000, 2005, and 2010. In this study, a census grid will be marked as "increase" when it satisfies either of the conditions listed in Table 2.

Here, expected population is calculated by applying the population change ratio for the entire target region to each census grid. The young population decreased by 8.3% from 2000 to 2005 and by 0.5% from 2005 to 2010, while the productive-age population decreased by 7.1% from 2000 to 2005 and by 1.2% from 2005 to 2010. Hence, it should be noted that the census grid may be categorized into "increase" even when the population of the census grid is slightly declining.

Then we develop cross-tabulation tables between population trends groups and the level of each living environment index shown on Table 1. Chi-square analysis and residual analysis are applied to these cross tabulation tables to test whether there is a significant relationship between the level of living environment and the population trends. Finally in the first part, we determine appropriate level preferred to the residents, which can be considered as the standard that the area should satisfy to attract residents, for each living environment index respectively.

In the second part, the analogy of discriminant analysis is used to derive the magnitude of impact on population change for each living environment index. As the result of residual analysis conducted in the first part, we have already obtained the standard shown in Table 3. From the

Table 2. Condition where the census grid is marked as "increase"

(a)	A population increased at either of combination of two Census results. [AND] Even for the other combination of two Census results, the population is larger than the expected population.
(b)	A population is at least 2% higher than the expected population for the comparison of both 2000-2005 and 2005-2010.

Table 3. Coefficient derived from discriminant analysis

Index	Young		Productive age	
	Standard	Coefficient	Standard	Coefficient
Distance to railway station	Less than 1500 m	0.162	Less than 1000 m	0.154
Distance to hospital	Less than 1500 m	0.254	Less than 1000 m	0.076
Distance to police	Less than 500 m	0.148	Less than 500 m	0.058
Distance to firefighting services	Less than 1000 m	0.210	Less than 1000 m	0.030
Presence or absence of parks	Presence	0.077	Presence	-0.214
Number of stores	Over 11	-0.042	Over 11	0.263
Number of businesses	Over 11	-0.019	Over 11	-0.474
Slopes	Less than 1 degree, excluding 0	0.091	Less than 1 degree	0.096
Population density	Over 20 person / ha	0.362	Over 40 person / ha	-0.135
Aging rate	Less than 25 %	-0.166	Less than 20 %	0.395
Average number of household members	Between 1.5 and 3	0.138	Less than 2.5	0.044
Vacant lot rate	Over 0 excluding absolutely 0	-0.091	Over 5 %	-0.132
Detached house rate	Less than 80 %	0.527	Less than 60 %	0.881

Translated into English based on Table 2 appears in Ai (2020)

discriminant analysis we obtain coefficient shown in Table 3, which is a relative magnitude of each explanatory variable on population change. Hence, we believe that the absolute value of this coefficient is a reliable substitution of the magnitude representing the priority order of residents' preference.

In the third part, which calculates the LES for each census grid, we compared the level of the 13 living environment indices in each census grid with the standard calculated in the first part. For the indices that satisfied the standard, we summed the discriminant coefficients obtained in the second part. This raw score is higher if the census grid satisfies the standard for more living environment indices or if the census grid satisfies the standard of the living environment with a large magnitude.

Finally, the LES was calculated by converting the raw score into a deviation value for the entire target region. A census grid with average attractiveness is marked as 50, and those with higher scores are considered to have a living environment that exceeds the average level from the standpoint of residential selection.

Figures 1 and 2 show the spatial distributions of the LES for young and productive-age generations, respectively. As shown in both figures, grids with high LES were found

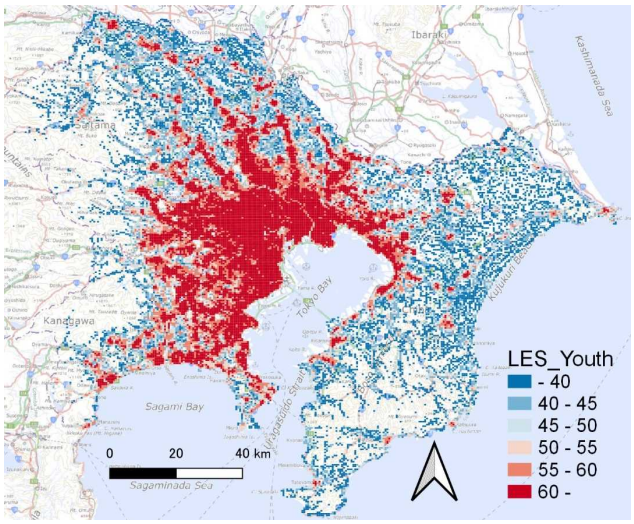

Fig. 1. LES for young generation
(Base map: GSI tile, Geospatial Information Authority of Japan)

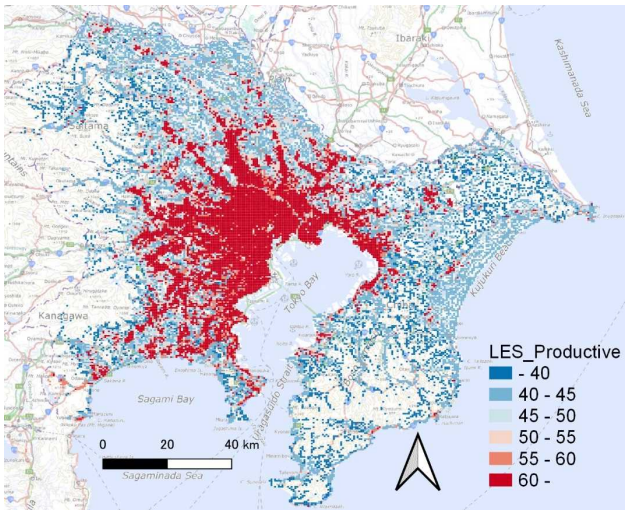

Fig. 2. LES for productive age generation
(Base map: GSI tile, Geospatial Information Authority of Japan)

in downtown Tokyo and the suburbs, mainly in the west direction. In the northern suburbs, some axes of the high LES grids are located along the inter-urban railway lines.

3. The LES and Population Trends

3.1. Definition of Population Trends

This report aims to discuss whether areas with a high LES experience an increase in population. If the LES, which is derived from population trends between 2000 and 2010, can explain population trends after 2010, it is useful for city planning decision-making because it can reflect the attractiveness of the area and be reliable for future population forecast. In this report, we calculated two types of population trends between 2010 and 2020: the first is a comparison of the 2010 census population and the 2020 census population, and the second is a comparison of the 2020 population forecast and the 2020 census population. Hereafter, we call the first and second types as "trend comparison" and "forecast comparison," respectively. Due to the data limitation of the population forecast, the young generation is redefined as those aged 0 to 14 years and the productive-age generation as those aged 15 to 64 years.

For trend comparison, population data for both 2020 and 2010 were obtained from the National Census; hence, they can be considered to reflect the real change in population. For forecast comparison, we compared the population forecast for 2020 calculated in 2010 with the real population of 2020 obtained from the National Census. The forecast comparison indicated that the area showing population change exceeded the expected level. If the forecast comparison shows a significant increase, this indicates that the area is attractive to residents.

3.2. Results of Trend Comparison

Table 4 shows the cross-tabulation table between the LES and the results of the trend comparison. Census grids with a population of less than 10 for either generation were excluded from the cross-tabulation. A block on the left side is the result of the young generation, and the right side is the result of the productive-age generation. The upper number in each cell shows the frequency, and the lower number shows the standardized residuals obtained from the residual analysis. Cells are highlighted in orange if the standardized residual is greater than 1.96, which means that significantly more cases are categorized into this cell; cells are highlighted in blue if the standardized residual is less than -1.96, which means that significantly fewer cases are categorized into this cell.

If the LES was high, the area was significantly likely to experience a population increase between 2010 and 2020. However, if the LES was low, the area was likely to experience a population decline. The threshold for population increase and non-increase is an LES of 60 for the young generation and an LES of approximately 50–55 for the productive-age generation.

The results show that the average level of the living environment, an LES of 50, is not sufficient to attract residents to the area. This can be confirmed by the fact that only 41.8% of the grids with LES of the young generation over 50 recorded a population increase, and only 46.0% of the grids with LES of the productive-age generation over 50 recorded a population increase.

Table 4. LES and trend comparison results

	Young		Productive	
	Increase	Decline	Increase	Decline
-40	557 -20.46	2481 20.46	442 -23.43	3013 23.43
40-45	828 -12.58	2465 12.58	1593 -28.39	7105 28.39
45-50	727 -6.28	1767 6.28	1200 -6.63	3449 6.63
50-55	837 -1.90	1691 1.90	535 1.52	1163 -1.52
55-60	1280 -1.92	2546 1.92	480 2.32	994 -2.32
60-	3728 30.97	3956 -30.97	4086 49.79	3844 -49.79

Figures 3 and 4 show the spatial patterns of the LES and trend comparison for young and productive-age generations, respectively. The red color illustrates that the LES of the grid is over 60 and that the population is

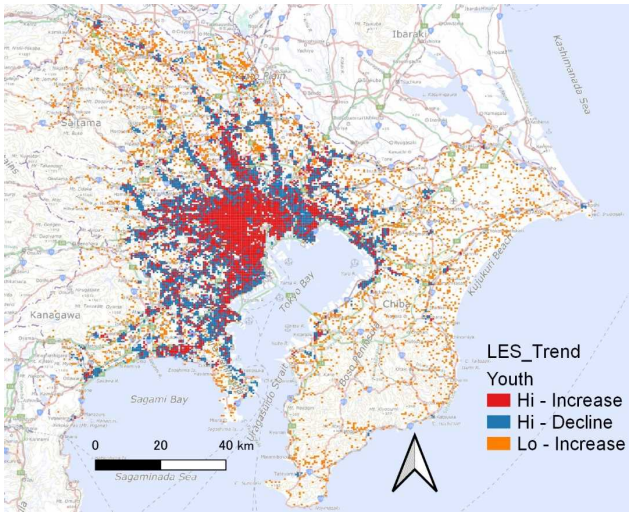

Fig. 3. LES and trend comparison, young
(Base map: GSI tile, Geospatial Information Authority of Japan)

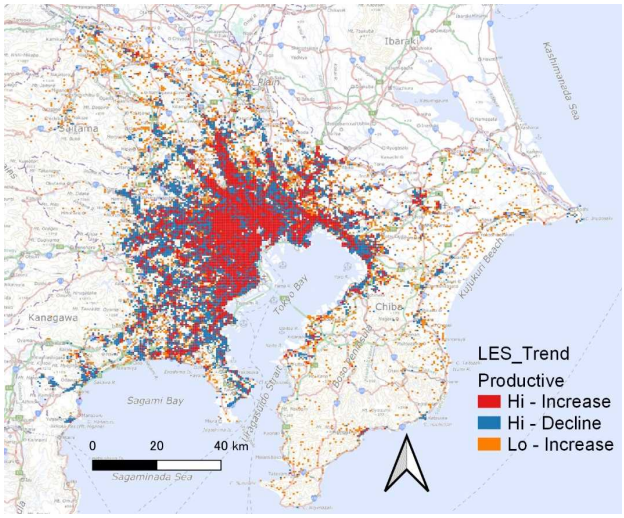

Fig. 4. LES and trend comparison, productive age
(Base map: GSI tile, Geospatial Information Authority of Japan)

increasing for the young generation (or the LES is over 55 for the productive-age generation); the blue color is the grid of the LES over 60 for the young generation and over 55 for the productive-age generation with population decline. The orange color is the grid of the LES under 50 with population increase; by comparing figures 1 and 3, or 2 and 4, we can visually understand that the high LES grids are divided into red and blue grids in figures 3 and 4, and that the red grids are mostly surrounded by the blue grids.

As shown in Table 4, there were 3,728 red grids and 3,956 blue grids for the young generation. In contrast, 2,112 orange grids were dispersedly distributed, as shown in figure 3. Similarly, there were 4,566 red grids, 4,838 blue grids, and 2,035 orange grids for the productive-age generation.

Here, blue grids are the majority in map visualization, which indicate the grids where we may overestimate the attractiveness of the living environment. Distinguishing the red grids from the blue grids without referring to population data will provide reliable information for setting urban cores for compact city planning before the city starts to shrink. However, both red and blue are grids with a high LES, which means that there are no clear differences between the living environment indices used in the LES calculation. Hence, we must discuss an additional living environment index to distinguish the red from blue grids.

3.3. Results of Forecast Comparison

Table 5 shows the cross-tabulation table between the LES and forecast comparison results. If the LES is > 60, the area's population is likely to exceed the forecasted level, whereas if the LES is < 45, the area's population is unlikely to reach the forecasted level. Because the population forecast is calculated by projecting the current change ratio for the future, the blue grids can be understood as areas that have started to lose their population.

Figures 5 and 6 show the spatial patterns of the LES and forecast comparisons for the young and productive age

Table 5. LES and forecast comparison results

	Young		Productive	
	Increase	Decline	Increase	Decline
-40	1120 -11.24	1918 11.24	1274 -8.71	2181 8.71
40-45	1359 -6.30	1934 6.30	3571 -6.11	5127 6.11
45-50	1161 0.23	1333 -0.23	2044 0.32	2605 -0.32
50-55	1214 1.80	1314 -1.80	738 -0.25	960 0.25
55-60	1784 0.40	2042 -0.40	637 -0.43	837 0.43
60-	3956 11.10	3728 -11.10	3945 12.72	3985 -12.72

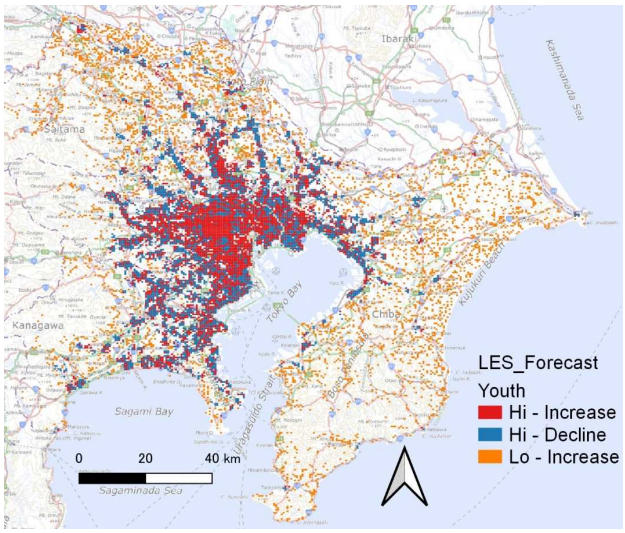

Fig. 5. LES and forecast comparison, young
(Base map: GSI tile, Geospatial Information Authority of Japan)

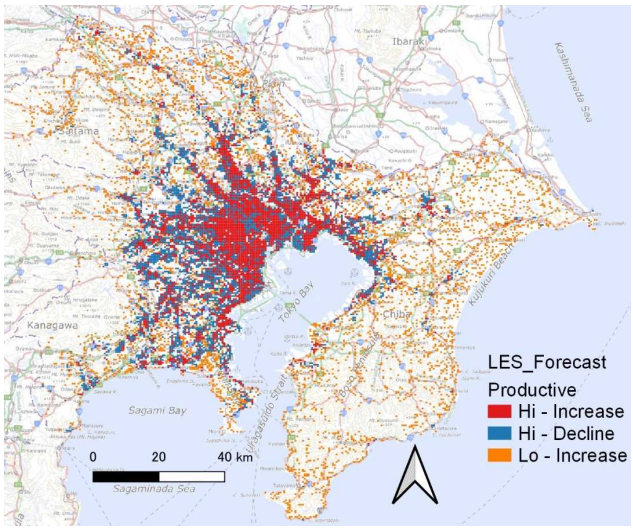

Fig. 6. LES and forecast comparison, productive age
(Base map: GSI tile, Geospatial Information Authority of Japan)

generations, respectively. Compared to figures 3 and 4, the blue grids of the forecast comparison are more likely to be distributed sparsely in a mosaic pattern than in the case of trend comparison.

Table 5 shows that for the young generation, there were 3,956 red grids, 3,728 blue grids, and 2,479 orange grids. For productive-age generation, there were 3,945 red grids, 3,985 blue grids, and 4,845 orange grids. Similar to the trend comparison, we found a certain number of blue grids where the population was overestimated.

Here, we focus on the grids categorized in blue for both trend and forecast comparisons; these grids are facing unexpected population decline. The number of grids was 2,918 for the young generation and 3,114 for the productive-age generation. Figures 7 and 8 show the spatial distributions of the grids for each generation. It is difficult to find any clear spatial patterns for these grids, except that we rarely find them in downtown Tokyo. Hence, in the suburbs, an area with unexpected population decline may occur, regardless of the distance from downtown or the prefecture to which the area belongs.

4. Conclusion and Future Challenges

Owing to the significant change in the Japanese

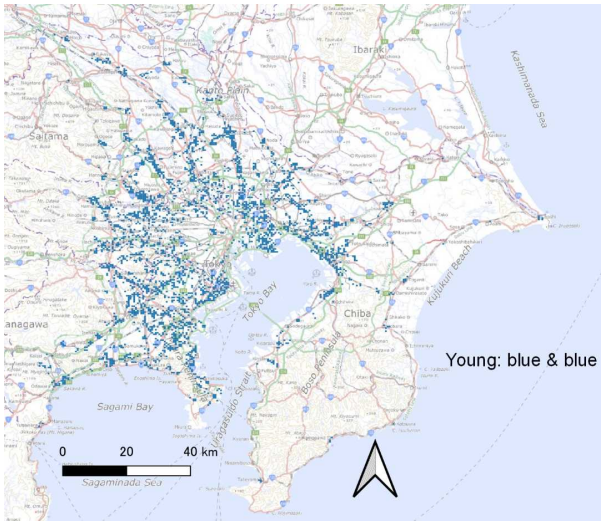

Fig. 7. Census grids with unexpected population decline, young
(Base map: GSI tile, Geospatial Information Authority of Japan)

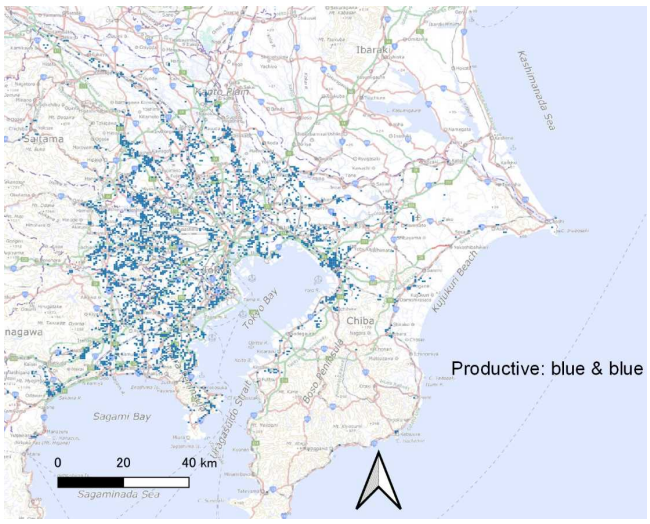

Fig. 8. Census grids with unexpected population decline, productive
(Base map: GSI tile, Geospatial Information Authority of Japan)

population trend from increasing to declining, the city planning system of Japan has changed its main issue from growth control to compact city planning. In compact city planning, it is important to identify areas that attract residents to their living environments. The living environment score (LES) is a comprehensive evaluation score derived from 13 living environment indices with the point of view of whether the area attracts residents. This study visualized the LES levels and population trends. Two types of population trends were employed in this study: trend comparison showing the increase or decline of the actual population, and forecast comparison showing over- or underestimation. Our main focus was on census grids showing population decline with a high LES. However, we could not find any clear spatial pattern of those grids; hence, we must further discuss the characteristics of these grids in future work.

Acknowledgement

This research is supported by the joint research program with the Center for Spatial Information Science, the University of Tokyo: JoRAS joint research No. 1156.

Notes

1) Item 2, Section 1, Chapter 3 in White Paper on Land, Infrastructure, Transport and Tourism in Japan, 2014. p121.

References

AI. H, (2014) How living environment indices effect on population change patterns of local districts - An analysis on urban area in the Greater Tokyo Area -, Journal of the City Planning Institute, 49 (3), pp. 567-572. In Japanese.

AI. H, (2016) Indexing of living environment attracts young and productive age generations - An analysis based on local districts within the Greater Tokyo Metropolitan Area -, Journal of the City Planning Institute, 51 (3), pp. 860-866. In Japanese.

AI. H, (2020) Calculating living environment index forecasting population increase in a grid based spatial units - Comparison of the result between a census grid basis and a basic unit block basis -, Journal of the City Planning Institute, 55 (1), pp. 41-48. In Japanese.

Applicability of alternative data for the identification of urban activity centers (UAC)

Vadim Boratinskii*, Toshihiro Osaragi**

Abstract: The spatial distribution of urban activities and places of their concentration in cities (urban activity centers – UAC) is one of the main issues within Urban Spatial Studies. However, due to the inaccessibility of corresponding data, the data not related to urban activities directly were used to study urban activities and detect UAC in most previous works. In this research, we use the results of Person Trip Survey for 23 special wards of Tokyo as the data describing urban activities directly to clarify the previously understudied relationship between the actual activities and alternative data commonly used to analyze them. Given the availability and relevance to the study area, Twitter data, Building Point data by Zenrin and POI of OpenStreetMap are used. This study clarifies the applicability of urban activity indicators extracted from these data by means of UAC modelling with machine learning algorithms.

Keywords: Urban activity, urban centers, spatial modelling, data selection, alternative data

1. Introduction

Since the second half of the 20th century, there is a trend to characterize the urban spatial structure through the analysis of urban centers and the relationships between them (Anderson et al., 1996). Accordingly, the detection and delimitation of urban centers became the major issue in Urban Studies.

Originally, urban centers and other elements of the urban spatial structure were studied from the perspective of the distribution of workplaces in a city. A widely known example of centers within this paradigm are central business districts (CBD) which are the core objects in ecological urban models of the Chicago School of Sociology (Schwirian, 2007). A particular example of urban centers identified based on employment patterns in Japan are the cores of Urban Employment Areas (UEA, 2015) that may be described as municipalities to which intensive commuting from suburbs takes place.

Although, as the case of UEA demonstrates, there are still methods for identifying urban centers based on the employment patterns, the primary trend in Urban Studies for the last decades has shifted to the analysis of multifunctional urban centers (De Goei, 2010; Pomorov & Zhukovsky, 2015).

The problem that emerged in relation to this shift is the search for the appropriate data to be used as an indicator of various urban activities concentrating in urban centers. Given the lack of data representing urban activities directly, scholars started to use indicators extracted from different alternative data sources (alternative indicators) such as social media and cell phone data, data on the location, area or revenue of businesses and other points of interest, satellite images and surveys' results (Frias-Martinez et al., 2012; Cai et al., 2017; Goncharov & Nikoghosyan, 2016; Riguelle et al., 2007).

In most of studies, alternative data is used without illustrating how it is related to the targeted variable (urban activity). The objective of this paper is to clarify the relationships between widely used alternative indicators and multifunctional urban activity occurred in cities. Taking 23 special wards of Tokyo for the study area, we intend to demonstrate which alternative indicators are more or less reliable for representing urban activities and, therefore, appropriate for the identification of UAC.

2. Data

2.1. Target indicator of urban activity

The role of the target data within this study is to represent the spatial distribution of urban activities directly. We use the results of the 6th Person Trip (PT) Survey collected in 2018 (Tokyo Metropolitan Area

* 学生会員 東京工業大 環境・社会理工学院 (Tokyo Institute of Technology) boratinskii.v.aa@m.titech.ac.jp
** 正会員 東京工業大 環境・社会理工学院 (Tokyo Institute of Technology)

Transportation Planning Council, n.d.) to extract the target indicator of urban activity (PT indicator). It represents the number of people visiting a certain place in Tokyo for a purpose that is related to outside-of-home activities such as work, eating out, leisure, shopping, etc. Thus, PT-indicator corresponds to the density of activities in a certain area within a single weekday. It is important to mention that PT data is collected only once in 10 years, so it does not reflect short- and mid-term changes occurred between surveys. Additionally, it is characterized by a certain sampling error, albeit relatively low.

2.2. Alternative indicators of urban activity

Alternative indicators reflect the data commonly used for UAC studies but are not related to urban activities directly. Given the availability, we used Twitter, Building Point (BP) data by ZENRIN and Points of Interest (POI) of OpenStreetMap (Table 1). The variables created from these datasets are presented in Table 2.

Table 1. Alternative data – datasets

Twitter data	Geotagged tweets posted from September to November 2018. Extracted using the Twitter API
Building Point (BP) data	Point data on buildings location and their characteristics such as the number of rooms by functions and total floor area occupied by functional types of facilities
Points of Interest (POI)	OpenStreetMap (OSM) dataset with coordinates of points that were found interesting. OSM is an open geographic database that is updated by the community of volunteers

Table 2. Alternative data – alternative indicators

Tweets-night	The number of users posted geotagged tweets from 0:00 to 6:00 (count)
Tweets-day	The number of users posted geotagged tweets from 6:00 to 24:00 (count)
BP-vacant	Total floor area (TFA) of vacant rooms in buildings (m^2)
BP-private	TFA of private residential rooms in buildings (m^2)
BP-target	TFA of government offices, public facilities (schools, medical institutions, etc.), shrines, and temples (m^2)
BP-business	TFA of business-occupied rooms in buildings (m^2)
BP-other	TFA of other facilities including apartment manager offices, warehouse, indoor parking lot, ATM corner... (e.g. warehouse, indoor parking) (m^2)
POI-tourism	Guesthouse, hostel, hotel, motel (number)
POI-open	Camp site, outdoor sports facilities, track, dog park, fountain, garden center, park, picnic site, playground, viewpoint, zoo (number)
POI-leisure	Attraction, cinema, mall, nightclub, theatre, arts center, artwork, museum, theme park (number)
POI-food	Café, pub, bar, fast food, food court, restaurant (number)
POI-daily	Bakery, convenience, department store, greengrocer, outdoor shop, pharmacy, supermarket, butcher (number)
POI-other	All stores other than those listed in the "daily" (e.g. book-, computer-, furniture-, gift-, shoe-, shop) (number)
POI-services	Bank, beauty shop, car rental, car wash, car sharing, doctors, library, dentist, hairdresser, veterinary, laundry, tourist info, tourist agent, post office (number)
POI-education	College, kindergarten, school, university (number)
POI-public	Clinic, community center, courthouse, embassy, fire station, police, shelter, town hall (number)
POI-vending	Vending machines (experimental group) (number)

3. Urban activity centers (UAC)

3.1. UAC – concept and applicability

In most general terms, UAC are areas of a city where the concentration of outside-of-home urban activities is significantly higher than in their surroundings. This definition is associated with the group of methods involving spatial-statistical modelling for the identification of urban centers. The feature of UAC-like methods is that they allow to identify centers attracting people on different scales (regional, intraurban, district and local), while by traditional methods (e.g. CBD identification) one may detect only points of the highest activity in a city (Fig. 1). UAC are believed to be a more effective and suitable option for targeting city-level planning measures precisely since they represent most attraction points of a city irrespective of their location and size in the urban structure.

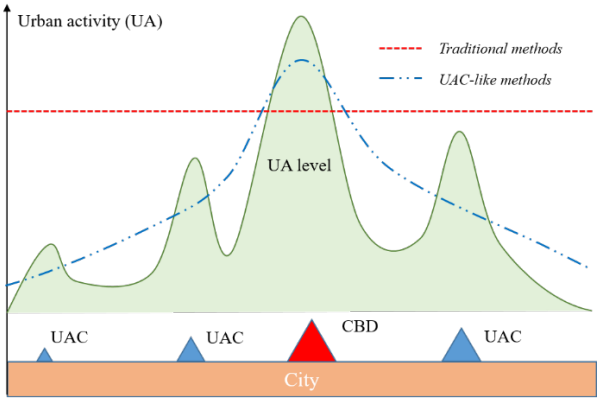

Figure 1. Scheme of the UAC detection method

3.2. UAC identification algorithm

A significant contribution to the development of spatial-statistical methods for the identification of urban centers was made by D.P. McMillen, J.F. McDonald (McMillen & McDonald, 1997; McMillen, 2001) and Vysokovsky (2005). Although McDonald, and McMillen worked within the paradigm of employment subcenters and Vysokovsky analyzed centers of commercial activity, their methodological findings are widely used for the studies of multifunctional urban centers (e.g. Riguelle et al., 2007; Cai et al., 2017; Goncharov & Nikoghosyan, 2016).

In 2019, Boratinskii proposed a new algorithm for the identification of UAC based on the same methodological

foundation (Boratinskii & Tikhotskaya, 2021). Its steps applied for this study are summarized below.

Before the analysis itself, the spatial grid is selected. Given the use of the matrix of neighbors in the later steps, the grid of regular hexagons is considered a preferable option. The size of cells is adjusted to the study area based on the desired balance between precision and generalization. We selected two grids with the side length of 173 m (0.078 km^2) and 144 m (0.054 km^2). Hereafter, they are called grid-L and grid-S respectively.

As the first step, the selected indicator of urban activity is aggregated by the grid(s) (Table 3 – step 1). Two crucial components of the UAC identification algorithm – local activity trend (y) and global activity trend (X) – are extracted from its actual distribution. The local activity trend is the urban activity level in the surrounding cells, while the global trend is the general decrease in urban activity level from the city center to the periphery. The latter is quantified as the distance from each cell to the closest of the global centers selected as the points of the highest urban activity in the urban structure. Global centers of Tokyo are outlined in the step 2 map in Table 3.

The second step is the modelling of urban activity based on X and y by means of the spatial autoregression:

$$\hat{Y} = \mu + Xb + pWy \qquad (1)$$

where $\hat{Y}$ is estimated urban activity, b – regression coefficient, W – matrix of neighborhood, p – autoregressive parameter and μ – regression bias. Local trend autoregressive component (pWy) allows to estimate urban activity in each cell based on values in neighboring cells, while global trend (Xb) is included to detect UAC equally in all parts of a city (see step 2 of Table 3).

The last step is the extraction of significant positive residuals from the model. Basically, residuals from the spatial autoregression represent the component of urban activity that is not explained by local and global trends. According to our definition, the urban activity in UAC should be significantly higher than in surroundings irrespective of the distance to the city center, so the significant positive residuals from the model correspond to UAC cells (step 3 in Table 3). The threshold for statistical significance is found by the following formula:

$$Sign_{res} > Q3 + 1.5 \times IQR \qquad (2)$$

where $Sign_{res}$ is significant residuals, $Q3$ – third quartile and IQR is the interquartile range of the residuals' distribution.

Table 3. UAC identification algorithm

Step #	Visualization of steps (grid-L)
1. Actual distribution of urban activity	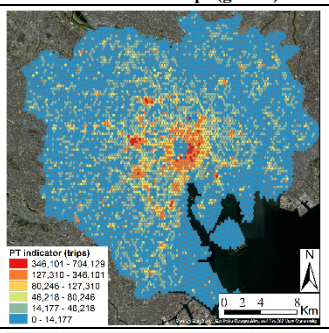
2. Modelled distribution of urban activity and the location of global centers	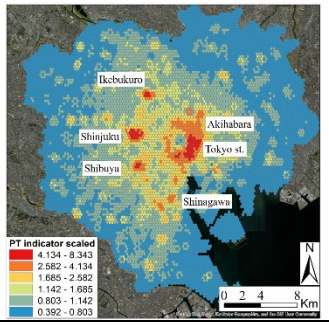
3. Significant positive residuals	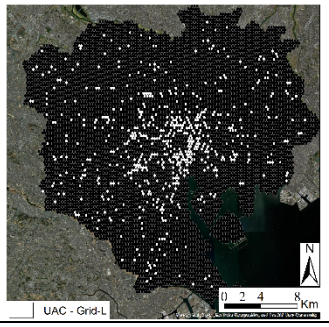

In Table 3, PT-indicator is processed through the UAC identification pipeline; however, any urban activity indicator may be used this way.

4. Methodology

4.1. Modelling approach

In this paper, the modelling of UAC from alternative indicators is a way to clarify which of them are the most reliable and relevant for urban activity studies and what is their potential for the UAC identification. The modelling consists of two steps. The first one is to estimate the distribution of the target indicator of urban activity (PT-

indicator) by regression model in which alternative indicators are used as predictors. The second step is the identification of quasi-UAC by applying the UAC identification algorithm to the regression-estimated values of the PT-indicator.

Taking our goal of clarifying the relevancy of alternative indicators for estimating actual urban activity level into account, the application of interpretable machine learning methods is prioritized over the accuracy of predictions. The simplest transparent and transferable tool satisfying such conditions is linear regression (LR). The problem is that this model has several limitations of applicability known as assumptions of LR. These assumptions are linear relationship between independent variables and the target variable, multivariate normality, no or relatively low collinearity, homoscedasticity of residuals and normality of their distribution.

If the data does not satisfy these conditions, there is a risk that model's prediction will be unstable and the interpretation of the model may be misguiding. Given this, the data is analyzed with respect to the main assumptions of LR before being used in modelling.

4.2. Preliminary data analysis

Although it is usually considered as the preliminary analysis not related to the targeted results directly, the LR assumption tests provide findings that are important for this study since they reveal how quantitatively (linearity test) and qualitatively (collinearity test) variables are interrelated.

In Figure 2, histograms showing the distribution of alternative indicators (left) and scatter plots illustrating their relationship with the target variable (right) are depicted. Only one or two variables from each dataset were selected to avoid plotting dozens of almost similar graphs. In histograms, there is a clear common pattern for all alternative indicators – their distribution by small grid is strongly skewed to the right. The degree of the skewness varies depending on the data, being the lowest for BP data. The significant number of zero values for Twitter and POI indicators may be also highlighted as a potential problem related to the use of small cells.

In the right part of Figure 2, the trend line with a 0.95 confidence interval is added to scatter plots. It corresponds to the LOESS curve which may be described as a locally weighted polynomial regression. It is clear from the plots that the relationship between alternative and target variables is not linear with the exception of BP-business. Another feature that may affect the performance of LR is that the majority of data instances is concentrated in the low-value range. Therefore, the linear algorithm will fit mostly to low-value data, whereas UAC by their nature are objects characterized by rather high values of activity indicators.

Several tests demonstrated that the data transformations often used for this purpose are insufficient to achieve neither normality nor linearity of the distribution of urban activity indicators aggregated by small cells (hexagon side below 500 meters). Since urban activity studies recently tend to be conducted by rather small regular or administrative grids, this may be highlighted as the major methodological problem. Taking into account our goal to clarify the relationship between variables and make the model interpretable, more complicated transformations were not considered.

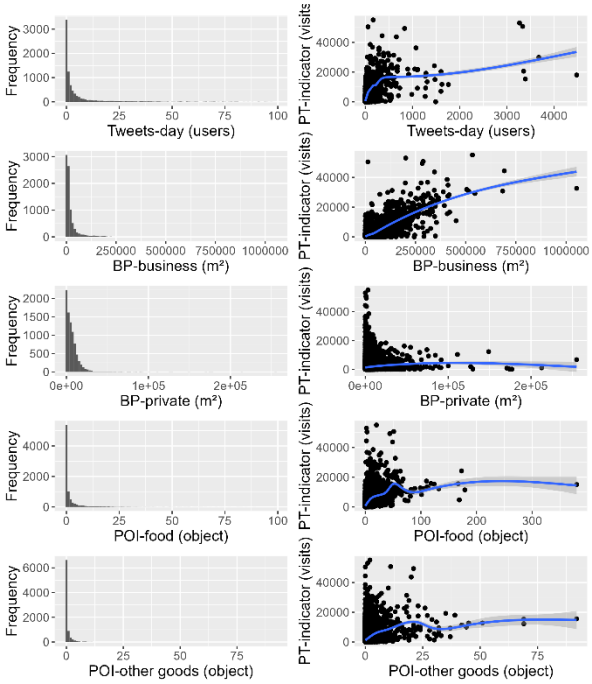

Figure 2. Normality and linearity tests (grid-S data)

The next assumption of LR – relatively low multicollinearity – may be checked using the correlation matrix (divided into two matrices for readability in Fig. 3). Since the distribution of variables is not normal, the Spearman's rank correlation coefficients were calculated.

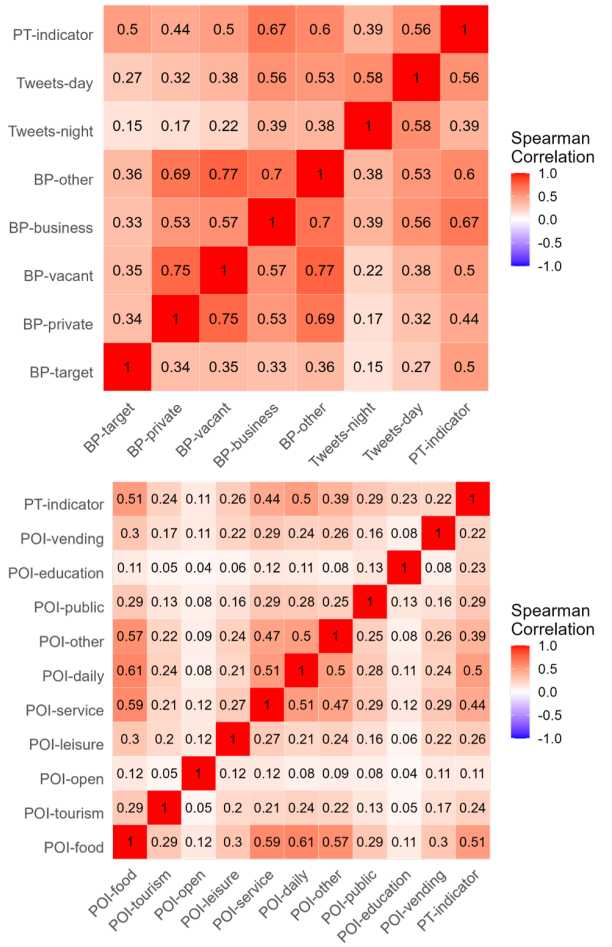

Figure 3. Correlation matrices (grid-S data)

The relationship between all alternative indicators and the PT-indicator is positive, however, the difference in the correlation degree is significant between datasets and variables within them. BP data, especially 'BP-business' and 'BP-target', are characterized by the highest correlation along with Tweets-day. The correlation with POI variables tends to be lower, however, POI-food, -service and -daily goods are almost on the same level. The problem for LR is that there is a relatively high correlation between alternative indicators within their groups and this correlation is in some cases higher than with the target variable. The example is commercial POI (namely 'food', 'daily goods', 'other goods' and 'service').

4.3. Linear regression

As follows from the preliminary analysis, the data distributed by small cells does not satisfy the assumptions of LR. Despite this, we decided to build the linear model after modifying the matrix of variables: highly correlating predictors were merged or removed. Table 4 summarizes these transformations and lists the resultant variables used in LR.

Table 4. Transformation of alternative variables

Original variables	LR variables
Tweets-night	Tweets-night
Tweets-work	Tweets-day
Tweets-leisure	
BP-vacant	-
BP-private	BP-private house
BP-target	BP-business (+target+other)
BP-business	
BP-other	
POI-tourism	POI-tourism
POI-open	POI-open
POI-leisure	POI-leisure
POI-food	POI-daily (+food)
POI-daily	
POI-other	-
POI-service	-
POI-education	POI-education
POI-public	POI-public
POI-vending	POI-vending

To increase the stability of model's performance and to make the regression coefficients comparable and, therefore, interpretable, the standard scaling is applied for independent variables.

The LR model built using all alternative indicators from Table 4 had two insignificant variables (95% confidence level) and three variables with negative coefficients. Since their correlation with the target variable (PT-indicator) is positive, such negative regression coefficients are caused by 'suppressed relationship' (Falk & Miller, 1992). After removing both insignificant variables and those with negative coefficients, the new model was built. Its summary is presented in Table 5.

4.4. Decision tree models

Obviously, merging or removing highly correlating predictors allowed to mitigate only the problem of multicollinearity, whereas non-linearity and non-normality were not addressed. As it was mentioned, the interpretation of a model built on such data and its results

may be misleading. To verify them, we built non-linear regression models based on the decision tree (DT) algorithm in addition to LR. DT models subdivide data instances by thresholds in independent variables in a way to create subgroups as homogenous by the target variable as possible. DT-based algorithms are considered a preferable option because they do not require a certain type of distribution or low multicollinearity and are suitable for finding relationships for different value ranges within a single dataset (Breiman, 2001). The latter is crucial for this study as UAC may vary significantly in urban activity level. The combined use of linear regression and decision-tree methods is expected to provide insights into the applicability of linear models for nonlinear spatial data.

Although single DT algorithms are generally suitable for the data with the distribution described above, they tend to either overfit or perform weakly. Due to this, the DT-based ensemble algorithms are used instead. In ensemble models, several trees are stacked horizontally – random forest (RF) or sequentially – Gradient Boosting (GBoost) – that allows to avoid overfitting and improve the accuracy of predictions (Breiman, 2001; CatBoost, n.d.).

Since non-parametric algorithms such as DT are not sensitive to multicollinearity and do not require the scaling of independent variables, we use all POI, Twitter and BP indicators listed in the left column of Table 4 for the prediction of the PT-indicator. Optimal hyperparameters of DT-based models were found by cross-validated grid-search over a parameter grid.

4.4. Train and test datasets

LR and DT-based models are fitted to 80% of randomly selected samples of grid-S. It was selected for training as the one having more cells and, therefore, providing more information from which algorithms may learn patterns. 20% of grid-S and all cells of grid-L were used for the testing of models. Although the study area for both grids is the same, the subdivision into cells between grids is different, so it is acceptable for validating the local patterns captured by models. To make the validation of models fitted for the grid of one size possible on the data aggregated by a grid of another size, all predictor values (alternative indicators) were divided by the area of cells. In this paper, we focus on the results for grid-L (test data).

5. Results

5.1. Linear regression

The summary of LR model presented in Table 5 provides the information on the overall accuracy of predictions for the test sample and the importance of predictors for estimating the target variable. In this chapter, we use adjusted R^2 as the regression accuracy metric for both LR and DT-based models.

Table 5. LR model summary

LR predictors	Estimate	p value	Adjusted R^2
(Intercept)	22392.89	0.00	$R^2 = \frac{\sum_{i=1}^{n}(y_i - \hat{y}_i)^2}{\sum_{i=1}^{n}(y_i - \bar{y}_i)^2}$
BP-business+ target+other	31611.53	0.00	
Tweets-day	9249.56	0.00	
POI-open	1215.00	0.00	$R^2_{adj} = 1 - (1 - R^2) \times \frac{(n-1)}{(n-k)}$
POI-daily+food	7003.42	0.00	y – target variable value, $\hat{y}$ – predicted value, $\bar{y}$ – mean value, n – sample size, k – number of predictors
POI-public	1623.21	0.00	
POI-education	3072.83	0.00	
Adjusted R^2 for test samples of grid-L			**0.7318**

Although the accuracy of linear model may seem relatively high and acceptable for the estimation of urban activity, we still highlight that not all conditions required for the stable performance of this type of algorithm are satisfied.

As for the significance of predictors, the BP-business (a variable also including BP-target and BP-other) is outstanding among alternative variables. In other words, the total floor area of facilities occupied by business and public facilities is the alternative indicator contributing to the prediction of urban activity the most. Based on the regression coefficients, the number of users who posted geotagged tweets in the daytime and the density of daily goods and food shops reflected in POI data are the second-third most reliable indicators of urban activity. These findings generally correspond to the correlation matrices (Fig. 3); however, they should be verified by non-linear algorithms given the specifics of the data.

5.2. Non-linear algorithms

The accuracy of estimation of the PT-indicator by both DT-based and LR models is outlined in Table 6. As we expected, the single decision-tree model performed even less precisely than linear regression, not to mention the ensemble algorithms. Due to this, the single-DT model is not used for the following steps of analysis.

In contrast to the single DT, RF and GBoost models appear to outperform LR by accuracy. The accuracy of GBoost is slightly higher than that of RF, however, it is unclear yet what potential three models provide for the UAC modelling.

Table 6. Regression models' accuracy (adj. R^2)

Model	Grid-S test set	Grid-L test set
DT	0.6451	0.7011
LR	0.6665	0.7318
RF	0.7090	0.7561
GBoost	0.7001	0.7683

The importance of features in three regression models is summarized in Figure 4. Originally, measures of importance differ depending on the model – it is regression coefficients in the case of linear regression and a metric indicating how effective the splits by a certain feature are for DT-based ensemble models (see CatBoost (n.d.), Scikit learn (n.d.)). To make a comparative summary of all models, we normalized the figures of feature importance using min-max scaling that transformed their values in a range from 0 to 1.

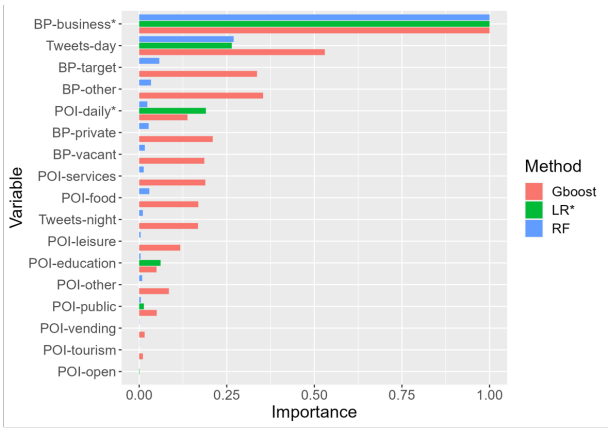

*Variables used for LR are different from other models as explained in chapter 4

Figure 4. Normalized importance of predictors

Irrespective of the method used, BP-business variable is characterized by the highest importance for the prediction of urban activity (PT-indicator) level, while Tweets-day is the second most important feature. This finding reveals that the alternative indicator used by, for instance, Goncharov & Nikoghosyan (2016) – the area of service facilities – is indeed a very decent choice for the analysis of urban activities. Given the relatively low availability of such data, the choice of geotagged tweets (e.g. Frias-Martinez et al., 2012; Boratinskii, Loopmans & Osaragi, 2023) may also be considered reasonable. An important finding is that, as we expected, the nighttime tweets are not so strongly related to weekday urban activities, so using only daytime tweets may be a more proper choice. Yet, the situation for weekends is likely to be different, so the importance of Tweets-night should be studied using the alternative target variable that provides information on activities on Saturday and Sunday.

The next most important features differ depending on the model. All predictors except BP-business and Tweets-day are much less significant in RF, but we can highlight BP-target, BP-other, POI-daily and POI-food among them. In GBoost, both BP-target and BP-other appeared to be almost as important as Tweets-day followed by the rest of the BP variables, POI-services, POI-food, POI-daily, and Tweets-night. Finally, based on the LR coefficients, POI-daily, POI-education, and POI-public explain a certain component of urban activity.

High importance of variables not related to urban activity by their nature in GBoost (BP-vacant and BP-private) is most likely caused by the overall correlation between floor area by all types of facilities (see Fig. 3).

5.3. Identification of quasi-UAC

The last step of clarifying the applicability of alternative indicators for the identification of UAC is the processing of PT-indicator values predicted by three models (LR, RF and GBoost) through the UAC pipeline (identification of quasi-UAC). Since the result of this step is the division of all cells into UAC and non-UAC cells, it may be considered as the result of classification task.

One of the common tools for the analysis of classification modelling is the confusion matrix. The logic

behind it and its main concepts are summarized in Table 7.

Table 7. Confusion matrix for the UAC modelling

	Predicted negative value	**Predicted positive value**
Actual negative value	True negative (TN) – cells correctly classified as non-UAC	False positive (FP) – cells that are actually not UAC but were classified as UAC
Actual positive value	False negative (FN) – cells that are UAC but were classified as non-UAC	True positive (TP) – cells correctly classified as UAC

The results of the UAC modelling by four classes of predictions of the confusion matrix are illustrated in Figure 5. Although it was highlighted earlier that LR is rather unsuitable for the given data, the spatial distribution of correct and incorrect prediction by linear and DT-based models is almost similar. The clearest difference is that the LR model's map is characterized by higher prediction accuracy in the city center and more FP detections in the southeastern periphery of Tokyo (Tokyo Bay zone). Unlike DT-based models that may detect various combinations of high and low values of features, LR with all positive coefficients can only sum features' values multiplied by coefficients. Thus, even if only one alternative indicator has a high value, the estimated urban activity will also be high irrespective of other indicators' values. In multifunctional areas, such as the city center of Tokyo, this one-direction summing worked well; however, it led to numerous errors in areas where, for instance, a significant concentration of workplaces is not associated with leisure or public food facilities.

For the quantitative assessment of the results mapped in Figure 5, the classification accuracy metrics are used (Table 8). F1-score equals 1 for the perfect model and 0 for the model with precision or recall equaling zero. ROC-AUC score equals 0.5 for the random model, 1 for perfect one and 0 for classifier providing reverse values (Hand & Till, 2001).

Table 8. UAC classification accuracy

	F1-score	**ROC-AUC**
LR	0.5579	0.7560
RF	0.5711	0.7703
GBoost	0.5707	0.7676

Despite the potential limitations described above, LR provides results comparable to DT-based ensemble models from the quantitative perspective as well.

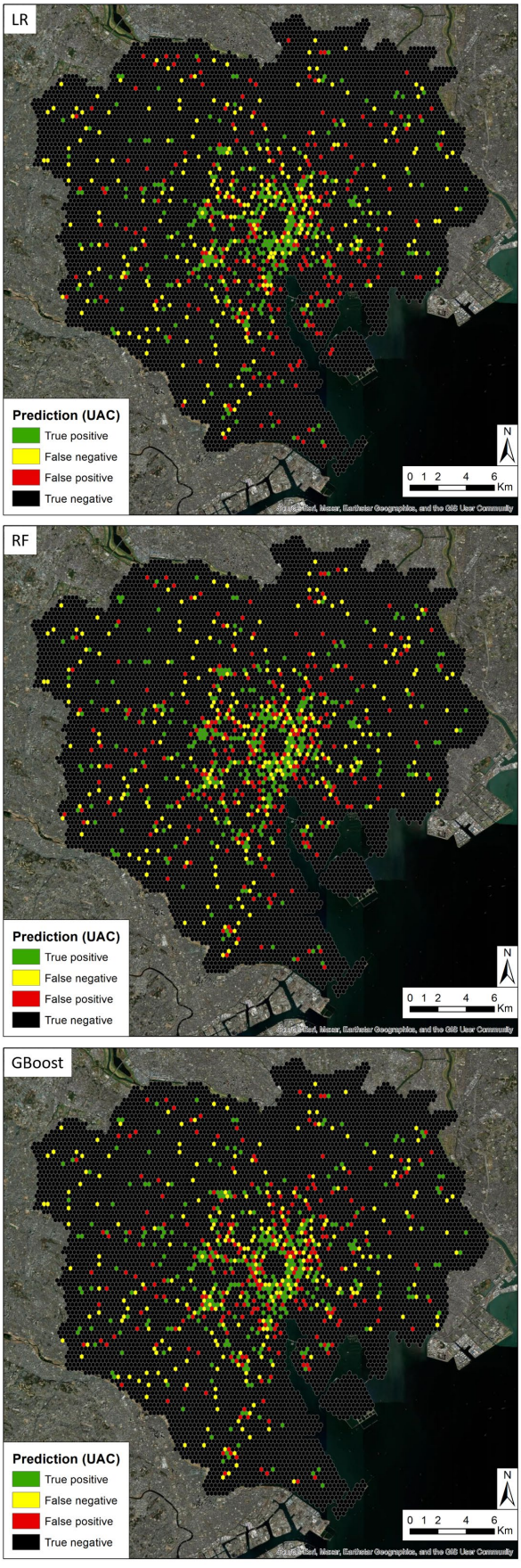

Figure 5. UAC classification by regression models

Although it is unclear whether it would affect other kinds of urban activity studies, we can state that the issues of non-linearity and non-normality of the data distributed by small cells have rather a minor impact on the UAC identification. Yet overall, about 35% of UAC are not detected by the modelling approach used in this study. It requires additional studies to clarify whether it is related to the nature of UAC, the selected indicator of urban activity, or whether supplementing the list of alternative indicators with other data may improve the result.

6. Conclusion

In this paper, we inspected the relevance of commonly used alternative indicators of urban activity for urban activity studies in general and UAC identification in particular. Linear regression and decision-tree-based ensemble algorithms were employed for it. Although the data used in this study seemed unsuitable for linear modelling given non-linearity, non-normality and relatively high multicollinearity between predictors, the results of LR and DT-based models appeared to be almost similar from both qualitative and quantitative perspectives.

Given this lack of controversy, we can state that urban activity reflected by the PT-indicator is associated with a high concentration of floor area occupied by businesses or target facilities (government offices, schools, hospitals, etc.). Thus, this type of data is the best for urban activity studies among datasets used for this study. Geotagged tweets, especially those posted in the daytime, may also be considered an adequate indicator of urban activity and a significant supplementary feature for the UAC identification. The number of facilities represented by POI demonstrated lower explanatory potential, however, it was found that urban activities are spatially related to the concentrations of POI representing commercial facilities such as cafes, shops, and various services.

As a major limitation of this study, it is crucial to highlight that these findings may be irrelevant to other Japanese cities, not to mention the international applicability. This issue provides a wide field for future studies.

Acknowledgement

We would like to thank Twitter for granting free and almost unlimited access to their data in a timely manner and the OpenStreetMap community for constantly working on their free-access database.

References

Anderson, W. P., Kanaroglou, P. S., & Miller, E. J. (1996). 'Urban Form, Energy and the Environment: A Review of Issues, Evidence and Policy', *Urban Studies*, 33(1), 7–35.

Boratinskii, V. and Tikhotskaya, I. (2021). 'Identification of Multifunctional Urban Activity Centers in Tokyo', *Geography, Environment, Sustainability,* 14 (2), 83-91.

Boratinskii, V., Loopmans, M., and Osaragi, T. (2023). 'Reshuffling city life: spatial and functional dynamics of urban activity in Tokyo during COVID-19', *International Journal of Urban Sciences*. Available at: https://doi.org/10.1080/12265934.2023.2172065.

Breiman, L. (2001). 'Random Forests', *Machine Learning* , 45 (1), 5-32.

Cai, J., Huang, B., and Song, Y. (2017). 'Using multi-source geospatial big data to identify the structure of polycentric cities', *Remote Sensing of Environment*, 202, 210-221.

CatBoost (n.d.). *CatBoost is a high-performance open source library for gradient boosting on decision trees*. Available at: https://catboost.ai/ (Accessed 14 April 2023).

De Goei, B., Burger, M.J., Van Oort, F.G., Kitson, M. (2010). 'Functional Polycentrism and Urban Network Development in the Greater South East, United Kingdom: Evidence from Commuting Patterns, 1981–2001', *Regional Studies*, 44(9), 1149–1170.

Falk, R., and Miller, N. (1992). *A Primer for Soft Modeling*. Akron, OH: The University of Akron Press.

Frias-Martinez, V., Soto, V., Hohwald, H. and Frias-Martinez, E. (2012). 'Characterizing Urban Landscapes Using Geolocated Tweets'. *International Conference on Privacy, Security, Risk and Trust;* 3-5 September. Amsterdam: The Netherlands.

Goncharov & Nikoghosyan (2016). 'Identification of centers of activity in the city: comparison of objective and cognitive data'. *XVII April International Academic Conference on Economic and Social Development*, April 18-22. Moscow: National Research University Higher School of Economics.

Hand, D. J. & Till, R. J. (2001). 'A simple generalization of the area under the ROC curve to multiple class classification problems', *Machine Learning*, 45, 171-186.

McMillen, D.P. (2001). 'Nonparametric employment subcenter identification', *Journal of Urban Economics*, 50 (3), 448–473.

McMillen, D.P., McDonald, J.F. (1997). 'A nonparametric analysis of employment density in a polycentric city', *Journal of Regional Science*, 37 (4), 591–612.

Pomorov, S.B. and Zhukovsky, R.S. (2015). 'Retrospective of the development of urban polycentrism and theoretical ideas about it', *Teoriya arhitektury (Architecture Theory)*, 52 (In Russian).

Riguelle, F., Thomas, I. and Verhetsel, A. (2007). 'Measuring urban polycentrism: a European case study and its implications', *Journal of Economic Geography*, 7 (2), 193–215.

Schwirian, K. (2007). 'Ecological Models of Urban Form: Concentric Zone Model, the Sector Model, and the Multiple Nuclei Model', in G. Ritzer (ed.). *The Blackwell Encyclopedia of Sociology*.

Scikit learn (n.d.). *Feature importances with a forest of trees*. Available at: https://scikit-learn.org/stable/auto_examples/ensemble/plot_forest_importances.html (Accessed 22 May 2023).

Tokyo Metropolitan Area Transportation Planning Council (n.d.). パーソントリップ調査 [Person Trip Survey]. Available at: https://www.tokyo-pt.jp/person/01. (Accessed Retrieved 1 February 2023).

UEA (2015). Urban Employment Area. Available at: https://www.csis.u-tokyo.ac.jp/UEA/uea_def_e.htm (Accessed: 13 July 2022).

Vysokovsky, A.A. (2005). *Land use and development rules: design guide. The experience of introducing legal zoning in Kyrgyzstan*, Ega-Basma, Bishkek (In Russian).

A machine learning-based Improved soil moisture estimation: Synergistic use of satellite observations and land surface model over CONUS

Jaese Lee*, Jungho Im**

This study aimed to enhance daily soil moisture (SM) data for the contiguous United States (CONUS) by combining three commonly used SM data sources: in-situ measurements, satellite observations, and land surface models (LSMs). Machine learning (ML) techniques including random forest, artificial neural networks, and support vector regression were employed, along with simple averaging ensemble approaches, to improve the quality of the data. Three different schemes were tested for each ML model, using satellite-derived variables, LSM-derived variables, or a combination of both as independent variables.

To address the issue of scale mismatch between in-situ and coarse gridded SM data, triple collocation analysis (TCA) was used. The proposed approach was evaluated using the International Soil Moisture Network (ISMN), Soil Moisture Active Passive Core Validation Sites (SMAP CVS), and TCA.

The evaluation based on ISMN demonstrated that the ML-based ensemble method consistently outperformed existing SM products, particularly in regions with complex topography and dense vegetation where the existing products showed poor performance. The evaluation using SMAP CVS data showed that the ML ensemble approach performed better than other SM datasets, resulting in a correlation coefficient of 0.78, an unbiased root mean squared difference of 0.035 m^3/m^3, and a bias of 0.006 m^3/m^3. Additionally, the TCA results confirmed that the ML-based ensemble exhibited better spatiotemporal quality compared to other SM products.

This study demonstrated that following three main findings: (1) the synergistic merging of various data sources using ML methods to improve SM data, (2) the robust performance of ML-based SM in areas with varying topography and vegetation, and (3) the additional improvement achieved through the average ensemble of three ML models. The SM time-series data generated by this approach are expected to be suitable for environmental and climate applications in CONUS. The findings suggest that ML algorithms can effectively model dynamic soil moisture.

Keywords: soil moisture, machine learning, satellite, land surface model

1. Introduction

Soil moisture (SM) is an important climate variable of hydrological and meteorological processes. To understand environmental processes and phenomena, various SM data have been used. For that purpose, the three primary sources of SM data—in-situ measurements, satellite observations, and land surface models (LSM)—are widely used.

In-situ measurements provide accurate SM data with a fine temporal resolution. However, in-situ SM data have limitations in spatial coverage and temporal continuity because of expensive cost of installation and maintenance Satellite observations and LSMs have been widely used to obtain spatiotemporally continuous SM information. Satellite-derived SM data have been retrieved from low-frequency microwave measurements. The satellite-based SM retrievals have uncertainties in the radiative transfer model parameterizations or sensor noises. The LSM provides SM estimates by numerical calculations from various environmental forcing data. however there are uncertainties comes from the model parameters and meteorological forcing data. Therefore, instead of using only one data source to use for environmental understanding, it would be plausible to use them with synergistic fusion.

Several studies have emphasized the synergistic use of both sources because of the varying characteristics of satellite and LSM-based SM estimates. Following the previous studies, this study tried to proposes a new methods to fuse three widely-used SM sources in a

* Student Member (KAGIS), Ulsan National Institute of Science & Technology (UNIST), wotp12@unist.ac.kr
** Vice-chairman (KAGIS), Ulsan National Institute of Science & Technology (UNIST), ersgis@unist.ac.kr

synergistic way by adopting the machine learning methods.

2. Data

2.1 Satellite data

ASCAT, operating at C-band frequency, has globally provided soil moisture (SM) data at a 1–3 day temporal resolution and 25 km spatial resolution since 2007. This study utilized near real-time (NRT) SM estimates based on the TU-Wien change detection algorithm, obtained from the EUMUETSAT data center. The data were transformed from degree of saturation to volumetric units (m3/m3) by incorporating soil porosity data, while excluding frozen grids through an internal flag in the ASCAT dataset.

AMSR2, a microwave radiometer, has been delivering global SM data with a 1–2 day temporal resolution and 25 km spatial resolution since 2012. This study employed X-band-based descending orbit SM estimates using the LPRM algorithm to avoid issues related to C-band ASCAT SM assumptions and unexpected performance degradation of C-band AMSR2 SM.

2.2 LSM data

The NLDAS-2 open-loop Land Surface Model (LSM) covers a spatial extent from 25°N to 53°N latitude and 125°W to 67°W longitude. This LSM, downscaled to 12.5 km with hourly resolution, effectively simulates land surface conditions and fluxes, showing improved agreement with in-situ measurements. Adopting the Noah LSM-based NLDAS-2, this study focuses on the first 10 cm layer to match satellite-based soil moisture (SM) measurements.

NCA-LDAS, another dataset built on the Noah LSM, incorporates assimilated satellite-derived geophysical variables using a 1-D ensemble Kalman filter. With a spatial resolution of 12.5 km and daily temporal resolution within the same domain as NLDAS-2, NCA-LDAS covers 1979 to 2016. This data-assimilated model has exhibited superior agreement with in-situ data compared to its open-loop counterpart. This study uses the NCA-LDAS SM data from the top 10 cm layer for analysis.

2.3 In-situ data

ISMN, established in 2009, provides sparse in-situ soil moisture (SM) measurements globally and is commonly used to validate satellite or land surface model (LSM)-based SM products. These measurements within the 0-10 cm surface layer were employed as dependent variables in machine learning (ML) modeling, after preprocessing steps including data quality filtering, temporal averaging, spatial representativeness assessment, and temperature-based filtering. Some ISMN data were retained as reference SM data. Meanwhile, SMAP Core Validation Site (CVS) offers dense in-situ SM networks, serving as a valuable reference for validation, with measurements upscaled to a 36 km grid. The CVS data, installed at a 5 cm depth, were used to evaluate the study's results.

2.4 Auxiliary data

This study incorporated six auxiliary data variables: day of year (DOY) transformed to account for seasonality, longitude, latitude, elevation (derived from GTOPO30 and aggregated to 25 km), total column (TC) standard deviation to address SM dataset limitations, and vegetation optical depth (VOD) obtained from AMSR2 X-band LPRM data. These variables were utilized to construct the machine learning models, with TC and VOD specifically employed to assess existing SM dataset constraints and to capture canopy structure and vegetation water content between 2015 and 2019.

3. Methods

3.1. Data preprocessing

Spatiotemporally fragmented data were aggregated from MODIS, NLDAS-2, and GTOPO30 to achieve a daily 25 km spatial resolution for ML modeling and

comparisons. When ASCAT provided multiple measurements in a day, they were averaged within each grid. To facilitate comparison, NCA-LDAS data were aggregated to daily 25 km resolution, while SMAP SM underwent bilinear resampling to match the 25 km scale. Additionally, for a thorough in-situ data-based assessment, ML outcomes and NCA-LDAS were resampled to a 36 km SMAP grid, accounting for disparities in spatial resolution and projection across SM datasets.

The Triple Collocation Analysis (TCA) is a method employed to assess the accuracy of geophysical data against an unknown true value, without relying on reference data. It employs three collocated datasets, assuming linearity, signal and error stationarity, independence between true target state and estimation error, and error independence among datasets (Stoffelen 1998).

To address spatial mismatch between grid-scale and point-scale data from individual ISMN stations, TCA was applied (Gruber et al. 2016; Chen et al. 2017). TCA triplet was considered as a following combination: [ISMN, ASCAT, and NLDAS-2]. TCA performance deteriorates when point measurements don't follow coarse gridded data variability. Thus, a criterion of TCA-based $R > 0.7$ was utilized to eliminate ISMN stations deviating from 25 km SM variation. For robust TCA estimation, data were excluded if collocated data was below 100 or if TCA-based R values were negative (Scipal et al. 2008).

3.2. Machine Learning methods

In this study, three widely used supervised machine learning (ML) algorithms, namely Random Forest (RF), Artificial Neural Network (ANN), and Support Vector Regression (SVR), were employed to enhance existing Soil Moisture (SM) datasets. Three distinct schemes were devised based on independent variables used in ML training: satellite-based variables (scheme S), Land Surface Model (LSM)-based variables (scheme L), and a combination of both (scheme A).

RF, a robust supervised learning technique comprising multiple decision tree estimators, was employed. It employs bagging to mitigate overfitting and averages the outputs of various trees. ANN, a biologically inspired approach involving multiple layers of neurons, was utilized, with backpropagation optimizing neuron weights and biases. SVR, which establishes a hyperplane to minimize error with regularization, was employed using the Python-based ThunderSVM for efficient computation.

An ensemble strategy, known as Ensemble (ENS), was adopted to further improve results by combining multiple model estimates. ENS was chosen due to its simplicity and demonstrated success in various domains, enhancing generalization performance and reducing overfitting issues associated with individual models.

4. Results

4.1. ISMN-based evaluation

The most favorable results were achieved using ENS (A), representing the ensemble of RF, ANN, and SVR models for scheme A. ENS (A) displayed metrics including R (0.78), ubRMSD (0.063), and bias (-0.007 m^3/m^3, or -0.006 m^3/m^3 for 2015-2019), outperforming other approaches except for bias.

Table 1 Assessment criteria for machine learning (ML) data compared to limited in-situ measurements were applied to different schemes during the period of 2015 to 2016 (metrics in parentheses encompassing 2015 to 2019). The combined sample sizes comprised 3649 data points between 2015 and 2016, and 8050 data points between 2015 and 2019. The most optimal outcomes for each metric were emphasized using bold typeface.

Metrics	R [-]	ubRMSD [m^3/m^3]	Bias [m^3/m^3]
ENS (S)	0.71 (0.73)	0.07 (0.069)	-0.014 (-0.01)
ENS (L)	0.77 (0.76)	0.064 (0.066)	-0.004 (-0.003)
ENS (A)	**0.78 (0.78)**	0.063 **(0.063)**	-0.007 (-0.006)
RF (S)	0.68 (0.71)	0.073 (0.071)	-0.004 (**-0.001**)

RF (L)	0.73 (0.76)	0.068 (0.069)	**0** (0.002)
RF (A)	0.75 (0.76)	0.066 (0.066)	-0.002 (-0.002)
ANN (S)	0.7 (0.71)	0.071 (0.071)	-0.025 (-0.02)
ANN (L)	0.77 **(0.78)**	0.064 (0.065)	-0.009 (-0.007)
ANN (A)	**0.78 (0.78)**	**0.062 (0.063)**	-0.011 (-0.009)
SVR (S)	0.7 (0.7)	0.071 (0.07)	-0.015 (-0.01)
SVR (L)	0.77 (0.76)	0.064 (0.066)	-0.005 (-0.003)
SVR (A)	**0.78 (0.78)**	0.063 (0.064)	-0.009 (-0.007)
AMSR2	0.55 (0.50)	0.123 (0.118)	0.077 (0.078)
ASCAT	0.58 (0.60)	0.092 (0.093)	-0.002 (-0.003)
SMAP	0.71 (0.75)	0.07 (0.067)	-0.02 (-0.016)
NLDAS-2	0.68 (0.68)	0.075 (0.076)	0.046 (0.046)
NCA-LDAS	0.67	0.07	0.07

4.2. CVS-based evaluation

The high-performing SM datasets (NCA-LDAS, SMAP, and ML result, ENS (A)) were further evaluated using SMAP CVS in-situ data. The NCA-LDAS and SMAP exhibited good performance, with average R values of 0.73 and 0.69 respectively, but ENS (A) outperformed with the highest average R (0.78). ENS (A) also displayed the smallest average ubRMSD (0.035 m3/m3) compared to NCA-LDAS and SMAP. ENS (A) met the required accuracy (ubRMSD < 0.04) for various applications. Both ENS (A) and SMAP demonstrated low averaged biases (0.006 and -0.005 respectively), while NCA-LDAS had a larger averaged bias (0.076 m^3/m^3).

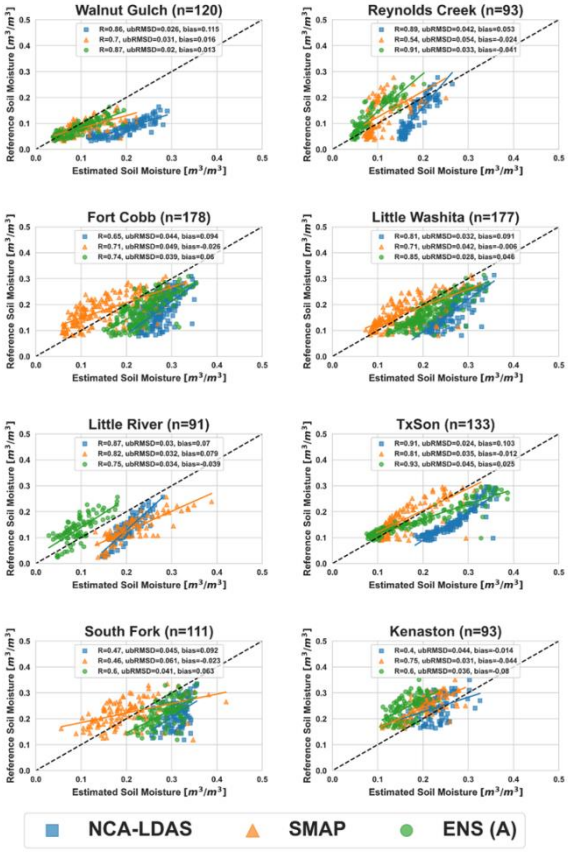

Figure 1 Graphs depicting the relationship between the area-weighted soil moisture from the CVS (Core Validation Sites) and the estimated soil moisture for the years 2015 to 2016 were generated. The lower bar plots showcase the correlation coefficient (R), unbiased root mean squared difference (ubRMSD), and bias for each CVS. The most notable results for each metric are emphasized using bold typography.

4.3. TCA-based evaluation

The TCA-derived Signal-to-Noise Ratio (SNR) for two SM data calculated using TCA triplets like [SM dataset, AMSR2, and SMAP], between 2015 and 2019, is depicted in **Figure 2**. Two example datasets which are not violating TCA assumptions are selected. In **Figure 2**, it is possible to check that the spatial distribution of SNR of ENS (A) is generally higher than the NLDAS-based SNR.

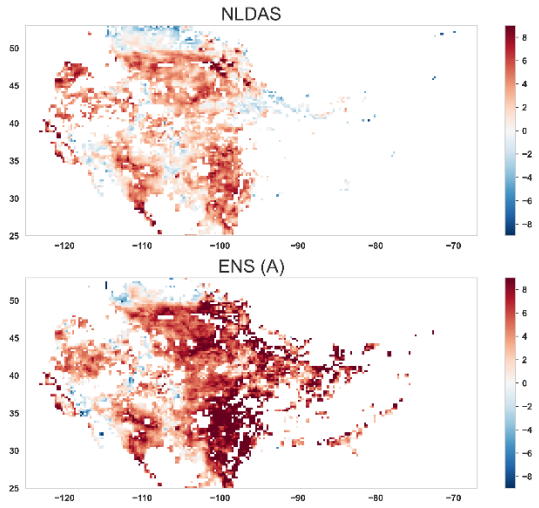

Figure 2 TCA-based signal-to-noise ratio (SNR). SNR values were calculated during 2015–2019.

5. Conclusion

This study introduces a novel data-driven approach that combines various SM datasets, including satellite, LSM, and in-situ data, through an ensemble of ML algorithms. The aim is to generate high-quality daily 25 km SM data across the CONUS region. Through evaluations utilizing sparse and dense in-situ measurements ISMN. The ensemble technique showed better quality than individual ML models and other SM datasets compared in this study.

Acknowledgement

This work was supported by Korea Environment Industry & Technology Institute(KEITI) through Project for developing an observation-based GHG emissions geospatial information map, funded by Korea Ministry of Environment(MOE) (RS-2023-00232066)

Reference

Chen, F., Crow, W.T., Colliander, A., Cosh, M.H., Jackson, T.J., Bindlish, R., Reichle, R.H., Chan, S.K., Bosch, D.D., Starks, P.J., Goodrich, D.C. & Seyfried, M.S., 2017, 'Application of Triple Collocation in Ground-Based Validation of Soil Moisture Active/Passive (SMAP) Level 2 Data Products', *IEEE Journal of Selected Topics in Applied Earth Observations and Remote Sensing*, 10(2), 489–502.

Gruber, A., Su, C.-H., Zwieback, S., Crow, W., Dorigo, W. & Wagner, W., 2016, 'Recent advances in (soil moisture) triple collocation analysis', *International Journal of Applied Earth Observation and Geoinformation*, 45, 200–211.

Scipal, K., Holmes, T., Jeu, R. De, Naeimi, V. & Wagner, W., 2008, 'A possible solution for the problem of estimating the error structure of global soil moisture data sets', *Geophysical Research Letters*, 35(24), 2–5.

Stoffelen, A., 1998, 'Toward the true near-surface wind speed: Error modeling and calibration using triple collocation', *Journal of Geophysical Research C: Oceans*, 103(3334), 7755–7766.

Oral presentation in IAG'i

Regional Analysis #2

Chair: Hisatoshi Ai (Showa Women's University)

Sat. Oct 28, 2023 10:40 AM - 12:20 PM Room D (C-201 2nd floor of Bldg. C)

[D2-01] Estimating hourly $PM_{2.5}$ using top-of-atmosphere reflectance from Geostationary Ocean Color Imagers I and II

*Hyunyoung Choi[1], Seonyoung Park[2], Jungho Im[1] (1. Ulsan National Institute of Science &Technology (UNIST), 2. Seoul National University of Science and Technology)

10:40 AM - 11:00 AM

[D2-02] Mapping Emotional Geographical Trends and User Behaviors Based on Japanese Tweets: A Case Study of Urban Green Spaces in Tokyo 23 Wards

*Mingchen Liu[1], Yuya Shibuya[2], Yoshihide Sekimoto[2] (1. Department of Civil Engineering, The University of Tokyo, 2. Center for Spatial Information Science, The University of Tokyo)

11:00 AM - 11:20 AM

[D2-03] Revealing Access Equity: An Examination of Walking Course Distribution and Streetscape Quality for Residents

*Xinyu Tang[1], Mamoru Amemiya[1], Sunyong Eom[1] (1. University of Tsukuba)

11:20 AM - 11:40 AM

[D2-04] Population Aging and the Community-based Integrated Care System in Akita Prefecture

*Ketian Chen[1], Mizuki Kawabata[1] (1. Keio University)

11:40 AM - 12:00 PM

[D2-05] Route Search Method of Alternative Bus for Rail Line Adopting Ant Colony Optimization

*Kei Nagaoka[1], Kayoko Yamamoto[1] (1. Graduate School of Informatics and Engineering The University of Electro-Communications)

12:00 PM - 12:20 PM

Estimating hourly $PM_{2.5}$ using top-of-atmosphere reflectance from Geostationary Ocean Color Imagers I and II

Hyunyoung Choi*, Seonyoung Park**, Jungho Im***

To produce real-time ground-level $PM_{2.5}$ information, many studies have investigated the applicability of satellite data, particularly AOD. However, traditional methods for retrieving AOD are computationally demanding. Thus, this study proposed a machine learning (ML)-based algorithm to directly estimate hourly $PM_{2.5}$ concentrations over South Korea using top-of-atmosphere (TOA) reflectance from the GOCI-I and its next-generation GOCI-II. A light gradient boosting machine (LGBM) was applied as an ML technique. Three schemes were examined based on the input feature composition of the GOCI spectral band. GOCI–II–based schemes 2 and 3 (R^2=0.85 and 0.85) performed slightly better than GOCI-I-based scheme 1 (R^2=0.83). The TOA reflectance at a new channel (380 nm) of GOCI-II was shown as the most contributing variable, given its high sensitivity to aerosols. The use of GOCI-II enables a more detailed spatial distribution of $PM_{2.5}$ concentrations compared to GOCI-I, thanks to its higher resolution of 250 m. Our results indicate that the proposed algorithm has great potential for estimating ground-level $PM_{2.5}$ concentrations for operational purposes.

1. Introduction

Fine particulate matter ($PM_{2.5}$) is not only an air quality problem closely related to human health, but also an important factor in the study of earth radiation and climate change. Therefore, the necessity of accurate monitoring of its global concentration distribution and movement is also emerging. Recently, ground-level $PM_{2.5}$ concentration estimation studies using satellite data that provide spatially continuous distribution with a high spatiotemporal resolution are actively conducted. The satellite-based aerosol optical depth (AOD), an indicator of the amount of aerosol in the atmosphere, was used as a key material in many previous studies, indicating the degree of reduction in radiant energy value by the atmospheric aerosol and expressing the amount of aerosol in the atmosphere. However, in the case of satellite-based AOD, the Top-of-Atmosphere (TOA) reflectance observed in the satellite is calculated according to the measured AOD and its optical characteristics, surface reflectance, and solar-satellite position conditions, and the look-up table (LUT) is created by comparing it with the observed TOA reflectance. This process requires a heavy computation, which takes a lot of computational time, and has a limitation that has a low spatial coverage that cannot be calculated for the high-reflective surface. Therefore, to overcome these limitations, this study aims to develop a machine learning-based algorithm that calculates the hourly ground-level $PM_{2.5}$ concentrations directly using the TOA reflectance from Geostationary Ocean Color Imager (GOCI) I and II without the AOD calculation process. The objectives of this study were to 1) develop a ML-based model that directly estimates ground-level $PM_{2.5}$ concentrations using satellite (GOCI-I and GOCI-II) TOA reflectance data over South Korea and 2) propose a long-term, continuous monitoring of satellite-based $PM_{2.5}$ concentrations using GOCI-I and GOCI-II.

2. Study area and data

The study area is South Korea, located in northeast Asia, a region known to have relatively poor air quality. The study area with elevation and $PM_{2.5}$ monitoring stations is shown in Figure 1. Data used in this study are ground observations as the target variable and remote-sensing data, model-based data, and other auxiliary data as

* Student Member (KAGIS), Department of Urban Environment Engineering, Ulsan National Institute of Science and Technology, Ulsan, Republic of Korea, hyong56@unist.ac.kr
** Professor Member (KAGIS), Department of Applied Artificial Intelligence, Seoul National University of Science and Technology, Seoul, Republic of Korea, sypark@seoultech.ac.kr
*** Professor Member (KAGIS), Department of Urban Environment Engineering, Ulsan National Institute of Science and Technology, Ulsan, Republic of Korea, ersgis@unist.ac.kr

explanatory variables. The ground observation data of $PM_{2.5}$ obtained from the AirKorea website (https://www.airkorea.or.kr/) from Jan 2020 to June 2021 were used as the dependent variable. Four satellite sensor systems were used in this study: Geostationary Ocean Color Imager (GOCI), Global Precipitation Measurement (GPM), Shuttle Radar Topography Mission (SRTM), and Moderate Resolution Imaging Spectroradiometer (MODIS). Along with remote-sensing data, the numerical model-based meteorological variables (e.g., temperature, relative humidity, wind speed and direction) and the auxiliary data were used as input data. All input data were resampled into GOCI grids (GOCI-I; 500 m, GOCI-II; 250 m) for use in machine learning models.

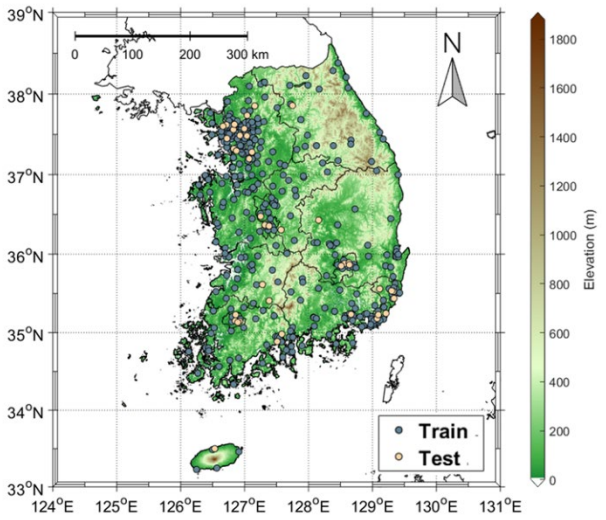

Figure 1 Study area with particulate matter ($PM_{2.5}$) monitoring stations in South Korea. The elevation is used as a background image.

3. Methods

Light Gradient Boosting Machine (LGBM) is applied as a machine learning technique for estimating the concentration of $PM_{2.5}$ in South Korea. LGBM is one of the gradient boosting techniques with a weak learner's weight ensemble structure. The model is constructed using the TOA reflectance and angle data from GOCI-I and its subsequent satellite, GOCI-II, meteorological variables from a numerical model, other auxiliary variables as independent variables, and the ground observation $PM_{2.5}$ concentration as a dependent variable. In this study, 10-fold cross-validation was performed to evaluate the model. To assess the accuracy of the proposed model, coefficient of determination (R^2), root mean square error (RMSE), relative RMSE (rRMSE) were used.

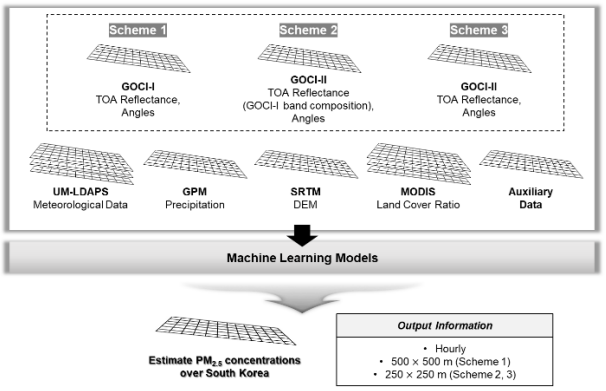

Figure 2 Process flow diagram for estimation of surface $PM_{2.5}$ concentrations proposed in this study.

4. Results and discussion

Table 1 presents the model validation results for LGBM model. The experiment was conducted during the overlapping period of the two sensors. There was a noticeable difference between scheme 1 and the other schemes. Because scheme 1 used GOCI-I data with a coarser spatial resolution (i.e., 500 m), it performed slightly worse than the other schemes. It is not surprising that the accuracy is high when using high-resolution data, which provides detailed surface information. When the GOCI-II data were used, there was no significant difference in the validation accuracy between the two schemes (schemes 2 and 3). The use of additional spectral bands scheme 3 did not significantly improve the performance for estimating $PM_{2.5}$ concentrations, resulting in a performance similar to that of scheme 2. However, scheme 3 had a slightly higher accuracy in SPCV and TPCV than scheme 2, implying improved spectral characteristics in estimating $PM_{2.5}$ concentrations.

Table 1 Results of model validation and comparison between the three schemes for each validation method.

RDCV, random cross-validation; SPCV, spatial cross-validation; TPCV, temporal cross-validation; TEST, hold-out validation.

		Slope	R^2	RMSE	IOA
RDCV	**Scheme 1**	1.07	0.83	8.49	0.95
	Scheme 2	1.05	0.85	7.69	0.96
	Scheme 3	1.05	0.85	7.82	0.95
SPCV	**Scheme 1**	1.05	0.76	9.88	0.92
	Scheme 2	1.02	0.77	9.42	0.93
	Scheme 3	1.03	0.77	9.40	0.93
TPCV	**Scheme 1**	1.15	0.63	12.56	0.85
	Scheme 2	1.09	0.70	10.95	0.90
	Scheme 3	1.08	0.70	10.90	0.90
TEST	**Scheme 1**	1.06	0.79	9.05	0.93
	Scheme 2	1.04	0.81	8.36	0.94
	Scheme 3	1.04	0.81	8.42	0.94

However, there are still some limitations and possible improvements. First, the proposed model resulted in relatively low performance for TPCV owing to the temporally dynamic characteristics of air pollutants. This can be overcome by continuously updating the training samples by weighting recent data through real-time learning. Second, the retrieval coverage was improved through a direct estimation approach using TOA reflectance, but it still has the limitation that it cannot be estimated under clouds. Gap-filling techniques such as regression kriging or state-of-the-art deep learning can significantly alleviate the limitation.

Mapping Emotional Geographical Trends and User Behaviors Based on Japanese Tweets - A Case Study of Urban Green Spaces in Tokyo 23 Wards

Mingchen Liu*, Yuya Shibuya**, Yoshihide Sekimoto**

Emotions are the basis of human behavior and an important part of spatial constructions. Social Network Service has become an important source of spatio-temporal big data due to many users sharing their emotions and behaviors, which helps us to clarify the relationship between sentiment changes and geographical locations. This research focuses on sentiment analysis of the one-year geo-tagged Japanese Tweets to understand the sentiment and behavioral patterns in urban green spaces in Tokyo 23 wards. We estimate the sentiment of Tweets with a fine-tuned pre-trained Japanese BERT model. The results show that the urban green spaces with more than 10 positive tweets were 131 out of 1,755 (7.46%), while the urban green spaces with more than 10 negative tweets were 27 (1.54%). In addition, we found that their behaviors are different when they are in different moods. People in positive moods engaged in behaviors such as walking, taking pictures, running, flower viewing, and painting, while keywords such as go home, tired, go to sleep, and give up appeared more often in negative moods.
Keywords: Sentiment Analysis, Natural Language Processing, Twitter, Machine Learning, Behavior Analysis

1. Introduction

In recent years, with the rapid development of mobile Internet technology and the upgrading of mobile social applications, Location Based Service (LBS) has become the main way to obtain spatial location information. Location Based Social Network (LBSN) is a combination of location and social network. In the application of LBSN, users can use mobile devices to publish their life logs at the places of interest, called Point-Of-Interest (POI), on the social network. The data generated with spatial location coordinates and time attributes has become a new source of spatio-temporal big data (Sadiq et al., 2015).

The number of social media users worldwide increased from 1.22 billion in 2011 (knowledge4policy.ec.europa.eu, 2018) to 4.26 billion in 2021 (Statista, 2023). Among them, the number of Twitter[1] users also reached 362.4 million in 2021 (Dixon, 2022). Users of social network platforms, especially Twitter, can post and share not only the news and events (Ye and Wu, 2013), but also users' opinions, emotions, behaviors and other details of their lives within 280 characters (Alshammari and Nielsen, 2018). Tweets posted on Twitter are publicly visible and can be collected through the official Application Programming Interface (API) launched by Twitter until 2023, unless the user sets his or her account as private.

According to the statistics published by ICT Research & Consulting (2022), the current population of Japan is about 125 million (Statistics Bureau of Japan, 2022), of which the number of SNS users was about 82.7 million in 2022. In Japan, the most popular SNS platform is LINE, a chat tool, with a usage rate of 79.5% of SNS users, while Twitter is the third most popular SNS platform with a usage rate of 55.9% (ICT Research & Consulting, 2022). Therefore, analyzing Japanese tweets posted by Japanese users can help researchers better understand both the sentiment of Japanese Twitter users and the relationship between behavior and geographic location.

Emotion is defined by the Lexico Dictionaries (2021) as "a strong feeling deriving from one's circumstances, mood, or relationships with others". Emotions have a significant impact on human cognitive processes and behaviors (Tyng et al., 2017), and changes in time, place, and social environment can cause changes in human emotions. In daily life, human emotion is an important part of spatial construction. When people analyze the emotional tendencies in a text, they are often influenced

* Student Member (GISA), Department of Civil Engineering, The University of Tokyo, liu-mingchen946@g.ecc.u-tokyo.ac.jp
** Member (GISA), Center for Spatial Information Science, The University of Tokyo
[1] "Twitter" was renamed to "X" in 2023. However, we use "Twitter" throughout this article because our target data consists of posts before renaming took place.

by their own subjective evaluations. Therefore, there is a greater need for a model that can objectively analyze the sentiment of a text to overcome the subjective emotional tendencies of humans (Liu and Zhang, 2012).

This study collects about 70.27 million of geo-tagged Japanese tweets posted in Japan in 2021 through Twitter's official Academic API. We collected the tweets in 2022 when the Academic API was still available. By fine-tuning a pre-trained Natural Language Processing (NLP) model for Japanese, we predict the sentiment of the above tweets, which are labeled as "positive", "negative", and "neutral" labels. In this study, all tweets located in urban green spaces in 23 wards of Tokyo are selected (N = 27,524), and the emotions and behaviors of users are analyzed to estimate the relationship between places with different functions in the city and the emotions and behaviors of Japanese users.

2. Literature Review

A geo-social network is a type of social network that links location data with information shared by users on the social network. Geo-social network applications usually use geospatial services to explore the relationships between users, locations, and content. At present, the research on geo-social network data analysis mainly focuses on the data of mainstream social media applications such as Twitter and Facebook.

Various studies have analyzed the relationships between people's emotions and real-world situations. For example, several studies have investigated social media emotions and disasters (Neppalli et al., 2017; Shibuya et al., 2018; Shibuya et al., 2019). Neppalli et al. (2017) analyzed the tweets during Hurricane Sandy and described how people's sentiments changed based on their distance from the hurricane. In marketing research, correlations between social media sentiment and sales (Rui et al., 2013), consumer choice (Liu et al., 2016), and stock prices (Rao et al., 2014) have been quantitatively analyzed. In public health, correlations between a pandemic and social media data have been studied with the aim of detecting epidemic outbreaks as soon as possible (Charles-Smith et al., 2015; Chew et al., 2015; Chunara et al., 2012). For geographic awareness, which refers to the users' perceptions of the surrounding geographic space, Xu et al. (2013) found that the geographical knowledge reflected in social media affects users' spatial behavior, and local residents have a much higher degree of geographic awareness than non-residents (Xu, Wong and Yang, 2013).

Furthermore, various scholars began to use social media emotion data to understand urban green spaces (Cui et al., 2021; Ghahramani et al., 2021; Zabelskyte et al., 2022). For example, Fan et al. (2023) studied tourist experiences at green spaces in China by analyzing Sina Weibo, finding that park types and green space ratio facilitated the touring experience. Wang et al. (2022) found that green spaces were associated with lower negative emotions in a Chinese city. Maas et al. (2009) analyzed whether the percentage of green space in people's living environment affects their feelings of social safety positively or negatively and found that green space generally enhances feelings of social safety. Cui et al. (2022) compared tweets for the three months of 2019-2021 and found differences in green space visiting patterns and people activity patterns there.

As shown above, there are various attempts to use emotional data from social media in order to comprehend the urban environment. Nevertheless, we have noticed that there is less research that explores the intertwined relationships between sentiments, behaviors, and places. In addition, there is a lack of long-term data, such as year-long communication data to understand green spaces. In particular, there is a lack of such research in the Japanese urban environment. Therefore, the purpose of this study is to contribute to the existing research by examining how social media sentiments can be used to gain an understanding of urban green spaces in Japan. Specifically, this study focuses on Tokyo 23 wards' green spaces and analyzes the year-long tweets of 2021.

3. Data and Methodology

This study's methods consist of three parts. The first part is data collection and preprocessing, where we preprocess the collected tweet data and construct the ground truth dataset for subsequent NLP model training. The second part is fine-tuning a pre-trained model to improve the accuracy of the model's sentiment prediction for our target tweet dataset. In the third part, all the urban green spaces located in Tokyo 23 wards are extracted using keywords and geographic location information. The tweets posted in these urban green spaces are subjected to sentiment classification and word frequency statistics to estimate the characteristics and changing patterns of users' sentiments and behaviors in the urban green spaces.

3.1 Data collection

Twitter Academic API allowed us to collect historical tweets with geo-location information. Tweets' geo-location information includes POI point (longitude and latitude), city name, admin-level area name, country name, and so on. These geo-location attributes are provided either by users or by Twitter. When a user posts a tweet with a geo-tagged feature, the coordinates are automatically provided. When a user's tweet or profile information contains a specific place, city name, or other geo-location information, Twitter labels the tweets with geo-location information, such as city names. As a result, some tweets may have specific coordinates, while others may only have city-name or wards-name information.

In this study, we use twarc2, a Python library, to collect and archive Twitter JSON data via the Twitter API v2.

This study constructs tweet datasets containing all Japanese tweets in Japan, 2021. To construct the datasets, this study queries all Japanese tweets that have geo-location information in 2021. Specifically, only tweets within 'Japan' and with 'Japanese' language are collected. We collected the data in 2022. In total, our datasets consist of 70,266,303 tweets, of which 5,773,959 tweets were posted with a POI location, accounting for 8.2% of the total.

3.2 Data preprocessing

Because this study's objective is to analyze urban green spaces in Tokyo 23 wards, we need to filter all the collected tweets to find out the tweets where the POI location is an urban green space.

Before filtering out the tweets related to urban green spaces, we first limit our target data to POI-type geo-tagged tweets located within the Tokyo 23 wards.

Next, we match the target tweets' POI information to urban green spaces. Two methods are used in this study to collect tweets where the POI location is an urban green space. The first method is to match the coordinates of the tweet POI locations with the urban park data in the Digital National Land Information provided by the Japanese government (Ministry of Land, Infrastructure, Transport and Tourism). Because the accuracy of the point coordinates of these two types of data is not the same, this study creates a buffer zone centered on the point of the urban parks that approximates the area of the parks, and counts the tweet POI data located within the buffer zone. The second method is to use keywords related to parks to filter out the target tweets. The specific keywords used are shown in Table 1. These inclusion and exclusion criteria are created by manually checking the target tweets and Tokyo 23 wards' green spaces.

Before using tweet text for model training and sentiment prediction, we need to preprocess the text. In this study, the preprocessing mainly includes removing URL links, usernames, and stop words (jp.mathworks.com, n.d.).

Finally, through the data preprocessing described above, this study obtained a total of 27,524 tweets posted in urban green spaces within Tokyo 23 wards, containing 1,755 POI locations and posted by 9,054 unique users.

3.3 Sentiment Analysis Model

3.3.1 Pre-trained model

Despite the fact that Japanese is known as one of the most difficult languages for non-native speakers to learn (Reza Rahutomo et al., 2019), with the advancements of NLP and machine learning technologies, Japanese NLP models can currently solve as many problems as models of other languages, such as translation, question answering, fill-

Table 1 Filtering keywords for tweets POI locations related to urban green space. Original Japanese keywords are shown in brackets.

Include Keywords	park [公園, パーク, Park], garden [庭園], Rikugien (a park name) [六義園], Gyoen (a park name) [御苑], Gaien (a park name) [外苑], Yuyake-Koyake-Fureai-no-Sato (a park name) [夕やけ小やけふれあいの里], Seibutsu-en (a zoo name) [生物園], Yushima-seido (a temple name) [湯島聖堂], Wanpaku-tengoku (a park name) [わんぱく天国], Mogusa-en (a park name) [百草園]
Exclude Keywords	Park Hyatt (a hotel name) [パークハイアット], Court (a part of apartment names) [コート], station [駅], Onsen (hot spring) [温泉], art museum [美術館], building [ビルディング], Park Tower (a part of hotel names) [パークタワー], Royal Park (a part of hotel names) [ロイヤルパーク], hotel [ホテル]、Park House (a part of apartment names) [パークハウス], restaurant [レストラン], Sirotan Friends Park (a shop name) [しろたんフレンズパーク], Nakano central Park (a building name) [中野セントラルパーク], gallery [ギャラリー], Park City (a part of apartment names) [パークシティ], Shopping Park [ショッピングパーク, RAIZEN], Prologis Park (a part of apartment names) [プロロジスパーク], Koen-dori Classics (a live house name) [公園通りクラシックス], Prince Hotel Shiba Park (a hotel name) [プリンス芝公園], attic (a part of restaurant names), Yu Park (a hot spring name) [湯パーク], studio [スタジオ], theater [シアター]

masks, and text classification. Text classification is defined as the task of assigning a label or class to a given text (Hugging Face, n.d.). The task of sentiment analysis is to assign sentiment labels to texts after prediction, which can be seen as a subset of text classification.

To analyze the sentiment of Japanese tweets, this study uses the pre-trained transformer model of Bidirectional Encoder Representations from Transformers (BERT), an unsupervised deep learning model developed by Devlin et al. (2018) from Google AI Language. BERT is designed to pretrain deep bidirectional representations from unlabeled text by jointly conditioning on both left and right context in all layers (Devlin et al., 2018). Unlike other deep learning neural network models that require large datasets for training, BERT is already pre-trained and only needs to be fine-tuned with smaller datasets for specific tasks.

Before fine-tuning the pre-trained model, this study compares the accuracy of several pre-trained Japanese BERT models provided by the NLP team from Tohoku University on the tweet dataset. These five pre-trained models compared in this study are all pre-trained for the masked language modeling task, and thus have low accuracy on the sentiment analysis task. The accuracy of sentiment analysis is shown in Table 2.

Finally, this study chooses 'bert-large-japanese' as the pre-trained model to fine-tune with our tweet dataset since it performs the best accuracy.

3.3.2 Constructing ground-truth dataset

This study classifies the sentiment of the text into 'positive', 'negative' and 'neutral', and generates the confidence score at the same time when the model predicts the sentiment. The sentiment labels of the text are classified according to the sentiment scores as shown in Table 3.

Table 2 Accuracy of pre-trained BERT models

Pre-trained model	Accuracy	F1	Precision	Recall
bert-large-japanese	0.76	0.76	0.76	0.77
bert-base-japanese	0.72	0.72	0.71	0.72
bert-base-japanese-whole-word-masking	0.75	0.72	0.72	0.71
bert-base-japanese-v2	0.60	0.60	0.61	0.60
bert-base-japanese-v3	0.60	0.60	0.60	0.60

Table 3 Setting of sentiment labels

Confidence score	Label predicted by model	Final label
0.9 < Score < 1.0	Positive	Positive
	Negative	Negative
	Neutral	Neutral
0 < Score < 0.9	Positive	Neutral
	Negative	Neutral
	Neutral	Neutral

3.3.3 Ground truth dataset

In order to improve the accuracy of this pre-trained model and optimize its performance on sentiment analysis tasks, this study builds its own ground truth dataset based on tweet texts for fine-tuning.

In this study, 6,000 tweets were randomly selected from the collected tweets, manually labeled by 14 Japanese speakers (13 of whom are native Japanese speakers), and the final sentiment labels are determined by the authors by majority decision.

We decided to construct our own ground truth datasets because there are no well-fitted training datasets for our datasets. Most of the previous studies in Japanese sentiment analysis used review datasets such as product reviews on an online retail platform, the Rakuten product review dataset (Enkhbold Bataa and Wu, 2019), to fine-tune their models. The sentiment tendency of these evaluation datasets is obvious compared to tweets in which people sometimes express their emotions in nuanced ways. In addition, the wording of product reviews is limited and different from the text posted by Twitter users. Therefore, we found that such well-used Japanese training datasets cannot improve the accuracy of sentiment classification models for our tweet dataset.

Nevertheless, for the purpose of comparing the developed models, this study uses 2 datasets for training, including both open training data and our own ground truth datasets (Table 4). The Recruit dataset comes with the usage of the text (train set, validation set and test set), while the ground truth dataset created in this study uses a ratio of 0.33 to divide the train set and the test set.

Table 4 The composition of train set

Dataset	Positive	Negative	Neutral	Accuracy
Recruit	3406	818	1329	0.63
Ground truth	1767	1187	3046	0.72

3.3.4 Fine-tuning model

The following hyperparameters are used during training: number of epochs is 10, training batch size is 16, evaluation batch size is 16, and learning rate is 2e-05.

This study uses 'Random Over sampler', an over-sampling model, on the train set to ensure that the number of samples per label in the train set is equal to the maximum number of 'neutral' labels. The prediction precision of each label after over-sampling without changing the test set is shown in Table 5. After over-sampling, there is a significant improvement in the prediction precision of the 'positive' and 'negative' labels.

Table 5 Prediction precision of each label with ground truth dataset (over-sampling)

	Precision	Recall	F1-score
Negative	0.70	0.69	0.69
Neutral	0.74	0.79	0.76
Positive	0.78	0.69	0.74
Accuracy			0.74

4. Results

4.1 Check-in maps of urban green spaces

Using the methods introduced in section 3.3, this study filters a total of 27,524 tweets posted in urban green spaces located within Tokyo 23 wards in 2021. The check-in maps show the distribution of POI locations attached to tweets posted by Twitter users, reflecting the urban green spaces and the hotspots within Tokyo 23 wards where users mainly organize various activities (Figure 1 and 2).

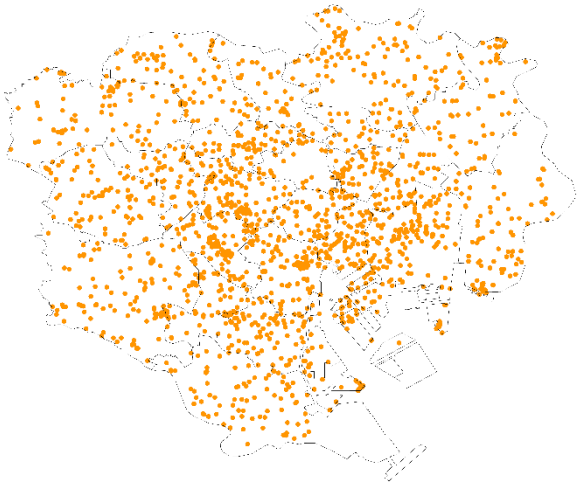

Figure 1 Distribution of tweets related to urban green spaces located in Tokyo 23 wards

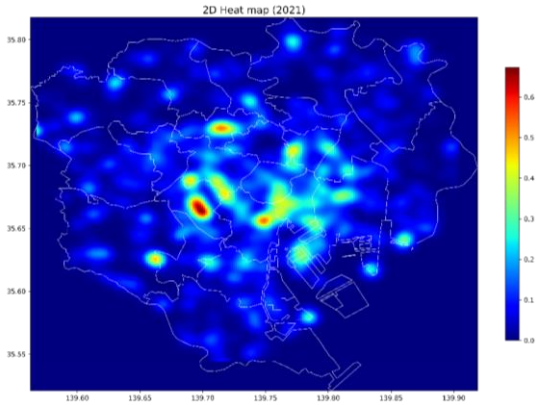

Figure 2 2D heat map of tweets related to urban green spaces located in Tokyo 23 wards

4.2 Basic statistical analysis

This study ranks the number of tweets for 1,755 POI locations (urban green spaces in Tokyo 23 wards) and finds that there are a total of 48 POI locations with more than 100 tweets, and the top 20 urban green spaces with the highest number of tweets account for 42% of all tweets. There are three urban green spaces with more than 1,000 tweets: IKE-SUNPARK, Yoyogi Park, and Jingu Gaien Ginkgo Avenue.

By counting the number of tweets by month, by weekday and by hour, this study finds that March and November had the highest number of tweets, and that tweets were more concentrated on weekends and from 11:00 to 17:00, shown as Figure 3. A general conclusion can be drawn that Twitter users prefer to go to urban green spaces for activities on weekends and during daytime, especially in March and November.

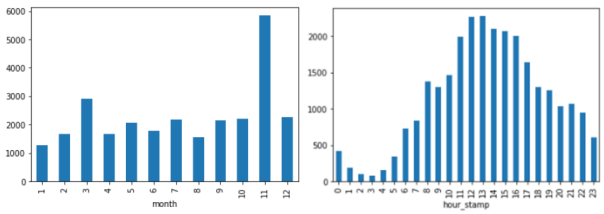

a) Tweets number per month b) Tweets number per hour

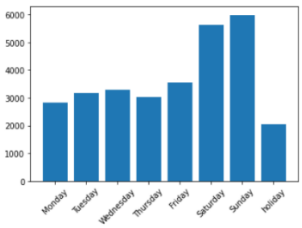

c) Number of tweets per weekday and national holidays

Figure 3 Basic statistic of related tweets

Based on Japan's holiday schedule for 2021, we count the number of tweets on different holidays as well as holidays that include weekends. Among the holidays, users prefer to visit the urban green spaces during the July and November holidays, especially on the Culture Day and Labor Thanksgiving Day (Figure 3). In 2021, there are a total of 116 days off in Japan, including holidays and weekends. On average, Twitter users posted 59 tweets per day on weekdays and 116 tweets per day on holidays.

4.3 Sentiment analysis

4.3.1 Result of sentiment prediction

By applying the fine-tuned Japanese BERT model for sentiment prediction on the tweet dataset, the dataset contains a total of 8,103 positive tweets, 1,557 negative tweets, and 17,864 neutral tweets, with 36% of the tweets having sentiment (positive or negative). Examples of tweets for different sentiments are shown in Table 6.

Table 6 Examples of sentimental tweets

Sentiment	Example (in Japanese)	Example (in English)
Positive	広尾でリラックスしながら打ち合わせした楽しい日曜日でした。	It was a fun Sunday with relaxing meetings in Hiroo.
Negative	なんか怖い＾＾	I'm scared^^
Neutral	練馬区民のオアシスオザキフラワーパーク	Ozaki Flower Park, an oasis for Nerima Ward residents.

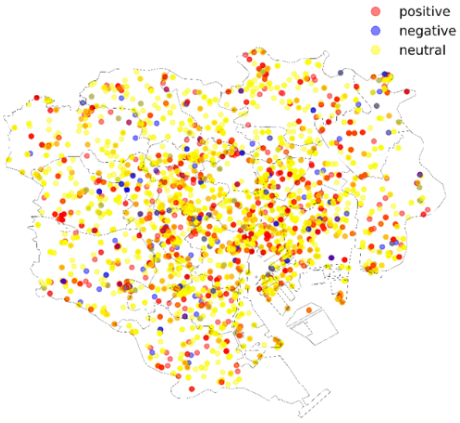

a) Positive, negative & neutral

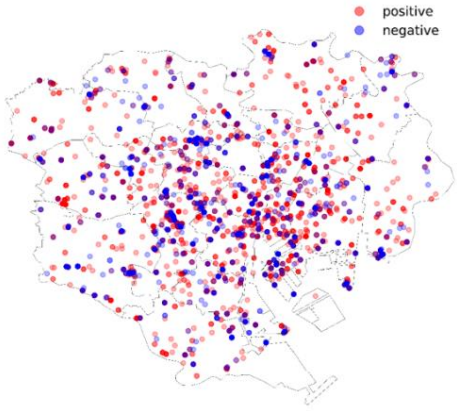

b) Positive & negative

Figure 4 Sentiment color map

4.3.2 Sentiment map

Based on the sentiment labels predicted by the fine-tuned model, this study assigns a different color to each sentiment, which is marked on the map with the POI location to more clearly represent the relationship between tweet sentiment and geographic location (Figure 4).

To explore the concentrated areas of different sentiments, this study generates 2D heat maps as shown in Figure 5 for positive tweets and negative tweets. We find that both sentiments are concentrated in Shibuya, Toshima, Taito, and Chiyoda wards. Positive sentiments are more concentrated in Yoyogi Park, Komazawa Park, IKE-SUNPARK, and Shiba Park, while the urban green spaces where negative sentiments are more concentrated include Kasai Rinkai Park and Ueno Park in addition to the aforementioned parks. Tweets like '指輪を手作りしてきたよ。細くて可愛いのが出来ました。(I made a ring myself. It's thin and cute.)' appeared in the areas concentrated with positive sentiments, while tweets such as '足がもうダメ、撤退します (My legs are tired, I'm going back.)' appeared in the areas concentrated with negative sentiments.

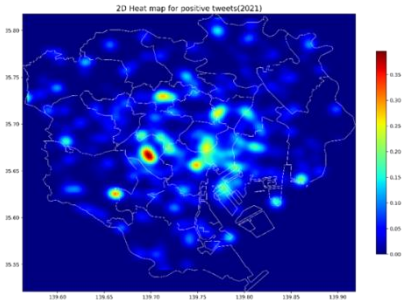

a) Positive

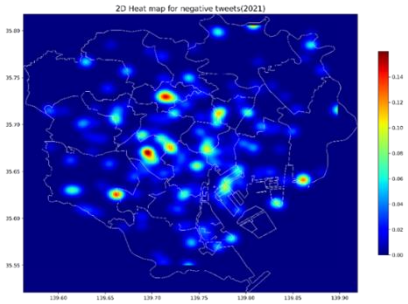

b) Negative

Figure 5 2D heat map for different sentiments

4.3.3 Sentiment perception in different wards

In this study, the percentage of positive and negative sentiments in all 1,755 POI locations are counted, and it is found that there are 181 POI locations with 100% positive sentiments, 44 POI locations with 100% negative sentiments, 830 POI locations with no positive sentiments at all, and 1,312 POI locations with no negative sentiments at all.

To further explore the concentrated areas of different sentiments, this study counts the number and percentage of tweets with different sentiments in each ward, as shown in Figure 7, and finds that among all tweets related to urban green spaces in Tokyo's 23 wards in 2021, the most positive ward is Arakawa, and the most negative ward is Bunkyo.

4.4 User behavior under different sentiments

Because users will share their lifelogs and behaviors on the SNS platform (Alshammari and Nielsen, 2018), we can roughly assume that the behaviors mentioned by users in the tweet texts are related to the specific POI location they attached in their tweets.

In this study, we use the same pre-trained tokenizer as the pre-trained model to tokenize the collected tweets. We count the word frequency in the tweet text to represent user behavior. Due to the lexical nature of the Japanese language, we retain nouns, verbs, adjectives, and phrases for the word frequency statistics. The word clouds plotted based on word frequency are shown in Figure 5.

a) All tweets

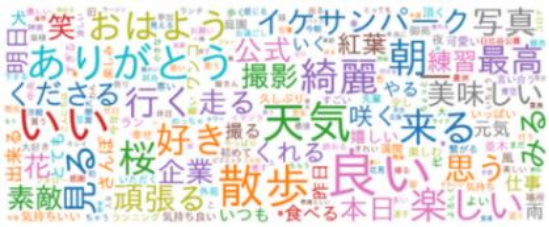

b) Positive

c) Negative

Figure 6 Word clouds of different sentiments

Based on the word frequency ordering we find that the common behaviors that users will perform in the urban green spaces are: walking (7.49%), taking pictures (5.38%), running (2.16%), flower viewing (1.50%), and painting (1.44%). The same behaviors as above are also observed when users have positive sentiment (8.38% walking, 5.68% taking pictures, 3.22% running, 2.09% flower viewing, and 1.48% painting). However, when users are in a negative mood, they are more likely to complain about the weather, and will feel tired, horrible and in pain, and they will post tweets with the keywords 'go home' (2.76%), 'go to sleep' (1.09%), and 'give up' (0.96%).

In the word cloud we note that there are also seasonal variations in the behaviors that users perform in urban green spaces, such as cherry blossom viewing in the spring and red leaf viewing in the fall. Therefore, this study also counts the frequencies by seasons and finds that the seasonal behaviors of users in urban green spaces in 2021 were: cherry blossom viewing in spring, discussing the Olympics and attending festivals in summer, enjoying the red leaves and ginkgoes in autumn, and plum blossom viewing in winter.

5. Conclusions

Geographical locations and places can affect people's emotions and behavior in a variety of ways. With the development of mobile devices and social networks, spatio-temporal big data on SNS platforms have provided researchers with a greater amount of real-time data, which provides a new source of data for studying the relationship between geographic locations and human emotions and behaviors.

This study collects geo-tagged Japanese tweets from all over Japan in 2021, from which 27,524 tweets posted in urban green spaces located within Tokyo 23 wards are filtered out. This study fine-tunes a pre-trained model (accuracy on our tweet dataset is 0.74) to analyze the differences in the distribution of Twitter users' sentiments within urban green spaces of Tokyo's 23 wards in 2021 by drawing POI location check-in maps and sentiment maps, and analyzes users' behaviors under different sentiments using word frequency statistics. The study finds: (A) Twitter users in Tokyo 23 wards are more likely to go to urban green spaces during the daytime on weekends. (B) The urban green spaces with more than 10 positive tweets were 131 out of 1,755 urban green spaces (7.46%), and the top of them were IKE-SUNPARK, Jingu Gaien and Yoyogi Park, while the urban green spaces with more than 10 negative tweets were 27 out of 1,755 urban green spaces (1.54%), and the top of them were Yoyogi Park, Jingu Gaien and Hibiya Park. (C) Positive sentiments accounted for 29.44% of all tweets in urban green spaces, while negative sentiments accounted for 5.66%. There were 181 POI locations with 100% positive sentiments, 44 POI locations with 100% negative sentiments, 830 POI locations with no positive sentiments at all, and 1,312 POI locations with no negative sentiments at all. IKE-SUNPARK, which had the highest number of tweets, had 29.71% positive sentiments and 1.02% negative sentiments. (D) In the central area of Tokyo 23 wards, there is a concentrated area of both positive and negative sentiments together. Positive sentiments are most

concentrated near Yoyogi Park in Shibuya Ward and tend to spread out in patches, while the areas of concentration of negative sentiments are scattered in a few large urban green spaces such as Kasai Rinkai Park and Ueno Park. (E) Users expressed positive emotions with behaviors such as walking (8.38%), taking pictures (5.68%), running (3.22%), flower viewing (2.09%), and painting (1.48%) in their tweets. When users are in a negative mood, the likelihood of the above behaviors decreases, and users are more likely to feel tired. Among all the negative tweets, 2.76% of them have the keyword 'go home', 1.86% of them have the keyword 'tired', 1.09% have the keyword 'go to sleep', and 0.96% have the keyword 'give up'. In addition, there are seasonal variations in user behavior in urban green spaces, usually related to the plants planted in the green spaces.

Overall, there are two main academic contributions of this study. First, since the penetration rate of Twitter is relatively high across all generations in Japan (Statista, 2023), the selection of geo-tagged tweets on Twitter as a data source can more accurately reflect the subjective emotions and behaviors of city residents. In addition, this study not only analyzes the concentration areas of different sentiments in the city, but also analyzes the users' behaviors through the word frequency statistics, which can also help urban planners to understand the residents' activities in urban green spaces.

In the future, this study will continue to analyze other functional places (such as transportation hubs) to find out the areas where sentiments are concentrated in the city and the impact of sentiments on user behavior.

This study has several limitations. First, there is a need to critically evaluate the possible risk of bias when using social media data, such as potentially biased information, a lack of socio-demographic data, and privacy settings on social media platforms (Zabelskyte et al., 2022). Another limitation of this study lies in sentiment analysis accuracy. As Roberts et al. (2018) pointed out, although social media data provides vast opportunities for urban planners to understand green spaces, there remains a need for increased innovation and development in the methodologies that would enable this data source to be engaged with most effectively, such as using semi-automated methods.

Reference

Alshammari, S.M. and Nielsen, R.D. (2018). Less is More. Proceedings of the 2018 International Conference on Computing and Big Data - ICCBD ' 18.

Charles-Smith, L.E., Reynolds, T.L., Cameron, M.A., Conway, M., Lau, E.H., Olsen, J.M., Pavlin, J.A., Shigematsu, M., Streichert, L.C., Suda, K.J. and Corley, C.D., 2015. Using social media for actionable disease surveillance and outbreak management: a systematic literature review. PloS one, 10(10), p.e0139701.

Chew, C. and Eysenbach, G., 2010. Pandemics in the age of Twitter: content analysis of Tweets during the 2009 H1N1 outbreak. PloS one, 5(11), p.e14118.

Chunara, R., Andrews, J.R. and Brownstein, J.S., 2012. Social and news media enable estimation of epidemiological patterns early in the 2010 Haitian cholera outbreak. The American journal of tropical medicine and hygiene, 86(1), p.39.

Cui, N., Malleson, N., Houlden, V. and Comber, A., 2021. Using VGI and social media data to understand urban green space: a narrative literature review. ISPRS International Journal of Geo-Information, 10(7), p.425.

Cui, N., Malleson, N., Houlden, V. and Comber, A., 2022. Using social media data to understand the impact of the COVID-19 pandemic on urban green space use. Urban Forestry & Urban Greening, 74, p.127677.

developer.twitter.com. (n.d.). Filtering Tweets by location. Available at: https://developer.twitter.com/en/docs/tutorials/filtering-tweets-by-location.

Devlin, J., Chang, M.-W., Lee, K. and Toutanova, K. (2018). BERT: Pre-training of Deep Bidirectional Transformers for Language Understanding. arXiv.org. Available at: https://arxiv.org/abs/1810.04805.

Dixon, S. (2022). Twitter: number of users worldwide 2019-2020 | Statista. Statista. Available at: https://www.statista.com/statistics/303681/twitter-users-worldwide/.

Fan, C., Li, S., Liu, Y., Jin, C., Zhou, L., Gu, Y., Gai, Z., Liu, R. and Qiu, B., 2023. Using Social Media Text Data to Analyze the Characteristics and Influencing Factors of Daily Urban Green Space Usage—A Case Study of Xiamen, China. Forests, 14(8), p.1569.

Ghahramani, M., Galle, N.J., Ratti, C. and Pilla, F., 2021. Tales of a city: Sentiment analysis of urban green space in Dublin. Cities, 119, p.103395.

Hugging Face (n.d.). What is Text Classification? - Hugging Face. Available at:

https://huggingface.co/tasks/text-classification.
ICT 総研 (2022). 2022 年度 SNS 利用動向に関する調査. Available at: https://ictr.co.jp/report/20220517-2.html/.
Knowledge4policy.ec.europa.eu. (2018). Number of social media users worldwide 2010-17 with forecasts to 2021 | Knowledge for policy. Available at: https://knowledge4policy.ec.europa.eu/visualisation/number-social-media-users-worldwide-2010-17-forecasts-2021_en.
Lexico Dictionaries. (2021). EMOTION | Definition of EMOTION by Oxford Dictionary on Lexico.com also meaning of EMOTION. Available at: https://web.archive.org/web/20211009004612/https://www.lexico.com/definition/emotion.
Liu, B. and Zhang, L. (2012). A Survey of Opinion Mining and Sentiment Analysis. Mining Text Data, pp.415‑463. doi: https://doi.org/10.1007/978-1-4614-3223-4_13.
Liu, Y. and Lopez, R.A., 2016. The impact of social media conversations on consumer brand choices. Marketing Letters, 27, pp.1-13.
Maas, J., Spreeuwenberg, P., Van Winsum-Westra, M., Verheij, R.A., Vries, S. and Groenewegen, P.P., 2009. Is green space in the living environment associated with people's feelings of social safety?. Environment and Planning A, 41(7), pp.1763-1777.
Neppalli, V.K., Caragea, C., Squicciarini, A., Tapia, A. and Stehle, S., 2017. Sentiment analysis during Hurricane Sandy in emergency response. International journal of disaster risk reduction, 21, pp.213-222.
Nio L, Murakami K. Japanese sentiment classification using bidirectional long short-term memory recurrent neural network[J]. The Association for Natural Language Processing, 2018: 1119-1122.
Rao, T. and Srivastava, S., 2014. Twitter sentiment analysis: How to hedge your bets in the stock markets. In State of the art applications of social network analysis (pp. 227-247). Cham: Springer International Publishing.
Reza Rahutomo, Lubis, F., Hery Harjono Muljo and Bens Pardamean (2019). Preprocessing Methods and Tools in Modelling Japanese for Text Classification.
Roberts, H., Resch, B., Sadler, J., Chapman, L., Petutschnig, A. and Zimmer, S., 2018. Investigating the emotional responses of individuals to urban green space using twitter data: A critical comparison of three different methods of sentiment analysis. Urban Planning.
Rui, H., Liu, Y. and Whinston, A., 2013. Whose and what chatter matters? The effect of tweets on movie sales. Decision support systems, 55(4), pp.863-870.
Sadiq, B., Faizan Ur Reliman, Ahmad, A., Md. Abdur Rahman, Sulaiman Ab Ghani, Murad, A., Saleh Basalamah and Lbath, A. (2015). A spatio-temporal multimedia big data framework for a large crowd. HAL (Le Centre pour la Communication Scientifique Directe).
Shibuya, Y. and Tanaka, H., 2018. Public sentiment and demand for used cars after a large-scale disaster: Social media sentiment analysis with Facebook pages. In Proceedings of the 5th International Workshop on Social Web for Disaster Management (SWDM’18).
Shibuya, Y. and Tanaka, H., 2019. Using social media to detect socio-economic disaster recovery. IEEE Intelligent Systems, 34(3), pp.29-37.
Statista (2023). Japan: Twitter penetration rate by age group 2021. Available at: https://www.statista.com/statistics/1077538/japan-twitter-penetration-rate-by-age-group/#:~:text=As%20of%20January%202021%2C%20the.
Statista (2023). Number of social media users worldwide from 2017 to 2027. Available at: https://www.statista.com/statistics/278414/number-of-worldwide-social-network-users/
Statistics Bureau of Japan (2022). Statistics Bureau Home Page/Population Estimates/Current Population Estimates as of October 1, 2022. Available at: https://www.stat.go.jp/english/data/jinsui/2022np/index.html.
Tyng, C.M., Amin, H.U., Saad, M.N.M. and Malik, A.S. (2017). The Influences of Emotion on Learning and Memory. Frontiers in Psychology, 8(1454).
Wang, R., Browning, M.H., Qin, X., He, J., Wu, W., Yao, Y. and Liu, Y., 2022. Visible green space predicts emotion: Evidence from social media and street view data. Applied Geography, 148, p.102803.
Xu, C., Wong, D.W. and Yang, C. (2013). Evaluating the ‘geographical awareness’ of individuals: an exploratory analysis of twitter data. Cartography and Geographic Information Science, 40(2), pp.103‑115.
Ye, S. and Wu, F. (2013). Measuring message propagation and social influence on Twitter.com. International Journal of Communication Networks and Distributed Systems, 11(1), p.59.
Zabelskyte, G., Kabisch, N. and Stasiskiene, Z., 2022. Patterns of urban green space use applying social media data: a systematic literature review. Land, 11(2), p.238.

Revealing Access Equity: An Examination of Walking Course Distribution and Streetscape Quality for Residents
- A Case Study in Tsukuba City -

Xinyu Tang*, Mamoru Amemiya**, Sunyong Eom**

Ensuring walkable neighborhoods for all residents is important for their health and well-being. This study aims to examine the distribution of the municipality-designated walking courses and its access equity to residents in terms of walkable course length per 30-minute walking trip and their quality and suggest implications for where to add or maintain courses. For this purpose, we conducted a field audit to assess the quality of the streetscape and applied a VRP (Vehicle Routing Problem) model to create routes that can maximize the use of designated walking courses. The main findings are as follows. First, there is a lack of designated working courses in suburban areas while designated working courses are concentrated in the city center and natural attraction sites. Second, we divided the area into five categories by length and quality of the designated walking course. Third, 12% of the population are in the categories that cannot reach walking course, 19% of the population are in the categories that have low quantity and quality, and 15 % of the population are in the categories that have high quantity but low quality. Fourth, based on the classifications, we suggested walking course improvement strategies.

Keywords: Walking Course, Resident, Access Equity, Quality

1. Introduction

Ensuring a walkable environment is important to improve the health and well-being of residents. In recent years, many cities have started to designate various walking courses for promoting exercise, providing a network for daily walking, and appealing to the unique sceneries of the city. Providing residents with opportunities to use good quality walking course can improve their physical activity level and let residents rediscover the attractiveness of their living environment (Okamoto et al., 2016) (Maegawa et al., 2022). Since proximity to facilities such as parks is one of the important factors to encourage resident usage (McCormack et al., 2010), it is also necessary to consider the closeness of resident homes while designing the course to improve the health and wellbeing of residents. Furthermore, microscale walkability aspects such as traffic volume and sidewalk quality also affect residents' motivation to use walking courses (Guzman et al., 2022; Raswol, 2020). Therefore, streetscape quality is also an important aspect to consider when designing and managing the courses.

However, resident access inequity in neighborhood environments that promote walking such as urban green spaces and parks is an ongoing issue in many countries according to people's race and income (Silva et al., 2018; Zandieh, 2015). However, walking course also being one of the aspects of the neighborhood environment, has not yet received much attention, with even the distribution pattern not yet known.

While existing research has extensively explored the built environment's influence on walking behaviors, the focus has largely been on promoting walkability rather than evaluating walking environments comprehensively. Notably, Frank et al. (2005) demonstrated the correlation between community design elements—such as land-use mix, street connectivity, and residential density—and moderate physical activity levels. Similarly, Moura et al. (2017) established a participatory framework—known as the 7C's layout—which encompasses seven key dimensions: connectivity, convenience, comfort, conviviality, conspicuousness, coexistence, and commitment. They revealed a strong correlation between

*: Student member; University of Tsukuba, Integrative and Global Majors, Bachelor's Program in Global Issues
Tenodai 1-1-1, Tsukuba, Ibaraki, Japan, 305-8573 E-mail: xy2019free@gmail.com
**: Regular member; University of Tsukuba, Institute of Systems and Information Engineering

measured walkability based on this framework and the walkability perceptions gathered through surveys.

However, current literature largely overlooks the nuanced evaluation of walking environments, specifically in terms of both the quantity and quality of streets designed for walking. For instance, Ozaki et al. (2011) examined the use of walking courses through registered IC cards and scanners but confined their analysis to variations in walking behavior based on individual characteristics such as sex and age. Similarly, Cui et al. (2022) quantified population coverage within a 200-meter buffer from designated walking courses and pedestrian-only streets. While their work elucidates disparities in access to walking spaces, it falls short in evaluating whether citizens can engage with a diverse range of walking environments in terms of both quantity and quality.

Recognizing this gap, our study posits that the length and streetscape quality of accessible walking courses may substantially impact residents' health and satisfaction levels with their local environments. Prior research has not holistically addressed these aspects, focusing either on quantity or quality but rarely both. This study aims to fill this void by investigating the equity of walking course access in Tsukuba City, specifically by considering both the quantity and quality of walking courses.

The research questions guiding this study are as follows:

1. What is the distribution of walking courses and their streetscape quality in Tsukuba City?
2. How equitable is access to walking courses in Tsukuba City, when considering both quantity and quality factors?

2. Methodology

2.1. Study site

The study site for this study is Tsukuba City, one of the cities that is implementing various walking courses. 6 walking courses in Table 1 were chosen and summarized in one map using GIS, with the total length being 290km, as shown in Figure 1.

2.2. Streetscape quality evaluation

We applied part of the walkability checklist (Table 2) by Hanibuchi et al. (2020), in table 2 with each question worth 0 or 1 point. For the evaluation process, we conducted an onsite audit by cycling and stopping at intersections to check each previously passed course splits. As mountain

Table 1. Data and sources

Data	Data source
Demographic information	Census 2020 (500m mesh)
ESRI Japan Road data	MLIT 2021
Health Road 10 courses	Ibaraki Prefecture Public Health Promotion Division
Tsukuba Running Map 9 courses	Tsukuba City Citizen Sports Promotion Division
Tsukuba landscape Map 5 courses	Tsukuba City Urban Planning Division
Footpass 5 courses	Tsukuba City Tourism Promotion Division
Tsukuba Pedestrian deck Main&sub	Tsukuba City Road Planning Division
Ringring road Mount Tsukuba Area	Ibaraki Prefecture Sports Promotion Division

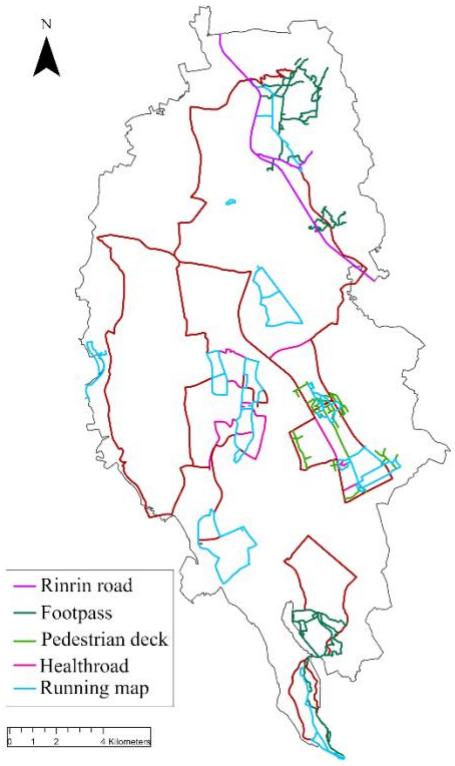

Figure 1. Walking courses network

areas do not fit the criteria for walkability in this checklist, this study excluded the walking courses in mountain areas and focused on the rest 260km courses for further analysis. The result quality scores were recorded in each course segment by adding a new field in the constructed course data.

2.3. VRP model building

Next, this study applied the course spatial data that contains quality scores on the Vehicle Routing Problem (VRP) model in ArcGIS. The detailed data settings and evaluation index calculated from the model are summarized in Table 3. The first half of the model consists of VRP analysis. It originally served as the function to select the optimal route for vehicles to conduct express delivery at many locations requiring settings for factors such as depots (OD), orders (delivery locations), and revenue (maximum income). In this study, we applied VRP to make a 30-minute walking route for each population mesh since conducting 30 minutes of exercise 2 times per week is recommended to all citizens for better health (MILT, n.d.). We transferred population mesh into central points as depots, excluding the points with 0 population and those that cannot reach courses within 30 minutes for model feasibility. As for order points, we split the courses on locations that are intersected by 3 lines, and transformed the course splits into central points as the blue line shows on the left side of Figure 2. The length of course splits was set as the revenue for the model to design routes with maximum course length.

Table 2 Walkability checklist

No.	Walkability checklist
1	Is there a sidewalk?
2	Is the sidewalk wide enough? (Width about 2 meters or more)
3	Are there any obstructions? (Surface irregularities)
4	Is there a steep slope?
5	Are there any cars parked in the street?
6	Is there heavy vehicle traffic? (Frequently or occasionally)
7	Is there heavy pedestrian traffic?
8	Is there a crosswalk?
9	Is the streetscape attractive? (Beautiful, interesting, comfortable, or not)
10	Is there any graffiti or abandoned trash?
11	Are there any abandoned buildings?

Source: Hanibuchi et al. (2020)

Table 3. Data setting and evaluation index

Index	Details
Maximum Walking time	30 min
Walking speed	4km/h
Walking distance	2160m
Network data	Constructed from ESRI road data
Depots	Mesh central points (1966 points)
Orders	Walking course road split central points
Revenue	Length of walking course road splits
Walked course length %	Walked course length / Total route length *100
Average walked course streetscape quality score	Quality score of walked course / Length of walked course

The outcome data are the percentage of walked course length, and the average streetscape quality score of walked course for each population mesh. These will be the evaluation index for determining resident access equity of walking courses. The example route A is shown in the right graph of Figure 2, with 45% of its length as walking course and its average quality score of 9 p/m.

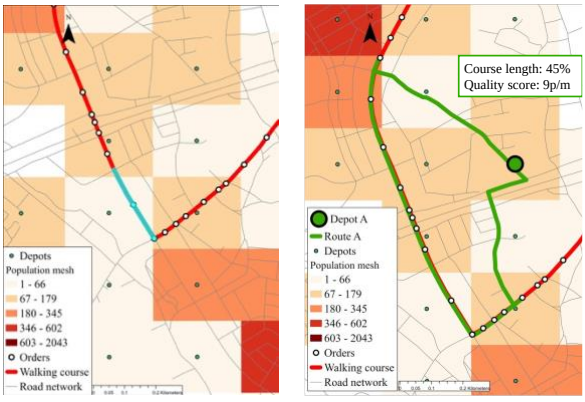

Figure 2. Example of VRP model output

3. Results

3.1. Course distribution and streetscape quality

Walking course mainly concentrates or overlaps in city centers, major parks, and natural attraction sites, with the

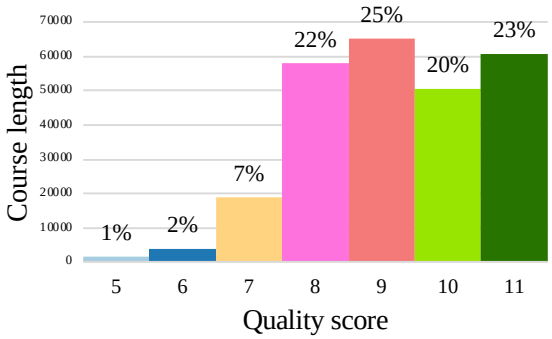

Figure 3. Course length for different quality scores

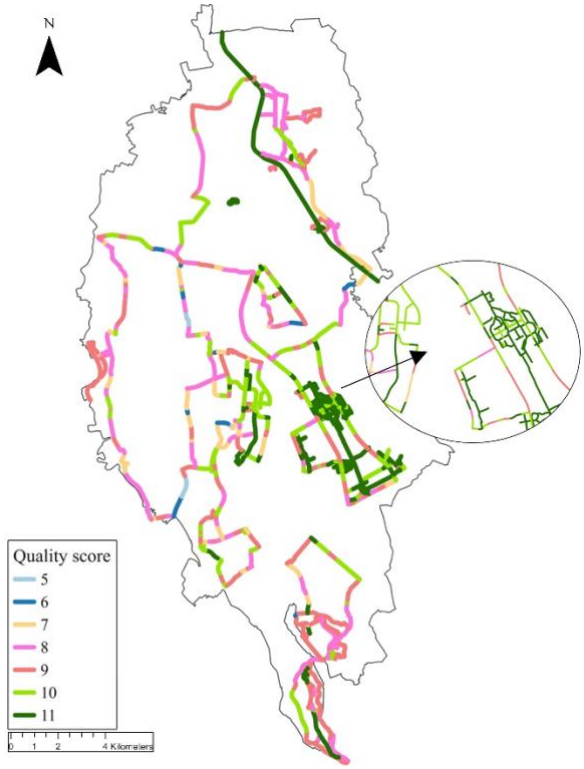

Figure 4. Walking course distribution and quality

suburban area having relatively few courses. As for streetscape quality, most with a total score being 11 and an average of 9.17, most course quality scores range from 8-11, with higher quality course concentrating around city centers and pedestrians, lower quality course at suburbs areas, city edge, and some major roads shown in Figure 3 and 4.

3.2. Resident access equity for walking course

In order to identify the gaps between access course length and quality for people who can reach walking course, we divided the population into 4 types based on the average

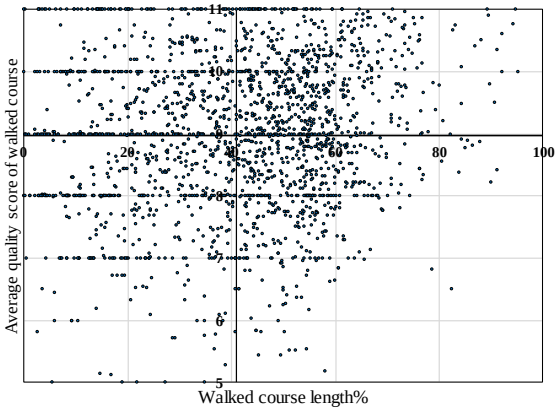

Figure 5. Population types by quantity and quality

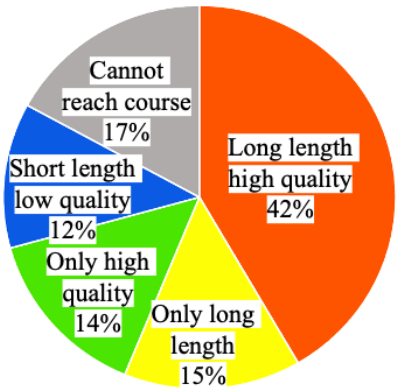

Figure 6. Proportion of population by types

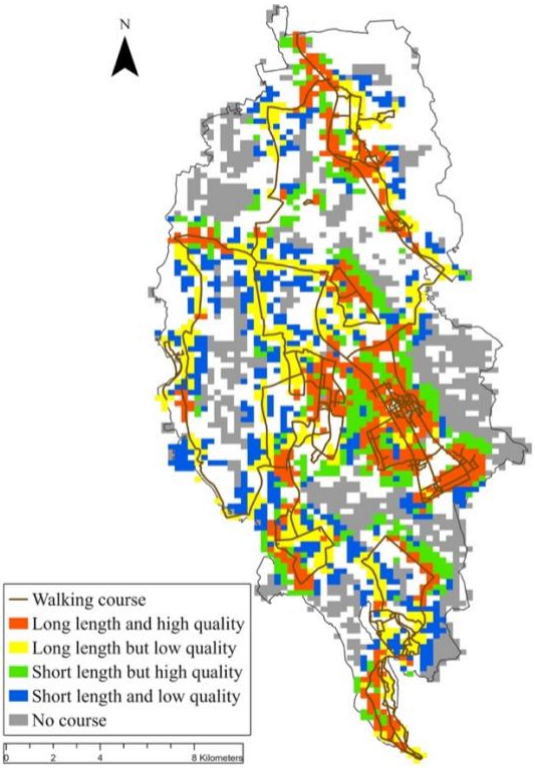

Figure 7. Spatial distribution of population types

of accessed course length and quality, as shown in Figure 5. Combined with the population who cannot reach courses, it was found that 42% of the population can enjoy both long and good quality course, while 29% of the population can only access either one of those aspects, the rest of the population lacks good quality walking course in their vicinity, with 12% of the population having walk short length and low quality course in their neighborhood, and another 17% having no access to course during a 30-minute walking trip. The spatial distribution of population types is illustrated on figure 7. It shows that the population lacking sufficient walking course in blue and grey is mainly concentrated in suburbs or the city edge. People living around city centers or natural attraction sites marked in orange can enjoy course with longer and better quality.

3.3. Area selection for adding new course

According to population types, there are 43% of the population with relatively less access to sufficient walking course length. In order to address this gap more efficiently, we set the priority level shown in Table 4, with the areas where people cannot reach courses or can only access short and low-quality walking courses being prioritized the most.

Table 4. Priority level for adding course

Population types	Percentage	Priority level
Cannot reach courses	17%	1
Short length low quality	12%	2
Only high quality	14%	3
Only long length	15%	4
Long length high quality	42%	5

3.4. Course maintenance

Not only adding new course, but improving the quality of walking courses for the residents is also necessary. The study chose to calculate the potential usage population for each course split by adding the overlapped mesh population number that passed each central point of the course split, as it can present the priority level for maintenance. Then, we divided the course into 4 types based on its average of

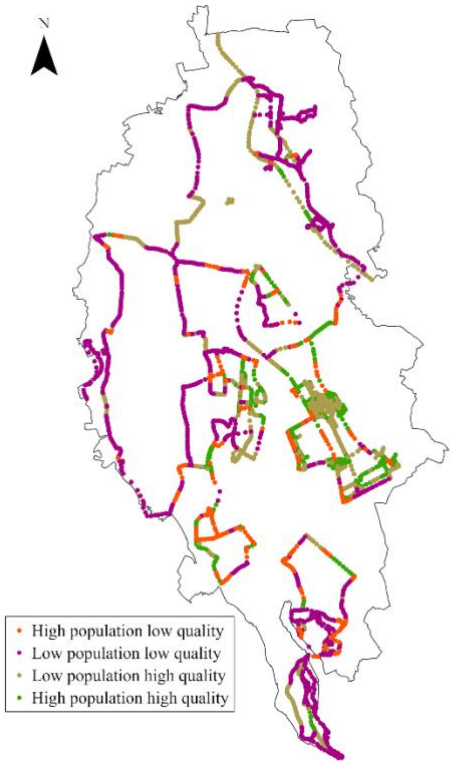

Figure 8. Spatial distribution of course types

course quality and usage number. Figure 8 illustrates that the course shown in orange has high population usage but in low streetscape quality. It is especially necessary to prioritize course maintenance in these areas.

4. Discussion

The current walking course mainly concentrates and overlaps at city centers and natural attraction spots. This indicates that the city center has better infrastructure management and responds to the fact that many course design purposes include appealing to the city's uniqueness and attractions. Simultaneously, since each course is designed by a different department, the overlapping situation may also indicate the lack of communication among departments, or they did not place importance on the overlapping situation.

Therefore, cities and departments that designate walking courses should be aware of the overall distribution of all walking courses to avoid excess overlap and achieve wider course distribution for a larger population. Increasing communication with departments is also beneficial to

understand each other's design purpose and maintenance plans.

While maintaining courses, streetscape aspects such as traffic amount fluctuate, certain roads may experience higher or lower traffic at different times of the day, leading to different comfort and safety levels while walking. Since this study only visited the course once, we cannot say that we were able to capture the traffic flow comprehensively. Therefore, the overall traffic should be monitored and considered as an aspect while setting course maintenance priority. In addition, information about the timing of traffic flow can also be shared with the citizens in course maps in addition to estimated calories and attraction spots. This can help residents decide the suitable time for taking a walk to achieve a better walking experience.

Furthermore, with the population that lacks adequate walking courses located in suburbs and city edge areas, it shows that the suburbs areas receive less attention, either because suburbs area may lack adequate walking courses or acknowledgeable unique sceneries, or that the roads were just not designated even though they are well-maintained. Therefore, future course design and maintenance should also place importance on suburban areas, since most populations in suburban areas are elderlies, who need to have regular exercise for health, and are the ones that utilize walking course the most (Okazaki et al., 2011). In addition, people in suburbs areas tends to use more private cars due to less easily accessible transportation, leading to increased sedentary behaviors, having walking course near resident's home can serve as a motivation for people to conduct physical activity.

In the meantime, as residents with various demographic characteristics have different preferences for a walkable environment, it is necessary to analyze the demographic traits of the area to determine how much to design or extend courses, and which aspects of streetscape quality to prioritize. Cooperating with residents when designing courses is also beneficial to understand their perspective of unique sceneries and achieve higher satisfaction for future course usage.

We suggested the above hypothesis for reasons leading to the current situation and provided several suggestions for course design and maintenance. Further research should conduct interviews with city departments and a comparison of different cities to verify the above reasons.

5. Conclusion

Walking course is one of the examples of the walkable environment. Resident proximity and streetscape quality are two important factors for walking course design. Insufficient consideration may lead to access inequity for residents. The result shows a concentration of course in city centers and natural attraction sites, with 29% of the population lacking good quality walking courses near their resident homes. Cities that are designating walking courses should understand the overall distribution of course and can apply the methodology adopted in this study to determine where to add or maintain courses, for better walkable environments and equal access to walking course for more residents.

Acknowledgments

This study was supported in part by JSPS KAKENHI Grant Numbers JP23K13460.

References

McCormack, G. R., Rock, M., Toohey, A. M. and Hignell, D. (2010). Characteristics of urban parks associated with park use and physical activity: A review of qualitative research. *Health and Place*, **16(4)**, 712–726.

Okazaki, K., Shibata, A., Ishii, K., Yako, S., Kawamura, Y., Imai, F., Moriya, K. and Oka, K. (2011). An Environment-Focused Project for Promoting Walking: The Misato City IC Walk Project. *Journal of Japan Society of Sports Industry*, **21(2)**, 235–244 (in Japanese with English abstract).

Silva, C. de S., Viegas, I., Panagopoulos, T. and Bell, S. (2018). Environmental justice in accessibility to green infrastructure in two European Cities. *Land*,

7(4).

Zandieh, R. (2015, July). *Inequality in Access to Local Facilities and Older Adults ' Walking Behaviour : An Environmental Justice Perspective*. 52nd International Making Cities Livable Conference on Achieving Green, Healthy Cities, Bristol, UK.

Maegawa, I., Ishiguro, T. and Hanawa, E. (2022). *How to Attract And Interact with Visitors in Post-Corona Areas*. Mitsubishi UFJ Research and Consulting <https://www.murc.jp/wp-content/uploads/2022/07/seiken_220704_01.pdf> (in Japanese).

Hanibuchi, T., Nakatani, T., Uesugi, M. and Inoue, S. (2020). Construction of Geographic Multilevel Data Through Internet Surveys and Systematic Social Observation. *Geographical review of Japan* **93–3**, 173–192 (In Japanese).

Okamoto, N., Kubota, A., Sun, F. and Nonaka, Y. (2016). Trial to Increase Physical Activity by the Recognition of the Neighborhood Environment Using GIS. Japan Journal of Lifelong Sport, **13(2)**, 75–83. (in Japanese with English abstract)

Frank, L. D., Schmid, T. L., Sallis, J. F., Chapman, J. and Saelens, B. E. (2005). Linking objectively measured physical activity with objectively measured urban form: Findings from SMARTRAQ. *American Journal of Preventive Medicine*, ***28***(2 SUPPL. 2), 117–125.

Moura, F., Cambra, P. and Goncalves, A. (2017). Measuring Walkability For Distinct Pedestrian Groups with a Participatory Assessment Method: A Case Study in Lisbon. *Landscape and Urban Planning*, **157**, 282-296.

Ministry of Land, Infrastructure, Transport and Tourism. (n.d.). the effects and benefits of "walking" and how to make it a habit. < https://www.mlit.go.jp/common/000022977.pdf>

Population Aging and the Community-based Integrated Care System in Akita Prefecture

Ketian Chen*, Mizuki Kawabata**

Abstract The Japanese government introduced "the community-based integrated care system" to provide health support for elderly residents in their communities. Focusing on Akita Prefecture, the most aged prefecture in Japan, this paper examines the spatial distribution patterns of the aged demographics and the accessibility to care facilities in this system. For the spatial distribution analysis, we use Moran's I and Getis-Ord Gi* statistics. The accessibility to the care facilities is measured using the two-step floating catchment area (2SFCA) method. We find that the elderly population is becoming more spatially clustered, and the degree of population aging is increasing across Akita Prefecture. The accessibility to elderly care facilities varies considerably, indicating issues of inequity in resource accessibility. These results can help officials identify future resource allocation plans to enhance accessibility and promote health equity in the community care system.

Keywords: Population aging, community-based integrated care system, Akita Prefecture

1. Introduction

Population aging is a global trend, with particular prominence in developed countries. Japan has the highest proportion of the elderly population in the world, leading to a "super-aging" social transformation across both rural and urban areas. Based on data from the Statistics Bureau of Japan, the population aged 65 and above has reached 35.89 million in 2019, which occupied 28.4% of the total population. This demographic shift is anticipated to persist and intensify over time. The process of population aging will bring severe challenges to the labor market, pension systems, retirement systems, health care resources, and other aspects (Bloom et al., 2015). In 2025, the post-World War II baby-boom generation in Japan will reach the age of 75 and above, which further increase the demand for healthcare services and exacerbate the aging problems.

To meet this demand and enable elderly citizens to spend senior years in their local communities, the Japanese government introduced "the community-based integrated care system" in April 2015, which aims to provide a comprehensive matrix of healthcare, nursing care, preventive care, housing, and livelihood support for elderly citizens within their local communities (Ministry of Health, Labour and Welfare of Japan, 2016). By coordinating various services within the communities, the system aims to ensure that necessary care and assistance are readily available to elderly individuals in their everyday residential zones. Since its initial launch, the system has been continuously evaluated and adapted to meet the evolving needs of Japan's aging population.

Among the 47 prefectures (*todōfuken*) in Japan, Akita Prefecture has the highest proportion of people aged 65 and above, standing at 37.2% in 2019. For context, an "aging society" is typically defined as one where 7% or more of its population is aged 65 or above. Akita Prefecture's figure of 37.2% far surpasses this threshold, underscoring the severity of aging problem. For a prefecture experiencing such pronounced aging, ensuring that care facilities for elderly population are both accessible and adequately equipped is a matter of public health and social equity. The easier access to care facilities can enhance the quality of life for the elderly by reducing travel times and potentially improve wellbeing and health. There exists extensive literature evaluating the accessibility of care facilities for elderly population. For example, Cho et al. (2021) evaluate the accessibility of elderly population to welfare facilities using walking and travel time in Daejeon, Republic of Korea. Carpentieri et al. (2020) analyzed the spatial accessibility of different elderly age groups to primary health services in Naples,

* Student Member, Graduate School of Economics, Keio University, chenketian@keio.jp
** Member, Faculty of Economics, Keio University, mizuki@econ.keio.ac.jp

Italy at health district level.

Despite its considerably aging population, the situation in Akita Prefecture remains under-studied. This paper aims to analyze the spatial pattern of the elderly population and their accessibility to care facilities in the community-based integrated care system in Akita Prefecture. Specifically, this study addresses two questions: First, what are the characteristics of the spatial distribution of the elderly population in Akita Prefecture? Second, is there a geographic inequity in the accessibility to elderly care facilities in the community-based integrated care system, including medical institutions, welfare facilities, cultural facilities, and care centers in Akita Prefecture?

2. Backgrounds

2.1 Population Aging in Akita Prefecture

Among the 47 prefectures in Japan, Akita Prefecture has the highest elderly population ratio (the proportion of people aged 65 and above of the total population), which was 33.8% in 2015. In the future, the elderly population ratio is estimated to exceed 40% in 2025 and reach 50.1% in 2045 (National Institute of Population and Social Security Research, 2018). On the other hand, the old-age dependency ratio, the ratio of those aged above 65 to the working-age population (those between age 15 to 64), increased dramatically from 25.8% in 2000 to 55.5% in 2020 (Figure 1).

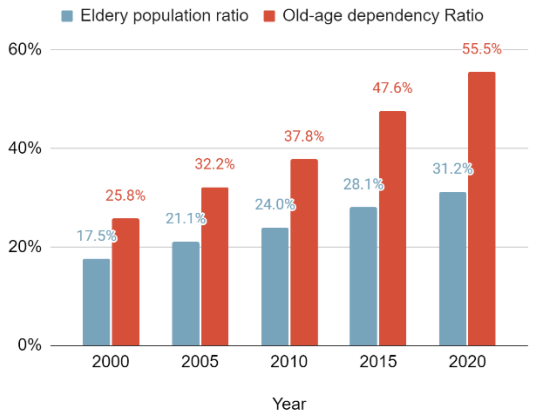

Figure 1 Elderly population ratios and old-age dependency ratios in Akita Prefecture from 2000 to 2020

The high old-age dependency ratio caused a great burden on social services and the pension system, which could lead to a long-run decline in the economy. These demographic trends highlight the pressing need for sustainable and comprehensive care solutions to address the challenges posed by an aging population in Akita Prefecture.

The prevailing factors contributing to the pronounced population aging and imbalanced age structure in Akita Prefecture are primarily rooted in the persistently low fertility and marriage rates, alongside a substantial outmigration of the younger population. The number of births in Akita Prefecture continued to decline (Figure 2). The birth rate (the number of births per 1,000 population) was 2.8 in 2021, ranked the lowest in Japan for 27 continuous years since 1994. The marriage rate (the number of married people per 1,000 population) and the number of marriages also show a declining trend except “Reiwa Marriage Boom” in 2019 (Figure 3). In addition, the marriage rate in Akita Prefecture ranked as the lowest in Japan for 21 continuous years since 2000 (Akita Prefectural Department of Planning and Promotion, 2021).

The social decrease of the young population also contributes to the severe population aging problem. There is a noticeable outflow of people aged 15 to 19 and 20 to 47 due to employment and postsecondary education outside the prefecture. According to System of Social and Demographic Statistics, nearly 80% of upper secondary school graduates in Akita Prefecture tend to enter the universities outside the prefecture. On the other hand, the outflow due to graduates getting jobs outside the prefecture also contributes to the social change in age structure. With fewer job opportunities and lower-income levels compared to the national average, approximately 30% of upper secondary school graduates from Akita Prefecture seek employment outside the prefecture every year, primarily in the Tokyo metropolitan area. Such a large outflow of the young generation not only leads to the shortage of labor force but also influences the birth rate inside the prefecture, which further affects the age

structure change and leads to population aging.

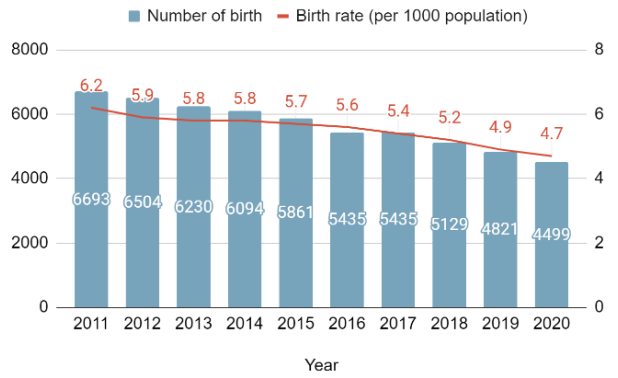

Figure 2 Number of birth and birth rate in Akita Prefecture from 2011 to 2020

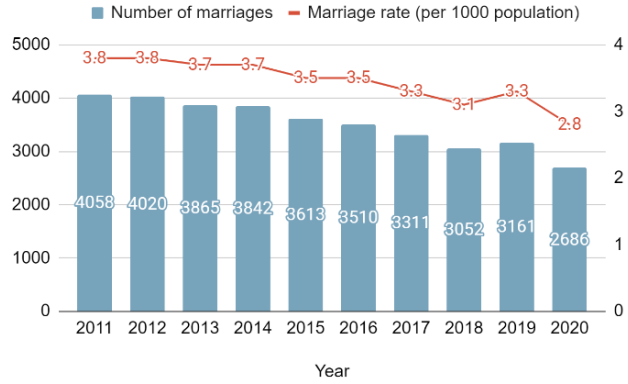

Figure 3 Number of marriages and marriage rate in Akita Prefecture from 2011 to 2020

2.2 The community-based integrated care system and care centers in Akita

The community-based care system in Akita Prefecture offers a range of services and initiatives to support the elderly population. These include promoting collaboration between home medical care and caregiving, facilitating the use of the adult guardianship system, providing information on dementia, conducting training courses and workshops for dementia supporters, and promoting safe monitoring for the elderly. Inside this system, the community-based care centers serve as accessible community hubs where elderly individuals can access a wide range of healthcare, caregiving, and social services tailored to their specific needs. One care center usually consists of team members with different professional qualifications, including public health nurse, certified social worker, life support coordinator, and care manager. The main functions and services of care center include (Ministry of Health, Labour and Welfare of Japan, 2016):

- Consultation support: The center responds to various consultations related to caregiving, welfare, healthcare, and other matters concerning the elderly population.
- Preventive care management: The center offers preventive care and life support services to individuals certified as requiring support levels 1 and 2 or those identified as potential candidates for long-term care.
- Right protection: For those who have problems with money management or contracts, the care center provides assistance with the procedures associated with the use of the adult guardianship system.
- Network building: In addition to providing support and guidance, the care center also works to build networks with medical institutions and other related organizations.

By 2021, there are 65 community-based integrated care centers operating in Akita Prefecture (Ministry of Health, Labour and Welfare, 2021). The average staff count per center stands at 4.8, with a range of 2 to 17 individuals. This number is lower than the national average of 6 staffs per center. One center receives an average of 1,654 consultations annually. This number is still below the national average of 2,601 consultations per center. The annual consultation figures per center exhibit notable disparities, varying from a minimum of 83 cases to a maximum of 104,171 cases. This is due to a difference in management between care centers that are directly managed by the local government and those outsourced. Moreover, the awareness of the existence of the care center is low in some areas, and the purpose and necessity of community-based care are not fully disseminated to residents. The quality of the community-based integrated care system in Akita Prefecture varies considerably from

region to region, due to the vast land area, dispersed population, and uneven distribution of medical and nursing care facilities (Akita Prefecture Official Homepage, 2018). A challenge is the insufficient publicity of this system and the lack of collaboration with related local organizations, including medical institutions and welfare facilities.

3. Methods

The study area is Akita Prefecture, located in the *Tōhoku* region of Honshu, with a total population of approximately one million, based on the 2015 Population Census. The spatial unit of analysis is small areas or districts (chocho aza etc.) in the 2015 Census data. The district refers to a geographical unit smaller than the municipality (*shikuchōson*, which represents cities, towns, villages, and special wards).

3.1 Spatial patterns of elderly population

We examine the spatial patterns of elderly population by using choropleth maps as well as the global Moran's I and Getis-Ord Gi* statistics of the elderly population ratios. The global Moran's I is a global indicator of spatial autocorrelation, which can be used to examine whether the spatial patten is random, clustered, or dispersed. Moran's I values range between approximately -1 and 1. Values that are not statistically significant indicate no spatial autocorrelation (a random distribution, or the null hypothesis). The expected value of Moran's I under the null hypothesis is $-1/(n-1)$, where n is the number of observations. When n is sufficiently large, $-1/(n-1)$ is nearly zero. Significant Moran's I values greater than the expected value represent positive spatial autocorrelation (a clustered distribution in which neighboring attribute values are similar). Significant values smaller than the expected value depict negative spatial autocorrelation (a dispersed distribution, where neighboring attribute values differ from one another). In this analysis, a 95% significance level is used. We use Moran's I statistics to indicate whether the spatial distribution of the elderly population in Akita Prefecture is clustered or dispersed. While the global Moran's I statistics demonstrate the overall spatial clustering, they do not identify the specific locations of clusters of high or low elderly population ratios. Therefore, we employ Getis-Ord Gi*, a local indicator of spatial autocorrelation. A significant positive Gi* statistic suggests a spatial clustering of high values, or a hot spot, with a larger value indicating more intense clustering of high values. A significant negative Gi* statistic represents a spatial clustering of low values, or a cold spot, wherein a smaller value denotes a more intense clustering of low values.

3.2 Accessibility measurements

The accessibility contains physical accessibility, affordability, and adequacy of supply (Gulliford et al., 2002). Physical accessibility or the geographical distance can be measured using geographic information systems (GIS). Other factors involving financial, organizational, and social barriers are more complex and difficult to compute using currently available data. In this study, we focus only on the physical accessibility to care facilities in the community-based integrated care system, including medical facilities, cultural facilities, and the community-based integrated care centers. By evaluating the geographical accessibility distribution, we examine disparities in accessing these care facilities.

There are various methods for measuring the geographical accessibility, including the nearest distance method, kernel density method, the gravity model (Joseph and Bantock, 1982), and the two-step floating catchment area (2SFCA) method (Luo and Wang, 2003). Given data limitations, we measure accessibility to the elderly care facilities using Thiessen polygons, Euclidean distance, and the 2SFCA method. First, we use Thiessen polygons, alternatively known as Voronoi polygons, to delineate the service areas of community-based integrated centers. If a person is within Thiessen polygon for care center A, then the nearest care center to that person is A. Second, Euclidean distance is used to calculate the distance between the population-weighted centroids of each district and the closest care facility to them. Third, we apply the

2SFCA method using the number of staff in each care center (supply) and the number of the aged population in each district (demand). The number of staff in each center are published by the Ministry of Health, Labour and Welfare (2021). We use the 2SFCA method to calculate accessibility in two steps: in the first step, we allocate the total elderly population in the 1km catchment area from a care center and then compute the supply-to-demand ratio. In the second step, the supply-to-demand ratios in the catchment area from population-weighted centroids are summed up to indicate the accessibility index at each district. In this way, the 2SFCA method incorporates a supply-to-demand ratio that extends beyond administrative boundaries.

3.3 Data

The care facilities that mentioned in the community-based care system includes medical institutions, welfare facilities and the community-based integrated care centers. In addition, cultural facilities are also considered as care facilities since they also contribute to elderly people's wellbeing by providing a platform for social activities that improve mental health (Phelan et al., 2004; Alidoust and Bosman, 2015). We derive point data on care facilities from 2014 Medical institutions, 2015 Welfare facilities for the elderly, and 2013 Cultural facilities published by the Ministry of Land, Infrastructure, Transport and Tourism. There are 1,332 medical institutions, including 73 hospitals and 1,259 clinics. There are 808 welfare facilities for the elderly, including different types of nursing homes and welfare centers for the elderly. The number of total cultural facilities is 1028, including museums, archives, memorials, libraries, aquariums, zoos, botanical gardens, and sports facilities. For the community-based integrated care centers, we geocoded the address into point data published from Akita Prefecture Official Homepage (2021). There are 65 community-based integrated care centers by 2021. Figure 4 shows the layout of medical institutions, welfare facilities for the elderly, cultural facilities, and the community-based integrated care centers in Akita Prefecture.

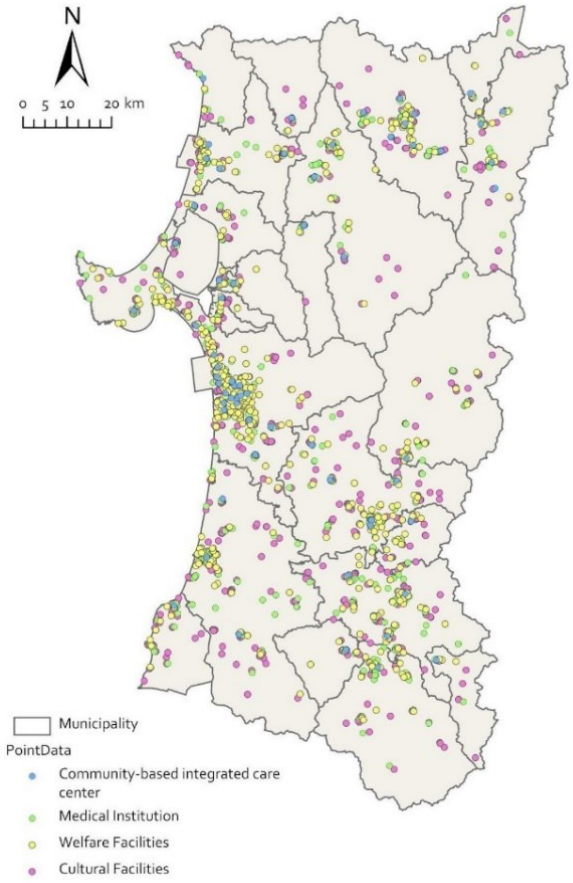

Figure 4 Distribution of care facilities in Akita Prefecture

4.Results

4.1 Spatial distributions of elderly population

To visually illustrate the spatial distribution of elderly population and its temporal changes, Figure 5 depicts the elderly population ratios in Akita Prefecture for 2005 and 2015. The maps reveal an overall increasing trend in population aging across most regions in Akita Prefecture. In 2005, there were still a few areas where the elderly population ratios were less than 20%. By 2015, however, almost all areas had ratios exceeding 20%. Additionally, there are notable variations in the elderly population ratios, even between neighboring areas.

Table 1 reports the global Moran's I statistics for the elderly population ratios in 2005 and 2015. The Moran's I values are both positive and statistically significant at the 1% level, indicating spatial clustering of the elderly population in Akita. Notably, from 2005 to 2015, the

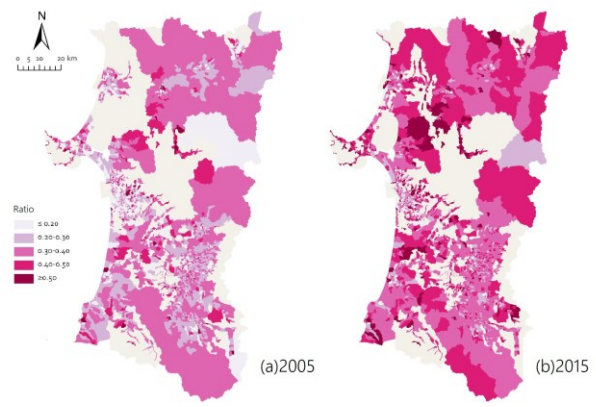

Figure 5 Spatial distribution of elderly population ratios in 2005 and 2015

Moran's I value rose from 0.198 to 0.251, accompanied by an increase in the associated z-score from 17.812 to 21.199. These findings indicate a discernible upward trend in the spatial clustering of Akita Prefecture's elderly population over the ten-year period.

Table 1 Global Moran's I statistics

Year	Moran's I	z-score	p-value
2005	0.198	17.812	＜0.000
2015	0.251	21.199	＜0.000

Figure 6 illustrates the spatial distribution of hot spots and cold spots for the elderly population ratios in Akita Prefecture, based on the Getis-Ord Gi* statistics for the years 2005 and 2015. In 2005, hot spots are primarily clustered in the southeast and northeast regions, signifying areas with higher elderly population ratios. Conversely, the cold spots were predominantly concentrated in the southwest coastal regions, Akita-shi and Yurihonjō-shi, indicating relatively low elderly population ratios in these areas. In 2015, the previous cold spots persisted, with additional cold spots emerging around Daisen-shi. Meanwhile, the hot spots shifted to the northern and central parts of the prefecture. These spatial patterns reveal the evolving distribution of elderly populations over the decade.

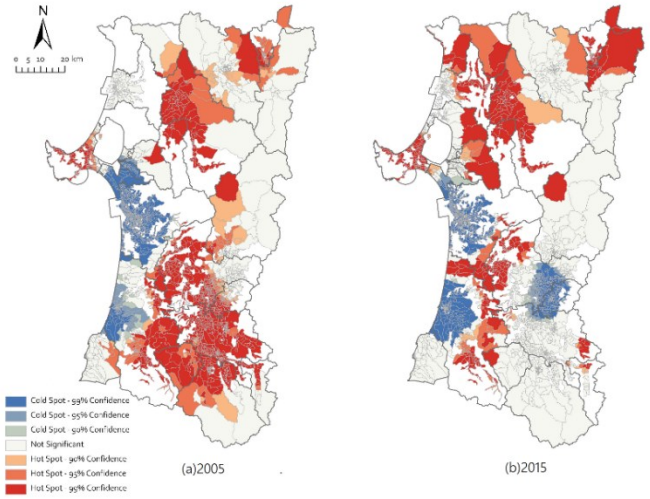

Figure 6 Hot and cold spots in elderly population ratios in 2005 and 2015

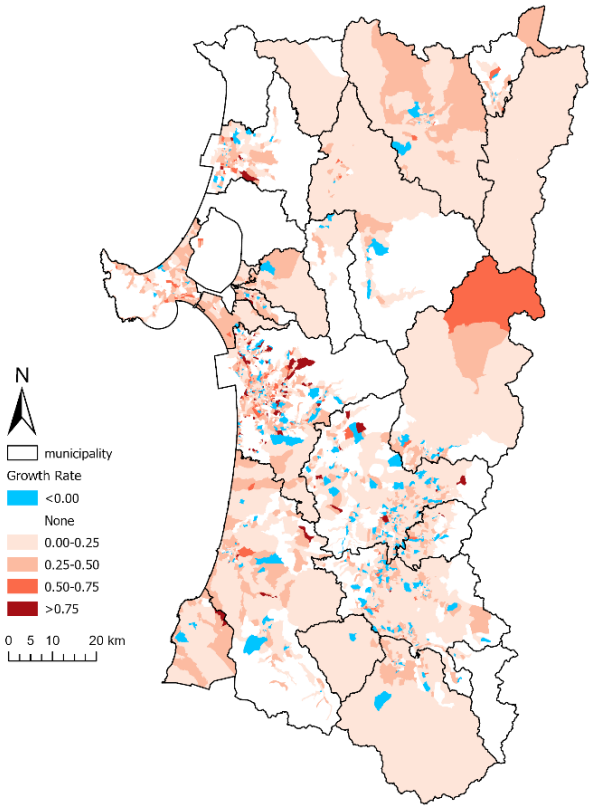

Figure 7 The growth rate of the elderly population ratio from 2005 to 2015

The overall elderly population ratio in the prefecture exhibit a substantial increase, rising from 21% in 2005 to 28% in 2015, representing a notable 7% growth rate over

the ten-year period. Figure 7 reveals that from 2005 to 2015, the majority of regions within Akita Prefecture experienced growth in their elderly population ratios. Conversely, only a few select areas (highlighted in blue on the map) show a decreasing trend in these ratios. These findings underscore the importance of recognizing the spatially heterogeneous nature of population aging in Akita Prefecture.

4.2 Accessibility to services in the community-based integrated care system

First, we show the service areas of the community-based integrated care centers using the Thiessen polygons (Figure 8). Each polygon delineates the catchment area of a specific care center. Individuals located within a particular polygon are considered the closest to the corresponding care center. The background of the Thiessen polygons depicts the density of the elderly population (elderly population/km^2). The distribution of these service areas tends to correlate with the spatial variation in the density of elderly population across Akita Prefecture. Care centers with expansive service areas are primarily located in regions with lower elderly population densities, predominantly in the middle-eastern and southern parts of the prefecture. In contrast, care centers with more confined service areas tend to exist in regions with higher elderly population densities. This pattern highlights that elderly individuals residing in larger service areas face longer travel distance to their respective care centers compared to those in smaller service areas. Such spatial disparity in accessibility emphasizes the need to address transportation and mobility issues faced by the elderly, especially in regions where the service area covers extensive geographic areas.

Table 2 presents the summary statistics for the Euclidean distance to the nearest elderly care facilities in Akita Prefecture. The urban area in this study is defined as the "urbanized area" published by the Ministry of Land, Infrastructure, Transport, and Tourism. All areas excluding the urban area are classified as non-urban areas. Based on the mean distance for the total area, among all

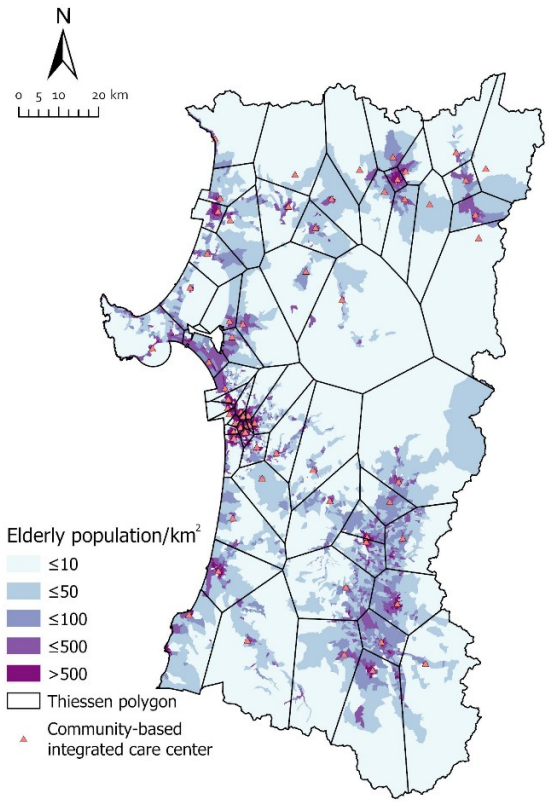

Figure 8 Thiessen polygons of the community-based integrated care centers

Table 2 Summary statistics for Euclidean distance (in meter) to nearest elderly care facilities

Elderly care facilities	Area	Mean	Median	SD	Max
Medical institutions	Total area	1,490	993	1,559	14,896
	Urban	846	493	883	6,279
	Non-urban	2,551	2,169	1,858	14,896
Welfare facilities for the elderly	Total area	1,642	1,037	1,738	16,586
	Urban	927	593	863	5,397
	Non-urban	2,836	2,308	2,148	16,586
Cultural facilities	Total area	1,653	1,232	1,427	9,907
	Urban	1,251	905	1,084	7,466
	Non-urban	2,313	1,969	1,658	9,907
The community-based integrated care centers	Total area	3,955	3,020	3,353	26,777
	Urban	2,719	1,832	2,418	7,674
	Non-urban	5,982	5,471	3,672	26,777

the facilities, medical institutions are the most accessible, while the community-based integrated care centers are the least accessible. This discrepancy can be attributed to the

relatively lower number of such care centers compared to other elderly care facilities. When analyzing accessibility by area, medical institutions are the most accessible elderly care facilities in urban areas, whereas cultural facilities are more prominent in non-urban areas. Remarkably, there exists a marked geographical disparity in elderly care facility accessibility between urban and non-urban areas. The latter face challenges in achieving the same accessibility level as the former, particularly concerning medical institutions and welfare facilities. The mean distance to these facilities in non-urban areas is almost three times that of urban areas. This disparity underscores the importance of addressing accessibility gaps and ensuring equitable accessibility across Akita Prefecture. Policies encouraging the elderly to relocate to central areas or near transit stations could enhance accessibility to care facilities. Furthermore, improving public transportation services in non-urban areas is crucial.

Figure 9 depicts the accessibility values calculated by the 2SFCA method. Most districts exhibit accessibility values below 0.005. Areas with values exceeding 0.0075 are mainly clustered in Happō-chō, Miharu-machi, and Gojōme-machi. In contrast, a large number of districts in Yurihonjō-shi and Yokote-shi have values below 0.0025. This discrepancy might be attributed to the limited number of care centers in these cities. Specifically, Yurihonjō-shi and Yokote-shi have only 4 and 3 care centers, respectively. Meanwhile, Akita-shi, despite a comparable land area, possesses 18 care centers.

To better understand the geographical disparities in accessibility across the prefecture, Figure 10 employs the quantile classification to illustrate accessibility measured by the 2SFCA method. The accessibility values are divided into five categories, with red and blue colors representing the lower and higher accessibility to care centers, respectively. It is evident that the northwestern regions and Ōdate-shi exhibit higher accessibility compared to other regions within the prefecture. Districts with lower accessibility are dispersed throughout various parts of Akita Prefecture.

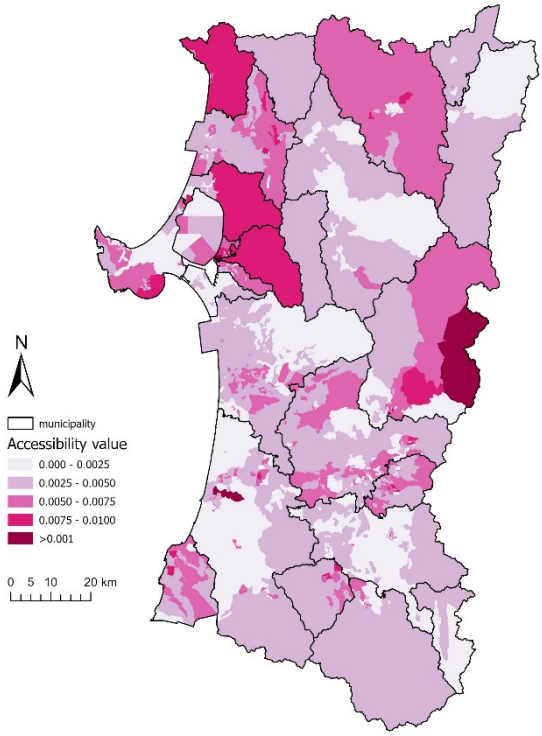

Figure 9 Accessibility to community-based integrated care centers: actual values

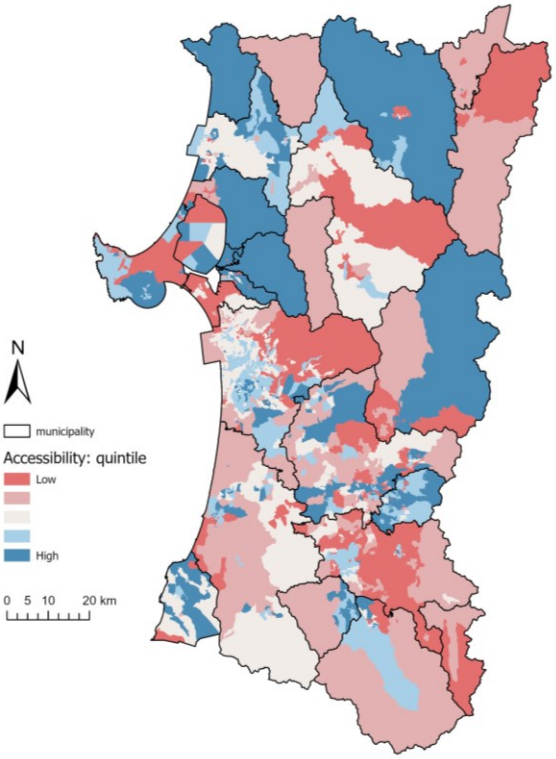

Figure 10 Accessibility to community-based integrated care centers: quintile classification

5.Conclusion

The global Moran's I statistics reveal an increasing trend in the spatial clustering of Akita Prefecture's elderly population during the ten years, from 2005 to 2015. The degree of population aging, however, varies from region to region in terms of the elderly population ratio and its growth rate. There are also geographical disparities in accessibility to elderly care facilities across the prefecture according to the results obtained from measuring the Euclidean distance to the nearest facilities. Non-urban areas have more difficulties in terms of accessing a variety of elderly care facilities than urban areas, especially accessing medical institutions and welfare facilities.

Furthermore, this paper applied the 2SFCA method to measure accessibility to care centers, taking into account both the capacity of these centers and the number of people aged 65 and above. The accessibility varies dramatically across regions due to disparities in the supply of care centers and variations in elderly population density.

The distribution of elderly care facilities plays an important role in delivering care services. Enhancing access to health and social engagement opportunities can improve well-being and quality of life of the elderly. However, the observed disparities in the accessibility to elderly care facilities raise concerns about the feasibility and equity of the services provided. The findings of this study can serve as an insight for officials in identifying potential locations for future care facilities, aiming to improve overall accessibility throughout Akita Prefecture and enhance health equity in community care. Strategic planning and resource allocation can bridge the accessibility divide, thereby ensuring that elderly individuals have more equal opportunities to access the care resources.

In recent years, the Japanese government has initiated efforts to promote the "residence for elderly people with services" system, with registration opening in October 2011. These residences are rental houses designed to provide a secure living environment for elderly singles or couples. Such an approach would facilitate the centralization of elder care services, enhancing their management and streamlining the provision of necessary care. Currently, there are 76 such residences in Akita Prefecture, providing a total of 1,907 slots. The government should consider implementing policies that encourage the development of more such residences in Akita Prefecture. These policies could include providing financial incentives for developers and streamlining the approval process for the construction of such residences. It is also essential to ensure that these residences are affordable for the elderly people. In the long run, considering the projected demographic shifts, by 2045, Akita Prefecture's total population is expected to decline by a staggering 41.2% compared to 2015 (National Institute of Population and Social Security Research, 2018). In light of such drastic population decline, promoting a compact city model might be able to address the challenges posed by the aging society. Travel distance and time can be reduced by consolidating essential elderly care facilities. Moreover, adopting a compact city model can result in diminished operational and maintenance expenses for elderly care facilities, given the efficient utilization of space. Such an approach holds particular relevance for regions facing serious aging problems like Akita Prefecture, enabling the reallocation of financial resources to augment the quality of care services, rather than dispersing funds across expansive and potentially underutilized facilities.

This study acknowledges several potential limitations that could be addressed in future research. Firstly, the lack of available population data in some districts poses a challenge in accurately capturing the real aging trend in Akita Prefecture. Secondly, employing either the Euclidean distance method or the 2SFCA method to measure accessibility does not fully consider transportation factors, such as the cost and time associated with different modes of transportation. As a result, the obtained results may carry inherent biases. Integrating transportation-related variables in future analyses would yield a more comprehensive understanding of accessibility.

Finally, only the elderly population ratio was used as the indicator of population aging. In fact, there are many other indicators measuring the different aspects of population aging, such as the oldest-old population rate and centenarian population rate. Future work addressing these issues enhances our understanding of the population aging and necessary care systems.

Acknowledgement

This research was supported by JSPS KAKENHI Grant Numbers JP23K17559 and JP 23H00448, as well as Keio Gijuku Academic Development Funds (Collaborative Research).

Reference

Akita Prefectural Department of Planning and Promotion. (2021) Analysis and Perspectives on Population: Decline Marriages, Births, and Social Changes.

Akita Prefecture Official Homepage. (2018) Deepening and Promoting the community-based integrated care system.<https://www.pref.akita.lg.jp/pages/archive/7916>.

Akita Prefecture Official Homepage. (2021) Status of Community-based Integrated Care Center < https://www.pref.akita.lg.jp/pages/archive/2202>.

Alidoust, S. and Bosman, C. (2015) Planning for an ageing population: links between social health, neighbourhood environment and the elderly. *Australian planner*, 52(3), pp.177-186.

Bloom, D.E., Chatterji, S., Kowal, P., Lloyd-Sherlock, P., McKee, M., Rechel, B., Rosenberg, L. and Smith, J.P. (2015) Macroeconomic implications of population ageing and selected policy responses. *The Lancet*, 385(9968), 649-657.

Carpentieri, G., Guida, C. and Masoumi, H.E. (2020) Multimodal accessibility to primary health services for the elderly: A case study of Naples, Italy. *Sustainability*, *12*(3), p.781.

Cho, H., Choi, J., No, W., Oh, M. and Kim, Y. (2021) Accessibility of welfare facilities for elderly people in Daejeon, South Korea considering public transportation accessibility. *Transportation research interdisciplinary perspectives*, 12, p.100514.

Joseph, A. E., and Bantock, P. R. (1982) Measuring potential physical accessibility to general practitioners in rural areas: a method and case study. *Social Science & Medicine*, 16(1), 85-90.

Luo, W., and Wang, F. (2003) Measures of Spatial Accessibility to Health Care in a GIS Environment: Synthesis and a Case Study in the Chicago Region. *Environment and Planning B: Planning and Design*, 30(6), 865–884.

Ministry of Health, Labour and Welfare. (2016) the Community-based Integrated Care System < https://www.mhlw.go.jp/stf/seisakunitsuite/bunya/hukushi_kaigo/kaigo_koureisha/chiiki-houkatsu>.

Ministry of Health, Labour and Welfare. (2021) Publication System for Long-Term Care Service Information. <https://www.kaigokensaku.mhlw.go.jp>.

National Institute of Population and Social Security Research. (2018) Future Population Projections by Region in Japan. <https://www.ipss.go.jp/pp-shicyoson/j/shicyoson18/t-page.asp>.

Phelan, E. A., Anderson, L. A., Lacroix, A. Z., and Larson, E. B. (2004) Older adults' views of “successful aging”—how do they compare with researchers' definitions?. *Journal of the American Geriatrics Society*, 52(2), 211-216.

Route Search Method of Alternative Bus for Rail Line Adopting Ant Colony Optimization

Kei Nagaoka*, Kayoko Yamamoto**

Abstract: In Japan, recently, unprofitable rail lines are hardly maintained and most of them are replaced with bus services, because the number of passengers has declined. Against such a backdrop, this study aimed to propose a route search method of bus service that replaces rail lines adopting ant colony optimization (ACO) and geographic information systems (GIS). Improve ACO can consider not only distances but bus stops and left-right turns. Road network data of an area around an unprofitable rail line was created and each road width was calculated using GIS. Routes between two stations in the area were searched adopting the improved ACO and Dijkstra's algorithm. Based on the comparison result, it made evident that the route search adopting Dijkstra method was the shortest route. However, no routes adopting the improved ACO has extremely long segment where the bus doesn't stop or extremely many left-right turns. Thus, it can be concluded that alternative bus routes can be searched taking various adopting the improved ACO.

Keywords: Ant Colony Optimization (ACO), Geographic Information Systems (GIS), Rail Replacement Bus Service, optimization algorithms

1 Introduction

Recent years, Japanese local railroads are struggling to manage. The West Japan Railway Company released a document titled "Recognition of Issues and Information Disclosure Concerning Local Lines". In the document, the revenues and expenditures for lines with a transit density of less than 2,000 in 2019. This includes 30 sections on 17 lines, including the JR Obama Line, the JR Etsumihoku Line and the JR Oito Line. According to the Act on Special Measures for Promoting the Reconstruction of Japanese National Railways (National Railway Reconstruction Act) in 1980, these railway lines should be replaced with buses, because they are difficult to maintain to be managed. JR West states in the document, "We believe that the characteristics of the railroad are not fully demonstrated in terms of mass transportation". The West Japan Railway Company and The Kyushu Japan Railway Company also faced similar problems and disclosed their revenues. The Hokkaido Japan Railway Company, which faced similar problems, has abolished some railroads including the JR Sassho Line and the JR Hidaka Line, and replaced buses with them for "sustainable transportation system".

In other areas, one possible way to address the issue is to discontinue local railroads and run alternative buses to ensure sustainable transportation for local people. Based on the above background, this study considers local railway lines that may be discontinued in the near future. This study aims to propose a method that introduces routes for railway replacement buses adopting the optimization algorithm called Ant Colony Optimization (ACO). In this study, we proposed the way to search the route of alternative buses for local rail lines by Ant Colony Optimization (ACO), which is one of the optimization algorithms.

* GISA member; Graduate School of Informatics and Engineering, The University of Electro-Communications; n2330086@edu.cc.uec.ac.jp
** GISA member; Graduate School of Informatics and Engineering, The University of Electro-Communications; kayoko.yamamoto@uec.ac.jp

2 Methodology

In this study, routes for alternative buses is searched by ACO. ACO is a probabilistic technique for solving computational problems which can be reduced to find good paths through graphs. When ants find a food source, they repeatedly return to the source and bring foods back to their nest. They return to their nests by applying pheromone, which is more concentrated on shorter routes. The pheromone of shorter paths is likely to more concentrate. The shorter paths ants take, the more concentrated the pheromone of the path is. The longer paths ants take, the more likely the pheromone of the path is to evaporate. Therefore, more ants will eventually take the shorter paths. Ant Colony Optimization is the algorithm for searching for the optimal solution that mathematically models the action of swarm of ants. The following is a flowchart of the ACO procedure. This procedure is described in Fig. 1.

2.1 Initialization

At first, ants and the graph are initialized. The amount of pheromone of edges are initialized and ants are placed in a start node.

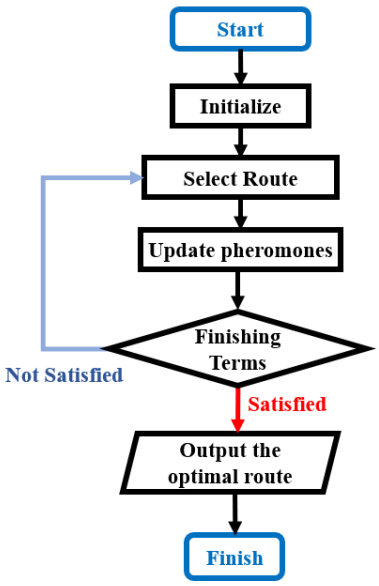

Fig 1. Procedure of ACO

2.2 Route selection

All of ants select next course to go. They probabilistically determine their routes. Ants probabilistically determine their routes and according to the following probability.

$$p_{im}^{k}(t) = \frac{a_{im}^{k}(t)}{\Sigma_{n\in\Omega} a_{in}^{k}(t)} \quad (1)$$

i: Current location
t: Number of steps
Ω: Set of adjacent nodes
a_{im}^{k}: Edge rating from i to m

a_{im}^{k} is a the rating value of edge connecting node *i and* node *m*. It is calculated as follows.

$$a_{ij}^{k}(t) = \frac{[\tau_{ij}(t)]^{\alpha}[\eta_{ij}]^{\beta}[tf(h,i,j)]^{\gamma}}{\Sigma_{l\in\Omega}[\tau_{il}(t)]^{\alpha}[\eta_{il}]^{\beta}[tf(h,i,j)]^{\gamma}} \quad (2)$$

t: Number of cycle
k: Ant number
h: The Node number passed last
τ_{ij}: The amount of pheromones of Edge ij
Ω: The set of vertices adjacent to i
η_{ij}: Inverse of the distance of the edge ij
α, β, γ: Weighting parameters
$tf(h,i,j)$: The function to weight turns

The higher the rating value of an edge, the more likely it is to pass through the edge. If an ant has reached the goal, the route the ant passed through is confirmed, if it is the optimal route at the point in time. The optimal route has to satisfy these constraint terms.

(1) The distance is 3 times shorter than the path searched by Dijkstra method
(2) The turns are 4 times less than the path searched by Dijkstra method
(3) Each non-stop section is shorter than 1,000m

These are the minimum requirements for being an optimal route. The route has to meets these conditions and the following converted distance of the route is shorter than the traditional one for being the optimal route. Converted distances is calculated as follows.

$$x + nT \tag{3}$$

$$\begin{pmatrix} x\text{: Total distance of path} \\ n\text{: The total turns} \\ T\text{: Weighting parameter of turns} \end{pmatrix}$$

2.3 Updating pheromone

The probability of a node moving on to the next node depends on the amount of pheromone on the edge. After all ants have selected their routes, pheromone concentration of edges is updated. The certain percent of pheromone of each edges evaporate and pheromone are added corresponding ants passed the edges. Equation for updating pheromone is follows.

$$\phi_{ij}(t+1) = \rho\phi_{ij}(t) + \sum_{k=1}^{N} \Delta\phi_{ij}^{k}(t) \tag{4}$$

$$\begin{pmatrix} \rho\text{: Evaporation Coefficient} \\ N\text{: The number of ants} \end{pmatrix}$$

$$\Delta\phi_{ij}^{k}(t) = \begin{cases} \dfrac{Q}{l_k(t)} & \text{Edge } ij \text{ is passed last and ants is homing} \\ 0 & otherwise \end{cases} \tag{5}$$

$$\begin{pmatrix} Q\text{:Total amount of pheromones a ant } secret \text{ in a cycle} \\ l_k(t)\text{: The distance of path of ant } A_k \text{ in step } t \end{pmatrix}$$

2.4 Confirming finishing terms

After updating pheromone, it is confirmed the finishing term has been satisfied. In this study, finishing term is "iteration is over 500 times". In the other words, if the process from section 2.2 to section 2.3 have repeated for 500 times, the process has to be finished. If it has been satisfied, output the optimal route. If not, start over from route selection.

3 Collecting and Processing GIS

3.1 Selection of target rail lines

The study area is selected based on these required conditions.

(1) The distance is not too long for bus route

(2) Other bus is not operated

(3) There are several roads wide enough for buses to pass. Management is unprofitable

The JR Kakogawa line between Nishiwaki-shi station and Tanigawa Station in the center of Hyogo Prefecture in the western part of Japan was selected as the target railway line. The JR Kakogawa line is operated by the West Japan Railway Company, and the line length between these two stations is 48.5km. 9 stations are located in this zone.

3.2 Selection of potential bus stops

In this study, the route considering bus stops is outputted. The potential bus stops are located in various places. They are located based on these conditions.

(1) Locate stops in spots near symbolic facilities

(2) Do not locate stops near traffic signals, intersections, or other locations where stops should not be located.

(3) Locate stops so that long no-stop sections do not exist.

(4) Locate stops along the rail lines.

3.3 Data and processing method

In this study, road network data is generated. It is the data which represent roads as graphs. It has various information about roads as attributes. Figs. 2 and 3 show examples of road centerline data and road edge data. Road network data is generated from road centerline data and road edge data.

Fig 2. Road centerline data

Fig 3. Road edge data

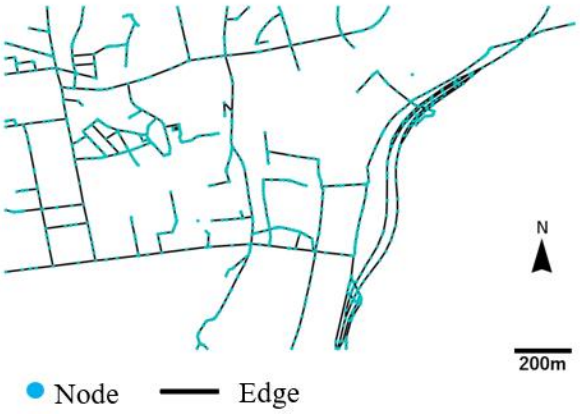

Fig 4. Road network data

Buses cannot pass through all of the roads. Road width for buses is limited by the cabinet order on vehicle restriction, which is Japanese law for vehicle. For example, typical small buses whose width is 2.1m can't pass thorough 4.7m or narrower roads. In this study, all of the road width in the target area are calculated, and 4.7m or narrower roads are deleted. The road network data is shown in Fig.4.

4 Route Searching

The route between all of adjacent two stations is separately searched to reduce the computational complexity. In this study, the section between from Nishiwaki City Station and Shin-Nishiwaki Station is taken up, and bus route in this section is searched. Figs. 5 and 6 respectively show the routes by Dijkstra method and the improved ACO.

Finally, Table 1 presents the compare results of these routes. As shown in Table 1, “distance” is the total distance of the route. “Number of turns” means how many times the bus turns right or left when it follows the route. “Number of bus stops” means the number of potential bus stops in the route. “Maximus non-stop section distance” means the longest section of all non-stop sections. “Non-stop section distance list” means the distances of each non-stop sections.

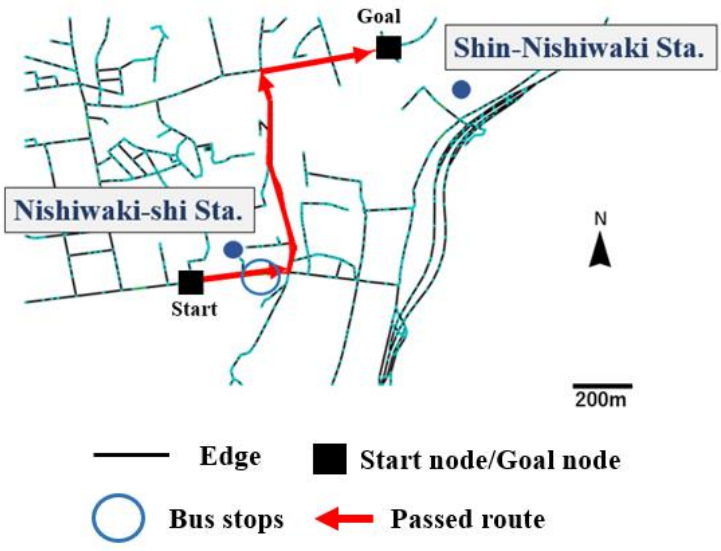

Fig 5. Route between Nishiwaki-shi Station and Shin-Nishiwaki Station by Dijkstra method

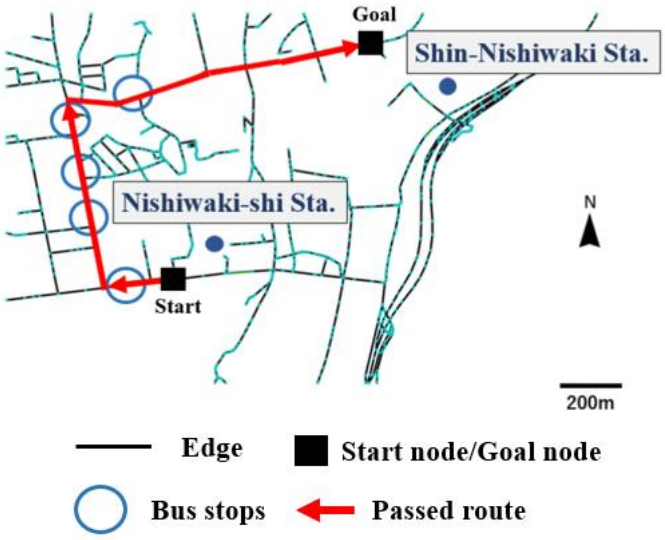

Fig 6. Route between Nishiwaki-shi Station and Shin-Nishiwaki Station by the improved ACO

Table1. Comparison results of Dijkstra Method and the Improved ACO

Method	Dijkstra method	Improved ACO
Distance(m)	1,585	2,041
Number of turns	2	2
Number of bus stops	3	7
Maximus non-stop section distance(m)	1,372	821
Non-stop section distance list(m)	[213, 1,372]	[179, 356 ,168, 218, 300, 821]

5. Discussion and Conclusion

Based on the route searching result, the route by Dijkstra method is shorter than the one by the improved ACO. Because the Dijkstra method can consider distance only and searched the shortest routes. However, comparing the Dijkstra method, the improved ACO is superior in considering other points (bus stops, left-right turns, etc.) in addition to distance.

Next, the numbers of turns are compared, but both of them are 2 times. Looking at Figs. 5 and 6, Theoretically, there is likely to be no routes with less than two times turns. Finally, characters of the bus stops are compared. The maximum non-stop section distance of the route by the improved ACO is 551m shorter than the route by Dijkstra method. This attributes to constraint terms (3) of route selection in section 2.2. In this study, though it is 1,000m, it can be changed another appropriate value in the improved ACO.

From the above, the improved ACO can optimize non-stop sections bus stops while considering the distance and the number of right and left turns. However, this method also has three future tasks. At first, start node and goal node must not be located near intersections, because they are the points of bus stops. Secondly, bus stops have to be searched prevent passing through the same road more than once in nearby sections. Thirdly, judgement accuracy of turns has to be improved.

References

[1] Hirotaka Goto,Asuka Ohta, Tomofumi Matsuzawa, Munehiro Takimoto, Yasushi Kambayashi, Masayuki Takeda (2005), ”Improved ACO algorithm by pheromone control for disaster evacuation guidance”, FIT2015, Vol.14, No.4, pp65-

70

[2] Koichiro Tani, Kayoko Yamamoto (2020),” Studied on evacuation route search method under heavy rain disaster using genetic algorithm”, Proc.82th National Convention of IPSJ, Vol.1, pp667-668

[3] Nagi Yoshitsugu, Shinya Abe, Kayoko Yamamoto (2019), ” Deriviation Method of Evacuation Routes Using Physarum Solver”, IPSJ Journal, Vol.60, No.12, p.2325-2329

[4] Yukinaga Izumida, Daisuke Kikuchi, Tetsuo Ikeda,Tsuyoshi Takayama(2015), ”Optimal Arrangement Method of Bus Stops in Regional Bus Route”, Proc.67th National Convention of IPSJ , Vol.1, pp.503-504

[5] Tsutomu Suzuki, “Optimal Locational Patterns of Bus-Stops for Many-to-One Travel Demand”, Journal of the City Planning Institute of Japan (1987), vol.22, p.247-252

[6] Takahito Shindo, Yoshiyasu Yanagisawa, Hirokazu Kato, Jun-ichi Takayama, Akihiro Masuo, Takeshi Sakatsume (2015),” PROCESS IN SERVICE PLAN DEVELOPMENT IN THE SUBSTITUTE BUS OF THE TASHIRO LINE AND ANALYSIS OF THE ACTUAL USAGE”, Proceedings of JSCE F5, Vol.70, No.2, p11-25

[7] JR West (2022), Recognition of Issues and Disclosure of Information Regarding Local Lines. <https://www.westjr.co.jp/press/article/items/220411_02_local.pdf>

Oral presentation in IAG'i

Disaster

Chair: Michinori Hatayama (Disaster Prevention Research Institute, Kyoto University)
Sat. Oct 28, 2023 3:20 PM - 4:40 PM Room D (C-201 2nd floor of Bldg. C)

[D4-02] A Comparison of Construction Sites for Temporary and Public Housing under Different Urban Reconstruction Policies - Based on Actual Cases in Japan and China

*Yang Zhou[1], Naoko Fujita[1], Suxueer Sun[1], Minghui Tang[1], Linda Gadhoum[1] (1. Art Program, Faculty of Comprehensive Human Sciences, University of Tsukuba)

3:20 PM - 3:40 PM

[D4-03] Assessing Urban Flood Susceptibility Maps Based on Machine Learning Models in Seoul, South Korea

*Julieber Toralde Bersabe[1], Byong-Woon Jun[1] (1. Kyungpook National University)

3:40 PM - 4:00 PM

[D4-04] Meteotsunamis in a Danshui River estuary, Taiwan

*Liching Lin[1], Wen-Cheng Liu[1], Chin H. Wu[2] (1. Department of Civil and Disaster Prevention Engineering, National United University, Taiwan, 2. Department of Civil and Environmental Engineering, University of Wisconsin-Madison, Madison, WI, USA)

4:00 PM - 4:20 PM

[D4-05] Comparison of the shorelines separately detected from Sentinel-1 and 2 satellite imagery acquired on the east coast of Korea

*Yun-Jae Choung[1] (1. Geo C&I Co., Ltd.)

4:20 PM - 4:40 PM

A Comparison of Construction Sites for Temporary and Public Housing under Different Urban Reconstruction Policies – Based on Actual Cases in Japan and China

Yang Zhou*, Naoko Fujita**, Suxueer Sun***, Minghui Tang***, Linda Gadhoum***

Abstract In the aftermath of disasters, the establishment of post-disaster resettlement housing is of paramount importance in ensuring secure and sustainable living environments for affected communities. Although governments actively engage in the construction of such housing, it remains uncertain whether the evolving needs of residents are adequately met over time. Few studies have investigated the long-term living conditions of these resettled populations. This study addresses whether the social infrastructure surrounding post-disaster resettlement housing effectively supports residents' daily requirements, and explores potential disparities in living conditions across urban, peri-urban, and rural contexts. Through case studies of China's Sichuan Province and Japan's Kumamoto Prefecture, this research progressively refines its focus from urban centers to peri-urban zones and rural areas, presenting a comprehensive and insightful perspective on the topic.

Keywords: post-disater resettlement housing, social infrastructure, post-disaster reconstruction

1. Introduction

During urban development, the challenges posed by natural disasters have garnered significant attention in many regions. Throughout the post-disaster reconstruction process, the construction of disaster resettlement housing has remained a critical issue, particularly in areas prone to frequent earthquakes. The impact of earthquakes compels governments and societies to reconsider how affected communities can be restored, ensuring that residents can access secure and sustainable housing environments.

In this context, the present study aimed to compare the distribution of post-disaster resettlement housing and the development of surrounding social infrastructure for disaster-affected populations in Sichuan Province, China, and Kumamoto Prefecture, Japan, under different urban reconstruction policies. Through practical case studies, we delved into various scales ranging from urban to rural areas, gradually narrowing the research scope. This approach provides us with a comprehensive and detailed perspective encompassing multiple factors, including government policy orientations, community needs, and resource allocation, which collectively shape disparities in the distribution of resettlement housing and infrastructure development. By gaining an in-depth understanding of these variations, we can offer valuable insights and guidance to enhance urban reconstruction policies and post-disaster recovery efforts.

The Wenchuan Earthquake in 2008 resulted in a displacement of approximately 18 million people. In response, the government implemented a series of emergency measures for post-disaster reconstruction and resettled 18 million individuals. Resettlement methods primarily include two approaches: self-reconstruction and unified reconstruction. Unified reconstruction refers to the government building new houses and distributing them to the resettled families (He, 2019). The resettlement approach for the Kumamoto Earthquake was similar to that of China. In the Kumamoto Prefecture, the local government conducted a post-earthquake questionnaire survey in 2018. The survey targeted 2,000 households affected by the earthquake and approximately half of the collected questionnaires were valid. Among the questions regarding residential building types, 10.6% of the respondents expressed a desire to live in post-disaster

GISA Members
* Student member; Graduate school of Comprehensive Human Science, University of Tsukuba; **s2330516@u.tsukuba.ac.jp**
** Member; Institute of Art and Design, University of Tsukuba; **fujita.naoko.gf@u.tsukuba.ac.jp**
*** Student member; Graduate school of Comprehensive Human Science, University of Tsukuba

resettlement housing in their study on the adequacy of resettlement facilities following the disaster caused by the Indian Ocean tsunami in Sri Lanka. They found that social infrastructure is a critical component in promoting the social well-being of disaster victims, particularly for the affected population, who had lost their tangible and intangible assets and had been resettled away from their familiar environments. Furthermore, they were able to confirm in their research findings that there is a lack of infrastructure near multiple resettlement sites, and that the life needs of the resettled disaster-affected population are neglected. The inconvenience of living has led to complaints from residents, and some individuals have even chosen to relocate elsewhere for habitation (Khaled, 2022) mentioned that a sustainable and successful community requires people to walk 10-20 minutes (800-1600 meters) to reach everyday facilities. These facilities should be located around most residences, and there is a need for sufficient amenities to meet their needs as well as spaces for various activities.

The study focuses on the Dujiangyan city, Beichuan county, and Hanwang town in Sichuan Province, China(figure 1), as well as Kumamoto City, Mashiki Town, and Minamiaso Village in Kumamoto Prefecture, Japan(figure 2). These areas have experienced severe earthquake disasters, resulting in significant changes in the lives of local residents and causing widespread casualties and property damage. Following these disasters, these regions have faced numerous challenges in terms of recovery, requiring responses to various social, economic, and environmental issues during the process of rebuilding and restoration.

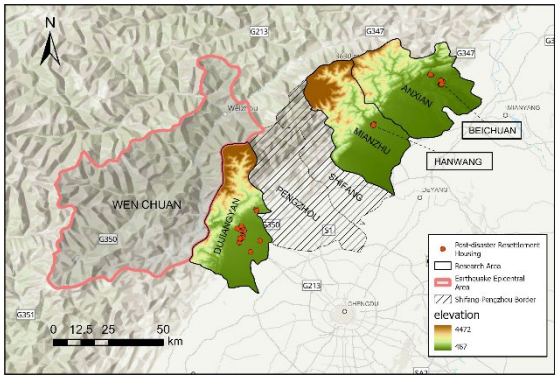

Figure 1 Survey area at China

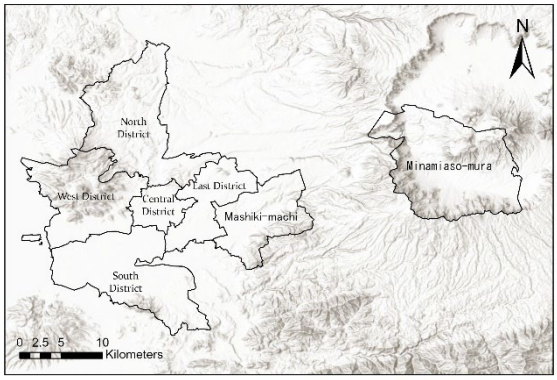

Figure 2 Survey area at Japan

1.3. Research Objectives

After the earthquake, the government implemented a series of emergency measures, one of which was to provide resettlement housing for affected residents. However, the distribution of these housing units and the state of the surrounding social infrastructure significantly affect the quality of life and daily convenience of disaster-affected residents. Therefore, this study aims to analyze the condition of social infrastructure near post-disaster resettlement housing in these areas, and whether these facilities meet the needs of disaster-affected residents. Through a comparative analysis of these regions, we can gain a better understanding of the issues and challenges

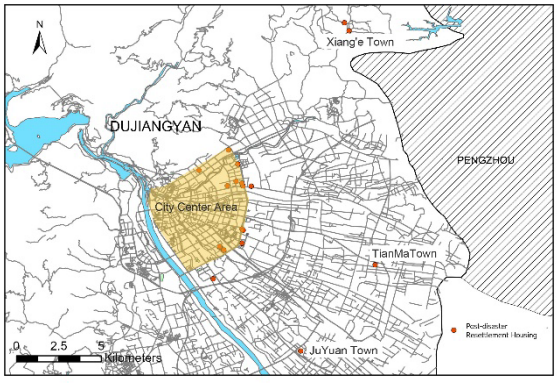

Figure 3 Dujiangyan central area map

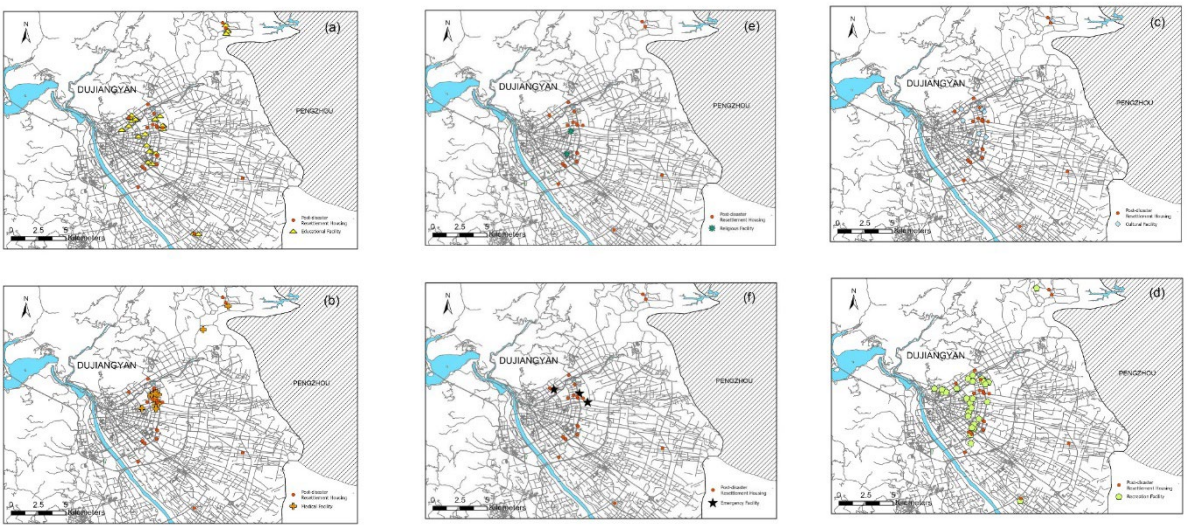

Figure 4 Infrastructure map around Dujiangyan post-dsaster resettlement housing

that different areas face in their recovery and development processes after earthquakes.

Furthermore, from the perspective of social infrastructure, we can assess the strategies and effectiveness of government efforts in terms of resident resettlement and community rebuilding, offering valuable insights and recommendations for future disaster-response situations. The chosen locations not only represent earthquake-affected areas in two different countries, but also encompass urban and rural regions as well as areas of varying scales. By thoroughly analyzing the state of social infrastructure in these areas, we can provide valuable insights and recommendations for improving the living conditions of disaster-affected residents and promoting urban-rural development.

2. Method

The research cases described in this paper were conducted in six earthquake-affected regions, with three each from China and Japan. Data for the case studies were collected from sources such as government announcements, reconstruction plans, preliminary research literature, and other relevant materials published on official government websites.

Taking post-disaster resettlement housing as the center, a radius of 1600 m was used as the statistical range to assess the status of various social infrastructure facilities within that range. Drawing upon the existing literature on social infrastructure across the world, this study focuses on essential life-supporting facilities, including education, medical, cultural, recreational, religious, and emergency services, within a specified radius.

3. Results

3.1. Dujiangyan City

In Dujiangyan City, there are 18 disaster relocation housing units, with 14 units located on the outskirts of the urban area. Two units are situated between Dujiangyan City and Xiang'e Township, whereas the remaining two units are positioned within Juyuan Town and Tianma Township (as shown in Figure 3, illustrating the specific locations of the central areas of Dujiangyan, Xiang'e Township, Juyuan Town, and Tianma Township).

Facilities within a 1600-meter radius around the post-disaster resettlement housing in Dujiangyan City are shown in Figures 4. In the vicinity of the 18 post-disaster resettlement houses. In Dujiangyan City, there are a total of 27 educational facilities, including 10 kindergartens, seven primary schools, nine middle schools, and one

university. Among them, the distribution of 16 adequately equipped areas provided residents with diverse school choices. However, only two areas, the southern community in the city center and Tianma Township, lack sufficient educational resources and require additional investment.

Regarding medical facilities, there were 20 facilities near post-disaster resettlement housing, including hospitals, health centers, and clinics. Adequate medical facilities are mainly concentrated near the northeastern part of the city center's resettlement housing, which helps ensure essential support for residents' health and medical needs. However, medical facilities near several other resettlement housing facilities require further resource allocation to meet residents' demands, and there are 12 cultural facilities near the post-disaster resettlement housing, including cultural centers, libraries, museums, and theaters. Diverse cultural amenities provide residents with opportunities for entertainment, learning, and social interaction. Although cultural facilities are generally well-equipped in most areas, some resettlement housing, such as those in the southern part of the city center, southeastern areas, Tianma Township, and Juyuan Town, still lack cultural facilities, and there are 31 recreational facilities near resettlement housing, including parks, sports venues, entertainment venues, and attractions. Overall, facilities are quite adequate; except for the limited recreational facilities near Jingling Garden, there are two temples in terms of religious facilities. The distribution of religious facilities is relatively uneven and warrants attention, as three police stations are distributed near the northeastern part of the city center's resettlement housing. However, other resettlement housing facilities lack sufficient emergency facilities.

3.2. Beichuan County

There are eight residential complexes for post-disaster resettlement housing in Beichuan County. Among these, 6 complexes are situated on the southeastern side of the county town, while the remaining 2 complexes are located on the northwestern side.The facilities within a 1600-meter radius of the Beichuan County post-disaster resettlement housing are depicted in Figures 5.

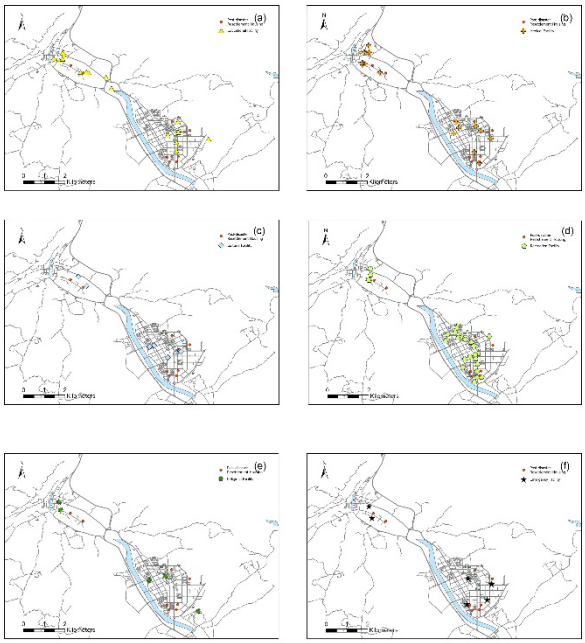

Figure 5 Infrastructure map around Beichuan county post-dsaster resettlement housing

Around the post-disaster resettlement housing in Beichuan County, there are 18 education facilities, including kindergartens, primary schools, middle schools, high schools, technical schools, universities, and administrative schools. All areas provide ample educational facilities, ensuring residents' educational needs are met.In terms of medical facilities, there are 16 in the vicinity of the resettlement housing, including hospitals, health centers, and clinics. All areas had sufficient medical facilities to ensure that residents had access to healthcare services at all times.

Regarding cultural facilities, there are a total of 9, including cultural centers, libraries, museums, and art centers. However, cultural facilities near resettlement housing in the southern part of the county town were inadequate. Consideration could be given to enhancing cultural resources in these areas.For recreational facilities, there are 27 near the Beichuan County post-disaster resettlement housing, including parks, sports venues, attractions, and entertainment centers. All areas offer a

variety of recreational options catering to residents' entertainment and leisure needs. There are five religious facilities: temples, mosques, and churches. Most areas have sufficient religious facilities to support residents' religious needs. For emergency facilities, there are six police stations, ensuring the safety of local residents and indicating a relatively sufficient presence of emergency facilities.

3.3. Hanwang Town

Hanwang Town has a total of 3 post-disaster resettlement housing. The facilities within a 1600-meter radius of the disaster relocation housing in Hanwang Town are shown in Figures 6.

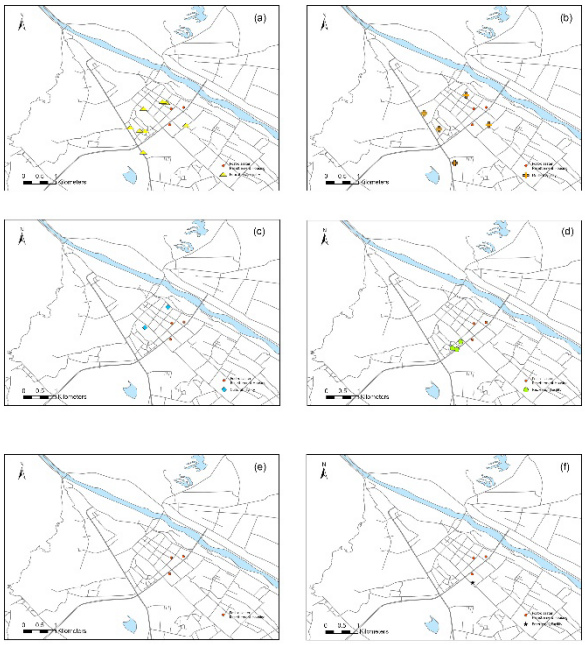

Figure 6 Infrastructure map around Hanwang town post-dsaster resettlement housing

Around the post-disaster resettlement housing in Hanwang Town, there are a total of eight educational facilities, including kindergartens, primary schools, and middle schools. All areas provide ample educational facilities.In terms of medical facilities, there are 5 near the post-disaster resettlement housing in Hanwang Town, including hospitals and clinics. All areas had sufficient medical facilities; for cultural facilities, there were two cultural centers. These facilities are relatively sufficient, providing residents with places for cultural exchange, there are 3 near the resettlement housing in Hanwang Town: parks, sports venues, and entertainment centers. All areas offer various recreational options, providing residents with opportunities for leisure and entertainment, and there are no religious facilities near resettlement housing. Attention should be paid to residents' religious needs, and regarding emergency facilities, the three resettlement housing units share one police station.

3.4. Kumamoto City

Kumamoto City has a total of eight post-disaster resettlement housing units, distributed across the central, eastern, and southern districts (Figure 7), providing residents with diverse housing options.

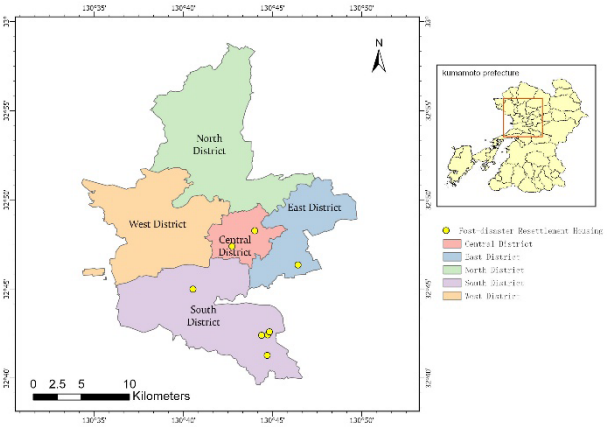

Figure 7 Distribution map of post-disaster resettlement housing in Kumamoto City

As shown in Figures 8, post-disaster resettlement housing in Kumamoto City has 32 educational facilities, including kindergartens, elementary schools, middle schools, high schools, technical schools, and universities. These facilities were distributed in the central, eastern, and southern districts, with the central and eastern districts having more abundant educational resources. In terms of medical facilities, there were 38 clinics and hospitals near the disaster relocation housing units. The central and eastern districts have more medical facilities, whereas the southern districts have relatively fewer facilities. There are 17 cultural facilities including libraries, museums, and

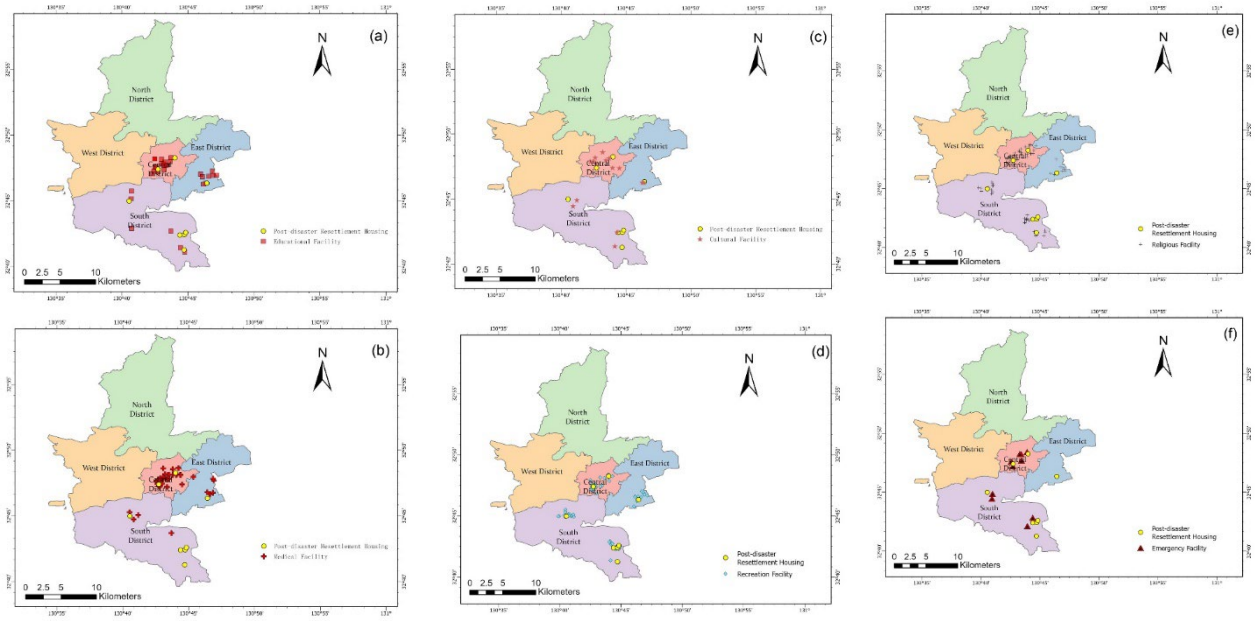

Figure 8 Infrastructure map around Kumamoto City post-dsaster resettlement housing

theaters. The central and southern districts offer more cultural amenities and provide residents with places for cultural and recreational activities. There are 74 recreational facilities near the resettlement housing in Kumamoto City, including parks and sports facilities. All areas offer various recreational options, providing residents with opportunities for leisure and entertainment. In terms of religious facilities, there were 78 in total, including shrines, temples, and Christian churches. Religious facilities are available in all areas, with the central and southern districts having extensive religious resources. For emergency services, there are 11 facilities, with the central and southern districts offering more emergency service resources.

3.5. Mashiki Town

There were 19 post-disaster resettlement houses in Mashiki Town, with nine homes distributed in the northwest and the rest scattered across various locations, as shown in figure 9. Around resettlement housing, there are a total of nine educational facilities, including kindergartens, elementary schools, and junior high schools. Among these, seven educational facilities are shared among the nine resettlement houses located in the northwest area, while the remaining ten homes have relatively fewer nearby educational facilities, with only two available. In terms of medical facilities, there were 10 in total, all concentrated around resettlement housing in the northwest area. Other resettlement housing facilities do not have medical facilities nearby. There are six cultural facilities, there are 6 in total, including art galleries and historical sites. The distribution of these facilities is relatively scattered, and within the scope of the 19 relocation homes, the level of cultural facilities is relatively low.There are 18 recreational facilities near the resettlement housing, mainly including parks and sports venues. These facilities can generally meet the entertainment needs of the area's residents, and there are 54 religious facilities in total, including shrines, temples, and Christian churches. Religious facilities within this area are relatively well-equipped. In terms of emergency services, there are two facilities: the police and fire stations. They are located near the central-northwest area of Mashiki Town, where the resettlement housing is located. For resettlement housing located on the outskirts of the town, reaching these emergency service facilities in the case of sudden needs might require more time.

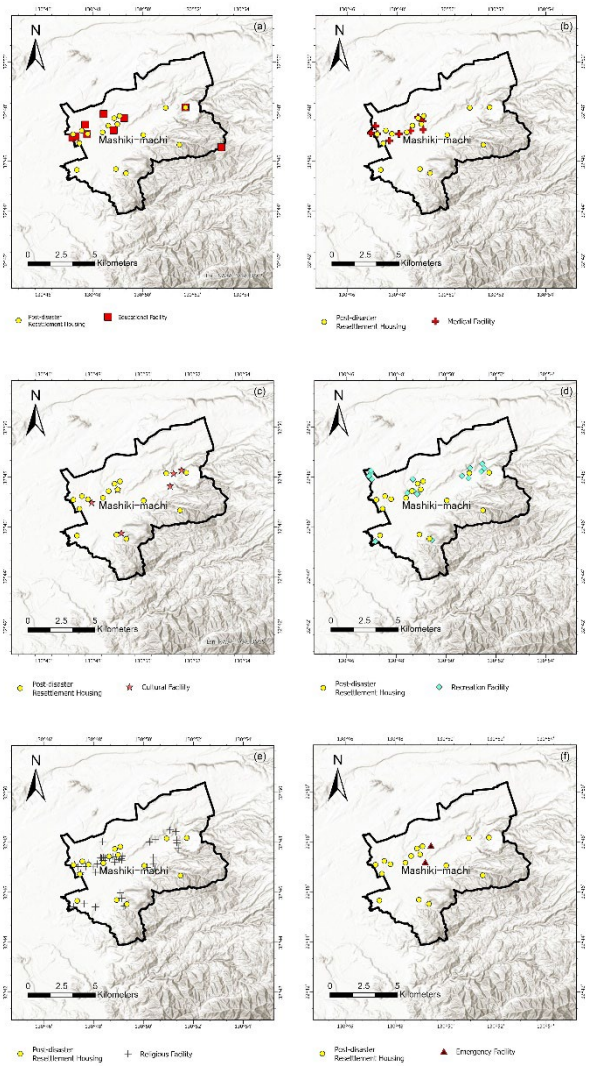

Figure 9 Infrastructure map around Mashiki Town post-dsaster resettlement housing

3.6. Minamiaso Village

There were four post-disaster resettlement houses in Minamiaso Village (Figure 10). Near-resettlement housing in Minamiaso Village has three educational facilities: elementary schools and junior high schools. The four resettlement housing facilities are relatively well equipped, providing essential educational resources for the rural area; there is only one hospital in terms of medical facilities. Among them, for Maridanchi, located in the northwest of Minamiaso Village, medical facilities are relatively well-equipped, whereas other resettlement housing facilities have insufficient medical facilities. There is only one cultural facility near resettlement housing, indicating limited cultural resources in the vicinity, and there are 15 recreational facilities, mainly parks and tourist attractions. The number of facilities is relatively high. There were nine religious facilities in total, including shrines and temples. The number of facilities is sufficient.There are 2 emergency service facilities, and they are relatively close. Emergency service facilities are well-equipped in the area.

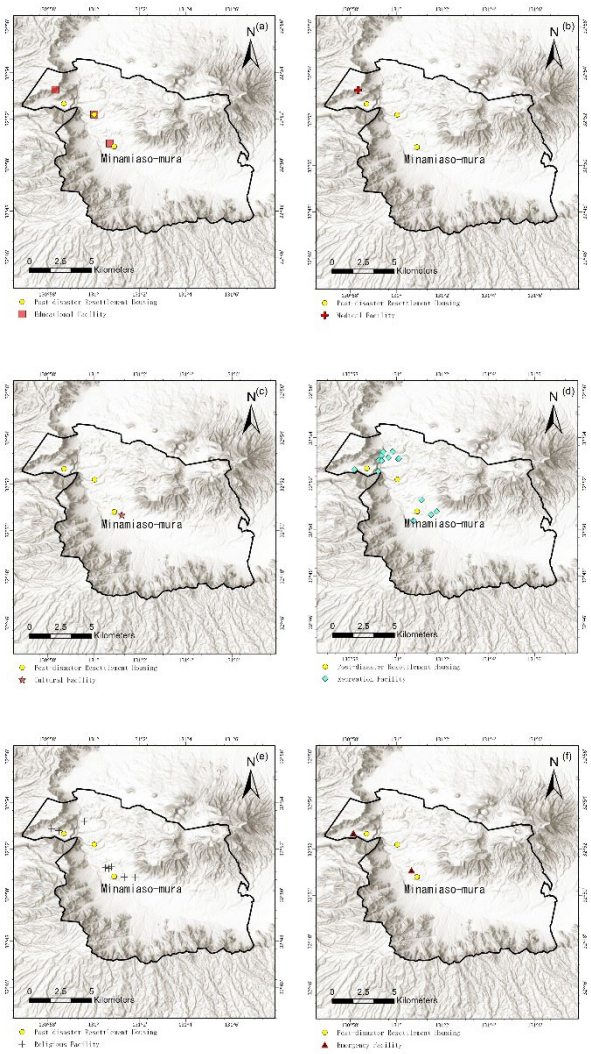

Figure 10 Infrastructure map around Minamiaso Village post-disaster resettlement housing

4. Dicussion and conclusions

In this study, we conducted extensive surveys and analyses of the earthquake-affected regions of the Wenchuan earthquake: Dujiangyan City, Beichuan County, and Hanwang Town in Sichuan Province, as well as the earthquake-affected regions of the Kumamoto earthquake

(Kumamoto City, Mashiki Town, and Minamiaso Village in Kumamoto Prefecture). The aim was to explore the distinct characteristics and compare urban, peri-urban, and rural areas within these two countries.

Through investigations of the distribution of social infrastructure related to education, medicine, culture, entertainment, religion, and emergency services in these areas, we identified significant differences between urban, peri-urban, and rural areas across the two countries.

In Sichuan Province, China, the distribution of infrastructure near post-disaster resettlement housing in Dujiangyan City is uneven. While education facilities are generally sufficient in most areas, additional resources are required for the southern community of the city center and Tianma Township. Medical facilities are relatively abundant in the northeastern area of the city center, but other areas require further allocation. Cultural facilities are relatively abundant but insufficient in the southern and southeastern communities. Recreational facilities are mostly adequate in most regions, but there is a lack of religious facilities and a need for increased emergency services, whereas the infrastructure in Beichuan County is comparatively balanced. Education facilities are sufficient to ensure the educational needs of residents. Medical facilities are widely distributed in various regions. Cultural facilities are abundant and have the potential to provide additional resources in the southern area. Diverse recreational facilities meet the leisure needs of residents. The distribution of religious and emergency facilities is relatively reasonable, catering to religious and safety needs.In Hanwang Town, there is sufficient availability of education and medical facilities, while cultural and recreational facilities are limited. The town lacks religious facilities, which should be noted. Emergency facilities are relatively scarce and require further provisions.

The distribution of infrastructure in Kumamoto City is relatively balanced. Educational facilities are reasonably distributed in all areas, and medical facilities are relatively abundant, with a slight shortage in the southern region. Abundant cultural and diverse recreational facilities cater to residents' cultural and entertainment needs. The distribution of religious and emergency facilities is reasonable, ensuring the religious and safety needs of the residents. In contrast, the distribution of infrastructure in Mashiki Town was uneven, mainly concentrated in the northwestern part of the town, with fewer facilities in other areas. Cultural facilities are relatively scarce and recreational facilities meet these needs. Religious facilities are relatively well established, but emergency services need to extend their coverage to the outskirts of the town. In Minamiaso Village, the distribution of infrastructure is relatively balanced. For the limited number of post-disaster resettlement housing units, education and medical facilities are sufficient, but cultural facilities are relatively lacking. Recreational facilities meet residents' needs, and the distribution of religious and emergency facilities is reasonable.

Among the research areas in Sichuan, there are a total of 18 post-disaster resettlement housing in Dujiangyan City, 8 units in Beichuan County, and 3 units in Hanwang Town. By combining the number of relocated housing units with a comprehensive analysis of their surrounding infrastructure (figure 11), we observed that the infrastructure within urban areas is not as developed as initially anticipated. However, infrastructure in urban-rural transition zones is relatively well established. In rural areas, there appears to be a state that meets basic needs. In typical circumstances, the economic level of urban areas surpasses that of urban-rural transition zones, which in turn surpasses that of rural areas. Consequently, one would expect the level of infrastructure development in urban areas to be positively correlated with economic status. However, this study yields a different outcome: within the Sichuan study region, the overall number of facilities follows the pattern: urban > urban-rural transition zones > rural, and the overall quantities of facilities were urban–rural transition zones > urban > rural. This contradicts the conventional expectation that infrastructure development is directly proportional to the economic level.

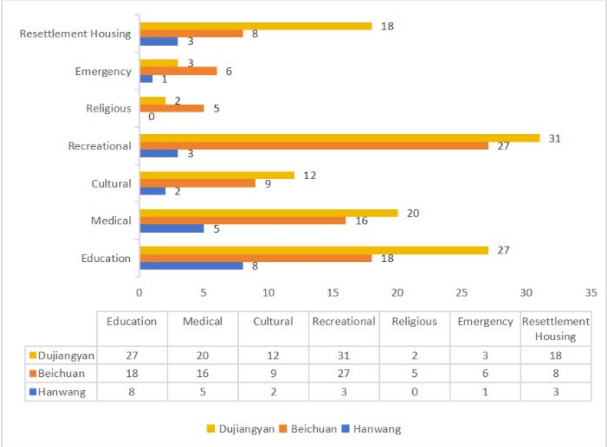

	Education	Medical	Cultural	Recreational	Religious	Emergency	Resettlement Housing
Dujiangyan	27	20	12	31	2	3	18
Beichuan	18	16	9	27	5	6	8
Hanwang	8	5	2	3	0	1	3

Figure 11 Post-disaster resettlement housing and infrastructure Data (China)

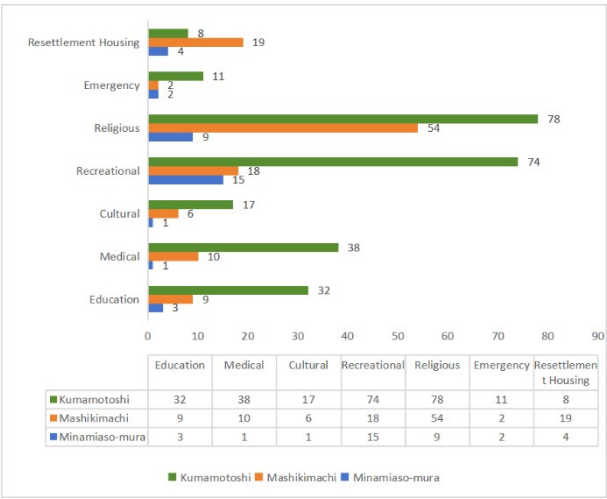

	Education	Medical	Cultural	Recreational	Religious	Emergency	Resettlement Housing
Kumamotoshi	32	38	17	74	78	11	8
Mashikimachi	9	10	6	18	54	2	19
Minamiaso-mura	3	1	1	15	9	2	4

Figure 12 Post-disaster resettlement housing and

Kumamoto Prefecture has eight post-disaster resettlement housing units in Kumamoto City, 19 units in Mashiki Towb, and four units in Minamiaso Village. We observed that the infrastructure surrounding resettlement housing within urban areas is relatively well-developed (figure 12), with the number of facilities far exceeding those in urban-rural transition zones and rural areas. Despite having the highest number of resettlement houses, Mashiki Town has a shortage of several types of basic facilities. In Minamiaso Village, the number of facilities was relatively evenly distributed, similar to Hanwang Town in Sichuan Province, indicating a state of meeting the basic needs. Within the Kumamoto study region, the overall number of facilities followed the pattern of urban > urban-rural transition zones > rural. the overall quantities of facilities, we found that the order is urban > rural > urban-rural transition zones.

By comprehensively analyzing the data, we also observed some differences between the two countries in terms of the selection of post-disaster resettlement housing locations and the establishment of a comprehensive infrastructure. In comparison to the relatively dispersed locations of resettlement housing within Kumamoto City, the placement of such units in Dujiangyan City is often on the outskirts of the urban center (Figure 3). This is attributed to local government reconstruction policies(The Regulations on Post-Disaster Recovery and Reconstruction of the Wenchuan Earthquake,2008) that aim to alleviate population pressure from the city center by dispersing excess population on the outskirts of the city. On the other hand, post-disaster reconstruction efforts in China's affected areas have placed less emphasis on the entertainment and religious needs of relocated residents and have focused more on fundamental requirements such as education and healthcare. Therefore, there is a greater need for support and development in these areas. In contrast, Kumamoto Prefecture in Japan demonstrates a relatively well-developed network of social service facilities, offering residents in both urban and rural areas a wide range of choices for comfortable and convenient living.

References

He,L.; Aitchison,J.C.; Hussey,K.; Chen,Y. Building new houses or long-term recovery? A combination of quantitative and qualitative evidence from earthquake-displaced households in Sichuan, China. Habitat international. 2019, vol. 83, p. 135-145.
Weerasena,N.; Amaratunga,D.; Hettige,S.; Haigh,R.; Sridarran,P. Provision of Social Infrastructure for Resettled Victims of the 2004 Tsunami: Evidence from the grass roots. Procedia engineering. 2018, vol. 212, p. 379-386.
Khaled Al Shawabkeh,R.; Alobaidat,E.; Ibraheem Alhaddad,M.; Alzouby,A.M. The role of social infrastructure services in developing the city centre planning: A framework for delivering sustainable cities in Jordan. Ain Shams Engineering Journal. 2022, vol. 13, no. 6, p. 101800.
The Regulations on Post-Disaster Recovery and Reconstruction of the Wenchuan Earthquake.2008
Kumamoto Earthquake Questionnaire Survey.2018
Kumamoto Earthquake Disaster Resettlement Housing Completion Record.2018

Assessing Urban Flood Susceptibility Maps Based on Machine Learning Models in Seoul, South Korea

Julieber Toralde Bersabe*, Byong-Woon Jun**

This study assessed flood susceptibility maps using logistic regression (LR), random forest (RF), and support vector machines (SVM) models in Seoul metropolitan city, South Korea. We constructed a flood inventory map consisting of 1,000 flood points and 1,000 non-flood points. These datasets were randomly divided into training and testing datasets in a 70:30 ratio. In addition, we selected 16 variables as flood conditioning factors considering previous literature and data availability. Various evaluation metrics such as accuracy, kappa, and AUC were computed to comprehensively evaluate the models' accuracy and predictive capabilities. The resulting flood susceptibility map was classified into five categories, ranging from very low to very high susceptibility. By comparing the evaluation metrics for each model, we concluded that the RF model outperformed the LR and SVM models, exhibiting an accuracy of 0.837 and an AUC of 0.902. Furthermore, our findings highlighted that the most significant flood conditioning variables were sewer pipe density, distance to storm drain, elevation, rainfall, and terrain ruggedness index.

Keywords: flood susceptibility, machine learning, random forest, support vector machine, logistic regression

1. Introduction

The incidence of extreme rainfall in South Korea has notably risen since 2002, reaching its peak in 2021 with 22 occurrences, followed by 19 occurrences in 2020. The interaction between urbanization processes, climate change risks, susceptibility, and exposure contribute to urban hazards and risks. An increase in population growth, particularly in vulnerable metropolitan regions, magnifies the potential impacts of future hazards within varying climatic contexts. Climate change influences urban systems, which can modify their operations reciprocally. Despite their climate change mitigation efforts, urban communities are predisposed to multiple hazards, including flooding, due to rapid urbanization. This vulnerability to flood risks is expected to surge 2.7 times between 2000 and 2030, fueled mainly by socioeconomic expansion, even without climate change considerations (Güneralp *et al.*, 2015).

In South Korea, the Ministry of Environment's flood control center has devised flood risk maps to share with local authorities to enhance disaster preparedness measures. These maps are constructed by applying scientific models, predicting potential flood scenarios, including embankment breaches and overflow situations.

Previously, flood risk maps were restricted from public access. However, with the escalating flood risk due to factors like intensified rainfall associated with the climate crisis, these maps are now available online. This accessibility accelerates the identification of flood-prone regions, thus expediting evacuation procedures. However, government-provided flood risk maps were not updated regularly and did fail to encompass shifts in urban development and the built environment. Consequently, this study aims to establish a new flood susceptibility map that will be developed using machine learning methods, factoring in geomorphological characteristics and human-induced variables.

2. Study Area

Seoul, the capital city of South Korea with coordinates 37° 33′ 51″ N and 127° 00′ 06″ E, was the selected study area for this research, which has an approximate area of 605.2 km^2 and a population of 9.5 million as of 2022. Due to its monsoon climate, Seoul's annual rainfall ranges from 1,200 to 1,600mm, and around 65% of this precipitation occurs during the summertime, which can cause flooding (Lei et al., 2021).

3. Data and Methods

The study aims to produce a new flood risk model that

* Julieber Toralde Bersabe, Kyungpook National University, jtbersabe@knu.ac.kr
** Byong-Woon Jun, Kyungpook National University, bwjun@knu.ac.kr

considers geomorphological and anthropologic characteristics and utilizes geospatial data representing actual flood events. While gathering data, it was identified that specific information was absent for Jongro-gu and Yongsan-gu. Consequently, these zones were omitted from the research to prevent potential misinterpretation. The objective was to uphold the precision and dependability of the analysis by excluding regions where data was incomplete.

This research was initiated by creating a geospatial database containing flood points and flood conditioning factors, forming the foundation for a susceptibility map generation model. The dependent variable comprised 1,000 randomly selected flood points from Seoul Metropolitan Government's inundation map and 1,000 non-flood points. Independent variables, as shown in Figure 1, included elevation, slope, aspect, curvature, topographic wetness index (TWI), terrain ruggedness index (TRI), stream power index (SPI), rainfall, distance to river (DRv), stream density (SD), sewer pipe density (SPD), distance to road (DRo), distance to storm drain (DSD), land use, soil type, and lithology. These variables were based on existing literature (Lei *et al.*, 2021; Lee *et al.*, 2017; Kim & Choi, 2022).

This database was divided into training and testing datasets, with training data used as input for three machine learning models—logistic regression (LR), random forest (RF), and support vector machines (SVM). Subsequently, the models were constructed, and flood maps were generated, followed by evaluation using the testing data. Various assessment metrics were applied to gauge model performance, helping identify the most effective model based on accuracy, precision, recall, and other relevant indicators. This process aimed to identify the optimal model for creating comprehensive flood susceptibility maps.

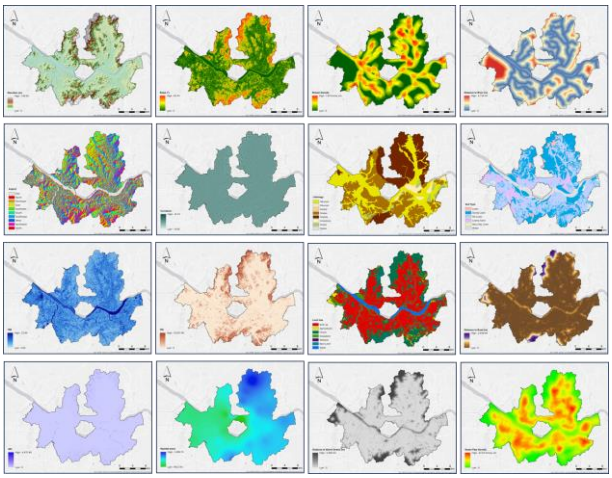

Figure 1 Flood conditioning factors

4. Results and Discussion

3.1 Correlation and Multicollinearity Analysis

Pearson's product-moment correlation coefficient (R) values for variable pairs were computed in IBM SPSS Statistics 25. Analysis revealed that the Distance to Road and Distance to Storm Drains variables exhibited the highest positive correlation (+0.903). In contrast, Stream Density and Distance to River variables exhibited the highest negative correlation (-0.729).

The outcomes of the multi-collinearity analysis were concisely presented in Table 1. Variance Inflation Factor (VIF) values spanned from 1.075 to 7.632, with tolerance values ranging from 0.131 to 0.930. Notably, the Aspect flood conditioning factor displayed the lowest VIF and the highest tolerance, whereas the Distance to Storm Drains variable exhibited the highest VIF and lowest tolerance. Importantly, all variables met the criteria (VIF $<$ 10, Tolerance $>$ 0.1), warranting the inclusion of all sixteen variables in evaluating the study area's susceptibility to flood risk.

Table 1 Collinearity Statistics

Variables	**Tolerance**	**VIF**
Elevation	0.169	5.905
Slope	0.171	5.848
Aspect	0.930	1.075

Curvature	0.842	1.187
TWI	0.513	1.948
TRI	0.286	3.496
SPI	0.847	1.181
Distance to River	0.471	2.123
Stream Density	0.422	2.369
Distance to Road	0.146	6.835
Rainfall	0.820	1.220
Soil Type	0.793	1.260
Land Use	0.646	1.548
Lithology	0.725	1.379
SPD	0.463	2.159
Distance to Storm Drain	0.131	7.632

3.2 Model Building

Machine learning models demonstrate varying performance due to different hyperparameters. While default settings are often used, fine-tuning these parameters is essential for achieving optimal outcomes.

The random forest models' precision and accuracy were influenced by key hyperparameters—the number of trees and features considered at each split—ultimately determined to be optimal at 500 trees and an automatic feature selection for splitting. In contrast, optimizing SVM models involved exploring various kernel functions, with the radial basis function (RBF) kernel demonstrating the highest mean test accuracy among options. Supported by prior research, this choice was substantiated by its reliability and interpolation capabilities.

3.3 Model Performance Evaluation

Predicted probabilities from each model were graphically represented using ArcGIS 10.8 software and presented in Figure 2.

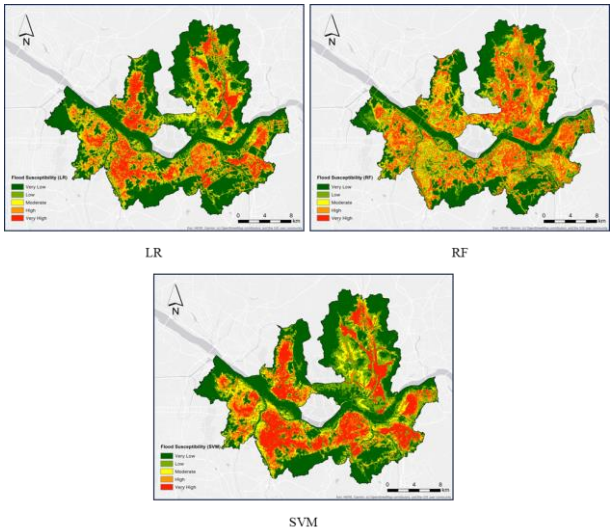

Figure 2 Generated flood susceptibility map

Furthermore, model performance assessment commonly involves a confusion matrix, offering detailed insight into predicted versus actual outcomes. This matrix reveals accurate and inaccurate classifications per class, facilitating an assessment of the model's predictive capability. The confusion matrix also provides critical metrics like accuracy, precision, sensitivity, specificity, and F1-score, collectively offering a comprehensive evaluation of model performance.

Accuracy estimates the proportion of correctly predicted outcomes among total outcomes in the dataset. Higher values denote superior model performance, while lower ones imply reduced reliability in flood occurrence prediction. The RF model showcased the highest accuracy at 83.67%, followed by the SVM model at 80.17% and the LR model at 79.50%. These values reflect the models' capacity to accurately identify flood occurrence, with RF models achieving the highest accuracy.

However, relying solely on accuracy as the sole evaluation metric may not comprehensively assess the machine learning model's performance, mainly when the dataset is imbalanced or when misclassification errors occur. Therefore, it is essential to consider additional evaluation metrics such as sensitivity, specificity, kappa, and F_1-score. The comparison of the evaluation metric values for each model is presented in Table 2.

Table 2 Comparison of Evaluation Metrics Values

Evaluation Metrics	LR	RF	SVM
Precision	0.877	0.873	0.887
Recall	0.756	0.814	0.758
Specificity	0.853	0.863	0.863
F_1-score	0.812	0.842	0.817
Kappa	0.593	0.673	0.603
Accuracy	0.795	0.837	0.802
AUC	0.872	0.902	0.854

Kappa, an evaluation metric measuring the agreement between predicted and actual classifications made by machine learning models, quantifies the overall agreement considering both accurate and potentially incorrect classifications. The LR, RF, and SVM models had kappa values of 0.593, 0.673, and 0.603, respectively. Sensitivity, representing the actual positive rate, yielded values of 0.814 for RF, 0.758 for SVM, and 0.756 for LR. For specificity, indicating the actual negative rate identified by the model, SVM and RF achieved 0.863, while LR had 0.853. Additionally, the F1-score, which balances accurately identifying positive outcomes and capturing all positives, was 0.842 for RF, 0.817 for SVM, and 0.812 for LR. All metrics range from 0 to 1, where 1 signifies optimal performance.

Models were evaluated using the receiver operating characteristic (ROC) curve's area under the curve (AUC), a standard metric in flood susceptibility. In Figure 3, ROC curves and AUC values are presented. The RF model led with an AUC of 0.902, distinguishing flood-prone from non-flood-prone areas. The LR model followed at 0.872, and the SVM model at 0.854. Higher AUC values signify superior accuracy in flood susceptibility classification.

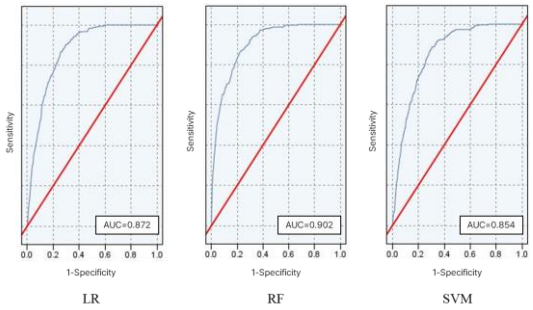

Figure 3 ROC curves and AUC values of each model

3.4 Predictor importance of variables

After selecting the RF model as the optimal machine learning approach, the predictor importance of variables within the RF model was further analyzed, as shown in Figure 4. The analysis revealed that certain variables had a more significant impact on determining flood occurrence than others. Among these variables, SPD, distance to storm drains, elevation, rainfall, and TRI in order stood out as the most influential factors.

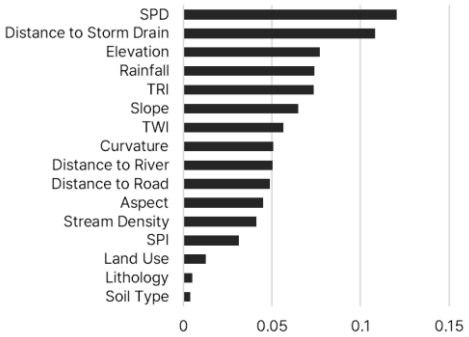

Figure 4 Predictor importance of variables of RF model

These variables' significance underscores their strong link with flood occurrences in the studied region. SPD reflects drainage channel density, guiding water flow during heavy rainfall. Distance to storm drains indicates proximity to drainage infrastructure, impacting water handling and flood risk mitigation. Lower elevation areas are more flood-prone than elevated areas due to reduced natural drainage capacity. Rainfall directly affects flooding likelihood. TRI measures elevation variability, influencing flood susceptibility.

3.5 Partial dependence by variables

Partial dependence plots (PDPs) are particularly useful in discerning the relationship between independent variables and the dependent variable, whether linear or non-linear (Breiman, 2001). Figure 5 depicts the PDP curves for each variable utilized in this study.

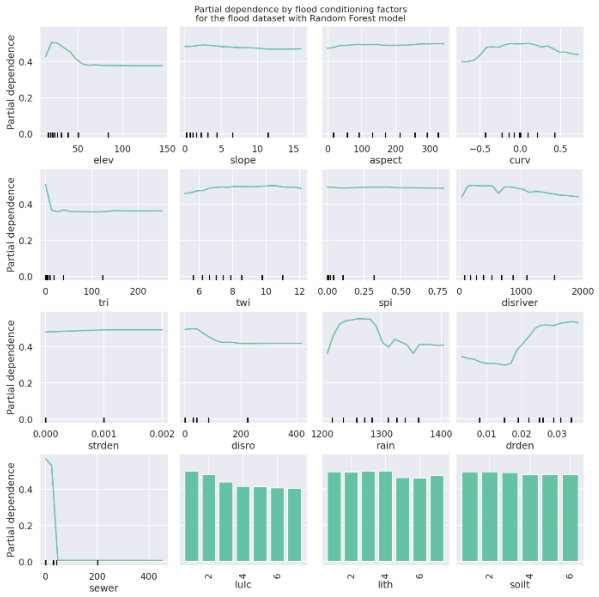

Figure 5 Partial dependence by variables in RF model

The results yield significant insights into flood occurrence patterns. Areas with higher sewer pipe density and closer proximity to roads, streams, and storm drains positively correlate with increased flood incidents. Conversely, regions with higher elevations tend to experience reduced occurrences of flooding. Furthermore, flood occurrence demonstrates an initial increase between average rainfall values of 1200 mm and 1280 mm, followed by a gradual decrease. Additionally, flood occurrence rises as the curvature of an area approaches zero and subsequently diminishes as curvature increases.

5. Conclusion

This research addresses the escalating challenges from climate-induced shifts, leading to intensified meteorological events like typhoons and heavy rainfall. Severe floods have become more frequent, necessitating an enhanced approach to managing flood risks. While current flood-risk maps help identify vulnerable areas, their effectiveness is hindered by their inability to account for evolving urban environments. Consequently, a precise flood susceptibility map based on quantitative analysis and vulnerability assessment is essential.

The study employs three machine learning techniques—logistic regression, random forest, and support vector machines—to comprehensively analyze flood susceptibility. The models determine areas at risk by identifying critical variables related to flooding. Notably, the random forest model proves superior and is chosen to generate flood-susceptibility maps for Seoul. The findings pinpoint high susceptibility zones along the southern Han River banks and southern districts of Seoul, while areas on the northern side demonstrate lower vulnerability due to elevated terrain. Key determinants include sewer pipe density, proximity to storm drains, and elevation. These insights provide valuable guidance for effective flood management strategies and urban planning efforts.

Acknowledgement

This research is partially supported by the Global Korea Scholarship (GKS) program sponsored by the Korean Government. The authors are very grateful to the Seoul Metropolitan Government for providing some data related to this research.

References

Breiman, L. (2001). 'Random forests', *Machine Learning*, 45(1), pp. 5–32.

Güneralp, B., Güneralp, İ. and Liu, Y. (2015). 'Changing global patterns of urban exposure to flood and drought hazards', *Global Environmental Change*, 31, pp. 217–225.

Kim, M. and Choi, J. (2022). 'Review on flood susceptibility prediction based on data-driven learning model', *Journal of The Korean Association of Regional Geographers*, 28(4), pp. 425–438.

Lee, Sunmin *et al.* (2017). 'Spatial prediction of flood susceptibility using random-forest and boosted-tree models in Seoul Metropolitan City, Korea', *Geomatics, Natural Hazards and Risk*, 8(2), pp. 1185–1203.

Lei, X. *et al.* (2021). 'Urban Flood modeling using deep-learning approaches in Seoul, South Korea', *Journal of Hydrology*, 601, p. 126684.

Meteotsunamis in the Tamsui River estuary

Li-Ching Lin *, Wen-Cheng Liu**, Chin H. Wu***

Meteotsunamis generated by atmospheric disturbances can be detected within the Tamsui River estuary. We present evidence of two meteotsunamis occurring in the river channels of Dahan River, Xindian River, and Keelung River. Meteotsunami waves with distinct oscillation periods, 23-26 min and > 30 min, are clearly observed. Both meteotsunamis exhibit the ability to propagate upstream with varying wave heights. The wave height associated with longer periods demonstrates a minor reduction, whereas waves with shorter periods experience a more pronounced reduction rate. These findings appear to be influenced by the river geometries, which could potentially pose hazards to the low-lying areas of the Tamsui River system.

Keywords: meteotsunamis, river estuary, hazards

1. Introduction

Meteotsunamis are long waves caused by a rapid movement of atmospheric disturbances (Monserrat et al., 2006), which have been officially classified as the tsunami phenomenon (Tsunami glossary, 2019) because of the scale and damage extent can also be produced by meteotsunamis. For example, the well-known and destructive damage of meteotsunamis occurs in the Vela Luka Bay of Croatia on 21 June 1978 (Orlić, 1980) and in Nagasaki Bay of Japan on 31 March 1979 (Hibiya & Kajiura, 1982). The extensive literature review and event-based report have summarized that the largest wave height is up to 4-6 m records and the spatial scale of meteotsunami impacts can be up to approximately 100–150 km (Rabinovich, 2020). Findings suggest that meteotsunamis occur not only under stormy conditions but also clam weather conditions. Such atmospheric disturbances induced meteotsunamis have been recognized by frontal passages, cyclones, and mesoscale convective systems (e.g., Monserrat et al.,2006).

Furthermore, meteotsunamis are frequently coincided with the sudden fluctuation in air pressure and winds which can travel fast and cover areas more than hundreds of kilometers in the coastal area. When the travel speed of atmospheric disturbances meets the propagation speed of meteotsunami waves, the meteotsunami can be amplified by the Proudman resonance (Proudman, 1929). In the shallow waters, multiple resonant effects, e.g, harbor and geometry resonance are likely to be the cause of destructive meteotsunami occurrences (Monserrat et al., 2006).

With regard to the meteotsunami generation and propagation toward the shoreline, the probability and impact of meteotsunami occurring in the river is high. However, the reports or literature reviews has received less study. For example, Šepić et al. (2018) reported the floods are triggered by meteotusnamis on the Mazaro River, Italy and the maximum height can be up to 1.0 m in the upstream channel observed by video footage. Findings indicate that floods are highly attributed by the rapid propagation meteotsunamis as a wave-like bore. One report also documents a ship damage by possible meteotsunamis induced strong currents (Pattiaratchi & Wijeratne, 2015).

The purpose of this study is to examine the evolution of meteotsunamis in the Tamsui River estuarine system and the relevant hazards/risks associated with atmospheric forcings.

* Department of Civil and Disaster Prevention Engineering, National United University, Miaoli, Taiwan, 360302, plihkimo@nuu.edu.tw
** Department of Civil and Disaster Prevention Engineering, National United University, Miaoli, Taiwan, 360302, wcliu@nuu.edu.tw
*** Department of Civil and Environmental Engineering, University of Wisconsin-Madison, Madison, WI, USA, 53706, chin.wu@wisc.edu

2. Study area and data sources

Situated in northern Taiwan, the Tamsui River has three significant tributaries of the Dahan River, Xindian River and Keelung River. These waterways experience the influence of semi-diurnal tidal forcing, as detailed in the study by Liu et al. (2001). The arrangement of the river system and the recorded data observations are illustrated in Figure 1. In particular, the Tamsui River estuarine system encompasses a densely populated area, with a resident population exceeding 6.8 million in the Taipei metropolitan region. Given this concentration, there exists a important need to focus on the potential impacts of meteotsunamis in the study area.

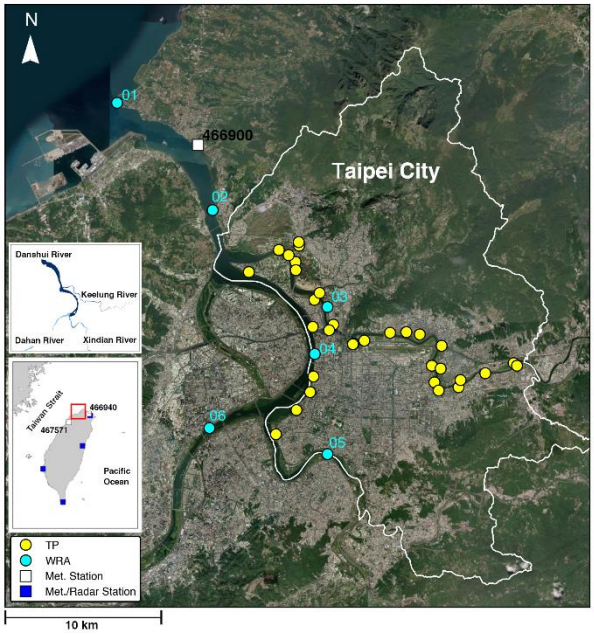

Figure 1 Study sites and locations of water level (circles). Insets show the Tamsui River with three tributaries, and meteorology stations with four weather radars (squares)

In the analysis, we utilize the water level and meteorological dataset to investigate the meteotsunami events and evolutions. Water level is acquired from the Water Resources Agency (WRA) of Taiwan, and Taipei City Government (TP), Taiwan illustrated as circles in Figure 1. Ground meteorological observations are obtained from Central Weather Bureau (CWB), Taiwan. In addition, atmospheric forcings may be originated by convective storms and can be identified by the radar reflectivity images from CWB and satellite-derived precipitation products from the Global Satellite Mapping of Precipitation (https://sharaku.eorc.jaxa.jp/GSMaP). The sampling rate of water level and ground observations is 10-min. The observation intervals of radar images and precipitation products are 30-min and one hour, respectively.

3. Meteotsunami identifications

We follow criteria given by Bechle et al. (2015) to identify meteotsunamis. First, we apply a high-pass filtering method to extract the water level oscillations between 2 minutes to 2 hours (Monserrat et al. 2006) as possible meteotsunamis. Second, the zero-crossing method is adpoted to estimate the wave height of possible ones. Lastly, meteotsunamis are identified in the condition that the rate of pressure changes in 1.5 hPa/10-min (Linares et al., 2018) or wind speed in excess of 5 m/s (Vilibić et al., 2005) is closely linked to those considered meteotusnamis.

In this study, we have demonstrated two meteotusnamis in the Tamsui River estuarine system shown in Figure 2.

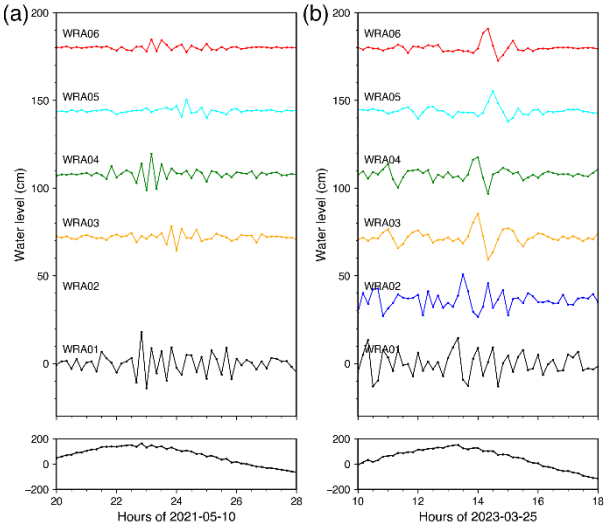

Figure 2 Meteotusnami occurrences on 10 May 2021(a) and 25 March 2023 (b). Upper panels are the filtered water level from the river mouth to upstream channels. Bottom panels indicate the tidal fluctuations in the river mouth (WRA01).

Two meteotsunamis are occurred in the time period of flood tides. On 10 May 2021, meteotsunami waves fluctuate in the period of 23-26 min. The fluctuation period of more than 30 min is occurred on 25 March 2023. In addition, the coincident pressure and wind changes indicates the close relations with the 2023 event, whereas the insignificant correlation seemingly occurs in the 2021 event shown in Figure 3 and 4. For the 2021 events, the pressure changes is insignificant and wind speed is less than 3 m/s. Seemingly, the atmospheric disturbances is not strong enough to trigger that meteotsunamis followed by above criteria.

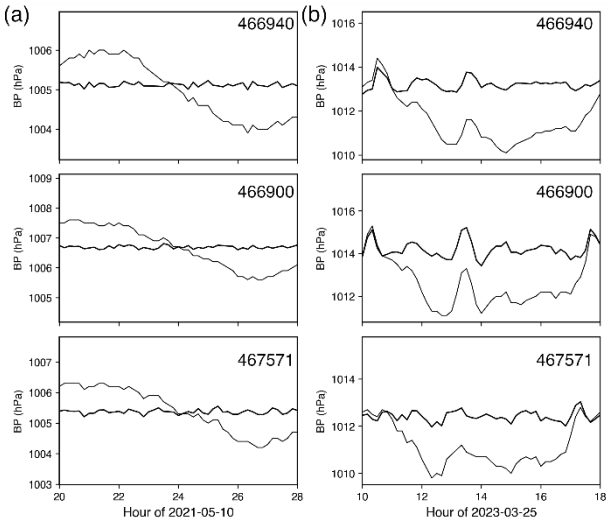

Figure 3 Barometric pressure and the rate of pressure change associated with meteotsunamis.466900 is the closest weather station around the Tamsui Rivers.

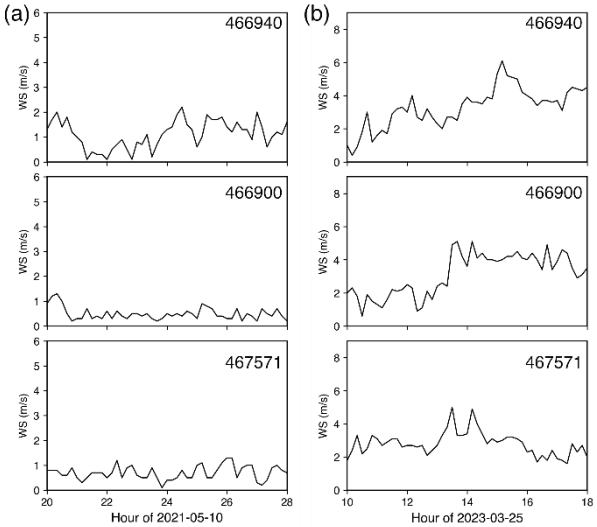

Figure 4 Same as Figure 3 but for wind changes.

Based upon radar reflectivity images, the convective storm of the 2021 event has no strong pattern around the northern Taiwan Strait area compared to the complex structure storm occurred in the 2023 event shown in Figure 5, which is well correlated with the satellite-derived precipitation results shown in Figure 6.

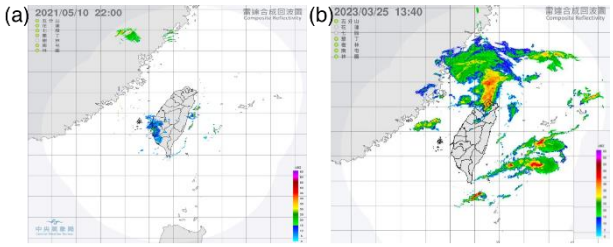

Figure 5 Radar reflectivity images for 2021 (a) and 2023 (b) events.

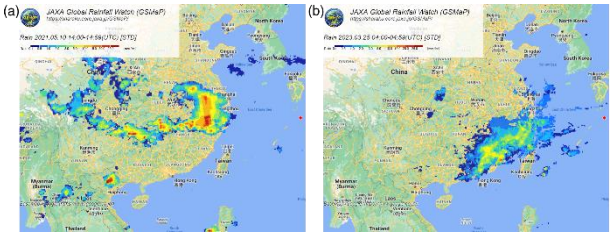

Figure 6 Same as Figure 5 but for satellite-derived precipitation.

4. Meteotsunami evolution in the Tamsui River

We have calculated the propagation of meteotsunami waves in the river systems. Notably, a mean velocity of 4 m/s is observed in the Keelung River, extending from WRA02 to WRA03. Along the main stream of the Tamsui River, the waves exhibit an approximate speed of 6 m/s, progressing through WRA01, WRA02, and WRA04. In the upstream portions of the Dahan River (from WRA04 to WRA06) and the Xindian River (from WRA04 to WRA05), the average velocity measures at 4.2 m/s.

In order to evaluate fluctuations in wave height within the rivers, we have employed a ratio-based approach. This ratio involves comparing the wave height measurements at various stations to the height recorded at WRA01. Figure 7 illustrates the application of this ratio to the two meteotsunami events. During the 2021 incident, where the river mouth's wave height is 0.3 m at WRA01, the ratio surpassing 0.6 is observed at 15 stations. In

contrast, the 2023 event displays a significant response at numerous stations, even including areas where waves propagate toward the outskirts of Taipei City, when the ratio is based on the 0.27 m wave height at WRA01. These findings suggest that longer-period meteotsunami waves, characterized by periods exceeding 30 minutes, tend to retain their energy within the specific channel geometries of the rivers. Conversely, shorter-period waves might experience more pronounced damping, particularly evident in the Keelung River.

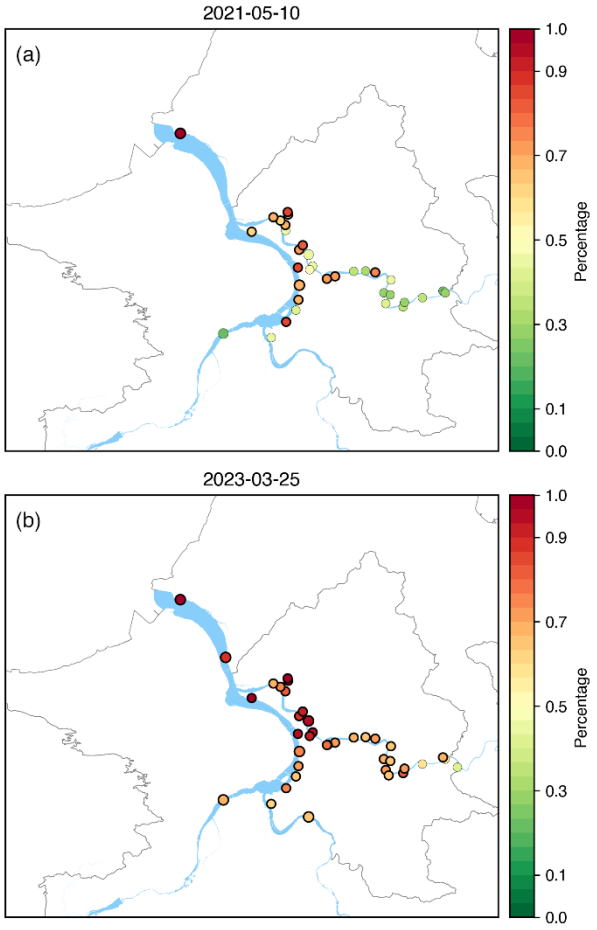

Figure 7 Wave height ratio of meteotusnami occurrences in the Tamsui rivers.

Concerning the 2021 occurrence, the wave oscillations only satisfy the first criterion for identifying meteotsunamis and exhibit a weaker correlation with atmospheric disturbances or convective storms. In light of this, we tend to look into a more detailed analysis of convective movement by examining changes in vertical velocity. Figure 8 illustrates the vertical velocity extracted from ERA5, the fifth generation ECMWF reanalysis (C3S, 2017) for the period spanning the two events. During the 2023 event, strong vertical motion is observed at 700 hPa, characterized by downward motion in the northern region and upward motion in the southern area, particularly around the northern Taiwan Strait. This pattern aligns well with the established identification criteria. In contrast, the 2021 event shows a distinct downward wind pattern in the northern Taiwan area, exhibiting rapid movement across the coastline. This finding suggests that convective forcing, even with precipitation-free signals, could potentially act as a trigger for meteotsunamis. Nonetheless, comprehensive investigations and detailed characterizations of convective movement in precipitation-free conditions are needed to fully understand this phenomenon.

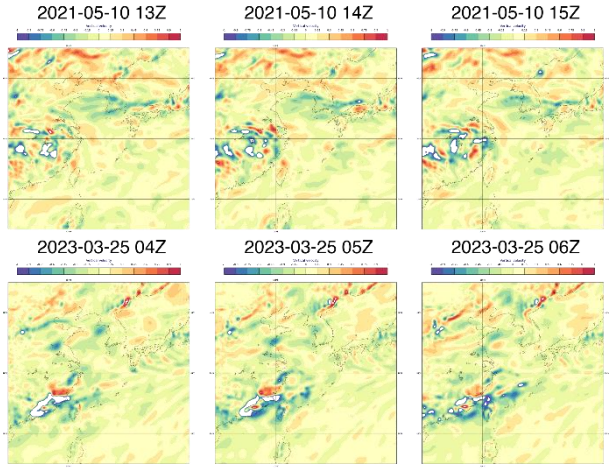

Figure 8 Vertical velocity of two meteotsunami occurrences at 700 hPa, ~3km a.m.s.l. Positive and negative value show the downward and upward winds, respectively.

5. Conclusion

In this study, we have examined the meteotusnamis with water level and meteorological dataset along the Tamsui Rivers. The demonstrations of meteotsunami occurrences reveal the strong association with atmospheric disturbances in 2023 but this association is not evident in 2021. Findings suggest that the convective movement in precipitation-free conditions could play an important role in generating meteotsunamis, as observed

in the 2021 event.

During the 2023 occurrence, the meteotsunami waves of longer periods (>30 min) exhibit a reduction rate in wave height of less than 40%, in contrast to the higher reduction rate of over 60% observed for short-period waves during the 2021 event. This different is particularly pronounced in the upstream channel of the Keelung River. Consequently, the specific river geometries appear to represent vulnerable areas for the emergence of long-period meteotsunamis, particularly in proximity to the low-lying regions of the Tamsui river system.

Reference

Bechle, A. J., Kristovich,D. A. R., Wu, C. H. (2015) Meteotsunami occurrences and causes in Lake Michigan. *Journal of Geophysical Research: Oceans*, 120, doi:10.1002/2015JC011317.

C3S Copernicus Climate Change Service (2017) ERA5: Fifth Generation of ECMWF Atmospheric Reanalyses of the Global Climate. Copernicus Climate Change Service Climate Data Store (CDS). Available online at: https://cds.climate.copernicus.eu/cdsapp#!/home

Hibiya, T., Kajiura, K. (1982) Origin of the Abiki phenomenon (a kind of seiche) in Nagasaki Bay. *Journal of the Oceanographical Society of Japan*, 38, 172-182.

Linares, Á., Bechle, A. J.,Wu, C. H. (2016) Characterization and assessment of the meteotsunami hazard in northern Lake Michigan. *Journal of Geophysical Research: Oceans*, 121(9), 7141-7158.

Liu, W. C., Hsu, M. H., Kuo, A. Y., Kuo, J. T. (2001) The influence of river discharge on salinity intrusion in the Tanshui estuary, Taiwan. *Journal of Coastal Research*, 544-552.

Monserrat, S., Vilibić, I., Rabinovich, A. B. (2006) Meteotsunamis: Atmospherically induced destructive ocean waves in the tsunami frequency band. *Natural Hazards and Earth System Sciences*, 6, 1035‑1051, doi:10.5194/nhess-6-1035-2006.

Orlić, M. (1980) About a possible occurrence of the Proudman resonance in the Adriatic. *Thalassia Jugoslavica*, 16(1), 79-88.

Pattiaratchi Charitha B., Wijeratne, E. M. S. (2015) Are meteotsunamis an underrated hazard? Phil. Trans. R. Soc. A. 373(2053), http://doi.org/10.1098/rsta.2014.0377

Proudman, J. (1929) The effects on the sea of changes in atmospheric pressure. *Geophysical Supplements to the Monthly Notices of the Royal Astronomical Society*, 2(4), 197-209.

Rabinovich, A. B. (2020) Twenty-seven years of progress in the science of meteorological tsunamis following the 1992 Daytona Beach event. *Pure and Applied Geophysics*, 177(3), 1193-1230.

Šepić, J., Vilibić, I., Rabinovich, A., Tinti, S. (2018) Meteotsunami (“Marrobbio”) of 25‑26 June 2014 on the southwestern coast of Sicily, Italy. *Pure and Applied Geophysics*, 175, 1573-1593.

Tsunami Glossary (2019) Intergovernmental Oceanographic Commission., Paris, UNESCO, IOC Technical Series, 85, rev.4 pp. 44.

Vilibić, I., Mihanović, H., Charrayre, F. (2015) Assessing meteotsunami potential of high-frequency air pressure oscillations observed in the middle Adriatic. Meteorological Tsunamis: The US East Coast and Other Coastal Regions, 217-232.

Comparison of the different types of shorelines detected from Sentinel-1 and 2 satellite imagery acquired on the east coast of Korea

Yun-Jae Choung*

In this research, the different types of shorelines detected from the Sentinel-2 satellite imagery with the multispectral bands and the Sentinel-1 satellite imagery with the Synthetic Aperture Radar (SAR) C-band were compared for detecting the accurate shoreline positions in the east coast of Korea. First, the Sentinel-1 Ground Range Detected (GRD) product was preprocessed, and Shoreline-1 was detected from the preprocessed Sentinel-1 GRD product by using the Otsu thresholding. Next, the Normalized Difference Water Index (NDWI) image was generated from the multispectral bands of the Sentinel-2 L2A product, and Shoreline-2 was detected from the NDWI image by using the Otsu thresholding. Both Shoreline-1 and Shoreline-2 were compared, and as a result, some of Shoreline-2's segments were not in the right places due to the misclassification errors caused by the Otsu thresholding, while most of Shoreline-1's segments were in the right places.

Keywords: Shoreline, Sentinel, SAR, NDWI, Otsu thresholding

1. Introduction

A shoreline is defined as "the land along the edge of an area of water" or "the edge of a sea, lake, or wide river" (The Britannica Dictionary, 2023; Cambridge Dictionary, 2023). Detecting the shoreline positions accurately is necessary in preserving the coastal properties, preventing the coastal disasters, describing the coastal shapes in detail, among other functions (Choung and Jo, 2016; Choung and Jo, 2017).

Remote sensing datasets such as high-resolution satellite imagery have been widely used in the shoreline mapping tasks due to their benefits in acquiring the geometric and surface information of coastal zones without human access (Choung, 2015; Choung and Jo, 2016; Choung and Jo, 2017). The types of satellite imagery are classified into optical imagery with the multispectral bands and microwave imagery with the Synthetic Aperture Radar (SAR) bands. Optical imagery with the multispectral bands is generally acquired by the passive sensors, while microwave imagery with the SAR bands is generally acquired by the active sensors (Fahey et al., 2021). Due to the complicated and irregular shapes of coastal zones, both optical and microwave satellite imagery should be compared in detecting the shoreline positions accurately.

Hence, in this research, the different types of shorelines were detected from the given optical and SAR satellite imagery to select the most appropriate sensor for detecting the shoreline positions in the east coast of Korea.

2. Dataset and study area

The east coast of Korea measuring 200 km in length was selected as the study area (see Figure 1).

Figure 1 East coast of Korea selected as the study area shown in Google Satellite Map

The east coast of Korea is eroded annually due to both natural and artificial causes (Lim et al, 2023). We used the Sentinel-1 Ground Range Detected (GRD) product with the SAR C-band acquired in the study area on 18 July 2023 and the Sentinel-2 L2A product with the

* Member (KAGIS), Geo C&I Co., Ltd., chyj@geocni.com

multispectral bands acquired in the same area on 9 May 2023.

3. Methodology

This section illustrates the procedure for detecting the two types of shorelines from the given Sentinel-1 and Sentinel-2 satellite imagery (see Figure 2).

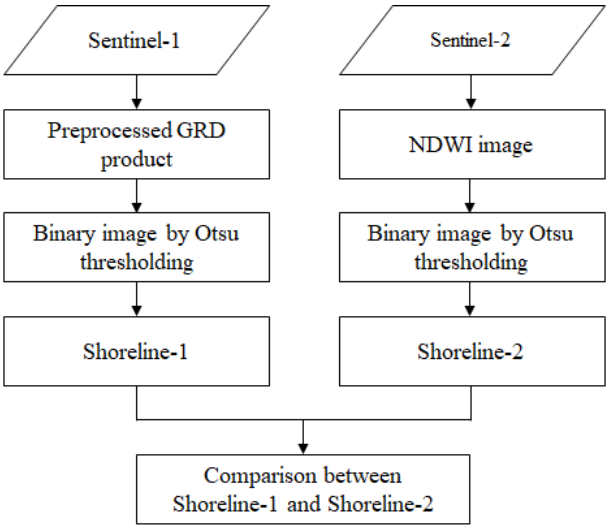

Figure 2 Flowchart showing the procedure for detecting the two types of shorelines from the Sentinel-1 and 2 satellite imagery

2.1 Detection of Shoreline-1 from the Sentinel-1 GRD product with the SAR-C band

The given Sentinel-1 GRD product was preprocessed through the multiple steps to remove the thermal and border noises, and to correct the radiometric and geometric distortions included in the given data (see Figure 3).

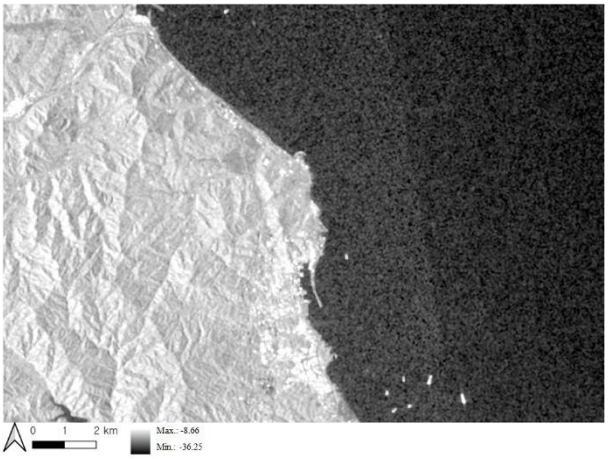

Figure 3 Preprocessed Sentinel-1 GRD product

Otsu thresholding was subsequently employed to generate the binary image that classify the land and water features from the preprocessed Sentinel-1 GRD product (see Figure 4).

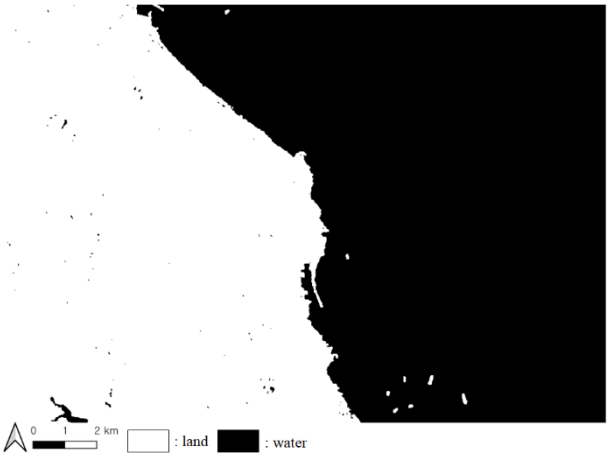

Figure 4 Binary image generated from the preprocessed Sentinel-1 GRD product

Finally, the boundary located between the land and water features in the binary image shown in Figure 4 was selected and defined as Shoreline-1 (see Figure 5).

Figure 5 Shoreline-1

2.2 Detection of Shoreline-2 from the Sentinel-2 L2A product with the multispectral bands

Normalized Difference Water Index (NDWI), a remote sensing-derived index estimating the liquid water features, was generated using the multispectral (green and near infrared) bands of the given Sentinel-2 L2A product using Equation 1.

$$NDWI = \frac{G-N}{G+N} \quad (1)$$

where G and N are the reflectance of the green and near infrared bands of the given Sentinel-2 satellite image, respectively (McFeeters, 1996).

In the generated NDWI image, the pixels located in the liquid water features have values higher than 0 and lower than 1, while the other pixels have values higher than -1 and lower than 0 (see Figure 6).

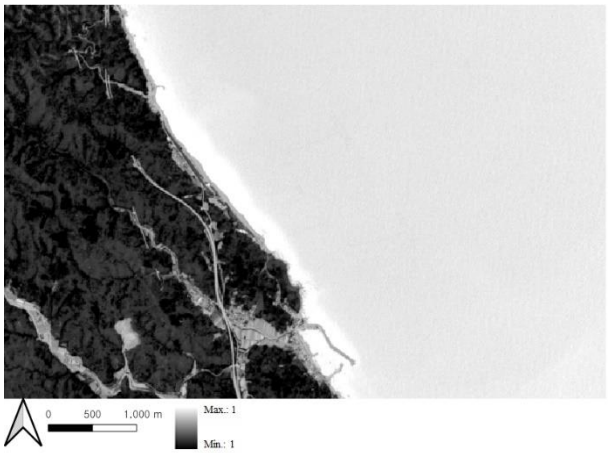

Figure 6 NDWI image

As with the previous step, the binary image classifying the land and water features was generated from the NDWI image using Otsu thresholding (see Figure 7).

Figure 7 Binary image generated from the NDWI image

Next, the boundary in the above binary image was selected and defined as Shoreline-2 (see Figure 8).

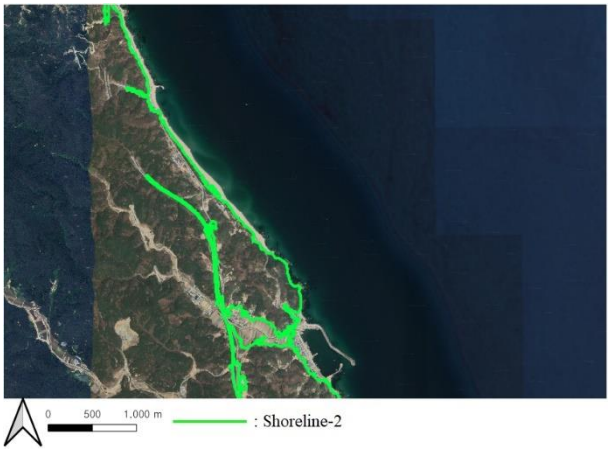

Figure 8 Shoreline-2

4. Result

As can be seen in Figures 5 and 7, most of Shoreline-1's segments are in the right places in the study area, while some of Shoreline 2's segments are in the wrong places. In the NDWI image (Figure 6), the pixels representing some land features including bare soil, beach, agriculture land and roads were misclassified into the water features by Otsu thresholding, and it causes some segments of Shoreline-2 to be located in the wrong places. In future research, the statistical results from these two types of shorelines would be computed to determine the most appropriate sensor for accurately detecting the shoreline positions in the east coast of Korea.

Acknowledgement

This research was supported by Korea Institute of Marine Science & Technology Promotion(KIMST) funded by the Ministry of Oceans and Fisheries, Korea(RS-2023-00256687).

References

Cambridge Dictionary (2023) *Shoreline*. Available at: https://dictionary.cambridge.org/dictionary/english/shoreline (Accessed: 26 April 2023).

Choung, Y.-J. (2015) 'Mapping 3D Shorelines Using KOMPSAT-2 Imagery and Airborne LiDAR Data', *Journal of the Korean Society of Surveying, Geodesy, Photogrammetry and Cartography*, 33(1), pp.23-30. doi:

http://dx.doi.org/10.7848/ksgpc.2015.33.1.23

Choung, Y.-J. and Jo, M.-H. (2016) 'Shoreline Change Assessment for Various Types of Coasts Using Multi-Temporal Landsat Imagery of the East Coast of South Korea', *Remote Sensing Letters*, 7(1), pp. 91-100. doi: https://doi.org/10.1080/2150704X.2015.1109157

Choung, Y.-J. and Jo, M.-H. (2017) 'Comparison between a Machine-learning-based Method and a Water-index-based Method for Shoreline Mapping Using a High-Resolution Satellite Image Acquired in Hwado Island, South Korea', *Journal of Sensors*, 2017, pp. 8245204. doi: https://doi.org/10.1155/2017/8245204

Fahey, T., Pham, H., Gardi, A., Sabatini, R., Stefanelli, D., Goodwin, I. and Lamb, D.W. (2021) 'Active and Passive Electro-Optical Sensors for Health Assessment in Food Crops', *Sensors*, 21(1), pp. 171. doi: https://doi.org/10.3390/s21010171

Lim, H.S.; Lee, H.J.; Kim, D. and Hong, S. (2023) 'Beach erosion along the eastern coast of Korea: A brief review', *Journal of Coastal Research*, 39(1), pp. 181–190. doi: https://doi.org/10.2112/JCOASTRES-D-22TM-00006.1

McFeeters, S.K. (1996) 'The use of the Normalized Difference Water Index (NDWI) in the delineation of open water features', *International Journal of Remote Sensing*, 17(7), pp. 1425–1432. doi: https://doi.org/10.1080/01431169608948714

The Britannica Dictionary (2023) *Shoreline*. Available at: https://www.britannica.com/dictionary/shoreline (Accessed: 26 April 2023).

Oral presentation in IAG'i

Data

Chair: Satoshi Kubota (Kansai University)
Sat. Oct 28, 2023 5:00 PM - 6:40 PM Room D (C-201 2nd floor of Bldg. C)

[D5-01] Enhancing large-scale footprint extraction evaluation: a two-level approach with proxy data and building-unit matching

*Shenglong Chen[1], Yoshiki Ogawa[1], Chenbo Zhao[1], Yoshihide Sekimoto[1] (1. University of Tokyo)

5:00 PM - 5:20 PM

[D5-02] Advancing Building Extraction in Thailand using the YOLOv8 Segment Model on Open-source Data across Diverse Land Use Types

*Bhanu Prasad CHINTAKINDI[1], Yoshiki OGAWA[1], Yoshihide SEKIMOTO[1] (1. The University of Tokyo)

5:20 PM - 5:40 PM

[D5-03] Marine Debris Monitoring and AI Application Optimization Plan by Geographic Characteristics and Research Devices

*BoRam Kim[1], Cholyoung Lee[1], Hynwoo Choi[1], TaeHoon Kim[1] (1. Korea Institute of Marine Science and Technology(KIOST))

5:40 PM - 6:00 PM

[D5-04] Another approach to terrain mapping method utilizing Unmanned Surface Vehicle and Light Detection and Ranging at shallow water area: A case study at Budai Port' s expansion sand filling project site.

*Amrico Hanafie[1], Kuan-Tsung Chang[2], Sheng-Yu Yu[3] (1. Master student, Dept. of Civil Eng. and Environmental Informatics, Minghsin Uni. of Science and Technology, 2. Corresponding author, Professor, Dept. of Civil Eng. and Environmental Informatics, Minghsin Uni. of Science and Technology, 3. Company, Manager, Strong Engineering Consulting Co.)

6:00 PM - 6:20 PM

[D5-05] The Public Sentiment During the Covid-19 Lockdowns in China: A Comparison of Wuhan and Shanghai

*Xuanda Pei[1], Yuzuru Isoda[1] (1. Tohoku university)

6:20 PM - 6:40 PM

Enhanced Evaluation Method for Large-scale Building Footprint Extraction: A Two-level Approach Using Proxy Data and Building Matching

Shenglong Chen*, Yoshiki Ogawa**, Yoshihide Sekimoto***

Abstract: Traditional evaluation metrics for footprint extraction depend on manually generated ground truth. Besides, certain areas lack authoritative reference data, and intrinsic methods are confined in limited regional applicability. Therefore, the study introduces a two-level approach. Initially, population and land use data serve as a proxy for grid-level completeness assessment. Secondly, an enhanced two-way area overlap method is employed to match extracted footprints with reference buildings, yielding a comprehensive evaluation of global and semantic accuracy. Validation conducted in Hyogo Prefecture and Numazu City demonstrate an enhancement in grid classification accuracy and completeness correlation by 2.6% and 0.53. Furthermore, the optimized matching method achieves an impressive 99% accuracy in semantic matching, displaying exceptional efficiency and robustness in multi-scale matching. This study presents an exhaustive and efficient solution for establishing a comprehensive large-scale building extraction evaluation system.

Keywords: Footprint quality evaluation, Completeness assessment, Proxy data, Building matching.

1. Introduction

Recent studies have investigated using deep learning technologies to automatically extract large-scale building footprints from remote sensing images (Chen et al., 2023). However, challenges related to reliability, accuracy, and usability still arise because of building feature diversity, sensor performance limitations, and so on. Consequently, evaluating extraction performance has become a crucial aspect of these methods.

Numerous studies have examined extraction results, mostly focusing on traditional accuracy assessments for image segmentation (Dey and Awrangjeb, 2020). However, this approach is limited by its dependence on reference data quality, often relying on manually created ground truth for assessment. The evaluation results can significantly differ based on the selected sampling area, potentially not representing overall extraction quality adequately. A viable solution involves maximizing the utilization of existing reference building data. Ensuring correspondence between extracted footprints and real-world objects requires geographic matching, presenting two significant challenges: discrepancies in position due to off-nadir angle in satellite images and complex semantic variations from chronological and detail disparities (Wang et al., 2022). Moreover, matching a wide range of footprints places high computational efficiency demands on the algorithm.

In certain developing regions, accessing reliable reference data poses challenges, particularly in evaluating aspects like positional accuracy and shape similarity. While some studies suggest utilizing indicators like building density and count as proxies for completeness, these quantitative relationships might not universally apply beyond specific target regions (Tian et al., 2019). Alternative proxy data, such as population statistics and land cover information, have been proposed for completeness assessment (Zhang et al., 2022). However, relying solely on population data disregards sparsely populated regions such as rural or industrial areas.

This study introduces a two-level approach, designed to evaluate large-scale footprint extraction results. Firstly, a grid-based approach utilizes WorldPoP population and Esri land cover data as proxies to assess footprint completeness (Zhou et al., 2022b). Secondly, an object-based method employs an optimized two-way area overlay (TWAO) technique to identify matches between

* GISA member College of Civil Engineering, The University of Tokyo **chen-sl@csis.u-tokyo.ac.jp**
** GISA member Center for Spatial Information Science, The University of Tokyo **ogawa@csis.u-tolyo.ac.jp**
*** GISA member Center for Spatial Information Science, The University of Tokyo **sekimoto@iis.u-tokyo.ac.jp**

extraction and reference data. (Fan et al., 2014). This yields global accuracy metrics and intricate semantic relationships. Finally, the methodology's efficacy is demonstrated through evaluations in Hyogo Prefecture, Japan using the grid-based approach, and in Numazu City using the object-based approach.

2. Related works

2.1 Footprint completeness assessment

To assess the completeness of footprint data, quantitative analysis is utilized to quantify various factors within a given region, by comparing it with a reference dataset (Zhou et al., 2022a). To tackle the challenge of insufficient building datasets, scholars have suggested using machine learning techniques or crowdsourcing methods to deduce or acquire reference footprint data. Herfort et al. (2022) applied a random forest regression to estimate building completeness in a megalopolis with 13,189 locations. However, training a machine learning-based model requires a substantial volume of training data and the fine-tuning of numerous hyperparameters and model architectures. Ullah et al. (2023) adopted a gamified crowdsourcing approach and engaged volunteers through the mobile application MapSwipe to classify building completeness. Nevertheless, there's room for improvement in both the quantity and quality of volunteer contributions. Moreover, several studies have employed building-related data as substitutes for the reference data (Zhou et al., 2022b). The availability of open-source population and land cover products with enhanced global resolution and precision has opened up new avenues for exploring innovative evaluation approaches.

2.2 Building-unit quality evaluation

Evaluation of the extraction involves two main steps: matching the results with the reference data and computing the corresponding quality metrics. The objective of building matching is to establish correlations between identical footprint characteristics from diverse sources. For polygons, the commonly used TWAO method accurately matches individual target positions but lacks precision in simultaneous matching of multiple targets (Memduhoglu and Basaraner, 2022). To enhance accuracy of complex semantic relations, researchers use techniques like minimum bounding rectangle combinatorial optimization (MBRCO) and relaxed labeling (Liu et al., 2023). However, these methods require exploring combinations and multiple iterations significantly increasing matching time. When considering evaluation metrics, Zeng et al. (2013) introduced three key aspects: matching rate, shape similarity, and positional accuracy. The matching rate, a crucial and commonly used measure, quantifies detection rate (recall) and accuracy (precision) based on building statistics (Chen et al., 2023). Shape similarity and positional accuracy assess quality through geometric criteria, relying on accurate reference data (Huang et al., 2021). This study primarily focused on the matching rate due to constraints in footprint extraction methods and available data.

3. Methodology

3.1 Study area and data

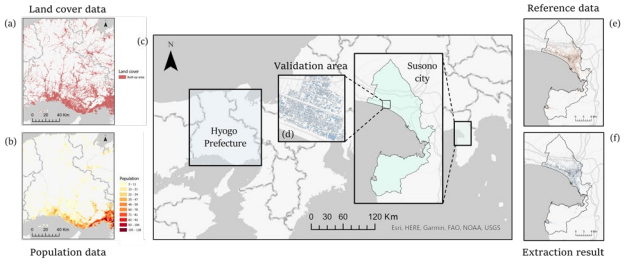

Figure 1. Study area and data.

In Figure 1c, Hyogo Prefecture and Numazu City were chosen as our study areas. The purpose of Hyogo Prefecture was to test the grid-level method's completeness using proxy data. Conversely, Numazu City was selected to assess the object-level method, specifically focusing on footprint semantic matching and quality evaluation based on reference data. For validation, a validation area containing around 5,000 buildings was randomly chosen (Figure 1d).

To assess grid-level completeness, we employed proxy

data, including Esri's land cover data (Figure 1a) and WorldPop population data (Figure 1b). Building footprint results (Figure 1e) were produced employing a super-resolution-based instance segmentation method (Chen et al., 2023). The reference data (Figure 1f) originated from the 1/2500 scale base map information officially provided by the Geospatial Information Authority of Japan (GSI).

3.2 Grid-level completeness assessment with proxy data

The completeness of extracted footprints was evaluated using a grid-based classification method inspired by Zhou et al. (2022b). This approach involves comparing extracted footprints with proxy data, specifically population count and built area in the land cover data. Initially, we overlaid the two datasets to align extraction results and proxy data. The count of footprints in each basic grid determined subsequent classification. Grid cells were then categorized into four groups based on population count, built-up area, and footprint count.

Type I: No footprints were identified ($N_{fe} = 0$) and had neither a population nor a built area ($N_p = 0\ and\ A_b = 0$). (e.g., A1 in Figure 2).

Type II: No footprints were identified but had evidence of a population or the presence of built areas ($N_p \geq 1\ or\ A_b > 0$). (e.g., C1 in Figure 2).

Type III: Footprints were identified ($N_{fe} \geq 1$) but had neither a population nor a built area. (e.g., A2 in Figure 2).

Type IV: Footprints were identified and had a population or built area. (e.g., B1 in Figure 2).

where N_{fe} represents the number of extracted footprints and N_p and A_b denote the population and built area in the grid. We assumed that the presence of a building signified either a population or built area.

With the provided classification method, determining the presence of buildings within a grid becomes feasible. Consequently, we adapted the completeness index introduced by Zhou et al. (2022b) to compute the proportion of grid cells containing accurately extracted building footprints in the alternative data (1).

$$C_e = \frac{N_{Type\,IV}}{N_{Type\,II} + N_{Type\,IV}} \times 100\% \qquad (1)$$

where the completeness index C_e represents the footprint completeness assessment factor for the target area. $N_{Type\,II}$ and $N_{Type\,IV}$ represent the numbers of grids classified as categories II and IV.

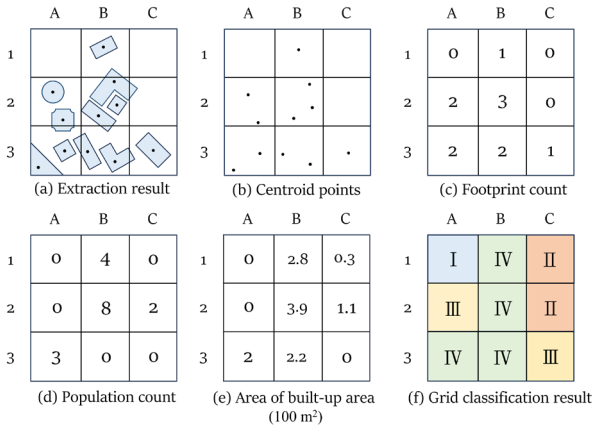

Figure 2 Illustration of grid classification method based on proxy data mapped onto 3 × 3 grids.

To evaluate the accuracy of the grid classification method and the completeness index, we compared the estimated assessment results obtained from reference data. The extracted footprint results were overlaid onto the reference building data by employing the same grid size and layout as those described earlier. Similarly, the grid was divided into four categories. Employing a confusion matrix, we quantitatively evaluated accuracy by comparing classification outcomes using both proxy and reference data. Moreover, to assess the validity of the completeness index, reference index C_r was derived from the reference data. The correlation between the estimated and reference completeness index values for different regions was analyzed through linear regression based on (2). Here, R^2 represents the correlation coefficient and $\overline{C_e}$ represents the average of the reference completeness index for each region.

$$R^2 = 1 - \frac{\sum(C_r - C_e)^2}{\sum(C_r - \overline{C_e})^2} \qquad (2)$$

3.3 Object-level matching and quality evaluation

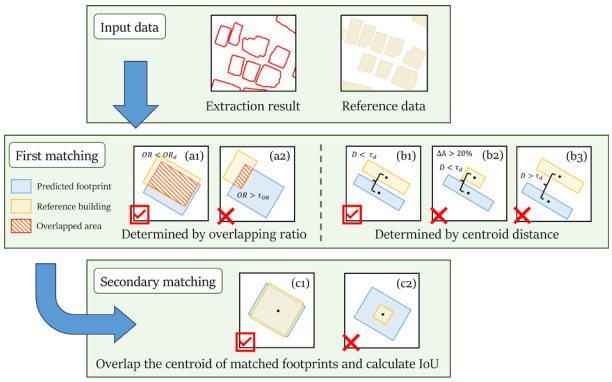

Figure 3. Flow chart of optimized footprint matching method.

To effectively address geometric inconsistencies and achieve a balance between accuracy and efficiency in large-scale geometric matching, we propose an optimized TWAO method. As illustrated in Figure 3, the optimized method incorporates a secondary matching strategy, where the first matching identifies possible relationships, and the secondary matching refines these matches by superimposing the polygon centroids of each pair. The first matching step employs two metrics, the overlap rate R_o and centroids distance. We set the thresholds corresponding to a 90% confidence interval of the geometric shifts of buildings in reference data as the criteria. The overlap rate is measured using (3), defined as the intersection area of the two footprint polygons ($A_{overlap}$) divided by the area of the smaller polygon in matching pairs (A_{fe} and A_{fr}) (Fan et al., 2014). If no overlapping footprints were found, other footprints within a specific range of the building centroid were searched, considering the impact of the geometric offset.

$$R_o = \frac{A_{overlap}}{\min(A_{fe}, A_{fr})} \tag{3}$$

After that, the reference buildings in all matched pairs were shifted such that their centroids were aligned with the predicted footprints, to consider the offset of the reference data. Then, the IoU is employed to perform secondary matching (4), where $A_{overlap}$ and A_{union} denote the intersection and concatenated areas of the predicted and reference footprints in the first matching.

$$IoU = \frac{A_{overlap}}{A_{union}} \tag{4}$$

To evaluate matching result in object-wise, precision, recall, and F-value were selected, as illustrated in (5). These metrics were calculated by quantitatively analyzing the relationship among three categories: TP, false positive (FP), and false negative (FN). Moreover, further analysis was conducted to evaluate the semantic accuracy. Six possible semantic relationships may exist.

$$Precision = \frac{TP}{TP + FP}$$

$$Recall = \frac{TP}{TP + FN} \tag{5}$$

$$F1 = \frac{2 \times Precison \cdot Recall}{Precision + Recall}$$

A) 1:1 relation: The predicted footprint corresponded to a single building in the reference data.

B) 1:n relation: The predicted footprint matched multiple buildings in the reference data.

C) 1:0 relation: The predicted footprint did not match any building in the reference data.

D) 0:1 relation: The reference building did not match any footprint in the predicted result.

E) n:1 relation: The reference building matched multiple footprints in the predicted result.

F) n:m relation: Multiple reference buildings and footprints in the predicted results matched.

Figure 4 graphically depicts the assessment of diverse semantic relationships. In datasets lacking correspondence between footprints, 1:0 and 0:1 relationships could be identified. When predicted footprints matched only one reference building, we encountered 1:1 and 1:n scenarios. In such cases, the match of the corresponding reference building was examined in reverse. If the corresponding reference building had a single match, a 1:1 relationship was indicated. Conversely, multiple matches signify a 1:n relationship. Similarly, when the predicted footprint corresponded to multiple reference buildings, n:1 and n:m

relationships were established.

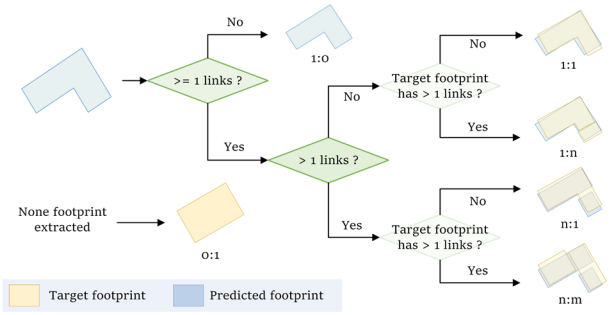

Figure 4 Flow chart and schematic diagram of semantic relationship between the extraction results and reference building.

4. Results

4.1 Grid-level completeness assessment

4.1.1 Grid classification and completeness results

Figure 5 illustrates different grid scenarios: Type I represents the background with no buildings; Type II indicates under-extraction; Type III signifies over-extraction; and Type IV denotes accurate building extraction at the grid level. The completeness assessment results, depicted in Figure 6a, illustrate the grid classification in Hyogo Prefecture. The analysis reveals that a significant majority of the grids fall under type I (61.8%) and type IV (27.7%), with a relatively low proportion of grids mistakenly identified as Type II and Type III at 7.2% and 3.3%. Overall, the extraction results demonstrate an accuracy rate approaching 90%.

Examining the spatial distribution of various grid types, Type IV predominated in the southern coastal area, coinciding with urban agglomerations in Hyogo Prefecture. In contrast, Type III grids were primarily situated in rural and wilderness areas. Type II grids were observed in regions featuring indistinguishable individual buildings and dense vegetation and were also found near topographical variations or built-up areas such as riverbanks. This is often caused by buildings exceeding the grid size (100 m).

Figure 6b presents the completeness of extracted footprint for various cities, represented in 10 bands (0.29–0.96). The histogram reveals that 54 of the 61 cities had completeness >0.6, with approximately half exceeding 0.8, indicating favorable footprint extraction for most urban areas. Spatially, the southern coastal urban agglomeration demonstrates higher completeness, which is consistent with the distribution of Type IV grids.

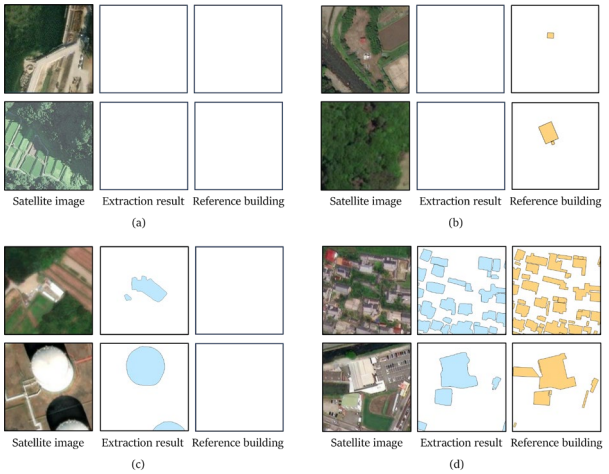

Figure 5. Typical scenarios representing different classified grids, including (a) Type I, (b) Type II, (c) Type III, and (d) Type IV.

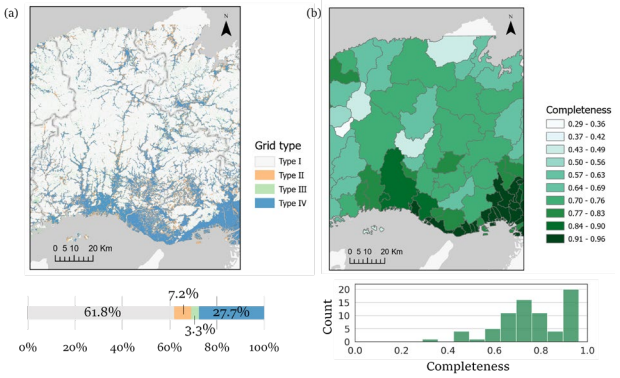

Figure 6. Spatial and frequency distribution results of grid-level completeness assessment in Hyogo prefecture, including (a) grid classification, and (b) estimated city completeness.

4.1.2 Evaluation results

To assess the completeness assessment accuracy, we employed two metrics: grid classification accuracy and correlation between the estimated and reference completeness. Figure 7 presents the confusion matrix and corresponding accuracies for various proxy data in grid classification. Combining population and land use data improved the grid classification accuracy by 1.6% and 2.6% compared to only using only land use and population

data. Upon analyzing the user's accuracy (UA) for each grid type, Type I and Type IV exhibited high UAs surpassing 0.9. The lower UA for Type II was due to misclassification due to non-building man-made surfaces (Figure 8a). In regions with a higher building probability like Type IV, this had a lower impact (Figure 8b). Type III presents challenges with reference to buildings in grids that lack population and built areas (Figure 8c). Nevertheless, the UA for Type III improved by 0.4 compared to a population-based approach, mainly due to unpopulated areas (Figure 8d). Incorporating land use data can considerably mitigate this misclassification.

Moreover, Figure 7 shows the relationship between the estimated and reference completeness using different proxy data (a2–c1). Incorporating population and land use data significantly improved the correlation by 0.22 and 0.53. Despite relatively confined result distribution, the linear equation slope was 0.7, indicating proxy data's tendency to underestimate result completeness (a3–c3 in Figure 7). This is attributed to the confusion matrix for grid classification, leading to an overall underestimation of completeness.

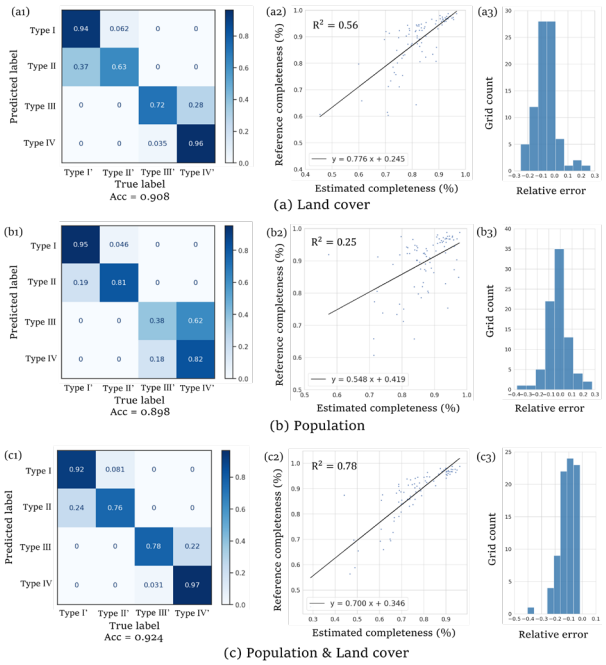

Figure 7. Accuracy evaluation of completeness assessment results by using (a) land cover, (b) population, and (c) population and land cover data as proxy data.

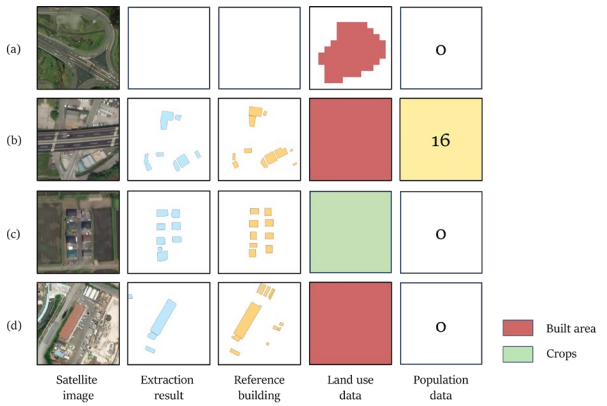

Figure 8. Illustration for reasons of special grid classification results, encompassing the following scenarios: (a) misclassification of Type I' as Type II, (b) correct classification of Type IV, (c) misclassification of Type IV' as Type III, (d) misclassification of Type IV' as Type III when sorely relying on population data.

4.2 Object-level quality evaluation

4.2.1 Overall and semantic accuracy results

Manual corrections were applied to the reference buildings within the validation area (Figure 1d) to establish the thresholds. To effectively address geometric errors in the reference buildings and include the majority of buildings in the first matching process, the matching algorithm employed a threshold value corresponding to a confidence level of 0.9. Consequently, the thresholds for the centroid displacement and overlap rate were set to 3 m and 0.4, strictly adhering to the specified requirements (Figure 9). This meticulous threshold selection ensured comprehensive and accurate matching results. The entire matching process for Numazu took 4 min 45 s, resulting in 74,822 TPs among the 92351 buildings. The precision of the extraction results, as listed in Table I was 0.842, whereas the recall was 0.803.

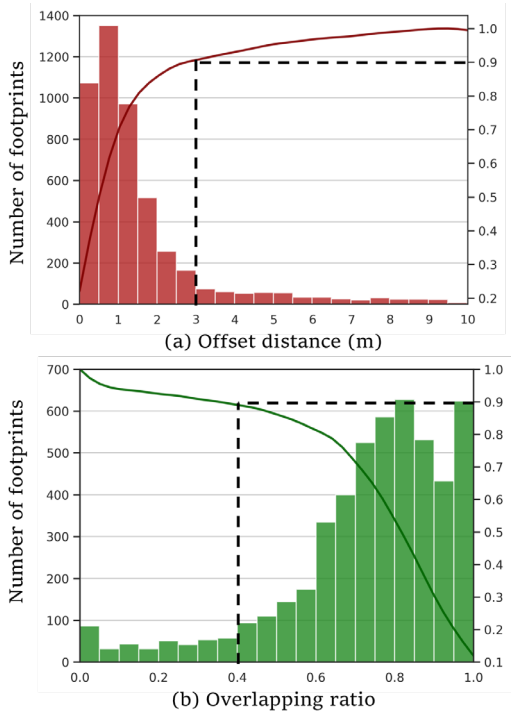

Figure 9. Frequency distribution histogram presented for (a) offset distance and (b) overlapping ratio between the reference building and the corrected ground truth in the validation area of Numazu.

After obtaining the matching results, the semantic relationships between the matched pairs were determined. Figure 10 illustrates the different semantic relationships, and Table II presents the related statistics for Numazu City. The table reveals 74,822 1:1 matching relationships, accounting for 68.7% of the total (Figure 10a). However, 8,402 extracted footprints (1:0) and 8,121 reference buildings (0:1) had no correspondence (Figure 10b and d), because of incorrect extraction and omission by the deep learning model. Furthermore, 17,529 complex semantic relationships existed, including 6,509 reference buildings (6%) with an n:1 relationship (Figure 10e). This suggests that the reference buildings contained more detailed semantic information than the extraction footprints. Additionally, 11,020 relationships, including 10,162 1:n relationships and 858 n:m relationships, had multiple neighboring extracted footprints that matched single or multiple reference buildings, forming a building group (Figure 10 c and f).

Table 1. Overall quality of footprint extraction in Numazu city

METRICS	PRECISION	RECALL	F1
VALUE	0.842	0.803	0.822

Figure 10. Illustration showcasing typical examples of different semantic relationships, namely (a) 1:1, (b) 1:0, (c) 1:n, (d) 0:1, (e) n:1, and (f) n:m relation.

Table 2. Statistics on the number of different semantic relations

Relation	1:0	1:1	1: n
Number of matched pairs	8402	74822	10162
Proportion	7.7%	68.7%	9.3%
Relation	**0:1**	**n:1**	**n:m**
Number of matched pairs	8121	6509	858
Proportion	7.5%	6.0%	0.8%

4.2.2 Evaluation results

To validate the accuracy of the quality evaluation

results, we assessed the extracted footprints within the validation area and compared the results with those obtained using different matching methods. Table 3 demonstrates that owing to the geometric disparities between the reference building and extraction results, the direct TWAO method exhibited a decrease in precision and recall by 0.080 and 0.114. Conversely, manual matching and the proposed method significantly mitigated the effects of geometric disparities in terms of precision, with marginal decreases of 0.005 and 0.013. The reductions in recall were 0.058 and 0.068, respectively, which were primarily attributed to discrepancies in the acquisition time of the reference data and satellite imagery used for extraction.

Furthermore, we assessed the accuracy of the semantic calculations using the proposed method and measured the precision and recall of various semantic relationships against manually matched semantic relations as the ground truth. As indicated in Table 4, the proposed matching method exhibits an overall matching precision and recall of over 99%. Moreover, for five of the six relationships (excluding n:m), the accuracy exceeded 0.98, validating the effectiveness of the method. The lower accuracy of the n:m relationship was attributed to the limited sample size.

Table 3. Evaluation results of different matching methods.

Matching Method	Reference Data	Precision	Recall	F1
IoU > 0.5	Corrected data	0.872	0.846	0.858
TWAO	Raw data	0.792	0.720	0.754
Manual	Raw data	0.867	0.788	0.826
Proposed method	Raw data	0.859	0.778	0.816

Table 4. Accuracy of different semantic relationships

Relation	1:0	1:1	1:n	0:1	n:1	n:m
Match recall	1.000	0.993	0.992	1.000	0.992	0.846
Match precision	0.991	0.997	0.985	0.990	0.985	0.786

5. Discussion

5.1 Grid size of completeness assessment

To test the effect of grid size, we assessed the completeness evaluation performance at different spatial resolutions (from 100 m to 1000 m) at 100 m intervals, as shown in Figure 11. First, increasing the grid resolution improves completeness. The average completeness difference between the 1000 m and the 100 m grids was 0.17 (Figure 11a). Second, Figure 11b illustrates the variation in the grid-type proportions with changing grid size. The proportions of the Types III and IV grids gradually increased, whereas those of the Types I and II grids decreased. Moreover, further analysis was performed to examine the effect of grid size on completeness accuracy (Figure 11c). Overall, the R^2 between the estimated and reference completeness values at different spatial resolutions (orange curves) decreased. Larger grid sizes lead to decreased classification accuracy, particularly for misclassified Type III grids, potentially resulting in an underestimation of completeness. So, selecting a 100 m grid size for this study is justified.

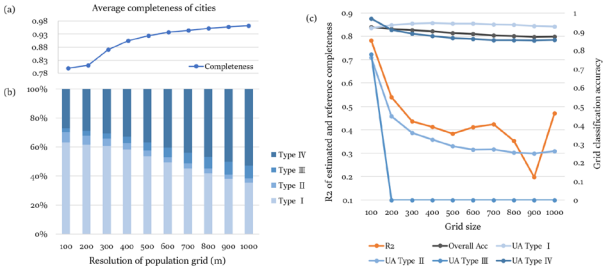

Figure 11. Impact of grid size on (a) estimated completeness, (b) different grid type proportions, and (c) completeness correlation and grid classification accuracy.

5.2 Thresholds of building matching

To comprehensively assess the chosen thresholds, we specify ten different sets (ranging from overlap rate 0 to 1 and centroid distance 0 to 10 m), aiming to understand their impact on matching results and semantic accuracy. Figure 12a illustrates the relationship between the overlap rate and precision-recall metrics. As the overlap rate

thresholds increased, TP precision improved from 0.71 to 1, while TP recall decreased from 1 to 0.78. Gradually increasing the overlap rate threshold reduced the number of recognized matching pairs, thus reducing the computation time. Regarding semantic accuracy, the overall precision and recall of the matching process exhibited varying patterns, as illustrated by b1 in Figure 12. Setting a small overlap rate threshold considers even minor overlaps as matches, leading to the misidentification of complex relationships (1:n, n:1, and n:m) and overlooking a relatively large number of 1:0, 1:1, and 0:1 relationships, resulting in lower matching recall and precision. Appropriate overlap rate threshold selection involves a tradeoff between algorithm accuracy and efficiency. Figure 12 suggests a threshold interval of 0.3–0.5 for optimal results and efficiency with higher semantic accuracy and minimized first matches. In contrast, the centroid distance minimally affected the TP determination accuracy, influencing the efficiency by approximately 1%, as shown in Figure 12 (a2). Furthermore, semantic accuracy declined slightly with increasing thresholds because of mistaken matches from the 0:1 to 1:1 relations.

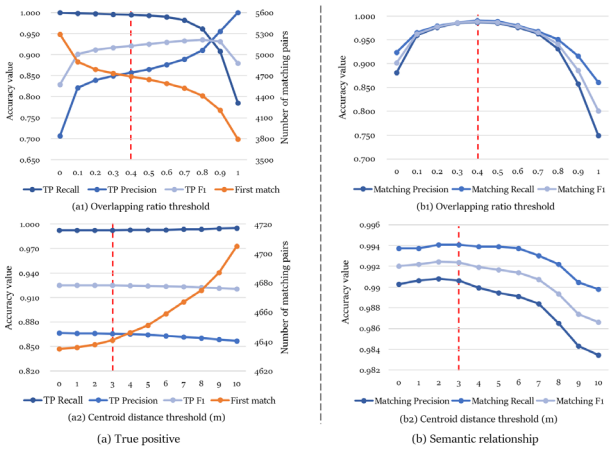

Figure 12. Influence of varying overlapping rate and centroid distance thresholds on (a) accuracy of true positives (TP) and number of matching pairs, and (b) matching accuracy of semantic relationships.

6. Conclusion

In this study, we proposed a two-level approach to evaluate large-scale building extraction results, comprising grid- and object-level assessments. At the first level, we classified the basic grid for each 100 m area using population data from the WorldPop dataset and built area information from the Esri land cover dataset as proxy data. This quantitative analysis helps assess extraction completeness when reference data are unavailable. At the second level, we enhanced the TWAO method by employing the overlap rate and centroid distance as matching metrics and introducing a two-step matching process. This approach effectively mitigated geometric errors and achieved extraction accuracy and semantic precision by meticulously comparing the extracted footprints with reference building data. The second level utilizes available reference data and provides a more detailed evaluation. To validate the effectiveness of the proposed method, we selected Hyogo Prefecture and Numazu City in Japan as the experimental areas. In Hyogo Prefecture, the results showed a 2.6% improvement in grid classification accuracy, and the R^2 of the estimated and reference completeness increased by 0.53 compared with single proxy data. In Numazu City, the quality evaluation of our method closely aligned with manually derived true values, outperforming the results obtained directly using the TWAO method. Furthermore, the improved matching method achieved a matching precision and recall of >0.99 in semantic relationship recognition, while maintaining high computational efficiency (4 min and 45 s for 92,351 buildings). In summary, our approach effectively assessed the large-scale building extraction results and interpreted the semantic relationships between the extraction results and actual buildings. This study provides crucial support and serves as a valuable reference for decision-making in urban planning and disaster risk assessment. In the future, we aim to enhance the accuracy of grid classification and address the complexities of semantic relationship matching. In addition, we aim to incorporate other dimensions, such as shape similarity, to offer a more

comprehensive evaluation of the results. Moreover, we plan to conduct experiments in diverse research regions, particularly in developing countries, to assess the applicability of this method on a global scale.

Reference

CHEN, S., OGAWA, Y., ZHAO, C. & SEKIMOTO, Y. 2023. Large-scale individual building extraction from open-source satellite imagery via super-resolution-based instance segmentation approach. *ISPRS Journal of Photogrammetry and Remote Sensing,* 195**,** 129-152.

DEY, E. K. & AWRANGJEB, M. 2020. A robust performance evaluation metric for extracted building boundaries from remote sensing data. *IEEE Journal of Selected Topics in Applied Earth Observations and Remote Sensing,* 13**,** 4030-4043.

FAN, H., ZIPF, A., FU, Q. & NEIS, P. 2014. Quality assessment for building footprints data on OpenStreetMap. *International Journal of Geographical Information Science,* 28**,** 700-719.

HERFORT, B., LAUTENBACH, S., DE ALBUQUERQUE, J. P., ANDERSON, J. & ZIPF, A. 2022. Investigating the digital divide in OpenStreetMap: Spatio-temporal analysis of inequalities in global urban building completeness.

HUANG, W., TANG, H. & XU, P. 2021. OEC-RNN: Object-oriented delineation of rooftops with edges and corners using the recurrent neural network from the aerial images. *IEEE Transactions on Geoscience and Remote Sensing,* 60**,** 1-12.

LIU, L., FU, Z., XIA, Y., LIN, H., DING, X. & LIAO, K. 2023. A building polygonal object matching method based on minimum bounding rectangle combinatorial optimization and relaxation labeling. *Transactions in GIS,* 27**,** 541-563.

MEMDUHOGLU, A. & BASARANER, M. 2022. An approach for multi-scale urban building data integration and enrichment through geometric matching and semantic web. *Cartography and Geographic Information Science,* 49**,** 1-17.

TIAN, Y., ZHOU, Q. & FU, X. 2019. An analysis of the evolution, completeness and spatial patterns of OpenStreetMap building data in China. *ISPRS International Journal of Geo-Information,* 8**,** 35.

ULLAH, T., LAUTENBACH, S., HERFORT, B., REINMUTH, M. & SCHORLEMMER, D. 2023. Assessing completeness of OpenStreetMap building footprints using MapSwipe. *ISPRS International Journal of Geo-Information,* 12**,** 143.

WANG, J., MENG, L., LI, W., YANG, W., YU, L. & XIA, G.-S. 2022. Learning to extract building footprints from off-nadir aerial images. *IEEE Transactions on Pattern Analysis and Machine Intelligence,* 45**,** 1294-1301.

ZENG, C., WANG, J. & LEHRBASS, B. 2013. An evaluation system for building footprint extraction from remotely sensed data. *IEEE Journal of Selected Topics in Applied Earth Observations and Remote Sensing,* 6**,** 1640-1652.

ZHANG, Y., ZHOU, Q., BROVELLI, M. A. & LI, W. 2022. Assessing OSM building completeness using population data. *International Journal of Geographical Information Science,* 36**,** 1443-1466.

ZHOU, Q., WANG, S. & LIU, Y. 2022a. Exploring the accuracy and completeness patterns of global land-cover/land-use data in OpenStreetMap. *Applied Geography,* 145**,** 102742.

ZHOU, Q., ZHANG, Y., CHANG, K. & BROVELLI, M. A. 2022b. Assessing OSM building completeness for almost 13,000 cities globally. *International Journal of Digital Earth,* 15**,** 2400-2421.

Advancing Building Extraction in Thailand using the YOLOv8 Segment Model on Open-source Data across Diverse Land-Use-Types

Bhanu Prasad Chintakindi*, Yoshiki Ogawa**, Yoshihide Sekimoto***

Abstract: The existing global building extraction models perform well in only a few land-use-types as each land-use-type comprises complex building patterns like low-rise buildings, high-rise buildings, isolated buildings, buildings surrounded by vegetation, and dense neighborhoods, and this limits the global extraction models to perform well across all land-use-types. This study addresses these challenges by devising seven dedicated building models for various land-use types in Bangkok, Thailand, through comprehensive training from scratch. Five of these models employ the YOLOv8 segment framework tailored for Commercial, Urban, SubUrban, Built-up, and Rural land-use types. Additionally, two models are trained to encompass all categories combined, using both YOLOv8 and YOLOv7 segment frameworks. The performance and adaptability of all seven models are meticulously compared. The findings underscore that, at an Intersection over Union (IoU) of 0.6, the five Building Models exhibit a precision ranging from 0.86 to 0.92, coupled with a recall of 0.69 to 0.83. In parallel, the two Building Models focused on all categories combined to achieve a precision of 0.69 and 0.70, alongside a recall of 0.56 and 0.55. These results illuminate the nuanced success of the specialized models across different land-use types.

Keywords: All Land-Use-Types (ALUT) Model, Individual Land-Use-Type (ILUT) Models, YOLOv8, YOLOv7

1. Introduction

The application of instance segmentation for building extraction from satellite imagery has yielded a range of methods catering to urban planning and digital city construction. Notable among these, Hu et al. (2021) introduced DABE-Net, incorporating squeeze-and-excitation operations and residual recurrent convolutional neural networks (RRCNN) for building extraction. Their innovation extended to an attention mechanism, enhancing accuracy, especially for small structures. Sirko et al. (2021) devised a U-Net model training pipeline, exploring diverse architecture, loss functions, regularization, pre-training, self-training, and post-processing techniques, resulting in improved instance segmentation performance, including challenging rural and urban scenarios, and generating the Open Buildings dataset. Chen et al. (2022) introduced a versatile approach involving reference-based color normalization and fine-tuning a mask R-CNN model for building footprint extraction from open-sourced satellite images. In 2023, Zhong et al. introduced the Multi-Swin Mask Transformer (MSMTransformer), a method for field extraction from remote sensing imagery that achieved exceptional performance and effectively resolved the issue of overlapping in dense scenes.

Challenges persist in the efficacy of global building extraction models across regions. Complex urban landscapes, diverse building structures, and low contrast between edifices and surroundings pose formidable hurdles (Yang et al., 2018). The intricate variability in building shapes and the environmental complexities impede automation efforts (Huang et al., 2019). One contributing factor to global models' limitations is the absence of spatial context within the loss function during training (Silvestre et al., 2023). Integrating spatial context in this way boosts the understanding of features in the surroundings, thereby enhancing building footprint extraction performance (Liu et al., 2023).

When considering model training strategies, the preference for training from scratch over fine-tuning emerges due to its enhanced generalization and efficacy in building extraction from low-resolution satellite imagery

* GISA member Department of Civil Engineering, The University of Tokyo **bhanu@g.ecc.u-tokyo.ac.jp**
** GISA member Center for Spatial Information Science, The University of Tokyo **ogawa@csis.u-tolyo.ac.jp**
*** GISA member Center for Spatial Information Science, The University of Tokyo **sekimoto@iis.u-tokyo.ac.jp**

through instance segmentation (NourEldeen et al., 2022). Contemporary research demonstrates that training from scratch yields performance comparable to fine-tuning, especially with increasing training iterations. On the other hand, fine-tuning may need help adapting to novel domains or few-shot scenarios due to a substantial semantic gap (Lo et al., 2022).

Moreover, it may fail to suppress extraneous information from earlier layers, undermining building extraction performance (Kong et al., 2023). Fine-tuning pre-trained models may also struggle with varied rooftop shapes, minor building omissions, and blurred edge predictions (Guo et al., 2022) (Wang et al., 2022). This underscores the preference for model training from scratch, promising enhanced performance and adaptability in building extraction from satellite imagery via instance segmentation.

In light of these considerations, this research endeavors to address the multifaceted challenges encountered in the realm of building extraction. It aims to bridge the gap between regional limitations, training strategy inefficiencies, and model performance. By advocating for training from scratch, this study seeks to enhance the accuracy, robustness, and adaptability of building extraction models when employing instance segmentation techniques.

2. Dataset

High-resolution satellite imagery poses challenges in developing countries like Thailand, often due to cost, limited resolution, cloud cover, and atmospheric interferences. Overcoming these obstacles, we leveraged 0.3m resolution satellite imagery from Mapbox for Bangkok province, Thailand. This open-source resource circumvents expenses and resolution limitations, though predominantly focusing on urban and commercial regions. To establish ground truth labels, we harnessed a repository of 2 million building footprints obtained from the Bangkok Metropolitan Administration GIS Portal, ensuring robust and open-source annotations for our study area.

Our research targets the development of distinct building models across varied land-use types, necessitating a coherent framework. Therefore, we adapted Bangkok's comprehensive land-use zoning plan, effective from 2013, as the reference framework, illustrated in Figure 1. We partitioned Bangkok Province into discrete zones representing Commercial, Urban, SubUrban, BuiltUp, and Rural Land-Use Types, each reflecting unique building patterns, densities, and characteristics, as portrayed in Figure 2. The distinctions are evident: Commercial areas host towering structures, while rural landscapes favor low-rise constructions. Urban domains showcase densely clustered buildings contrasted against suburban areas featuring solitary structures. In built-up zones, concentrated buildings are cloaked by vegetation.

Tailoring our research objectives, we aligned Bangkok's land-use plan with our study, ensuring relevance and accuracy, as demonstrated in Figures 1 and 2. To create our dataset, we cropped satellite imagery patches measuring 640 × 640 pixels, preserving a 30% overlap to prevent partial segmentation of edge buildings. Notably, the datasets were divided into training (70%), validation (20%), and testing (10%) subsets for each distinct land-use type, culminating in Table 1. The tabulation encapsulates image and instance counts, representing the number of satellite images and annotated buildings for each land-use category.

Creating the comprehensive All Land-Use-Types (ALUT) dataset demanded a nuanced approach. For its training subset, a balance was maintained by randomly selecting an equivalent number of images from Commercial, Urban, SubUrban, BuiltUp, and Rural Land-Use Types. This methodology curbed bias towards specific land-use categories while fostering a balanced training environment. The process was mirrored for the validation and testing subsets of ALUT, ensuring consistency and accuracy across datasets.

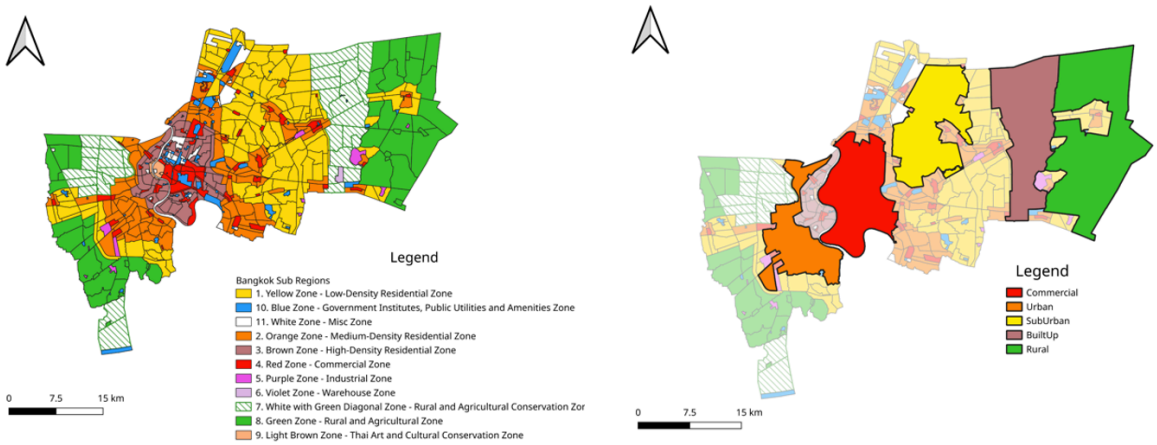

Fig:1 Bangkok's last comprehensive land-use zoning plan (effective from 2013) within the 50 district-bound is customized to the Bangkok Land-Use Plan for this research study.

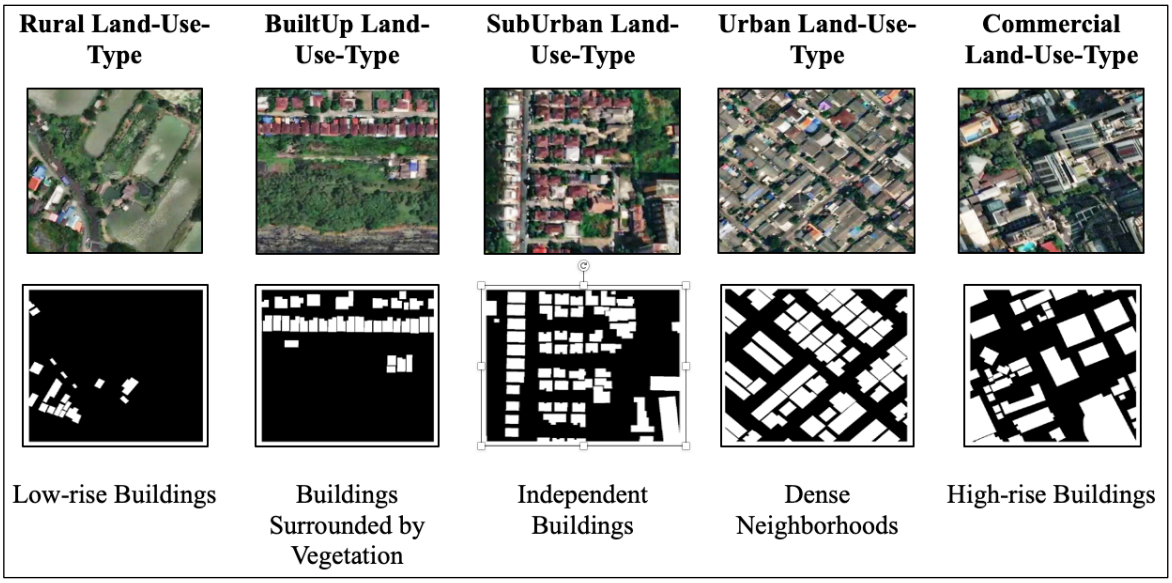

Fig:2 Examples of Rural, BuiltUp, SubUrban, Urban, and Commercial Land-Use-Types Training Data containing the Ground Truth Images and Ground Truth Labels.

Datasize		Rural	BuiltUp	SubUrban	Urban	Commercial	All Land-Use-Types
Total	*Images*	6755	5897	7935	5817	7789	6357
	Instances	121886	125302	391054	313558	445073	257336
Train	*Images*	4729	4128	5555	4072	5452	4442
	Instances	86334	86800	273487	221524	313039	179556
Test	*Images*	676	590	793	582	779	644
	Instances	12249	13176	38588	30877	42435	24770
Valid	*Images*	1350	1179	1587	1163	1558	1271
	Instances	23303	25326	78979	61157	89599	53010

Table 1: Dataset Size of the Individual Land-Use-Type Building Models

In essence, our dataset amalgamates meticulously curated satellite imagery and annotated building footprints, aligning with diverse land-use types and encompassing specialized training subsets as well as a comprehensive All Land-Use-Types dataset, which was strategically fashioned to eliminate bias and ensure impartial model training and evaluation.

3. Methodology

To overcome the challenges posed by intricate land-use patterns and complex urban environments, this study introduces a comprehensive methodology involving the development of seven specialized building models tailored to diverse land-use types within Bangkok, Thailand. The core strategy revolves around training these models from scratch, ensuring a robust and contextually accurate building extraction process.

Five of the seven models were meticulously developed utilizing the YOLOv8 segment framework. This framework is uniquely configured for each land-use type: Commercial, Urban, Suburban, BuiltUp, and Rural. This tailored approach optimizes the model's ability to discern distinct building patterns characteristic of each land-use type, resulting in enhanced accuracy and segmentation performance.

Moreover, the methodology encompasses creating two models intended to operate across All Categories. These models, constructed using both YOLOv8 and YOLOv7 segment frameworks, demonstrate the comprehensive applicability of our approach. A thorough assessment is conducted to evaluate and compare the efficacy of these seven models. Performance metrics encompassing precision, recall, and mAP 50 are meticulously examined to ascertain the models' adaptability to diverse land-use scenarios.

Specifically, the YOLOv8x-seg model is chosen as the focal point of this study due to its formidable capabilities (Jocher *et al.*, 2023). At the same time, the YOLOv7-seg model is also trained from scratch to validate its performance against the YOLOv8 segment models (Wang et al., 2022). These models are selected based on their compatibility with the dataset and the research objectives.

The training process is methodically conducted for each land-use type, ensuring optimal accuracy. The YOLOv8x-seg model undergoes rigorous training for all distinct land-use types (Commercial, Urban, SubUrban, built-up, Rural, and All-Categories combined land-use types). In contrast, the YOLOv7-seg model is trained exclusively for the All-Categories scenario. This systematic approach ensures the models' effectiveness in capturing intricate building patterns across the diverse Bangkok Province.

The validation process focuses on benchmarking the models against each other, emphasizing performance metrics and adaptability. By meticulously analyzing precision and recall rates, our methodology establishes a robust foundation for extracting buildings with unparalleled accuracy.

The ultimate goal of this study's methodology is to augment building extraction across varied land-use types within Bangkok, Thailand. We ascertain the models' capabilities in effectively addressing complex building patterns and urban environments through rigorous training, meticulous validation, and robust performance comparison.

4. Results

4.1 Accuracy Matrices

To ensure the accuracy of the building footprints extracted from the Individual-Land-Use-Type Building Models and ALUT Models, thorough cross-validation was conducted across all land-use categories. Evaluation metrics such as precision, recall, and mAP 50 were scrutinized for each model, and the results are tabulated in Tables 2, 3, and 4. An Intersection over Union (IoU) greater than 0.6 between predictions and ground-truth data was considered a true positive (TP) for reliable detection.

When assessing the performance of the Individual-Land-Use-Type Building Models, each trained and tested within its respective land-use category, the Rural Model stood out with the highest mAP 50 score of 0.90.

Table 2: Precision Matrix of the Individual Land-Use-Type Building Models in Different Land-Use-Types

Model Architecture	Individual Land-Use-Type Building Models	Precision (iou = 0.6, conf = 0.25)					
		Rural	Built-UP	Sub-Urban	Urban	Commercial	All Land-Use-Types
YOLOv8x-seg	Rural	**0.92**	0.54	0.09	0.30	0.15	0.36
	Built-UP	0.51	**0.91**	0.15	0.28	0.15	0.33
	Sub-Urban	0.48	0.52	**0.91**	0.45	0.49	0.63
	Urban	0.31	0.24	0.23	**0.88**	0.44	0.53
	Commercial	0.20	0.13	0.54	0.63	**0.86**	0.65
	All Land-Use-Types	0.76	0.72	0.71	0.72	0.63	**0.69**
YOLOv7-seg	All Land-Use-Types	0.75	0.72	0.74	0.74	0.64	**0.70**

Table 3: Recall Matrix of the Individual Land-Use-Type Building Models in Different Land-Use-Types

Model Architecture	Individual Land-Use-Type Building Models	Recall (iou = 0.6, conf = 0.25)					
		Rural	Built-UP	Sub-Urban	Urban	Commercial	All Land-Use-Types
YOLOv8x-seg	Rural	**0.83**	0.44	0.061	0.23	0.11	0.22
	Built-UP	0.30	**0.78**	0.10	0.21	0.09	0.21
	Sub-Urban	0.18	0.28	**0.77**	0.17	0.24	0.35
	Urban	0.12	0.14	0.11	**0.76**	0.26	0.34
	Commercial	0.04	0.04	0.25	0.34	**0.69**	0.36
	All Land-Use-Types	0.63	0.61	0.57	0.61	0.48	**0.56**
YOLOv7-seg	All Land-Use-Types	0.62	0.57	0.55	0.60	0.46	**0.55**

Table 4: mAP 50 Matrix of the Individual Land-Use-Type Building Models in Different Land-Use-Types

Model Architecture	Individual Land-Use-Type Building Models	mAP 50 (iou = 0.6, conf = 0.25)					
		Rural	Built-UP	Sub-Urban	Urban	Commercial	All Land-Use-Types
YOLOv8x-seg	Rural	**0.90**	0.45	0.06	0.22	0.10	0.25
	Built-UP	0.39	**0.87**	0.10	0.19	0.09	0.25
	Sub-Urban	0.31	0.38	**0.86**	0.28	0.34	0.49
	Urban	0.19	0.15	0.14	**0.85**	0.32	0.45
	Commercial	0.11	0.07	0.38	0.47	**0.80**	0.51
	All Land-Use-Types	0.70	0.67	0.65	0.67	0.55	**0.63**
YOLOv7-seg	All Land-Use-Types	0.68	0.65	0.64	0.67	0.54	**0.62**

It was closely followed by the BuiltUp Model at 0.87, the SubUrban Model at 0.86, the Urban Model at 0.85, and the Commercial Model at 0.80. The ALUT YOLO8 Model scored 0.63, while the ALUT YOLO7 Model exhibited the lowest mAP 50 of 0.62.

However, the scenario changed when cross-validating the Individual-Land-Use-Type Building Models across other land-use types. The ALUT YOLO8 and YOLO7 Models exhibited superior overall performance and generalizability. On the other hand, the other Individual Land-Use-Type Building Models demonstrated less favorable outcomes.

For instance, the Rural Model's precision was highest in its native Rural Land-Use-Type (0.92), declining to 0.54 in BuiltUp, 0.36 in All Land-Use-Types, 0.30 in Urban, 0.15 in Commercial, and finally 0.09 in SubUrban. In contrast, the ALUT YOLO8 and YOLO7 Models showcased precision ranging from 0.63 to 0.76 in other land-use types. Similar patterns were observed in recall and mAP 50 tables.

Directly comparing the ALUT YOLO8 and YOLO7 Models, the ALUT YOLO7 Model exhibited slightly better precision, outperforming the ALUT YOLO8 Model by nearly 1% in each land-use type. However, regarding recall and mAP 50, the ALUT YOLO8 Model beat its counterpart by a similar margin in all land-use types. This performance trend was visually corroborated by prediction plots, demonstrating the ALUT YOLO8 Model's slight superiority over the ALUT YOLO7 Model and its dominance over other Individual Land-Use-Type Building Models. This dynamic is vividly illustrated in Figures 3 and 4, where predicted building footprints from the models are showcased alongside a randomly selected Land-Use-Type test image and its corresponding ground truth label.

4.2 Prediction Inference

Examining Figures 3 and 4 reveals the exceptional capability of ALUT Models in accurately segmenting building footprints, even in challenging scenarios where buildings are closely situated or possess intricate structures, small connections, vegetation surroundings, or minute size. The performance of the ALUT YOLO8 and YOLO7 models consistently shines, exhibiting predictions closely aligned with ground truth labels.

This pattern persists across various land-use types. While individual land-use-type building models excel within their designated categories, the ALUT YOLO8 and YOLO7 models exhibit remarkable versatility, performing adeptly in all land-use scenarios. Notably, although underperforming in other contexts, the Rural Model detected small buildings in suburban, urban, and commercial zones, eluding the respective individual models. Similarly, the BuiltUp Model identified buildings surrounded by vegetation in SubUrban and Urban settings, surpassing the capabilities of its corresponding individual models despite lower accuracy levels.

Further examination of Tables 2, 3, and 4 in conjunction with Figures 3 and 4 reveals a significant insight: the All Land-Use-Type Building Model proves suitable for diverse areas encompassing low-rise, high-rise, isolated, vegetated, and densely populated building patterns. These patterns transcend their specific land-use designations and coexist across various categories. A comprehensive approach involving individual, and all land-use-type building models yields optimal results for accurate building identification across diverse land-use scenarios and intricate urban environments.

It is essential to acknowledge the study's limitations, particularly the models' inability to detect new buildings absent from the ground truth labels but present in satellite imagery. Future investigations will focus on enhancing the models' recall while maintaining precision, striving to capture newly emerging structures, and alleviating these challenges.

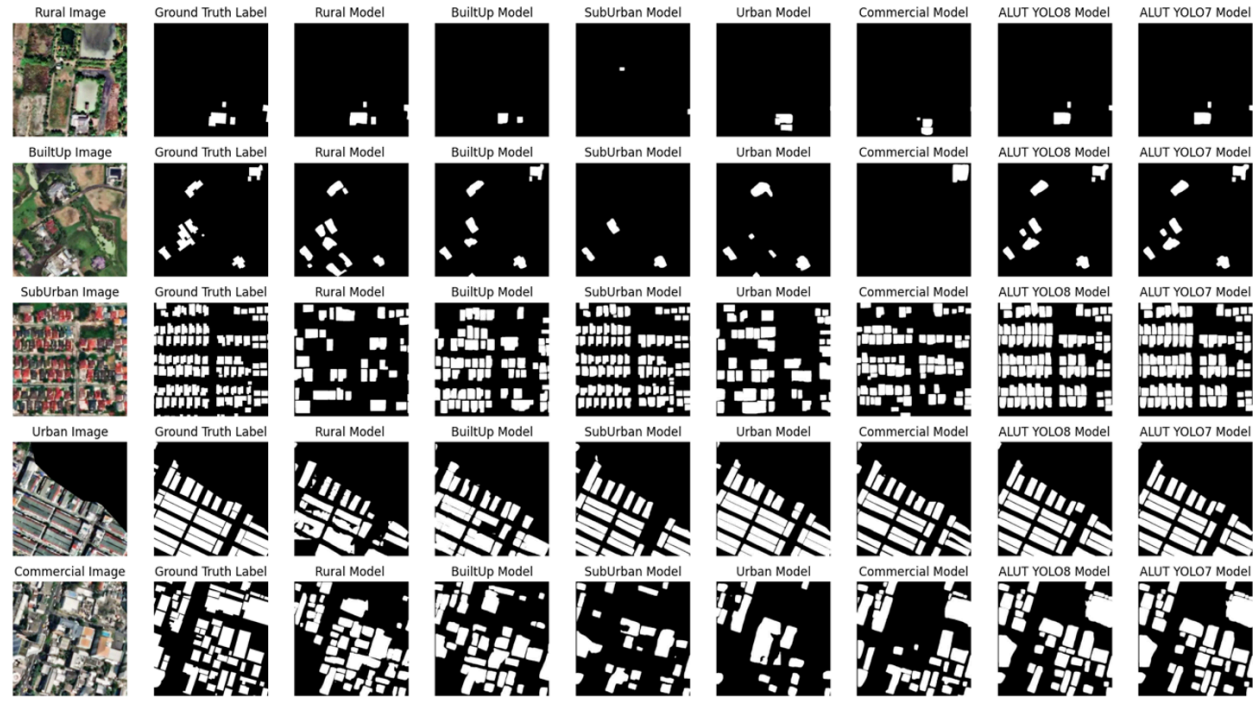

Fig 3: Predicted results by Individual Land-Use-Type Models and corresponding source image and ground truth label in

(a) Rural Area, (b) BuiltUp Area, (c) SubUrban Area, (d) Urban Area, and (e) Commercial Area

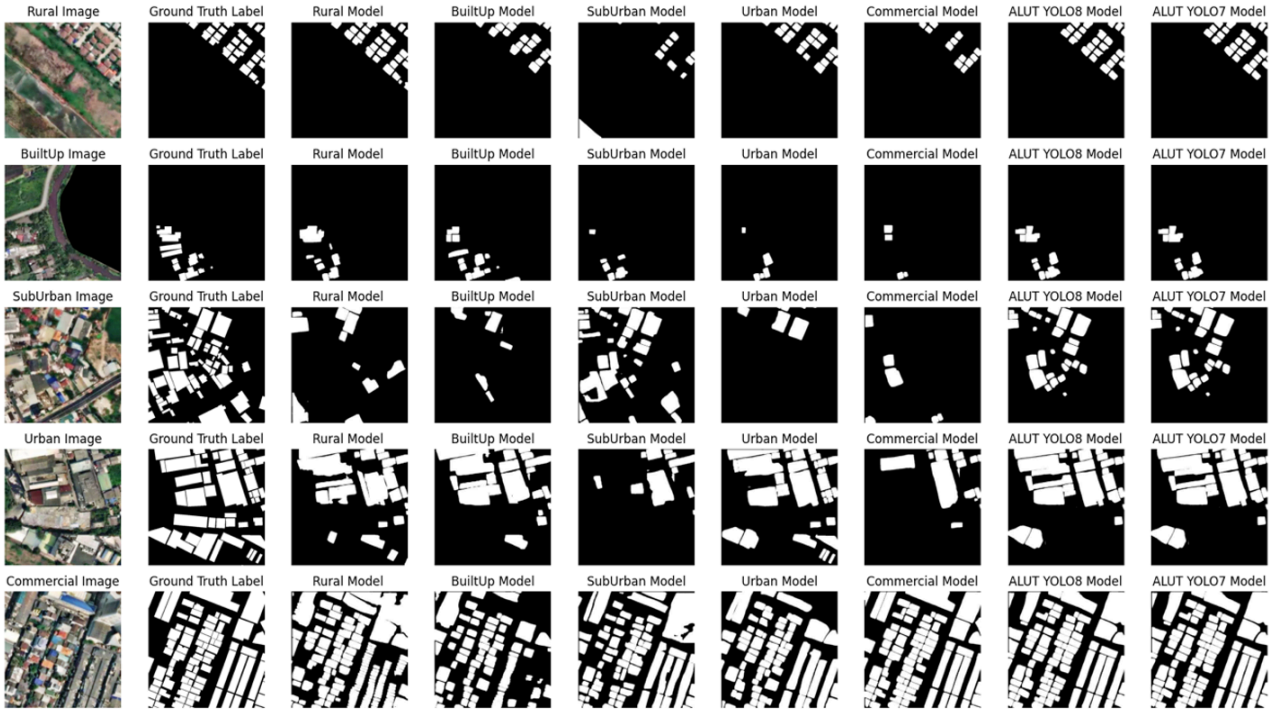

Fig 4: Predicted results by Individual Land-Use-Type Models and corresponding source image and ground truth label in

(a) Rural Area, (b) BuiltUp Area, (c) SubUrban Area, (d) Urban Area, and (e) Commercial Area

In conclusion, our study underscores the efficacy of utilizing individual and all land-use-type building models for precise building identification across Thailand's multifaceted land-use types and intricate urban landscapes. The results illuminate the potential of such models in addressing complex scenarios while shedding light on avenues for future improvements to achieve a comprehensive and accurate building detection solution.

5. Conclusion

In this study, we harnessed the potential of open-source data. We leveraged a training-from-scratch approach to validate the precision and resilience of the YOLOv8 model across Thailand's diverse land-use types. Our findings significantly contribute to the progression of building extraction techniques, shedding light on Thailand's intricacies and distinct characteristics. By delving into the challenges and nuances specific to Thailand's building detection landscape, our research advances the field and offers valuable insights that can drive further developments.

Our cross-validation efforts, including a comparative analysis with the YOLOv7 model, shed light on the performance and adaptability of the models developed. The comprehensive evaluation demonstrates the effectiveness of our approach, particularly the YOLOv8 model, in accurately identifying buildings across various land-use contexts. These findings hold promise for Thailand and other regions facing similar complexities in building detection.

However, like any research endeavor, our study comes with its limitations. While we achieved commendable results, the models currently need more ability to detect new buildings not present in the ground truth labels. This presents an avenue for future investigations, where we intend to enhance the recall capabilities of our models while upholding their precision. As we look ahead, our research offers a strong foundation for developing refined building extraction techniques that can transcend the unique challenges faced by Thailand's diverse land-use types. We envision continued efforts in refining our models, addressing their limitations, and expanding their applicability to other regions with analogous complexities. In doing so, we anticipate a significant impact on building extraction and its broader applications in urban planning and digital city construction.

References

Hu, Q. et al. (2021). “Automated building extraction using satellite remote sensing imagery,” Automation in Construction, 123, p. 103509. Available at: https://doi.org/10.1016/j.autcon.2020.103509.

Sirko, W., Kashubin, S., Ritter, M., Annkah, A., Bouchareb, Y.S.E., Dauphin, Y., Keysers, D., Neumann, M., Cisse, M. and Quinn, J., 2021. Continental-scale building detection from high-resolution satellite imagery. arXiv preprint arXiv:2107.12283.

Chen, S. et al. (2022). “Large-Scale Building Footprint Extraction from Open-Sourced Satellite Imagery via Instance Segmentation Approach,” IGARSS 2022 - 2022 IEEE International Geoscience and Remote Sensing Symposium [Preprint]. Available at: https://doi.org/10.1109/igarss46834.2022.9884762.

Zhong, B. et al. (2023). “Multi-Swin mask transformer for instance segmentation of agricultural field extraction,” Remote Sensing, 15(3), p. 549. Available at: https://doi.org/10.3390/rs15030549.

Yang, H.L. et al. (2018.) “Building extraction at scale using convolutional neural Network: Mapping of the United States,” IEEE Journal of Selected Topics in Applied Earth Observations and Remote Sensing, 11(8), pp. 2600–2614. Available at: https://doi.org/10.1109/jstars.2018.2835377.

Huang, J. et al. (2019). “Automatic building extraction from high-resolution aerial images and LiDAR data using gated residual refinement network,” Isprs Journal of Photogrammetry and Remote Sensing, 151, pp. 91–105. Available at: https://doi.org/10.1016/j.isprsjprs.2019.02.019.

Silvestre, J. and Prasad, S., 2023, June. Spatially constrained deep semantic segmentation of geospatial imagery for building footprint extraction. In Geospatial Informatics XIII (Vol. 12525, pp. 46-50). SPIE.

Liu, Y. et al. (2023). “Powering Fine-Tuning: Learning compatible and Class-Sensitive representations for domain adaption few-shot relation extraction,” in Lecture Notes in Computer Science, pp. 121–131. Available at: https://doi.org/10.1007/978-3-031-30678-5_10.

NourEldeen, A. et al. (2022). “Building Footprint Extraction from Low-Resolution Satellite Imagery using Instance Segmentation,” Frontiers in Scientific Research and Technology (Print), 0(0), p. 0. Available at: https://doi.org/10.21608/fsrt.2022.123397.1058.

Lo, E.Y.-M. et al. (2022) “Efficient Building Inventory Extraction from Satellite Imagery for Megacities,” Photogrammetric Engineering and Remote Sensing, 88(10), pp. 643–652. Available at: https://doi.org/10.14358/pers.21-00053r2.

Kong, H., Ling, C. and Zhang, K., (2023, April). Satellite Image Parcel Segmentation and Extraction Based on U-Net Convolution Neural Network Model. In 2023 IEEE International Conference on Control, Electronics and Computer Technology (ICCECT) (pp. 95–100). IEEE.

Guo, H. et al. (2022). “A coarse-to-fine boundary refinement network for building footprint extraction from remote sensing imagery,” Isprs Journal of Photogrammetry and Remote Sensing, 183, pp. 240–252. Available at: https://doi.org/10.1016/j.isprsjprs.2021.11.005.

Wang, A. and Zhang, P., (2022, August). Automatic Building Extraction based on Boundary Detection Network in Satellite Images. In 2022 29th International Conference on Geoinformatics (pp. 1–7). IEEE.

City Planning Department, Bangkok Metropolitan Administration. 2013. [Online]. http://iad.bangkok.go.th/sites/default/files/21.City%20Planning%20Department.pdf

Mapbox Satellite – Accessed on January 22, 2023 (https://docs.mapbox.com/data/tilesets/reference/mapbox-satellite/)

Bangkok Metropolitan Administration GIS Portal (open-source) – Accessed on April 24, 2023 https://bmagis.bangkok.go.th/portal/home/

Jocher, G., Chaurasia, A., & Qiu, J. (2023). YOLO by Ultralytics (Version 8.0.0) [Computer software]. https://github.com/ultralytics/ultralytics. (n.d.).

Wang, C.-Y., Bochkovskiy, A. & Liao, H.-Y.M. (2022). “YOLOv7: Trainable bag-of-freebies sets new state-of-the-art for real-time object detectors,” arXiv (Cornell University) [Preprint]. Available at: https://doi.org/10.48550/arxiv.2207.02696.

Marine Debris Monitoring and AI Application Optimization Plan by Geographic Characteristics and Research Devices

BoRam Kim*, Cholyoung Lee, Hynwoo Choi, TaeHoon Kim**

Abstract
As a problem arises with marine debris that is introduced into or discharged into the ocean and has harmful effects on the marine environment, research using various devices such as drones and CCTVs is being conducted. Considering the characteristics of marine debris distributed over a wide area, research based on remote sensing using artificial intelligence is currently underway. In this study, we compared and analyzed the optimal monitoring method for each research device and the use of artificial intelligence for efficient marine debris management. It is expected that it will be possible to establish a marine debris management plan tailored to the characteristics of each region by using different monitoring altitudes and cycles for each device and using appropriate artificial intelligence algorithms and analysis methods.

Keywords: Marine Debris, AI, OSHW, Drone, Remote Sensing

1. Introduction

Marine waste refers to solids that are intentionally or inadvertently left on the coast or are introduced and discharged into the sea and adversely affect the marine environment, regardless of material, type, and existing use. The National Oceanic and Atmospheric Administration (NOAA) says marine waste can hurt or kill marine life, interfere with safe navigation, and threaten human health. In addition, marine waste flows into the sea through various inflow sources, and the overall amount and type are reported.

Marine waste is recognized as a common problem in the world and requires international cooperation to solve it as it crosses borders along the ocean current and has a wide range of influences. Accordingly, international organizations and consultative bodies such as the G7, G20, APEC, ASEAN, and the EU are discussing or promoting various measures to solve the problem of marine waste.

South Korea is working with China, Japan, Russia, and North Korea to solve the problem of marine waste in the Northwest Pacific Ocean based on the Northwest Pacific Action Plan (NOWPAP) to manage marine waste that causes international conflicts. It is engaged in activities such as sharing the current status of marine waste in each country, discussing ways to manage marine waste, and promoting joint monitoring projects. Additionally, the 3rd Marine Environment Management Act's plan includes initiatives to strengthen the response to foreign garbage, eliminate blind spots in management, and improve the efficiency of the collection system. In accordance with the enforcement of the Marine Waste and Marine Pollution Deposits Management Act, plans for systematic management of marine waste and marine pollution deposits are being established and policies for collection and purification treatment are being promoted in earnest.

Various policies for collection and management are implemented, but standards for clear monitoring measures for the purpose of investigation and objects are still insufficient. For efficient collection and management of marine waste, distribution investigation, and research, it is necessary to present a new standard for monitoring marine waste by gas in consideration of the purpose of the survey, the object of investigation, and the characteristics of each point.

Therefore, in this study, the characteristics of marine waste monitoring for each gas were compared using gases used in marine waste monitoring methods before presenting a standard proposal for marine waste monitoring.

2. Study Method

In this study, marine waste was observed in actual waters using drones, self-made CCTVs, and mobile phones to compare the monitoring characteristics of each marine waste survey gas. Marine waste image data were collected for each gas, and monitoring characteristics for each gas were compared through this. In addition, existing marine waste monitoring measures were examined through literature review such as prior research and policies.

2.1. Study Area

The acquisition of research data by aircraft was conducted at a point near Guyeong Beach in Geoje Island. Geoje Island is the second largest island in Korea, located in the southern part of the country. The northeastern coast of Geoje Island is heavily affected by the estuary of the Nakdonggang River between Gimhae-si and Busan, and in particular, the Nakdonggang River estuary is open, or Nakdonggang River waste is flooded and accumulated in the event of floods or typhoons. In addition, many fish farms are distributed, so a lot of trash such as styrofoam and ropes due to fishing causes are also marked. Most of Geoje-si is used as a means of livelihood and tourism, such as fish farms, fishing, and pensions, but regular management is not conducted for the entire sea area, which is a problem. Therefore, it was judged as an area suitable for monitoring research on various marine waste objects, and the area was selected as a research target site (Figure 1). A simulation standard was designed using image data collected in the area.

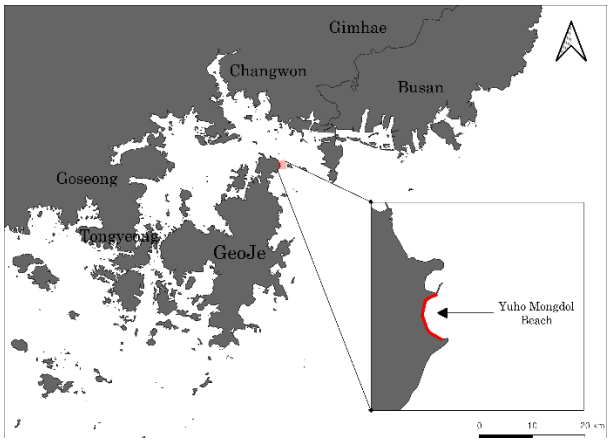

Figure 1. Study Area.

Figure 2. Photographs of the study site.

2.2. Acquisition of real-world data

The altitude of the drone was designated as 5m, the highest altitude for detecting marine waste, according to previous studies on the results of the drone's altitude and speed affecting the detection of marine waste. The drone collected data using DJI's Phantom 4 Pro 2 gas using a manual photographing method. Flags were planted at intervals of 5m in the area to be studied, and how well

KAGIS and TGEO members
The format of affiliation of authors is as follows.
* KAGIS member Kiost; marob@kiost.ac.kr, cylee82@kiost.ac.kr, **hwchoi@kiost.ac.kr**
** KAGIS member Kiost; thkim00@kiost.ac.kr, correspondence author

marine waste was distinguished at the distance between flags by altitude was compared.

CCTV was self-produced and used using open source hardware Raspberry Pi and Camera Module 3. Open source hardware has the advantage of being cheaper and easier to change shape than standard products because it assembles parts directly. Among them, the most popular Raspberry Pi 3B+ model was used. Unlike previous generation cameras, camera module 3 has characteristics of automatic focus and wide viewing angle (wide model limited). In the case of general CCTV, various accessories such as Internet connection and power connection are required, and it is convenient to check video information in a situation where a network environment is established, but marine waste generally occurs in areas where it is difficult to enter and exit with network connections and large equipment. Therefore, CCTV was self-produced and used for research using Raspberry Pi, which can easily collect data even with small equipment such as auxiliary batteries even in a barren environment. Data were collected by designating the altitude as 3m, the height at which CCTV best recognizes the license plate of the car.

Cell phone cameras have the advantage that anyone can easily film and report. Typically, marine waste management using mobile phones is carried out in the Sea Knights Terran activities. In the Bada Knights activity, the weight and volume of marine waste are estimated by taking pictures of the cell phone every 10m interval. However, in this study, images of marine waste were collected at intervals of 5m to compare and evaluate the degree of identification of marine waste by gas. Afterwards, in order to analyze marine waste, the degree of identification and analysis of marine waste within a length of 5m was checked, and the degree of identification of marine waste within a length interval of 10m was estimated by applying it. The iPhone 13PRO was used as the model, and the specs of all the gases used in the study are as follows.(Table 1)

	Drone	CCTV	Cellphone
Model	Phantom 4 Pro v.2	Raspberry Pi 3B+, Camera 3	iPhone 13 Pro
Pixel	5472x3684	4608x2592	4032x3024
Altitude	5m	3m	-

Table 1. Research Equipment

2.3. Monitoring Application Review

Prior research, research projects, and policies in Korea, the United States, and Japan were examined to investigate the current status of using monitoring measures for marine waste research. In order to compare the artificial intelligence methods used in marine waste research, trends were examined through search terms in Google Scala academic search. The search terms were <marine debris>, <ai>, <detection>, <monitoring>, <drone>, <cctv>, and <phone>, and the methods were compared for studies that performed image analysis by searching and combining the above words alone. Through a total of 10 documents, the research and artificial intelligence application trends of marine waste were examined.

3. Results and Considerations

Research trends and artificial intelligence application trends were examined through data collection and literature review in waters where marine waste remains. Matters to be considered when preparing a plan to monitor marine waste for each gas and details of each matter are as follows. (Table 2)

	Drone	CCTV	Cellphone
Pixel (Camera)	5472x3684	4608x2592	4032x3024
Power	5870mAh	Power connection	3095mAh
Available time	30m	All time	20h
Research cycle	month	hour	Event
Monitoring Application Plan	Production of distribution map Calculation of distribution area Count calculation (detection)	Estimation of inflow Estimation of inflows Time series change calculation	weight estimation volume estimation

Table 2. Research by Device

As a result of comparing and analyzing studies that monitor marine waste by gas, research using drones can confirm the map mapping of marine waste, the distribution area of marine waste on the beach, and the number of marine waste. CCTV research is conducting monitoring and management to track the movement of marine waste and observe long-term changes. Research using mobile phones included estimation of weight and distribution through the operation of the foundation for reporting marine waste through citizen participation.

As a result of the experiment, there were limitations in that the length, width, accessibility, and number of passengers were not considered for each sea area, and it is expected that a clearer and systematic standard design will be possible.

In addition, all gases were analyzed after collecting image data, and image collection may be missing due to differences in the amount of light that changes according to changes in solar altitude and weather, and this phenomenon occurred in objects such as styrofoam in an actual research data collection environment. Therefore, it is expected that the standard plan can be made in more detail by adjusting the camera exposure factor.

In addition, in the case of CCTV and cell phone cameras that do not shoot vertically, distortion may occur depending on how the direction of shooting the object is set. There is no problem in research that simply identifies the number and distribution, but studies that require accurate behavioral analysis such as distribution area, amount of existence, and weight estimation are considered to require research in the direction of reducing distortion.

4. Conclusion

In this study, the monitoring characteristics of drones, CCTV, and mobile phones were examined through a review of image data collection literature for each gas for monitoring marine waste monitoring. In the case of drones, it is suitable to monitor the degree of change in marine waste in the entire sea area at a monthly period, and CCTV and mobile phones are used to collect long-term data for time-series changes and monitor information on event marine waste. In the future, we would like to present a new installation standard for marine waste monitoring by analyzing the degree of identification and detection of marine waste on the image through more detailed items and artificial intelligence. The results of this study are expected to be used as basic data when designing standards.

Acknowledgement

This research was supported by Development of source identification and apportionment methods for toxic substances in marine environments program of Korea institute of Marine Scinece & Technology Promotion(KIMST) funded by the Ministry of Oceans and Fisheries(KIMST-20220534)

References (in Harvard style)

J. Lee and H. So, “A Strategy for Marine Litter Management in Gyeonggi-Do,” Gyeonggi

Research Institute, Dec. 2012, pp. 35

L. Cha, H. Han, H. Cho, U. Aan, and S. Kim, "Marine life damage Characteristics and Marine debris of Korea coast," J. of the Korean Society for Marine E

M. Jeong, N. Kim, M. Park, and H. Yoon, "The Characteristics of the Compositions and Spatial Distributions of Submerged Marine Debris in the East Sea," J. of the Korean Society of Marine Environment & Safety, vol. 27, JKIECS, vol. 17, no. 06, 1249-1258,

K. Topouzelis, D. Papageorgiou, A. Karagaitanakis, A. Papakonstantinou, and M. Ballesteros, "Remote Sensing of Sea Surface Artificial Floating Plastic Targets with Sentinel-2 and Unmanned Aerial Systems(Plastic Litter Project 2019)," Remote Sensing, vol. 12, no. 12, 2020, https://doi.org/10.3390/rs12122013

S. Jang, S. Lee, S. Oh, D. Kim, and H. Yoon, "The Application of Unmanned Aerial Photograpy for Effective Monitoring of Marine Debris," J. of the Korean Society of Marine Environment & Safety, vol. 17, no. 04, 2011, pp. 307-314.

S. Kako, A. Isobe, and S. Magome, "Sequential monitoring of beach litter using webcams," J. of Marine Pollution Bulletin, vol. 60, no. 5, May 2010, pp. 775-779.

J. Oh, 2021, "Target Identification and Classification Based on Side-Scan Sonar Images of Submarine Debris," Master's Thesis, Soongsil University Graduate School, 2021.

Another approach to terrain mapping method utilizing Unmanned Surface Vehicle and Light Detection and Ranging at shallow water area: A case study at Budai Port's expansion sand filling project site.

*Amrico Hanafie[1], Kuan-Tsung Chang[2], Sheng-Yu Yu[3] (1. Master student, Dept. of Civil Eng. and Environmental Informatics, Minghsin Uni. of Science and Technology, 2. Corresponding author, Professor, Dept. of Civil Eng. and Environmental Informatics, Minghsin Uni. of Science and Technology, 3. Company Manager, Strong Engineering Consulting Co.)

Light Detection and Ranging or known as LiDAR is a great tool to capture the terrain map in a wide range in a short time, however there is one problem ground LiDAR has, it cannot penetrate below surface of water. Especially in the shoreline, lake, swamp, shallow water area. LiDAR most definitely feasible to scan the area however not under the water, thus where Unmanned Surface Vehicle, USV for short aiding the terrain mapping process. A small boat, small enough to be able to collect data close enough to surface up to 15cm of depth water while carrying a single beam. By taking a look at data that gathered at Budai Port's expansion sand filling project site both by USV and LiDAR, the data taken at the same time with a three different set of time period. This utilization of two tools will be explained in detail, combining together to create new terrain mapping method that is more efficient and viable in rough terrain.

Keywords: 3D Terrain Models, LiDAR, USV, Shallow water scanning

1. Introduction

Both Topography and Bathymetry have been studied independently (Gesch et al. 2016; Collin et al. 2018). However nature's risk such as coastal erosion, coastal defenses and flooding risk loom the scientific questionnaire as it required integrated approach to be able to understand (Collin et al. 2018). Thus performing Topography and Bathymetry separately are not optimal, risk such as different format, projection, accuracy and datum are present in complex way (Genchi et al. 2020). Nature challenges also presents such as strong winds, strong wave, alteration of low and high tides companied with strong waves.

Small number of studies have been performed with different set of equipment, in USA Coast by merging LiDAR data and hydrographic surveys (Gesch & Wilson 2001). In Philip Bay, Australia have performed scan using Bathymetric and topographic LiDAR (Quadros, Collier & Fraser 2008). Others studies have been reported even using airborne green LiDAR to create seamless topobathymetry map even in environmentally challenging coastal zones (high-turbidity water and high-energy tidal environment) model (Andersen et al. 2017). Over the French Polynesia Pleiades-1 triplet imaginary were used to retrieve a seamless map of the islands which the topography was achieved from stereo and tri-stereo photogrammetry and the bathymetry was achieved from quasi-nadiral multispectral data; the validation was performed by using airborne LiDAR topobathymetry measurements (Collin et al. 2018). And in the recent years study in Argentina have been performed in coastal zone aiming for low-cost price with high accuracy available (Genchi et al. 2020).

1.1. Methodology

This paper proposed the method of topobatymetry aiming at shallow water area such as shoreline and coastal zone or water body area filled with dense vegetation such as swamp, mangrove, lake, and manmade dam. By using Stationary LiDAR as reference to Backpack LiDAR both are integrated with USV for bathymetry. The key focus are proving utilization of Backpack LiDAR is much faster and flexible to use in rough terrain than the use of stationary LiDAR or UAV. Therefore using LiDAR equipment are separated by time frames whereas USV and GNSS are to be kept operating for interpolation and alignment (Figure 1).

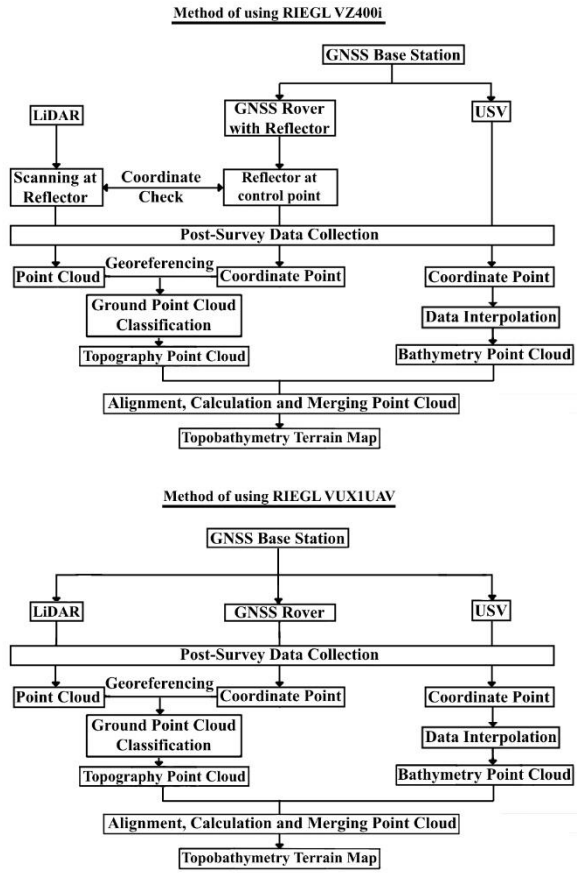

Figure 1 The process of using Stationary LiDAR (above) and Backpack LiDAR (below)

1.2. Study Area

Budai port official has laid out a blueprint to expand their port to the west side of the port from 2022. The port has long laid their foundation shown by below (figure 2).

Figure 2 Top-view of budai port sand-filling site taken via google earth (2022)

To get accurate data in calculating how much volume of sand needed to fill the water inside the seawall. The contractor of the site requested that the area needed to be thoroughly scanned using LiDAR and possibly under the water as well. Scanning seaside area using LiDAR yielded excellent result on the land, however the laser cannot penetrate anything under the water surface, the smallest boat available are bigger than what the shallow water areas are possible to scanned, resulting small area underwater scanning, and redundant manpower and time wasted. There is solution to this problem, with recent deployment in Taiwan starting the year 2021, The Surveyor companies started adopting Unmanned Surface Vehicle, USV in short. With size 100*65*30cm dimension and able to carry single beam with 15cm at the lowest possible depth data captured, a boat that small is highly optimal with this scenario. With 72,787.47 m^2 wide area have been scanned using Backpack LiDAR RIEGL VUX1UAV and Ground LiDAR RIEGL VZ-400i. These LiDAR data are to be taken at the same time as USV boat GEOMATE Model 1 the small boat that scanned under the water surface.

2. Discussion

2.1. Preparation on-field

There are three main tools to be used in this terrain mapping method, firstly by setting base point and rover using the GNSS receiver. There are two GNSS receiver used at once per project. One used as a base, which can

also be linked by rover, LiDAR, and USV simultaneously. And another GNSS receiver used to rover to capture the coordinate taken on-field, CHCNAV iBase (Figure 2) used as base station and PrinCe i30 (Figure 2) used as rover, both are used at October 2022 and May 2023 survey mission. And CHCNAV iBase (Figure 3) used as base station and STONEX S9 (Figure 3) are used as rover at July 2023. With this coordinate data collected at the same time as operating LiDAR and USV, it will be used as georeference point for LiDAR cloud points.

Figure 2 CHCNAV iBase as base station (left) and PrinCe i30 as rover (right)

Figure 3 CHCNAV iBase as base station (left) and STONEX S9 as rover (right)

Secondly, the use of LiDAR. To capture the project site's Cloud points, in this paper will be using RIEGL product, specifically RIEGL VUX1UAV (Figure 4) that is used at October 2022. The striding speed will be around 1 - 1.08m/s or roughly around 2 knot as stride as slowest and has most stability of average Asian (Rahman et al. 2012). LiDAR laser pulse repetition rate are recorded at 100 KHz. Another LiDAR that have been used in this project is RIEGL VZ-400i (Figure 5) at May 2023 and July 2023. The specification can be shown table 2 below. The laser pulse repetition rate used are 100 KHz for close distance and 300 KHz for far and wide place. These cloud data will be transformed into readable DEM file.

Figure 4 RIEGL VUX1UAV (left) and the use of the LiDAR strapped to Backpack on the field (right)

Figure 5 RIEGL VZ-400i (left) and operation of the equipment scanning the while port visible (right)

Lastly, as the solution to a shallow water in this paper will be using USV. GEOMATE Model 1 (Figure 6). The specification can be seen table 1 below.

Table 1. GeoMate Model 1 Underwater Mapping System Specifications

Size	100*65*30cm
Draft depth	10cm
Satellite system	BOS B1/B2, GPS L1/L2, GLONASS L1/L2, GALILEO E1/E5, SBAS, QZSS
RTK positioning accuracy Plane	±8mm+1ppm
Inertial navigation accuracy	6°/h

Table 1. Cont.

Remote control signal	**2.4 GHz radio, network bridge and 4G**
Depth range	0.15-200m
Sounding accuracy	±1cm+0.1% D (D is water depth)
Sounding frequency	200Khz
Beam angle	6.5°±1°

The entirety of shallow water in this project will be scanned by this USV and its single beam. The data captured will be treated as another single beam boat project with 50 KHz sounding frequency, and the final product of this USV will be served as CSV file. Which later will be integrated with DEM file and will be mashed together forming Terrain map that encompassing both under the shallow water body and above the water surface.

Figure 6 top view of GEOMATE Mode l (left) and USV being operated at the port shallow water (right)

2.2. On-field data acquisition

Normally, the mission proceed with one personnel placing a GNSS receiver as base station linked it with USV and GNSS receiver as VRS Rover, Stationary LiDAR such as RIEGL VZ-400i Needed at least two personnel to operate with, and the personnel holding the VRS Rover also needed to hold Reflector to be placed on top of reference point when scanned with LiDAR later to be replaced with VRS Rover to record said point, this steps needed to be repeated for each reference point. USV itself is operated with two personnel at least and can be operated along with LiDAR scanning or at different time (Figure 7).

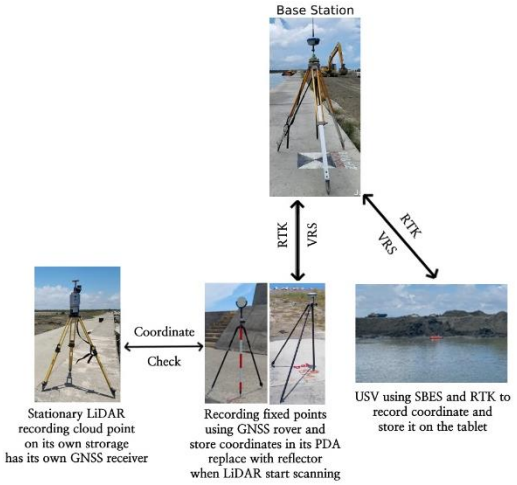

Figure 7 Visual schematic of Operation on-field using Stationary LiDAR and USV

The operation started at May 23rd 2023 from 10:57 to 14:00 detailing from establishing base station for 5 minutes, continuing with LiDAR scanning and RTK-VRS at the same time in 145 minutes starting from 11:35 to 14:00, while USV has its own schedule seeing the tide rises around 11:33 begin surveying until 12:20 taking 47 minutes to complete. The operation totally took roughly 3 hours or 192 minutes to complete. While at July 11th 2023, the operation started from 10:54, from establishing base station for 5 minutes, followed by RTK-VRS at control points from 10:59 to 11:35 taking 36 minutes, continued by LiDAR scanning in 127 minutes starting from 12:38 to 14:45, while USV still following the time when tides is high, although the tides are no longer a concern since at this point of time the contractor already plugged off the connection of water inside the lagoon from open seas, starting from 11:30 to 12:00 taking 30 Minutes to scan. Whole operation taken time totaling 193 minutes.

On the other hand using RIEGL VUX1UAV strapped on backpack, with one GNSS receiver used as base station that is linked with GNSS receiver as VRS Rover, LiDAR, and USV all at the same time. And depend on the manpower this method can be used by up to five personnel to save time, with one personnel assembling a GNSS receiver set as base station, two personnel operating the USV and two personnel

operating Back pack LiDAR and VRS Rover. This method will also increase accuracy since all the surveying mission taken at the same time. Another option that this method can be done by one personnel, which is in order of operation of using Bag pack LiDAR First and getting the coordinate checks using VRS Rover when the tide is low, followed by USV when the tide is high (Figure 8).

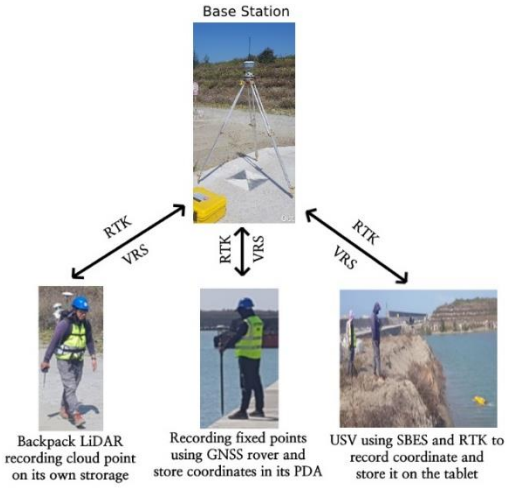

Figure 8 Visual schematic of Operation on-field using Backpack LiDAR and USV

At October 28th 2022, starting from establishing base station at 10:00 take 6 minutes. Continued by Backpack LiDAR to stride around the project sites for 59 minutes from 10:06 to 11:05, while the other operator record the project's control points using GNSS rover for 35 Minutes from 10:35 to 11:10. Lastly operating USV when the tide is high from 12:35 to 13:05 taking 30 minutes, taking whole 2 hours or 125 minutes to map the project site.

2.3. Data Processing

When processing the cloud data starting from Sampling the land surface, generating a surface model, correcting errors, deriving land-surface parameters and objects, lastly application of the resulting parameters and objects (Reuter & Hengl 2008), the processing part from raw data into point cloud performed using Riscan pro, and the rest of the process are using Lidar 360. The point cloud thus cleaned of the unnecessary object, and set classification of ground point cloud and clean as accurate as possible, after the data classified, processing the ground point cloud into DEM format data (figure 9).

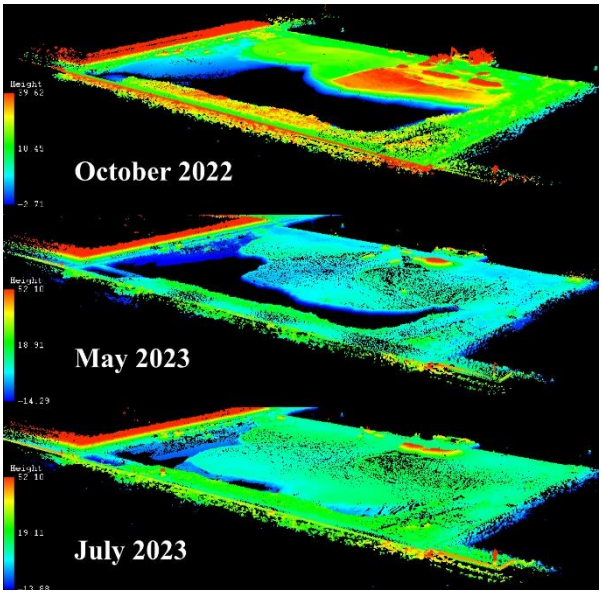

Figure 9 Point cloud data of progression of sand filling project October 2022-July 2023.

As for USV after data procession, following Figure 10, these are the same location taken however since 2022 the sand filling project has been progressing, the area of water to be able to survey is getting smaller, at glance the project will be done by early 2024.

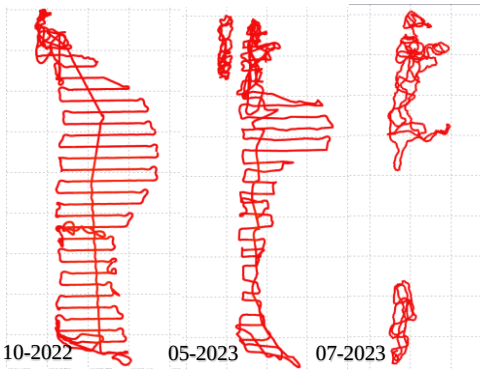

Figure 10 from left to right sand filling project has been progressing October 2022 – July 2023

The data are taken in parallel box trajectory with single lines in perpendicular trajectory with the parallel box, afterwards in the existing data, noises and unnecesarry point will be removed manually (figure 11).

Figure 11 Above data are before data cleaning and below data are after data cleaning, the purple line represent per meter data recorded.

After data cleaning the data will be refined, and shown per meter interval, finally exported into CSV file creating BPC (bathymetric point cloud) to be used together in topobathymetry.

The final step after converting Ground poinit cloud of the LIDAR and coordinate data taken from USV SBES, is to combine both data together into one, meerging it into one file afterwards to be able to process into DEM data (figure 12).

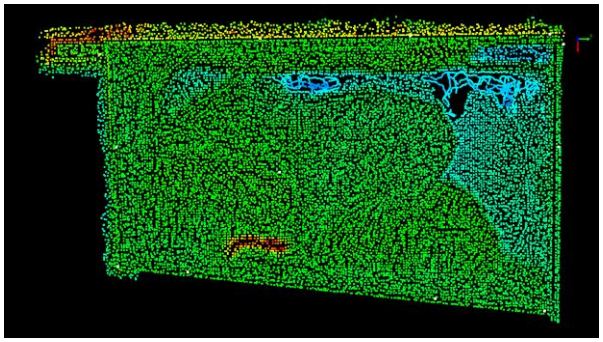

Figure 12 Merging both LiDAR and USV data together into 1 terrain map project

2.4. Result and Analysis

For this paper, will be showing the result of October 2022 to July 2023, the first step is to check the accuracy of the ground point cloud (GPC) prevalent to GNSS coordinate taken on the field, according to (Andersen 2017; Genchi et al. 2020). The mean absolute deviation (MAD) obtained from average of absolute value of each control point (CP) error, and root mean square error (RMSE) acquired from gap of GNSS coordinate and LiDAR GPC, which is formulated as follows:

$$MAD = \frac{1}{n}\sum_{i=1}^{n}|xi - \bar{X}| \qquad (1)$$

$$RMSE = \sqrt{\frac{1}{n}\sum_{i=1}^{n}(pi - ai)^2} \qquad (2)$$

Where xi are individual values and $\bar{X}$ are mean of observed values, and pi are coordinate of GNSS recorded on control points and ɑi are coordinate extracted from GPC of LiDAR. There are nine control points sample that recorded by GNSS and the center of the observed from GPC of Backpack LiDAR and Stationary LiDAR are extracted as closely as possible from GNSS coordinate and visually visible center of the control points.

The value of RSME of observed GPC of backpack LiDAR and stationary LiDAR both are lower than ±0.10m which is in x, y, z direction are 0.001m, 0.004m, 031m and 0.005m, 0.001m, 0.005m respectively, qualifies as highly accurate. However it is considered relative accuracy as some of the control point GPCs are not in the exact center of the observed control points and GNSS coordinate. In table 2, RMSE of the backpack LiDAR are bigger than stationary LiDAR, this can be explained by confidence level of the point clouds (see Aguilar et al. (2008) for further details), where the thinner the spread of the point clouds the higher accuracy level of said point clouds, since backpack LiDAR laser RMSE are 0.031m and stationary LiDAR are 0.005m, it is within reason as to why the point cloud spreads of backpack LiDAR are higher than Stationary LiDAR. In backpack LiDAR case the GPC is easier to extract the center of the control point's coordinate, hence in practice backpack LiDAR are carried by personnel that can stride freely on-site and are capturing point cloud closer to center of control point than stationary LiDAR even in high frequency as 300 KHz.

Table 2. Ground control point (GPC) error in x,y,z coordinates. All values are expressed in m. SD: standard deviation; MAD: mean absolute deviation; RMSE: root mean square error

GNSS 10/2022-Backpack LiDAR			
GPC	X	Y	Z
NO04	0.009	0.002	0.000
Z928	0.001	-0.006	-0.003
P01	0.008	0.006	-0.016
P02	-0.006	0.002	-0.014
P03	-0.006	0.005	-0.015
P04	0.006	0.001	-0.011
P05	-0.006	0.003	-0.006
P06	-0.007	0.005	-0.006
P07	0.003	-0.006	-0.022
Mean	0.000	0.001	-0.010
SD	0.007	0.004	0.007
MAD	0.006	0.003	0.006
RMSE	0.001	0.004	0.031
GNSS 07/2023-Stationary LiDAR			
GPC	X	Y	Z
NO04	0.001	0.005	0.010
Z928	0.017	-0.007	0.004
P01	0.001	0.001	-0.002
P02	0.000	-0.003	-0.006
P03	0.004	0.003	0.004
P04	-0.005	0.000	0.002
P05	0.002	-0.002	-0.004
P06	-0.006	0.001	0.008
P07	0.002	0.005	-0.002
Mean	0.002	0.000	0.002
SD	0.007	0.004	0.005
MAD	0.004	0.003	0.004
RMSE	0.005	0.001	0.005

To check the accuracy of USV there is method called Cross Section, it is when two lines are connected in perpendicular, when said lines are close, the depth can be compared, thus can be check how much differential of that depth (figure 13). The details of the calculation can be seen in this (Genchi et al. 2020) paper.

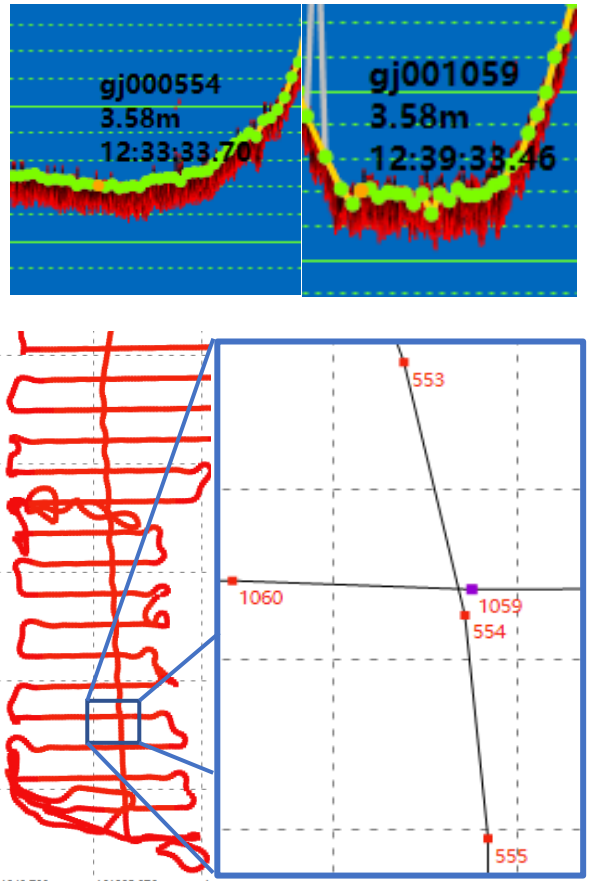

Figure 13 The Cross section method

Accuracy assessment of USV can be determined by using October 2022 data, considering it has the most water area surface before the sand filling project started in full swing in 2023. To determine accuracy of USV depth by picking up cross section point up to 30 samples in vertical direction are extracted and calculated in RMSE, mean absolute error (MAE) and other formula as follows:

$$MAE = \frac{1}{n}\sum_{i=1}^{n}|xi - yi| \quad (3)$$

$$R^2 = \left[\frac{\frac{1}{n}\sum_{i=1}^{n}(xi - \bar{x}i)(yi - \bar{y}i)}{\sqrt{\frac{1}{n}\sum_{i=1}^{n}(xi - \bar{x}i)^2 \frac{1}{n}\sum_{i=1}^{n}(yi - \bar{y}i)^2}}\right]^2 \quad (4)$$

Where R^2 are coefficient of determination and MAE are mean average error, xi are line in x axis and yi are line in y axis of crossed sectioned data. The RMSE and MAE value of USV are 0,062m and -0,006m respectively, in R^2

value showing 0,997 which is align with study conducted by (Curtarelli et al. 2015; Wu et al. 2019).

After assessing the accuracy of both LiDAR with filtered GPC and USV with filtered BPC, combining them together into one DEM data using Surfer, afterwards used to calculate the volume of sand moved out of dredging to the sand-filling site (figure 14).

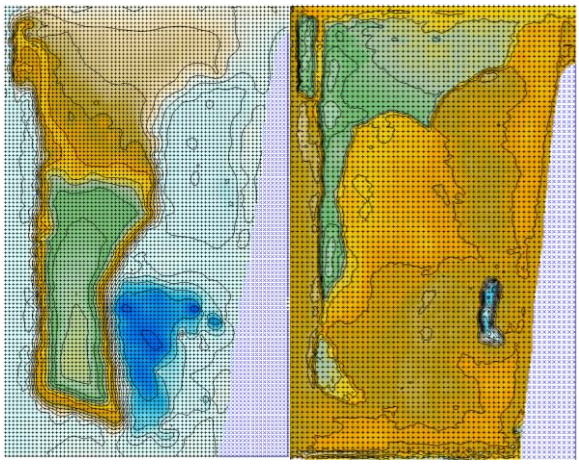

Figure 14 (Left) DEM and contour of October 2022 (Right) DEM and Contour of July 2023. Where green hue show water elevation, brown hue show ground elevation and blue hue show a height that is higher than ground elevation.

Lastly the data will show three lines of interest to intersect to show in this paper at 0K+080, 0K+190, and 0K+300. Which is showing significant changes of amount sand moved, other intersection showing similar result in October 2022–July 2023 period (figure 15).

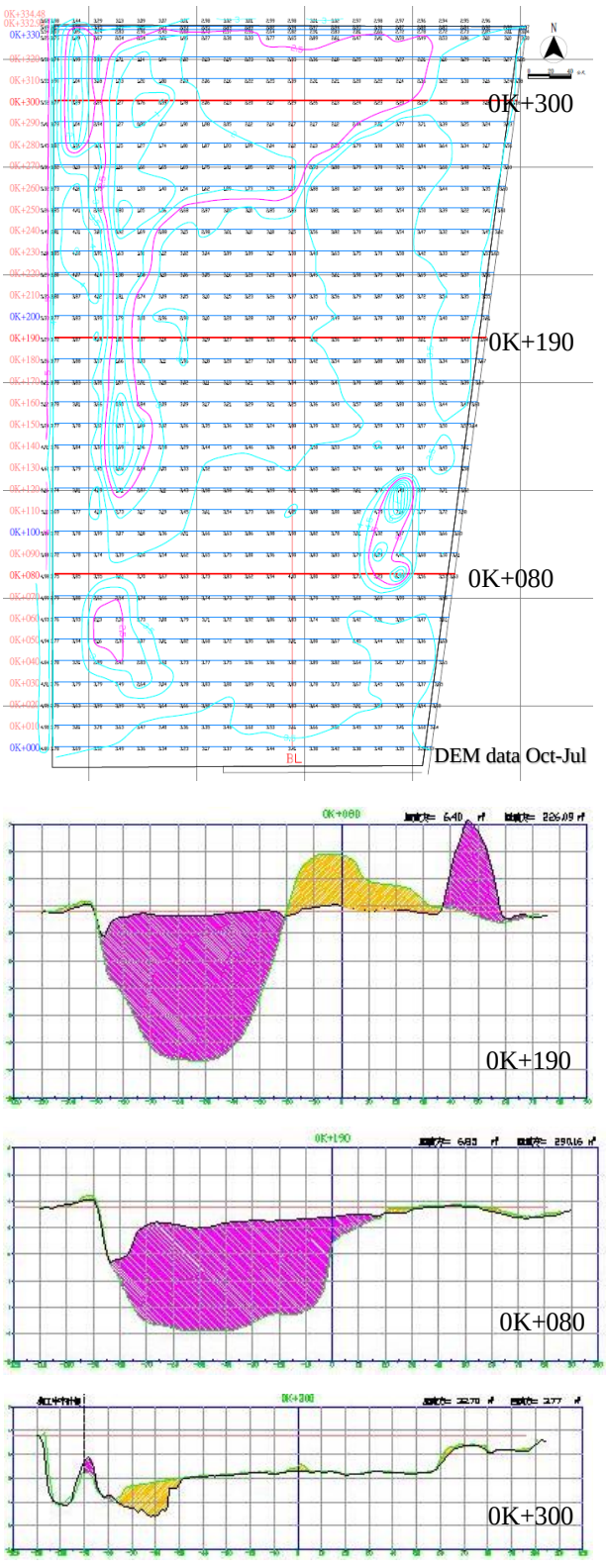

Figure 15 Terrain map of sand filling project of Budai port October 2022 –July 2023 period, the intersection shows how much sand have been moved, purple showing sand filled and yellow showing sand taken out.

To calculate the volume of the sand moved will be using common method of volume calculation. By calculating total of sand backfilled and reduced by total sand compacted.

$$\left(\sum\left(\frac{af+bf}{2,2}\right)\times t\right)-\left(\sum\left(\frac{ac+bc}{2,2}\right)\times t\right) \quad (5)$$

af = Area of previous sandfill

bf = Area of next sandfill

ac = Area of previous sand taken

bc = Area of next sand taken

t = Interval of distance between Intersection = 10m

From this calculation the amount of sand moved in October 2022 – July 2023 Period are 37,614.30 M^3.

3. Conclusion and future prospect

The combination of backpack LiDAR and USV can also be considered to use when facing upheaval and challenging geographic projects, where backpack LiDAR can course through rigorous open area with waterbody, where small UAV cannot operate due to strong wind or unable to go through the density of the0 swamp, or normal boat with single beam equipped unable to enter small pond of water in the area. The RMSE value of backpack LiDAR are bigger than stationary LiDAR 0.031m > 0.005m which is affecting the confidence level of the spreads of the point clouds (Aguilar et al. 2008), in spite of that the value were still small enough for backpack LiDAR to be alternative to stationary LiDAR in open space of challenging geographical feature.

When comparing time saving capability of backpack LiDAR and stationary LiDAR, it is visibly faster considering stationary LiDAR have to be stand of its tripod in stable and safe place first before placing the equipment on top of it and start scanning, not to mention a reflector must have been placed at control point during scanning process to create tie point. Where backpack LiDAR can be operated immediately once configuration setup is completed. The stationary LiDAR spent 145 minutes with recording the control points with GNSS and 127 minutes without recording the control points with GNSS, while backpack LiDAR only operates in 59 minutes, margin of time saved by using backpack LiDAR are 68~86 minutes in 72,787.47 m^2 wide scan area.

As for the USV data which is having RMSE of 0.062 and MAE of -0.006, which showing minimal depth error and statistically speaking the data are crowded in the middle tilted towards left side of graph. And the USV boat showing a good accuracy of R^2 equal to 0.997, when comparing to another study (Curtarelli et al. 2015; Wu et al. 2019; Genchi et al. 2020).

When both GPC and BPC data are obtained, combining them together into DEM resulting generating the contour lines that can be used as a reference in creating intersection line to calculate the volume of the sand moved in this project, this paper shows that combination of LiDAR and USV are a good tools to use when the intention is to create topobathymetric model and comparing two existing models at the different time frame to create for example changes in geographical area that has waterbody like swamp, lake, shoreline, man-built dam for inspection or in post-disaster event, or when comparing volume moved in suspected regression of water area in river or seaside caused by natural phenomenon, or just simply wanted to know the amount of sand moved precisely in that period of time, so the project owner can calculate exactly how much more sands needed to move and when the project is finished.

Acknowledgement

This paper was supported by Strong Engineering Consultants Co., Ltd. By providing the Budai's port data [110-112 annual channel water dredging project in Budai Port, ID:765] taken on-field to advance the method of on-field surveying technique notably in using USV in the recent year. And the academic program development of Minghsin University Science and Technology Department of Civil Engineering and Environmental Informatics in LiDAR application.

Reference

Andersen, MS, Gergely, Á, Al-Hamdani, Z, Steinbacher, F, Larsen, LR, Ernstsen, VB 2017, 'Processing and performance of topobathymetric lidar data for geomorphometric and morphological classification in a high-energy tidal environment', *Hydrology and Earth System Science*, Vol. 21, No. 1, pp. 43–63, DOI:10.5194/hess-21-43-2017.

Aguilar, FJ & Mills JP 2008, 'Accuracy Assessment of LiDAR-Derived Digital Elevation Models', *The Photogrammetic Record*, Vol. 23, No. 122, pp. 148-169, DOI:10.1080/13658810601079783.

Collin, A, Hench, JL, Pastol, Y, Planes, S, Thiault, L, Schmitt, RJ, Holbrook, SJ, Davies, N, Troyer, M 2018, 'High resolution topobathymetry using a Pleiades-1 triplet: Moorea Island in 3D', Remote Sensing of Environment, Vol. 208, No.4, pp.109–119, DOI:10.1016/j.rse.2018.02.015.

Curtarelli, M, Leão, J, Ogashawara, I, Lorenzzetti, J, Stech, J 2015, 'Assessment of Spatial Interpolation Methods to Map the Bathymetry of an Amazonian Hydroelectric Reservoir to Aid in Decision Making for Water Management', *ISPRS International. Journa of. Geo-Information*, Vol. *4*, No. 1, pp. 220-235, DOI:10.3390/ijgi4010220.

Genchi, SA, Vitale, AJ, Perillo, GME, Seitz, C, Delrieux, CA 2020, 'Mapping Topobathymetry in a Shallow Tidal Environment Using Low-Cost Technology', *Remote Sensing*, Vol. 12, No. 9, DOI:10.3390/rs12091394.

Gesch, D & Wilson, R 2001, 'Development of a seamless multisource topographic/bathymetric elevation model of Tampa Bay', *Marine Technology Society Journal*, Vol. 35, No. 4, pp.58–64. DOI:10.4031/002533201788058062.

Gesch, DB, Brock, JC, Parrish, CE, Rogers, JN, Wright, CW 2016, 'Introduction: Special Issue on Advances in Topobathymetric Mapping', *Advances in Topobathymetric Mapping, Models, and Applications*, Vol. 76, No. 1, pp. 1–3, DOI:10.2112/SI76-001.

Jin, J, Zhang, J, Shao, F, Lyu, Z, Wang, D 2018, 'A Novel Ocean Bathymetry Technology Based on an Unmanned Surface Vehicle', *Acta Oceanol Sinica*, Vol. 37, pp. 99–106, DOI:10.1007/s13131-018-1269-2.

Michel, J, Thierry, O, Antonio, A, Marc-Henri, D, Loye, A, Richard, M, Andrea, P 2012, 'Use of LIDAR in landslide investigations: A review', *Natural Hazards*, Vol. 61, pp. 5-28, DOI:10.1007/s11069-010-9634-2.

Quadros, ND, Collier, PA & Fraser, CS 2008, 'Integration of Bathymetric and Topographic LiDAR: A Preliminary Investigation', *Remote Sensing and Spatial Information Sciences*, Vol. 37, No. 1, pp. 1299–1304.

Rahman, K, Ghani, N, Kamil, A, Mustafa, A 2012, 'Analysis of Pedestrian Free Flow Speed in a Least Developing Country: A Factorial Design Study' *Research Journal of Applied Sciences, Engineering and Technology*, Vol. 4, No. 21, pp. 4299-4304.

Reuter, HI & Hengl, T 2008, *Geomorphometry: Concepts, Software, Applications*, Elsevier Science, Netherlands.

Wu, CY, Mossa, J, Mao, L, Almulla, M 2019, 'Comparison of different spatial interpolation methods for historical hydrographic data of the lowermost Mississippi River', *Annals of GIS*, Vol. 25, No. 1, pp. 1-19, DOI:10.1080/19475683.2019.1588781.

The Public Sentiment During the COVID-19 Lockdowns in China: A Comparison of Wuhan and Shanghai

Pei Xuanda*, Yuzuru Isoda**

Abstract In the context of the COVID-19 pandemic, most governments implemented lockdown policies to contain the spread of the virus. These policies elicited a broad range of responses from the population. This paper presents a spatiotemporal analysis of the differing reactions of the populations in Wuhan and Shanghai, aiming to understand shifts in public sentiment on social media during the lockdown. The methodology employs sentiment analysis using the BERT model to classify posts into six emotional categories, ranging from negative to positive. We found that Wuhan was generally more positive and optimistic towards the government-promoted lockdown policies.

Keywords: COVID-19, Sentiment Analysis, Phase of Disaster, Public Health

1. Introduction

Since 2019, the global onset of the novel coronavirus (COVID-19) has posed profound epidemiological and public health challenges (Dodds et al., 2020). In response, the Chinese government implemented the "Dynamic Zero COVID" strategy, prioritizing epidemiological containment with the potential for eradicating the virus. The inaugural deployment of these countermeasures occurred in Wuhan in 2020 and subsequently extended to numerous other urban centres in China. These measures included restrictions on interpersonal mobility, meticulous oversight of industrial operations, stringent regulation of transportation modalities—both private and public—and a categorical moratorium on private and public congregations (Sun et al., 2020). By 1 March 2022, Shanghai initiated a comprehensive lockdown, encompassing its entire population of 25 million. Rigorous testing regimes and lockdown protocols persisted until 25 June 2022 to quell potential COVID-19 resurgence nodes (Burki, 2022).

In a contrasting epidemiological paradigm, the "living with the virus" strategy emphasizes mitigation over eradication. Recognizing the multifaceted socio-economic and psychosocial reverberations of sustained lockdowns, this modality underscores coexistence with the virus under a robust protective regimen within the populace. It necessitates strategically disseminating empirically validated information and promoting behaviours to minimize transmission risk. This policy matrix pivots on three cardinal objectives: decelerating viral transmission trajectories, ensuring the resilience and optimal functionality of healthcare infrastructures, and modulating controlled viral circulation within communities without an explicit extermination agenda (Emanuel, 2022; Burki, 2022).

Expanding on policy dynamics, Parviainen et al. (2021) argue that in scenarios emblematic of "Building a Ship while Sailing It," the dynamism and immediacy of social media engender a "regime of futurity." This framework amplifies the urgency of policy decisions, particularly within disaster and crisis management paradigms. Therefore, a granular understanding of public sentiment and behavior becomes pivotal for effective policy articulation and implementation in COVID-19 containment.

In conclusion, this study aims to employ BERT's sentiment analysis model to classify posts into six emotional categories, ranging from negative to positive, to

* 学生会員　東北大大学院理学研究科　(Graduate School of Science, Tohoku University)　**peixuanda@gmail.com**
** 正会員　東北大学大学院理学研究科 (Graduate School of Science, Tohoku University) **isoda@tohoku.ac.jp**

compare and understand public sentiment during lockdowns. This will be juxtaposed with the phase of disaster model to explore the stages of public psychology under the lockdown policy during the significant crisis of COVID-19.

2. Literature Review

2.1 Phase of Disaster

The phases of disaster were developed to help psychologists map out individuals' psychological reactions during various stages of a disaster. Initially conceptualized by Zunin and Meyers (2000), this framework aims to aid people in recovering from disasters and prevent the development of mental health disorders. The model divides the phases into Pre-disaster, Impact, Heroic, Honeymoon, Disillusionment, and Reconstruction.

In the Pre-disaster phase, disasters provide varying degrees of advance notice to affected communities. In the Impact phase, Zunin and Meyers (2000) note that the loss of life and property due to a natural disaster is directly proportional to psychosocial reactions; a lack of warning leaves individuals feeling frightened and vulnerable. During the Heroic phase, individuals prioritise survival, assist others in need, and seek safety. While the actions of surviving individuals and first responders are often altruistic, their efforts may lack efficiency and productivity. The Honeymoon phase is characterised by increased hope and solidarity, particularly when government and volunteer aid are readily available; however, this psychological state may be short-lived. In the Disillusionment phase, disillusionment sets in as aid fails to restore people to their pre-disaster lifestyles, and losses become evident. Hostility towards the community is common during this phase. Finally, in the Reconstruction phase, individuals come to the realization that they must rebuild their lives and communities independently. Despite the suffering and losses, people begin to find meaning and opportunities for growth.

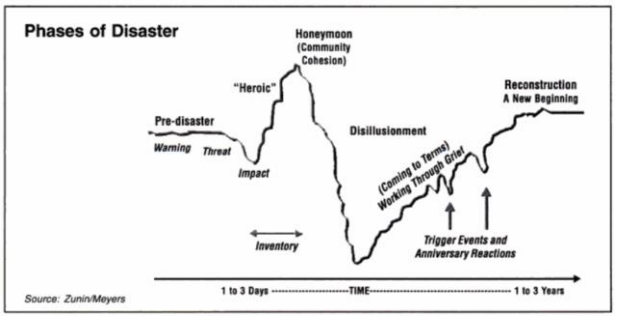

Fig. 1 The Phase of Disaster. Reprinted from DeWolf (2000:5).

To understand public sentiment during the pandemic elimination process, the following steps should be progressively undertaken:

1) collect social media data.

2) utilize a sentiment analysis model to evaluate public sentiment.

2.2 Sentiment Analysis

Graham et al. (2015) found that social media is extensively used during disasters. Sutton et al. (2008) explored the use of social media as shared knowledge and examined the characteristics of social media data during wildfire events. Vieweg et al. (2010) extracted disaster-related information from social media platforms, and Imran et al. (2013) proposed a method for automatically extracting information from disaster-related microblog posts. Singh et al. (2018) argued that many outbreaks and pandemics could have been more effectively controlled if experts had considered social media data, particularly during pandemics.

2.3 Sentiment Analysis and Lockdowns

Several studies have examined sentiment during lockdowns in China and globally (Barkur et al., 2020; Gupta et al., 2020; Sharma & Sharma, 2021). Scholars have identified that the increasing number of cases worldwide, the lack of interpersonal interactions, and restricted access to natural environments can lead to psychological distress among individuals (Cao et al., 2020; Mucci et al., 2020; Killgore et al., 2020). However, most existing studies focus primarily on the binary classification of sentiment from social media content, categorising posts as positive, neutral, or negative (Bhat et al., 2020;

Chakraborty et al., 2020; Wang et al., 2020). Such oversimplification of emotion classification hampers the identification of nuanced correlations between specific emotions (Xu et al., 2017). This lack of detail could result in overlooking the public's messages or misinterpreting the actual demands and public opinion.

2.4 Research Objective

While most sentiment studies concerning disasters have predominantly focused on assessing mental health and human behavior, there has been limited attention on integrating these findings with the phase of disaster model. Extending beyond previous research that utilized binary sentiment classifications to understand public sentiment during disasters, our study employs a more nuanced approach by incorporating six distinct emotions. This enriched classification not only complements the existing body of research but also addresses gaps in the literature by providing more comprehensive information. Therefore, this study aims to explore the differences between two distinct lockdown periods by comparing them with the phase of disaster model and broadening the sentiment classifications to prevent information loss.

3. Data and Methodology

3.1 Study Area

3.1.1 Wuhan and Shanghai

Wuhan, the capital city of Hubei province and the economic centre of central China, had a population of 12 million in 2020 (Wuhan Statistics Bureau, 2021). It ranks as the ninth most populous city in China. Wuhan was the initial epicentre of the COVID-19 pandemic and served as the first testing ground for lockdown policies. The lockdown in Wuhan commenced on January 23, 2020, and concluded on April 8, 2020, lasting a total of 76 days (BBC, 2020). Concurrently, the Chinese government executed a series of nationwide measures, such as establishing checkpoints at community entrances and instructing residents to remain indoors, to curtail public gatherings and maintain social distancing (National Health Commission of the People's Republic of China, 2020).

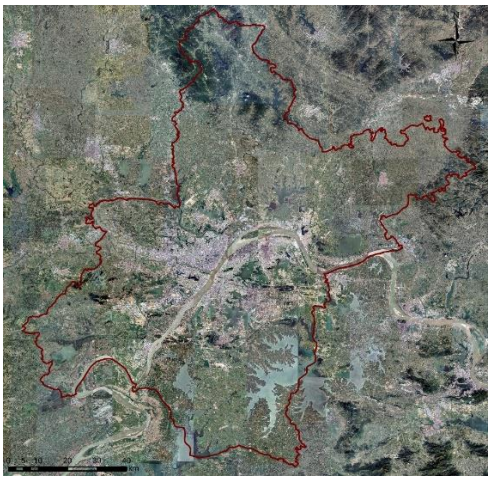

Fig. 2 Wuhan (Source: Google Earth, 2022)

In contrast to Wuhan, the lockdown in Shanghai commenced on March 1, 2022. All 25 million residents were locked down as part of China's national "dynamic zero COVID" policy. Mass testing and rigorous quarantine measures persisted until June 1, though some sources indicate an extension until August 7.

Fig. 3 Shanghai (Source: Google Earth,2022)

3.2 Methodology

Bidirectional Encoder Representations from Transformers (BERT) is a pre-training model that has shown significant effectiveness in improving tasks related to Natural Language Processing (NLP), particularly in languages other than English (Cui et al., 2020). Several scholars have employed the BERT model in Chinese language studies across various domains, including sentiment analysis of tweets, educational research, and

stock reviews (Xiang et al., 2021; Zheng et al., 2020; Li et al., 2021).

This study adopts a Chinese multi-emotion classification model based on BERT, as proposed by Peng et al. (2021). Peng's model utilizes six categories for emotion classification in social media content. We employ Scikit-learn and Ekphrasis libraries to process the data, that allow us to handle irregular syntax, emoticons, abbreviations, and other language anomalies that could otherwise adversely affect emotion classification.

The analysis will consist of the following steps. First, we will collect data from the Weibo platform. Second, we will classify tweets through Peng's model. The results will be divided into six categories: Happy, Sad, Neutral, Angry, Fear, and Surprise. This model can assign scores to each Weibo text from six emotional angles, with a total score of 100, and the one with the highest proportion will be judged as the main emotion. Third, we will visualize the daily emotional proportion and extract the words with the highest frequency of emotion-related ccurrences.

3.3 Data

The data for this study are collected from the social media platform Weibo, a Chinese-language microblogging service akin to Twitter launched in 2009. As of 2019, Weibo had over 463 million daily users. The retrieved data encompassed several variables: (1) the user's name and ID, (2) the publication date, (3) the content of the Weibo post, (4) metrics like the number of retweets, comments, and likes, and (5) the type of device used for posting—either a cell phone or a browser. Ethical considerations were rigorously observed throughout the data collection process. Data collection was executed using specific keywords associated with possessive particles in Chinese ("的"), and covered various periods: pre-lockdown, during lockdown, and post-lockdown. Moreover, data extraction during the lockdown was limited to keywords such as "lockdown," "control," "prevention," and "PCR." After pre-processing, the dataset comprised over 6 million Weibo posts.

4. Result

4.1 Trends in Daily Emotions

In Wuhan, happiness was the dominant emotion, especially during the lockdown. This period saw easily discernible spikes in positive sentiment. Following the city's reopening, there appeared to be a balance between negative and positive sentiments. Of the negative emotions, anger was most prominent, while other negative emotions were less evident. Shanghai presented a more intricate emotional tapestry. Unlike the clear emotional divisions seen in Wuhan, emotions in Shanghai were dispersed and multifaceted. Positive sentiments were notably less frequent in Shanghai than in Wuhan, and there was a surge in negative emotions during the city's lockdown. Yet, as the lockdown measures eased, positive sentiments began to resurface in Shanghai, albeit interspersed with occasional peaks of negativity.

(a) Wuhan

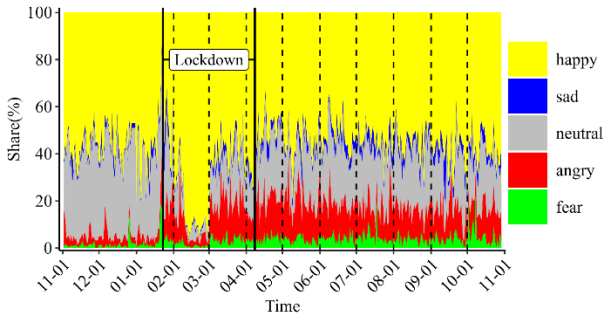

(b) Shanghai

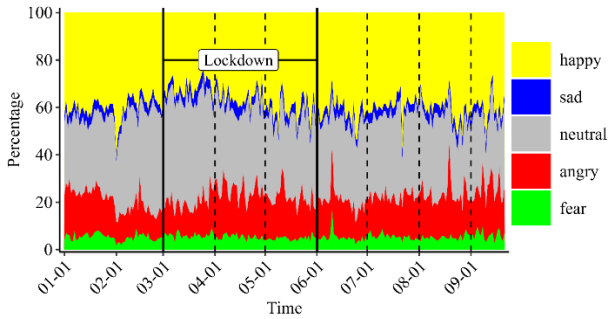

Fig 4. Trends in daily emotional expressions in Wuhan and Shanghai (Dashed lines indicate the commencement of each month).

When comparing the emotional landscapes of the two cities, Shanghai displayed a noticeable dip in happiness around the midpoint of its lockdown. The city also

exhibited more pronounced fluctuations in emotions like fear and sadness when compared to Wuhan. In Wuhan, at the beginning of the lockdown, both sadness and fear remained at consistently low levels. These emotions only experienced brief surges before swiftly declining again. A distinctive difference between the two cities during their respective lockdowns was the rate at which happiness levels recovered.

4.2 Words Frequency by Emotions

This section analyses the most commonly used words during the lockdown periods in Wuhan and Shanghai. As happiness saw a significant spike in Wuhan and anger was more prevalent in Shanghai, we will focus on presenting the word frequency results for these two emotions.

4.2.1 Wuhan – Happy

Fig.5 Wuhan word frequency for 'Happy' (From January to April)

In Wuhan, the phrase "Cheer up" stands out in expressions of happiness, signalling a prevalent theme of mutual support and encouragement. A significant portion of tweets expressing happiness revolves around words of encouragement and gratitude. Notably, a considerable number of these appreciative messages are directed towards healthcare professionals.

4.2.2 Wuhan - Angry

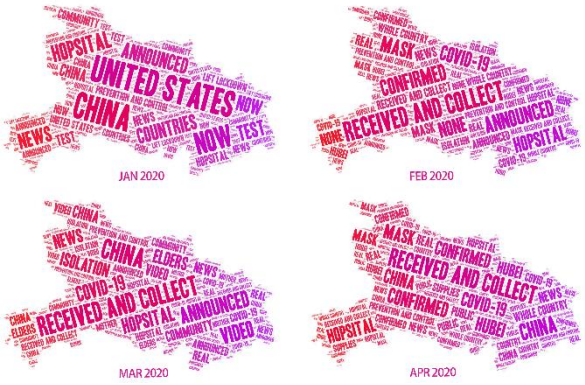

Fig.6 Wuhan word frequency for 'Angry' (From January to April)

For the 'angry' sentiment in Wuhan, the majority of tweets address issues such as the distribution of resources and rising food prices. Notably, the source of this anger isn't directly associated with COVID-19, but rather with the societal challenges that emerged in its wake and the perceived inadequate reactions from governmental entities.

4.2.3 Shanghai - Happy

Fig.7 Shanghai word frequency for 'Happy' (From March to May)

Regarding the 'happy' sentiment in Shanghai, a large portion of tweets relate to the receipt of supplies, whether from the government, professional entities, or from family and friends. This aligns with Maslow's hierarchy of needs, underscoring that fundamental needs, such as sustenance and water, remain priorities, even amidst a lockdown.

4.2.4 Shanghai – Angry

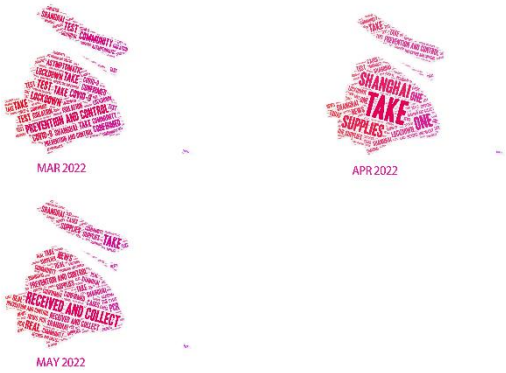

Fig.8 Shanghai word frequency for 'Angry' (From March to May)

Expressions of anger in Shanghai predominantly fall into two categories: the regularity of PCR tests and grievances related to the escalation in food prices or resource distribution. Often, this sentiment manifests as disappointment with the measures or responses from the local government. During the lockdown, the allocation of essential resources, especially food, remained at the forefront of public discourse. Contrasting with the tweets from Wuhan, where mutual encouragement was the norm, those from Shanghai leaned more towards calls for tangible support.

5. Discussion and Conclusion

5.1 Sentiment During Lockdown

Our findings indicate a consistent positive sentiment in Wuhan throughout the lockdown. In contrast, Shanghai exhibited a positive sentiment that generally fell below the average during the early and mid-phases of the lockdown. Notwithstanding, a commonality in both cases emerged in the trajectory of negative sentiment: an early surge, a middle-to-late decline, and sporadic fluctuations upon the cessation of the lockdown.

Though both Wuhan and Shanghai are densely populated urban hubs that underwent extended lockdowns due to substantial outbreaks, their public sentiments markedly diverged. This disparity can be attributed to the timeline of the lockdowns: Wuhan's occurring in the early days of the pandemic and Shanghai's two years post the initial outbreak. Government strategies, particularly those involving lockdowns, redirected the public's focus from their regular routines to prioritising COVID-19 prevention. The commencement of these strategies induced an array of emotions: early doubts regarding new guidelines, anxiety about the unfamiliar virus, and discontentment due to restricted outdoor engagements, all culminating in a downturn of public sentiment. Yet, Wuhan witnessed a swift uplift in positive sentiment during the initial phase of the lockdown, underpinned by a community spirit of mutual encouragement.

Contrastingly, the variance in sentiment between the two cities can be ascribed to differential public awareness structures. Being better informed about COVID-19, Shanghai's populace displayed a different emotional landscape than their Wuhan counterparts. As Vartti et al. (2009) elucidate, the decision-making in response to Emerging Infectious Diseases proved efficacious in Wuhan. The resilience of the Wuhan public was evident when, despite a mid-lockdown extension announcement by authorities, the prevailing sentiment bounced back promptly. When confronted with an array of risks and uncertainties, the collective reactions and choices of the public reflect their real-time circumstances. Further extending this analysis, She et al. (2022) spotlight cultural dynamics, such as xenophobia, as a potential driver of adverse sentiment. In the context of Shanghai, the primary catalyst for the outbreak was identified as imported cases from abroad.

5.2 Phase of Disaster

Within the unfolding saga of COVID-19, our observations align with those of Stowe et al. (2022) regarding introducing a 'Sandbar' phase. They defined the sandbar phase as a touching bottom of an opportunity to rest and reflect during the COVID-19 outbreak. Through our analysis of Wuhan, the sequential phases of impact, heroism, honeymoon, and disillusionment are distinctly discernible. The early uptick in negative sentiment and a dip in happiness characterizes the 'Impact' phase. A surge in positive sentiment, commencing in early February and plateauing by mid-month, demarcates the 'Heroic' and

'Honeymoon' phases. Post-lockdown, oscillating sentiments predominantly anchored in negativity are indicative of the 'Disillusionment' phase. An intriguing spike in negative sentiment possibly points towards the Sandbar phase, resonating with reflections on past policies or speculations on forthcoming strategies.

Examining Shanghai, we note that its 'Impact' phase extends considerably from March to the outset of April. When juxtaposed with Wuhan, the 'Heroic' and 'Honeymoon' phases in Shanghai manifest as transient and introduce elements of instability as early as May. We posit that this dynamic is intricately linked to the ripple effects of the Sandbar phase. Given its evolved position in the COVID-19 timeline, Shanghai's policy framework naturally expands, influenced in part by the populace's heightened cognisance and their experiential backdrop. Such evolution directly moulds public sentiment. Moreover, the distinct approaches to high-frequency PCR testing adopted in Shanghai could be a determinant in the truncated Heroic and Honeymoon phases. Following the cessation of the lockdown, a resurgence in positive sentiment might be construed as an extended Honeymoon phase, but its entanglement with negative undertones corroborates characteristics of the 'Disillusionment' phase.

In summation, the recognition of the Sandbar phase emerges as pivotal in our comprehension of COVID-19's trajectory. We contend that the pair of lockdowns examined are not mere episodic occurrences but represent extensions or reverberations of preceding policy interventions. Echoing Yue et al. (2021), our analysis underscores that public perceptions adopt a multifaceted approach rather than a linear one. Decision-making is predominantly influenced by prevailing challenges, where deliberations transcend the realm of public health, encompassing adherence to COVID-19-centric directives. Importantly, the risk perception isn't tethered exclusively to the disaster in isolation.

5.3 Conclusion

COVID-19 represents not an abrupt disaster but rather a protracted, intertwined, and recurrent calamity. The inaugural decision to initiate a lockdown was resoundingly effective, swiftly enacted upon. In such circumstances, a lockdown curtails the rampant spread of COVID-19, manages mortality rates to a degree, and quells public trepidation. In Shanghai, particular junctures witnessed a dominance of fluctuating negative sentiments. Employing the 'Phase of Disaster' framework to elucidate these temporal markers highlights a more structured progression in Wuhan, where the 'Impact' and 'Sandbar' phases manifest succinctly compared to Shanghai. Conversely, the 'Heroic' and 'Honeymoon' phases render a divergent tableau. Fast-forwarding two years, the focal point of public sentiment transitions towards Shanghai, now grappling with intricate societal challenges. As a sequel to the primordial lockdown strategy, elements such as the communal milieu and inhabitants' resilience merit consideration.

Moreover, the academic consensus underscores the potential repercussions of protracted lockdowns, encompassing a spectrum of psychological distress, spanning anxiety to depression. In summary, harnessing the 'Phase of Disaster' paradigm could provide policymakers with invaluable insights for future recalibrations. Real-time scrutiny facilitates the prompt identification and rectification of policy lacunae. In our forthcoming research endeavours, we aspire to discern consistent patterns across diverse lockdown settings. The objective remains to substantiate the hypothesis that the culmination of a lockdown in a given locale can potentially delineate benchmarks, calibrating public anticipations subsequently.

5.4 Limitations

This research is not devoid of limitations. Foremost, the behaviour of social media users, especially their posting patterns, remains elusive to our purview. It's untenable to verify with certainty the consistent posting trends of users throughout the three lockdown epochs. Consequently, we predicate our findings on the presumption that our voluminous dataset resonates with the broader demographic. Further, the enormity of the

dataset spanning the three delineated durations strains our computational capacities, thereby curbing our scope of data collection. This precipitates queries regarding the representative efficacy of our dataset. Secondly, the inclusion of detailed user profiles from social media platforms is hampered by ethical and privacy imperatives. To circumnavigate this predicament, we've endeavoured to anonymise all user-related data, thereby safeguarding individuals potentially reticent about publicising their emotional evolutions or attitudinal shifts.

Acknowledgment

This work was supported by JST SPRING, Grant Number JPMJSP2114.

References

Alford, J., & Head, B. W. (2017). Wicked and less wicked problems: A typology and a contingency framework. *Policy and Society*, *36*(3), 397–413. https://doi.org/10.1080/14494035.2017.1361634

Barkur, G., Vibha, & Kamath, G. B. (2020). Sentiment analysis of nationwide lockdown due to COVID 19 outbreak: Evidence from India. *Asian Journal of Psychiatry*, *51*, 102089. https://doi.org/10.1016/j.ajp.2020.102089

BBC. (2022, April 28). Shanghai Closed the City for One Month: The Official Insists on the "Dynamic Clearing" Policy Unchanged, How to Resolve the Crisis. BBC News. https://www.bbc.com/zhongwen/simp/chinese-news-61242081

Bhat, M., Qadri, M., Beg, N.-A., Kundroo, M., Ahanger, N., & Agarwal, B. (2020). Sentiment analysis of social media response on the Covid19 outbreak. *Brain, Behavior, and Immunity*, *87*, 136–137. https://doi.org/10.1016/j.bbi.2020.05.006

Briggs, D., Telford, L., Lloyd, A., Ellis, A., & Kotzé, J. (2021). *Lockdown: Social Harm in the Covid-19 Era*. Springer Nature.

Burki, T. (2022). Dynamic zero COVID policy in the fight against COVID. *The Lancet Respiratory Medicine*, *10*(6), e58–e59. https://doi.org/10.1016/s2213-2600(22)00142-4

Cao, W., Fang, Z., Hou, G., Han, M., Xu, X., Dong, J., & Zheng, J. (2020). The psychological impact of the COVID-19 epidemic on college students in China. *Psychiatry Research*, *287*, 112934. https://doi.org/10.1016/j.psychres.2020.112934

Ceci, L. (2022, January 18). *Top U.S. mobile social apps by session length 2019*. Statista. https://www.statista.com/statistics/579411/top-us-social-networking-apps-ranked-by-session-length/

Chakraborty, K., Bhatia, S., Bhattacharyya, S., Platos, J., Bag, R., & Hassanien, A. E. (2020). Sentiment Analysis of COVID-19 tweets by Deep Learning Classifiers—A study to show how popularity is affecting accuracy in social media. *Applied Soft Computing*, *97*, 106754. https://doi.org/10.1016/j.asoc.2020.106754

Chen, Z., Deng, X., Fang, L., Sun, K., Wu, Y., Che, T., Zou, J., Cai, J., Liu, H., Wang, Y., Wang, T., Tian, Y., Zheng, N., Yan, X., Sun, R., Xu, X., Zhou, X., Ge, S., Liang, Y., … Yu, H. (2022). *Epidemiological characteristics and transmission dynamics of the outbreak caused by the SARS-CoV-2 Omicron variant in Shanghai, China: A descriptive study*. https://doi.org/10.1101/2022.06.11.22276273

Cui, Y., Che, W., Liu, T., Qin, B., Wang, S., & Hu, G. (2020). Revisiting Pre-Trained Models for Chinese Natural Language Processing. *Findings of the Association for Computational Linguistics: EMNLP 2020*. https://doi.org/10.18653/v1/2020.findings-emnlp.58

DeWolfe, D. J. (2000). *Training manual for mental health and human service workers in major disasters*. US Department of Health and Human Services, Substance Abuse and Mental ….

Dodds, K., Broto, V. C., Detterbeck, K., Jones, M., Mamadouh, V., Ramutsindela, M., Varsanyi, M., Wachsmuth, D., & Woon, C. Y. (2020). The COVID-19 pandemic: Territorial, political and governance dimensions of the crisis. *Territory, Politics, Governance*,

8(3), 289–298. https://doi.org/10.1080/21622671.2020.1771022

Dyer, J., & Kolic, B. (2020). Public risk perception and emotion on Twitter during the Covid-19 pandemic. *Applied Network Science*, *5*(1). https://doi.org/10.1007/s41109-020-00334-7

Emanuel, E. J., Osterholm, M., & Gounder, C. R. (2022). A National Strategy for the "New Normal" of Life With COVID. *JAMA*, *327*(3), 211. https://doi.org/10.1001/jama.2021.24282

Graham, M. W., Avery, E. J., & Park, S. (2015). The role of social media in local government crisis communications. *Public Relations Review*, *41*(3), 386–394. https://doi.org/10.1016/j.pubrev.2015.02.001

Gupta, P., Kumar, S., Suman, R. R., & Kumar, V. (2021). Sentiment Analysis of Lockdown in India During COVID-19: A Case Study on Twitter. *IEEE Transactions on Computational Social Systems*, *8*(4), 992–1002. https://doi.org/10.1109/tcss.2020.3042446

Imran, M., Elbassuoni, S., Castillo, C., Diaz, F., & Meier, P. (2013). Extracting information nuggets from disaster-Related messages in social media. In T. Comes, F. Fiedrich, S. Fortier, J. Geldermann, & T. Müller (Eds.), *10th Proceedings of the International Conference on Information Systems for Crisis Response and Management, Baden-Baden, Germany, May 12-15, 2013*. ISCRAM Association. http://idl.iscram.org/files/imran/2013/613_Imran_etal2013.pdf

Jie, L. H., Ayyasamy, R. K., Sangodiah, A., Jalil, N. B. A., Krishnan, K., & Chinnasamy, P. (2023, January). The Role of ERNIE Model in Analyzing Hotel Reviews using Chinese Sentiment Analysis. *2023 International Conference on Computer Communication and Informatics (ICCCI)*. https://doi.org/10.1109/iccci56745.2023.10128534

Killgore, W. D. S., Taylor, E. C., Cloonan, S. A., & Dailey, N. S. (2020). Psychological resilience during the COVID-19 lockdown. *Psychiatry Research*, *291*, 113216. https://doi.org/10.1016/j.psychres.2020.113216

Kim, K.-S., Sin, S.-C. J., & Yoo-Lee, E. Y. (2014). Undergraduates' Use of Social Media as Information Sources. *College & Research Libraries*, *75*(4), 442–457. https://doi.org/10.5860/crl.75.4.442

Li, M., Chen, L., Zhao, J., & Li, Q. (2021). Sentiment analysis of Chinese stock reviews based on BERT model. *Applied Intelligence*, *51*(7), 5016–5024. https://doi.org/10.1007/s10489-020-02101-8

Marken, G. A. (2006). Social Media…the Hunted Can Become the Hunter. *Public Relations Quarterly*, *52*(4), 9–12.

Mayfield, A. (2006). *What is Social Media?* Spannerworks. http://www.spannerworks.com/fileadmin

Meyers, D., & Zunin, L. M. (2000). *Training Manual for Human Service Workers in Major Disasters*. US Department of Health and Human Services.

Mucci, F., Diolaiuti, F., & Mucci, N. (2020). Lockdown and isolation: Psychological aspects of COVID-19 pandemic in the general population. *Clinical Neuropsychiatry*, *17*(2), 63–64. https://doi.org/10.36131/CN20200205

National Health Commission of the People's Republic of China. (2020, January 26). Notice on Strengthening Community Prevention and Control of the COVID-19 Pandemic (Issued by Joint Prevention and Control Mechanism) . https://www.gov.cn/xinwen/2020-01/26/content_5472235.htm

Peng, S., Zeng, R., Liu, H., Chen, G., Wu, R., Yang, A., & Yu, S. (2021). Emotion Classification of Text Based on BERT and Broad Learning System. In *Web and Big Data* (pp. 382–396). Springer International Publishing. https://doi.org/10.1007/978-3-030-85896-4_30

Sharma, S., & Sharma, S. (2020). Analyzing the depression and suicidal tendencies of people affected by COVID-19's lockdown using sentiment analysis on social networking websites. *Journal of Statistics and Management Systems*, *24*(1), 115–133. https://doi.org/10.1080/09720510.2020.1833453

She, Z., Ng, K.-M., Hou, X., & Xi, J. (2022). COVID-19 threat and xenophobia: A moderated mediation model of

empathic responding and negative emotions. *Journal of Social Issues*, *78*(1), 209–226. https://doi.org/10.1111/josi.12500

Singh, J., Singh, G., & Singh, R. (2017). Optimization of sentiment analysis using machine learning classifiers. *Human-Centric Computing and Information Sciences*, *7*(1). https://doi.org/10.1186/s13673-017-0116-3

Stowe, A., Upshaw, K., Estep, C., & Lanzi, R. G. (2021). Getting to the Sandbar: Understanding the Emotional Phases of COVID-19 Among College and University Students. *Psychological Reports*, *125*(6), 2956–2980. https://doi.org/10.1177/00332941211028105

Su, Y., Jin, J., Zhu, L., & Cai, J. (2022). Emerging psychological crisis issues during lockdown in Shanghai. *The Lancet Regional Health - Western Pacific*, *25*, 100536. https://doi.org/10.1016/j.lanwpc.2022.100536

Sun, Z., Zhang, H., Yang, Y., Wan, H., & Wang, Y. (2020). Impacts of geographic factors and population density on the COVID-19 spreading under the lockdown policies of China. *Science of The Total Environment*, *746*, 141347. https://doi.org/10.1016/j.scitotenv.2020.141347

Sutton, J., Palen, L., & Shklovski, I. (2008). Backchannels on the front lines: Emergent uses of social media in the 2007 southern California wildfires. In F. Fiedrich & B. Van de Walle (Eds.), *Proceedings of the Fifth International ISCRAM Conference* (pp. 1–9).

Tsou, M.-H. (2015). Research challenges and opportunities in mapping social media and Big Data. *Cartography and Geographic Information Science*, *42*(sup1), 70–74. https://doi.org/10.1080/15230406.2015.1059251

Vartti, A.-M., Oenema, A., Schreck, M., Uutela, A., Zwart, O. de, Brug, J., & Aro, A. R. (2009). SARS Knowledge, Perceptions, and Behaviors: A Comparison between Finns and the Dutch during the SARS Outbreak in 2003. *International Journal of Behavioral Medicine*, *16*(1), 41–48. https://doi.org/10.1007/s12529-008-9004-6

Vieweg, S., Hughes, A. L., Starbird, K., & Palen, L. (2010). Microblogging during two natural hazards events: What twitter may contribute to situational awareness. In E. D. Mynatt, D. Schoner, G. Fitzpatrick, S. E. Hudson, W. K. Edwards, & T. Rodden (Eds.), *Proceedings of the 28th International Conference on Human Factors in Computing Systems, CHI 2010, Atlanta, Georgia, USA, April 10-15, 2010* (pp. 1079–1088). ACM. https://doi.org/10.1145/1753326.1753486

Wang, T., Lu, K., Chow, K. P., & Zhu, Q. (2020). COVID-19 Sensing: Negative Sentiment Analysis on Social Media in China via BERT Model. *IEEE Access*, *8*, 138162–138169. https://doi.org/10.1109/access.2020.3012595

Wuhan Statistics Bureau. (2021, May 28). *Bulletin of the Seventh National Population Census in Wuhan (No.4)*. Wuhan Statistics Bureau. https://tjj.wuhan.gov.cn/tjfw/tjgb/202105/t20210528_1707401.shtml

Xiang, N., Jia, Q. Q, & Wang, Y. D. (2021, July). Sentiment analysis of Chinese Weibo combining BERT model and Hawkes process. *2021 5th International Conference on Deep Learning Technologies (ICDLT)*. https://doi.org/10.1145/3480001.3480007

Xu, Y., Liu, Z., Zhao, J., & Su, C. (2017). Weibo sentiments and stock return: A time-frequency view. *PLOS ONE*, *12*(7), e0180723. https://doi.org/10.1371/journal.pone.0180723

Yuan, S. (2022). Zero COVID in China: What next? *The Lancet*, *399*(10338), 1856–1857. https://doi.org/10.1016/s0140-6736(22)00873-x

Yue, Ri., Lau, B. H. P., Chan, C. L.-W., & Ng, S.-M. (2021). Risk perception as a double-edged sword in policy compliance in COVID-19 pandemic? A two-phase evaluation from Hong Kong. https://doi.org/10.31234/osf.io/g523h

Zhuang B. B. (2022, March 19). *Shanghai Announced the Results of Recent Local Confirmed Cases Traceability*. Shanghai Publication. https://web.archive.org/web/20220319041947/http://www.dzwww.com/xinwen/guoneixinwen/202203/t20220311_9942069.htm

Oral presentation in IAG'i

Landscape

Chair: Maki Kishimoto (Tokyo Institute of Technology)
Sat. Oct 28, 2023 9:00 AM - 10:20 AM Room E (C-301 3rd floor of Bldg. C)

[E1-01] Capturing Walking-related Perceptions and Willingness within Tokyo's Station Areas: Leveraging Crowd-sourced Methods and AI Approach

*LU HUANG[1], TAKUYA OKI[1], SACHIO MUTO[2], YOSHIKI OGAWA[2] (1. Tokyo Institute of Technology, 2. The University of Tokyo)

9:00 AM - 9:20 AM

[E1-02] The Generation Process and Data Characteristics of Volunteered Street View Imagery for Streetscape Monitoring: A Case Study in Tokyo

*Xinrui Zheng[1], Mamoru Amemiya[1] (1. University of Tsukuba)

9:20 AM - 9:40 AM

[E1-03] Analyzing the Authenticity and Integrity of Cultural Landscapes Using Geographic Data - A Case Study of Pickle-making in Sichuan Province, China.

*Suxueer Sun[1], Naoko Fujita[1], Hideki Kobayashi[2], Yang Zhou[1], Suzu Shimada[1], Zile Tian[1] (1. University of Tsukuba., 2. Kanazawa University)

9:40 AM - 10:00 AM

[E1-04] Geographic information analysis of the transmission of cultural landscape values through farmers' guesthouses in Aso

*Linda Gadhoum[1], Naoko Fujita[1], Yang Zhou[1], Suxueer Sun[1], Hideki Kobayashi[2] (1. University of Tsukuba, 2. Kanazawa University)

10:00 AM - 10:20 AM

Capturing Walking-Related Perceptions and Willingness within Tokyo's Station Areas: Leveraging Crowd-Sourced Methods and AI Approach

Lu Huang*, Takuya Oki**, Sachio Muto*** and Yoshiki Ogawa****

Abstract In order to formulate strategies pertaining to pedestrian activities, it is imperative to develop an understanding of the pedestrian-oriented characteristics inherent to rail transit station areas. However, existing research in this field predominantly espouses an objective outlook. In contrast, this study adopts a subjective stance, centering its focus on the pedestrian perceptions and willingness within these station areas. Initially, by using crowd-sourced and AI approaches, the study conducts an analysis within the context of Tokyo's Setagaya Ward to quantify various facets associated with pedestrian perceptions and their willingness in a spectrum of transit station areas. Furthermore, an examination of the heterogeneity in these characteristics is undertaken through the process of clustering the transit station areas.

Keywords: pedestrian perceptions, pedestrian willingness, crowd-sourced method, AI, transit station areas

1.Introduction

In today's modern urban environment, walking has surpassed its functional role and has evolved into a multifaceted experience that deeply engages individuals with their surroundings. Beyond being a mere mode of transportation, walking has transformed into a sensorial and experiential journey that fosters a meaningful connection with both the built environment and the local residents and visitors (Chan & Li, 2022). This transformation is notably accentuated within rail transit station areas, typically denoting the approximate 500-meter radius encompassing public rail transit stations.

Certainly, to provide effective policy recommendations for urban and transport planning, the walking-related characters of rail transit station areas should be understood thoroughly firstly. However, the existing studies of walking-related characters concerning rail transit station areas largely stem from an objective perspective, highlighting disparities and shared characteristics in behavior patterns (Jin, et al., 2023), land use characters (Huang, et al., 2018), or other functional and demographical characters (Lyu, et al., 2016). Nonetheless, research delving into the characteristics and patterns of station areas from a subjective standpoint, with a specific emphasis on pedestrian perceptions and willingness remains relatively limited.

This study is a sub-research of walkability research project empowered by AI and Big Data. In the first phase, we introduced the index and methods to measure street-level walking characteristics (Huang, et al., 2023). This study, however, delves more deeply into the subjective walkability measurement that wasn't thoroughly discussed in the first phase. It strives to bridge the previously recognized gaps in research knowledge. First and foremost, it seeks to quantify different aspects of pedestrian perceptions and the willingness across different station areas within Setagaya Ward. Moreover, it aspires to gain an initial understanding of the spatial pattern of perceptions and willingness of station areas by examining disparities in levels. Additionally, it explores a deeper understanding of the heterogeneity from a perspective that takes into account the relative proportional relationships among different perception and willingness indicators within each station area.

To accomplish the outlined research objectives, this study capitalizes on contemporary trends in urban big data and harnesses the progressions in crowd-sourcing method and artificial intelligence (AI).

* 学生会員　東京工業大学　環境・社会理工学院 (Tokyo Institute of Technology) huang.l.ac@m.titech.ac.jp
** 正会員　東京工業大学　環境・社会理工学院 (Tokyo Institute of Technology)
*** 東京大学連携研究機構 不動産イノベーション研究センター (The University of Tokyo)
**** 正会員　東京大学　空間情報科学研究センター (The University of Tokyo)

2. Data and method

2.1 Study area

This study is centered on Setagaya Ward, a special ward of Tokyo, characterized by an approximate area of 58.06 square kilometers and one of the highest population densities among Tokyo's wards. It is worth highlighting that Setagaya Ward boasts a well-established rail transit infrastructure, intricately weaving its localities into the larger urban tapestry. Comprising a network of 40 strategically positioned rail transit stations, dispersed across 8 distinct railway lines, these stations play a pivotal role as conduits for seamless connectivity (Setagaya City, 2023) (Fig. 1). Beyond enhancing accessibility to key destinations, these stations, along with their station areas, serve as foundational pillars in bolstering Setagaya Ward's socio-economic vibrancy and urban life.

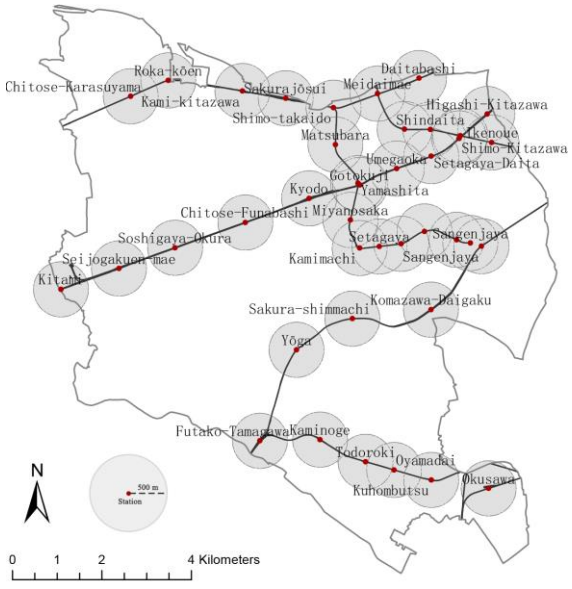

Fig. 1. Transit station areas of Setagaya ward, Tokyo

2.1 Data source

This research makes use of two distinct categories of data: Street View imagery and Geographic Information System (GIS) data. Specifically, Street View images (SVIs) are sourced from Zenrin Corporation, constituting a dataset akin to Google Street View. In order to strike a balance between computational efficiency and the overall dataset size, a 30-meter interval was adopted along the road network for capturing Zenrin SVIs.

To enable subsequent analytical procedures, the panoramic images were transformed into front-view perspectives, creating a viewpoint similar to that of a pedestrian at eye level.

Furthermore, the study integrated GIS data, encompassing administrative boundary information sourced from the Ministry of Land, Infrastructure, Transport and Tourism (MLIT) of Japan, along with street network data and rail transit station locations extracted from OpenStreetMap.

2.2 Analytical framework

The analysis methodology of this study is delineated through a three-step process (Fig. 2). Initially, it formulates precise definitions for pedestrian perceptions and willingness, thereby establishing a clear framework for measurement. Subsequently, it undertakes extensive data collection of perceptions and willingness through crowd-sourced surveys on a sizable scale. Following this, deep learning techniques are applied to model the survey data, thus quantifying diverse indicators of walking perceptions and willingness in the 500m buffers of Setagaya Ward's rail transit stations, offering a preliminary understanding of the perceptual and willingness characteristics of station areas. Lastly, through clustering analysis, an in-depth exploration is conducted to uncover

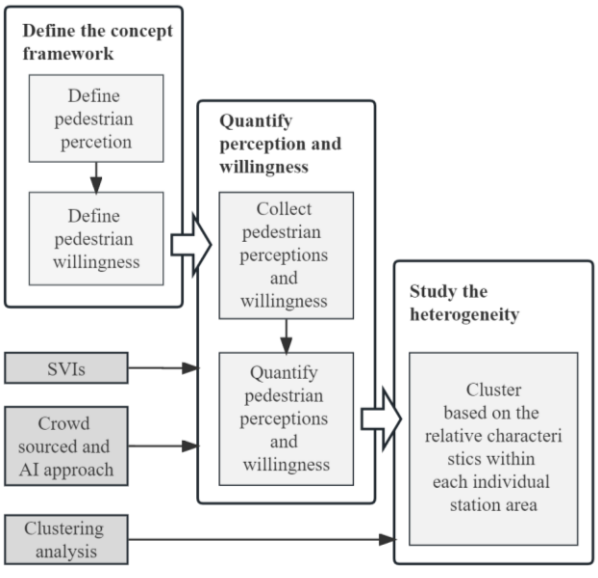

Fig. 2. Analytical framework

the heterogeneity of pedestrian perceptions and willingness across distinct station areas.

2.3. Defining pedestrian perceptions and willingness

Walking activities, especially non-utilitarian pedestrian activities, encompass not only walking behaviors but also stationary behaviors (Mehta, 2008; Gehl, 1987). Walking behaviors entail actions like crossing busy streets, traversing through parks, and navigating diverse urban areas. Conversely, stationary behaviors involve actions such as appreciating street art, taking pauses at corners, or engaging in conversations with other people. The perceptions of these walking and stationary behaviors within these two behavioral states diverge due to their engagement in distinct contexts and cognitive processes. Consequently, these perceptions exert a notable influence on individuals' comprehension, evaluation, and modes of interaction within the urban environment.

In addition, the pedestrian perceives different hierarchical needs. Drawing from Alfonzo's (2005) five-level hierarchy of walking needs, the needs associated with pedestrian perception can be categorized into five dimensions, ascending from feasibility, accessibility, safety, comfort, to enjoyment. Although Southworth (2005) is not concerned with feasibility in his research. In order to better adapt to our research context, we have modified a four-tiered hierarchy based on Alfonzo's (Fig. 3).

Building upon the theoretical foundation mentioned above, the notion of pedestrian willingness within spatial contexts can be equivalently grouped into the classifications of "willingness to walk" and "willingness to stay." These classifications distinctly mirror individuals' intentions to traverse a street by selecting walking as the mode of transportation and to pause at a location while engaged in walking activities (Fig. 3).

2.4 Quantifying pedestrian perceptions and willingness

Ordonez et al. (2014) and Dubey et al. (2016) introduced a pipeline that harness crowd-sourced

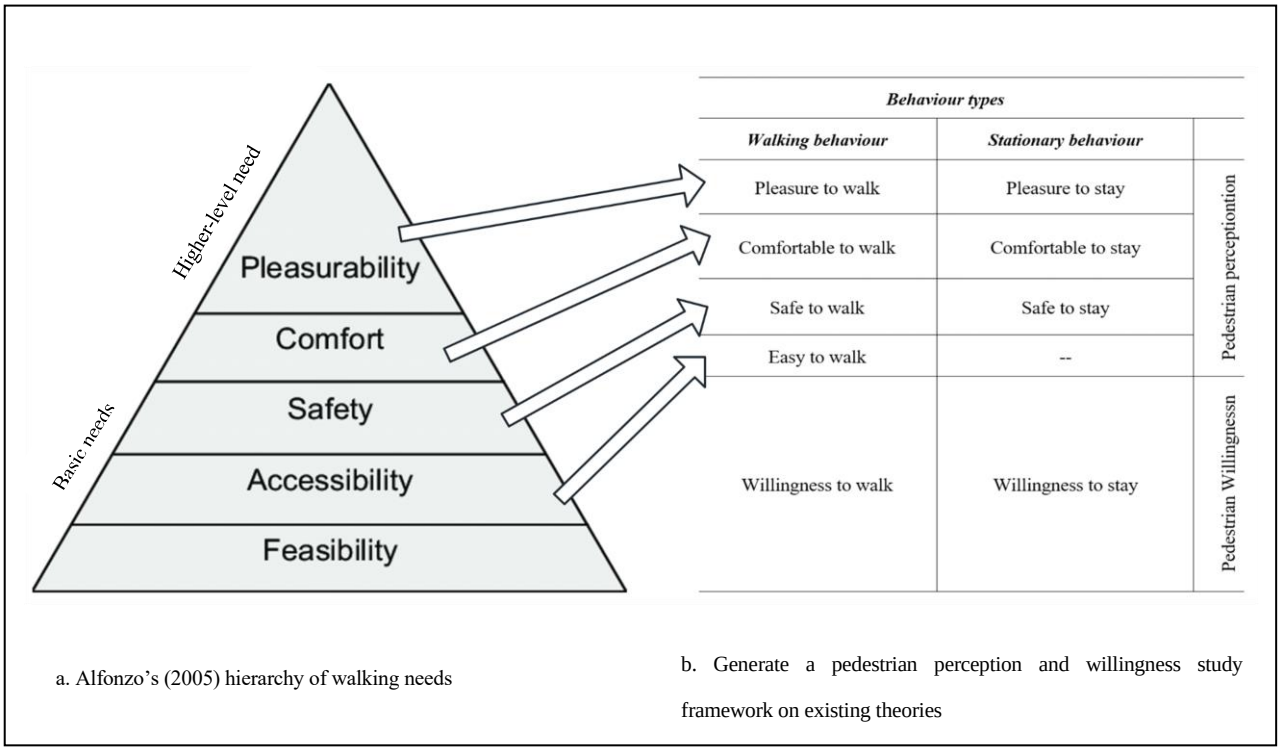

a. Alfonzo's (2005) hierarchy of walking needs

b. Generate a pedestrian perception and willingness study framework on existing theories

Fig. 3. Generate a framework with indicators for measurement

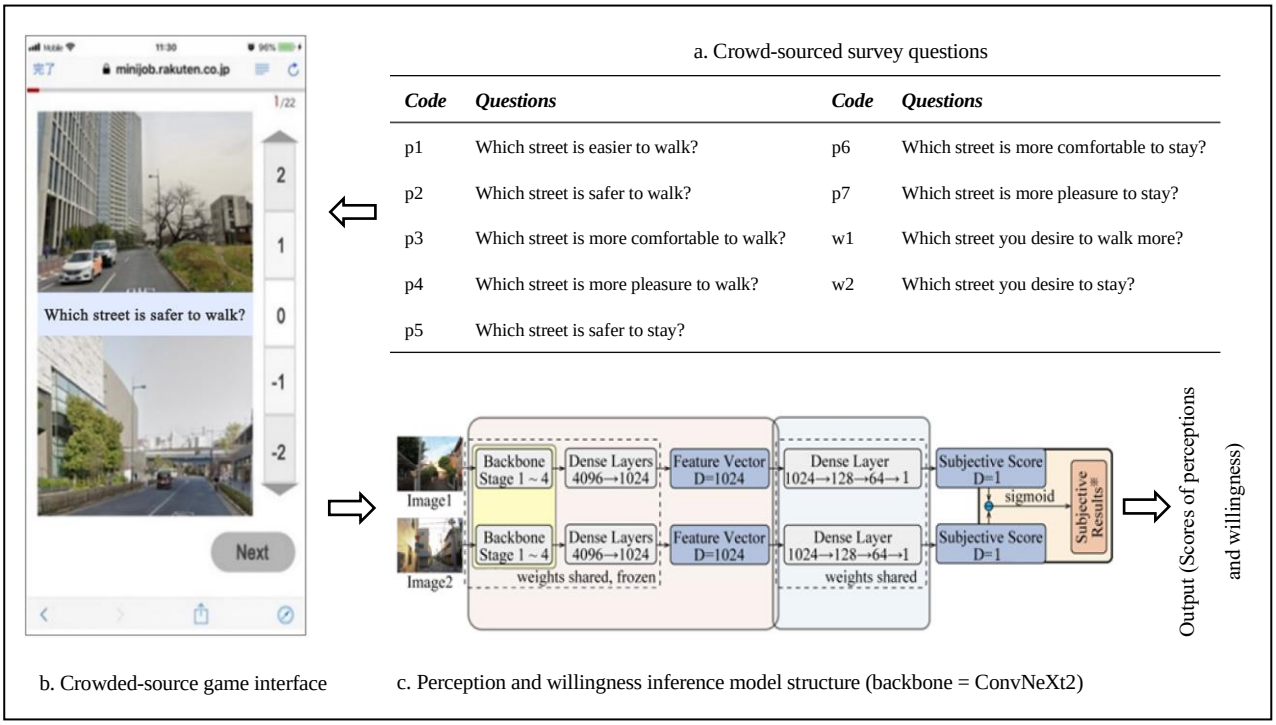

Fig. 4. The pipeline of quantifying pedestrian perceptions and willingness

approaches and deep learning techniques for the extensive measurement of visual environmental perceptions. Presently, this pipeline is progressively being adopted to delve into the intricate dynamics between a city's physical environment and subjective perceptions of people (Zhang, et al., 2018; Oki & Kizawa, 2022; Ogawa, et al., 2022).

We also intend to investigate pedestrian perceptions and willingness from a visual perspective. Our approach involves fine-tuning existing methodologies. On one hand, we utilized online mobile platforms and Japanese street view images to collect data on individual's perceptions and willingness related to walking. Furthermore, we enhanced the predictive accuracy by replacing the backbone of the deep learning model.

2.4.1 Collect individuals' perceptions and willingness related to walking

In terms of collect individuals' pedestrian perceptions and willingness, we utilized an online survey conducted through cell phones to gather data. This survey was adeptly fashioned as an interactive comparative game interface (Fig. 4b). Within this interactive context, respondents engaged with a series of questions aligned with the dimensions defined in Section 2.3. These questions included prompts such as "Which street is safer to walk (Fig. 4a)?"

2.4.2 Quantify pedestrian perceptions and willingness

To quantify the pedestrian perceptions and willingness of all station areas of Setagaya Ward, we leveraged data collected from image pair comparisons and images' feature vectors as variables, and then employed an advanced deep learning approach to establish our model. It is capable of precisely predicting various indicators of pedestrian perceptions and willingness from a single input SVI. The foundation of these models is rooted in the Deep Convolutional Neural Network (DCNN) Architecture, with a ConVneXt-V2 (Woo, et al., 2023) as the backbone (Fig. 4c). This model adeptly processed the comparison scores acquired from the survey as well as the image features. This intricate processing enabled the extraction of human attitude scores through a process of multi-label classification, ultimately leading to the prediction of 9 different indicators.

Considering the study's focus on rail transit station areas, we visualized the results on a per-station area basis.

After acquiring the distinct scores for each of the 9 indicators corresponding to individual street view images, we geolocated these scored street view images based on their coordinates within ArcGIS. Subsequently, a spatial join tool was employed to calculate the mean scores for each indicator of street views associated with each station area. However, to ensure visual clarity in portraying score divergences across various indicators, we normalize data from various scales to fit within the 0 to 1 range, ensuring consistency and ease of analysis.

2.5 Clustering based on the relative proportions among different indicators within each station area

By quantifying various perceptions and willingness indicators, we can observe the varying levels of these indicators across different station areas. However, the relative proportion characteristics among different indicators within station areas cannot be depicted using this approach. To address this, we utilized the K-means clustering method to further investigate the heterogeneity of features associated with pedestrian perception and willingness in distinct station areas within Setagaya Ward.

K-means is a foundational clustering algorithm known for its efficiency in categorizing data into distinct and compact clusters (Li & Wu, 2012). However, determining the optimal number of clusters is crucial when using K-means clustering. To achieve this objective, the elbow method was employed, plotting the cost function values corresponding to different values of K. At a particular K value, there is a notable decrease in the cost function, which then stabilizes after further increments of K. The K value that corresponds to the point where the reduction in distortion diminishes the most can be identified as the optimal number of clusters (Kodinariya & Makwana, 2013).

In order to enhance the clustering algorithm's capacity to precisely discern the relative discrepancies in scores across indicators for each station area, we conducted a normalization process on the variations in characteristics among different indicators for each station area prior to the implementation of K-means.

3. Experiment results

In this section, Setagaya Ward was taken as a case study, and a total of 18,000 front-view street images representing rail transit station areas were prepared using the designated preprocessing methodology. Among these, 1,200 images that exhibited distinctive regional characteristics were selected to comprise the dataset for the crowd-sourced survey.

3.1 Crowd-sourced survey results

By utilizing the selected 1,200 survey images, we constructed a collection of 12,000 image pairs in order to facilitate the collection of comparative scores.

Carried out in February 2023 within Japan, the online-based questionnaire collected from a wide range of respondents primarily focused on Japanese individuals. The survey attracted over 18,000 anonymous respondents, encompassing major cities and prefectures throughout Japan. The gender breakdown of the respondents displayed a nearly balanced distribution. Overall, the representativeness of the survey results is satisfactory.

3.2 Prediction accuracy

We employed the method proposed in section 2.4 to train a DCNN model, enabling the prediction of 7 perceptual indicators and 2 willingness indicators. Subsequently, we evaluated the precision of the model's predictions, with the accuracy values presented in Table 1.

Table 1. Indicator prediction accuracy

Code	*Indicators*	*Accuracy*
p1	Easy to walk	0.8420
p2	Safe to walk	0.8393
p3	Comfortable to walk	0.8135
p4	Pleasure to walk	0.8502
p5	Safe to stay	0.8249
p6	Comfortable to stay	0.8210
p7	Pleasure to stay	0.8082
w1	Willingness to walk	0.8195
w2	Willingness to stay	0.7999

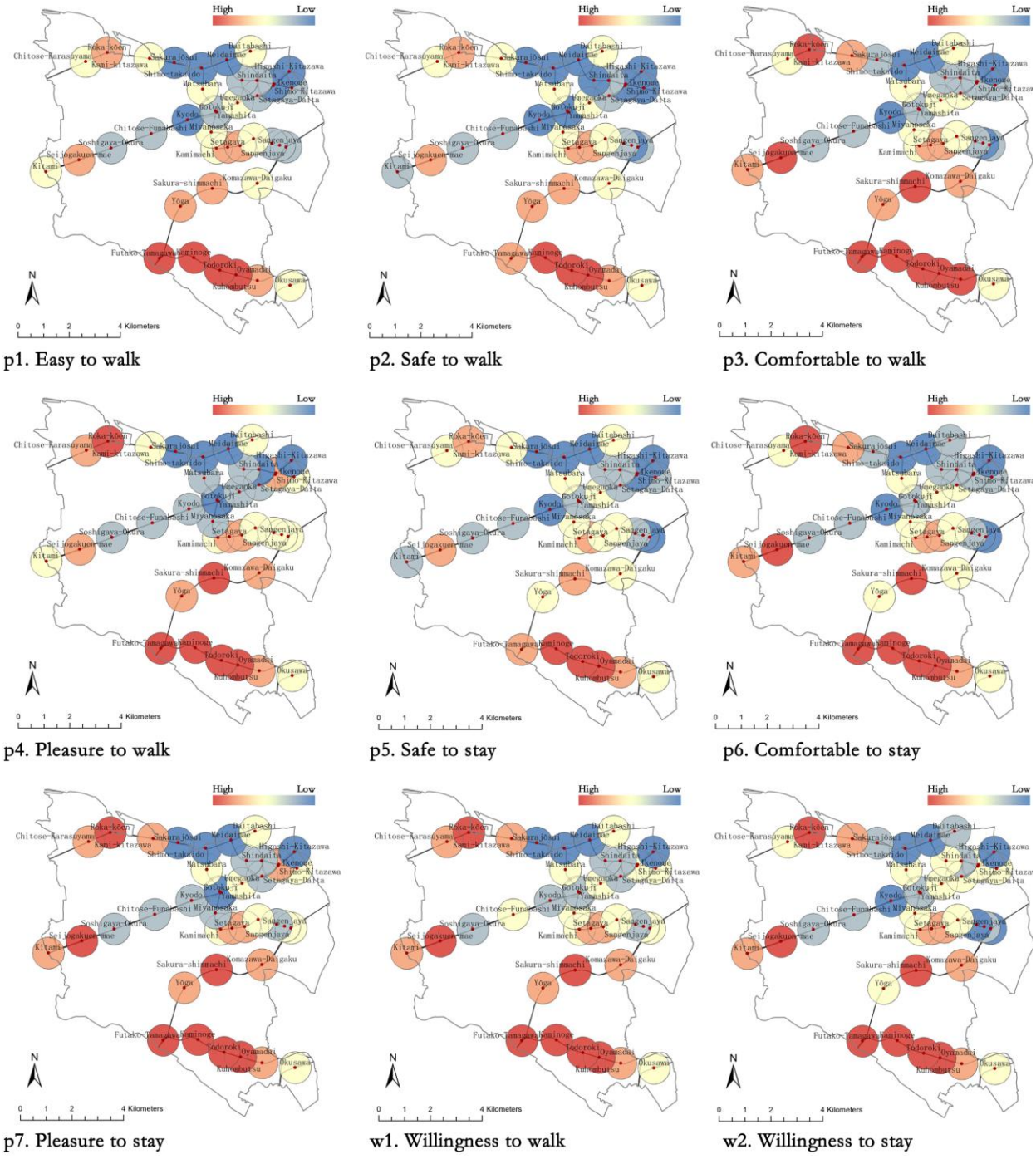

Fig. 5. Mapping pedestrian perceptions and willingness

3.3 Map pedestrian perceptions and willingness

The analysis of Fig. 5 (p1 to w2) allows us to draw several initial conclusions. Firstly, the station areas, such as Futako-tamagawa and Kaminoge, located along the Tokyu Oimachi Line and adjacent to the southern Tama River exhibit higher score in both perception and willingness indicators compared to the majority of other station areas. Conversely, several station areas, such as Shimo-takaido and Meidaimae, situated along the Keio Line and neighboring the northern Suginami Ward show the opposite trend, performing relatively poorly across nearly all indicators. Some station areas exhibit significant contrasts across different indicators. For example, the station area of Shimo-Kitazawa, Shoin-jinja-mae, and

Sangenjaya display lower scores in indicators such as "safe to stay (p5)," "safe to walk (p2)," and "comfortable to walk (c)." However, they achieve relative higher scores in indicators like "pleasure to walk (p4)," "pleasure to stay (p7)," and "willingness to walk (w1)." These findings underscore the intricate nature of perceptions and willingness within the station areas of Setagaya Ward.

3.4 Clustering results

By employing the elbow method, we determined that the optimal number of clusters for the K-means clustering from second perspective is 3 (Fig. 6). Accordingly, we divided the station areas into three clusters based on the relative proportional relationships among different dimensions of indicators within each station area. Considering their comprehensive features, we assigned the following names to the three clusters: (1) Comprehensive Developed Station Areas, (2) Comfortable and Safe Station Areas, and (3) Engaging Exploration Station Areas. Furthermore, the average values of different indicators within each cluster are calculated to reflect and visualize the characteristics of that cluster (Fig. 7).

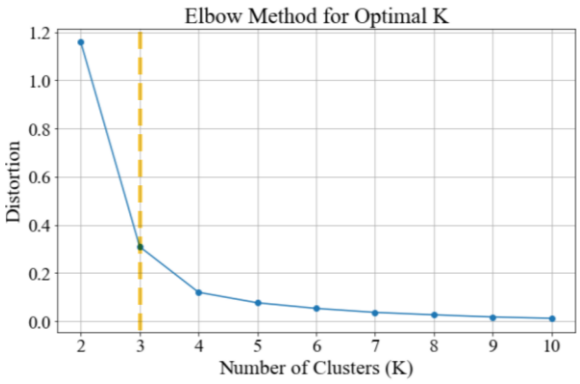

Fig. 6. Decide the optimal K for clustering for the second perspective

Cluster 1: Comprehensive Developed Station Areas.

Cluster 1 comprises 10 station areas, namely Yōga, Shimo-kitazawa, Nishi-Taishidō, Oyamadai, Shoin-jinja-mae, Setagaya, Chitose-Funabashi, Daitabashi, Soshigaya-Okura, and Sakurajōsui. Within this cluster, the station areas exhibit a relatively balanced performance across various pedestrian perceptions. In terms of pedestrian willingness, these station areas show a relatively higher willingness to walk compared to their willingness to stay.

Cluster 2: Comfortable and Safe Station Areas

Cluster 2 encompasses 13 station areas where people's perceptions of basic-level walking needs, especially indicators such as "easy to walk" and "safe to walk/stay," are relatively high. However, within this cluster, station areas tend to receive a relatively lower scores in terms of satisfying higher-level walking needs (pleasure to walk). Regarding willingness, these station areas exhibit relatively higher scores for "willingness to stay" compared to "willingness to walk." Specifically, the stations included in this cluster are Shindaita, Matsubara, Setagaya-daita, Kaminoge, Kamimachi, Yamashita, Wakabayashi, Umegaoka, Kuhombutsu, Gōtokuji, Miyanosaka, Higashi-Matsubara, and Okusawa.

Cluster 3: Engaging Exploration Station Areas

Cluster 3 encompasses a total of 17 station areas, characterized by relatively higher evaluations of the higher-level walking need "pleasure to walk." This signifies that these station areas play a more prominent role in stimulating people's desires for exploration and engagement with interesting environments. Regarding pedestrian willingness, this cluster demonstrates a relatively balanced distribution between the "willingness to walk" and "willingness to stay". The station areas included in this cluster are Sakura-shimmachi, Shimo-Kitazawa, Shimo-Kitazawa, Kitami, Kamikitazawa, Sangenjaya, Sangenjaya, Chitose-Karasuyama, Meidaimae, Ashihama-Koen, Komaba-Todaimae, Kyodo, Futako-Tamagawa, Higashi-Kitazawa, Todoroki, Ikenoue, and Seijōgakuen-Mae.

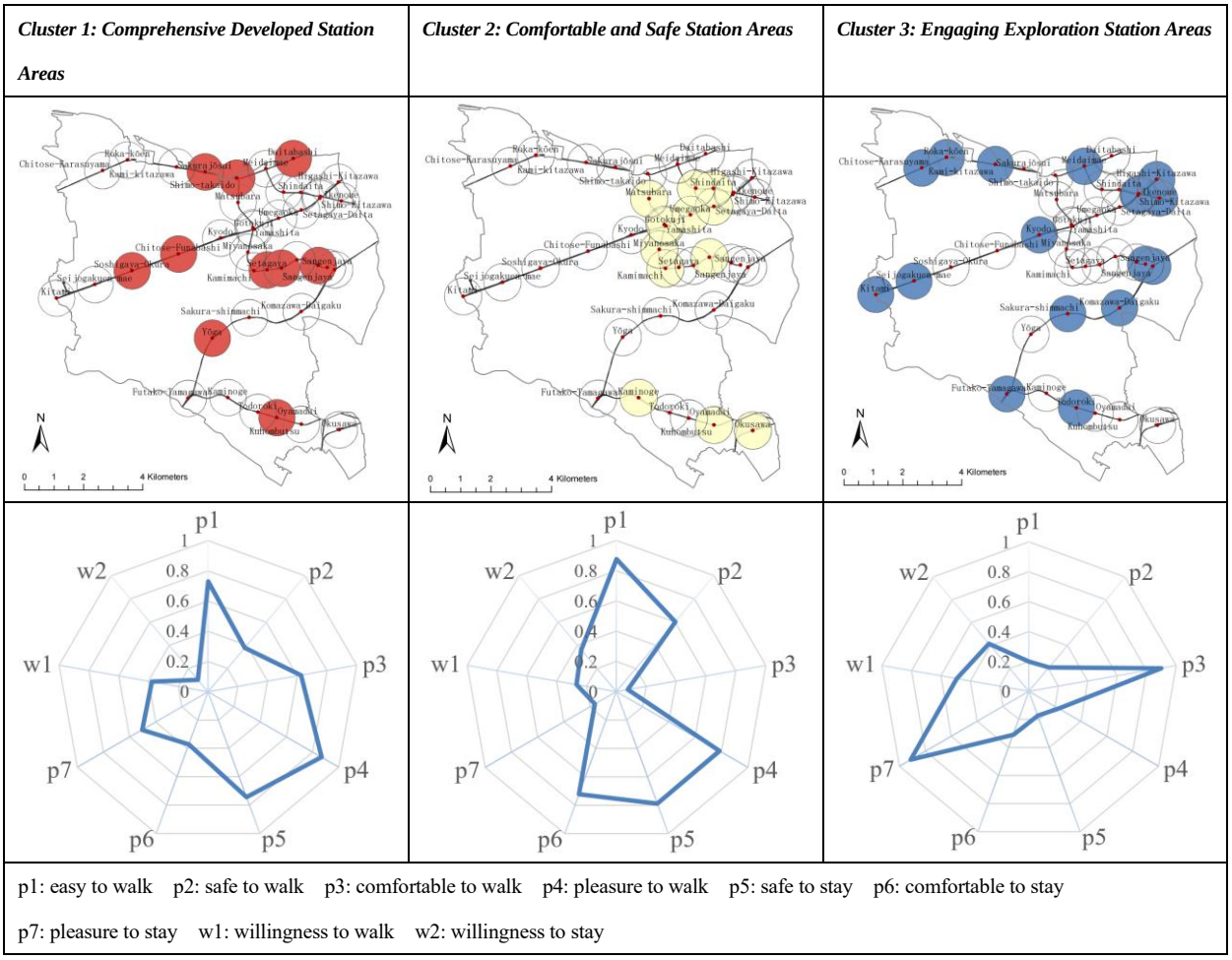

Fig. 7. Clustering results based on the relative proportional relationships among different dimensions of indicators within each station area

4. Discussion

By leveraging SVI big data, crowd-sourcing methods, and AI techniques, we have achieved large-scale quantitative predictions of pedestrian perceptions and willingness. In terms of score level discrepancies, we have identified variations in subjective pedestrian perceptions and willingness among different stations across individual or all dimensions. Notably, these differences exhibit spatial clustering in distribution. These insights are instrumental in identifying station areas that excel or lag behind in terms of pedestrian perceptions and willingness. Such findings hold the potential to provide guidance to policy makers and urban planners in recognizing spatial imbalances and in prioritizing strategic spatial interventions for forthcoming developments in station areas.

By undertaking K-means clustering analysis, we are able to categorize station areas with similar characteristics from the viewpoint centered on the relative proportional relationships among various dimensions of indicators within each station area. In this context, we have clustered station areas into three distinct groups: (1) Comprehensive Developed Station Areas; (2) Comfortable and Safe Station Areas; and (3) Engaging Exploration Station Areas. This classification has the potential to guide further investigations into whether the distribution of perceptions and willingness in these areas aligns with their regional Transit-Oriented Development (TOD) visions and land use policy.

However, it is essential to acknowledge the limitations of this study. Relying solely on visual perceptions may introduce biases, as pedestrian experiences involve multiple sensory dimensions. Future

research should incorporate auditory, olfactory, and other sensory aspects to provide a more holistic understanding. Moreover, while our study harnessed established indicators to capture pedestrian perceptions, it is worth noting that these dimensions may not fully encapsulate the intricate tapestry of pedestrian encounters within transit hubs situated in densely populated urban cores. As such, future endeavors in this field should contemplate the integration of innovative indicators that can more accurately and comprehensively capture the nuances of experiences in station areas characterized by intricate multi-layered and high-density attributes. Finally, the study's reliance on daytime street view data might underestimate station areas with vibrant nighttime activities. Incorporating nighttime data in future studies could help mitigate this bias.

5. Conclusion

This paper aimed at focusing on the subjective aspects that characterize rail transit station areas within Setagaya Ward. Its primary aim is to quantify the variables of pedestrian perceptions and willingness, followed by a preliminary exploration into the heterogeneity of these indicators across the different transit station areas.

The outcomes of this research contribute to a deeper comprehension of the patterns linked to pedestrian perceptions and willingness within Setagaya Ward's transit station areas and serves as a valuable guide for the future TOD in Japan. Furthermore, it establishes the groundwork for upcoming investigations that delve into the relationship between pedestrian perceptions and willingness.

Acknowledgement

This work was supported by JSTSPRING under Grant Number JPMJSP2106, and JSPSKAKENHI under Grant Number JP22K04490. We extend our gratitude to Zenrin Corporation for providing valuable street view data, to all survey respondents for their participation, and to Rakuten Corporation for their cooperation during the survey.

References

Alfonzo, M. A., 2005. To walk or not to walk? The hierarchy of walking needs. *Environment and behavior,* 37(6), pp. 808-836.

Chan, E. T. & Li, T. E., 2022. The effects of neighbourhood attachment and built environment on walking and life satisfaction: A case study of Shenzhen. *Cities,* Volume 130, p. 103940.

Dubey, A., Naik, N., Parikh, D., Raskar, R. and Hidalgo, C.A., 2016. Deep learning the city: Quantifying urban perception at a global scale. In *Computer Vision–ECCV 2016: 14th European Conference, Amsterdam, The Netherlands, October 11–14, 2016, Proceedings*.

Gehl, J., 1987. *Life Between Buildings: Using Public Space.* s.l.:Van Nostrand Reinhold

Huang, R., Grigolon, A., Madureira, M. & Brussel, M., 2018. Measuring transit-oriented development (TOD) network complementarity based on TOD node typology. *Journal of transport and land use,* 11(1), pp. 305-324.

Huang, L., Oki, T., Muto, S., Kim, H., Ogawa, Y. and Sekimoto, Y., 2023. Automatic Evaluation of Street-Level Walkability Based on Computer Vision Techniques and Urban Big Data: A Case Study of Kowloon West, Hong Kong. In *International Conference on Computers in Urban Planning and Urban Management*, pp. 231-259. Cham: Springer Nature Switzerland.

Jin, Y. et al., 2023. Understanding railway usage behavior with ten million GPS records. *Cities,* Volume 133, p. 104117.

Kodinariya, T. M. & Makwana, P. R., 2013. Review on determining number of Cluster in K-Means Clustering. *nternational Journal,* 1(6), pp. 90-95.

Li, Y. & Wu, H., 2012. A clustering method based on K-means algorithm. *Physics Procedia,* Volume 25, pp. 1104-1109.

Lyu, G., Bertolini, L. & Pfeffer, K., 2016. Developing a TOD typology for Beijing metro station areas. Journal of Transport Geography. *Journal of Transport Geography,* Volume 55, pp. 40-50.

Mehta, V., 2008. Walkable streets: pedestrian behavior, perceptions and attitudes. *Journal of Urbanism,* 1(3), pp. 217-245.

Ogawa Y, Oki T, Zhao C, Sekimoto Y, Shimizu C., 2022. Development of a Model for Evaluating Subjective Impressions of Streetscapes Using Omnidirectional Street Image Big Data. The *31st Annual Conference of Geographical Information Systems Association*, *Proceedings.*

Oki, T. & Kizawa, S., 2022. Model for Evaluating Impression of Streets in Residential Areas Based on Image Big Data and A Large Questionnaire. *Journal of Architecture and Planning,* 87, pp. 2102-2113.

Ordonez, V. and Berg, T.L., 2014. Learning high-level judgments of urban perception. In *Computer Vision–ECCV 2014: 13th European Conference, Zurich, Switzerland, September 6-12, 2014, Proceedings*.

Pearson, K. & Lee, A., 1903. On the laws of inheritance in man: I. Inheritance of physical characters. *Biometrika,* 2(4), pp. 357-462.

Setagaya City, 2023. *Setagaya City.* [Online] Available at: https://www.city.setagaya.lg.jp/index.html?SLANG=ja&TLANG=en&XMODE=0&XCHARSET=utf-8&XJSID=0 [Accessed 10 8 2023].

Southworth, M., 2005. Designing the walkable city. *Journal of urban planning and development,* 131(4), pp. 246-257.

Woo, S., Debnath, S., Hu, R., Chen, X., Liu, Z., Kweon, I.S. and Xie, S.C., V2: Co-Designing and Scaling ConvNets with Masked Autoencoders. arXiv 2023. *arXiv preprint arXiv:2301.00808*.

Zhang, F. et al., 2018. Measuring human perceptions of a large-scale urban region using machine learning. *Landscape and Urban Planning,* Volume 180, pp. 148-160.

The generation process and data characteristics of Volunteered Street View Imagery (VSVI) for streetscape monitoring
- A case study in Tokyo -

Xinrui Zheng*, Mamoru Amemiya**

Abstract The emergence of the Web 2.0 era has enabled individuals to contribute to Volunteered Street View Imagery (VSVI), which has the potential to provide more open and comprehensive geographic information but is subject to several criteria (e.g., data completeness and quality). In order to better understand the value of VSVI in streetscape monitoring studies, this study aims to analyze the generation process and examine the relevant characteristics in Tokyo using Mapillary. The generation process of Mapillary from 2014 is analyzed in terms of spatial expansion and revisit behavior. For data characteristics, we analyzed data completeness and quality in terms of temporal (update frequency and temporal diversity) and spatial resolution (spatial density, viewing angle completeness, and perspective diversity) using GSV as a benchmark.

Keywords: crowdsourcing, Volunteered Street View Imagery (VSVI), Mapillary, contribution behavior, data quality

1. Introduction

In urban audit studies, Street View Imagery (SVI) facilitates the examination of visual features of street environments from a human perspective. In recent years, SVI as an important data source in virtual audits has been catalyzed by the proliferation of large-scale street-level imagery platforms, advances in computer vision, machine learning, and availability of computing resources (Biljecki and Ito, 2020). With the shift from on-site surveys to virtual audits for various analysis tasks, traditional SVI (e.g., Google Street View (GSV), Baidu Total View) provided by government agencies or companies has been criticized for their limitations in providing more precise and dynamic environmental monitoring due to uniform data collection methods and restrictions on old image downloads (Biljecki and Ito, 2021; Li, 2021; D'Andrimont et al., 2018; Inoue et al., 2022).

The emergence of the Web 2.0 era has enabled individuals to access and contribute information through the internet, facilitating the collection of Volunteered Street View Imagery (VSVI) on a large scale and at a low cost (Goodchild, 2007; Zhen, Wang, and Weis, 2014). The availability of various data sources and free access to data may contribute to a higher quality SVI dataset. However, use of user-generated data in environmental audit studies is currently limited. This is partially due to the extensive coverage and popularity of traditional SVI (especially GSV). More importantly, it is due to the inherent spatial heterogeneity of VSVI contributions (Juhász and Hochmair, 2016) and the unknown mechanisms governing quality control of this data. If the mechanisms by which contribution activities contribute to the growth of required data quality related to environmental audits can be understood, it can confirm the feasibility of this contribution method in constructing high-quality datasets, and it can also provide an easy-to-calculate method for quality evaluation.

Recognizing the need, we aimed to perform an intrinsic analysis of the evolution of relevant data characteristics of VSVI with increasing contributions. The analysis comprises two parts that inspect different VSVI data characteristics whose growth is assumed to be determined by distinct aspects of contributions. The first part examines the data growth encompassing the growth rate and the spatial expansion process. VSVI does not provide any data coverage guarantees and often reports less complete comparing with traditional SVI (Juhasz and Hochmair, 2015). Examining the growth of VSVI data can

* Student member (GISA); University of Tsukuba; **s2236007@u.tsukuba.ac.jp**
** Member (GISA); University of Tsukuba; **amemiya@sk.tsukuba.ac.jp**

offer new insights into the dynamics of VSVI mapping to help estimate data coverage at different contribution stages.

The second part of this study investigates the evolution of data quality elements at street level as revisits increase. A distinguishing feature of VSVI compared to traditional SVI is that user-generated services enable downloading imagery from various users captured at different moments and perspectives along the same road. That provides an opportunity to create a more comprehensive SVI dataset in terms of higher spatial and temporal resolution for environmental audits. Modeling data quality as a function of revisits represents a discovery of novel links between contribution behavior and various aspects of VSVI data quality.

The VSVI data used in this study was downloaded from the Mapillary platform, which is the world's largest crowdsourcing-based street view platform. The study was conducted in Tokyo, one of the hotspots of Mapillary activity in Japan. The rest of the paper is structured as follows: Section 2 introduces the sources of data and its preparation process. In Section 3, we discuss the expansion process of data, followed by Section 4, which explores the evolution of data quality as revisits increase. The above results were discussed in Section 5 and concluded in Section 6.

2. Data Description

2.1. Mapillary Data

As shown in Figure 1, a total of 5,626,656 imagery data points were downloaded through the Mapillary API for Tokyo as of the date of data collection (July 16-18, 2022). To facilitate temporal analysis, images without timestamps and those taken before the launch of Mapillary in 2014 were excluded. Images more than 55 meters away from the road centerline (accounting for road width and GPS drift) were removed as they were deemed to not been captured along roads. Additionally, we excluded points located in railways which is not the subject of the study. These procedures were carried out in ArcGIS using tool of *nearest facility* to match the image points with the roads.

2.2. Reference Road Data

The reference roads for evaluation were obtained from the centerline road data of the digital map published by the Geospatial Information Authority of Japan in 2021. These roads are categorized into five groups including national expressways, national highways, prefectural roads, municipal roads, and parkways/garden paths. These roads were separated at road intersections for ordinary roads, and at intervals of 100 meters (which is commonly used in urban audit studies; Li, et al., 2015; Li, 2021) for national expressways, tunnels, and other roads longer than 1km after division at intersections. After preprocessing, 767,228 road segments were used to construct a road network for data connecting (185,832 of them contain Mapillary data) (Figure 1).

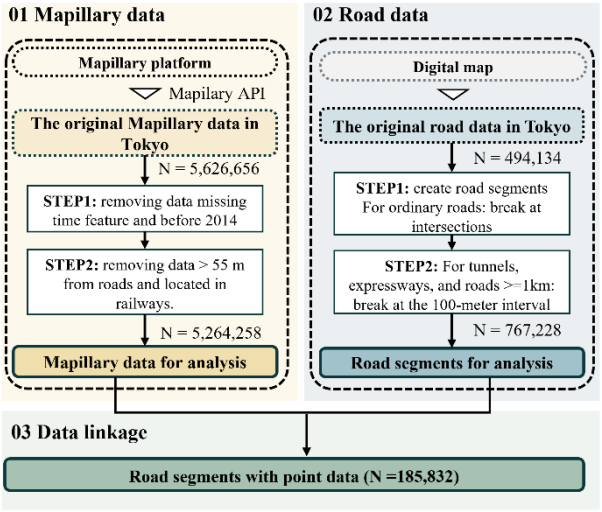

Figure 1 Data retrieval and preprocessing

3. Street Network Growth

As shown in Figure 2, Mapillary contributions in Tokyo increased during the study period, reflecting a similar trend observed in prior studies across Japan (Seto and Nishimura, 2022) and other countries (Ma et al., 2019). The following two sub-sections further explored the growth of the Mapillary street network in terms of growth rate and the spatial expansion process respectively.

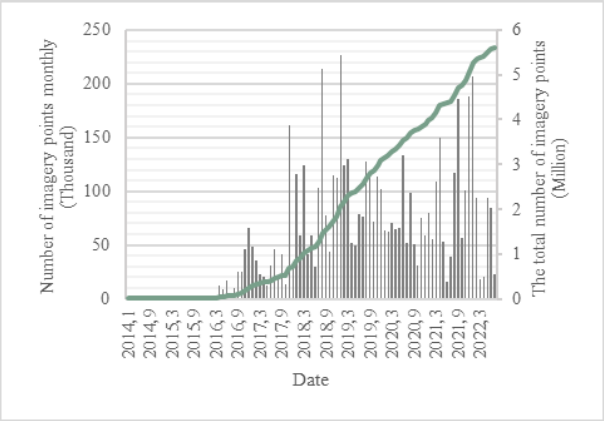

Figure 2 Contribution growth

3.1. Rate of Growth

Figure 3 displays the street length growth during study period on a monthly basis. By July 2022, the total length of the Mapillary network reached nearly one-third of the total length of roads in Tokyo. From 2014 to March 2016, a limited number of images were contributed (Figure 2), resulting in slow growth. However, network expansion gained momentum after April 2016, with an increase of over 50 km almost every month. By June 2022, the minimum monthly growth rate is 24.8 km observed in June 2021, while the maximum rate recorded is 428.2 km in November 2017.

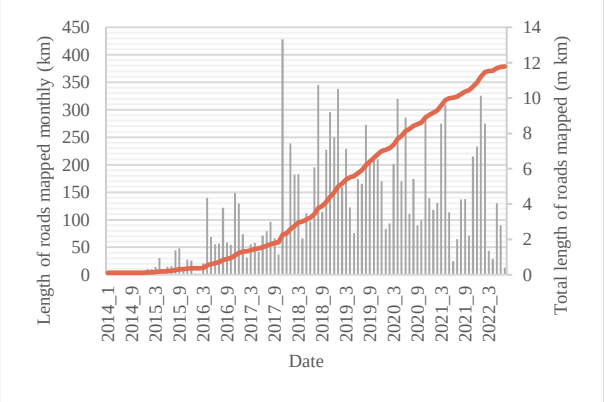

Figure 3 The growth of the length of street network

Figure 4 displays the growth of data completeness values across diverse road types in Tokyo. Generally, higher grade roads demonstrate a higher level of data completeness. All road types grow slowly in the earlier years, however, from 2016 onward, national expressways and national highways experience a rapid increase, reaching over 80% coverage following four years of swift growth. Subsequently, contributions along these two road types slow down, achieving over 90% coverage by the time of data collection. For prefectural roads, rapid growth began in approximately 2017 and subsequently slowed after reaching about 70% coverage in 2021. At the time of data collection, road coverage had reached 73.5%. The contributions made by the two types of low-grade roads, namely municipal roads, and parkways/garden paths, experienced a gradual increase at a relatively low rate compared to high-grade roads. As of the time of data collection, the road coverage values for them are relatively low, with results of 24.0% and 16.7% respectively.

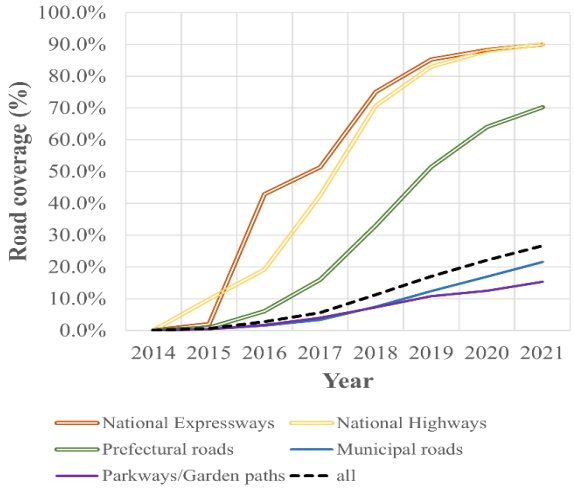

Figure 4 Completeness growth for different road types

3.2. Spatial Expansion Process

Figure 5 shows the spatial expansion of the roads that were mapped in Tokyo spanning from 2014 to 2021. Generally, it was discovered that the data gradually increased from the center of Tokyo to its outskirt. In 2013, Corcoran et al. reported two elementary spatial process of *exploration* (which is responsible for the expansion of the network into new areas) and *densification* (which is responsible for increasing the local density of the street network) in OSM street network representations (Corcoran et al., 2013). Additionally, as the network grows, *densification* becomes more dominant relative to *exploration*. Even though there is distinct difference in

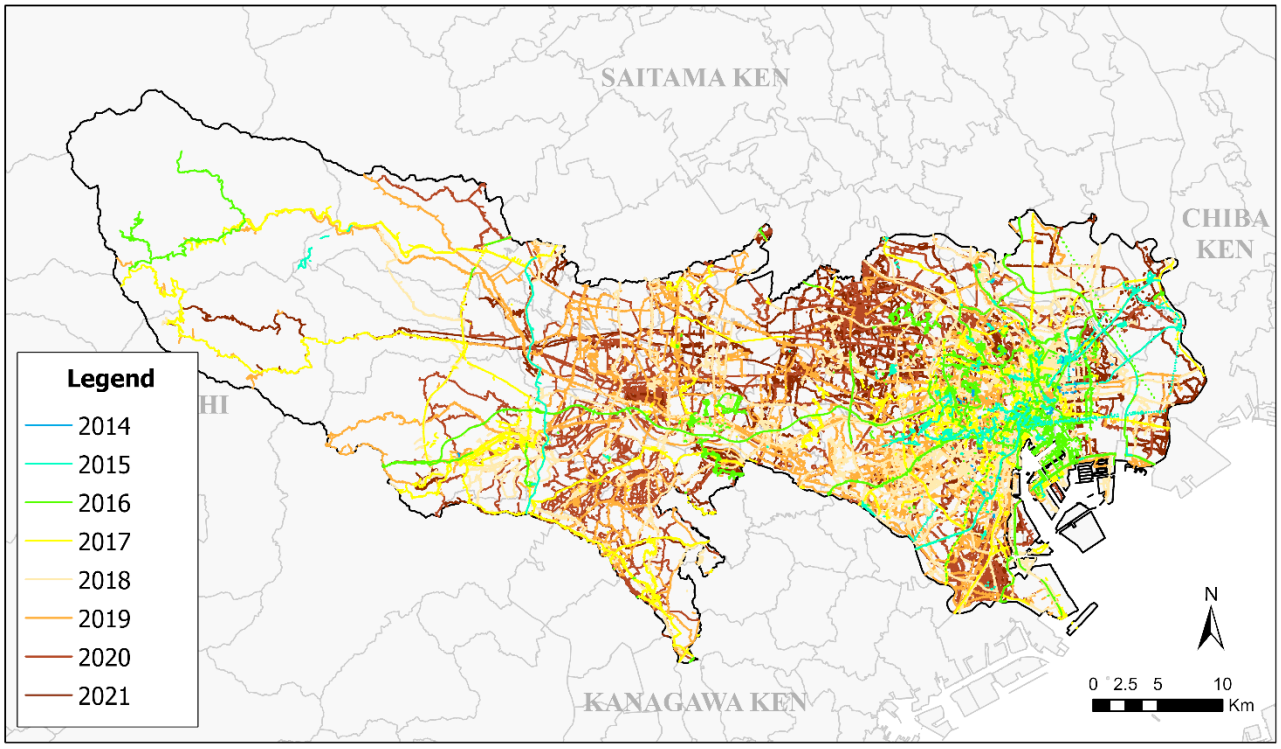

Figure 5 Completeness growth for different road types

data collection methods between OSM and Mapillay, a similar expansion pattern is found in this study. It also identified the existence and temporal sequence of those two elementary spatial patterns of *exploration* and *densification* for Mapillary. Prior to 2017, *exploration* appears to have been more dominant than *densification* in Tokyo, where data tends to be contributed along the major roads. From 2018 to 2021, the spatial pattern of *densification* along lower-grade roads became increasingly dominant compared to *exploration*. Notably, *exploration* began at an earlier stage for roads surrounding the center of Tokyo, resulting a high level of data coverage and virtually no new contributions after 2020.

4. Street Revisits and Data Quality Evaluation

Like other VGI platforms, Mapillary allows users to access all the historical data (unless removed by its contributors). This allows the data to be overlaid in both temporal and spatial dimensions, potentially improving its quality. GSV serves as the benchmark for these evaluations.

4.1. Street Revisits

We first analyzed the composition of roads contributed each year. As shown in Figure 7, a significant proportion of contributions are made towards previously mapped roads. We then calculated the revisit frequency for each road by calculating the number of unique dates of data contributions. In Tokyo, the mean value of revisit frequency is 3.1 days (SD: 6.6), ranging from 1 to 120 days. As illustrated in Figure 8, the distribution of revisit time is less geographically influenced, and the higher value is found on the major roads.

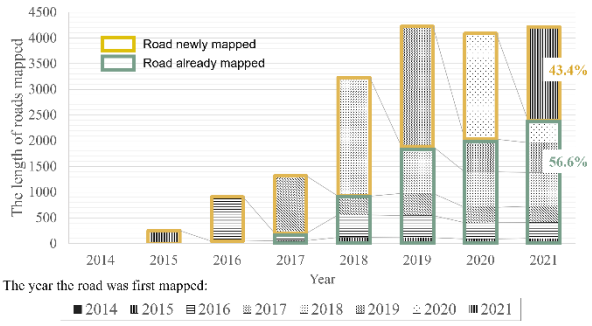

Figure 6 Composition of roads

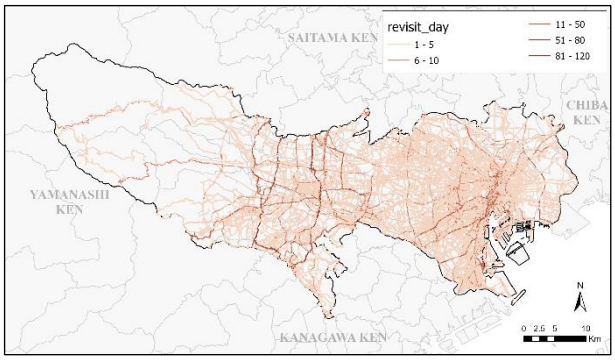

Figure 7 Distribution of revisit days

Table 1 Descriptive statistics of temporal features

	Years of updates		Hourly diversity		Seasonal diversity	
	M	*SD*	*M*	*SD*	*M*	*SD*
National Expressways (N=4436)	3.46	1.62	5.68	3.77	2.90	1.08
National Highways (N=5350)	2.95	1.50	4.90	3.26	2.54	1.05
Prefectural Roads (N=31,275)	2.09	1.20	3.15	2.71	2.03	1.04
Municipal Roads (N=129,399)	1.46	0.82	1.81	1.55	1.44	0.76
Parkways/ Garden paths (N=15,359)	1.43	0.80	1.76	1.45	1.38	0.71

Table 2 Correlations with revisits

	Years of updates	Hourly diversity	Seasonal diversity
National Expressways	.877**	.972**	.845**
National Highways	.849**	.958**	.866**
Prefectural Roads	.865**	.953**	.898**
Municipal roads	.872**	.939**	.884**
Parkways	.894**	.923**	.878**

4.2. Evolution of data characteristics

This section examines the evolution of data characteristics along with street revisits in terms of temporal and spatial features.

4.2.1 Temporal features

For temporal features, years of updates represent the span of years of data for each road, enabling yearly comparisons of streetscapes. Hourly and seasonal units are used to analyze temporal diversities, reflecting VSVI's ability to observe dynamic streetscape features. Table 1 presents descriptive statistics of these variables for different road types. Generally, Mapillary is found to be better than GSV for temporal features, including a wider time span (1.43-3.46 years per road), greater hourly diversity (1.76-5.68 hours per road), and more seasons (1.38-2.90 seasons per road), The strength of temporal diversity decreases as the road grade decreases. Addtionally, as shown in Table 2, all three temporal features have a strong correlation with revisits for all road types.

4.2.2 Spatial features

As for the spatial feature, we examined spatial density, viewing angle coverage, and the existence of pedestrian perspectives. Regarding spatial density, GSV provides about one image per 10 meters, which remains constant over time, whereas VSVI may indicate more strength in this area. With respect to viewing angle completeness, as all GSV images are panoramas that provide complete viewing coverage, we explore whether the revisit behavior compensates for the drawback in VSVI. Finally, we investigated whether VSVI can offer more pedestrian view photos, which GSV often omits.

Results in Table 3 show that Mapillary generally outperforms GSV in spatial density (0.40-1.22 points per meter) and reflecting pedestrian perspective (23.9% - 59.4% of roads contain pedestrian view photos) but falls short in viewing angle completeness. Correlation between revisits and spatial density is strong for high-grade roads (0.771**-0.825**) while weak for low-grade roads (0.385**-0.406**) (Table 4). Moderately strong to weak correlations were found for the angle of view (0.436**-0.732**). Regarding the feature of containing pedestrian pictures, prefectural roads without pedestrian pictures had a higher value of revisit, while no significant difference

was found for national highways (Table 5).

Table 3 Descriptive statistics of spatial features

	Spatial density		Viewing angle coverage (%)	
	Mean	*SD*	*Mean*	*SD*
National Expressways (N=4436)	0.71	0.72	64.2	31.0
National Highways (N=5350)	1.22	1.30	56.4	28.3
Prefectural Roads (N=31,275)	0.76	1.20	46.5	27.3
Municipal Roads (N=129,399)	0.40	0.80	38.7	27.3
Parkways/ Garden paths (N=15,359)	0.76	2.24	53.2	35.3

Table 4 Correlations with revisits

	Spatial density	Viewing angel coverage
National Expressways	.813**	.627**
National Highways	.825**	.673**
Prefectural Roads	.771**	.732**
Municipal roads	.406**	.700**
Parkways	.385**	.436**

Table 5 Independent samples t-test for revisits

	Containing pedestrian pictures		Without pedestrian pictures		p
	M	*SD*	M	*SD*	
National Highways	9.89	10.46	9.90	15.88	0.980
Prefectural Roads	5.02	7.601	6.07	12.069	<.001

5. Discussion

By analyzing Mapillary data in Tokyo, this study presents an analysis of VSVI's contribution behavior, and the evolution of data characteristics under this contribution behavior, using GSV as a benchmark.

5.1. Street network growth

Contribution inequality in different road types has been previously reported in VGI studies and VSVI studies conducted in other countries (Juhasz & Hochmair, 2015). The relative abundance of posting users on major roads (Seto & Nishimura, 2022) may explain the observed completeness inequality.

After more than 8 years of contribution, high-grade roads (e.g., national expressways, national highways) have achieved a dataset that is nearly as complete as GSV in Tokyo (GSV is reported with completeness values ranging from 77.11% to 91.44% for selected cities in Germany in 2015; Juhasz & Hochmair, 2015). For VSVI where volunteers have to travel along streets to collect data, the mapping behavior is subject to the travel environment. Specifically, the speed of travel modes impacts the mapping speed, and higher traffic volumes increase potential contributors, resulting faster completeness rates for high-grade roads. This finding suggests that the unplanned VSVI contribution method can produce a complete dataset like other commercial SVI dataset especially for high-grade roads, while may facing data unavailability for low-grade roads.

Notably, only 16.7% of garden paths/parkways contain Mapillary data, and the value has increased slowly. Pictures of traditional SVI are predominantly collected by devices mounted on cars, bikes, or other transportation means. Mapping non-motorized paths is time-consuming and costly for them and therefore limited to a few densely populated areas. As a result, VSVI is often reported to provide better coverage than traditional SVI for these non-motorized roads in previous study (Juhasz & Hochmair, 2015) and this study (Figure 8). Therefore, VSVI may serve as complementary data to traditional SVI in studies on non-motorized roads.

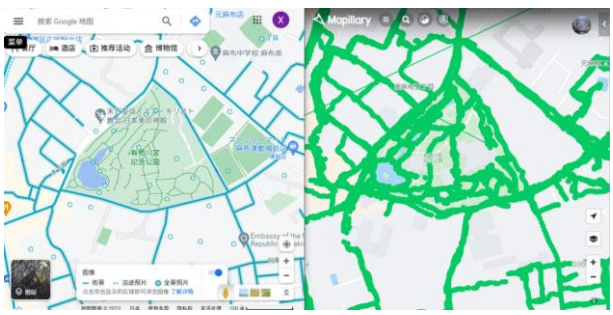

Figure 8 Comparison of data coverage for a park between GSV (left) and Mapillary (right)

Investigations on the spatial expansion process is to

understand the availability of VSVI data at different development stages. Given the differences in data collection methods between VSVI and other VGI, it seems that the expansion process is governed by the spatial distribution of contributors and their activity patterns. The spatial heterogeneity could be explained by the unequal distribution of users, likely caused by the fact that this novel VSVI platform became prevalent earlier in the city center than in the outskirt. *Exploration* tends to occur and complete earlier than *densification* may have different explanation with other VGI related to travel patterns. Contributions from high-speed roads are considerably more efficient than contributions from low-speed roads for street-level image collection.

5.2. Street revisits and quality evolution

As contributions increase, revisits appear to be more dominant than network expansion. Regarding the spatial distribution of revisit activity, it is found that higher revisits in the city center are limited to a small area and mostly subject to road grade. The higher number of users resulted from high population density in city center (Mahabia et al., 2020) may partially explain the higher level of revisits. For the result that higher revisits along major roads could be due to the high number of users and more active contribution activity for users along these roads (Seto & Nishimura, 2023). The possible explanations to this phenomenon include large traffic volume and higher network connectivity for major roads.

Unlike other geographic information such as building shape or location name, the visual information of SVI is more sensitive to time. This study also confirmed the unique contribution of VSVI in achieving a dataset with high temporal resolution through volunteered contributions. It demonstrates the strength of VSVI in temporal diversity at the street level and confirmed the potential to achieve greater temporal diversity with increasing revisits.

Spatial resolution is critical in conducting accurate environmental assessments, such as surveys of small items (e.g., trash). Result in this part indicates that contribution behavior patterns have a greater effect on spatial features than the number of contributions. For example, users who collect pictures while walking are more likely to achieve data with high density and use professional equipment such as panorama cameras. Additionally, VSVI has shown the ability to solve the problem of reflecting pedestrian perspectives well for some motorized roads. However, the assumption that more revisits bring higher possibility for pedestrian contributions may not hold true. The possible explanation is that, unlike contributors traveling by car, who tend to select major roads with higher levels of connectivity, pedestrian contributors are more inclined to select roads that are safer, more interesting for taking pictures, and easier to access through walking.

6. Conclusion

To better understand the data quality improvement mechanisms for the VSVI, this study examined VSVI's data characteristics from the perspectives of completeness and quality and investigated links between these features and contribution activity. While contribution inequality is inevitable in this volunteered data, VSVI may serve as complementary data to traditional data, offering a wider data coverage and perspective due to its unique and various data collection methods. The accumulation of data through revisits can improve some elements of data quality, such as spatial density and temporal diversity. However, it has been found that the increasing revisits may not offset image quality deficiencies resulting in insufficient viewing angle even though for the major roads. This concern could be resolved by more widespread use of advanced photography equipment.

Reference

Biljecki, F. and Ito, K. (2021) "Street view imagery in urban analytics and GIS: A review," *Landscape and Urban Planning*, 215, p. 104217. Available at: https://doi.org/10.1016/j.landurbplan.2021.104217.

Corcoran, P., Mooney, P. and Bertolotto, M. (2013) "Analysing the growth of OpenStreetMap networks," *Spatial Statistics*, 3, pp. 21–32. Available at:

https://doi.org/10.1016/j.spasta.2013.01.002.

D'Andrimont, R. *et al.* (2018) "Crowdsourced Street-Level imagery as a potential source of In-Situ data for crop monitoring," *Land*, 7(4), p. 127. Available at: https://doi.org/10.3390/land7040127.

Goodchild, M.F. (2007) "Citizens as sensors: the world of volunteered geography," *GeoJournal*, 69(4), pp. 211–221. Available at: https://doi.org/10.1007/s10708-007-9111-y.

Inoue, T. *et al.* (2022) "Landscape value in urban neighborhoods: A pilot analysis using street-level images," *Landscape and Urban Planning*, 221, p. 104357. Available at: https://doi.org/10.1016/j.landurbplan.2022.104357.

Juhasz, L. and Hochmair, H.H. (2015) "Exploratory Completeness Analysis of Mapillary for selected cities in Germany and Austria," *Gi_Forum J. Geogr. Inf. Sci.*, pp. 535–545. Available at: https://doi.org/10.1553/giscience2015s535.

Juhász, L. and Hochmair, H.H. (2016) "User contribution Patterns and completeness evaluation of Mapillary, a crowdsourced street level photo service," *Transactions in GIS*, 20(6), pp. 925–947. Available at: https://doi.org/10.1111/tgis.12190.

Li, X. (2021) "Examining the spatial distribution and temporal change of the green view index in New York City using Google Street View images and deep learning," *Environment and Planning B: Urban Analytics and City Science*, 48(7), pp. 2039–2054. Available at: https://doi.org/10.1177/2399808320962511.

Li, X. *et al.* (2015) "Assessing street-level urban greenery using Google Street View and a modified green view index," *Urban Forestry & Urban Greening*, 14(3), pp. 675–685. Available at: https://doi.org/10.1016/j.ufug.2015.06.006.

Ma, D. *et al.* (2019) "The State of Mapillary: An Exploratory analysis," *ISPRS International Journal of Geo-information*, 9(1), p. 10. Available at: https://doi.org/10.3390/ijgi9010010.

Permissions – *Google* (no date). Available at: https://www.google.com/intl/ja_ALL/permissions/geoguidelines/.

Seto, T. and Nishimura, Y. (2022) "Analysis of the spatiotemporal accumulation process of Mapillary data and its relationship with OSM road data: A case study in Japan," The International Archives of the Photogrammetry, Remote Sensing and Spatial Information Sciences, XLVIII-4/W1-2022, pp. 403–410. Available at: https://doi.org/10.5194/isprs-archives-xlviii-4-w1-2022-403-2022.

Zhen, F., Wang, B. and Wei, Z. (2014) "The rise of the internet city in China: Production and consumption of internet information," *Urban Studies*, 52(13), pp. 2313–2329. Available at: https://doi.org/10.1177/0042098014547369.

Analyzing the Authenticity and Integrity of Cultural Landscapes Using Geographic Data
- A Case Study of Pickle-making in Sichuan Province, China -

Suxueer Sun*, Naoko Fujita**, Hideki Kobayashi***, Yang Zhou****, Suzu Shimada****, Zile Tian****

Abstract Pickle production embodies regional traits that encompass cultural and geographical dimensions as a secondary food-processing activity deeply embedded in local contexts. This study employed geographic information data to evaluate the genuineness and coherence of cultural landscapes through an analysis of transportation accessibility and land-use dynamics within the landscape. Our findings highlight how the vicinity of residents' living areas shapes the cultural landscape, intertwined with time-honored food-processing traditions. The adjustments and alterations carried out by local inhabitants in response to their surroundings and traditional food-processing practices can be viewed as visible markers of authenticity inherent in cultural landscapes.

Keywords: cultural Landscape, pickle-making, transportation accessibility, authenticity

1. Introduction

Cultural landscapes inscribed on the World Heritage List are cultural properties and represent the 'combined works of nature and of man,' (UNESCO World Heritage Centre, no date). The protection of cultural landscapes can contribute to contemporary techniques of sustainable land use and can help maintain or enhance natural values in the landscape (UNESCO World Heritage Center, no date). Although landscapes are appropriate units for the sustainable assessment of biodiversity and cultural heritage (Liu and Taylor, 2002), we currently lack specific evaluations of cultural heritage and biodiversity (Neumayer, 2001).

Authenticity and integrity serve as indicators for assessing cultural landscapes, with conditions to fulfill authenticity, including aspects such as form and design, materials and substance, location and setting, etc. These elements can intricately describe the specific artistic, historic, social, and scientific dimensions of cultural landscapes (UNESCO World Heritage Center, no date). Additionally, Silva et al. (2022) point out that the authenticity of intangible heritage is closely intertwined with a community's cultural, social, and natural evolution and how these transformations are understood by the community in relation to their identity. When evaluating the integrity of cultural landscapes, it is essential to examine whether all the elements expressing their Outstanding Universal Value are included, whether there is sufficient spatial coverage, and whether they are adversely affected by development and/or neglect (UNESCO World Heritage Center, no date).

While some scholars have pointed out that the nomination and inscription of World Heritage Sites have historically been dominated by Europe (Brumann and Gfeller, 2021b), in recent years, discussions about Asian cultural landscapes and intangible heritage have increased (Taylor and Altenburg, 2006). Certain studies are now focusing on agricultural and cultural landscapes in Asia. For several years, the Japan Cultural Agency has conducted investigative reports on Japan's traditional way of life and food culture. In both Japan and South Korea, substantial research has been conducted on the cultural landscapes of rice terraces and paddy agriculture (Piras et al., 2022; Kieninger et al., 2012; Jung and Ryu, 2015).

However, the lack of evaluation criteria for the intangible aspects of cultural landscapes makes it difficult

GISA Members
* Student member, Graduate School of Comprehensive Human Science, University of Tsukuba; 1-1-1 Tennodai, Tsukuba, Ibaraki, Japan; s2130487@u.tsukuba.ac.jp
** Member; Institute of Art and Design, University of Tsukuba; fujita.naoko.gf@u.tsukuba.ac.jp
*** Institute of Art and Design, Kanazawa University
**** Student member, Graduate School of Comprehensive Human Science, University of Tsukuba

to properly assess cultural landscapes that heavily involve intangible elements related to life and livelihoods (Silva et al., 2022). Existing research assessing the authenticity and integrity of cultural landscapes often employs qualitative analysis. Kawashima (2021), using the example of Hidden Christians' Villages in Nagasaki, illustrates the challenges faced in the United Nations' assessment of authenticity for cultural landscapes that predominantly lack tangible heritage components. Nezhad, Eshrati, and Eshrati (2015) propose a theoretical framework for evaluating the authenticity of cultural landscapes through data analysis. Gao and Jones (2020), through ethnographic research, uncover the shared complexities surrounding authenticity in both China and Scotland. Garcia-Esparza, Juan (2018) discusses vernacular habitats, suggesting that the concept of "authenticity" results from cognitive processes influenced by conscious and unconscious perspectives. Li and Wang (2023), through field surveys, gather tourist perceptions of the authenticity of traditional village cultural landscapes, asserting that authenticity plays a role in traditional rural tourism.

Many scholars have conducted research on the authenticity and integrity of cultural landscapes using geographical information data analysis. Yang and Han (2020) assert that Geographic Information Systems (GIS) represent the most revolutionary method for recording and conserving cultural heritage, especially cultural landscapes. They exemplify this by considering the Slender West Lake Scenic Area, where different database features are employed to represent both the physical environment and the intangible cultural heritage components of the site. Angelstam et al. (2003) evaluated the authenticity of cultural heritage levels through visual inspection of satellite images. Al-Saad (2017) employed GIS to analyze land use changes in the cultural landscape of the Jerash Archaeological Site and to identify the impacts of modern urbanization on it. Moreover, a wealth of previous research has utilized GIS analysis, including studies by Tena (2018), Cuca and Agapiou (2018), and Li and DeLiberty (2021).

This study focuses on the assessment of lifestyle- and livelihood-oriented cultural landscapes in Asia. Pickle-making, a food processing activity rooted in local traditions, creates landscapes that reflect regional characteristics. With its long history and stability, pickle-making satisfies the integrity requirements of cultural landscapes (Taylor and Lennon, 2011). Furthermore, its widespread worldwide presence has led to distinct variations in pickle-making and the resulting landscapes, each with unique features. We contend that such landscapes possess outstanding universal value and align with UNESCO's definition of an "organically evolved landscape" within cultural landscapes (UNESCO World Heritage Centre, no date).

As an example of a landscape formed through traditional livelihoods and lifestyles, the boundaries of the landscape formed by pickle making are vague and encompass numerous intangible elements that cannot be directly observed. To address this, we employed geographical data analysis to analyze and assess the landscape features, authenticity, and integrity of the cultural landscape associated with pickle-making. This approach enables quantification and analysis of intangible elements within the cultural landscape as tangible data. The conclusions drawn from this research contribute to the preservation of traditional living cultures, culinary traditions, and related landscapes. Given the differences in values between Eastern and Western perspectives, particularly in discussions about vernacular aspects (Silva et al., 2022), an Asian perspective is necessary to highlight Asian culinary and lifestyle cultures and to enhance their influence.

2. Methods

To achieve the research objectives of this study, we selected the distribution areas of Sichuan pickle-making, which boasts high recognition and a rich history. The research regions included Guangyuan, Chengdu, Mianyang, Meishan, Ziyang, and Luzhou in Sichuan Province, China (Figure 1). Onsite investigations were

conducted from June 1st to June 19th, 2022, and the study was divided into three approaches.

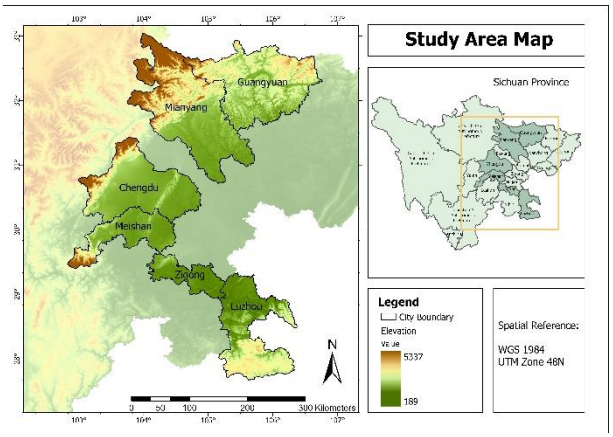

Figure 1 Study area

2.1. approach1

Through data analysis and on-site investigations, specific research sites were identified for detailed analysis. Geographic analysis was conducted on the primary distribution areas of the research sites.

Data Collection: High-resolution 12.5m DEM (Digital Elevation Model (DEM) data for each research region were obtained from EARTHDATA. The data source was ©JAXA/METI ALOS PALSAR L1.0 2009, accessed through ASF DAAC on August 18, 2023.

Data Analysis: The DEM data for these areas were subjected to slope, aspect, contour, and hillshade analysis. The Slope tool identifies the steepness of each cell on a raster surface. Lower slope values indicate flatter terrain, whereas higher values indicate steeper terrain (How Slope Works-ArcGIS Pro | Documentation, no date). The Aspect tool identifies the direction of the downhill slope face (How aspect works—ArcGIS Pro | Documentation, no date). The distribution of the contour lines depicts how the values change across a surface. A wider spacing of contour lines indicates minimal value change, whereas a closer spacing corresponds to rapid value fluctuations (How contouring Works—ArcGIS Pro | Documentation, no date). The Hillshade tool generates hypothetical surface illumination by calculating illumination values for each cell in a raster, simulating the shadow effect on the terrain (How Hillshade Works—ArcGIS Pro | Documentation, no date). Through these analyses, the land characteristics of these regions were determined and factors that could impact the lifestyles and dietary habits of local residents were examined to understand the significance of pickle-making activities in these areas.

2.2. approach2

Aerial images were captured using drones at various research sites. In this study, research sites with valid aerial images were referred to as "data collection sites" for differentiation, named as SC01 to SC20. These aerial images were georeferenced to obtain the geographic coordinates of the cultural landscape elements within each data collection site. Compared to existing map data, the high clarity of aerial images captured by drones allows for the easy identification of element features. This assists in clarifying the elements that reflect the authenticity and integrity of the cultural landscape of Sichuan pickle-making. Additionally, these elements were categorized and analyzed to decipher patterns within the cultural landscape.

Data Collection: A total of 284 overhead photographs were captured using unmanned aerial drones at various research sites related to pickle-making. The real-time locations of each capture were recorded using ArcGIS Earth Mobile. ArcGIS Earth Mobile enables the creation of geographic reference points, markers, pathways, polygons, annotations, and data manipulation (3D Earth Map | Earth App for Desktop & Mobile | ArcGIS Earth, no date). The drones used for this study were of the DJI Mini 2 model, known for its portability and user-friendliness, weighing less than 199 g (DJI Mini 2 - Make Your Moments Fly - DJI, no date), leading to fewer flight restrictions. The drones used in this study were purchased from Japan and registered on the Unmanned Aircraft Registration Web Portal/Japan. All captures were conducted within authorized flight zones and below the restricted maximum flight altitude of 150 m. All photographs were taken with the permission of the local residents and their awareness of the intended usage of the images. During drone photography, we paid particular

attention to the following elements and informed residents that we would be capturing them: rivers, vegetation, farmland (for economically cultivated crops), farmland (for household-consumed crops), unused land, residential houses (primary residences), residential houses (former residences), other structures connected to primary residences (storage warehouses, work sheds, storage rooms, etc.), structures not connected to primary residences, courtyards, and paths. We invited residents to review the captured photographs, asking them to identify plant species in farmland and other cultivated areas, mark areas where ingredients for pickling were grown, and describe the distribution of spaces used for pickle-making (including both outdoor and indoor spaces).

Data Analysis: First, we exported the locations of the research sites in KMZ format from ArcGIS Earth Mobile. The research sites were divided into 60 survey points and 20 data-collection sites. The location information of these two types of points was imported into ArcGIS Pro, a widely used mapping software that integrates multiple data sources, visualizes and edits data, and conducts analysis (2D, 3D, and 4D GIS Mapping Software | ArcGIS Pro, no date). Under the WGS 1984 UTM Zone 48N projection coordinate system, distribution maps were created for both the survey and data collection sites.

Next, we analyzed the data collection sites with valid aerial images in ArcGIS Pro. Despite the lightweight and limited flight restrictions of DJI Mini 2, it lacks GPS and its aerial images lack coordinate information. To address this, georeferencing was applied in ArcGIS Pro to position drone-captured aerial images. Georeferencing tools align raster data without spatial reference information or register them to a map coordinate system (Overview of Georeferencing—ArcGIS Pro | Documentation, no date). Import the drone-captured images without coordinates and, using ArcGIS Earth point data, locate the points on satellite imagery basemaps with the WGS 1984 Web Mercator (auxiliary sphere) projection coordinate system. Georeferencing control points were added based on prominent features such as buildings, roads, and public facilities in clearer satellite imagery. Once the aerial images are accurately positioned, mark the ranges of elements related to pickle-making within each representative site: ingredient area, cooking and preserving area, eating area, processing area, path, residential house, heritage site, farmland, and fishpond. This process aims to clarify the landscape composition elements of pickle-making cultural landscapes at each representative site and to develop element pattern maps.

2.3. approach3

Visual interpretation was conducted by comparing historical maps of the study area to derive conclusions regarding changes in the cultural landscape of pickle-making and its impacts on the local environment.

Data collection: Aerial photographs of data collection sites SC01–SC20 were downloaded from Google Earth Pro at two different scales (Source of Map Data: Google Earth Pro application. Google LLC. Maxar Technologies.) allowing for enhanced observation. The time span covers 2002–2023.

Data analysis: Visual Interpretation was performed on historical maps spanning approximately 20 years for the same locations. For each site, three to five years were chosen and arranged from left to right in chronological order to interpret the characteristics of both small and large-scale changes in the surrounding landscape elements.

3. Results

3.1. Distribution and Geographic Features of Research Sites

Through on-site investigations, we identified 60 landscape sites related to pickle making, conducted field observations, and conducted brief interviews. The distribution of the survey points is shown in Figure 2.

Representative and diverse points with pickle-making activities and landscape features were selected as Data

Collection Sites for further investigation and analysis. Their locations are shown in Figures 3, 5, and 7, primarily concentrated in Guangyuan, Meishan, and Zigong, respectively. The Data Collection Sites were classified into five types: residence (marked in yellow), Vegetable Farm (green), Vegetable Market (light blue), restaurant (blue), and Historical Sites (pink).

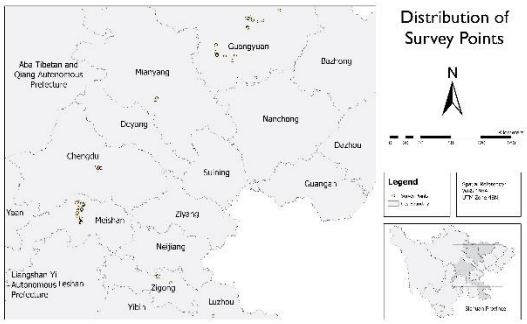

Figure 2 Distribution of survey points

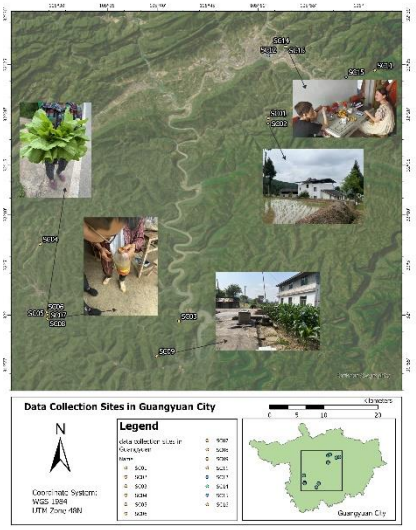

Figure 3 Data collection sites in Guangyuan city

As shown in Figure 4, the sites in Guangyuan were predominantly located on land with very gentle to moderate slopes, with slope values ranging from 1.811248 to 15.04016. This terrain is suitable for both residential and agricultural activities. The main river and mountain range on the northern side are visible. SC03, which relies on cultivating mustard green, a key ingredient for pickle production, along with other vegetable farmers, has developed fields near this river to ensure a stable irrigation water source.

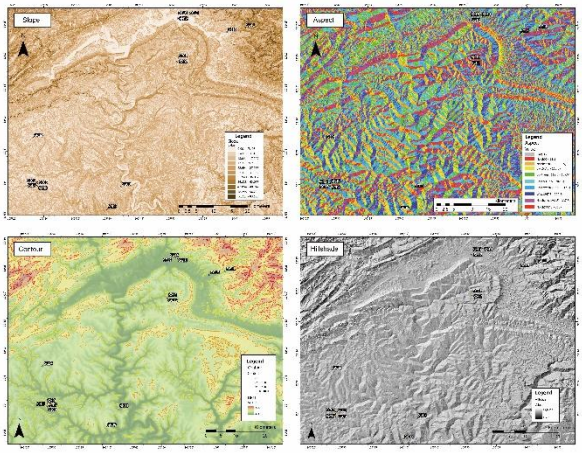

Figure 4 Geographic features of guangyuan

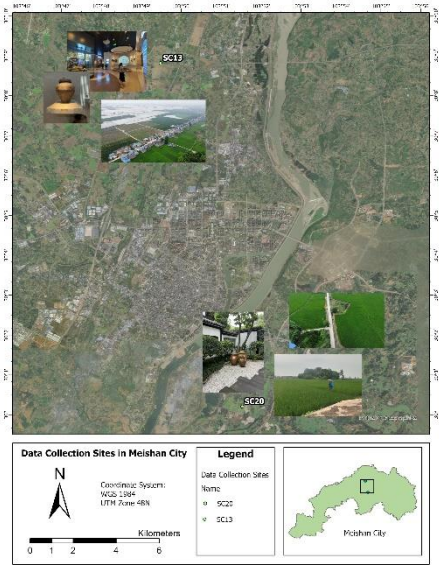

Figure 5 Data collection sites in Meishan

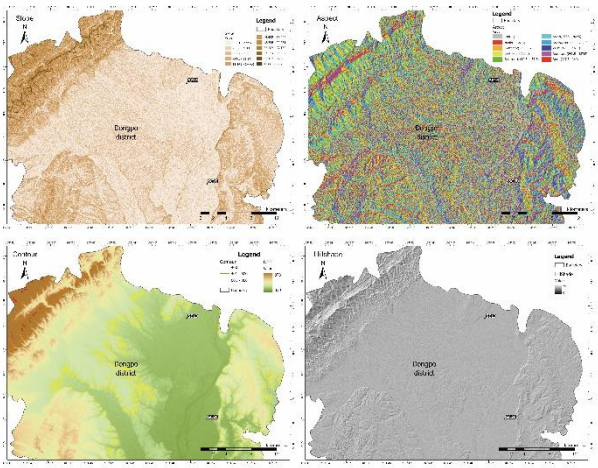

Figure 6 Geographic features of meishan

As shown in Figure 6, the main urban area of Meishan, located in Dongpo District, lies in a gently sloped area

between the mountain ranges. The research sites consisted of two vegetable farms that practiced rotation of rice and mustard green cultivation. Adjacent to these farms are a mustard green processing company and a pickle museum, benefiting from a strategically advantageous geographical location. The slopes of these two sites are 3.237688 and 4.573921, respectively, which are generally considered moderate slopes, conducive to soil conservation and water infiltration, making them suitable for agricultural activities.

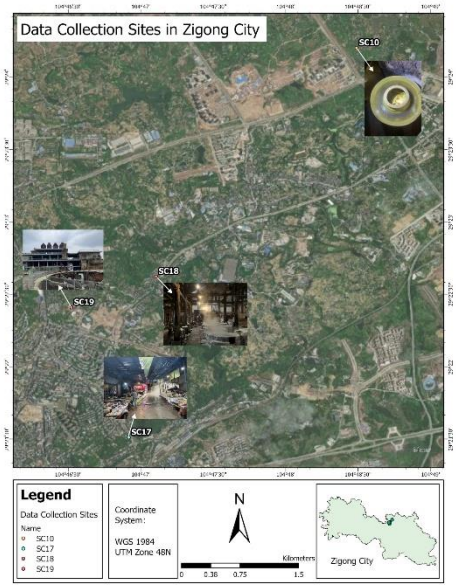

Figure 7 Data collection sites in Zigong city

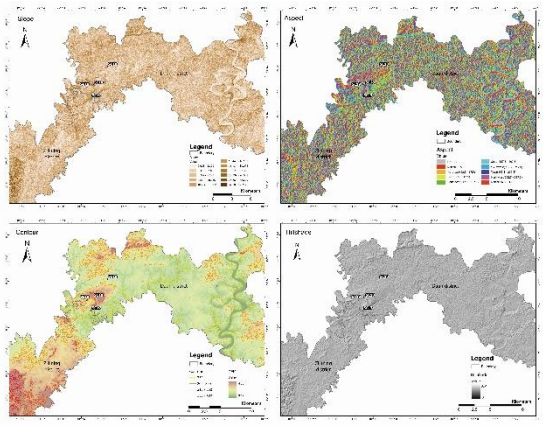

Figure 8 Geographic features of zigong

Zigong City possesses numerous remnants and sites of salt industry culture, such as the SC18 Shenhaijing Ancient Salt-making Site and SC19 Old Salt Field in 1957. The source of high-quality salt ensures the production of salt-soaked pickled vegetables in Sichuan Province. As shown in Figure 8, Zigong City exhibits a diverse range of slope variations, although the numerical differences are not significant and the intensity of the mountain shadow is relatively mild.

3.2. Landscape composition and patterns of research sites

Through georeferencing of aerial images captured by drones and marking of element extents, we obtained geospatially referenced landscape composition maps (Figure 9) and landscape composition pattern maps (Figure 10) for the data collection sites. We found that pickling was predominantly carried out by households for personal consumption, specifically in SC01, SC02, SC08, SC09, and SC10. The cultivation and processing of pickled vegetables is closely linked to residential houses. Common pickling vegetable cultivation areas include vacant spaces alongside paths, personal courtyards, and spaces between self-cultivated economic crop fields (or fishponds), leading to cost-effective pickling production. Drying pickling ingredients often takes place in front of courtyards, whereas the pickling process is conducted in outdoor corridors under house eaves. Consecutive pickling steps are conveniently executed in close proximity, making the combination of outdoor corridors and courtyards a crucial space for pickling. Furthermore, this space also serves to dry grains and other crops, as well as process vegetable oil, showcasing significant representative agricultural activities in rural areas alongside the pickling production cultural landscape.

SC03, engaged in industries related to pickling production, witnessed changes in the types of vegetables used for personal pickling consumption in accordance with the varieties used by pickling factories. The vegetables used for personal consumption are cultivated in corners adjacent to fields used to produce vegetables for sale in pickled form, with trees acting as natural dividers, serving as an embodiment of how humans use natural resources to shape the landscape. Similarly, farmers residing near vegetable bases SC13 and SC20 ingeniously utilized their spaces by creating their own small vegetable gardens in irregular spaces adjacent to the enterprise's

mustard fields. From SC16 and SC17, it can be observed that urban residents within relatively confined spaces also have diverse sources for pickling ingredients: markets connected to residences, rooftop gardens/home gardens, and vegetable stalls along the streets.

The convenient acquisition of ingredients, low manufacturing costs, and skillful space utilization collectively contribute to the significant factors that underpin the cultural landscape of pickle-making in Sichuan.

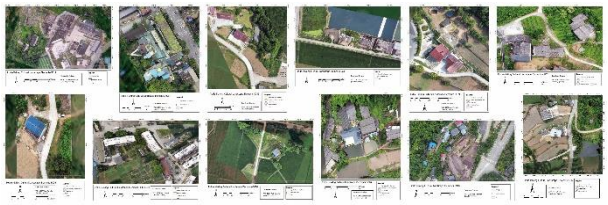

Figure 8 Landscape composition of research sites

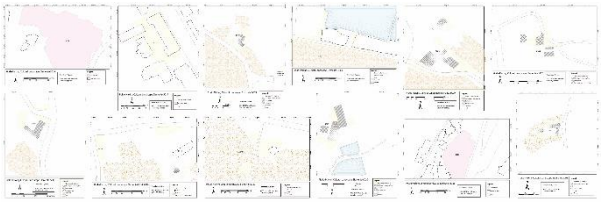

Figure 9 Landscape patterns of research sites

3.3 Changes in Landscape Elements

The selected data collection sites, SC01 to SC20, represented different types: residential houses, heritage sites, and pickle-making vegetable cultivation sites.

Residential Houses: In the past 20 years, local residents' dwellings have experienced relatively stable land use and village structures. In most areas, more land has been developed for cultivation and more and wider roads have been opened, improving local transportation convenience. SC10 serves as a more dramatic example of change, with newly constructed amusement parks, hotels, and modern high-rise buildings around the settlement. This significantly segmented the original village structure and reduced cultivated land. However, the small settlements surrounding SC10 and neighboring villages have maintained stability since 2007, with little change in their form and structure.

Pickle-making vegetable cultivation sites: Through map comparisons, we found that lands designated for cultivation have consistently been used for crop planting without being affected by development or other factors. The practice of rotating rice and pickling vegetables was inherited. Such landscape elements can be viewed as carriers for intangible elements in the cultural landscape, reflecting the tangible embodiment of local circular livelihoods and traditional ways of life. SC03, located adjacent to a vegetable farm used for pickle making, revealed that the introduction of a pickle factory into the existing environment did not alter the composition of the original cultivation area. However, it also introduced living spaces for factory workers, enriching landscape composition elements.

Heritage site: SC19 is a salt culture exhibition base transformed from an abandoned salt factory. Changes in maps from 2015 to 2018 indicate the local process of renovating and redesigning the discontinued factory without affecting the form of the surrounding buildings and landscapes. This was similarly observed in SC18. It is evident that the region has a certain understanding of heritage sites and is organized in their protection, contributing to the maintenance of the authenticity and integrity of the cultural landscape.

4. Discussion

This study discusses how to better assess the authenticity and integrity of cultural landscapes in the realms of daily life and livelihoods, where intangible elements play a significant role. Existing research emphasizes the "authenticity" as a measure of heritage quality, demanding legitimacy, truthfulness, and credibility of intangible heritage and cultural landscapes （Taylor, 2022）. We attempted to employ geographic information analysis to analyze and measure the tangible landscapes that serve as carriers of intangible elements within the pickle-making cultural landscape. This approach allowed us to grasp the authentic scope, timescale, and genuine landscape composition patterns of the cultural landscape under study. An effective assessment of the "authenticity" of the pickle-making

cultural landscape was conducted, yielding results beneficial for the preservation and development of local cultural landscapes. In addition, these findings can facilitate the discovery and evaluation of culturally rich landscapes with significant intangible components in other regions.

The cultural landscape sites related to pickle-making investigated and analyzed in this study are representative and diverse. These sites can be regarded as tangible landscapes that embody the authenticity and integrity of the cultural landscapes. The geographical features of these sites were showcased, quantifiable, and further analyzed. The intangible elements of cultural landscapes are documented and reflected in the corresponding tangible landscapes. These landscape sites can be considered representative of the cultural landscape of pickle making in Sichuan Province.

Based on the self-sufficiency of pickle-making within small-scale living circles, the widespread presence of home gardens, the common exchange and sharing of pickle brine and vegetables for pickling within settlements and neighborhoods, the continued intergenerational transmission of pickle jars within families, the abundant use of pickles in household recipes, and the preference for their taste, we speculate that the cultural landscape formed through pickle-making contributes to maintaining the form and composition of settlements. This in turn aids in preserving the green environment around residences, thereby promoting biodiversity and ecological balance.

While traditional pickle-making practices in these regions might fade or change in the future, the landscape elements of their cultural landscapes could endure as carriers of new purposes and behaviors. They will persistently remain in the environment, bearing witnesses to people's transformation and utilization of nature in the pursuit of life.

Regarding the limitations of this study, it has been noted that authenticity is not solely based on physical attributes but also requires discussions on cultural traditions, symbolic meanings, cultural diversity, and changes over time as criteria for assessing authenticity (Taylor, 2022). We also recognize the historical context, transmission, and inherent evolution of the traditional food processing practice of pickle-making, which synchronizes with the passage of time. Investigation of the "authenticity" and "integrity" of these elements will be conducted in future research.

Furthermore, this study only collected data from 20 sites across six cities, analyzing the cultural landscape characteristics of these locations. They cannot represent all areas within Sichuan Province, and these six cities are predominantly inhabited by the Han ethnic group, excluding the characteristics and composition of the pickle-making cultural landscapes of minority ethnic groups. In the future, we will continue to survey and document landscape sites influenced by pickle-making across more regions in Sichuan Province, continually enriching the description and assessment of the cultural landscape of pickle-making in the province.

5. Conclusion

This study focuses on the assessment of cultural landscapes related to life and livelihoods in the Asian region. The pickle-making cultural landscape of Sichuan Province, China, which is based on traditional livelihoods and ways of life, was selected as the research subject.

Through geographical analysis of the study area, we found that the land characteristics of the region are suitable for various agricultural activities and habitation. The slopes were gentle, which promoted soil retention and water infiltration.

By analyzing aerial photographs taken by drones after geographic registration, we evaluated the authenticity and integrity of the pickle-making cultural landscape in Sichuan Province. Landscape elements can be viewed as carriers for intangible elements within a cultural landscape. They embody tangible expressions of local cyclical livelihoods and traditional ways of life. These elements can be quantified, calculated, and analyzed. High-resolution drone images make it easier to identify

landscape features and present them comprehensively on the maps. For example, we can visually observe how trees serve as natural dividers between fields for pickling ingredients and fields for economic crops. This can be seen as a manifestation of human utilization of natural resources to shape the landscape. We discovered that convenient and quick access to ingredients, low manufacturing costs, and skillful spatial arrangements are important factors underpinning the pickle-making cultural landscape in Sichuan.

Through the visual interpretation of historical maps of the study area, we observed that the land use and village structures of most research sites have remained relatively stable over the past 20 years. In many regions, more land has been developed for agricultural purposes and additional and wider roads have been constructed to enhance regional accessibility. In areas influenced by economic development and urban planning, the small settlements surrounding the research sites have also maintained stability with little to no change in their form and structure.

Furthermore, we identified a certain level of understanding and organized the preservation of heritage and relics in the study area. This conditional and organized approach to conservation is conducive to maintaining the authenticity and integrity of the cultural landscape.

This study grasped the authentic scope, true time scale, and genuine landscape composition patterns of the cultural landscape in the study area. An effective assessment of the "authenticity" of the pickle-making cultural landscape was conducted, yielding results that contribute to the preservation and development of the local cultural landscape. Additionally, these findings are beneficial for identifying and evaluating cultural landscapes rich in intangible elements in other regions.

The cultural landscape sites investigated and analyzed in relation to pickle-making behaviors are both representative and diverse. The intangible elements of cultural landscapes are documented and reflected in the corresponding tangible landscapes. The categories represented by these landscape sites can serve as references for identifying and evaluating other cultural landscapes.

The cultural landscape formed through pickle-making contributes to the maintenance of the morphology and composition of settlements. This facilitates the preservation of the green surroundings around residences. While traditional pickle-making practices in these areas may change or even disappear in the future, the landscape elements of their cultural landscapes might serve as carriers for new purposes and human activities. They can persist in the environment and continue to bear witness to people's transformation and utilization of nature in the pursuit of life.

Acknowledgement

This research was supported by SPRING (Support for Pioneering Research Initiated by the Next Generation) program of Japan Science and Technology Agency (JST) (JPMJSP2124).

References

Al-Saad, S. (2017) Sustainable tourism management at potential world heritage sites: land use analysis by using gis: case study: Jerash Archaeological Site, Jordan. *PEOPLE: International Journal of Social Sciences*, **3(2)**, 614–636.

Angelstam, P. *et al.* (2003) Assessing village authenticity with satellite images: a method to identify intact cultural landscapes in Europe. *AMBIO: A Journal of the Human Environment*, **32(8)**, 594–604.

Brumann, C. and Gfeller, A. (2021b) Cultural landscapes and the UNESCO World Heritage List: perpetuating European dominance. *International Journal of Heritage Studies*, **28(2)**, 147–162.

Cuca, B. and Agapiou, A. (2018) Impact of land-use change and soil erosion on cultural landscapes: the case of cultural paths and sites in Paphos district, Cyprus. *Applied Geomatics*, **10(4)**, 515–527.

DJI Mini 2 - Make Your Moments Fly - DJI (no date).

Gao, Q. and Jones, S.L. (2020) Authenticity and heritage conservation: seeking common complexities beyond the 'Eastern' and 'Western' dichotomy. *International Journal of Heritage Studies*, **27(1)**, 90–106.

Garcia-Esparza, J. (2018) Clarifying dynamic authenticity in cultural heritage. A look at vernacular built environments. *ICOMOS University Forum*, **1**, 1-12.

How aspect works—ArcGIS Pro | Documentation (no date).

How contouring Works—ArcGIS Pro | Documentation (no date).

How hillshade works—ArcGIS Pro | Documentation (no date).

How slope works—ArcGIS Pro | Documentation (no date).

Jung, H. and Ryu, J. (2015) Sustaining a Korean traditional rural landscape in the context of cultural landscape. *Sustainability*, **7(8)**, 11213–11239.

Kawashima, T.D. (2021) The authenticity of the hidden Christians' villages in Nagasaki: issues in evaluation of cultural landscapes. *Sustainability*, **13(8)**, 4387.

Kieninger, P., Penker, M. and Yamaji, E. (2012) Esthetic and spiritual values motivating collective action for the conservation of cultural landscape—A case study of rice terraces in Japan. *Renewable Agriculture and Food Systems*, **28(4)**, 364–379.

Liu, J. and Taylor, W.W. (2002) *Integrating Landscape Ecology into Natural Resource Management*, Cambridge University Press eBooks.

Li, Q. and DeLiberty, T.L. (2021) Integrating drones, participatory mapping and GIS to enhance resiliency for remote villages. *Transactions in GIS*, **00**, 1– 21.

Li, X. and Wang, C.Y. (2023) Understanding the relationship between tourists' perceptions of the authenticity of traditional village cultural landscapes and behavioural intentions, mediated by memorable tourism experiences and place attachment. *Asia Pacific Journal of Tourism Research*, **28(3)**, 254–273.

Neumayer, E. (2001) The human development index and sustainability — a constructive proposal. *Ecological Economics*, **39(1)**, 101–114.

Nezhad, S.F., Eshrati, P. and Eshrati, D. (2015) A definition of authenticity concept in conservation of cultural landscapes. *ArchNet-IJAR*, **9(1)**, 93.

Overview of Georeferencing—ArCGIS Pro | Documentation (no date).

Piras, F., Fiore, B. and Santoro, A. (2022) Small Cultural Forests: landscape role and ecosystem services in a Japanese cultural landscape. *Land*, **11(9)**, 1494.

Silva, K.D., Taylor, K. and Jones, D. (2022) *The Routledge Handbook of Cultural Landscape Heritage in The Asia-Pacific*, Routledge eBooks.

Taylor, K. (2022) Concerning intangible associations and authenticity in cultural landscapes. In Silva, K.D., Taylor, K., & Jones, D.S. (Eds.). *The Routledge Handbook of Cultural Landscape Heritage in The Asia-Pacific*, Routledge, 49–59.

Taylor, K. and Altenburg, K. (2006) Cultural landscapes in Asia‐Pacific: potential for filling world heritage gaps1. *International Journal of Heritage Studies*, **12(3)**, 267‐282.

Taylor, K. and Lennon, J. (2011) Cultural landscapes: a bridge between culture and nature?. *International Journal of Heritage Studies*, **17(6)**, 537–554.

Tena, P.A. (2018) The perception of heritage values and their analysis by using GIS tools in vernacular heritage landscapes. *Vitruvio*, **3(1)**, 12.

UNESCO World Heritage Centre (no date) The Operational Guidelines for the implementation of the World Heritage Convention.

Yang, C. and Han, F. (2020) A digital information system for cultural landscapes: the case of Slender West Lake scenic area in Yangzhou, China. *Built Heritage*, **4**,3.

2D, 3D & 4D GIS Mapping Software | ArcGIS Pro (no date).

3D Earth Map | Earth App for Desktop & Mobile | ArcGIS Earth (no date).

Geographic information analysis of the transmission of cultural landscape values through farmers' guesthouses in Aso

Linda Gadhoum*, Naoko Fujita**, Suxueer Sun***, Yang Zhou***, Hideki Kobayashi****

Abstract This research indicates that farmers' guesthouses contribute extensively to The upkeep of the cultural historical past and sustainable lifestyles by adhering to FAO values. Aso in Kumamoto Prefecture has been distinctive as a World Agricultural Heritage Site and is in the process of being registered as a World Cultural Heritage Site. Through GIS evaluation, we capture the vicinity of farmers' guesthouses and reveal the geographic arrangement of neighborhood assets associated with the houses. This includes elements, such as land use, terrain, weather, and herbal assets. This highlights the importance of sustainable agricultural practices that defend natural assets, reduce environmental effects, and sell resilience in the face of weather changes.

Keywords: farmers guesthouses, FAO, biophilic design, sustainable tourism

1. Introduction

Globalization and urbanization have caused individuals to become disconnected, eroding their regional identities and culture. Traditional practices and knowledge vanish quickly, and young people increasingly seek economic opportunities. Recognizing and protecting heritage is now more important than ever before. The Food and Agriculture Organization of the United Nations (FAO) has proposed strategies to protect heritage and the environment. Design is a powerful tool that integrates elements into the architecture and cities. This concept seeks to reconnect people, nature, and cultures.

A significant aspect of this movement involves the establishment of farmers' guest houses as agents of change in communities. These guesthouses are dwellings or farmhouses that are transformed into welcoming accommodations for tourists. Through these arrangements, visitors can immerse themselves in culture and heritage. Moreover, these guesthouses provide a source of income for farmers, encouraging them to maintain their agricultural methods while embracing sustainable practices.

The FAO works to promote sustainable rural development, conserve biodiversity, and protect cultural heritage by advocating for biophilic design in the hotel's construction and renovation. This includes using local materials, sustainable construction, natural light and ventilation, green interior spaces, and integrating land into architecture. GIS technology is essential for mapping and analyzing cultural heritage, natural resources, and local customs. It preserves and complements cultural identity. This project combines biophilic design, the FAO's sustainable development goals, and GIS technology to create a balance between cultural heritage, economic growth, and ecological sustainability. Revitalizing farmers' guesthouses strengthens rural communities, allowing them to share their traditions, knowledge, and way of life with visitors.

GISA Members
* Student member, Graduate School of Comprehensive Human Science, University of Tsukuba; 1-1-1 Tennodai, Tsukuba, Ibaraki, Japan; **s2321629@u.tsukuba.ac.jp**
** Member; Institute of Art and Design, University of Tsukuba; **fujita.naoko.gf@u.tsukuba.ac.jp**
*** Student member, Graduate School of Comprehensive Human Science, University of Tsukuba
**** Institute of Art and Design, Kanazawa University

2. Objectives

This study seeks to suggest a more sustainable production and building approach by combining Biophilic Design and Sustainable philosophy. Biophilic Design, which emphasizes nature, can be used to suggest eco-friendly building strategies that integrate human habitats and nature, creating a healthier and more sustainable future.

This study explores the importance of farmers' guesthouses in preserving cultural history. It aims to demonstrate their capacity to sustain and promote local customs, traditions, and lifestyles, thereby contributing to the preservation and appreciation of cultural diversity.

Studies will explore sustainable tourism and its role in promoting farmers' guesthouses, focusing on the positive effects of responsible and eco-aware tourism practices. It emphasizes the importance of showcasing a country's cultural and environmental heritage in a sustainable and respectful manner. This approach not only ensures the preservation of natural resources but also enhances the nation's reputation as a responsible global citizen dedicated to environmental conservation and cultural appreciation.

3. Methods

This research surveys people of different ages and backgrounds to achieve three objectives and record results.

Chapter 1 reviews the research from articles, theses, and reliable websites. GIS will analyze sustainable and biophilic guesthouses' geographic arrangement, resources, land use, terrain, climate, natural resources, and FAO's role. Thus, farm stays and sustainable tourism could be combined. Chapters 2 and 3 examine a case study. We focused on sustainable experiences and green tourism by visiting case study sites and collecting local data through observations and professional research. In Aso, Kumamoto, we have immersed ourselves in the local community. Purposive sampling identifies key informants from farmers' guesthouses, agriculture, and culture. Semi-structured interviews were conducted to explore their views on guesthouses, culture, and sustainability. Engagements range from casual conversations to formal conversations, providing a comprehensive overview. Ethnographic observations at farmers' guesthouses will collect qualitative data on guests' engagement with the local culture and farming activities.

This study examined sustainable and biophilic designs and FAO's role. Chapter 4 compares the advantages and disadvantages of both study cases. This study shows how guesthouses can promote sustainability and the importance of preserving a region's heritage and identity. The conclusion summarizes the main points of this study. The study area was determined after multiple analyses, comparisons, and assessments.

4. Results

A crucial aspect of this research pertains to the strategic distribution of Farmers' Guest Houses (Figure 1). Farmers' guesthouses offer a unique and authentic experience in rural settings. They provide more than traditional hospitality, immersing visitors in agricultural activities and local farm life. These accommodations blend traditional hospitality, sustainable farming, and community involvement. Farmers' guesthouses offer more than a place to stay; they provide a chance to experience the local agricultural lifestyle. Guests can participate in farming activities such as tending crops, harvesting, milking cows, and collecting eggs. This concept provides urbanites the opportunity to reconnect with nature and appreciate their agricultural heritage. Guesthouses provide cultural exchanges, allowing travelers to learn about local customs, traditions, and

lifestyles. Guests can interact with farmers and artisans to deepen their understanding of the region's culture. Sustainability is key, as farmers' guesthouses promote eco-friendly practices and sustainable food systems. Organic farming, waste recycling, and energy-efficient operations are used to reduce the environmental impacts. The FAO's conservation efforts and biophilic design principles, integrated into sustainable tourism practices, will boost human well-being and foster a deep, lasting connection with nature. This integration is expected to shift tourists' attitudes and behaviors towards environmental conservation and sustainable living, preserving cultural heritage, and creating a more resilient and sustainable environment for current and future generations.

The results are expected to improve human well-being, with tourists feeling a deep connection to nature. This transformative experience is likely to change tourists' attitudes and behaviors towards environmental conservation and sustainable living. The results of the two cases may differ because sustainable tourism and biophilic design are still new in Tunisia, although there are some steps towards sustainability and eco-friendly tourism. We suggest solutions that combine FAO, biophilic design, and farmers' guesthouses to create a sustainable environment. This fusion highlights the region's culture, creates a distinct identity, and promotes local cuisine and its ingredients. This will also benefit the region's economy and landscape.

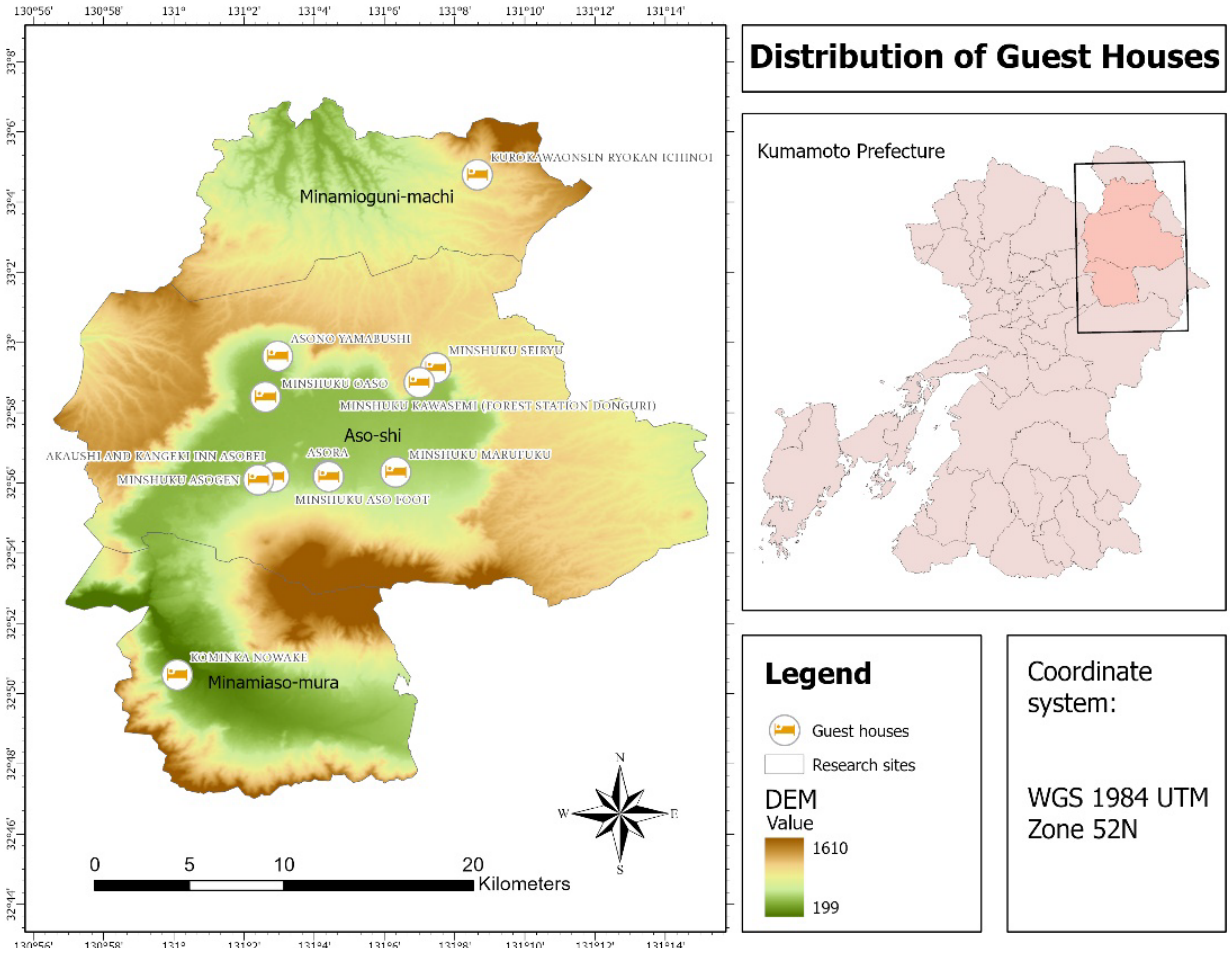

Figure 1 Distribution of Guest House

5. Discussion

GIS, sustainable practices, and cultural upkeep were integrated into the study. A deeper look at agroecology and permaculture concepts and their connections to farmers' guesthouses can expand our understanding of their transformative power. Let us explore the practical applications of these concepts to accommodation. Agroecology, which is a sustainable farming system, is embraced by farmers' guesthouses. This includes natural farming, reduced chemical inputs, and biodiversity promotion, which aid conservation and reduce environmental impacts. For instance, local farmers in guesthouses use agroecology by combining vegetation and animals to create symbiotic relationships that enhance soil fertility and pest control. These practices match the FAO's sustainable agricultural goals and protect cultural heritage sites.

.Permaculture, as a design tool, is used by farmers' guesthouses to foster harmony between humans and nature. The benefits include reducing waste with efficient recycling, creating sustainable water control, and producing diverse and resilient food systems. For example, guesthouses use rainwater harvesting and waste recycling to reduce their environmental impact, while cultivating organic gardens to provide fresh produce for guests. These practices reflect permaculture's core values and preserve cultural traditions connected to sustainable practices. Agroecology and permaculture principles are embraced by farmers' guesthouses, which combine agricultural practices with ecological integrity and protect cultural heritage. These sustainability-based ideas have had positive effects, making guesthouses agents of exchange and sustainability in communities.

6. Conclusion

GIS technology is essential to this research as it provides a comprehensive spatial analysis of the relationship between farmers' guesthouses, cultural heritage, and sustainable practices. GIS reveals the intricate geographic arrangement of local resources associated with these guesthouses, such as land use, terrain, climate, and natural resources. This spatial understanding helps to identify optimal locations for guesthouses and shows how they interact with their environment. GIS maps the relationship between farmers' guesthouses and their environment, exploring the synergy between cultural heritage, sustainable agriculture, and landscape. GIS visualizes these dynamics, providing insights into how they coexist and aiding the research's goal of achieving a balance between culture, economy, and ecology.

This research explored the role of farmers' guest houses in preserving cultural heritage, promoting sustainability, and reconnecting humanity and nature. Biophilic Design principles and GIS technology have illuminated the transformative potential of such accommodations. By immersing guests in the agricultural rhythm of the region, farmers ' guest houses foster an understanding of local traditions and demonstrate a commitment to eco-friendly practices. The FAO's sustainable development goals, Biophilic Design, GIS analyses, and on-the-ground investigations demonstrate the importance of guesthouses in balancing cultural heritage preservation, economic prosperity, and ecological resilience. Agroecology and permaculture further enrich this exploration, showing a symbiotic relationship between sustainable farming, environmental integrity, and cultural continuity. This study highlights the transformative power of sustainable tourism and thoughtful design, emphasizing the potential to create a more harmonious and sustainable environment for present and future generations, where communities protect their heritage while embracing responsible growth.

Oral presentation in IAG'i

Environment

Chair: Tsutomu Suzuki (University of Tsukuba)

Sat. Oct 28, 2023 10:40 AM - 12:00 PM Room E (C-301 3rd floor of Bldg. C)

[E2-01] Seasonal ARIMA Prediction of Streamflow: Sobat River Tributary of the White Nile River

*MANZU GERALD SIMON KENYI[1], KAYOKO YAMAMOTO[1] （1. The University of Electro-Communications）

10:40 AM - 11:00 AM

[E2-02] Analysis of Thermal Environment of Greening Vacant Houses in Old Downtown Metropolitan Areas: A Case Study on Busan Metropolitan City*clear*

*YOKO KAMATA[1], Kwang Woo Nam[1] （1. Kyungsung University）

11:00 AM - 11:20 AM

[E2-03] An advanced tropical cyclone center estimation approach using geostationary satellite-based infrared channels

*Juhyun Lee[1], Jungho Im[1] （1. Ulsan National Institute of Science and Technology）

11:20 AM - 11:40 AM

[E2-04] COMPARATIVE ANALYSIS OF URBAN GREENING EVOLUTION AND IMPLICATIONS IN GLOBAL NORTH AND SOUTH CITIES OVER A 30-YEAR PERIOD

*Ahmed Derdouri[1], Yuji Murayama[1], Takehiro Morimoto[1] （1. Faculty of Life and Environmental Sciences, University of Tsukuba）

11:40 AM - 12:00 PM

Seasonal ARIMA Prediction of Streamflow: Sobat River Tributary of the White Nile River

Manzu Gerald Simon Kenyi*, Kayoko Yamamoto**

Abstract: This study analyzes historical monthly streamflow time series data collected over the Sobat River in South Sudan using the Seasonal Auto-regressive, Differencing, and Moving Average (Seasonal ARIMA) Model. The time series data was found to be non-stationary, as an Augmented Dickey-Fuller (ADF) test on the data strongly rejected the null hypothesis of the existence of unit root (p-value: 0.00195, ADF statistic: -3.91, critical values at 1%:-3.449; 5%:-2.869; and 10%:-2.571). An optimal Seasonal ARIMA model, ARIMA(2,1,0)(2,0,1) was selected and fitted with a training set and used to forecast/predict streamflow values for four years with results compared against the validation/test set. The residuals of the fitted model were not correlated with a constant mean of zero as further proved by a Lung-Box p-value of 0.03, which is lower than the significant level ($\alpha = 0.05$). A coefficient of determination score of 0.931, a Mean Absolute Error of 0.864, a Root Square Mean Error of 1.132, and a mean absolute percentage error of 0.1489, indicate that the model is good enough and reliable to be used for predictions/ forecasts on the Sobat River in South Sudan.

Keywords: Time series prediction, Time series forecasting, streamflow prediction, streamflow forecasting

1. Introduction

Understanding the patterns and behavior of streamflow based on reliable past and present information is imperative for effective water projects including water resources planning, design and development, usage optimization and management, and forecasting for flood plannings and warnings (Box et al., 1976).

Some authors have categorically used the terms prediction and forecasting independently. Brown (1963) describes 'prediction' as a subjective method and forecasting as an objective method, but Brass (1974) describes a 'forecast' as looking into the future and 'prediction' as a systematic procedure to look into the future (Chatfield, 2003). In this paper, we use the two terms interchangeably. Observations such as streamflow values of a river recorded over a discrete time - only at specific times usually, equally spaced like daily, weekly, or monthly are referred to as discrete time series (Chatfield, 2003).

Chatfield defines time series as "a collection of observations made sequentially in time" (Chatfield, 2003). A time series is deterministic if its future values can be predicted exactly (Chatfield, 2003). A lot of time series observations are stochastic in such a sense that to be able to predict the future, the probability distribution of future values is correlated with the knowledge of past values (Chatfield, 2003). Streamflow is not deterministic in nature since a river's flow can be affected by several factors like changes in climate and topography of the river. A probability model or a stochastic model is used to calculate the probability of a value in the future if it lies between two specified limits, for instance, streamflow values. With time series, stochastic models, especially stationary models which in practice assume that the "stochastic process remains in equilibrium about a constant mean level", have had a lot of attention (Reinel et al., 2021). Stochastic forecasting using Autoregressive Differencing and Moving Average Models (ARIMA) and Seasonal Autoregressive Differencing and Moving Average Models (Seasonal ARIMA) have been applied to streamflow prediction in several studies.

Reinel et al., (2021). compared the performance of a Seasonal ARIMA model against a Holt-Winters model based on mean monthly forecasts at the 'V Aniversario' basin in western Cuba. The SARIMA

* Student Member (GISA), Graduate School of Information Science and Technology, The University of Electro-Communications, k2244001@edu.cc.uec.ac.jp
** Member (GISA), Graduate School of Information Science and Technology, The University of Electro-Communications, kayoko.yamamoto@uec.ac.jp

model was found to be more reliable for longer lead-time forecasts while limitations associated with the model came from training on shorter observations, thereby resulting in over-fitting problems.

A study on the monthly streamflow for the Blue Nile at Eldiem Station in Ethiopia using stochastic forecasting models strongly recommended Seasonal ARIMA as the model's coefficient of determination (R2) score was 0.94 compared to others (Elganainy, 2018).

Mohamed used Seasonal ARIMA to forecast the monthly flow of the White Nile River at Malakal gauging station in South Sudan (Nhial, 2021). The model's coefficient of determination of 0.869, a Root Mean Squared Error of 8.660, and a Mean absolute Error of 5.473, were adequate to be used for forecasting. Moreover, Malakal Station is just a few kilometers from the confluence of the White Nile River and the Sobat River, in South Sudan.

Malakal and other towns in South Sudan have in the past few years been largely hit by devastating, disastrous floods. These floods make South Sudan one of the countries in Africa with high recorded flood disasters in recent decades (Nhial, 2021; OCHA, 2022; The Nile Basin). With no single gauging station over the Sobat River in South Sudan at the time of this study, our objective and novelty is to develop an optimal stochastic model to forecast/predict streamflow on the Sobat River and we hope that such a model can be used for predictions once a gauging station exists. We evaluate the performance of our forecasting/prediction model with four metrics; RMSE, MAE, MAPE, and R2.

2. Data and Methods

2.1.Description of Study Area

The Sobat-Sub basin: The Baro-Akobo-Sobat Sub-basin (The Nile Basin, online) is a sub-basin of the Nile River that gets its name from the rivers that drain it. The Pibor River which flows from within South Sudan joins the Akobo River flowing from western Ethiopia. The confluence of the Akobo, Pibor and the Baro rivers (flowing from the highlands of Ethiopia) forms the Sobat River (Britannica) (a major tributary of the White Nile River) at the South Sudan-Ethiopia border. The Sobat River then flows westwards to join the White Nile River in the South Sudanese town of Malakal. Only one gauging station on the Sobat River in South Sudan was operational between 1912 and 1982. Since the Sobat starts flowing only after the confluence of the Pibor River and the Akobo Rivers, in this paper we refer to the Baro-Akobo-Sobat Sub-basin in South Sudan as the "Sobat Sub-basin" (The Nile Basin).

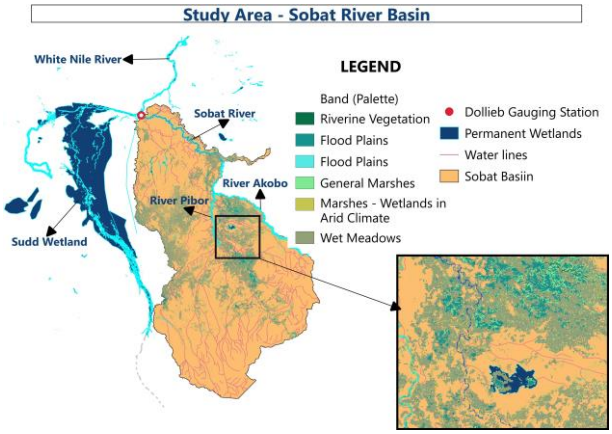

Figure 1 Study Area

2.2. Data Collection

Monthly historical stream-flow data from Dollieb station on the Sobat River between 1912 and 1982 were used. The century-old data provides an insightful understanding of the long-term stream-flow patterns in the station and the Sobat Sub-basin in general. The station is located on a latitude of 5.2 and a longitude of 31.77 with a catchment area of about $450,00 KM^2$ (The Nile Basin, online).

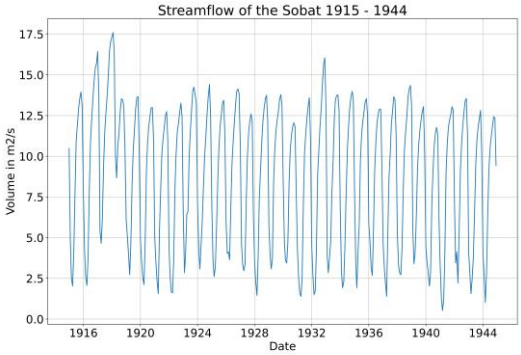

Figure 2 Streamflow data

2.2.Method(s)

The Seasonal Auto-regressive Integrated Moving Average (Seasonal ARIMA) was chosen for forecasting/prediction of the streamflow at the station. Seasonal ARIMA is a widely used time series forecasting model that incorporates auto-regressive, differencing, and moving average components, particularly useful for analyzing data with seasonal patterns, which is often observed in hydro- logical time series [4]. The SARIMA model involves selecting the appropriate non-seasonal orders accounting for auto-regressive (p), differencing (d), and moving average (q) components, as well as seasonal orders of auto-regressive (P), differencing (D), and moving average (Q) components. These orders are selected depending on the analysis of the autocorrelation (ACF) and partial autocorrelation (PACF) functions which provide insights into the long-term trends and seasonality present in the monthly stream-flow time-series data. The general form of a Seasonal ARIMA model is given by:

$$SARIMA(p, d, q)(P, D, Q)s \ldots\ldots\ldots (1)$$

A series is said to exhibit periodic behavior with period s when similarities in the series occur after $\boldsymbol{s}$ basic time intervals. In the monthly streamflow data for instance, since it is recorded monthly, the period is $s = 12$. $\boldsymbol{s}$ can also have quarterly or semi-annual data (where periodicity is more than one).

The general $SARIMA(p, d, q)(P, D, Q)s$ model is expanded to give a basis for the general multiplicative seasonal models. The fundamental fact about seasonal time series with period $\boldsymbol{s}$ is that observations that are $\boldsymbol{s}$ intervals apart are similar. Observations for a particular month are related to those of previous months. This can be represented by [1]:

$$\varphi(B^s)\nabla^D z_t = \Theta(B^s)\alpha_t \ldots\ldots\ldots\ldots (2)$$

Where:

- s = 12, $\varphi(B^s)$, $\Theta(B^s)$ are polynomials of degrees P and Q respectively.

However, it is possible to link behaviors of a given month to a few months prior with a seasonality (s). For instance, streamflow data for August could be correlated to streamflow values for June and July. Such can be represented in a model as:

$$\varphi(B^s)\nabla^D{}_s Z_{(t-1)} = \Theta(B^s)\alpha_{(t-1)} \ldots\ldots\ldots\ldots (3)$$

Where:

- α_t and α_{t-1} ...., are components which might be correlated.
- α_t in equation one could be related to $\alpha_{(t-1)}$ in equation 2.

Such relationships are combined to form a better repre-sentation as below [1]:

$$\varphi(B)\nabla^D\alpha_{(t)} = \Theta(B)\alpha_{(t)} \ldots\ldots\ldots (4)$$

Where:

- α_t is a white noise process, θB and θB are polynomials in B of degrees P and Q, and $\nabla = \nabla 1 = 1 - B$

Substituting equation 3 in equation 1 gives the general multiplication model written as [1]:

$$\varphi_p(B)\,\Phi_p(B^s)\,\nabla^d\nabla^d{}_s Z_t = \theta_q(B)\,\Theta_q(B^s)\,\alpha_t \ldots\ldots (5)$$

Where:

- S = 12

- subscripts p, P, q, and Q capture the seasonal and non-seasonal components yielding a multiplicative process of order SARIMA(p, d, q)(P,D, Q, s)

3. Results and Discussion

3.1. Train-Test

The collected data was divided into a training set and a testing set for model validation. The training set consisted of data from 1915 to 1940, while data used for validating the performance of the model consisted of data from 1941 to 1944.

Stationarity Test

The decomposition of the data shows the presence of both seasonality and trend, as shown below.

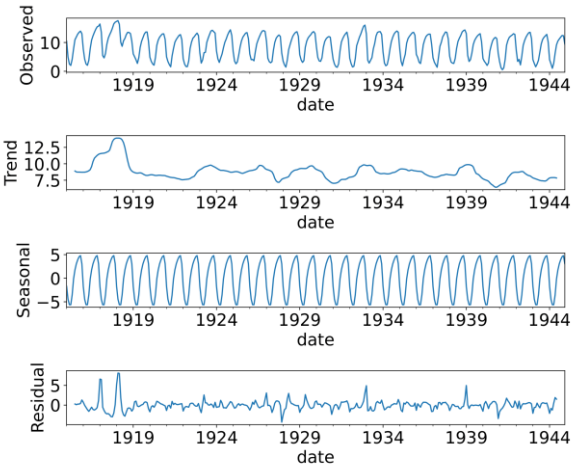

Figure 3 Decomposition of the data

The stream-flow data as well as the ACF and the PACF graphs were visualized and showed both components of trend and seasonality. To determine whether the data was stationary or not, a Unit Test was carried out using the Ad fuller-Dickey-Fuller test. The stationarity test on the data strongly rejected the null hypothesis that the stream- flow data is stationary. The computed p-value of 0.1235 indicated that indeed, the stream-flow data from the station was non-stationary since it was greater than the significant level (α = 0.05). Furthermore, the computed ADF Statistic was greater than any of the critical values (ADF-Statistic: -2.467733, Critical Values at 1%: -3.4384, Critical Values at 5%: -2.8651 Critical Values at 10%: -2.5687) thereby rejecting the null hypothesis. With a seasonal period of 12 months, a seasonal differencing (D=1) was performed to remove the seasonality of the time series stream-flow data. After the seasonal transformation, a unit test with the Ad fuller-Dickey-Fuller test was carried out again. The p-value was significantly less than the significant level of α = 0.05 (p-value=-6.55). The resulting ADF Statistic was also largely less than any of the computed critical values (ADF-Statistic: -7.311, Critical Values at 1%: -3.4384, Critical Values at 5%: -2.8651, Critical Values at 10%: -2.5687).

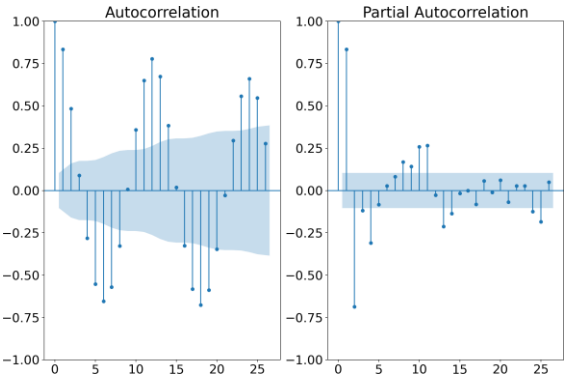

Figure 4 The ACF and PACF graphs

3.2. Model Selection

Selecting a model based only on observations of the ACF and the PACF is prone to errors. An auto-arima method using grid search performs an ARIMA hyperparameter optimization for both the seasonal and nonseasonal parameters of SARIMA(p, d, q)(P,D,Q)s and returns candidate models based on a probabilistic model selection or information criteria. The model with the least Akaike Information Criterion (AIC) value or Bayesian Information Criterion (BIC) is chosen out of candidate models. For this study, the model ARIMA(2,0,1)(2,1,0)12 was chosen with an AIC value of 1,188.759 and a BIC value of 1,211.873. The data was then fit into the model.

3.3. Model Performance

The residual plot and the correlogram of the fitted model ARIMA(2,1,0)(2,0,1) indicate that the residuals are not correlated and have a constant mean of zero. The histogram plot of the residuals also indicates that the residuals are normally distributed with a bell shape. The Lung-Box test of the residuals of the fitted model has a p-value of 0.03, hence rejecting the null hypothesis.

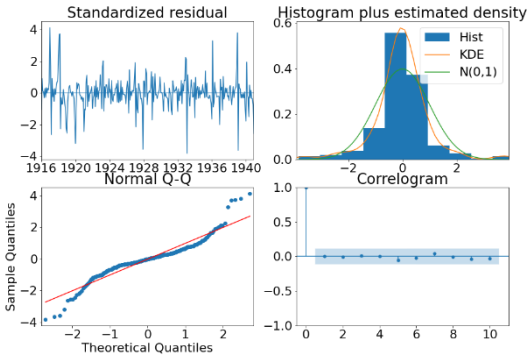

Figure 5 Residual Plot

3.4. Performance Evaluation

Four statistical indexes were used in the evaluation of the performance of the chosen model. These include: The Root Mean Square Error (RMSE), the Mean Absolute Error (MAE), and the Mean Absolute Percentage Error (MAPE). The Root Square Mean Error is computed from the Equation:

$$RMSE = \sqrt{\frac{1}{N}\sum (S_0 - S_f)^2} \qquad (6)$$

The Mean Absolute Error is computed from the Equation:

$$MAE = \frac{1}{N}\sum |(S_o - S_f)| \qquad (7)$$

The Mean Absolute Percentage Error is computed from the Equation:

$$MAPE = \frac{\sum (\frac{|A-F|}{A}) * 100}{N} \qquad (8)$$

The coefficient of determination, r2 is computed from the Equation:

$$r2 = \left[\frac{\sum (S_0 - \overline{S_0})(S_f - \overline{S_f})}{\sqrt{\sum (S_0 - \overline{S_0}) \sum ((S_f - \overline{S_f})^2)}}\right] \qquad (9)$$

3,5. Summary

The selected model of ARIMA(2,0,1)(2,1,0) was used to forecast the monthly streamflow values for four years from 1941 to 1944, a period of four years. The results of the prediction were compared against the test set of observations within the same period of time, for goodness of fit. Results indicate that the model can be used for predictions, given a reliable coefficient of determination score of 0.931, a Mean Absolute Error of 0.864, a Root Square Mean Error of 1.132, and a mean absolute percentage error of 0.1489. These results indicate that the model is good enough to be used for predictions/ forecasts on the Sobat River in South Sudan.

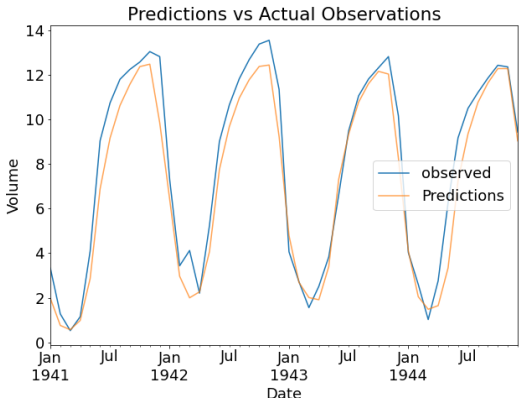

Figure 6 Prediction vs Actual Observations

4. Conclusion

Monitoring and forecasting streamflow is vital in managing water resources and water-related disasters. In this work, we utilized the available historical univariate stream-flow time series data collected between 1915 and 1944 over the Sobat tributary of the White Nile River, at Dollieb Station along the Sobat River using a stochastic model, the Seasonal ARIMA. We specifically chose this model due to the seasonal behavior of rivers in the Nile Basin as noted by others (Mohamed, 2018; Nhial, 2021) and backed by the univariate nature of the available data and further proved by the tests of stationarity carried out in this study. We have found this model to be effective for long-term predictions of streamflow on the Sobat River. Since the Seasonal ARIMA model is only limited to univariate data and since streamflow is affected by other external factors like precipitation, we propose the use of multivariate time series data that will give a further understanding of stream flow and its dynamics on the

Sobat Sub-basin of the White Nile. This would be possible in the utilization of other methods including Machine and deep learning models for better inference.

Overall, this study highlights the potential of the Seasonal ARIMA model in analyzing univariate historical streamflow data and providing reliable forecasts. The findings contribute to the understanding and management of water resources, emphasizing the importance of incorporating advanced forecasting techniques in water resource planning, water-related disaster planning (floods) and decision-making processes.

References

G. E. Box, G. M. Jenkins, G. C. Reinsel, and G. M. Ljung, Time series analysis: forecasting and control. San Francisco, USA: Holden-Day, 1976.

R. Brown, Smoothing, Forecasting and Prediction. Englewood Ciffs, New Jersey, U.S.A: Prentice Hall, 1963.

W. Brass, "Perspectives in population prediction: Illustrated by the statistics of england and wales," Journal of the Royal Statistical Society Series A: Statistics in Society, vol. 137, no. 4, pp. 532–570, 1974.

C. Chatfield, Time Series Forecasting. Chapman HALL/CRC, 2003.

A. B. G. Reinel, R. V. Anaily, L. Quan, and A. R. P. M. Elena, "Comparison between sarima and holt-winters models for forecasting monthly streamflow in the western region of cuba," 05 2021.

M. A. Elganainy and A. E. Eldwer, "Stochastic forecasting models of the monthly streamflow for the blue nile at eldiem station," pp. 326–337, 2018.

T. M. Mohamed, "Forecasting of monthly flow for the white nile river (south sudan)," pp. 103–112, 2021.

Nhial Tiitmamer, "South sudan's devastating floods: why there is a need for urgent resilience measures," 2020, nhial Tiitmamer.

Office for the Coordination of Humanitarian Affairs (OCHA), "Flooding situation report by the inter-cluster coordination group," 2022, uNOCHA.

The Nile Basin Initiative, "Our nile - our benefit," 2020. [Online]. Available: https://www.nilebasin.org/index.php/information-hub/documents-publications

Nile Basin, "The baro-akobo-sobat nile sub-basin," N/A. [Online]. Available: https://atlas.nilebasin.org/treatise/thebaro-akobo-sobat-nile-sub-basin/

Encyclopedia Britannica, "Sobat river," July 20 1998. [Online]. Available: https://www.britannica.com/place/Sobat-River

Analysis of Thermal Environment of Greening Vacant Houses in Old Downtown Metropolitan Areas
- A Case Study on Busan Metropolitan City -

Yoko Kamata*, Kwang Woo Nam**

This study investigates land cover characteristics of vacant lots in the densely populated residential areas of Ami-dong and Chojang-dong, located in Busan Metropolitan City's old downtown area. Furthermore, it evaluates the thermal environment mitigation effects of greening vacant lots after demolition vacant houses using ENVI-met simulation. The simulations were conducted on four zones, considering building density and slope direction, and four greening scenarios were evaluated within these zones. The study found that about 83% of vacant lots were left neglected with concrete pavement. Compared to the current scenario, the concrete scenario showed a 0.51℃ increase in Physiological Equivalent Temperature (PET), indicating significant deterioration in the thermal environment. Conversely, planting trees led to notable improvements, resulting in a 0.65℃ decrease in PET. This study provides crucial data to support intelligent greening strategies for sustainability.
Keywords: vacant housing, greening, thermal environment, ENVI-met, old downtown

1. Introduction

In South Korea, a country facing a declining population due to low birth rates and an aging society, even metropolitan cities are experiencing depopulation in their downtown areas, primarily driven by population outflow to the Seoul metropolitan area and suburbanization. Consequently, the number of vacant houses is increasing. In particular, residential areas in the city center, which were densely populated by low-wage workers during the industrialization process, are now suffering from severe aging and decline (Kamata and Kang, 2021). As the city centers with concentrated buildings are susceptible to the urban heat island effect (Hwang, 2020), addressing vacant houses and simultaneously implementing thermal environment improvements for vulnerable populations are urgently needed.

In response to the vacant housing issue, the Fifth Comprehensive Land Development Plan (2020–2040) suggests sustainable smart-shrinking strategies, such as removing vacant houses with low development demand or that are difficult to reuse, and creating green spaces instead of replacing them with artificial structures, such as buildings (Ministry of Land, Infrastructure and Transport, 2019, pp.89-90). On the other hand, the reality is that many vacant houses remain neglected for extended periods, and in the case of vacant houses being demolished in the old city centers, numerous instances are observed where the sites are left with concrete pavements (Jung and Woo, 2019). While the condition of the sites after the removal of vacant houses has not been well understood, it can be said that this situation contradicts the national policy goal of sustainable vacant housing management.

It is vital to assess the consequences of such practice from multiple aspects in order for the vacant house management plan, which is stressed in policy, to be adopted and disseminated in practice. The effects of greening vacant houses and idle spaces have been evaluated from various aspects in other countries, such as rising real-estate prices, crime suppression, health improvement (Branas et al., 2011; Heckert and Mennis, 2012; South et al., 2015). However, because there are few such cases in South Korea, and the region is small, it is difficult to test the effectiveness of greening strategy experimentally or empirically. Furthermore, in the era of climate change, there is a lack of research focusing on the thermal mitigation effects of greening vacant houses.

The only research case concerning the thermal mitigation effects of greening vacant houses is presented by Lee (2021). Lee (2021) utilized a Computational Fluid

* Member (KAGIS), Kyungsung University, okamatayoko@gmail.com
** Member (KAGIS), Kyungsung University, kwnam4794@gmail.com

Dynamics (CFD)-based simulation model to analyze the temperature changes when vacant houses were removed, and small green spaces were created. However, the study did not observe significant thermal environment improvement effects. Nevertheless, this research did not consider the type of vegetation grown, and it did not assess aspects related to thermal comfort, such as improved airflow resulting from vacant house removal or the shading effects of trees.

Therefore, to address these challenges, this study focuses on evaluating the thermal environment improvement effects resulting from the removal of vacant houses and the implementation of greening strategies in declining high-density urban areas. To achieve this goal, the study specifically targets the representative declining areas of Ami-dong and Chojang-dong in the old city center of Busan Metropolitan City (BMC), South Korea.

We conducted a comprehensive on-site survey to assess the post-removal conditions of vacant properties and to understand the status of greening. Additionally, we established a GIS database (DB) that incorporates building information, including vacant houses, and land cover information for the areas including vacant lots. This DB is then integrated into the ENVI-met simulation model to assess the thermal environment improvement effects at a microscale. The simulations were conducted on four zones, considering building density and slope direction, and four greening scenarios were evaluated within these zones. The thermal environment was evaluated using atmospheric temperature (T_a), wind path, and physiological equivalent temperature (*PET*). *PET* is a thermal comfort index used to quantify how the human body perceives temperature. It considers factors like air temperature, humidity, wind speed, and radiation to provide a comprehensive assessment of the comfort or discomfort a person might experience in a given environment (Höppe, 1999). Through the calculation of *PET*, it becomes possible to comprehensively assess the thermal environment, considering enhancements in air circulation and the creation of shaded regions that arise from the greening of vacant properties. This study provides crucial data to support intelligent greening strategies for sustainability.

2. Methodology

2.1 Study area and data

The areas selected in this study are Ami-dong and Chojang-dong in BMC, representative areas of urban decline in the original downtown areas of South Korea (see Fig. 1). The study areas, totally 1.169 km^2, are typical high-density sloped residential areas, where defective and illegal detached houses were spontaneously built on steep slopes. Urban decline has progressed, leading to an increase in vacant houses.

In this study, we focus on long-term neglected vacant houses and barren sites that have been left after the demolition of vacant houses as targets for greening strategies. The vacant house data were obtained from Kamata and Kang (2021) for both 2017 and 2020. According to this study, the vacancy rate in the study area was 13.6% as of 2020. Among the vacant houses in 2017, 72.4% were confirmed to remain vacant in 2020. These vacant houses that persist over this period are considered targets for greening strategies. Persistently vacant houses need to be prioritized for management, as they accelerate

Figure 1 The location of the study area (top), Photographs of vacant houses (left), barren sites (center), and maintenance sites (right)

neighborhood decline.

To understand the condition of sites after the removal of vacant houses, the research team conducted a comprehensive on-site survey of the barren sites in November 2020. Among the sites where buildings were demolished, some sites have been repaired and used as parking lots, and some were neglected and unused. In this study, the used and idle sites are referred to as "maintenance" and "barren" sites, respectively (see Fig. 1). The maintenance and barren sites were investigated together with the land cover condition and purpose of use. The barren sites are targeted for greening strategies.

The data pertaining to vacant houses and post-vacant house removal sites that were collected were incorporated into a GIS DB, utilizing the Road Name Address electronic map (2020) as the foundational source for geospatial information.

2.2 The flow of the study

The flow of the study is depicted in Fig. 2. First, we assessed the condition of post-vacant house removal sites in the study area. Subsequently, these data were integrated into the GIS DB along with vacant house data from Kamata and Kang, land cover data, and building data. Next, we selected zones for thermal environment evaluation. Due to the computational limitations of ENVI-met for the entire study area, we identified four 50m-grid zones with concentrated vacant houses, considering building density and slope direction. For the selection of the zone, we used GIS DB of vacant houses and post-vacant house removal sites, the Road Name Address electronic map (2020) for calculation of building density, and the inclination map created using the Digital Topographic Map v1 (1/5000, 2020). These tasks were performed using ArcGIS Pro. In the third phase, we proceeded with ENVI-met simulations across four distinct scenarios. These greening strategies encompassed the current situation (S1) serving as the baseline; the concrete pavement approach (S2), involving the clearance of vacant houses and barren sites followed by the application of concrete surfacing; the ground cover plantation strategy (S3), entailing the removal of vacant houses and barren sites in favor of ground cover plantings; and the tree plantation scheme (S4), encompassing the removal of vacant houses and barren sites followed by the introduction of ground cover plants and trees. Finally, we evaluated the local and overall thermal environment using T_a, wind path, and *PET* indices.

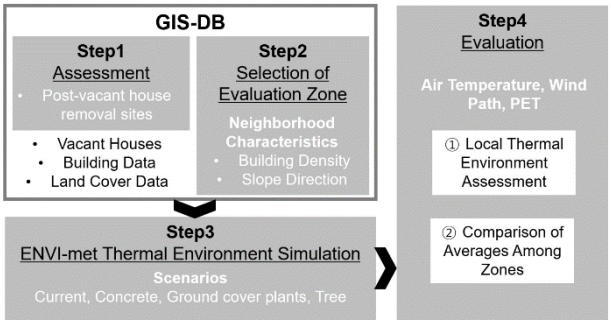

Figure 2 Study flow

2.3 ENVI-met simulation

ENVI-met is the most widely used three-dimensional CFD-based simulation software for modeling urban microclimates. ENVI-met can utilize spatial information and attributes from shapefile (shp) format files as input data. In this study, the GIS DB of vacant houses and post-vacant house removal sites, along with building data from the Road Name Address electronic map (2020), and land cover data from the Land Characteristics Graphic Information (2020), were employed as input data for ENVI-met.

The simulation settings are presented in Table 1. The

Table 1 Settings for the ENVI-met simulation

Item		**Setting**
Simulation date and time		2021.8.6. 11:00–15:00
Climate conditions	Temperature	Min. 31.1 ℃ - Max. 32.5 ℃ (Full Forcing)
	Relative humidity	Min. 41.4 % - Max. 47.0 % (Full Forcing)
	Wind	Speed: 4.55 m/s, Direction: 94°(E)
Boundary condition		Installation of building-free buffer at a range of 5 m outside the 50 m grid. 15 nesting grids in total.

simulations focused on a summer daytime scenario, evaluating the thermal environment at 14:00. The meteorological data used for input were obtained from the SAHA weather station, located 2.5 km away from the study area, on August 6, 2021. The weather on this day was sunny, with the highest temperature recorded at 32.5°C at noon. The spatial resolution of the simulations was set at 0.5m. We assumed broadleaf trees with a height of 5 meters and a canopy diameter of 3 meters for greening purposes, along with grass as ground cover. All thermal indices were calculated and mapped at a height of 1.25 meters above the ground, considering the height at which humans perceive temperature.

3. Current state of demolished vacant housing sites

Table 2 summarizes the surface states of the demolished vacant housing sites as of 2020. In the study area, 313 sites were demolished building sites. Although the previous uses or reasons for demolition of the buildings could not be known, it was presumed that most of the sites were detached houses, owing to the characteristics of the area. Moreover, many vacant houses that were demolished owing to the vacant-house maintenance project carried out by the local government must also be included.

A total of 213 sites were left as barren sites after demolition, accounting for 68.1% of the total demolished sites. Among them, the surfaces of 177 sites (83.1%) were impermeable pavement with concrete. In the case of barren sites on permeable surfaces, there were seven cases where gravel was laid to suppress plant propagation. Most permeable barren sites were neglected with overgrown weeds. Among the demolished sites, 100 sites were maintained and actively utilized. A review of the usage status of maintenance sites showed that roads or sidewalks, spaces for residents, parks or sports facilities, vegetable gardens, parking lots.

Overall, when vacant houses were removed, 80.2% of the sites were characterized by vegetation-free land

Table 2 Surface states of demolished sites in 2020 (number of sites)

Type of site	Perviousness	Vegetation		Total number of sites
		Absent	Present	
Barren	Impermeable	177	-	213
	Permeable	7	29	
Maintenance	Impermeable	63	-	100
	Permeable	4	33	

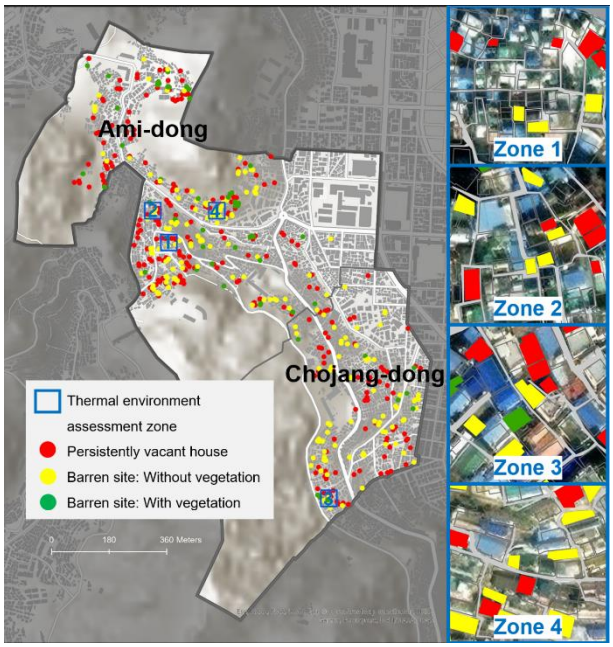

Figure 3 The distribution of vacant houses and barren sites in study area.

cover. The distribution of vacant houses and barren sites targeted for greening is depicted in Fig. 3.

4. Thermal Environment Mitigation Effects through Greening Strategies

4.1 Zones' Conditions and Traits

As outlined in Section 2, four specific zones were selected for the evaluation. The geographical locations and detailed descriptions of these zones can be found in Fig. 3. All of these zones are situated on steep slopes with an inclination of 13° or more.

Table 3 illustrates the characteristics of each zone. Zone 1 is situated within the Tombstone Culture Village,

representing the area with the highest building density. Notably, the removal of vacant houses holds the potential to enhance both ventilation and thermal comfort within this zone. Zones 1, 2, and 3 are positioned on north-facing slopes and exhibit varying building densities. Consequently, these zones offer an opportunity to contrast the impact of greening against building density. Meanwhile, Zones 2 and 4 share the same building density but differ in slope orientation, facilitating a comparison between slope direction and the influence of greening. The thermal environment simulation models of each greening scenario are shown in Fig. 4.

4.2 Local thermal environment

Figures 5 and 6 present the spatial distribution of indicators such as T_a, wind, and *PET* across each zone and scenario. Notably, Zone 4, oriented toward the south, exhibits notably elevated temperature patterns in comparison to the north-to-northeast-facing Zones 1 and 2. Similarly, Zone 3, which faces northeast, experiences relatively higher temperatures across all indicators when contrasted with Zones 1 and 2. This disparity can be attributed to the direct infiltration of solar radiation through the buildings, a phenomenon linked to the lower building density in Zone 3.

The variation in T_a among scenarios remains within the 0.4°C range, indicating a lack of significant difference. The wind enters from the east at a speed of 4.55 m/s and gradually diminishes to below 0.5 m/s upon entering the alley, displaying consistency across all cases and scenarios. The absence of substantial wind in the alley during summer is anticipated to lead to discomfort. Conversely, in S2 where vacant houses were removed, an airflow pathway is created, resulting in an increase in wind speed (observed as a white circle in S2 of Fig. 5). Notably, some ventilation limitations are observed around the trees (noted as a white circle in S4 of Fig. 5), while in S3, the airflow remains consistent.

The distribution of *PET* did not always correspond to the T_a distribution, showing notable variability within the same zone. In areas directly exposed to sunlight, the *PET* ranged from 47 to 59 °C. Notably, a sunny alley with limited ventilation exhibited a high *PET* value of 59 °C

Table 3 Overview of the zones

Zone	1	2	3	4
Number of vacant houses (area, m²)	5 (98.9)	5 (139.4)	6 (177.7)	4 (127.7)
Number of barren sites (area, m²)	3 (64.6)	7 (109.4)	6 (171.5)	11 (262.6)
Building density	High	Medium	Low	Medium
Slope direction	N	NE	NE	S

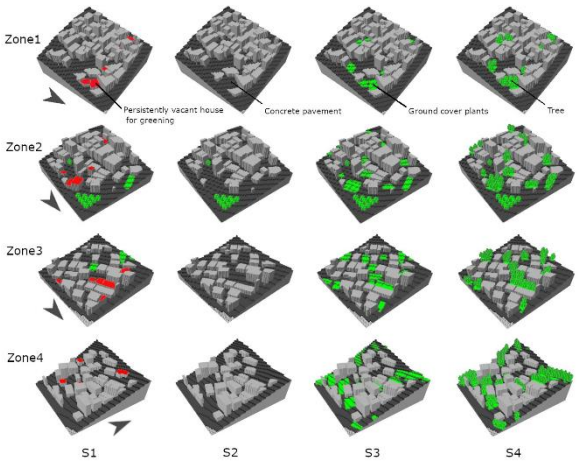

Figure 4 Simulation model by scenario

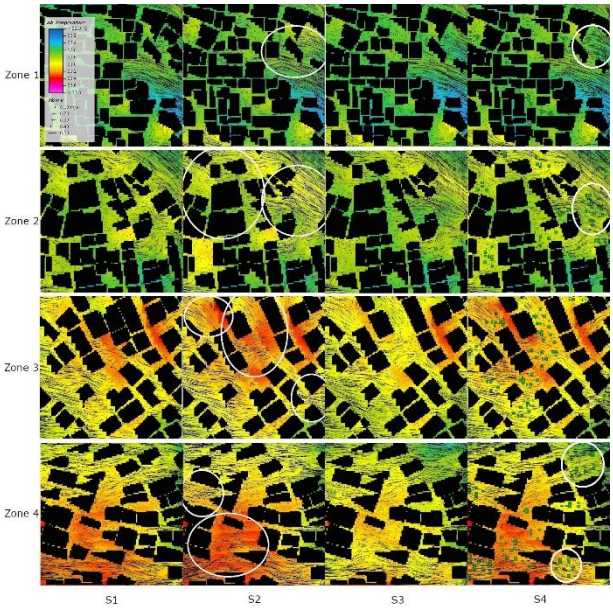

Figure 5 T_a and wind by zone and scenario.

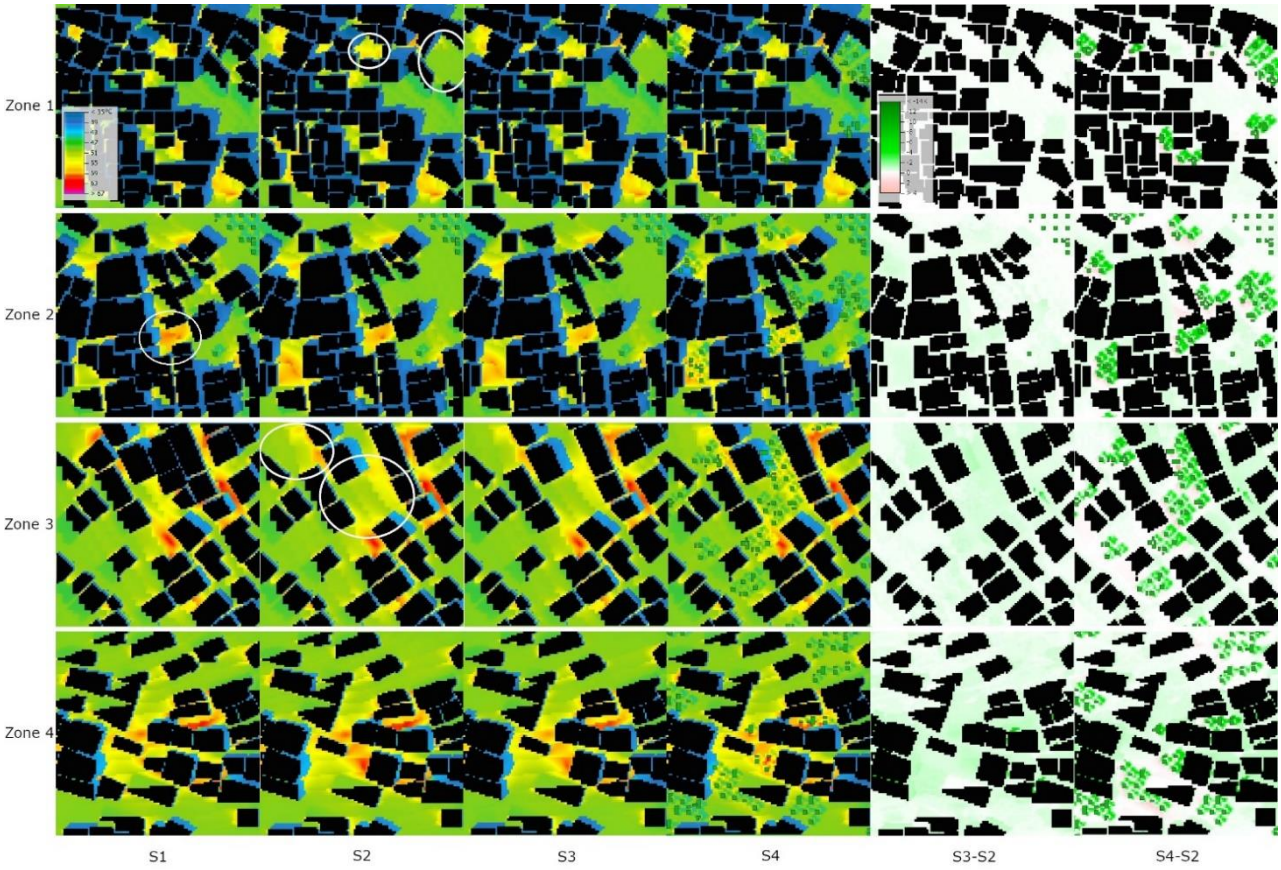

Figure 6 Difference in *PET* by zone and scenario.

(highlighted by a white circle in Zone 2 S1 of Fig. 6). These values significantly surpass the threshold for the 'Very Hot' category of thermal sensitivity (Matzarakis and Helmut, 1996). For instance, in Fig. 6, the two areas emphasized by white circles in Zone 1 S2 are both sunlit concrete sections. Despite no significant T_a difference between the two areas (as shown in Fig. 5), the *PET* recorded 51 °C on the right and 55 °C on the left. As previously mentioned, the relatively higher wind speed in the circle on the right may contribute to this variation in *PET* between the two areas, as evident from its impact on the *PET* values.

4.3 Comparison of average among zones

Table 4 presents the calculated and summarized average values of each index across the different zones. Upon analyzing the overall averages for the four zones, it becomes apparent that S2 exhibited the highest temperatures for all indicators, with T_a and *PET* increasing by 0.04 ℃ and 0.51 ℃, respectively, in comparison to S1. Notably, there were no substantial differences in T_a observed among the various scenarios. Interestingly, S4 yielded the lowest *PET* temperature. In S4, the *PET* values were reduced by 0.15 °C compared to those in S1, and notably by 0.65 °C in contrast to the *PET* values observed in S2. Wind speeds are slightly lower in zones with higher building density. Additionally, it can be observed that the removal of vacant houses has led to a marginal increase in wind speeds.

When examining Zones 1 through 3 with an emphasis on building density, the influence of greening was most evident in the area characterized by the least dense construction. In Zone 3, the introduction of greening resulted in a decrease of 0.03°C in *PET* for S3 and a reduction of 0.26°C for S4, when compared to the baseline S1. These figures point to a more substantial decline in *PET* compared to Zones 1 and 2.

Regarding slope direction, Zone 4, oriented towards the south, exhibited the highest temperatures across all surfaces, leading to an unfavorable thermal environment. In contrast, the introduction of greening had a significant

Table 4 Average values by zone

Item	Zone	S1	S2	S3	S4
T_a (°C)	1	32.65	32.68	32.64	32.66
	2	32.79	32.84	32.76	32.80
	3	33.05	33.11	32.99	33.07
	4	33.08	33.10	32.95	33.05
	Avg.	32.89	32.93	32.84	32.90
Wind speed (m/s)	1	0.39	0.41	0.41	0.40
	2	0.48	0.56	0.56	0.55
	3	0.50	0.52	0.52	0.50
	4	0.59	0.62	0.61	0.56
	Avg.	0.49	0.53	0.53	0.50
PET (°C)	1	44.45	45.11	44.96	44.55
	2	46.48	47.28	47.02	46.60
	3	49.83	50.21	49.80	49.57
	4	50.07	50.27	49.76	49.52
	Avg.	47.71	48.22	47.89	47.56

positive influence. In the baseline scenario, the average T_a and *PET* values in Zone 4 exceeded those in Zone 2 by 0.29 and 3.59°C, respectively, despite both zones sharing the same building density level. On the other hand, the thermal mitigation effects of trees were more pronounced in Zone 4 compared to Zone 2. When comparing S1 and S4, it becomes evident that Zone 4 experienced a greater thermal mitigation effect. In Zone 4, the cooling impact resulted in a T_a decrease of 0.04°C and a *PET* decrease of 0.67°C compared to Zone 2. The greater impact of greening in Zone 4 could be attributed to its larger concrete open area in comparison to Zone 2, which incorporated more greenery.

5. Discussion

The findings of this study yield several implications. First, it's evident that in densely populated urban areas undergoing decline in South Korea's city centers, the consideration of greening strategies for vacant house management is lacking. To effectively implement the sustainable smart-shrinking strategy of converting vacant spaces into green areas, it's essential to emphasize the benefits of such strategies. In the case of Ami-dong and Chojang-dong in BMC, the locations studied, it was observed that after vacant houses were removed, 83% of the resulting sites were paved with concrete. This is likely due to the ease of maintenance. However, as demonstrated in this study, greening these spaces can lead to improved thermal comfort. In addition to emphasizing the benefits of greening, it's important to establish green space management plans that gain community support. For instance, the Philadelphia Land Care Program, which creates jobs for locals through green space management, could serve as a useful reference (Parks and Recreation Department of Philadelphia, n.d.).

Second, continuing the practice of post-vacant house removal concrete pavement could significantly worsen the thermal environment in densely populated residential areas. Simulation results indicate that S2, involving concrete pavement, leads to the highest temperatures among all scenarios. The outdoor thermal comfort worsened by 0.51 °C in terms of *PET* when compared to the S1. This is believed to be a result of converting all previously vegetated vacant spaces into concrete pavement and the removal of building-generated shadows due to vacant house removal. This highlights the need for more environmentally friendly strategies that consider thermal comfort and overall livability.

Third, greening strategies, particularly the planting of trees after removing vacant houses, can substantially improve the thermal comfort of exterior spaces in densely populated urban areas. Contrary to previous studies (Lee, 2021; Shu and Hioki, 2011) that found limited temperature reduction from small-scale green spaces, this study demonstrates that a combination of improved airflow due to vacant house removal and shading effects from trees can lead to enhanced thermal comfort. This improvement is not limited to localized areas but can be seen on a larger scale. Even in scenarios where vacant houses were removed and concrete surfaces were introduced, the introduction of trees led to a comprehensive reduction in thermal discomfort. This effect was particularly

pronounced in scenarios where concrete pavement was identified as the least favorable option.

Fourth, in environments with low building densities, greening with trees proves to be more effective. In particular, the zone with the lowest building density, Zone 3, showed the significant improvement in thermal comfort due to greening. One potential rationale for this phenomenon is that zones characterized by lower development densities afford greater open spaces and more expansive areas for implementing greening initiatives. However, previous research has substantiated that the positive effects of greening are particularly pronounced in street canyons featuring low aspect ratios, as noted in studies by Wu et al. (2022). In comparison to single-story houses standing at a maximum height of 4 meters, the efficacy of greening interventions became even more evident due to the extensive shade provided by trees reaching a height of 5 meters. The strategic placement of taller trees relative to the height of the structures being demolished has proven to be an effective approach.

Lastly, in south-facing slopes, it's crucial to prioritize greening strategies, especially tree planting, due to the initial poor thermal conditions. Despite having the same building density as Zone 2, Zone 4 exhibited higher temperatures across all indicators due to its south-facing orientation. However, the positive impact of tree planting was evident, leading to improved thermal conditions. The removal of building-induced shadows coupled with the introduction of tree shading led to a significant decrease in *PET* by 0.65 °C compared to S2. This emphasizes the importance of targeted greening strategies, particularly in environments with challenging initial thermal conditions.

6. Conclusion

This study aimed to examine how introducing green spaces could address the issue of vacant properties in the declining central area of a metropolitan city, characterized by densely populated residential neighborhoods in the old downtown district. Therefore, this study focused on Ami-dong and Chojang-dong, representing the old city core of BMC, to investigate post-vacant house removal site usage and land cover. The research confirmed the insufficient consideration of greening strategies. Furthermore, the study evaluated the thermal environment improvement effect of replacing vacant houses with green spaces using ENVI-met simulations. The results highlighted the enhanced thermal comfort through vegetation-based greening.

By comprehensively evaluating the effects of vacant house greening from the overlooked perspective of post-removal site conditions and addressing the previous research limitations in terms of thermal comfort, this study contributes valuable insights. This research offers crucial insights into the application of greening as a smart and sustainable approach to managing vacant properties.

However, due to the computational limitations of the computer resources available, this study was unable to conduct a comprehensive assessment of the thermal environment across the entire study area. Consequently, there's a need for future studies to expand the assessment to a wider geographical area where extensive computational capabilities are accessible.

Acknowledgement

This work was supported by the [Basic Science Research Program through the National Research Foundation of Korea (NRF), funded by the Ministry of Education] under Grant [2021R1I1A3056691]

Reference

Address-based Industry Support Service. Road Name Address electronic map. 2020. https://business.juso.go.kr. (Accessed October 9, 2020)

Branas, C.C., Cheney, R.A., MacDonald, J.M., Tam, V.W. and Jackson, T.D., Ten, T.R. 2011. “Have, A difference-in-differences analysis of health, safety, and greening vacant urban space.”, Am. J. Epidemiol. 174(11), 1296‑1306.

Han, H.S. 2014. “The impact of abandoned properties on

nearby property values." Housing Policy Debate, 24(2), 311-334.

Heckert, M. and Mennis, J. 2012. "The economic impact of greening urban vacant land: A spatial difference-in-differences analysis.", Environ. Plan. A. 44(12), 3010-3027.

Höppe, P. 1999. "The physiological equivalent temperature: a universal index for the biometeorological assessment of the thermal environment." International Journal of Biometeorology 43(2), 71-75.

Hwang, H.S. 2020. "Analysis of Spatial Distribution Characteristics and Greening Reduction Effects of Urban Heat Island and Urban Pollution Island: Focused on Busan Metropolitan City." (Pusan National University Master's Thesis).

IPCC. 2022. IPCC Sixth Assessment Report. Working Group III: Mitigation of Climate Change. Retrieved from [https://www.ipcc.ch/report/ar6/wg3/]

Jung, I.A. and Woo, S.K. 2019. "Analysis of the vacant spaces occurrence and areal characteristics in old hillside residential area: Focused on hillside residential areas surrounding old downtown in Busan." J. Archit. Inst. Korea, 35(2), 115-125.

Kamata, Y. and Kang, J.E. 2021. "A study on the occurrence, persistence, and reuse of vacant houses in deteriorated high-density residential areas of old downtowns of large cities: Focused on Ami-dong and Chojang-dong in Busan." J. Korea Plan. Assoc., 58(3), 73-86.

Lee G.W. 2021. "The Impacts of Creation of Small Green Areas Within Urban Regeneration Projects on the Formation of Wind Paths and the Thermal Environment: Focused on Indongchon, One of the Urban Regeneration and Revitalization Areas in Daegu." Korea Institute of Ecological Architecture and Environment, 21(5), 91-100.

Matzarakis, A. and Mayer, H. 1996. "Another kind of environmental stress: Thermal stress." WHO Collab. Cent. Air Qual. Manag. Air Pollut. Control. 18, 7-10.

Ministry of Land, Infrastructure and Transport. 2019. Fifth National Land Use Plan of Korea (5th Plan).

National Geographic Information Institute. Digital Topographic Map. 2020. https://www.ngii.go.kr/kor/main.do. (Accessed December 11, 2021).

National Spatial Data Infrastructure Portal. Land Characteristics Graphic Information. 2020. http://www.nsdi.go.kr/. (Accessed December 11, 2021)

Parks and Recreation Department of Philadelphia. (n.d.). Philadelphia Horticultural Society. [Online] Available at: https://phsonline.org/ [Accessed 29 August 2023].

Shu, M. and Hioki, Y. 2011. "Comparison of Thermal Environment Improvement Effect for Parking Lots between Different Types of Greening." Journal of the Japanese Society of Revegetation Technology, 37(2), 318-329.

South, E.C., Kondo, M.C., Cheney, R.A. and Branas, C.C. 2015. "Neighborhood blight, stress, and health: A walking trial of urban greening and ambulatory heart rate.", Am. J. Public Health. 105(5), 909-913.

Wu, J., Chang, H. and Yoon, S. 2022. "Numerical Study on Microclimate and Outdoor Thermal Comfort of Street Canyon Typology in Extremely Hot Weather: A Case Study of Busan, South Korea." Atmosphere, 13(2), 307.

An advanced tropical cyclone center estimation approach using geostationary satellite-based infrared channels

Juhyun Lee* and Jungho Im*

Since the tropical cyclone (TC) is one of the most destructive natural disasters, accurate monitoring is crucial. Operational monitoring of TC still relies on the forecasters' subjectivities, this study proposed advanced fully automatic TC center estimation using geostationary satellite. The approach consists of two approaches: automatic setting of regions of interest (ROI) and TC center estimation using an advanced logarithmic spiral band (LSB) and score matrix (SCM). The setting of ROI enables to mask out the region where has less potential of TC center, and then, the accurate TC center would be determined considering TC size, length of rain band in relating on the intensity. Two schemes (i.e., schemes A and B), depending on the initial guess setting method, and two models (i.e., models A and B), whether SCM was considered with LSB or not, were examined. While both proposed models improved comparing to previous studies, the best performed model, considering both SCM and LSB, performed skill score of 20.8% in the scheme B. Especially, for the strong TC cases, the proposed model achieved the skill score of 72.3% for the scheme

Keywords: Tropical cyclone, Geostationary satellite, Center estimation, Spiral band fitting

1. Introduction

A tropical cyclone (TC) is a large-scale atmospheric system that is the result of ocean-atmosphere interactions. When a TC forms in the open ocean, it regulates the heat and mass balance between the ocean and atmosphere. Due to its enormous destructive power, the landfall of a tropical cyclone frequently results in a substantial number of fatalities and economic losses (Jacob and Shay, 2003; Weinkle et al., 2012). To mitigate the damages, accurate and rapid TC monitoring is crucial. The most relatable TC monitoring tool is a geostationary satellite. Using satellite data to monitor tropical cyclones requires two steps: 1) identifying the initial estimate location of a TC and 2) identifying the precise center of the TC. Several techniques exist for identifying the initial location of a TC in satellite images, including manual delineation, the use of forecasting data, and the utilization of the best track previously reported. Due to the fact that TCs typically possess distinct spatial characteristics, such as the rotating comma construction (Dvorak, 1975), it is relatively straightforward to determine their approximate location. Historically, satellite data were used to manually identify TC locations (Dvorak, 1975). Due to the operational difficulty of using manual identification for automated tracking of TCs, predictive fields of numerical models and extrapolated fields based on previous TC tracks have been extensively used to estimate the initial location of a TC (Wimmers and Velden, 2016; Lu et al., 2019). In the numerical model and location-based TC center estimation algorithms, it is presumed that the actual TC center exists close to the initial estimate. After the initial position of a TC has been estimated, its exact center must be determined. There are two ways to determine the center of a tropical cyclone: wind vector analysis and cloud pattern recognition. While the former can determine the actual circulation center based on wind vectors, it requires an active sensor system and is not suitable for TC monitoring with high temporal resolution (hourly) geostationary satellite data. On the other hand, the latter can be utilized with geostationary satellite-based observations and is extensively utilized for operational TC center estimation systems. The purpose of this study is to investigate an advanced technique for TC center estimation using geostationary satellite observations. The proposed approach is novel in two ways: 1) Determining TC candidate regions (i.e., TC ROI) utilizing satellite observations; 2) Introducing an improved spiral pattern fitting-based TC center estimation algorithm via an ensemble of water vapor (WV) and infrared window (IRW) channels. This research evaluated two schemes and

* Member (KAGIS), Department of Urban & Environmental Engineering, Ulsan National Institute of Science and Technology, Ulsan, Republic of Korea, wngus_0225@unist.ac.kr (J.Lee); ersgis@unist.ac.kr (J.Im)

two models for identifying the initial location of TCs and determining their precise location. The detection outcomes were evaluated based on the TC intensity and phase.

2. Data

2.1 Geostationary satellite-based meteorological imager

Communication, Ocean, and Meteorological Satellite (COMS) Meteorological Imager (MI)-based observations were utilized to estimate TC centers. It has four infrared and one visible channel with a spatial resolution of 4 and 1 km, respectively. In here, the WV (6.7 m) and IR1 (10.8 m) channels-based observations from 2011 to 2019 were utilized..

2.2 Typhoon track data

Initial TC center estimation is indispensable for operational TC surveillance. This study employed two forms of initial estimates: 1) TC center based on a numerical model forecast and 2) TC center location reported in previous time, typically 6 hours prior. Using the Korea Meteorological Administration's (KMA) real-time TC warning and forecasting data, these two initial estimates were compared. Meteorological Information Portal Service System from KMA (http://afso.kma.go.kr/) provides access to warning and forecasting datasets in real time.

3. Method

The TC center estimation model proposed comprises of two steps: 1) establishing the ROI and 2) detecting the TC center (Fig. Initially, a square image containing a TC system was extracted from unprocessed satellite imagery using KMA-based real-time track information or forecast data (schemas 1 and 2). Then, clouds comprising the TC with low luminance temperatures were extracted to designate the TCCS, allowing the parameters for logarithmic spiral band (LSB) construction to be established. Prior to matching the LSB to the TCCS, the ROI was established using a score matrix (SCM), which was proposed to eradicate regions with a low likelihood of containing the center. In the second stage, the location of the TC center was determined using two models (A and B). These procedures were repeated for both the IRW and WV images, and the final TC center was identified as the center of the two-channel results. The estimation performance was evaluated utilizing the best trace from the Joint Typhoon Warning Center (JTWC) as the reference data.

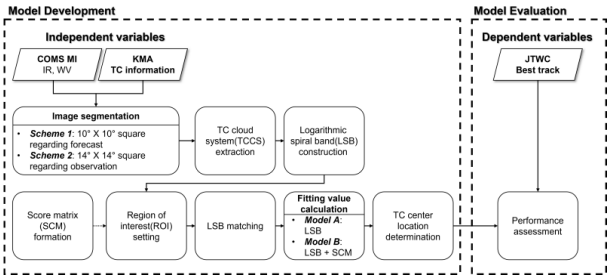

Figure 1 Study flow of the proposed TC center estimation approach

One-hundred ninety TC cases reported by KMA from 2011 to 2019 were used to evaluate the proposed TC center estimation models. To evaluate the two models by scheme, median error (ME), mean absolute error (MAE), root mean squared error (RMSE), and an MAE percentage less than 0.5° (P05) were utilized. The skill score (SS) was used to evaluate the improvement in performance of the proposed models relative to the control model (Lu et al., 2019).

$$\text{MAE} = \frac{distance(y - \hat{y})}{n} \quad (1)$$

$$\text{RMSE} = \sqrt{\frac{distance(y - \hat{y})}{n}} \quad (2)$$

$$\text{P05} = Proportion\ of\ under\ 0.5°\ error \quad (3)$$

$$\text{SS} = \left(1 - \frac{MAE_{model}}{MAE_{control}}\right) * 100 \quad (4)$$

where y represents the TC reference center reported by KMA-based observations and y represents the estimated location of the center using the proposed method. MAE_{model} represents the proposed model-based MAE, while $MAE_{control}$ represents the control model-based MAE. P05 refers to the proportion of well-estimated cases where the distance error is less than 0.5°, whereas MAE and

RMSE are used for general quantitative evaluation of models. Both the MAE and the RMSE are expressed in degrees. P05 is ununited and ranges between 0 and 1, whereas SS is expressed as a percentage.

4. Results

The MAEs of the control model, model A, and model B were respectively 0.53°, 0.49°, and 0.44°. Models A and B outperformed the control model by 6.6% and 17.4%, respectively. As the TC intensified, each model's errors decreased. In category 1, the MAEs of the control model, models A and B were comparable (0.59°, 0.63°, and 0.58°, respectively), whereas in category 5, they were substantially different (0.40°, 0.25°, and 0.11°, respectively). Compared to the control model, category 5 models A and B improved by 38.7% and 72.8%, respectively. P05 increased alongside the intensification of TC. Model B had the highest P05, at 60%, compared to the control model's 44%. Specifically, model B demonstrated that 84% of category 4 cases and 97% of category 5 cases were correctly identified with MAE values of less than 0.5°. Model B had the highest P05, 0.42, 0.49, 0.65, 0.84, and 0.97 from categories 1 to 5, indicating that it has a high probability of identifying the center location of the TC with precision. The quantitative errors of scheme 2-based TC center estimation for each category are summarized in Table 5. In scheme 2, models A and B improved performance in terms of MAEs by 19.3% and 20.8%, respectively, compared with the control model. P05 for both models (0.27 for model A and 0.29 for model B) was more than double that of the control model (0.13). However, there were significant differences in the SS between models A and B based upon intensity. In the case of weak and normal TCs with categories 1 to 3, SSs in models A and B were comparable, whereas differences were significant for the strong TC cases with categories 4 to 5: model A resulted in SSs of +3.8%, 12.5%, +32.1%, and model B resulted in SSs of +2.8%, +13.5%, +33.8% for categories 1 to 3, respectively, whereas model A yielded SSs of +35.5% and +53.2%, and model B resulted in SSs of +41.2% and +72.3% for categories 4 and 5, respectively.

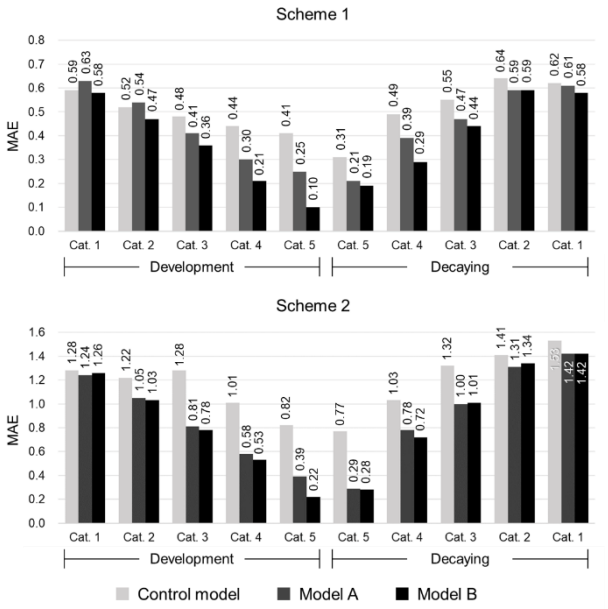

Figure 2 Mean absolute error (MAE) of the TC center estimation models (i.e., control model, models A and B) according to the schemes (schemes 1 and 2)

5. Conclusions

This study's primary objective is to propose a fully automated operational TC center estimation method based on geostationary satellite data. There are two stages involved in estimating TCs: establishing the ROI and determining the TC center. While the majority of previous research has concentrated on the second phase, ROI specification is essential for accurate and efficient TC center estimation. In this study, SCM and enhanced LSB were suggested for a more precise TC center determination and ROI configuration. To determine the optimal method for TC center determination, two models (A and B) and two schemes (schemes 1 and 2) were evaluated. Using the finest track reference data, the results were compared to those of the control model based on the intensity and phase of TCs. Compared to the control model, the proposed models enhanced performance with errors of less than 0.5° by 10% and 16%, respectively, for schemes 1 and 2. Specifically, for powerful TCs (category 4), the models enhanced the MAE by 35% and 43% for category 4 and category 4, respectively. Model B

performed the best among the proposed models, with MAEs of 0.44° and 0.98° for schemes 1 and 2, respectively. Compared to the control model, model B's overall performance increased by 17.4% for scheme 1 and by 20.8% for scheme 2. Specifically, the performance of model B improved by 72.8% and 72.3% for Category 5 in both schemes. Compared to model A, model B improved scheme 1 and 2 performance by approximately 56.0% and 39.5%, respectively. These results indicate that specifying the ROI using SCM can effectively reduce false detections, and the combination of SCM and enhanced LSB, proposed in this study as model B, improved the accuracy of TC center detection using geostationary satellite data.

Acknowledgement

This research was supported by “The Technical Development on Weather Forecast Support and Fusion Service using Meteorological Satellites” of the NMSC/KMA

Reference

Dvorak, V. F. (1975). Tropical cyclone intensity analysis and forecasting from satellite imagery. Monthly Weather Review, 103(5), 420-430.

Jacob, S. D., & Shay, L. K. (2003). The role of oceanic mesoscale features on the tropical cyclone‐induced mixed layer response: A case study. Journal of physical oceanography, 33(4), 649-676.

Lu, X., Yu, H., Yang, X., Li, X., & Tang, J. (2019). A new technique for automatically locating the center of tropical cyclones with multi-band cloud imagery. Frontiers of Earth Science, 13, 836-847.

Moore, T. W., & Dixon, R. W. (2012). Tropical cyclone-tornado casualties. Natural Hazards, 61, 621-634.

Weinkle, J., Maue, R., & Pielke, R. (2012). Historical global tropical cyclone landfalls. Journal of Climate, 25(13), 4729-4735.

COMPARATIVE ANALYSIS OF URBAN GREENING EVOLUTION AND IMPLICATIONS IN GLOBAL NORTH AND SOUTH CITIES OVER A 30-YEAR PERIOD

Ahmed Derdouri*, Yuji Murayama**, Takehiro Morimoto***

Abstract As urbanization continues to surge in the 21st century, the significance of urban greening becomes paramount in addressing challenges of climate change, resource constraints, and socio-economic disparities. This study analyzes the urban greening evolution in Berlin, Casablanca, Phoenix, and Riyadh from 1990-2020 using GIS and remote sensing in terms of coverage, accessibility, and equity of access. Results reveal diverse trajectories in urban green space (UGS) rates and varied human exposure to UGS. While Berlin experienced significant fluctuations, Casablanca, Phoenix, and Riyadh showed relative stability. Equity assessments, utilizing the Gini index, uncover disparities in green space access across urban sectors. These insights underscore the interconnectedness of urbanization, socio-economic dynamics, and environmental considerations, stressing the importance of city-specific urban planning strategies.

Keywords: Urban greening evolution, Green Space Accessibility, Equity in green space access

1. Introduction

As urbanization continues to surge in the 21st century, cities across both the global north and south face the multifaceted challenges of climate change, resource constraints, and socio-economic disparities (Seto et al., 2012; United Nations, 2018). These complex challenges emphasize the increasing need for innovative and sustainable urban planning solutions. A key strategy that has garnered significant attention in addressing these urban dilemmas is urban greening. Urban greening not only offers a pathway to environmental sustainability but also has the potential to enhance human well-being, foster community integration, and bridge the prevailing social inequalities within urban ecosystems (Elmqvist et al., 2018). However, the spatial distribution and temporal evolution of these greenspaces, along with their equitable accessibility across different urban demographics, remain under-explored areas of study.

Given this backdrop, the primary objectives of this research are twofold. First, we aim to undertake a spatio-temporal assessment of urban greenspace (UGS) coverage from 1990 to 2020, charting out their expansion, contraction, or stability over this period. This will provide insights into the evolving urban landscape and the place of greenspaces within it. Secondly, we seek to analyze the equity of these greenspaces, exploring whether their benefits are accessible to all urban residents.

2. Related Work

The critical importance of urban vegetation in the context of sustainable urban development has increasingly caught the attention of scholars in recent times. Specifically, research has focused on the distribution and human exposure to UGS amidst the backdrop of burgeoning urbanization.

Utilizing tools such as the Google Earth Engine (GEE), Richards and Belcher (2019) and Huang et al. (2021) successfully mapped urban vegetation cover across extensive global regions. A common thread in their findings indicates that while certain urban areas, notably in eastern North America and parts of Europe, have experienced an increase in vegetation, a decline in proportional vegetation cover is evident, especially in the

* Psodoc Researcher; University of Tsukuba; derdouri.ahmed.gn@u.tsukuba.ac.jp
** Professor Emeritus, Adjunct Researcher; University of Tsukuba; mura@geoenv.tsukuba.ac.jp
*** Professor; University of Tsukuba; tmrmt@geoenv.tsukuba.ac.jp

Global South. Huang et al. (2021) extend this discussion by highlighting a concerning equity disparity: cities in affluent regions generally have superior green space coverage and accessibility compared to their counterparts in less prosperous areas. Drilling down to the nuances of green space exposure, Chen et al. (2022) delineated a striking disparity between the Global North and the South. They observed that green space exposure in the South is just a fraction of what populations in the North experience, a gap exacerbated by factors such as the provision and spatial configuration of these green spaces. Adding layers to this discourse, Zhang et al. (2022) presented a more complex narrative around urbanization. While the direct impacts of urban growth often diminish vegetation, there exists a hidden, indirect positive influence. The relationship between these contrasting effects is mediated by factors including climate and population density.

Collectively, these studies underscore a pressing need for equitable, sustainable, and comprehensive urban planning, emphasizing the wellbeing of urban inhabitants in the years to come. Broadening the scope beyond these findings, the present study seeks to provide a detailed spatio-temporal analysis of the evolution of urban UGS in select cities (i.e., Berlin, Casablanca, Phoenix, and Riyadh,). By focusing on these cities across diverse contexts, we aim to shed light on the unique patterns, challenges, and opportunities that arise within varied urban settings from 1990 to 2020.

3. Materials and Methods

3.1. Target Cities

The cities selected for this study, namely Berlin, Casablanca, Phoenix, and Riyadh, represent a diverse cross-section of urban landscapes across the Global North and South. Their unique geographies, socio-economic backgrounds, and urbanization trajectories offer a rich tapestry of insights into the evolution of urban greening.

Berlin: As the capital city of Germany, Berlin stands as a key representative of European urban development. With its historical background, including the fall of the Berlin Wall and the reunification of East and West Germany, Berlin has undergone significant urban changes in the last few decades.

Casablanca: This bustling metropolis serves as a major hub in Morocco and North Africa. The city's rapid urbanization, driven by both rural-urban migration and economic development, presents an intriguing contrast to its European counterparts.

Phoenix: Located in the arid region of the American Southwest, Phoenix provides an example of urban sprawl in an environment characterized by water scarcity. The city's exponential growth over the past few decades, and its efforts to maintain and expand green spaces amidst such conditions, provide a distinctive angle of urban greening analysis.

Riyadh: As the capital city of Saudi Arabia, Riyadh exemplifies the challenges associated with urban greening in hyper-arid regions. The city's rapid urban development, spurred by its oil-driven economy, juxtaposed against its desert environment, sheds light on the relationship between economic development, land use, and urban greening.

The selection of these cities encompasses a range of urbanization challenges, from the water-scarce deserts of Phoenix and Riyadh to the historical intricacies of Berlin and the rapid developmental pressures in Casablanca. By encompassing such a variety, this study aims to offer a holistic view of urban greening trends across different global contexts.

3.2. Data and Sources

This study employed key datasets that facilitated an in-depth exploration of urban greening evolution against the backdrop of population dynamics.

- Landsat imagery, available at a resolution of 30m, served as our primary source for satellite imagery data. We leveraged imagery from multiple Landsat platforms via GEE (Level 2 Collection 2 Tier 1), ensuring that selections were based on data availability for the years

of interest and a commitment to images with the least cloud cover (less than 10%).

- The Global Urban Boundaries (GUB) from Li et al. (2020) provided detailed urban boundary definitions using 30m global artificial impervious area (GAIA) data. The dataset was derived through a blend of kernel density estimation and cellular-automata based urban growth modeling, further refined using a morphological approach. Covering seven distinct years, from 1990 to 2018, with data points provided at five-year intervals.
- Population Data (GHS-POP): Population dynamics were mapped using the GHS-POP R2023A dataset by the European Commission, Joint Research Centre (JRC) as documented by Schiavina et al. (2023). This dataset offers residential population distribution from 1975 to 2020 in 5-year intervals, with projections up to 2030. The population data, disaggregated to grid cells, was guided by the Global Human Settlement Layer (GHSL). We leveraged its 250m resolution in the World Mollweide coordinate system (EPSG:54009) for precision.

3.3. Methodology

To comprehensively analyze urban greening evolution, we employed a multi-step methodology as follows.

- Landsat Image Collection & Processing: For each target city and year, we sourced Landsat images (Level 2 Collection 2 Tier 1) from all seasons, with an exclusion of winter. This exclusion was made based on the rationale that winter months typically exhibit limited greenery and plant growth, hence, might not be representative of the annual greenery (Huang et al., 2021). Post collection, we masked clouds to ensure clarity and composited the images employing the greenest spectral compositing method (Richards and Belcher, 2019). This method essentially consolidates pixel values from the image which recorded the highest NDVI value amongst all available images, culminating in the formation of a newly composited image that showcases the greenest vegetation for that period.
- Image Classification and Accuracy Assessment: LULC training and validation samples were collected for each city and year based on a combination of visual inspection from high-resolution Google Earth imagery and spectral indices like NDVI, MNDWI, and EVI. Utilizing the random forest algorithm, we classified LULC into six distinct categories: Water, Impervious, Baresoil, Trees/Shrubs, Grassland, and Cropland as suggested in (Huang et al., 2021). Upon classification completion, an accuracy assessment was carried out, yielding Kappa coefficients for all cities between the range of 0.8 and 0.92.
- UGS Coverage Rate Calculation: With the classified images at hand, we determined the UGS coverage rate by overlaying the greenspace (primarily the Trees/Shrubs and Grassland classes) and urban population within the urban area boundaries pertinent to the target city and year. A noteworthy point is the adoption of the urban boundary data of 2018 for the year 2020 due to data availability from the previously mentioned sources.
- Human Exposure to Greenspace: Human exposure to greenspace within a 500m vicinity was computed next. To this end, we employed a population-weighted exposure model as delineated by Chen et al. (2022), which provided insights into the proximity of population clusters to green spaces.
- Equity of Greenspace Exposure: Lastly, the equity in human exposure to greenspace was evaluated using the Gini index—a statistical measure ranging between 0 and 1. A Gini index of 0 represents perfect equality, meaning everyone has equal exposure to greenspace, while a value of 1 indicates maximum inequality, where only a specific segment of the population has access to greenspaces, and others have none. This index quantified the distribution equity, allowing us to deduce whether the exposure to greenspaces was uniformly distributed or skewed towards certain population segments.

4. Results

4.1. UGS Rate Evolution

Over the three-decade study period, the four cities exhibited varied trajectories in terms of their UGS rates (**Figure 1** and **Table 1**). Berlin, for instance, faced significant fluctuations, starting with a UGS rate of 0.48 in 1990 and declining drastically to 0.14 by 2020. On the other hand, Casablanca's green space rates showed relative stability, beginning at 0.21 in 1990, facing a dip, and finally stabilizing at 0.16 by 2020. Phoenix's rates, while starting at a modest 0.13 in 1990, saw a gradual decline and a slight recovery to 0.11 by 2020. Riyadh, on the other hand, showcased a notable increase from 0.04 in 1990 to a peak of 0.12 in 2000, before declining to 0.03 by 2020.

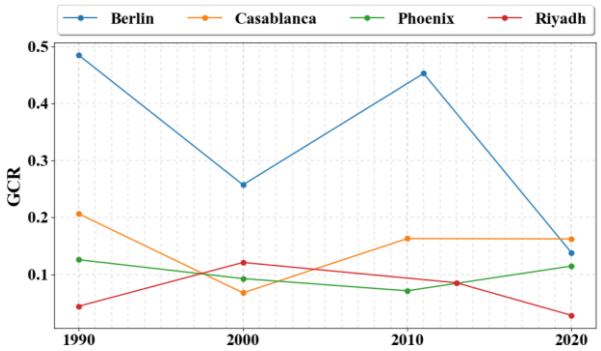

Figure 1. Trend of UGS Coverage Rate (%) in Selected Target Cities from 1990 to 2020.

Target Cities	1990	2000	2010s	2020
Berlin	0.48	0.26	0.45	0.14
Casablanca	0.21	0.07	0.16	0.16
Phoenix	0.13	0.09	0.07	0.11
Riyadh	0.04	0.12	0.09	0.03

Table 1. UGS coverage rate (%) in selected cities from 1990 to 2020. Note: The term "2010s" was used because, due to data availability issues, Berlin and Riyadh were analyzed for the years 2011 and 2013 respectively, instead of the exact year 2010. This notation applies to all subsequent tables.

4.2. UGS Exposure Dynamics

When analyzing human exposure to UGS within a 500m radius (**Figure 1** and **Table 1**), Berlin once again displayed a declining trend, with rates dropping from 0.40 in 1990 to 0.09 in 2020. Casablanca, meanwhile, showed a recovery in green space exposure, increasing from 0.13 in 1990 to 0.10 by 2020. Phoenix's exposure rates were relatively stable, with a minor dip from 0.13 in 1990 to 0.10 in 2020. Riyadh displayed an initial increase, with rates rising from 0.03 in 1990 to 0.11 in 2000, before declining to 0.02 by 2020.

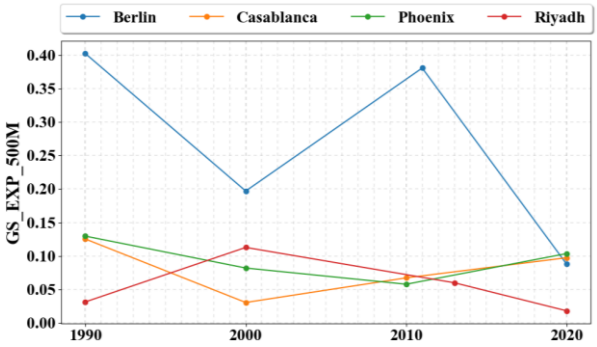

Figure 2. Trend of UGS Exposure in Selected Target Cities from 1990 to 2020.

Target Cities	1990	2000	2010s	2020
Berlin	0.40	0.20	0.38	0.09
Casablanca	0.13	0.03	0.07	0.10
Phoenix	0.13	0.08	0.06	0.10
Riyadh	0.03	0.11	0.06	0.02

Table 2. UGS Exposure (500m) in selected cities

4.3. Equity in UGS Exposure

The equity in UGS exposure (**Figure 3** and **Table 3**), as indicated by the Gini index, reveals the disparities in access across different urban sectors. A higher Gini index indicates greater inequality. Berlin's Gini index showed fluctuations, increasing from 0.55 in 1990 to a peak of 0.73 in the 2010s, and then reducing to 0.54 by 2020. Casablanca experienced a significant rise in inequality from 0.67 in 1990 to 0.86 in 2000, followed by a slight reduction in the subsequent years. Phoenix showed a steadily increasing trend in inequality, starting at 0.76 in 1990 and rising to 0.83 in the 2010s before a minor reduction to 0.75 in 2020. Riyadh, however, experienced a notable decline in the Gini index from 0.85 in 1990 to 0.67 in the 2010s, but this was followed by a sharp increase to 0.93 by 2020, indicating a significant disparity in green space exposure in the latter years.

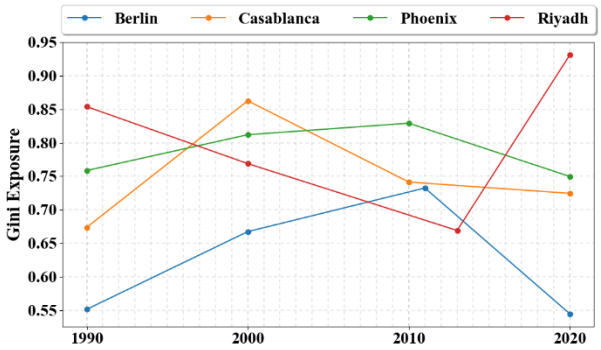

Figure 3. Trend of UGS Exposure Equity in Selected Target Cities from 1990 to 2020.

Target Cities	1990	2000	2010s	2020
Berlin	0.55	0.67	0.73	0.54
Casablanca	0.67	0.86	0.74	0.72
Phoenix	0.76	0.81	0.83	0.75
Riyadh	0.85	0.77	0.67	0.93

Table 3. UGS Exposure Equity in Selected Target Cities from 1990 to 2020.

5. Discussion

A comprehensive examination of the evolution of urban greening in Berlin, Casablanca, Phoenix, and Riyadh over three decades offers significant insights into the intricate relationship of urbanization processes, socio-economic factors, and environmental priorities.

5.1. Diverse Urban and Greening Trajectories

The observed greenspace rates across the selected cities portray a mosaic of urban greening trajectories influenced by a myriad of factors. Berlin's fluctuating greenspace rate potentially reflects its transformative urban history. The city, post-reunification in the 1990s, likely experienced developmental pressures leading to the drop in 2000. Its recovery in the 2010s might have been a result of increased environmental consciousness and policy implementation. However, the sharp decline by 2020 warrants further investigation. Perhaps changing land-use policies, economic factors, or competing developmental needs contributed to this reduction. Casablanca's relatively stable greenspace rate post-2000 could signify a balancing act between developmental pressures and attempts at urban greening. Phoenix's trend, especially the slight recovery in 2020, highlights possible shifts in city planning, recognizing the imperative of green spaces in water-scarce environments. Riyadh's pattern underscores the challenges desert cities face, balancing rapid urbanization and the intrinsic need for greenspaces for societal well-being.

5.2. Accessibility and the Urban Fabric

Accessibility to green spaces, as inferred from exposure rates, offers a lens into the urban fabric's inclusivity. Berlin's trajectory underscores the importance of not just having green spaces, but ensuring they are well-distributed to maximize human exposure. Its decline in 2020 could be indicative of urban expansion where newer areas lack sufficient green space provision. Casablanca's improvement, albeit from low initial figures, is a positive sign. It suggests efforts towards making urban greening more integral to the city's development, or perhaps an increased focus on public parks and accessible green corridors. Phoenix's steady figures, in contrast, reveal the challenges of increasing accessibility amidst an expansive urban layout. Riyadh's declining trend, particularly after the initial rise, is concerning, suggesting potential inequities in green space distribution as the city expands.

5.3. Equity in UGS

The Gini coefficients offer a lens to explore the societal dimensions of urban greening. Green spaces, while ecologically vital, have distribution patterns that can mirror socio-economic gradients within cities (Rigolon, 2016). The disparities in Berlin might be influenced by uneven development dynamics, while Casablanca's persistent high Gini values suggest deep-rooted socio-economic divides potentially impacting green space accessibility. Phoenix exemplifies the complexities of ensuring equitable green space distribution in cities with expansive geographies. The sharp rise in Riyadh's coefficients in 2020 warrants exploration into possible development disparities or exclusive green initiatives.

5.4. Policy Implications for Urban Planning

The data emphasizes the need to incorporate green space considerations within wider urban planning discussions. Beyond their ecological significance, green spaces play essential roles in promoting social integration, mental well-being, and environmental resilience. However, the diverse trends observed suggest that universal policy approaches may be less effective. The unique challenges of each city call for strategies that blend local needs with globally recognized best practices.

6. Conclusion

This study reveals the complex dynamics shaping urban greening trajectories across diverse city contexts. The observed fluctuations in UGS coverage underscore the relationship of urbanization patterns, land use priorities, and sustainability initiatives. Declining accessibility and exposure trends highlight socio-economic divides impacting equitable green space distribution. As urbanization accelerates, tailored policies balancing developmental needs and environmental resilience will be critical. Urban planners must recognize green spaces as tools for ecological sustainability, community building and social equity. Further research integrating socio-economic factors can inform locally rooted urban greening strategies. Overall, the study provides a spatio-temporal analysis of urban green evolution across distinct city archetypes. It sets the foundation for longitudinal assessments guiding policies that balance liveability, sustainability and community well-being as cities reshape their urban fabrics.

Acknowledgement

The authors would like to express their sincere gratitude to JSPS KAKENHI for their generous support and funding of this research under Grant Numbers 22F22303 and 22KF0054. Their contribution has been instrumental in the realization of this ongoing study.

References

Chen B, Wu S, Song Y, et al. (2022) Contrasting inequality in human exposure to greenspace between cities of Global North and Global South. *Nature Communications* 13(1): 4636. DOI: 10.1038/s41467-022-32258-4.

Elmqvist T, Bai X, Frantzeskaki N, et al. (eds) (2018) *Urban Planet: Knowledge towards Sustainable Cities*. 1st ed. Cambridge University Press. DOI: 10.1017/9781316647554.

Huang C, Yang J, Clinton N, et al. (2021) Mapping the maximum extents of urban green spaces in 1039 cities using dense satellite images. *Environmental Research Letters* 16(6): 064072. DOI: 10.1088/1748-9326/ac03dc.

Li Xuecao, Gong P, Zhou Y, et al. (2020) Mapping global urban boundaries from the global artificial impervious area (GAIA) data. *Environmental Research Letters* 15(9): 094044. DOI: 10.1088/1748-9326/ab9be3.

Ma J, Li J, Wu W, et al. (2023) Global forest fragmentation change from 2000 to 2020. *Nature Communications* 14(1): 3752. DOI: 10.1038/s41467-023-39221-x.

Richards DR and Belcher RN (2019) Global Changes in Urban Vegetation Cover. *Remote Sensing* 12(1): 23. DOI: 10.3390/rs12010023.

Rigolon A (2016) A complex landscape of inequity in access to urban parks: A literature review. *Landscape and Urban Planning* 153: 160–169. DOI: 10.1016/j.landurbplan.2016.05.017.

Schiavina M, Freire S and MacManus K (2023) GHS-POP R2023A - GHS population grid multitemporal (1975-2030). European Commission, Joint Research Centre (JRC). DOI: 10.2905/2FF68A52-5B5B-4A22-8F40-C41DA8332CFE.

Seto KC, Güneralp B and Hutyra LR (2012) Global forecasts of urban expansion to 2030 and direct impacts on biodiversity and carbon pools. *Proceedings of the National Academy of Sciences* 109(40): 16083–16088. DOI: 10.1073/pnas.1211658109.

United Nations (2018) *World Urbanization Prospects:*

The 2018 Revision. New York: Department of Economic and Social Affairs, Population Division. Available at: https://population.un.org/wup/Publications/Files/WUP2018-Report.pdf (accessed 4 April 2023).

Zhang L, Yang L, Zohner CM, et al. (2022) Direct and indirect impacts of urbanization on vegetation growth across the world's cities. *Science Advances* 8(27): eabo0095. DOI: 10.1126/sciadv.abo0095.

Oral presentation in IAG'i

Mobility, Transportation and Navigation

Chair: Wataru Nakanishi (Kanazawa Univerisity)

Sat. Oct 28, 2023 3:00 PM - 4:40 PM Room E (C-301 3rd floor of Bldg. C)

[E4-01] Generating Human Daily Activity Sequences Using Neural Networks Models

*Weiying WANG[1], Toshihiro Osaragi[1] (1. Tokyo Institute of Technology)

3:00 PM - 3:20 PM

[E4-02] Towards Pseudo People Flow: Developing a Deep Generative Model based on Person Trip Survey Data to Reproduce Large-Scale Daily People Activity Profiles.

*Yurong Zhang[1], Yoshihide Sekimoto[1], Yanbo Pang[1], Kunyi Zhang[1] (1. The University of Tokyo)

3:20 PM - 3:40 PM

[E4-03] Location-Based Content Tourism Support System on Foot

*Nobuaki Nagano[1], Kayoko Yamamoto[1] (1. Graduate School of Informatics and Engineering, University of Electro-Communications)

3:40 PM - 4:00 PM

[E4-04] Development of Food Tourism Support System Adopting Location-Based AR

*Makoto Hirano[1], Kayoko Yamamoto[1] (1. Electro-Communications Univ.)

4:00 PM - 4:20 PM

[E4-05] Effect of Speed Control for Travel Time and Emission Reduction in Connected Vehicle Environment

*Yuheng Liu[1], Sunyong Eom[1], Tsutomu Suzuki[1] (1. University of Tsukuba)

4:20 PM - 4:40 PM

Generating Human Daily Activity Sequences Using Neural Network Models

Weiying WANG*, Toshihiro OSARAGI**

Abstract: Human activity patterns have raised broad interests across disciplines, and they have been studied using various data sources in terms of different attributes. In the field of traffic research, it is widely believed that most travel behaviors are driven by activities to be conducted. In this paper, we present neural network models to generate synthetic datasets for daily activity sequences, which may be further utilized to replicate daily people's movements in the city. Generation results are compared, and the models are discussed in detail.

Keywords: Human daily activities, Generation model, Neural network, Person Trip survey data

1. Introduction

Knowledge about human activity-travel patterns is one of the key elements of traffic management and urban planning. It is commonly assumed that most travel behaviors are triggered by activities to be conducted, and thus activity-based approaches are often adopted to forecast travel demands. Activity-based models usually include the following steps: (1) generation of a synthetic population; (2) prediction of people's daily activity agendas (what to do in the day); (3) prediction of the start time and the duration for each activity; (4) prediction of the location for each activity; (5) prediction of the travel mode for each movement. The second and third steps are termed activity scheduling. They have significant impacts on travel demand forecasting. Previously, researchers have applied probabilistic models and machine learning-based approaches (e.g., multinomial logit model, decision tree, and random forest tree) to predict people's daily agenda (i.e., what activities to conduct) (Kitamura et al., 1997; Hafezi et al., 2021; Drchal et al., 2019). The start time and duration of each activity were then predicted with another model (e.g., the hazard model) or probabilistically drawn from datasets.

Activity agenda is generally represented by a sequence of characters, which is similar to the representation of natural language. This similarity was explored, and conventional language models were applied to generate activity agenda (Li and Lee, 2017). In recent years, one of the most popular neural network frameworks, namely transformer (Vaswani et al., 2017), was developed and applied to various language models (e.g., ChatGPT). In this paper, this framework is applied to generate daily activity sequences. Its performance is then compared with the time-varying Markov Chain model.

2. Datasets and activity sequences

In this study, we use a dataset named Person Trip survey data. A brief introduction to this dataset and our method of getting activity sequences is presented in the following.

2.1. The Person Trip survey data

The Person Trip survey has been conducted every ten years by the Ministry of Land, Infrastructure, and Tourism of Japan in major urban areas. It is conducted to households and collects information about their travels on a given day. "Trips" defined in the Person Trip survey data (hereafter PT data) are illustrated in Fig. 1. Place and time of departure and arrival, travel purpose, and means of trips,

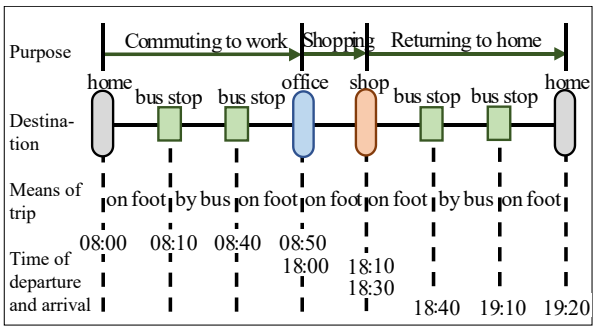

Fig. 1. Example of trips in the Person Trip survey data.

* 学生会員 東京工業大学 環境・社会理工学院 (Tokyo Institute of Technology)
〒152-0086 東京都目黒区大岡山 2-12-1 E-mail：wang.w.al@m.titech.ac.jp
** 正会員 東京工業大学 環境・社会理工学院 (Tokyo Institute of Technology)

as well as personal attributes (age, gender, occupation, car ownership, etc.), are included in the dataset. In our research, the surveys were conducted in 1978, 1988, 1998, and 2008. Each survey covers an area of a circle with a radius of 70 km centered on the Tokyo Railway station (Osaragi and Kudo, 2020). Fig. 2 shows the surveyed administrative regions over the years. The day starts at 3:00 AM and ends at 3:00 AM the next day. We further filtered out samples whose trip information, such as trip purpose, travel time, and location, is missing.

2.2. Activity sequences

In this paper, we classify activities into three types: being at home (denoted by R); working or educational-related activities (denoted by C); other activities (denoted by O, including shopping, entertainment, personal activities, etc.). A day is divided into 48 slots (30 min for each slot), and for each person, we assign each slot the person's activity during that 30-minute interval so that we have a sequence of activities for each person (Fig. 3). Following existing studies, traveling activity is omitted so that the next activity is connected to the current activity rather than a travel behavior. If one trip lasts for more than 30 minutes, the activity after the trip is assigned to the current slot. An activity sequence includes information on the start time and the duration of each activity.

3. Methodology

In this paper, we employ the transformer model to generate daily activity sequences and compare its performance with the time-varying Markov Chain model (MC model hereafter). The transformer model will be applied to generate the activity sequences for the whole population first. A slightly different version will be applied to reproduce activity sequences for any specific region. Similar generation tasks will be conducted using the MC model. In Subsection 3.1, the transformer model is presented. In Subsection 3.2, the MC model is introduced.

3.1. The transformer model

A transformer model is a neural network that learns the structure of sequential data and makes predictions for the next instance. In terms of natural language, the input is a sequence of words, and the output is the probabilities of words in the next position. In our case, the input is a sequence of activities (characters), and the output is the probabilities of activities in the next time slot. Activities are generated one by one. Given the current incomplete sequence of activities, the next activity is selected randomly based on the output probabilities. The incomplete activity sequence and the selected activity are connected to a new sequence, which is used to predict the next following activity.

The transformer model learns through a mechanism called self-attention (or attention sometimes). A diagram of its architecture is shown in Fig. 4. It includes three blocks. In the first block (left), each activity and the position of the activity in the sequence are embedded into two vectors of the same length. The two vectors are added up (i.e., the sum operation) to one vector indicating the positional (time of day) and actional characteristics of this activity. A sequence of activities is converted into a

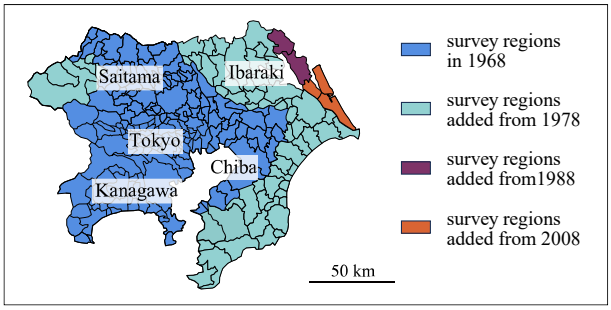

Fig. 2. Surveyed administrative regions.

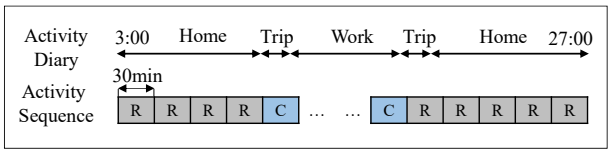

Fig. 3. An example of activity sequences.

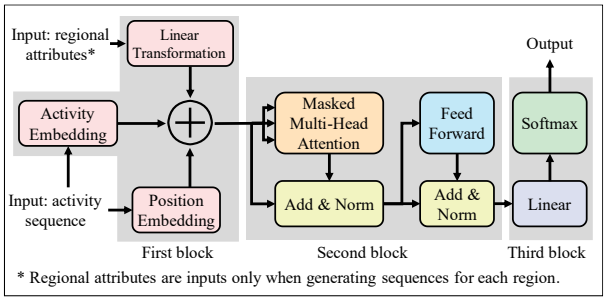

Fig. 4. The transformer model.

sequence of vectors (i.e., a matrix), which is the input into the second block (middle). Here the self-attention mechanism and residual networks are applied and this block outputs a vector. Due to the complexity, the details are not introduced here. In the third block (right), the vector goes through a linear and a softmax layer. It is converted into a list of values that sum up to one, indicating the probabilities for activities at the next time slot. Interested readers can read the paper by Vaswani et al. (2017) for more details about the transformer model.

We trained another model to make predictions for each region. The only difference is that the new model takes regional attributes as input in the first block. For any region, land use, population density, average land value, average family size, and the distance to the city center are concatenated into a vector. Through a linear transformation, this vector is converted to a vector of the same length as the vectors embedded from activity and position. In the new model, these three vectors are summed up to one vector as the input to the second block when making predictions.

The second block (commonly named head) can be duplicated multiple times in one layer and different layers can be stacked to create deeper models. The number of heads in one layer and the number of layers determine the complexity of the model. For the model to generate activity sequences for the whole population (i.e., the original transformer model), we used ten heads in one layer and three layers. For the model to generate activity sequences for each region (i.e., the new transformer model), we adopted thirty heads and three layers.

3.2. The time-varying Markov Chain model

A simple Markov process is one where the future state is only dependent on the current state and independent of previous states. In a mathematical sense, the process assumes that:

$$P(X_{t+1} = x_{t+1} | X_t = x_t, X_{t-1} = x_{t-1}, \dots, X_0 = x_0) = P(X_{t+1} = x_{t+1} | X_t = x_t) \quad (1)$$

where the top is the transition probability that the next state is x_{t+1} conditioned on all previous states $(x_t, x_{t-1}, \dots, x_0)$ and the bottom is the probability that the next state is x_{t+1} conditioned on the current state x_t. In this paper, we consider a MC model where the probability of transition varies with time. Mathematically,

$$P_t(X_{t+1} = x_{t+1} | X_t = x_t, X_{t-1} = x_{t-1}, \dots, X_0 = x_0) = P_t(X_{t+1} = x_{t+1} | X_t = x_t) \quad (2)$$

P_t varies with time, indicating the transition probability from one activity to another during time t and $t+1$. For each time t, transition probabilities from all activities to all others were aggregated from the activity sequences. Illustratively, the model is shown in Fig. 5. Each node indicates conducting one activity at a specific time interval of 30 minutes, and each edge (arrow) is assigned a probability indicating an activity transition. When generating activity sequences for the whole population, the transition probabilities at each time were calculated using all the activity sequences obtained in Section 2. When generating activity sequences for one specific region, one MC model is constructed based on activity sequences in the region.

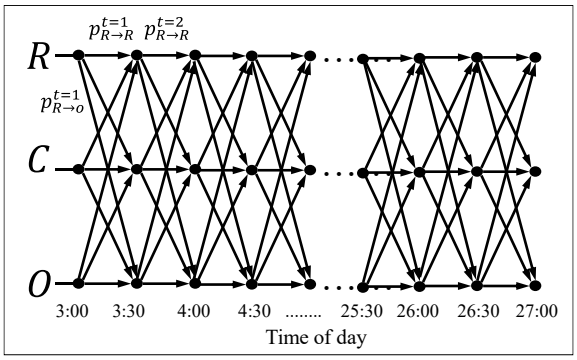

Fig. 5. Illustration of the MC model.

4. Results

In this section, generation results and model evaluation are presented in Subsections 4.1 and 4.2.

4.1. Visual evaluation of the generation results

Generation results for the whole population are shown in Fig. 6 for the most frequent 4,000 activity sequences. Each dot stands for one activity sequence with a length of forty-eight. The x-axis value is the proportion of the activity sequences from the original dataset, whereas the y-axis value is the proportion from the generated datasets. For the whole population, the results are good in both

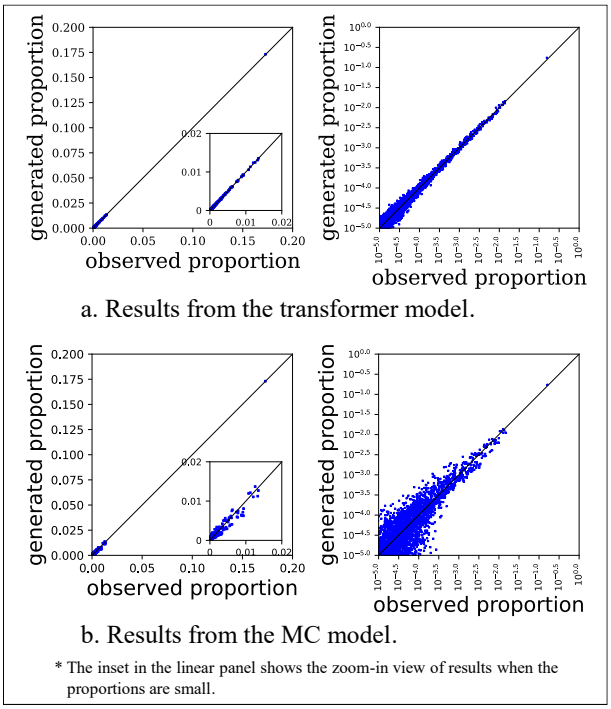

a. Results from the transformer model.

b. Results from the MC model.

* The inset in the linear panel shows the zoom-in view of results when the proportions are small.

Fig. 6. Results for the whole population.

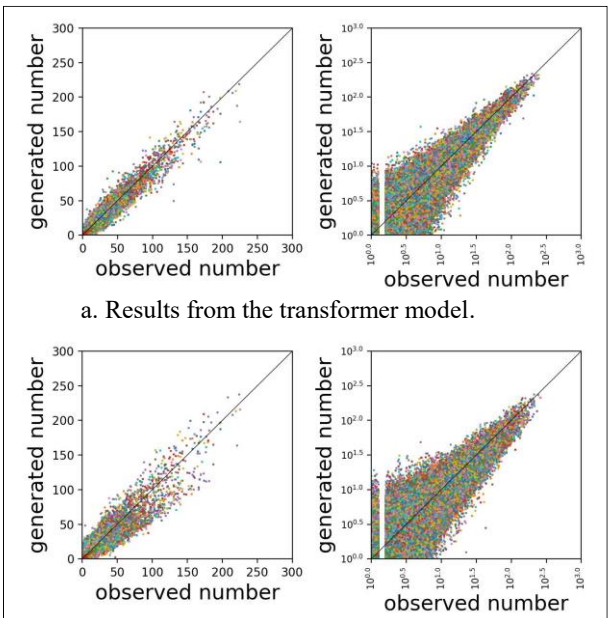

a. Results from the transformer model.

b. Results from the MC model.

* The above figures show the results for activity sequences except staying at home all day (i.e., sequence with only *R*).

** The above figures show the observed numbers of activity sequences rather than the proportions because some regions have too few people surveyed, which causes inaccurately high proportions of some activity sequences.

*** One color indicates one region.

Fig. 7. Results for each region.

linear (left panels) and logarithmic representations (right panels). Compared with the MC model, the transformer model shows better performance, especially for activity sequences of small proportions. Results for each region are shown in Fig. 7, where one color indicates one region. Since detailed land use data are only available for 1978 and 1988, Fig. 7 shows the results for surveyed regions in these two years. Overall, Fig. 7 suggests similar results to Fig. 6. Generally, the two modes perform well, while the transformer model outperforms the MC model.

4.2. A deeper evaluation of the two models

For any specific group of people, the transformer model and the MC model predict the probability of the next activity given the previous activities. The transformer model considers all the previous activities and their orders, while the MC model only considers the last one and the time. Given all the previous activities before time t, if the probabilities for activities in the next time slot are perfectly predicted, all dots in Fig. 6 and Fig. 7 should be on the line of $y = x$. In this section, a deeper evaluation of the two models is presented by comparing the predicted probabilities and the real probabilities. First, let's define a metrics to evaluate the prediction accuracy for any group of people:

$$L = -\frac{1}{n}\sum_t \sum_{i=1}^{n} \sum_{a\in A} I_{i,t}(a) \ln\left(\hat{p}\left(a|s_{i,t-1}\right)\right) \qquad (3)$$

where n is the number of people; t is the index of the time slot (48 slots one day); i is the index of a person; a is an activity and A is the total set of activities including R, C, and O; $I_{i,t}(a)$ is one if person i does activity a at time t otherwise zero; $\hat{p}\left(a|s_{i,t-1}\right)$ is the predicted probability of conducting activity a given the previous activity sequence (i.e., predicted probability of the person doing a at time t). L is defined in a similar form as cross-entropy. The smaller the value of L, the better the prediction. When $\hat{p}\left(a|s_{i,t-1}\right)$ equals the real probability of conducting activity a at time t given the previous activity sequence $s_{i,t-1}$, L is minimized. In the following, the real probability is denoted by $p\left(a|s_{i,t-1}\right)$.

For the whole population (Fig. 6), we can evaluate the values of L using predicted probabilities by the transformer model and the MC model (denoted by L_{Trans} and L_{MC} for the transformer model and the MC model respectively). By comparing them with the value

calculated from real datasets (i.e., the theoretical minimum calculated with $p(a|s_{i,t-1})$, denoted by L_{Min}), we know the prediction accuracy for probabilities. For the results of each region (Fig. 7), we may evaluate the L value for each region and sum them up weighting on the population total size:

$$K = \frac{\sum_r n(r)L(r)}{\sum_r n(r)} \quad (4)$$

where r is the region; $n(r)$ is the number of people in the region; $L(r)$ is the value calculated using Equation (3) for the region. The value of K can be evaluated by the new transformer model, the MC model for each region, and the real datasets from the region. They are denoted by K_{Trans}, K_{MC}, and K_{Min} respectively. Fig. 8 shows the values of $L(r)$ calculated for each region versus the surveyed population in the region. The values of L and K calculated from various models and datasets are marked with arrows (they share the same y-axis). It can be observed that the L values from the transformer and the MC model are both close to the theoretical minimum, while L_{Trans} is closer. It implies that the probabilities for activities at each time slot are well-predicted. The theoretical minimum of the K value is around 5.547, which is significantly smaller than those from the two models. However, it is also noticed that, as the number of people surveyed grows, the theoretical minimum grows. One extreme case is that, when only one person is surveyed in a region, the theoretical minimum value of $L(r)$ for this region is zero because $p(a|s_{i,t-1})$ is one when $I_{i,t}(a)$ is one and is zero when $I_{i,t}(a)$ is zero in this case. Since K_{Min} is the weighted sum of $L(r)$ value from each region, the theoretical minimum can be underestimated because of the insufficient number of respondents from some regions. Given the growing trend of the $L(r)$ value with the number of people surveyed in Fig. 8, K_{Min} is approximately around 5.8 to 6 when the number of people surveyed is large enough. To conclude, the performances of the two models are good but can be further improved. In addition, the transformer framework is flexible, and many variations can be further examined.

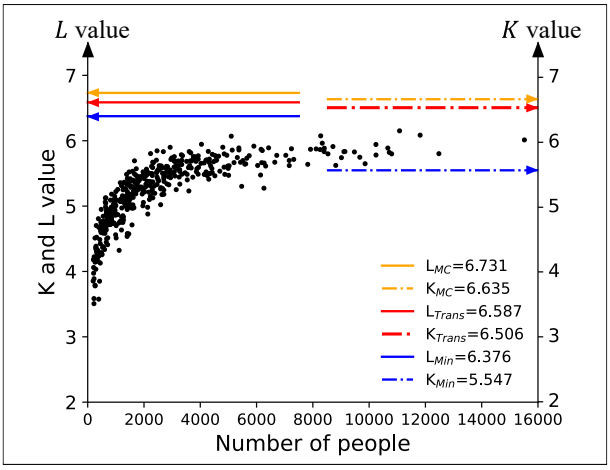

Fig. 8. Values of L and K.

Table 1. Summary of the two models.

	Metric	Trans model	MC model	Theoretical
For population	L value	6.587	6.731	6.376
	Number of parameters	29,760	426	N.A.
For each region	K value	6.506	6.635	5.547
	Number of parameters	252,450	184,884	N.A.

5. Discussions and conclusion

The transformer mode and the MC model provide decent performance, while the transformer model is better. Table 1 shows the summary of the two models regarding their performance and the number of parameters. When we focus on the whole population, the transformer model needs many more parameters. However, when constructing models to generate activity sequences for people in each region separately (which is a common task for demand prediction), we should construct one MC model for one region, and thus the number of parameters for the MC model would grow linearly with the number of regions. When the characteristics of a region change (e.g., land use), the current transformer model can be applied to make predictions, while the MC model is incapable of this. On the other hand, the transformer model is almost a black box, and we can get little knowledge about how the activity plans are made. The MC model clearly provides the logic of activity scheduling.

The transformer model for regions can be further improved by considering other regional attributes, such as

the distance to train stations for commuters in each region, and other contextual information, such as the land use attributes of regions near the target region. In addition, the encoder-decoder framework developed for transformer models can be applied to generate daily movements from activity sequences. They will be our future topics.

References

Drchal, J., Čertický, M., Jakob, M., 2019. Data-Driven Activity Scheduler for Agent-Based Mobility Models. Transportation Research Part C: Emerging Technologies 98, 370–390. https://doi.org/10.1016/j.trc.2018.12.002

Hafezi, M.H., Daisy, N.S., Millward, H., Liu, L., 2021. Ensemble Learning Activity Scheduler for Activity Based Travel Demand Models. Transportation Research Part C: Emerging Technologies 123, 102972. https://doi.org/10.1016/j.trc.2021.102972

Kitamura, R., Chen, C., Pendyala, R.M., 1997. Generation of Synthetic Daily Activity-Travel Patterns. Transportation Research Record 1607, 154–162. https://doi.org/10.3141/1607-21

Li, S., Lee, D.-H., 2017. Learning Daily Activity Patterns with Probabilistic Grammars. Transportation 44, 49–68. https://doi.org/10.1007/s11116-015-9622-1

Osaragi, T., Kudo, R., 2020. Enhancing the Use of Population Statistics Derived from Mobile Phone Users by Considering Building-Use Dependent Purpose of Stay, in: Kyriakidis, P., Hadjimitsis, D., Skarlatos, D., Mansourian, A. (Eds.), Geospatial Technologies for Local and Regional Development, Lecture Notes in Geoinformation and Cartography. Springer International Publishing, Cham, pp. 185–203. https://doi.org/10.1007/978-3-030-14745-7_11

Vaswani, A., Shazeer, N., Parmar, N., Uszkoreit, J., Jones, L., Gomez, A.N., Kaiser, Ł., Polosukhin, I., 2017. Attention is All You Need, in: Advances in Neural Information Processing Systems. Curran Associates, Inc.

Towards Pseudo People Flow: Developing a Deep Generative Model based on PT Data to Reproduce Large-Scale Daily People Activity Profiles

Yurong ZHANG[1], Kunyi ZHANG[2], Yanbo PANG[3], Yoshihide SEKIMOTO[4]

Abstract
The lack of cost-effective access to the human mobility dataset constrains deeper scientific investigations and restricts policymakers' ability to evaluate policy effectiveness. Recent achievements in generative pre-training models have made it possible to generate high-quality synthetic data as a practical substitute. In this study, we explore how existing generative pre-training models can be harnessed to reconstruct human daily behavior by modeling it as a sequence of activity choices. We evaluate the performance of our proposed approach using the Person Trip survey data collected from 20 metropolitan areas in Japan, encompassing approximately 6 million individuals' typical daily activities. Our experimental results show that the proposed approach is proficient at generating representative, realistic, and diverse synthetic human daily activity pattern data. This research significantly contributes to the generation of synthetic human mobility datasets, such as the Pseudo People Flow. Consequently, it aids in enhancing our understanding and accuracy of human mobility, demonstrating a promising avenue for future studies in this domain.

Keywords: Generative Model, Pseudo People Flow, PT Data

1. Introduction

1.1 Background

With the acceleration of urbanization, people's behavioral patterns are becoming increasingly complex. Understanding and predicting an individual's daily activity choices are crucial for areas such as traffic planning, urban planning, and environmental impact assessments. Moreover, with the advancement of data technology and the mobile internet, we have more means to acquire and process large-scale travel data, such as PT data and GPS data, providing more possibilities for modeling individuals' daily activity choices.

However, the privacy concerns arise due to potential personal identification, visits to sensitive locations, and data aggregation, even after anonymization. Strick regulations, while protecting privacy may stifle innovation and limit data granularity affecting research quality. Thus, generating and providing synthetic dataset is vital for research community.

1.2. Purpose

The primary objective of this research is twofold. Firstly, we aspire to explore an effective deep generative model structure capable of replicating large-scale daily activity profiles of individuals. Secondly, we aim to pinpoint an optimal training approach using person trip survey data. Moving forward, our aim is to leverage the developed model to support Pseudo People Flow generation. Additionally, we plan to apply the pre-trained model from data-rich areas to data-poor regions, harnessing fine-tuning techniques to enhance model performance. With this study, our ambition is to introduce an innovative tool for transportation and urban planning sectors. Furthermore, we hope to emphasize the versatility of deep generative models, particularly the GPT model, in an array of practical applications.

2. Related studies

In recent years, leveraging open statistical data, efforts

[1]Student Member (GISA), Graduate School of Frontier Sciences, the University of Tokyo, Kashiwa, Chiba 277-0882, Japan (e-mail: zyr0520@iis.u-tokyo.ac.jp).
[2]Student Member (GISA), Department of Civil Engineering, the University of Tokyo, Bunkyo-Ku, Tokyo 113-0032, Japan (e-mail: kyzhang@iis.u-tokyo.ac.jp).
[3]Member(GISA), Center for Spatial Information Science, the University of Tokyo, Meguro-Ku, Tokyo 153-8505, Japan (e-mail: pybdtc@csis.u-tokyo.ac.jp).
[4]Member(GISA), Center for Spatial Information Science, the University of Tokyo, Meguro-Ku, Tokyo 153-8505, Japan (e-mail: sekimoto@csis.u-tokyo.ac.jp).

have been made to construct Pseudo People Flow data [1], which replicates the typical daily behaviors of people across Japan. This synthesized data has been provided to various research communities, spanning both academia and the corporate world. Nevertheless, research related to Pseudo People Flow is still in its nascent stages. Enhancing its accuracy is imperative for practical applications, especially considering the inherent uncertainties in human decision-making and the intricate relationships dictated by urban structures and sizes. The demand for deep learning models capable of capturing and replicating these phenomena is on the rise.

Drawing from the advancements in deep learning, particularly in the field of natural language processing (NLP), there are indications that large computational models can accurately predict human behavioral patterns [2, 3]. However, much of the existing research remains tailored to specific regions or scenarios, with comprehensive, versatile models still underdeveloped. Acknowledging this backdrop, our study is inspired to harness vast mobility data to construct a generalized model, adaptable to diverse tasks and cities.

Generative pre-trained models, especially the Generative Pre-trained Transformer, have shown significant promise in the realm of deep learning and NLP [4]. OpenAI's introduction of the GPT architecture emphasizes unsupervised learning on extensive text corpora, suggesting potential applications beyond language tasks, including replicating intricate sequences like human behaviors [5]. In transportation, while understanding and predicting travel behaviors remains paramount, challenges such as data scarcity and privacy concerns persist. Recognizing these challenges, innovative approaches, like those of Pang et al. [2], have sourced trip semantics information from national censuses and other open repositories. Such data offers a feasible solution to the constraints present in transportation research, laying the groundwork for our current investigation.

3. Methodology

3.1. Data source

Person Trip survey data primarily records the movement of individuals within a certain area or region. The aim is to understand travel behavior, including reasons for travel, modes of transportation used, duration, distance, and frequency. Governments and transportation planners often use PT data to shape public transportation policies, urban planning, and infrastructure development.

The Person Trip (PT) survey in Japan captures residents' daily travel behaviors, covering various modes like walking, cycling, driving, and public transport. Conducted periodically, participants detail their trips using travel diaries, noting origins, destinations, modes, purposes, and times. This data informs urban and transportation planning, helping authorities understand travel demand and plan infrastructure projects. Additionally, demographic details are collected to analyze specific group patterns. The survey aids in decision-making regarding transportation infrastructure and policy in Japan's densely populated cities. However, challenges like respondent recall errors and underreporting of trips exist.

3.2. Activity sequence tokenizer

Tokenization is a fundamental step in many data processing tasks. At its core, tokenization involves breaking down larger data sets or texts into smaller, more manageable pieces, often referred to as "tokens." These tokens can then be used for various analyses, model training, or further processing. In our context, the data of interest is the activity sequences of individuals, and the tokenization process is applied to these sequences.

To begin with, we tokenize the PT (Personal Trip survey) data of every individual. This involves transforming the per-minute records into distinct time intervals based on changes in latitude and longitude. In simpler terms, instead of logging data for every single minute, we only recorded data points when there was a change in an individual's location. This method reduces redundancy and focuses only on moments of movement or change in activity.

Table 1 Purpose-to-Activity Mapping

purpose	activity
Commute	Office
Go School	School
Back Home	House
Shopping Daily	Store Daily
Shopping Nondaily	Store Nondaily
Go Eat	Socializing
Go Recreational Facility	Socializing
Pick up & Drop off	Welcoming
Go Sightseeing	Tourist Spot
Private Movement	Private Space
Delivering	Business Place
Attend Meeting	Business Place
Go Occupation	Business Place
Go Agricultural Work	Natural Area
Go Other Business	Business Place
Go Exercise	Pitch
Volunteering	Public Space

Once the data is consolidated in this manner, we proceed to generate 'trip chains'. A trip chain can be visualized as a sequence of activities an individual engages in. Each link in this chain denotes the type of activity and its duration, recorded in 15-minute intervals. For example, if an individual was stationary at a particular location (say, a coffee shop) for 30 minutes, this would be represented as two consecutive tokens of the same activity type, each of 15-minutes.

Fig 1 Illustration of Activity Sequence Tokenization

3.3 Model selection

The GPT (Generative Pre-trained Transformer) models are a series of language models developed by OpenAI. They have been released in several versions, each with increasing complexity and capabilities. Smaller models are faster, require less memory, and are more cost-effective, making them suitable for rapid prototyping or less complex tasks. Larger models, while computationally intensive, offer better performance and can handle more complex tasks or datasets. The choice often involves a trade-off between computational cost and desired performance.

The GPT model aligns perfectly with my objective of generating hypothetical pedestrian flow data. What's noteworthy is that the GPT model undergoes an initial pre-training on vast amounts of unlabeled data. During this phase, it grasps the fundamental structure, vocabulary, and features of the language. Subsequently, it can be fine-tuned for specific tasks, ensuring a high level of adaptability to the data I'm training on. Given that my data involves textual representations, like descriptions or records, GPT emerges as an optimal choice due to its prowess in generating continuous, logical text that mirrors genuine data.

3.3 Model architecture

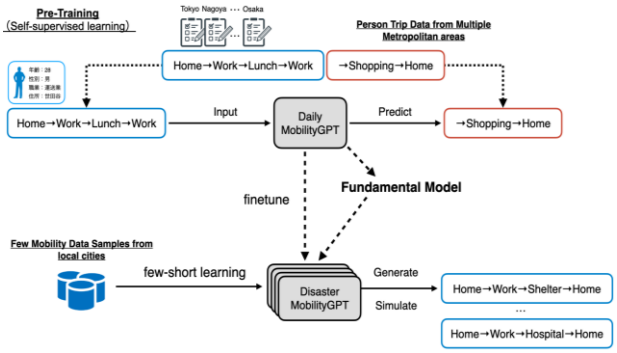

Fig 2 Framework of the proposed method

3.4. Model training

Since every 15 minutes a person's travel activity type is recorded, each generated travel activity chain contains 96 words. Considering that people are likely at home during the first and last 6 hours of the day, data from both ends were removed, leaving only the middle 48 words to complete the travel chain. We chose the GPT model to train our data, using the AdamW optimizer with a learning rate set at 0.0001 and a weight decay of 0.2. The model will iterate over the entire dataset 10 times, i.e., for 10 epochs. At the end of each epoch, an evaluation is performed on the validation dataset, recording metrics such as loss and perplexity for ease of observation in the later stages.

4. Experiment

4.1. Details of the study area

We selected Person Trip data from various cities in Japan to train our model, with each dataset coming from different collection years. These datasets include data from Sendai metropolitan area in 2002, the northern-Kyushu metropolitan area in 2005, Hokkaido metropolitan area in 2006, Tokyo metropolitan area in 2008, Kinki metropolitan area in 2010 and Chukyo metropolitan area in 2011. We selected these 6 datasets for model training because these cities have large data volumes and are geographically dispersed throughout Japan, rather than being confined to a single region. And we also trained them separately by using one metropolitan area, multiple metropolitan areas and all areas data to observe the different results.

As illustrated in the figure2, we utilized data pertaining to the following regions for the model training and validation. After pre-processing and conversing the data, as demonstrated in the table1, different areas yielded datasets of varying sizes, cumulatively encompassing a total of 1,749,773 individual data entries.

Table 2 Statistics of Person Trip Data used in this study

Metropolitan area	No. of people	No. of samples
Kinki	22,018,058	590,514
Tokyo	39,719,677	576,805
Chukyo	11,205,326	200,916
Northern-Kyushu	5,903,031	194,390
Sapporo	1,959,512	101,928
Sendai	305,030	85,220

Table1. Statistics of Person Trip Data used in this study

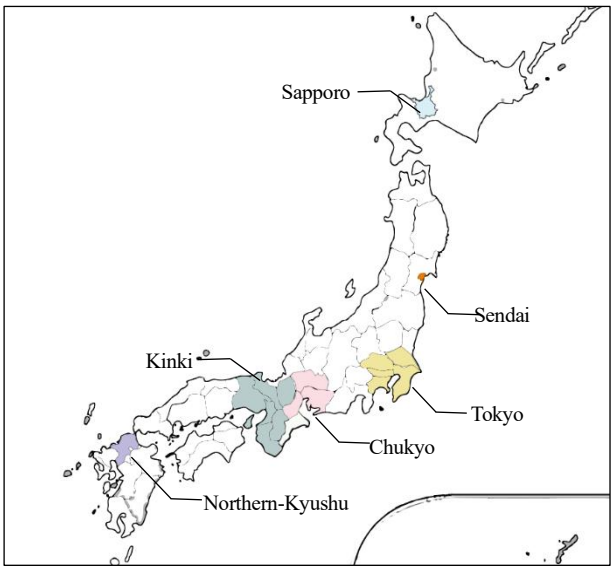

Fig 3 Target areas in experiment

Green: Kinki metropolitan area. Pink: Chukyo metropolitan area. Yellow: Tokyo metropolitan area. Blue: Sapporo metropolitan area. Purple: Kita-Kyushu metropolitan area. Orange: Sendai metropolitan area.

4.2. Details of the implementation

We trained the model with three different data strategies as:

Tokyo only: Only use the activity sequence derived from Tokyo PT dataset.

3 Metropolitan areas: use the activity sequence derived from Tokyo, Kinki and Chukyo PT dataset.

All Metropolitan areas: use the activity sequence derived from Tokyo, Kinki, Chukyo PT, Northern Kyushu, Sapporo, and Sendai PT dataset.

We split each dataset by 9:1 as training and validation dataset.

To evaluate the prediction performance of the proposed task, we feed variable-length of initial activities and let model to predict the remained activity sequence. For example,

Input (n=5): House → House → House → House → Commute

Output of GPT (n=43): → Commute → Commute → Office → … → Dine → Office → BackHome → BackHome → House → House → House

We tested the initial length from 1(15 mins) to 47 (11hour 45 mins).

Table 3 The details of hyper-parameters used in the model

Hyper-parameters	value
Parameter Number	361,856
Learning rate	0.0001
Batch size	1024
Training epochs	10
Loss function	Cross-Entropy Loss

4.3. Evaluation matrices

In this study, we employ the Jaccard Similarity Index as a pivotal metric to quantify the degree of similarity between generated activity sequences and ground truth data. This measure is particularly advantageous when handling expansive datasets where the primary concern revolves

around the presence or absence of items, rather than their quantity or order. Historically, the Jaccard Similarity has been a preferred choice in domains such as document clustering and text mining, offering a robust means to ascertain the similarity between texts or documents.

$$J(A,B) = \frac{|A \cap B|}{|A \cup B|}$$

Where:

$|A \cap B|$ denotes the cardinality of the intersection of sets A and B.

$|A \cup B|$ denotes the cardinality of the union of sets A and B.

Scores residing between 0 and 1 depict the proportion of common elements between the two sets.

4.4. Results

We first show the learning curves in Figure 4 for different datasets. The green lines represent the model's training and validation for Tokyo Only dataset, blue lines represent the model's training on three metropolitan areas: Tokyo, Osaka, and Nagoya. The solid lines depict the model's performance when trained solely on data from Tokyo.

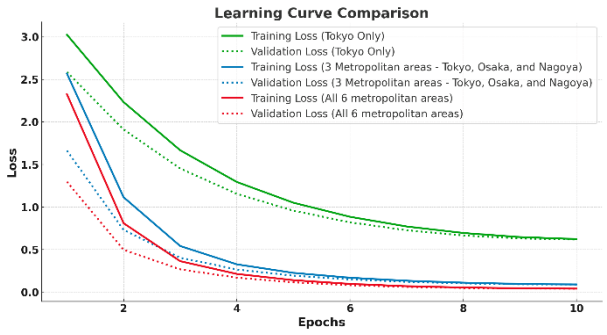

Figure 4 Comparison of the learning curves.

As depicted, training on a more diverse dataset (three metropolitan areas and all metropolitan areas) yields a distinct loss pattern compared to training on data from Tokyo alone.

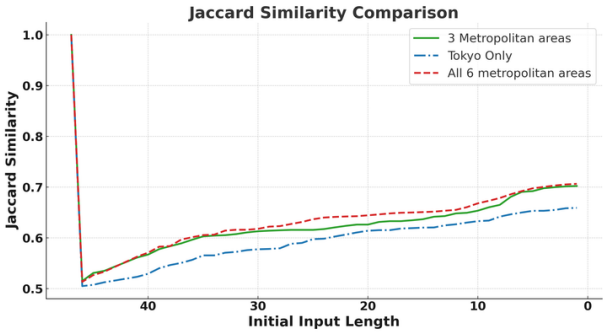

Figure 5 Comparison of the predicted activities accuracy.

Figure 5 illustrates the predicted activity sequence accuracy based on varying initial input lengths for three models: "3 Metropolitan areas," "Tokyo Only," and "All 6 metropolitan areas." Notably, all three models display an accuracy of 1.0 when the input length is 47, indicating that with sufficiently long initial inputs, these models can accurately predict the subsequent activity. However, as the initial input length diminishes, there is a noticeable decline in the Jaccard Similarity. This decline suggests that shorter sequences tend to deviate more from the norm compared to their longer counterparts. Such an observation is consistent with many textual datasets, where shorter sequences often exhibit greater variability. Moreover, the close overlap of trends across the three datasets implies consistent patterns or shared linguistic characteristics across Tokyo, the three metropolitan areas, and all six metropolitan areas, reinforcing the idea of shared behavioral patterns across these regions.

5. Conclusion

In this study, we proposed a novel daily activity sequence prediction model based on the neural language model Generative Pretrained Transformer (GPT). By converting people's daily activities into token time sequences with the People Flow dataset, the GPT model can automatically learn the daily activity patterns of individuals using self-supervised learning.

Our investigation focused on the prediction accuracy of the models when utilizing different volumes of metropolitan individuals' daily activity data. We demonstrated that even a basic GPT-1 level model could be

trained effectively using the daily activity data from 2% of the population across three metropolitan areas. When using the dataset from all regions, the model exhibits a favorable learning curve, with both the average loss and validation values dropping to 0.04, and the Jaccard similarity exceeding 0.7.

However, this work still presents several limitations. First, the model's prediction accuracy could benefit from both an increase in model size and more extensive training data. While we employed the GPT-1 level model in this study, future efforts will explore the potential of larger models like GPT-2. Second, this study did not take into account individual demographics, resulting in homogeneous predicted activities, which may decrease accuracy. Lastly, we exclusively evaluated results using the Jaccard Similarity index. Incorporating activity patterns such as Motif may provide deeper insights and further refine our results.

Moving forward, our aim is to leverage the developed model to support Pseudo People Flow generation. Additionally, we plan to apply the pre-trained model from data-rich areas to data-poor regions, harnessing fine-tuning techniques to enhance model performance.

References

[1] Kashiyama, T. et al. (2022) Pseudo-PFLOW: Development of nationwide synthetic open dataset for people movement based on limited travel survey and Open Statistical Data, arXiv.org. Available at: https://arxiv.org/abs/2205.00657 (Accessed: 31 August 2023).

[2] Y. Pang and Y. Sekimoto, (2022) *IEEE International Conference on Big Data (Big Data),* "Deep Learning for Destination Choice Modeling: A Fundamental Approach for National Level People Flow Reconstruction," pp. 1900-1905. doi: 10.1109/BigData55660.2022.10020165.

[3] Yabe, T., Tsubouchi, K., Shimizu, T., Sekimoto, Y., & Ukkusuri, S. V. (2020, August). Unsupervised translation via hierarchical anchoring: functional mapping of places across cities. In Proceedings of the 26th ACM SIGKDD International Conference on Knowledge Discovery & Data Mining (pp. 2841-2851).

[4] Radford, A., Narasimhan, K., Salimans, T., & Sutskever, I. (2018). Improving language understanding by generative pre-training.

[5] Mizuno, T., Fujimoto , S. and Ishikawa , A. (2022) Generation of individual daily trajectories by GPT-2, Frontiers. Available at: https://www.frontiersin.org/articles/10.3389/fphy.2022.1021176/full (Accessed: 31 August 2023).

Location-Based Content Tourism Support System on Foot

Nobuaki Nagano*, Kayoko Yamamoto**

Abstract: Content tourism, or trips to places modeled after works such as anime and movies, is gaining popularity in Japan. Content tourism differs from conventional forms of tourism in that the places tourists visit are known only to the fans of the works including animation, novel and the like. Therefore, it is also very important for people living in the area to know the information about places related to contents of the works. Therefore, the purpose of this study is to design and developed a system that supports content tourism not only for funs but also for residents. This system has the function of creating sightseeing routes and allowing the use of such routes. This system displays the routes and nearby sightseeing spots using the users' location information. This system will also provide a function that allows users to share information by viewing and rating sightseeing routes created by other users. This system is expected to help residents deepen their understanding of their community and improve their health by walking around the area.

Keywords: Content Tourism, Location Information, Sightseeing Spots, Sightseeing Route, Tourism Support

1. Introduction

In recent years, the rapid development of advanced information and telecommunications networks has made it possible to obtain a wide variety of information via the Internet. In addition, the spread of social networking services (SNS) has made it possible for anyone to not only acquire but also disseminate information. The same is also true for tourism information, which can be obtained not only through traditional methods such as guidebooks and tourism information magazines but also increasingly via the Internet. Furthermore, it has also be-come possible for people to easily acquire tourism information that matches their own particular tastes, so tourism has taken a more diverse range of forms.

One of these is "content tourism". Contents tourism is defined as "tourism intended to promote tourism and the related industries by utilizing local contents (movies, TV dramas, novels, manga, games, etc.) in a survey conducted by the Ministry of Land, Infrastructure, Transport and Tourism in 2005. In Japan, travel to places related to subcultures such as anime has been attracting attention in recent years. According to the Development Bank of Japan (DBJ), the number of tourists who visit Kuki City in Saitama Prefecture had increased, this city became the model for a famous Japanese anime. As a result, according to the DBJ, the economic ripple effect of Kuki City over 10 years is approximately $20,000,000.

Places related to anime and other content are known only to its fans and are often unremarkable to the general public who are not fans. According to the Japan Travel Bureau (JTB), one of the challenges for successful content tourism is to gain an understanding of residents. In other words, it is important that residents living in the area also know information about content tourism. Therefore, a system that simultaneously provides information on conventional tourist attractions and information on places that appeared in the works is needed. Most of the existing systems that support content tourism are work-based, and no system comprehensively deals with the places that appeared in the works that exist in the area. In addition, it is expected that content tourism by residents on foot will not only deepen their understanding of the region but also improve their health. In this case, by utilizing the location information of users, the system can improve convenience of the system by providing route navigation and information on the surrounding area.

* Student Member (GISA), Graduate School of Information Science and Technology, The University of Electro-Communications, n2230104@edu.cc.uec.ac.jp
** Member (GISA), Graduate School of Information Science and Technology, The University of Electro-Communications, kayoko.yamamoto@uec.ac.jp

Based on the above social and academic backgrounds, the purpose of this study is to develop a system that supports not only tourists but also residents to engage in content tourism on foot by utilizing location information. To this end, a location-based walking content tourism support system will be first designed and developed (sections 3 and 4). It will then be operated (section 5). After the operation, we will evaluate the system by conducting a questionnaire survey for users and access analysis of log data.

2. Related Work

This study is related to three academic fields; (1) studies on tourism support systems, (2) studies on content tourism support systems, and (3) studies on location-based systems. In the following, representative previous studies of three academic fields is introduced and the originality of this study is demonstrated.

In (1) studies on tourism support systems, Maruyama et al. (2004) developed a personal navigation system (P-Tour) that supports the creation of sightseeing schedules and provides route guidance. Ueda et al. (2015) developed a tourism support system that generates posterior information from tourists' activities during sightseeing and shares this information among users as advance information during sightseeing. Ikizawa- Naitou et al. (2020) integrated a travel route recommendation system, Web-GIS and augmented reality (AR) in order to develop a sightseeing planning support system. Robert et al. (2008) developed a recommender system for visiting tourist attractions in Macau that manage travel schedule and travel time.

In (2) studies on content tourism support systems, Yamazaki et al. (2016) developed a system that records detailed action histories by analyzing global positioning system (GPS) logs and has a check-in function for sightseeing spots of people who visited places related to animes. Akiyoshi et al. (2017) developed a system with functions for effectively recommending nearby tourist spots and for planning sightseeing in a fun way to support anime content tourism. Echigo et al. (2018) developed a conectAR that provides an opportunity to talk with residents using AR when visited places related to anime.

In (3) studies on location-based systems, Fränti et al. (2017) developed O-Mopsi, which is an orienteering game that uses location information to visit many destinations. Simcock et al. (2003) developed a tourist guide application that uses location information to guide visitors to destinations and create sightseeing tours.

In (1) studies on tourism support systems, the routes created by the systems of Maruyama et al. (2004), Ikizawa et al. (2020) and Robert et al. (2008) can be viewed only by creators, and no functions to view routes created by other users are implemented in the above systems. In addition, since only sightseeing spots that have been registered in the database in advance are displayed, users cannot submit new sightseeing spot information and create their sightseeing routes. The systems of Maruyama et al. (2004) and Ueda et al. (2015) required ex-post information on the sightseeing behavior of other tourists as advance information, and it is difficult to obtain sufficient useful advance information when the number of users is small. The previous studies in (2) studies on content tourism support systems assumed that only fans of the content use the system, and no systems have been proposed that targets other people as well. In addition, the system of Akiyoshi et al. (2017) only registers information about spots of a single anime work. In (3) studies on location-based systems, the system of Fränti et al. (2017) can also be used for sightseeing, but it only displays the order of visits efficiently and does not display routes, etc. The system of Simcock et al. (2003) can create sightseeing tours using users' location information and upload them. However, it does not allow users to evaluate tours created by others.

Compared with the previous studies mentioned above, the first originality of this study is that even users who do not know the contents can enjoy content tourism by referring to sightseeing routes created and comments submitted by other users. The integration of Web-GIS,

tourist information system, location information system, and SNS makes it possible. The second originality is that both tourists and residents can use location information to conduct content tourism on foot, thereby deepening their understanding of the region and improving their health. The third originality is that the system developed in this system handles not only information on places appearing in multiple contents such as anime, movies, dramas, and special effects and sightseeing spots but also various types of information such as restaurants and parks.

3. System Design

3.1. System Characteristics

This system consists of a Web-GIS, a tourist information system, a location information system and an SNS. Figure 1 shows the characteristics of each system. When using this system for the first time, users set their ID, nickname and passwords, and register their user information in the database. After logging in to the system, users can register new sightseeing spot information on the digital map of Web-GIS. Users can decide which sightseeing spots to visit and create a sightseeing route to visit them. The sightseeing route will be used to display the route and nearby spots based on the user's location information. In addition, users can view and evaluate sightseeing routes created by other users. The total distance traveled, total number of steps taken and total calories consumed are calculated for each user based on the information on the sightseeing route used. The top five sightseeing routes with the longest total distance traveled, and the most frequently used sightseeing routes are displayed in a ranking format. New sightseeing spots registered by users and sightseeing routes created by them are stored in the database.

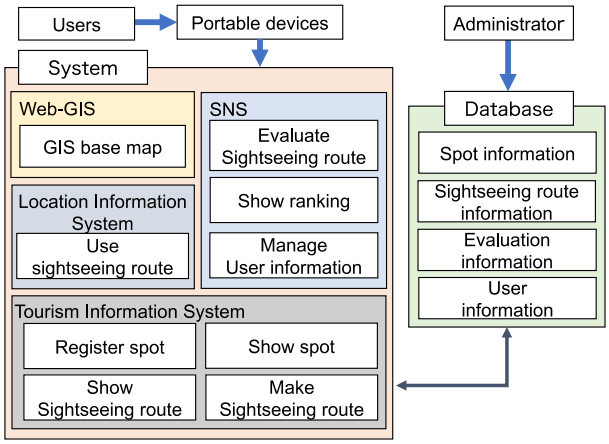

Figure 1 System design

3.2. System Effectiveness

The effectiveness of this system is summarized into the following three points.

(1) Users do not need prior information when sightseeing.

Even users with no knowledge of the contents can learn about contents from the sightseeing spot information. In addition to sightseeing spots, users can also browse information on restaurants, parks, etc. Users do not need to browse other systems or web pages, thereby reducing the burden of information collection.

(2) Abundance of information

This system registers sightseeing spots that have appeared in works regardless of the medium of the work, allowing users to browse and visit spots that interest them from among a wide variety of spots. In addition, since users can register new spots, the system can be used to fill in missing information.

(3) Health promotion along with sightseeing

Users can obtain information on their total travel distance traveled, total number of steps taken, and total calories consumed. In addition, by obtaining the user's location information, it is easy to determine the relationship between each spot and the location of the user, thus supporting content tourism on foot by the user. Users can easily check the amount of exercise they have done and improve their health.

3.3 Calorie Consumption Calculation Method

User information is managed, and the total distance traveled, total number of steps taken, and total calories consumed by the user are calculated and displayed based on the information on the sightseeing routes used by the user. The equation for calculating the number of steps is based on information from OMRON corporation website. The equation for calorie consumption is based on the "Physical Activity Standards for Health Promotion 2013" established by the Ministry of Health, Labour and Welfare.

The user's distance traveled was added each time the sightseeing route was used, using the values measured by Web-GIS. The number of steps taken by the user is calculated from Equation (1). The travel distance l uses the value measured by Web-GIS. The height h is calculated as $h \times 0.45$ as the stride length, referring to the average height by gender and age in the National Health and Nutrition Survey (2018) by the Ministry of Health, Labour and Welfare.

$$s=(l\times1000)/(h\times0.45) \quad \ldots(1)$$

s : Number of steps

l : Distance traveled (km)

h : Height(cm)

The calorie expenditure of the user of this system is calculated from equation (2). The metric value m used is a value that indicates how many times the energy expenditure due to exercise is compared to that at rest, and in this study, three metric values at 67 m/min (4.0 km/h) are used. For body weight w, we use the average weight by gender and age from the National Health and Nutrition Survey (2018) of the Ministry of Health, Labour and Welfare. The time taken to walk the distance measured on the Web-GIS at a speed of 67 m per minute is calculated and used as the exercise time t. The time taken to walk the distance measured on the Web-GIS at a speed of 67 m per minute is used as the exercise time t.

$$cal = m \times w \times t \times 1.05 \quad \ldots(2)$$

cal : Calories consumed (kcal)

m : METs

w : Weight(kg)

t : Exercise time (m)

4. System Development

4.1. Frontend of the System

This system implements 5 unique functions for users, which will be mentioned below, in response to the purpose of the present study as mention in section 1.

(1) Function of new user registration and login

First-time users of this system must first register as new users. On the new user registration screen, the user registers "ID", "Nickname", "Password", "Gender" and "Age". Users who are using the system for the second time or later will enter their "ID" and "password" to access the system.

(2) Function of sightseeing pot information registration

By selecting "Add Spot" from the menu bar at the top of the home page of the system, users can move to the "Register Spot Function" screen and submit spot information. At this time, users enter the "name of the spot," "category," and "whether the spot appears in a work. If the spot is a place that appears in a work, "related content" and "links to related content" are additionally entered. The "Category" can be selected from 11 types: "Places of Interest/Historical Sites", "Parks/Botanical Gardens", "Public Facilities", "Restaurants", "Temple/Shrine", "Museums", "Hot Springs", "Hanami", "Festival/Event", "Theme Park" and "Others".

(3) Function of sightseeing route creation

By selecting "Create Sightseeing Route" from the menu bar at the top of the home page of the system, users can move to the screen of the make sightseeing route function and create a sightseeing route. By selecting an icon on the digital map, a pop-up window appears, allowing users to enter information on sightseeing spots included in the sightseeing route. Selecting multiple sightseeing spots on this screen and selecting the "Selection Complete" button will take users to the sightseeing route registration screen. A sightseeing route can be created by entering the title and

introduction of the sightseeing route and selecting the "Route Complete" button.

(4) Function of sightseeing spot display

Users select "Display Spot" from the menu bar at the top of the home page of the system, and then selects either "View from List" or "View from Map" on the next screen to move to the "View Spots" screen. When "View from List" is selected, users can view a list of sightseeing spot information ("Sightseeing Spot Name", "Category", "Place Appears in a Work", "Related Content" and "Links to Related Content"). By selecting a category that matches users' preferences, users can search for sightseeing spots in that category.

When "View from Map" is selected, the sightseeing spots can be viewed on a digital map. A pop-up window appears when users select an icon of a sightseeing spot. The pop-up displays the "name of the sightseeing spot", "category", "related content" and "links to related content". Users can also select a layer to narrow down the spots to be displayed to a specific category of drinking, and if users have location information turned on, only spots in the user's vicinity are displayed on the map (Figure 2).

Figure 2 Show Spot Function (Image)

(5) Function of sightseeing route display

Users move to the sightseeing route viewing function screen by selecting "Display Sightseeing Routes" from the menu bar at the top of the home page of the system. This screen displays the date and time the sightseeing route was created, the creator's nickname, title, introduction, time required, number of times used, and number of likes. By selecting the "Details" button on this screen, the user is taken to a screen where he/she can view the details of the sightseeing route. Furthermore, by selecting the "Adopt this route" button on this screen, the user can move to the screen for adopting the sightseeing route.

(6) Function of sightseeing route selection

By selecting the "Select this route" button on the sightseeing route details screen, user moves to the sightseeing route use screen (Figure 3). On this screen, users' location information and the sightseeing route are displayed. The user moves along the created sightseeing route, and when user's location information matches the sightseeing spots registered in the route, the system judges that the user has visited those spots. The system judges that the user has used the sightseeing route by visiting all the sightseeing spots registered on the route, and their total distance traveled, total number of steps taken, and total amount of calories consumed are updated. In addition, when users have turned off location information or when they are not judged to have visited a sightseeing route, the user is judged to have used a sightseeing route by pressing the "Used route" button. Users can check the sightseeing route used on the screen of the manage user information function.

Figure 3 Use Sightseeing Route Function (Image)

(7) Function of sightseeing route evaluation

Users can evaluate sightseeing routes created by other users by posting comments from the comment input screen at the bottom of the sightseeing route details viewing screen. Users can also simply evaluate the sightseeing route by clicking the "Like" button. Users can view the sightseeing routes they have commented on and liked on their My Page.

(8) Function of user information management

By selecting "My Page" from the menu bar at the top of the home page of the system, the user is transferred to the user information management function screen. On this screen, users can view their ID, nickname, total distance traveled, a total number of steps taken, total calories consumed, comments posted, likes, and sightseeing routes used or created. Users can log out of the system by selecting the "Logout" button on this screen.

(9) Function of user ranking

By selecting "Ranking" from the menu bar at the top of the home page of the system, the user is transferred to the user and sightseeing route ranking function screen. On this screen, the top five sightseeing routes with the longest total distance traveled and the most frequently adopted sightseeing routes are displayed in a ranking format. The "nickname" and "total distance traveled" are displayed as information on the user, and the "title," "creator's nickname," "introduction," and "number of times used" are displayed as information on the sightseeing route. By selecting the "Details" button on this screen, the Users move to the screen for viewing the details of the sightseeing route.

4.2. Backend of the System

In the backend of the system, the following 6 processes are conducted in response to 7 functions in the frontend.

(1) Processes related to user information registration and login

User information is stored in a database. At this time, passwords are hashed to prevent misuse by third parties. The login process is performed only when the ID and password match and an error message is displayed when they do not match.

(2) Update of spot information

When a user submits new spot information, the backend performs a process to store the information in the database.

(3) Processing related to the creation of sightseeing routes

The backend stores the information entered by users using the sightseeing route creation function in two tables in the database. The first table stores the date and time of creation, title, creator's nickname, introduction, time required, and number of times the route has been used, while the second table stores the center coordinates and zoom factor of the digital map, names of sightseeing spots, categories, and Related Content.

(4) Processing related to the evaluation of sightseeing routes

The backend stores the comments posted on the sightseeing routes in two tables in the database. These two tables store the comments of the user who created the route and the comments of other users on the route.

(5) Processing related to the use of sightseeing routes

When a user uses a sightseeing route, the backend calculates the total distance traveled, the total number of

steps taken, and the total number of calories consumed, and updates the number of times the sightseeing route is used and the user information. The backend also arranges the number of times a sightseeing route has been used and the total distance traveled by users and displays the top five users with the longest total distance traveled and the most frequently used sightseeing routes on the user and sightseeing route ranking function screen.

(6) Processing related to location information

When a user uses a sightseeing route, the system acquires the user's location information and displays it on the map. When the user's location information and a spot on the sightseeing route match within a certain range, the system determines that the user has visited that sightseeing spot.

4.3. System Interface

This system is developed with the assumption that it will be used by mobile information terminals. In consideration of the case where users may be reluctant to use location information, an interface for the case where location information is not used will also be produced.

5. System Operation

5.1. Selection of the area for operation

The area around Chofu City, Tokyo, was selected as the target area for this system. The reason for this selection was the existence of the “Very Detailed Map of Locations Featured in the Work in Chofu City” created by Chofu FM, which is a community radio station in Chofu City. The “Very Detailed Map of Locations Featured in the Work in Chofu City” contains a wide range of places appearing in works in Chofu City contributed by ordinary viewers, and the system's functions can be widely used immediately after the start of its operation.

The following three types of people can be assumed as users of this system. Those who are familiar with the target area and have knowledge of sightseeing spots related to the works will disseminate information by posting new sightseeing spots and creating sightseeing routes. Those who are familiar with the target area but do not know the sightseeing spots related to the works will collect information provided by other users and create sightseeing routes. Those who are not familiar with the target area can browse information on sightseeing spots and sightseeing routes created by other users, and plan their sightseeing plans efficiently.

5.2. Data Collection of Sightseeing Spots

Four types of data were collected in advance to make the functions of this system available immediately after the start of operation.

(1) Sightseeing spot information

Data on 78 sightseeing spots was collected from "Fortlavel.

(2) Restaurant information

Data on 1,083 restaurants was collected from "Tabelog.

(3) Park information

Data on 75 parks was collected from "Ikoyo," a website that supports outings with children.

(4) Information on spots that appeared in the content

Data on 1,083 spots that appeared in the works was collected from “Very Detailed Map of Locations Featured in the Work in Chofu City”

A total of 1,524 of these spots are registered in the system.

5.3. System Operation

The system will be in operation for approximately two months, targeting people of all ages in and outside the target area. When the system is operated, the authors will call for it via their laboratory's website, SNS, etc.

6. Conclusions

In this study, the system was designed and developed (Sections 3 and 4), and it will be operated (Section 5). This study can be summarized in the following two points.

(1) This study designed and developed a system integrating Web-GIS, a tourist information system, a location information system, and an SNS to support content tourism on foot. The system enables users to create and use sightseeing routes and to post, store, and

browse information on sightseeing spots. The usefulness of this system is that users do not need prior information before sightseeing, that the information is abundant, and that the system promotes health along with sightseeing.

(2) This system is intended to be operated in Chofu City, Tokyo, and information on 1524 sightseeing spots was collected in advance. After the system is developed, it will be operated and evaluated.

To evaluate the system developed in this study, an online questionnaire survey for users and an access log analysis will be conducted. In the questionnaire survey, the use of the system and the functions of the system will be evaluated. In the access log analysis, Google Analytics will be adopted to analyze the access logs using the log data of users during the operation of the system.

Reference

Tourism and Regional Development Division, Policy Bureau, Ministry of Land, Infrastructure, Transport and Tourism; Cultural and Information Related Industries Division, Commerce and Information Policy Bureau, Ministry of Economy, Trade and Industry; and Arts and Culture Division, Agency for Cultural Affairs (2005), Survey on Regional Development through Production and Use of Video and Other Content.

Development Bank of Japan. Content and Regional Revitalization - 100 Years of Japanese Anime, Focusing on Pilgrimage to Holy Places. https://www.dbj.jp/topics/region/ industry/files/0000027774_file2.pdf

JTB Boken, "Adding Value to Tourism Resources: The Key to Successful Content Tourism." <https://www.jtbbokun.jp/column/22031401#:~:text=%E5%BE%93%E6%9D%A5%E3%81%AE%E3%80%8C%E3%83%%95 95%E3%82%A3%E3%83%AB%E3%83%A0%E3%83%84%E3%83%BC%E3%83%AA%E3%82%BA%E3%83%A0%E3%80%8D%E3%80%8C,%E3%82%8F%E3%82%8C%E3%81%A6%E3%81%84 E3%82%8B%E3%81%A8%E3%81%84%E3%81%86%E3%81%93%E3%81%A8%E3%80%82>, accessed August 5, 2023

Maruyama, A., Shibata, N., Murata, Y., Yasumoto, K. and Ito, M. (2004) P-Tour: A Personal Navigation System to Support Creation of Sightseeing Schedules and Provide Guided Sightseeing Along the Schedule. Transactions of Information Processing Society of Japan, 45 (12), 2678-2687.

Ueda, T., Ooka, R., Kumano, K., Tarumi, H., Hayashi, T., and Yaegashi, R. (2015) A tourism support system for generating/sharing tourism information. IPSJ Research Report (Information Systems and Social Environment (IS)), 2015-IS-131 (4), 1-7.

Ikizawa-Naitou, K. and Yamamoto, K. (2020) A Support System of Sightseeing Tour Planning Using Public Transportation in Japanese Rural Areas, Journal of Civil Engineering and Architecture, 14, 14, 1-7. Journal of Civil Engineering and Architecture, 14, 316-332.

Yamazaki S and Tajima K (2016) A study of action history recording methods suitable for regional sightseeing applications. Proceedings of the IPSJ Entertainment Computing Symposium 2016, 277-278.

Akiyoshi T., Takayama T. (2017) A system to support the activation of pilgrimages to anime holy places. Proceedings of the 79th National Convention of Information Processing Society of Japan, 995-996.

Echigo H, Kobayashi M (2018) conectAR: A proposal of communication support system using AR for pilgrimage to anime holy places. IPSJ Research Report (Groupware and Network Services (GN)), 2018-GN-105 (12), 1-8.

Fränti P., Mariescu-Istodor R., and Sengupta L.. 2017. O-Mopsi: Mobile orienteering game for sightseeing, exercising, and education. ACM Transactions on Multimedia Computing, Communications, and Applications (TOMM) 13, 4 (2017), 1–25.

Simcock, T., Hillenbrand, S., Thomas, B. 2003. Developing a location based tourist guide application. In Proceedings of the CRPITS '21 at ACSW frontiers

Omron Corporation, "What is the standard stride length?", <https://www.faq.healthcare.omron.co.jp/faq/show/4195?site_domain=jp>, accessed July 25, 2023.

Ministry of Health, Labour and Welfare (2013), "Physical Activity Standards for Health Promotion 2013.

Ministry of Health, Labour and Welfare National Health and Nutrition Survey (2018) <https://www.e-stat.go.jp/dbview?sid=0003224177>, accessed 25 July 2023.

Fortravel <https://4travel.jp/>, accessed 6 May 2023.

Tabelog <https://tabelog.com/>, accessed 6 May 2023.

Ikoyo|Children and Outing Information <https://iko-yo.net/>, accessed May 6, 2023.

Very Detailed Map of Locations Featured in the Work in Chofu City <https://www.google.com/maps/d/viewer?mid=1RCpfgHrgMWYyujmo42NOwwZDM3GFvu0&ll=35.654976093147965%2C139.55779518254025 &z=13>, accessed July 2, 2023.

Development of Food Tourism Support System Adopting Location-Based AR

Makoto Hirano*, Kayoko Yamamoto**

In recent years, the objectives tourists have for visiting sightseeing areas are becoming more diverse all over the world. The form of tourism known as “food tourism” has become especially widespread. In addition, though some tourists wish to create sightseeing plans, others wish to visit tourist destinations without advance planning. Against such a backdrop, this study aimed to develop a system that integrates a tourism planning system, Web-GIS and AR in order to support both planned and unplanned tourism especially for eating and drinking in urban tourist destinations. The system has original functions including the functions of food tourism plan creation, search for nearby sightseeing spots, and navigation adopting location-based AR. The function of food tourism plan creation allowed users to efficiently create food tourism plans. The function of navigation adopting location-based AR allowed users to visit restaurants in addition to nearby sightseeing spots included in food tourism plans they have created.

Keywords: Web-GIS, Tourism Planning System, Augmented Reality (AR), Food Tourism

1. Introduction

1.1 Background

In recent years, the objectives tourists have for visiting sightseeing areas are becoming more diverse all over the world. The form of tourism known as "food tourism" has become especially widespread. Food tourism is composed of activities that provide experiences of consumption and appreciation of food and beverages, presented in such a way that values the history, the culture and the environment of a particular region. Furthermore, food tourism was selected as a theme of projects conducted by the Japan Tourism Agency for attracting tourists to provincial areas between 2016 and 2020. Because of this, hopes are high for the spread of food tourism to revitalize local economies and communities, and a variety of related measures have been carried out in urban and rural areas all around Japan.

In addition, there is a certain demand among sightseeing users who want to go sightseeing without creating a sightseeing plan in advance. According to a survey conducted by "Jaran Research Center" (2022), 42.1% of tourists answered that they decide their sightseeing routes and plans in advance. Whereas a survey conducted in "Dekakeru JP" (2015), 59.0% of tourists answered that they travel without creating detailed sightseeing plans in advance. From these results, it is desirable to support tourists who create sightseeing plans in advance and who want to sightsee without planning.

1.2 Augmented Reality

Supporting local tourism can take various forms, and an innovative approach is augmented reality (AR) which is a technology that seamlessly blends digital information with the "real space (physical space) " using portable devices such as smartphones and tablets. There are three primary methods for implementing AR; location-based, marker-based, and marker-less. Among these, location-based AR, which utilizes the global positioning system (GPS) included into the user's mobile device, can be utilized for information collection and navigation. As a result, it effectively enhances the mobility support of tourists. Therefore, it can be said that location-based AR is valuable tool for effectively supporting tourists in sightseeing destinations.

1.3 Purpose

Based on the above, in order to support both planned and unplanned tourism for the purpose of eating and drinking, the purpose of this study is to integrates a tourism planning system, Web-GIS and Web-AR to

* Student Member (GISA), The University of Electro-Communications, h2230116@gl.cc.uec.ac.jp
** Member (GISA), The University of Electro-Communications, kayoko.yamamoto@uec.ac.jp

develop a system that can both create tourism plans and support on-site tourism. This system has unique functions such as the function of sightseeing spot search, sightseeing plan creation and navigation adopting location-based Web-AR.

2. Related works

This study is related to three academic fields: (1) studies on tourism planning support, (2) studies on information provision adopting AR, and (3) studies on food tourism. The representative previous studies in the above three academic fields are introduced and the originality of this study is demonstrated.

In (1) studies on tourism planning support, Maruyama et al. (2004) developed a system that supports the creation of sightseeing routes and navigation according to the user's level of preference; Kurata et al. (2015) developed CT-planner, which is a system that can recommend tourist attractions and sightseeing routes according to user preferences, and interactively create detailed plans based on these recommendations.

In (2) studies on information provision adopting AR, Morozumi et al. (2016) developed a restaurant search system that can display nearby restaurants on AR in order to make a comparison of restaurants easier than a listable display method. Takahashi et al. (2012) developed a system that navigates sightseeing routes adopting AR, which allows users to transmit information based on their location and view and share sightseeing information more actively. (2) Ikizawa-Naitou et al. (2020) developed a system that recommends travel routes and provides information adopting AR to assist tourists to create sightseeing plans, reflecting public transportation timetables.

In (3) studies on food tourism, Miyoshi et al. (2018) developed a restaurant recommendation system adopting knowledge-based recommendation to recommend regionally unique cuisine that considers tourists' preferences and circumstances. Michail et al. (2019) also developed a system that provides users with a platform for sharing and rating information about restaurants in order to search for restaurants focusing on cuisines rather than location. Kosugi et al. (2014) developed a system that recommends users sightseeing routes to restaurants that provide local gourmet food based on the calculation of Twitter attention.

The systems developed in (1) studies on tourism planning support have functions that allow users to create sightseeing plans that reflect their preferences, but these do not consider sightseeing for the purpose of eating and drinking. In (2) studies on information provision adopting AR, the system developed by Takahashi et al. (2012) can only provide a navigation of sightseeing routes prepared in advance. The system developed by Ikizawa-Naitou et al. (2020) developed as separate Web systems and applications, while all functions of the system developed in this study are available on the Web. In addition, these two systems only display tourist information adopting AR functions, while the system developed in this study has the functions of navigation and search. Thought the system developed by Morozumi et al. (2016) and (3) studies on food tourism have the function of providing restaurant information as the main function, the system developed in this study has the functions to support all of the activities of food tourism. Thought the system developed by Kosugi et al. (2014) has the function to recommend sightseeing routes with local gourmet food as a secondary purpose of general sightseeing, the system developed in this study can support the creation of sightseeing plans with the main objectives of eating and drinking. Compared to the above previous studies, this study has two elements of originality. The first element is that this study develops a unique system by integrating a tourism planning system, Web-GIS and Web-AR in order to support food tourism with the main purpose of eating and drinking. The second element is that this system allows users to use all of the functions on the Web, and there is no need to install a specific application into users' PCs and mobile information terminals.

3. System design

3.1. System Characteristic

This system consists of a tourism planning system, Web-GIS, and location-based Web-AR. The features of each system are shown in Figure 1. The sightseeing planning system first sets the starting and ending stations for sightseeing, and searches and determines restaurants that serve lunch and dinner. Then, from the list or the digital map of Web-GIS, sightseeing spots around the sightseeing route are incorporated into the sightseeing route to create a sightseeing plan focusing on restaurants. A system adopting Web-AR allows users who visit without creating a sightseeing plan to view nearby restaurants and sightseeing spots using their mobile information terminals, and create a sightseeing plan on site. In addition, this system navigates users to the next destination through the AR display. The above functions can support users to sightsee according to their created sightseeing plans and create sightseeing plans in tourist destinations.

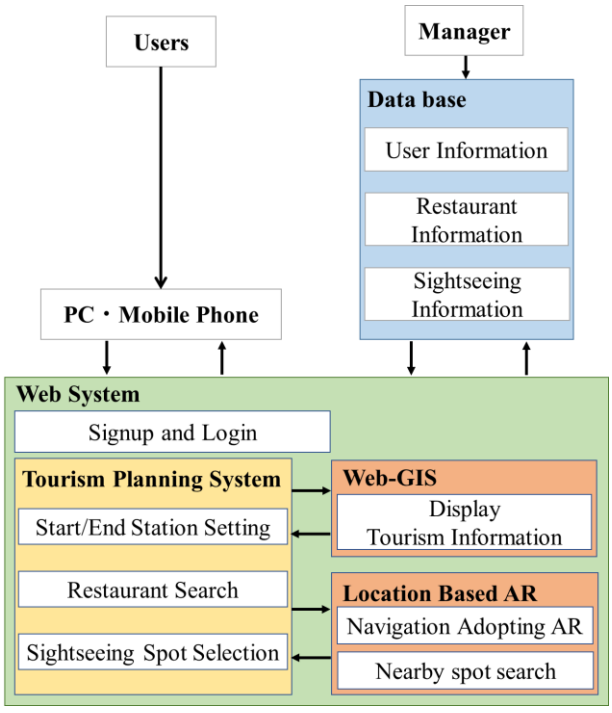

Figure 1 System Design

3.2. Usefulness of the System

The usefulness of this system is summarized into the following four points.

(1) Improved overview by displaying information adopting AR

Users can intuitively understand their location by displaying information adopting location-based AR. Therefore, users can easily grasp the location relationship between restaurants and each sightseeing spot.

(2) Support of planned and unplanned sightseeing

The functions of sightseeing plan creation and navigation adopting location-based Web-AR support users' activities both before and during sightseeing. In addition, the functions of nearby sightseeing spots search and sightseeing plan creation can support not only pre-planned sightseeing but also unplanned sightseeing by collecting sightseeing information on site.

(3) Ease of creating sightseeing plans

Users decide a restaurant for lunch or dinner first, and then select nearby sightseeing spots and create sightseeing route connecting start and end stations and these locations. This makes it easier for users to set their destinations and create favorite sightseeing plans. In addition, users can search for and determine the restaurants they wish to visit as their main destinations as well as the sightseeing spots they will visit and create a sightseeing route. This allows users to make decisions on sightseeing routes all at once without respectively collecting information on restaurants and sightseeing spots.

(4) Ease of use conditions

As all functions adopting AR can be used as a web system, there is no need to install a specific application into users' mobile information terminals. Therefore, the system can be used without being affected by the OS types of users' mobile information terminals. Also, because it is a web system, it can be used by anyone with mobile information terminals that can connect to the Internet.

3.3. Design of Each System

3.3.1. Tourism Planning Systems

Tourism planning system has a restaurant search system to search for desired restaurants, and a system to select nearby sightseeing spots and create sightseeing routes.

3.3.2. Web-GIS

Thought there are various types of Web-GIS, it must be appropriately selected according to the purpose of use. Since this system is intended for use by a wide range of people of all ages, it is desirable that the system can be used simply by connecting to the Internet from a browser, without requiring users to install specific software or applications. For this reason, this study will develop a Web-GIS adopting the ArcGIS API for JavaScript provided by the Environmental Systems Research Institute, Inc. (ESRI).

3.3.3. AR

As mentioned in section 1.2, there are three main types of AR implementation methods. In this study, the purpose is to use AR for tourism support, and it is assumed to be mainly used outdoors. Therefore, an AR system based on location information obtained from the GPS of users' mobile information thermals is developed, adopting location-based AR that can present contents such as photos and videos to the user. A-frame, which is a framework for VR, and AR.js, which is a framework for Web-AR system development, are adopted.

4. System Development

4.1. System Frontend

4.1.1. Function of New User Registration and Login

In order to use the system, users move from the login screen to the user registration screen to register their use of the system. On the user registration screen, users register their ID, password, gender and age as user information. Once the information is submitted, users will log into the system with the registered information.

4.1.2. Functions of Start/End Stations Setting

After logging into the system, users can set the stations where they want to start and end of their sightseeing. Stations can be set from the select box or from the pop-up window that appears by clicking the icon on the digital map of Web-GIS.

4.1.3. Function of Restaurant Search

Users can search for favorite restaurants for lunch and dinner during sightseeing. The search conditions include WIFI, private room, credit card payment, non-smoking area, number of seats, budgets of lunch and dinner, restaurant genre and name and search word (input box). In addition, the time required and calorie intake (optional) can be registered when registering a sightseeing plan.

4.1.4. Function of Sightseeing Spot Selection

Users can select favorite sightseeing spots by referring to either the distance from the current sightseeing route or the category of the sightseeing spot, and the result of the selection can be displayed in the list or on the digital map of Web-GIS. In the list view, users can click "Visit before lunch", "Visit after lunch" or "Visit after dinner" to incorporate these spots to a plan. In addition, users can enter the amount of time they will stay at each sightseeing spot.

4.1.5. Function of Sightseeing Plan Creation

Users can create a sightseeing plan to tour the spots selected by the functions introduced in sections 4.1.2, 4.1.3 and 4.1.4. Information on the created sightseeing plan can be viewed using the function described in section 4.1.7 below.

4.1.6. Function of Nearby Spot Search

Information on restaurants and sightseeing spots based on specified conditions is visualized on users' mobile information terminals adopting AR. This enables the display of information with a high degree of visibility. The search conditions are the same as for the functions of restaurant search and sightseeing spot selection. In

addition to this, the system sorts sightseeing spots by distance from the current location and budget, then displays information on each spot. Figure 2 shows the screen of this function.

4.1.7. Function of Navigation Adopting Web-AR

Navigation from the user's current location to the next destination is conducted adopting Web-AR on a mobile information terminal. The system displays information on the direction of a destination and the distance from the user's current location by adopting location-based-AR. This makes it possible to provide intuitive and easy-to-understand guidance to the user. Figure 3 shows the screen of this function.

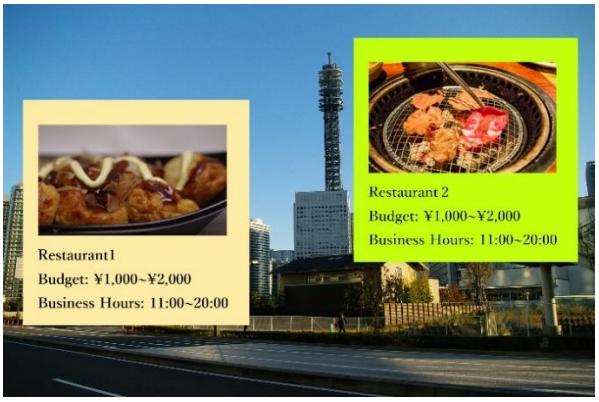

Figure 2 Screen of the function for nearby spot search

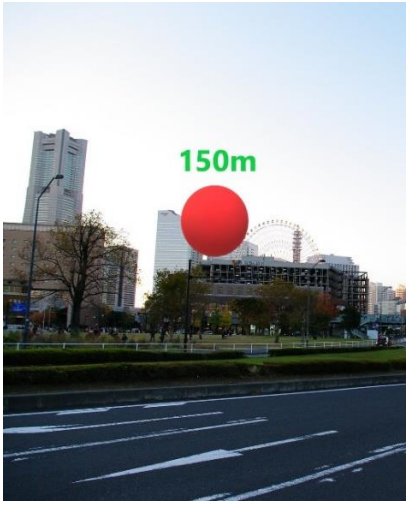

Figure 3 Screen of the function of navigation adopting Web-AR

4.1.8. Function of Sightseeing Plan Information Display

Information on sightseeing plans created by users can be viewed. The information on sightseeing route, total walking distance, total walking time, total time required for sightseeing and net calories (total calories consumed - total calories consumed) can be viewed on the digital map of Web-GIS, and the sightseeing plan can be saved by clicking "Save Sightseeing Plan".

4.2. System Backend

4.2.1. Processing Related to the Function of New User Registration and Login

New user registration information is stored in the database of Heroku PostgreSQL. At the time of registration, the entered password is hashed adopting the PHP hash function and stored in the database. When logging into the system, the password is hashed in the same way, and if the ID and password match in the database, the login process is performed. If they do not match, an error message is displayed and the login information is entered again.

4.2.2. Processing Related to the Function of Restaurant Search

Each restaurant stored in the database has an ID number respectively. As for the function of restaurant search, in the backend, the IDs of restaurants that match the search conditions and contain the search words set by users are extracted from the database, and displays them in the list or on the digital map of Web-GIS, along with the related information.

4.2.3. Processing Related to the Function of Sightseeing Spot Selection

As for restaurants, each sightseeing spot stored in the database is assigned an ID number. For narrowing down sightseeing spots, a route for the current sightseeing plan is created, and the IDs of sightseeing spots around the route that match the narrowing conditions set by users are extracted from the database ,and displayed in the list or on

the digital map of Web-GIS, along with the related information.

4.2.4. Processing Related to the Function of Nearby Spot Search

The IDs of restaurants that match the search conditions are extracted from the database. The process then displays the top 10 nearby sightseeing spots on users' mobile information terminals adopting location-based AR, along with the related information.

4.2.5. Processing Related to the Function of Navigation Adopting Web-AR

The distance from the coordinates of the user's current location and the next destination are derived, and it is displayed on users' mobile information terminals adopting location-based AR when user's location information is updated.

4.2.6. Processing Related to the Function of Sightseeing Plan Information Display

The sightseeing route is displayed on the digital map of Web-GIS based on the created sightseeing plan information. The total walking distance, total walking time, total time required for sightseeing and net calories (total calories consumed - total calories consumed) are also displayed. In addition, the process of saving the created sightseeing plans in the database is conducted. The saved sightseeing plans are restored, and displayed as the current sightseeing plans when the user logs in again.

4.3. System Interface

The interface of this system has two types; the PC and mobile information terminals (smartphones and tablets) screen of users, and the PC screen of the administrator. As the system is developed as a web system, all functions can be used on any terminal with Internet access. Thought the interface may differ depending on the terminal used, there is no difference in functionality, and the same functions can be used from either terminal. In addition, for the administrator's page, users' information can be managed. By utilizing graphic user interface (GUI), malicious users can be deleted without being affected by the information technology (IT) literacy of the administrators.

5. Operation

Regarding the operation target area, Minato Mirai District in Yokohama City of Kanagawa Prefecture in Japan, was selected. The following three reasons were given for the selection. The first reason for this selection is that many tourists visit Yokohama City as it is a popular urban sightseeing area, and there is an abundance of information submitted and released, making it difficult for tourists to efficiently obtain the necessary information. The second reason is that a citizen group called the YOKOHAMA FOOD LOVERs spontaneously conducts the activity to increase the attraction of the culinary culture in Yokohama City. The third reason is that the system can be used to efficiently search for eateries and sightseeing spots that match the many preferences of each user, because the great variety of such information is already accumulated in the system. Namely, as there are new eateries and sightseeing spots discovered one after another, it can be anticipated that the system will be used to efficiently collect such information and create sightseeing plans.

6. Future research plans

Currently, data on restaurants and sightseeing spots is collected and formatted, and the system is developing. After the system is developed, test operations and evaluations will be conducted, and the system will be reconfigured and improved based on these evaluations. Subsequently, the system will be put into the operation and evaluation.

References

[1] Japan Tourism Agency, "The Project to Attract Visitors to Rural Areas through Thematic Tourism", <https://www.mlit.go.jp/kankocho/shisaku/kankoch

i/theme_betsu.html>, accessed August 8, 2023.

[2] Jalan Research Center, "Domestic Lodging Travel Needs Survey as of May 2022 (13th).", <https://jrc.jalan.net/wp-content/uploads/2022/06/8c8fc74199c0cf1e3c6b85815f66af60.pdf>, accessed July 7, 2023.

[3] Dekakeru JP, "Do you need a travel plan, we surveyed 300 people to find out the percentage of those who do or do not plan a travel plan!", <https://dekakeru.jp/lab/theme/kanko-reserch-20150218/>, accessed July 8, 2023.

[4] Atsushi Maruyama, Naoki Shibata, Yoshihiro Murata, Keiichi Yasumoto, Minoru Ito, (2004). "P-Tour: A Personal Navigation System to Support Creation of Sightseeing Schedule and Route Guidance along the Schedule", Transactions of Information Processing Society of Japan, Vol.45, No.12, p.2678-2687.

[5] Yohei Kurata, Yasutaka Shinagawa, Tatsunori Hara, (2015). "CT-planner5: A Computer-Aided Tour Planning Service Which Profits Both Tourists and Destinations", Proceedings of the Workshop on Tourism Recommender Systems, Vol. 15. ACM, p.35-42.

[6] Shingo Morozumi, Yoshiyuki Yamazaki, Yasutami Chikusa, Taizo Hattori, (2016). "Development of Restaurant Navigation System Using AR", Proceedings of the 78th National Convention of Information Processing Society of Japan, p.4-361-362.

[7] Kosuke Takahashi, Hitoshi Furuta, Koichiro Nakatsu, Ken Ishibashi, Asami Aira, (2012)."Proposal of a Personalized Tourist Guidance Application Using Augmented Reality", Proceedings of the 28th Fuzzy System Symposium, p.398-401.

[8] Kana Ikizawa-Naitou and Kayoko Yamamoto, (2020). "A Support System of Sightseeing Tour Planning Using Public Transportation in Japanese Rural Areas", Journal of Civil Engineering and Architecture, Vol.14, No.6, p.316-332.

[9] Yoshiya Miyoshi, Taku Okuno, (2018). "Developion of a food tourism support system using knowledge-based recommendation", Proceedings of the 80th National Convention of Information Processing Society of Japan, p.1-443-444.

[10] Aimilia-Myriam Michail, Damianos Gavala, (2019). "Bucketfood: A Crowdsourcing Platform for Promoting Gastronomic Tourism" 17th IEEE International Conference on Pervasive Computing and Communications (PerCom'2019), p.9-14.

[11] Masashi Kosugi, Osamu Uchida, (2014). "Recommendation of sightseeing routes considering restaurants offering local gourmet foods", Proceedings of the 13th Forum on Information Science and Technology, p.177-178.

[12] YOKOHAMA FOOD LOVERs, 2022, "Human Gourmet Site' to enhance the appeal of Yokohama's food culture",
< https://media.new-port.jp/ >, accessed August 29, 2023.

Effects of Speed Control for Travel Time and Emission Reduction in Connected Vehicle Environment

Yuheng Liu*, Sunyong Eom**, Tsutomu Suzuki***

Abstract An increasing number of speed control methods at signalized intersections have been developed integrating geographic information with vehicle speed control technology. However, efforts to reduce travel delay time and emissions of vehicles traveling through multiple intersections are limited. To address this gap, this article aims to develop a new speed control model considering multiple intersections based on Vissim, by utilizing the traffic signal timing information and vehicle platoon data. First, we varied the number and range of intersections that were simultaneously controlled and compared the performance of the speed control in different scenarios. Second, the performance of the speed control is also evaluated by vehicle delay and emission reduction considering traffic volume and the penetration rate of connected vehicles. The results of this study will provide valuable insights for traffic engineers aiming to construct effective intelligent traffic system.

Keywords: Connected vehicles, Vehicle queue estimation, Speed control

1. Introduction

With the rapid rise of travel demand, traffic issues hindering traffic congestion, CO_2 emissions and fuel consumption are greatly increasing in recent years (Shi et al., 2023). This traffic congestion increases the travel time of driver (Coppola et al., 2023). In addition, vehicles stalled in traffic waste 3.3 billion gallons of fuel per year, representing a three-fold increase in wasted fuel over the 27 previous years (Louati et al., 2023). Within the urban traffic road network, signalized intersections witness frequent instances of vehicle acceleration, deceleration, and idling, all of which contribute to considerable fuel consumption and emissions (Zeng et al., 2023).

Various studies have established a connection among traffic congestion, CO_2 emissions, fuel consumption and certain driving behaviors (Zhao et al., 2023). These behaviors include recurring acceleration and abrupt stops, maintaining speeds exceeding 60 km/h, sluggish movement in congested traffic, and extended periods of idling (Ma et al., 2023). Given these findings, it becomes imperative to minimize instances of rapid acceleration, sudden deceleration, and abrupt stops at signalized intersections (Mosharafian et al., 2023).

The advancement of Vehicle-to-Infrastructure (V2I) and Vehicle-to-Vehicle (V2V) technologies has paved the way for the integration of connected vehicles (Wang et al., 2023). This innovative technology allows individual vehicles to communicate with both roadside infrastructure and the central control system within a connected vehicle environment (Li, 2023). Collected data from connected vehicles in the intersections can contribute to devising optimal speed trajectories that effectively curtail traffic congestion, CO_2 emissions and fuel consumption at multiple signalized intersections (Ma et al., 2023).

In recent years, with the goal of minimizing fuel consumption and emissions many speed control algorithms that assist drivers in their travel along signalized intersections appeared. Agafonov et al. (2023) examined a cooperative transportation system, which allows vehicles to accept trajectory instructions from the speed control system and they found that this system is highly beneficial in terms of mobility and fuel consumption. Mei et al. (2023) studied main urban roads and proposed a speed control strategy considering factors such as the location of vehicles, status of signal controls, acceleration and deceleration time of vehicles, and drivers'

* Student member; Master's Program in Risk and Resilience Engineering, University of Tsukuba; 1-1-1 Ten-nodai, Tsukuba, Ibaraki, 305-8573, Japan, Email: s2220554@u.tsukuba.ac.jp
** Regular member; Institute of Systems and Information Engineering, University of Tsukuba

acceptance. The strategy analyzed the feasibility of dynamic speed control and discussed its potential benefits in the field of traffic control. Additionally, Gokasar et al. (2023) leveraged real time traffic data from V2V and V2I communication to develop a speed control method. The simulation results suggested the potential to improve vehicle fuel economy around the intersection. These studies are mainly focused on isolated intersections. Their stability and reliability will be affected by long interval between adjacent intersections, complicated vehicle composition and multiple driving behavior, which is difficult to achieve the goal of reducing fuel consumption and emissions when the vehicle passes through the arterial road.

Some researchers worldwide have been investing considerable efforts to develop better strategies on optimal control of multiple signalized intersections. Ren et al. (2023) studies the interaction between multiple vehicle platoons in different paths before entering an unsignalized intersection supported by connected vehicles. The simulation results show that this method is generally efficient and outperforms the benchmark methods. Li et al. (2023) systematically analyzed the regularity of intersection crossing mode and solved the collision-free trajectories generating problem iteratively and offline. Deng et al. (2023) presented a vehicle platoon optimization algorithm to coordinate the merging of connected vehicles at unsignalized intersections. They used the real-time traffic conditions to jointly optimize the vehicle passing sequence and timeslot with the platoon configuration scheme to improve operational efficiency and fairness. Most of these methods can only achieve the ideal control effect when all vehicles are connected and follow the control. However, such situation will not happen in the near future (Xiao et al., 2021; Zheng and Liu, 2017) .

This study aims to improve transportation efficiency and vehicle fuel economy, by proposing a new vehicle speed control method for multiple signalized intersections. There are three primary contributions. Firstly, this study suggests the speed control considering multiple intersections. Even though several studies (Gelbal et al., 2023; Chen et al., 2023) considered the multiple intersections, our model will give speed control dynamically for every two adjacent intersections, considering the unique traffic condition of each intersection. Secondly, this study considers take into account the preceding vehicle conditions and the queue estimation into the speed control algorithm to apply the developed model to actual traffic condition. Thirdly, this study tests the performance of speed control with different penetration rates of connected vehicles. Previous studies (Hesami et al., 2023; Lv et al., 2023) assumed that all vehicles in the traffic network as connected vehicles. However, penetration rate of connected vehicle varies according to regions. Considering different penetration rate can give useful information to find the necessary level of penetration to maximize the effect of speed control.

The subsequent sections of this paper are structured as follows. In Section 2, the research issue addressed in this paper is delineated, accompanied by the introduction of the new speed control technique designed for addressing multiple signalized intersections. This technique takes into account the impact of preceding vehicles and vehicle queues in the control process. Section 3 provides insights into some simulation scenarios. Section 4 describes the consequent outcomes, serving as an assessment of the efficacy demonstrated by the proposed speed control approach. Concluding remarks and potential directions for future research are expounded in Section 5.

2. Methodology

2.1. Problem statement

Within urban signalized intersections, instances of stop-and-go behaviors are intrinsic. The scope of this investigation centers around the scenario delineated in Figure 1. This diagram illustrates a scenario wherein a vehicle approaches signalized intersections. Employing the speed control approach, vehicles can leverage the remaining distance to the subsequent traffic light, coupled

with the sequential pattern of signals, to ascertain its intended speed. This strategy aims to circumvent the detriments associated with halting at signalized intersections. The proposed speed control method dynamically considers two adjacent intersections simultaneously and aims to find the optimal speed that the vehicle can pass multiple signalized intersections without any stop.

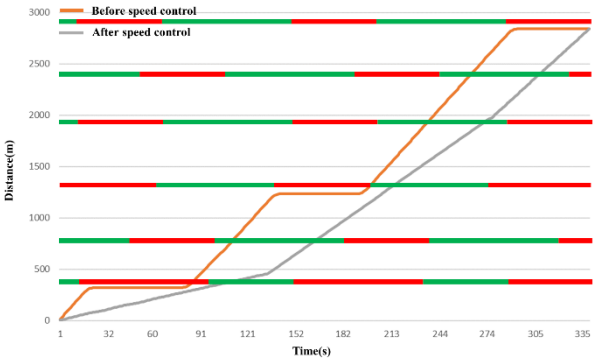

Figure 1. An example of a vehicle passing through multiple intersections under speed control and without speed control

Figure 2 shows the flowchart of the proposed speed control method. The speed control model consists of four steps. In order to calculate the optimal speed of each connected vehicle, five parameters are needed: the speed of the connected vehicle, the position of the connected vehicle, the length of the vehicle queue at the intersection, the queue dissipation time, and the signal control scheme of the intersection. Therefore, firstly, the speed control system will collect the speed and location of each connected vehicle through the communication between the connected vehicle and the speed control system. Then the queue length estimation method proposed in this paper will be used to calculate the necessary parameter: vehicle queue length. Secondly, the queue dissipation time will be calculated according to the estimated queue length. Thirdly, the speed control system will collect the necessary parameter: traffic signal time information and calculated the optimal speed for two adjacent intersections simultaneously and find the optimal speed that the vehicle can pass multiple signalized intersections without any stop. Fourthly, the optimal speed for isolated signalized intersections will be calculated when the common optimal speed for two adjacent intersections cannot be found.

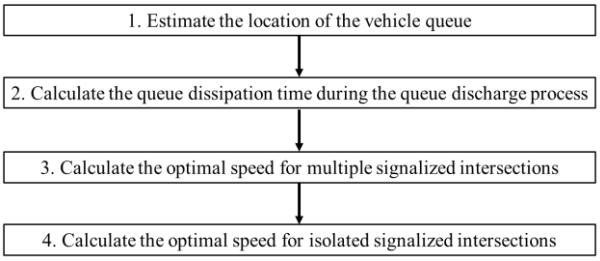

Figure 2. Flowchart of the speed control system

2.2. Queue estimation at intersections

Queuing vehicles are defined as vehicles that arrive at the intersection entrance load with the speed reduced to zero and wait for the green light to pass. The connected vehicle needs to send the following information to the roadside unit: vehicles ID, location, queue time and speed. Assuming that the vehicle arrives in a Poisson distribution, forms a queue with the corresponding arrival rate and passes back in the form of a wave during the red light. Based on the number of connected vehicles, this paper takes the single lane situation as an example for simplified analysis of queue estimation.

Figure 3 shows the diagram of queue estimation when there are n connected vehicles. The solid rectangle is the connected vehicle and n represents the number of connected vehicles. Penetration rate of connected vehicles is defined as the ratio of the number of connected vehicles to the total number of vehicles. r_s represents the start time of the red light, r_e represents the end time of the red light. According to shockwave model established by (Comert et al., 2015), when there is only one connected vehicle, the speed of the shockwave (v_1) can be determined as follows:

$$v_1 = \frac{l_b}{t_1 - r_s} \tag{1}$$

where t_1 is the stop time of this connected vehicle, l_b represents the queue length in front of this connected vehicle, which is determined by the distance between the connected vehicle and the stop line.

Therefore, when there is only *n* connected vehicles, we can assume that the speed of the shockwave is determined as follows:

$$v_n = \frac{1}{n-1}\sum_{i=1}^{n-1}\frac{l_b^n - l_b^i}{t_n - t_i} \quad (i = 1,2,\cdots,n-1) \tag{2}$$

where i is the connected vehicle, l_b^n is the queue length of the last connected vehicle, l_b^i is the queue length before the i th connected vehicle, which is determined by the difference between the position of the last connected vehicle and the stop line, t_n is the stop time of the nth connected vehicle, and t_i is the stop time of the i th connected vehicle.

The queue length of unconnected vehicles after the *n* th connected vehicle (l_a) is determined as follows:

$$l_a = v_n(r_e - t_n) \tag{3}$$

The total queue length can be calculated by Equation (4):

$$l_i = l_a + l_b^n = v_n(r_e - t_n) + l_b^n \tag{4}$$

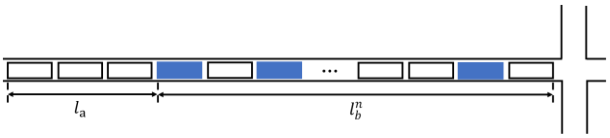

Figure 3. Diagram of *n* connected vehicles

2.3. Queue discharge process at a signalized intersection

Assume that the traffic flow entering the intersection is q_0 with a density of p_0. The traffic state upstream of the intersection is A during the green time, as shown in Figure 4. When the signal turns to red, the subsequent arrival of the vehicle has to wait at the stop line that leads to queue formation. Assume that the jam density is p_j and the discharge rate is reduced to zero. During this period the upstream state becomes B, and a shock wave is generated and propagates backward. Once the signal turns to green again, the intersection begins to discharge vehicles at the saturation flow rate q_c and the density of this state is p_c.

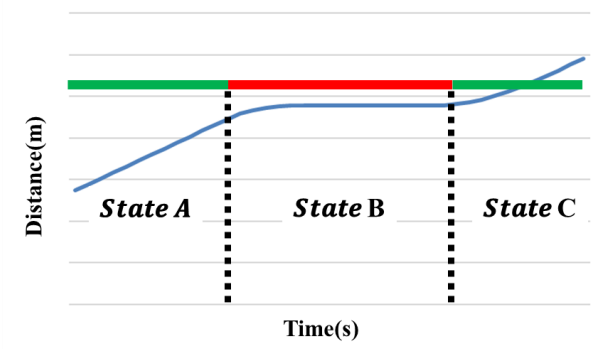

Figure 4. Queue discharge process at a signalized intersection

According to the traffic flow theory in (Wu et al., 2015), the speed v, traffic volume q and the traffic density p has the following relationship:

$$v = \frac{q}{p} \tag{5}$$

Therefore, the speed of traffic wave spreads v_s can be calculated as follows:

$$v_s = \frac{q_c}{p_c - p_j} \tag{6}$$

Then, the queue clearance time Δ_{ij} after the green light turns on can be calculated by the estimated queue length and the speed of traffic wave spreads:

$$\Delta_{ij} = \frac{l_i}{v_s} \tag{7}$$

It should be noted that the parameters of the model are dynamically changing and do not need to be calibrated in advance.

2.4. Speed control method for multiple signalized intersections

According to the speed control method established by (Wu et al., 2015), the key to speed control is to ensure that when a vehicle reaches the end of the queue, which is caused by the red light, the shock wave is just transmitted to the end of the queue. Inspired by such concept, we assume that the distance between the vehicle and the next several traffic lights are known at each time t and shown by L_i ($i = 1,2,3 \ldots N$). The subscript i denotes the light number in a sequence of the upcoming traffic lights. Suppose g_{ij} is start of the j th green time of the i th traffic light and r_{ij} is start of the j th red time after the first green time of the i th traffic light. Then the feasible speed set of the vehicle that can pass the i th signalized intersection during its green time can be expressed as follows:

$$[\frac{L_i}{r_{ij}}, \frac{L_i - l_i}{g_{ij} + \Delta_{ij}}] \cap [v_{min}, v_{max}] \quad (8)$$

where v_{min} and v_{max} are the minimum speed limit and maximum speed limit, respectively. They are determined according to the speed limit and capacity of different sections of the arterial road; l_i is the length of the queue before the ith signalized intersection, which is estimated by Equations (3) or Equation (6); Δ_{ij} is the queue clearance time of the vehicles ahead. If

$$\left[\frac{L_i}{r_{ij}}, \frac{L_i - d_i}{g_{ij} + \Delta_{ij}}\right] \cap \left[\frac{L_{i+1}}{r_{i+1j}}, \frac{L_{i+1} - d_{i+1}}{g_{i+1j} + \Delta_{i+1j}}\right] \cap [v_{min}, v_{max}]$$

$$= [v'_{min}, v'_{max}] \neq \emptyset \quad (9)$$

Then the vehicle can pass through the i th intersection and i+1 th intersection with a constant speed chosen from $[v'_{min}, v'_{max}]$ without having to stop, where v'_{min} and v'_{max} are the minimum feasible speed limit and maximum feasible speed limit.

However, an empty set above does not signify that the vehicle must have to stop at the stop line. It only indicates that passing the i th intersection and i+1 th intersection with one constant speed is not practicable.

In this situation, the speed of the i th intersection and i+1 th intersection will be optimized separately using the method of vehicle trajectory optimization for isolated intersection.

2.5. Speed control method for isolated signalized intersections

The strategy of speed control method for isolated signalized intersections is to ensure that when a vehicle reaches the end of the queue which is caused by the red light, the shock wave is just transmitted to the end of the queue, that is, the vehicle at the end of the queue starts to move. In this context, this vehicle can smoothly clear the intersection following the shock wave. Therefore, the optimal speed can be calculated as follows:

$$v = \frac{L_i - l_i}{g_{ij} + \Delta_{ij}} \quad (10)$$

In the above equation, the numerator indicates the distance between the vehicle and the stop line (L_i) minus the road space occupied by all the queueing vehicles (l_i), which is estimated by Equations (3) or Equation (6). The denominator indicates the time duration between the time that the last vehicle in the queue begins to move.

In the model of the speed control method for isolated signalized intersections, the suggested driving speed for a vehicle after control must have the following:

$$v = \begin{cases} \frac{L_i - l_i}{g_{ij} + \Delta_{ij}}, & v_{min} \leq v \leq v_{max} \\ v_{max}, & v > v_{max} \\ v_{min}, & v < v_{min} \end{cases} \quad (11)$$

Equation (11) illustrates that the suggested speed must be constrained within the upper and lower bounds, namely v_{max} and v_{min}.

2.6. Evaluation of fuel consumption

We utilized EnViVer Pro, an add-on for PTV Vissim, to calculate emissions based on the VERSIT+ microscopic exhaust gas/emission model (PTV GROUP, 2023). EnViVer Pro imports vehicle record files from PTV Vissim and computes CO2 emissions within the study area at a spatially detailed level. This emissions model is also referenced in related research (Quaassdorff et al., 2023; Severino et al., 2023).

3. Simulation setting

3.1. Simulation area

The performance of the proposed speed control model is tested in Vissim and Visual Basic simulation. The optimization function is solved in Visual Basic, and the solution is transferred to Vissim through COM interface. Meanwhile the Vissim parameters could be adjusted to simulate connected vehicle environment. Figure 5 shows the actual location of the research area, which consists of an arterial with eleven adjacent intersections of Gakuen Higashiōdōri in Tsukuba, Ibaraki, Japan.

3.2. Traffic volume and signal settings

The traffic volume and signal scheme data of the simulation area are collected from a field survey during

the evening peak and the data collection period is one hour. The survey data of the current traffic volume is shown in Table 2. The traffic volume on the arterial road during the evening peak is around 1200 veh/h, while the traffic volume during the morning peak is around 1800 veh/h and traffic volume during 12 o'clock is around 900 veh/h.

In order to examine the effectiveness of the proposed speed control algorithm in different traffic volume situations, four demand patterns were used in the case study of the whole network:

1- 500 veh/h on the arterial road (free flow)

2- 750 veh/h on the arterial road (undersaturated flow)

3- 1,000 veh/h on the arterial road (normal flow)

4- 1,250 veh/h on the arterial road (rush hour flow)

The trajectory of vehicles on the north arterial and the south arterial road are both collected by Vissim to evaluate the effect of the speed control model. The vehicle composition of each lane consists of 98% cars and 2% of buses.

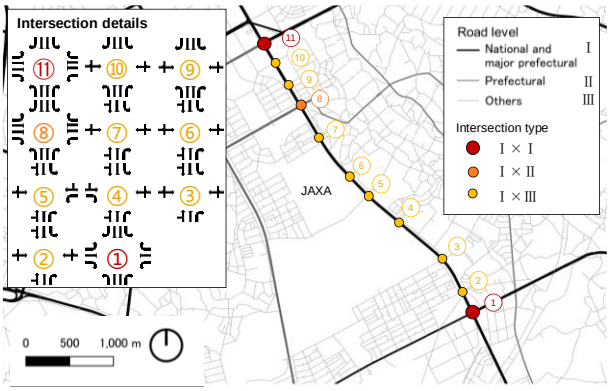

Figure 5. Simulation area: Gakuen Higashiōdōri in Tsukuba, Ibaraki, Japan

Table 2. Traffic volume of each intersection (Evening peak)

Int. No.	North Entrance (veh/h)			South Entrance (veh/h)			West Entrance (veh/h)			East Entrance (veh/h)		
	L	S	R	L	S	R	L	S	R	L	S	R
11	144	1251	89	215	1265	90	213	1254	150	187	1298	89
10	57	1247	58	48	1206	63	54	52	59	62	137	56
9	100	1208	68	86	1203	119	52	50	91	137	170	137
8	68	1287	85	82	1294	91	98	141	493	102	224	159
7	49	1283	52	47	1220	157	57	69	52	74	61	61
6	149	1265	142	73	1206	59	116	0	202	100	0	60
5	69	1260	64	58	1228	50	160	48	56	37	40	50
4	193	1286	70	100	1280	116	89	94	76	70	76	317
3	43	1298	168	108	1284	270	205	130	62	167	262	113
2	54	1290	103	100	1275	71	44	90	164	56	48	60
1	264	1281	128	241	1228	185	269	1217	211	230	1294	202

The proposed speed control model is based on the current signal control scheme during the evening peak. The signal interval data is also collected by the field survey during the evening peak.

4. Simulation results

4.1. Scenario 1: Comparison of simulation results with different speed control methods

To verify the feasibility of the joint control model, we select the single-intersection speed control model to be simulated as reference results. In the simulation, we select delay, number of vehicles stops, fuel consumption and CO_2 emissions as evaluation indexes to test the optimal effect. In this scenario, we select the road section from intersection 1 to intersection 11 as the data analysis area. The vehicles travel from intersection 1 to intersection 11.

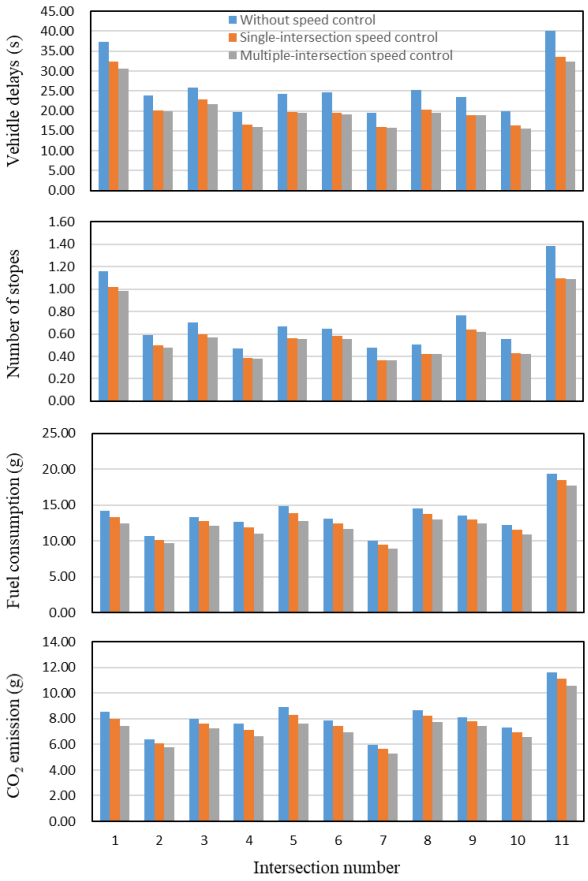

Figure 6. Comparison of simulation results with different speed control methods

Figure 6 shows the vehicle delay, number of vehicles stops, fuel consumption, and CO_2 emissions comparison results among the current situation (without speed control), the conventional speed control method of single intersection and the proposed speed control method (multiple intersections speed control method). It is clearly showed that the four evaluation indexes are significantly reduced under the proposed speed control method. Vehicles can pass through the intersection with less stops. The results show the traffic capacity of the arterial road and green time utilization are improved based on the proposed speed control method. The difference between the maximum reduction of vehicle delay and fuel consumption and the minimum reduction is not more than 5%. Therefore, the location of the intersections may not have an influence on the effect of the proposed vehicle speed control method.

4.2. Scenario 2: Comparison of simulation results with different traffic volume

Figure 8 show the vehicle delay, number of vehicles stops, fuel consumption, and CO_2 emissions comparison results between four different cases under different traffic flow density. It can be found from Figure 7 that the fuel consumption and CO_2 emissions for the vehicles with speed control method under connected environment are reduced by around 10% to 24% approximately. Moreover, the reduction in fuel consumption and CO_2 emissions is

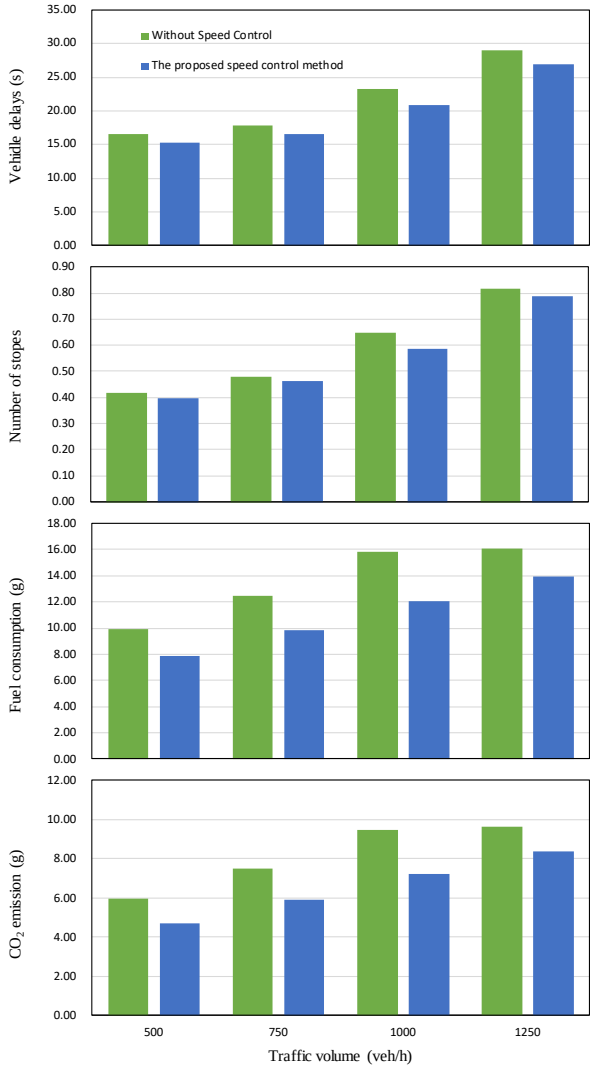

Figure 7. Comparison of simulation results with different traffic volume

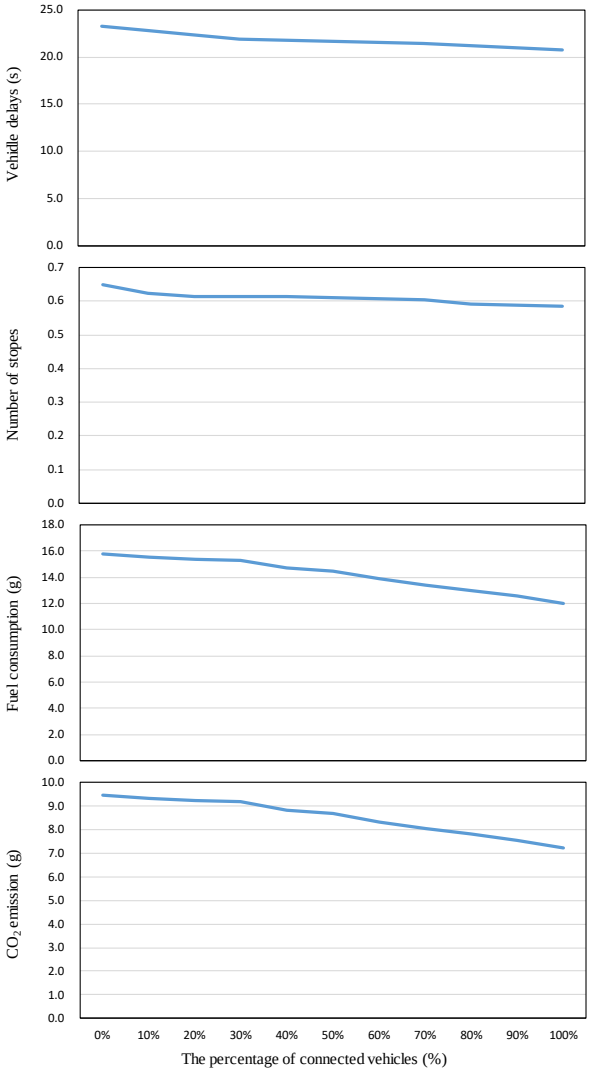

Figure 8. Comparison of simulation results with different penetration rate of connected vehicles

more significant under the medium traffic flow density (the traffic volume is below 500 veh/h). This is because of the reduction of the sharp acceleration or deceleration during the driving process. However, under the high traffic flow density (the traffic volume is over 1,000 veh/h), the effect of the speed control method is weakened because of the strong car-following conditions. Thus, the reduction in fuel consumption and CO_2 emissions is not obvious compared to the medium traffic flow density.

4.3 Scenario 3: Comparison of simulation results with different penetration rate of connected vehicles

In order to examine the effectiveness of the proposed speed control algorithm in different penetration rate of connected vehicles, we varied the penetration rate of connected vehicles from 0% to 100%, eleven different scenarios were used in the case study of the whole network:

Figure 8 shows that by using the proposed method, as the penetration rate of connected vehicles increases from 0% to 100%, the reduction of average fuel consumption can be improved to about 24%. Furthermore, when the penetration rate of connected vehicles is small, for instance 30%, the proposed method can still reduce the average fuel consumption by around 10%. More than 30% of the penetration rate of connected vehicles is needed to guide the vehicle speed and the possible reason is that the car following phenomenon becomes more obvious when the penetration rate of connected vehicles is more than 30%. In such situation, vehicles may form as a platoon and more vehicles can reach the optimal vehicle speed.

5. Conclusion

This study introduces a system for regulating vehicle speeds across multiple signalized intersections within the context of a connected vehicle environment. By factoring in the influence of preceding vehicles and the presence of vehicular queues at signalized intersections, this mechanism enables a vehicle to make informed decisions regarding acceleration or deceleration. This choice aims to evade red signals by utilizing information such as signal timing and distance from the stop line, provided in advance.

To evaluate the effectiveness of the proposed speed control approach, a simulation framework is established, which emulates the environment of connected vehicles. Notably, first the proposed multiple intersection speed control method achieved reduced about 5% more reduction in vehicle delay and fuel consumption than the previous single intersection vehicle speed control method. Second, in scenarios characterized by medium traffic density, the proposed speed control strategy achieves better results than low or high traffic density. Specifically, the method demonstrates the capacity to reduce fuel consumption by around 24% and decrease the vehicle delay by around 10%. Third, more than 30% of the penetration rate of connected vehicles is necessary to guide the vehicle speed. Such penetration rare is possible to realize in the foreseeable future and the proposed vehicle speed control model can be equipped in the real world afterwards.

It should be noted that the speed control method for arterial road in this paper may have some negative effects on vehicles on the side street. Collaborative optimization of arterial and the side street are worthy of further study. Future research should consider more complex traffic scene, for example, multiple lanes with lane-change behavior. In addition, the current studies are primarily focused on vehicles adjusting their speed based on fixed time signals. Adaptive signal control is the future research direction of traffic control at the multiple signalized intersections. It is expected that even further fuel and emission benefits will be possible by the coordination between speed adjustment of vehicles and traffic signal timing adjustment of the signal controllers.

Acknowledgments

This study was supported in part by JSPS KAKENHI Grant Numbers JP 21H01559 and Obayashi Foundation.

References

Agafonov, A., Yumaganov, A., & Myasnikov, V. (2023) Cooperative Control for Signalized Intersections in Intelligent Connected Vehicle Environments. *Mathematics*, **11**(6), 1540.

Alanazi, F. (2023) A Systematic Literature Review of Autonomous and Connected Vehicles in Traffic Management. *Applied Sciences*, **13**(3), 1789.

Chen, H., Rakha, H. A., Jeihani, M., Sadeghvaziri, E., & Center, E. (2023) Optimum Connected Vehicle Speed Control on Signalized Roadways in Mixed Flow. *Morgan State University. Urban Mobility & Equity Center*, **24**(4), 4320-4332.

Comert, G., and Cetin, M. (2009) Queue length estimation from probe vehicle location and the impacts of sample size. *European Journal of Operational Research*, **197**(1), 196-202.

Coppola, A., Di Costanzo, L., Pariota, L., and Bifulco, G. (2023) Fuzzy-based Variable Speed Limits System under Connected Vehicle environment: A Simulation-Based Case Study in the city of Naples. *IEEE Open Journal of Intelligent Transportation Systems*, **123**, 106239.

Deng, Z., Yang, K., Shen, W., and Shi, Y. (2023) Cooperative platoon formation of connected and autonomous vehicles: toward efficient merging coordination at unsignalized intersections. *IEEE Transactions on Intelligent Transportation Systems*, **14**(2), 55.

Gelbal , S., Zhu, S., Anantharaman, G., Guvenc, B., and Guvenc, L. (2023) Cooperative collision avoidance in a connected vehicle environment. *IEEE Transactions on Intelligent Transportation Systems*, **24**(4), 4320-4332.

Gokasar, I., Timurogullari, A., Deveci, M., and Garg, H. (2023) SWSCAV: Real-time traffic management using connected autonomous vehicles. *ISA transactions*, **132**, 24-38.

Hesami, S., De Cauwer, C., Rombaut, E., Vanhaverbeke, L., and Coosemans, T. (2023) Energy-Optimal Speed Control for Autonomous Electric Vehicles Up-and Downstream of a Signalized Intersection. *World Electric Vehicle Journal*, **14**(2), 55.

Li, J., Fotouhi, A., Pan, W., Liu, Y., Zhang, Y., & Chen, Z. (2023) Deep reinforcement learning-based eco-driving control for connected electric vehicles at signalized intersections considering traffic uncertainties. *Energy*, **128139**.

Li, Y. (2023) Traffic Control Method Review of Signalized Intersection under Connected Vehicles Environment. *Highlights in Science, Engineering and Technology*, **44**, 377-389.

Louati, A., & Kariri, E. (2023) Enhancing Intersection Performance for Tram and Connected Vehicles through a Collaborative Optimization. *Sustainability*, **15**(12), 9231.

Lv, W., Dang, J., Zhang, Z., Min, Y., & Zuo, J. (2023) Collaborative Trajectories Optimization for Tram and Connected Vehicles at Signalized Intersection. *Applied Sciences*, **13**(3), 1514.

Ma, H., An, B., Li, L., Zhou, Z., Qu, X., and Ran, B. (2023) Anisotropy safety potential field model under intelligent and connected vehicle environment and its application in car-following modeling. *Journal of Intelligent and Connected Vehicles*, **24**(4), 4320-4332.

Ma, Y., Liu, Q., Fu, J., Liufu, K., and Li, Q. (2023) Collision-avoidance lane change control method for enhancing safety for connected vehicle platoon in mixed traffic environment. *Accident Analysis and Prevention*, **184**, 106999.

Mei, P., Karimi, H. R., Xie, H., Chen, F., Huang, C., and Yang, S. (2023) A deep reinforcement learning approach to energy management control with connected information for hybrid electric vehicles. *Engineering Applications of Artificial Intelligence*, **123**, 106239.

Mosharafian, S., and Velni, J. (2023) A hybrid stochastic model predictive design approach for cooperative adaptive cruise control in connected vehicle applications. *Control Engineering Practice*, **130**, 105383.

Ren, C., Wang, L., Yin, C., Wang, Z., Chen, X., & Li, J. (2023) Research on the Platoon Speed Guidance Strategy at Signalized Intersections in the Connected Vehicle Environment. *Journal of Advanced Transportation*, **123**, 106239.

Shen, M., He, C. R., Molnar, T., Bell, A., and Orosz, G. (2023) Energy-efficient connected cruise control with lean penetration of connected vehicles. *IEEE Transactions on Intelligent Transportation Systems*, **24**(4), 4320-4332.

Shi, Y., Wang, Z., LaClair, T., Wang, C., and Shao, Y. (2023) Real time control of connected vehicles in signalized corridors using pseudospectral convex optimization. *Optimal Control Applications and Methods*, **14**(2), 55.

Wang, Z., Dridi, M., & El Moudni, A. (2023) Co-Optimization of Eco-Driving and Energy Management for Connected HEV/PHEVs near Signalized Intersections: A Review. *Applied Sciences*, **13**(8), 5035.

Wu, W., Li, P. K., and Zhang, Y. (2015) Modelling and simulation of vehicle speed guidance in connected vehicle environment. *International Journal of Simulation Modelling*, **14**(1), 145-157.

Zeng, J., Qian, Y., Li, J., Zhang, Y., and Xu, D. (2023) Congestion and energy consumption of heterogeneous traffic flow mixed with intelligent connected vehicles and platoons. *Physical A: Statistical Mechanics and its Applications*, **609**, 128331.

Zhao, J., Li, W., Wang, J., & Ban, X. (2015) Dynamic traffic signal timing optimization strategy incorporating various vehicle fuel consumption characteristics. *IEEE Transactions on Vehicular Technology*, **65**(6), 3874-3887.

Zhao, W., Gong, S., Zhao, D., Liu, F., Sze, N. N., and Huang, H. (2023) Effects of collision warning characteristics on driving behaviors and safety in connected vehicle environments. *Accident Analysis and Prevention*, **186**, 107053.

Oral presentation in IAG'i

Spatial Analysis

Chair: Takahiro Yoshida (Center for Spatial Information Science, The University of Tokyo)
Sat. Oct 28, 2023 5:00 PM - 6:20 PM Room E (C-301 3rd floor of Bldg. C)

[E5-01] Evaluating spatial design in office buildings through behaviors identified by Wi-Fi sensing and Bluetooth technology

*Xinting Gao[1,2], Toshihiro Osaragi[2], Weimin Zhuang[2] （1. Tsinghua University, 2. Tokyo Insitute of Technology）

5:00 PM - 5:20 PM

[E5-02] Exploring Separation Strategies for Car-Bicycle Integration

*Liling Liu[1], Sunyong Eom[1], Tsutomu Suzuki[1] （1. University of Tsukuba）

5:20 PM - 5:40 PM

[E5-03] Regional-Spatial Analysis and Comparison of Social Farming in Japan and the Netherlands by Using GIS

*Zile Tian[1], Naoko Fujita[2], Max Hanssen[1], Ding Ma[3], Suzu Shimada[1] （1. Doctoral Program in Arts, Graduate School of Comprehensive Human Sciences, University of Tsukuba, 2. Institute of Arts and Design, University of Tsukuba, 3. Master Program in Arts, Graduate School of Comprehensive Human Sciences, University of Tsukuba）

5:40 PM - 6:00 PM

[E5-04] Accessibility of Third Places around a University Campus: A Spatial Analysis on Travel Times and Usage Patterns

*Max Hanssen[1], Naoko Fujita[1], Ding Ma[1], Suzu Shimada[1], Zile Tian[1], Linda Gadhoum[1], Joris Zandbergen[2], André Jacob Lodewijks[2], SeungHee Lee[1] （1. University of Tsukuba, Graduate School of Comprehensive Human Science, Art, 2. University of Technology Eindhoven, Industrial Design）

6:00 PM - 6:20 PM

Evaluating spatial design in office buildings through behaviors identified by Wi-Fi sensing and Bluetooth technology

Xinting Gao*, Toshihiro Osaragi**, Weimin Zhuang

Abstract Workplace vitality influences employees' perception, performance, and contentment. Office staff's extended sedentary periods pose health risks. Utilizing non-invasive positioning systems like Wi-Fi and Bluetooth could offer insights into sedentary behavior within office spaces. However, such systems lack comprehensive testing, particularly in large public buildings. This study aims to gauge the feasibility of measuring and locating workplace vitality non-intrusively. It establishes an assessment framework integrating subjective behavior data with objective spatial attributes. This approach provides a data-centric method for evaluating workspace vitality in sizable office complexes.

Keywords: Environment behavior, spatial vitality, indoor localization, office buildings

1. Introduction

Traditional methods of collecting user behavior involve on-site observation and image recording. Artificial intelligence (AI) tools and data mining methods offer new perspectives for environmental monitoring and assessment. The rapid development and expansion of Internet of Things (IoT) and communication technologies (such as smart sensors, smart meters, and smartphones) make it easier to obtain data on energy consumption and environmental conditions (e.g., temperature, humidity, light, and illumination) (Varlamis et al., 2022). Ubiquitous sensing technology provides long-term, large-scale, multidimensional, and non-intrusive data. Diverse wireless sensing technologies like Wi-Fi (Huang et al., 2019), RFID (Li et al., 2012), visible light (Monti et al., 2022), Bluetooth (Arai et al., 2019), and ultra-wideband (UWB) (Alarifi et al., 2016) are applied in spatial perception and behavioral information detection due to their range, latency, accuracy, and energy efficiency. (Himeur et al., 2022; Li et al., 2017; Varlamis et al., 2022) Each user in a space becomes a sensor, voting for space availability with their movements. Time-sharing processing yields positional information from different users to assess the rationality of architectural space design. Technological advancements transition spatial behavior detection from "presence" to "fine-grained behavior," collecting data at different resolutions in spatial, temporal, and behavioral aspects (Zhang et al., 2022). Involving individual users in data collection serves valuable information for spatial assessment. Previous research on location-based technology in built environments focuses mainly on outdoor spaces in planning areas, such as enclosed parks (Huang, 2017) and university campus squares (Osaragi et al., 2021). Limited research addresses indoor spaces from an architectural design perspective, with some studies exploring usage behavior patterns in residential, educational (Alfalah et al., 2022), and airport buildings (Huang et al., 2019). Much of the existing research emphasizes improving the accuracy of indoor positioning technology, often through hybrid systems combining inertial, radio frequency, acoustic, and vision systems. However, applications of data, particularly non-intrusive techniques for assessing architectural space design, remain less explored. Current evaluations of

* 学生会員 清華大学 建築学科 (Tsinghua University) &東京工業大学 環境・社会理工学院 (Tokyo Institute of Technology)) 〒152-0086 東京都目黒区大岡山 2-12-1 Email: gxt22@mails.tsinghua.edu.cn
**正会員 東京工業大学 環境・社会理工学院 (Tokyo Institute of Technology)

indoor spatial positioning technology for architecture often involve invasive sensing devices, recruiting participants to wear emitting devices for a period before retrieval. While this approach provides fine-grained trajectory data, it may suffer from the Hawthorne effect and limited data volume. Non-intrusive sensing technologies can mitigate these limitations, enhancing the reliability and validity of spatial assessments through large-scale data analysis.

2. Methodology

2.1. Architectural features

The research site is the headquarters of an internet company located in Beijing, with a seven-story building (Fig. 1). The office building has dimensions of 180 m x 180 m, with each floor covering 32,000 square meters. There are two outdoor courtyards and three indoor atriums in total. The standard office floor is divided into 12 office units of 45m x 45m each, accommodating workstations, manager offices, and meeting rooms. The office units are arranged around outdoor courtyards and indoor atriums, allowing comfortable sunlight to diffuse into the units. The focus of this study is on the standard F6 floor of the building. F6 floor features an open layout, with individual workstations for each employee, multiple open discussion areas, enclosed meeting rooms, and several pantry spaces. The internal floor area (excluding utility rooms, courtyards, etc.) is 28,438 square meters, providing 1,916 workstations.

Figure 1. Architectural features

To begin, the research units are determined based on the dimensions of the building's column grid and the precision of the indoor positioning system. The column grid of the building is 9m, accommodating varying numbers of workstations within each grid, ranging from 0 to 40. Analysis units are set at a 9m grid to analyze the correlations between different elements within the column grid (Fig. 2).

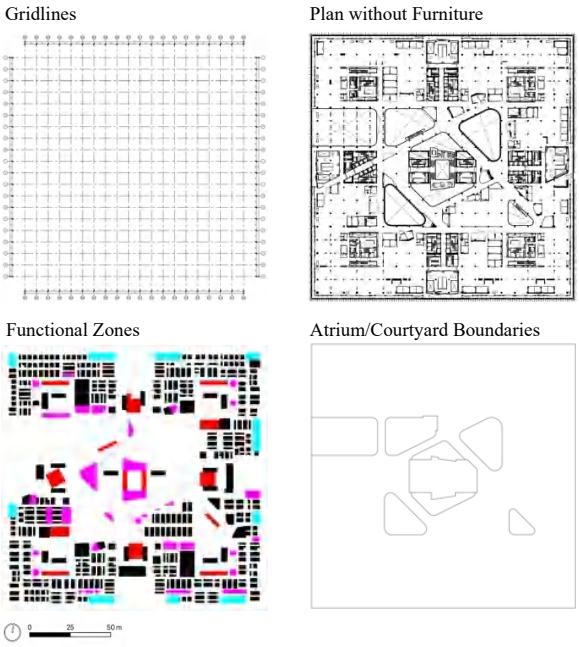

Figure 2. CAD plan of Floor 6

2.2 Data acquisition method

The indoor positioning system (IPS) used in the study was developed by Tencent, a company based in Beijing, China. Leveraging the popularity of Tencent Map, a widely-used map application in China, the researchers utilized existing Wi-Fi and GPS data, including access point (AP) names and building names, to initialize their fine-grained indoor localization service (Fig. 3). This initial stage benefited from a substantial user base, especially in bustling commercial centers, allowing for rapid bootstrapping within just 1-2 weeks through user-contributed updates.

Tencent's IPS technology incorporates a unique feature, termed the "number of requests" (NoR), which adds an additional dimension to traditional WiFi-based fingerprinting methods that rely solely on Received Signal Strength Indicator (RSSI) readings from multiple access points. The NoR feature is derived from a large dataset, representing a data-driven enhancement. This supplementary feature enhances the accuracy of

localization.

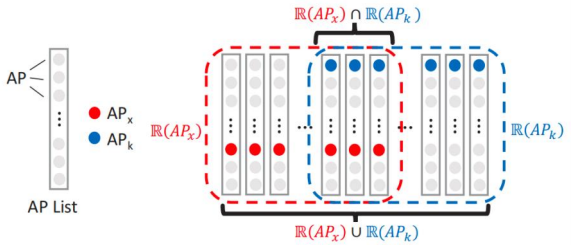

Figure 3. Each device reports a list of APs overheard

Bluetooth indoor positioning involves two main steps: the mobile device obtains nearby location information through Bluetooth beacon signals, and the server performs positioning calculations. The positioning algorithms employed include Bluetooth distance-based positioning, Bluetooth fingerprint positioning models, and the fusion of Pedestrian Dead Reckoning (PDR). Additionally, floor identification models and floor switching algorithms are applied to achieve floor-level positioning.

In the research, both WiFi and Bluetooth devices were deployed within the study area (Fig. 4). The average distance between 195 WiFi devices was 9 m, while the average distance between 753 Bluetooth devices was 4.7 meters. When users initiate a location request, they upload the Bluetooth and WiFi information they have scanned at that moment to the server. Using this information, the server calculates the user's location and sends it back. Bluetooth probe devices upload collected data to the platform every 5 seconds, while WiFi probe devices do so every 30 seconds, with data further processed and stored.

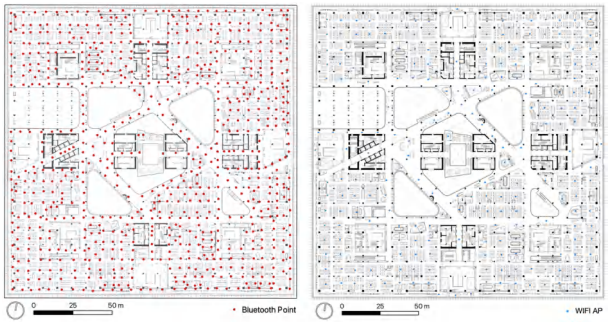

Figure 4. Device Placement Map

The accuracy of WiFi-based positioning is approximately 5-7 meters, while Bluetooth-based positioning achieves an accuracy of about 3-5 meters. When combined with Pedestrian Dead Reckoning (PDR) from motion sensors, accuracy can improve to 1-3 meters. Floor identification accuracy exceeds 97.5%. In transitional areas between indoor and outdoor spaces, the accuracy of indoor-outdoor differentiation is also above 90%. This research provides a significant opportunity to better understand crowd density inside the building, the influence of indoor physical environments on this movement, and the development of effective interventions to promote increased movement during work.

2.3 Analysis workflow

This study follows these steps (Fig.5) : 1. Analyzing user location data captured by indoor positioning, exploring statistical patterns across hours, days, weeks, and different floors.2. Investigating spatial traits of architectural elements like column layouts, atrium boundaries, functional zones, and furniture arrangements. 3. Projecting user locations onto floor plans using coordinates, merging subjective behavior with objective spatial features for user-centric maps. 4. Defining analysis units, assessing location density, calculating spatial compatibility, and evaluating behavioral preferences in key areas. 5. Ultimately, assessing the effectiveness of spatial layout design.

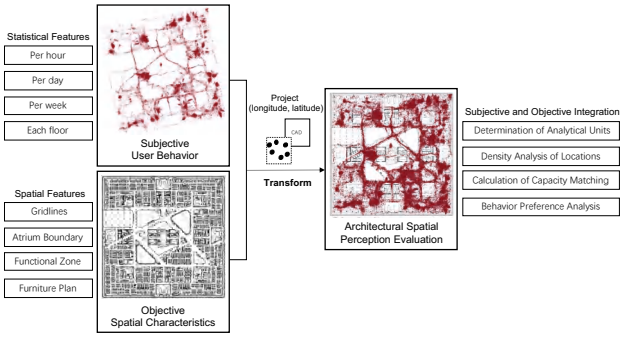

Figure 5. Analysis Process

3. Spatio-temporal data analysis

Extract a total of 364,030 records data for July 2023, a total of 31 days, and analyze the behavioral characteristics associated with spatial location information. There are variations in the spatial point density distribution across different time slices (Fig.6).

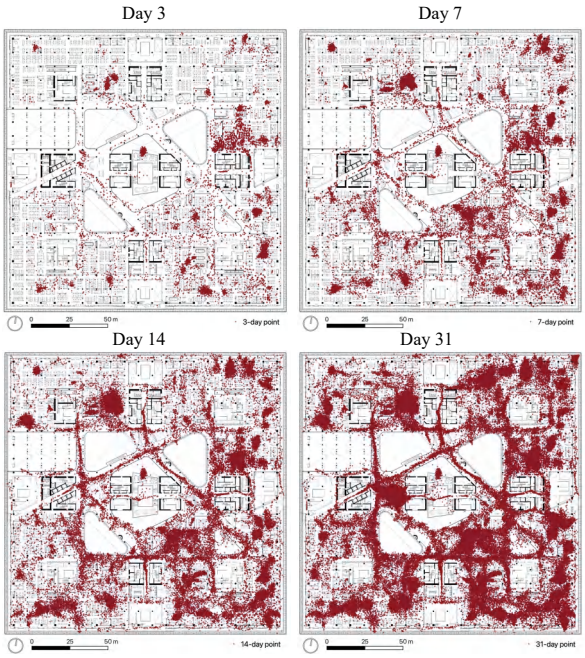

Figure 6. Spatial projections at different time slices.

The data points for the 31-day period occupy approximately 52.8% of the space, and there are variations in the proportions of different functional spaces (Fig.7). Next, we will analyze the spatiotemporal distribution characteristics of different functional spaces and attempt to explain the reasons behind them.

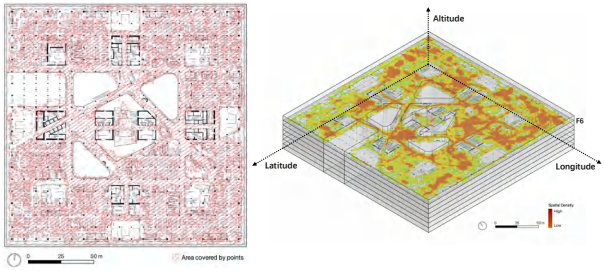

Figure 7. Space utilization rate and heat map.

3.1 Exterior Landscape Facade

The study focuses on distinctive characteristics of large urban commercial office buildings. The building is surrounded by tall glass curtain walls, providing excellent panoramic views and adequate natural lighting for occupants. However, this design may lead to indoor discomfort in terms of lighting and thermal conditions (Fig. 8).

Per Hour: during weekdays, peak usage of the courtyard is noticeable, particularly during lunch hours. Peaks are concentrated on the north and south sides where reclining chairs offer a space for employees to rest. Therefore, a significant peak is observed during lunch breaks. On the east side, peaks occur in the afternoon and overtime periods, correlating with high workstation usage. Employees show a preference for passing by the exterior landscape facade during breaks to alleviate work stress.

Per Day: usage of the courtyard over weekends shows less distinct variations over time. This could be attributed to a more relaxed work atmosphere during weekends.

Each Side: due to the building's location within a well-planned landscape, views from the landscape windows are evenly distributed across all four sides. Usage trends of the exterior landscape facade are consistent across different orientations, with variations in point density linked to workstation utilization. The higher number of employees accommodated on the east side leads to higher point concentration.

The utilization of the exterior landscape facade is closely tied to workstation usage. The question of whether employees prefer to take routes with better landscape views or through workstation corridors while heading to their destinations warrants consideration.

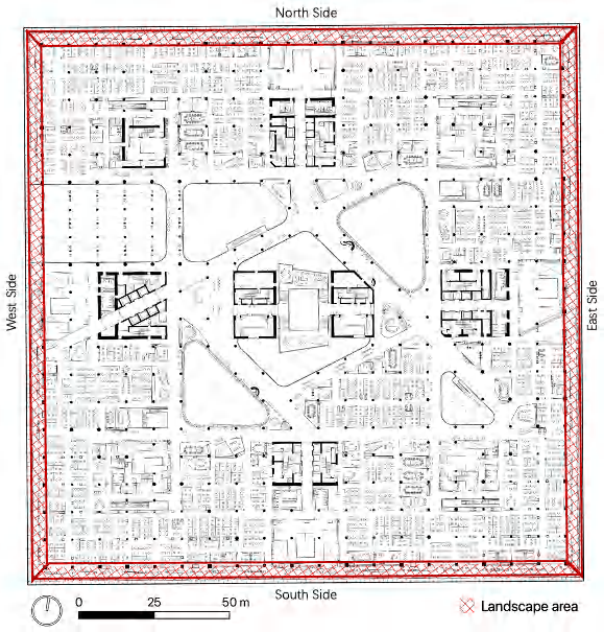

Figure 8 (a). Exterior landscape façade research area

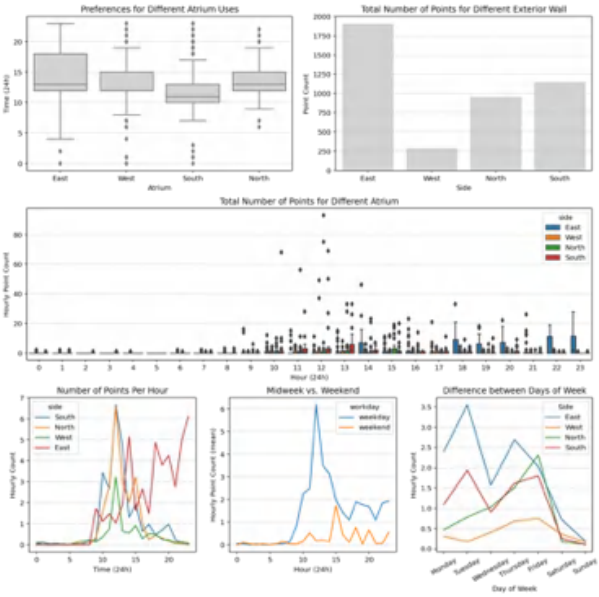

Figure 8 (b). Exterior landscape façade features

3.2 Atrium

The 6th floor features a total of 7 atriums, categorized based on their functions and views into Landscape, Traffic, and Structural types (Fig.9).

Landscape Atrium: These central atriums host therapeutic elements like plants for healing. Atriums ② and ④ represent this category.

Traffic Atrium: These atriums have staircase and traffic facilities at their center. Atriums ①, ③, ⑤, and ⑥ are examples of this category.

Structural Atrium: This category includes atriums positioned considering structural factors. Atrium ⑦ serves as an example.

Therefore, atriums ②, ③, and ⑦ are chosen as representatives of the three types. A 4.5m buffer zone is set, allowing the calculation of spatiotemporal features within these atrium categories (Fig.10).

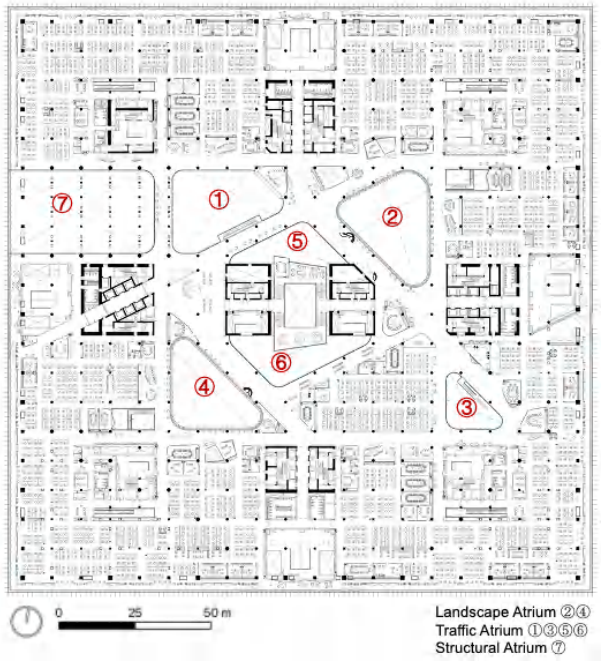

Figure 9 (a). Atrium classification

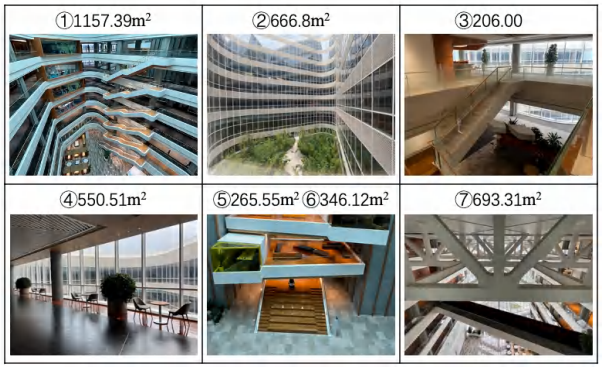

Figure 9 (b). Atrium view

Usage Analysis: From the total number of points, it's evident that Landscape-type atriums have a higher utilization rate compared to the other two categories.

Per Hour: Strategic atrium placement can moderately alleviate employee fatigue. Due to the natural lighting in the atriums, their primary usage occurs during daylight hours, particularly during working hours. This complements the usage pattern of elevators. Moreover, the peak usage is concentrated in the afternoon, likely related to employee fatigue. As work hours increase, usage gradually rises.

Per Day: Weekday atrium usage peaks are prominent, primarily during working hours in the morning and afternoon. Weekend atrium usage shows less distinct

variations over time, possibly due to a more relaxed weekend work atmosphere.

Each Side: Differential usage patterns exist among different functional atriums. The frequency of usage extracted from the three atrium categories follows Landscape, Traffic, and Structural types. This aligns with our understanding of spatial preferences, as a pleasant landscape view can alleviate stress, leading to higher occupancy. Traffic-oriented atriums follow due to their functional nature.

During daylight hours, there's a positive correlation between work hours and atrium usage. Rational atrium placement aids in alleviating worker fatigue and establishing a healthier work environment.

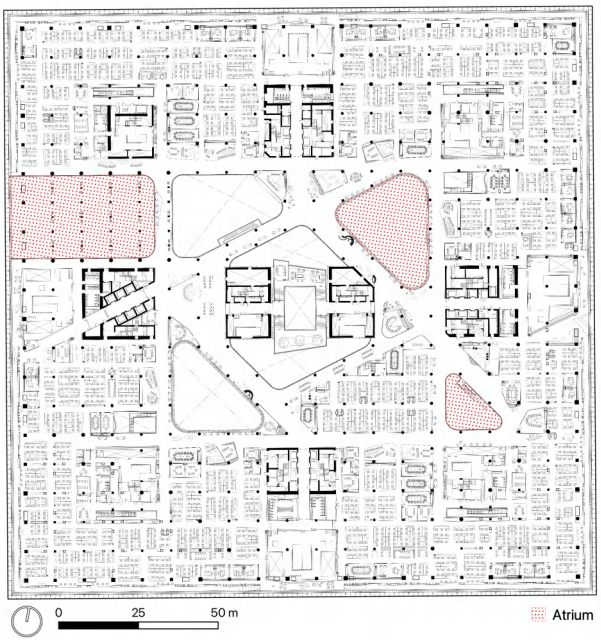

Figure 10 (a). 10 Atrium research area

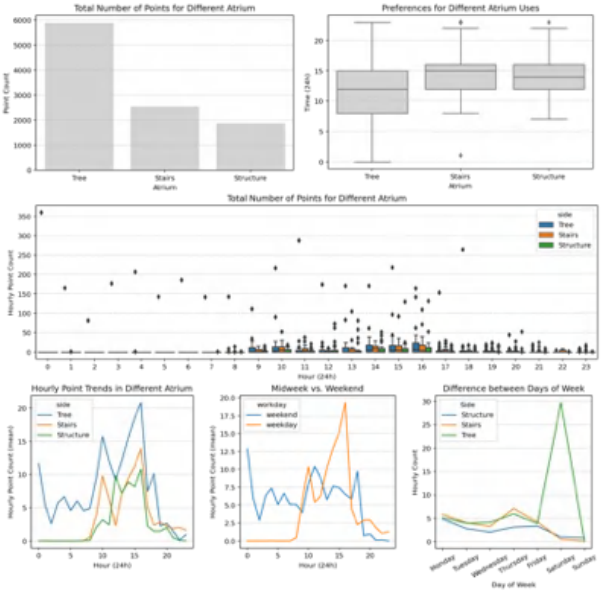

Figure 10 (b). Atrium features

The boxplot reveals that the data has a high degree of dispersion and does not follow a perfect normal distribution. (fig. 10) There are significant differences between the results of median and mean analysis, taking the usage analysis of the weekend landscape atrium as an example. Median analysis indicates a usage trend approaching 0, while mean analysis shows a higher usage rate. Median analysis is less affected by outliers, providing a more robust measure of the data's central tendency. However, using the median might result in some information loss.

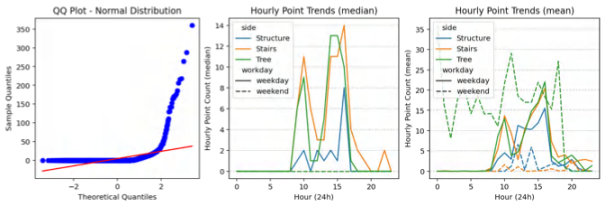

Figure 11. Normal distribution test

3.3 Elevators

Four elevator traffic areas are situated on the building's north, south, east, and west sides. The point distribution within these traffic areas suggests similar usage rates, and their usage trends over 24 hours are consistent. This indicates a high level of data reliability (Fig. 12).

Per Hour: Elevator usage during weekdays exhibits

noticeable peak patterns: 9 AM, 2 PM, and 6 PM, corresponding to the start, lunch break, and end of work hours. Lower point counts indicate concentrated work periods when employees are around their workstations or stationary. After 10 PM, the usage of the east-side elevator traffic area is notably higher than others in July, suggesting an intense overtime period for the workgroups situated on the east side.

Per Day: Elevator usage during weekdays is significantly higher than on weekends. Among weekdays, elevator usage on Tuesday stands out, likely due to weekly group meetings. Employees from branch offices gather at headquarters for reporting on Tuesdays.

Each Side: The average point density per hour indicates the following density order: east, north, south, west. However, the total point count doesn't reflect the usage rate's temporal changes accurately. Precise indoor positioning technology provides data accurate to milliseconds, necessitating more accurate preference analysis at higher time resolutions, such as daily, hourly, or even minute-based analysis. Variability in data is higher for the south and north directions, possibly due to variations in group activities. Higher usage rates on weekends are mainly in the afternoon and evening, likely due to employee overtime habits. Hourly point counts show similar trends, peaking around 9 AM, 2 PM, and 6 PM.

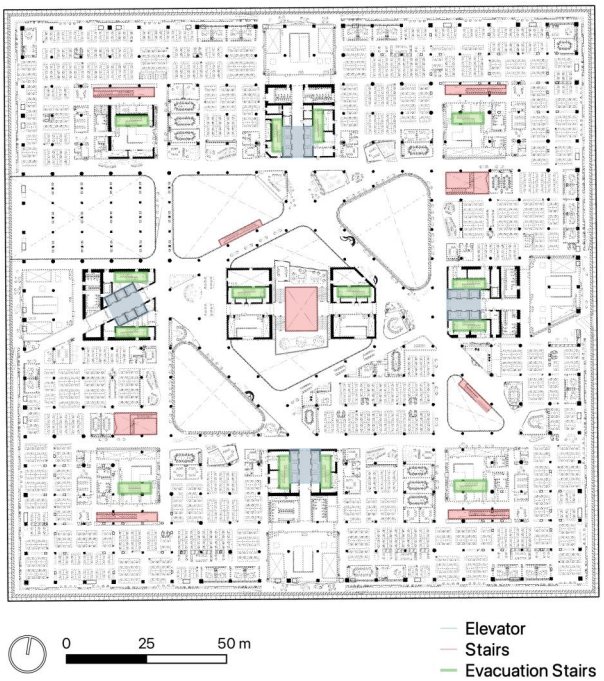

Figure 12 (a). Elevator features

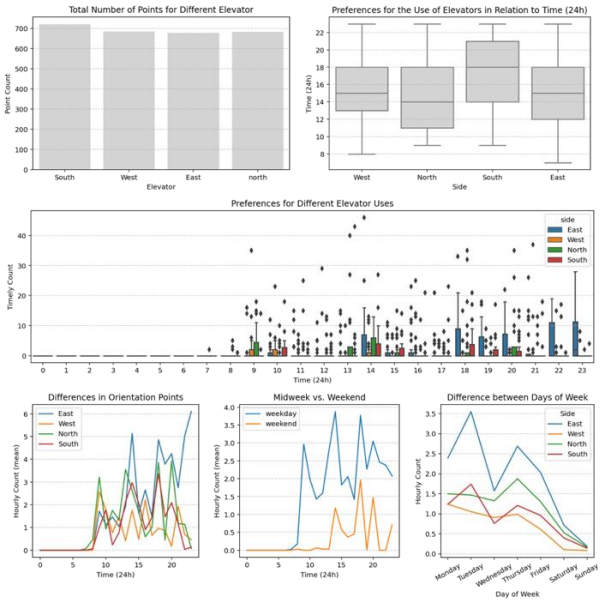

Figure 12 (b). Elevator features

4. Discussion

4.1 Finer Data Slicing

The current data slicing resolution is relatively coarse. To achieve smoother vitality curves over time, it's advisable to reduce the time interval from hours to minutes when creating slices. The present analysis focuses on landscape atriums, façade curtain walls, and elevator areas. Future

efforts could incorporate more analysis elements, such as amenities supporting work environments (pantries, discussion spaces, meeting rooms), transportation spaces (emergency staircases, stairwells, elevators), etc.

4.2 Health metrics focus

Physical Environmental Factors. Correlate indoor physical environmental data, including thermal, lighting, acoustic, and indoor air quality aspects, with human movement behavior. Analyze variations in space vitality across different seasons.

Effect of Different Workspace Performances. Future analyses could consider incorporating calculations for the proximity of each workstation to traffic hubs, scenic windows, atriums, and service areas. This could provide a score for the accessibility of each workstation. By combining subjective behavioral data, relationships between workstation vitality, accessibility, and comfort scores can be derived.

4.3 Potential and limitations of the Data

In future research, an attempt will be made to apply point data to analyze and calculate the density of points in different functional areas. Time will be segmented into shorter intervals to analyze the number of points within each minute, aiming to distinguish between stationary and mobile behaviors. Additionally, there is potential to analyze the data based on activities rather than specific spatial locations.

Data inaccuracies might arise due to biases in capturing Bluetooth positioning and errors in mapping points to the building's layout. Furthermore, due to privacy concerns, the absence of trajectories restricts the availability of valuable behavioral information.

5. Conclusion

The paper introduces a novel approach for assessing the vitality of large public building spaces using indoor Wi-Fi and Bluetooth positioning. It establishes a framework for evaluating the perceptual attributes of office spaces through an indoor positioning system, employing a data-driven approach to describe behaviors and subsequently assess spaces. Tailored spatial analysis methods are required for different analysis indicators. The results indicate that this method effectively evaluates office building spaces by quantifying spatial perception through the analysis of behavioral data distribution, clustering, and correlations, thereby enhancing the understanding of spatial design from a data perspective. Rationalizing the relationship between office workspace and rest areas proves beneficial in alleviating worker fatigue and creating a healthy work environment, offering actionable insights for architects, engineers, and managers to enhance space design.

Acknowledgement

This manuscript is grateful for the help of Osaragi Research Laboratory and the data support provided by China Tencent.

References

Alarifi A, Al-Salman A, Alsaleh M, et al. (2016) Ultra Wideband Indoor Positioning Technologies: Analysis and Recent Advances. Sensors 16(5). 5. Multidisciplinary Digital Publishing Institute: 707. DOI: 10.3390/s16050707.

Alfalah B, Shahrestani M and Shao L (2022) Identifying occupancy patterns and profiles in higher education institution buildings with high occupancy density–A case study. Intelligent Buildings International. Taylor and Francis Ltd. DOI: 10.1080/17508975.2022.2137451.

Arai T, Yoshizawa T, Aoki T, et al. (2019) Evaluation of Indoor Positioning System based on Attachable Infrared Beacons in Metal Shelf Environment. In: 2019 IEEE International Conference on Consumer Electronics (ICCE), January 2019, pp.

1–4. DOI: 10.1109/ICCE.2019.8662007.

Himeur Y, Rimal B, Tiwary A, et al. (2022) Using artificial intelligence and data fusion for environmental monitoring: A review and future perspectives. Information Fusion 86–87: 44–75. DOI: 10.1016/j.inffus.2022.06.003.

Huang W (2017) Spatial-Temporal Behavior Analysis Using Big Data Acquired by Wi-Fi Indoor Positioning System. In: P. Janssen, P. Loh, A. Raonic, M. A. Schnabel (eds.), Protocols, Flows, and Glitches - Proceedings of the 22nd CAADRIA Conference, Xi'an Jiaotong-Liverpool University, Suzhou, China, 5-8 April 2017, pp. 745-754, 2017. CUMINCAD. Available at: https://papers.cumincad.org/cgi-bin/works/paper/caadria2017_113 (accessed 29 June 2023).

Huang W, Lin Y, Lin B, et al. (2019) Modeling and predicting the occupancy in a China hub airport terminal using Wi-Fi data. Energy and Buildings 203: 109439. DOI: 10.1016/j.enbuild.2019.109439.

Li H, Shrestha A, Fioranelli F, et al. (2017) Multisensor data fusion for human activities classification and fall detection. In: 2017 IEEE SENSORS, October 2017, pp. 1–3. DOI: 10.1109/ICSENS.2017.8234179.

Li N, Calis G and Becerik-Gerber B (2012) Measuring and monitoring occupancy with an RFID based system for demand-driven HVAC operations. Automation in Construction 24: 89–99. DOI: 10.1016/j.autcon.2012.02.013.

Monti L, Tse R, Tang S-K, et al. (2022) Edge-Based Transfer Learning for Classroom Occupancy Detection in a Smart Campus Context. Sensors 22(10): 3692. DOI: 10.3390/s22103692.

Osaragi T, Yamada Y and Kaneko H (2021) Pedestrian Behavior Characteristics Based on an Activity Monitoring Survey in a University Campus Square. In: Geertman SCM, Pettit C, Goodspeed R, et al. (eds) Urban Informatics and Future Cities. The Urban Book Series. Cham: Springer International Publishing, pp. 211–231. DOI: 10.1007/978-3-030-76059-5_12.

Varlamis I, Sardianos C, Chronis C, et al. (2022) Smart fusion of sensor data and human feedback for personalized energy-saving recommendations. Applied Energy 305: 117775. DOI: 10.1016/j.apenergy.2021.117775.

Zhang W, Wu Y and Calautit JK (2022) A review on occupancy prediction through machine learning for enhancing energy efficiency, air quality and thermal comfort in the built environment. Renewable and Sustainable Energy Reviews 167: 112704. DOI: 10.1016/j.rser.2022.112704.

Exploring Separation Strategies for Car-Bicycle Integration

Liling Liu*, Sunyong Eom**, Tsutomu Suzuki**

Abstract This study focuses on the conflicts between cars and bicycles in mixed traffic and their impact on speed and safety. It aims to improve the situation by investigating an approach that separates bicycles and cars onto different roads within a network. Various scenarios were compared to a baseline, considering factors such as traffic volume, modal share, and road hierarchy. The performance of each scenario was evaluated from the perspectives of motorists and cyclists, considering car and bicycle efficiency for different trip lengths and the level of cycling stress assessed using the LTS score. The methodology involved estimating travel times using a traffic simulator and generating reachable areas for bicycles and cars using ArcGIS. The study contributes to providing insights for designing multi-modal transportation systems that consider both the benefits of shared road spaces and the potential advantages of separating bicycles and cars onto different roads.

Keywords: Car-bicycle conflict, Road space allocation, Separation Strategies, Microscopic model, Transport efficiency

1. Introduction

Cycling is being promoted in many places as a sustainable and healthy means of transportation. In Japan, a law on bicycle promotion was enacted and a roadmap plan based on this law was decided in 2016 and 2018. Since bicycles are regulated to use car lanes, car-bicycle conflicts in mixed traffic can hinder car speed and can raise cycling safety concerns, especially on narrow roads in urban areas. Cycling promotion requires a scope of multi-modal transportation design.

While there is a wide variety of approaches to allocating road space between bicycles and cars−including shared space, bicycle boulevards, sharrow, bike lanes, and bike paths − the importance of excluding cars and creating cycling dedicated facilities are revealed by studies using stated preference survey and GPS tracking data (Broach *et al.*, 2012; Stinson and Bhat, 2003; Winters *et al.*, 2010). Cyclists show their preference for facilities that reduce the impact of intervening with motorized vehicles to provide a comfortable and safe ride. Cyclists value off-street bike paths most, followed by bicycle boulevards (Broach *et al.*, 2012). Samples from European cities show the determinants of overall cycling satisfaction are most related to limited hindrance from other transportation modes and smoothness (Susilo and Cats, 2014). A study based on self-reported accidents shows that accidents between bicycles are less severe and frequent than bicycle-car ones (Shinar *et al.*, 2018). Assessments on enlarged cycling areas on original car lanes are conducted (Noland *et al.*, 2015), but the strategy to systematically separate bicycles from cars at the road network scale lacks investigation.

To simulate bicycle traffic and bicycle-car interaction, microscopic simulation methods are applied recently. It is reported to be a useful tool in evaluating road allocation in fronts of costs and benefits in travel-time delay and environmental impacts (del Carmen Almanza Mendoza *et al.*, 2018), and bicycle considered intersection treatments (Kothuri *et al.*, 2018).

In the scope of multi-modal transportation design, this study attempts to investigate an approach where bicycles and cars are separated into different roads at a network scale. The separation of road space between automobiles and bicycles can serve a dual purpose: it can not only fit the cyclists' preference for comfort and right-of-way, but also benefit motorists with a smooth drive without roads

* GISA student member; Doctoral Program in Risk Engineering, University of Tsukuba; 1-1-1 Ten-nodai, Tsukuba, Ibaraki, 305-8573, Japan, Email: s1930157@u.tsukuba.ac.jp
** GISA regular member Institute of Systems and Information Engineering, University of Tsukuba

being narrowed down by bicycle facilities or hindered by cyclists. However, such separation may diminish travel efficiency by limiting the routes available to minimize travel distance. This suggests that there is a trade-off between comfort and efficiency when considering the separation of road space.

Insights are required on both the benefits of shared road lanes and the potential advantages of separating bicycles and cars onto different roads. More specifically, we want to answer in what kind of cases separating bicycles and cars can be preferred: on which kind of hierarchy of road, with low or high traffic volume, with high or low bicycle modal share, in short or long trips? To address these research questions, we design various scenarios and assess their performance through two key metrics: 1) the efficiency of travel, and 2) the traffic stress imposed on cyclists. These evaluations are conducted by varying parameters including traffic volume, modal share, and road hierarchy when segregating bicycles and cars.

2. Methodology

2.1. Network Outline and Road Allocation

Evaluation is conducted on grid-like virtual road networks that infinitely extend. To comprise such networks, we design square community units with a side length of 1km. It is assumed that the same community units are endlessly connected. Within each community, 2*12 roads are arranged in a grid pattern with an even centerline-to-centerline distance of 83.3m. The road network features three levels of hierarchical organization (A-, B-, and C-class). This general layout (upper left corner in Fig. 1) of the community unit is constant in all network scenarios.

The width of each hierarchy of roads is determined, and then based on each class of road, different road segment separating strategies are designed, bicycle-car mix use, car-only, and bicycle-only (Table 1). For example, based on B-class road with a width of 8m, three sub-classes, B1, B2, and B3, are designed. Table 1 summarizes the settings of three hierarchies, their sub-classes, lengths of each class per community, and road space allocation for a single road.

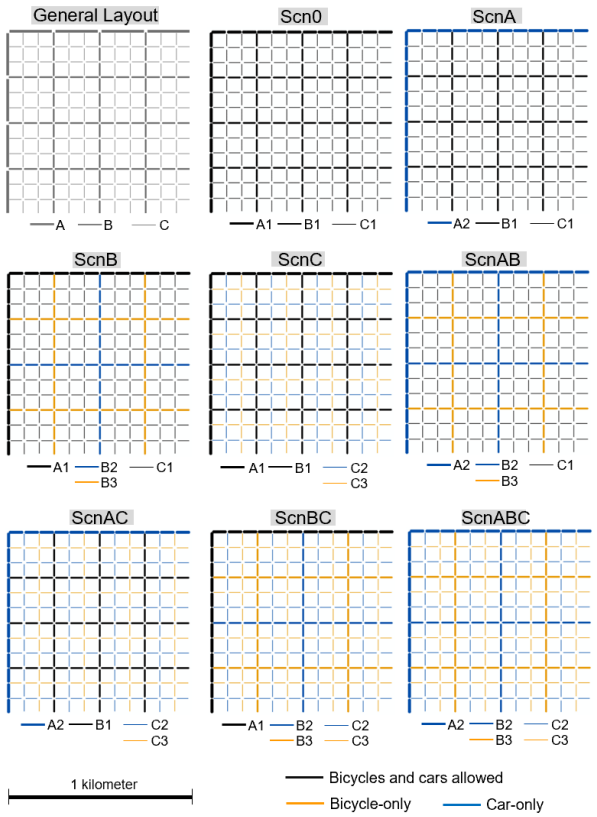

Figure 1. General community unit layout and network scenario layouts.

Table 1. Road allocation settings for road segments

Class	Width [m]	Length [km]	Speed limit [km/h]	Sub-class	Road cross section				Figure
					Sidewalk [m]	Bikeway [m]	Car lane [m]	Direction	
A	20	2	50	A1	2	2	6 (2 lanes)	Two-way	
				A2	1	0	9 (3 lanes)	Two-way	
B	8	6	40	B1	0	1	3 (1 lane)	Two-way	
				B2	1	0	3 (1 lane)	Two-way	
				B3	1	3	0	Two-way	
C	5	16	30	C1	1	mix 4m		One-way	
				C2	0	0	(1 lane)	Two-way	
				C3	1	1.5	3	Two-way	

Car lane Bikeway Sidewalk

2.2. Network Scenario Settings

Combining the road allocation scenarios in Table 1, eight network scenarios are set following the general

layout (Fig.1). They are named ScnX, where the X includes A, B, and C, indicating the hierarchies of roads on which bicycles and cars are separated into different roads. The Scn0 is the baseline scenario where all roads have bicycle lanes adjacent to car lanes. When allocating roads to community units, we attempt to set both cars and bicycles can obtain a similar chance to traverse the whole network. When car-only roads exist, they are set to be through the center of the community network, considering car-only roads perform a higher hierarchy than bicycle-only roads.

Based on space allocation in each network scenario, traffic volume on each road is calculated. Traffic flow f_a^m of mode *m* on road *a* in scenario *k* is proportional to its area in the gross area for mode *m* in the scenario *k*:

$$f_{ak}^m = F^m \frac{l_{ak}^m w_{ak}^m}{\sum_{i=1}^{N_k^m} l_{ik}^m w_{ik}^m} \quad (1)$$

where l_{ik}^m and w_{ik}^m are road length and road width of mode m on road *i* in scenario *k* in one community unit, N_k^m is the number of roads for vehicle m in one community unit in scenario *k*. Mode *m* indicates *bicycle* or *car*. F^m, the total input volume of mode *m* in one community unit, is constant across the network scenarios. F^{car} is calculated using Eq. (1) when keeping car traffic *f* on road A1 in baseline scenario Scn0 to be 200 vehicle-per-hour (vph), 300vph, or 400vph. 200vph is the hourly average traffic volume of a road class nationwide in the real world that similar to A1 in the setting. 400vph is the highest possible volume to input into the microscopic models the authors built that the queue length those models can hold. Then $F^{bicycle}$ is calculated as

$$F^{bicycle} = \frac{bicycle\ share\ F^{car}}{1 - bicycle\ share} \quad (2)$$

where bicycle modal share is set to three levels, 10%, 20%, or 30%. The traffic volume on each road resulting from here is used as input into microscopic models.

2.3. Vehicle Features in Microscopic Model

The travel time through road segments and intersections is estimated using a microscopic traffic simulator software PTV Vissim, version 10. Three kinds of vehicles are simulated, conventional bicycle, electrical assistant bicycle ("Bicycle" is used as the general term for these two kinds in this paper, and all analyses are conducted on them as a whole without distinction), and car.

Desired speed distributions are required to define vehicles. For cars, three kinds of design speeds are set, 50km/h, 40km/h, and 30km/h. Based on each kind of design speed, the desired speed distribution is set to be linear ranging from design speed ± 5 km/h, and with 85th percentile of the desired speed is set to be design speed. For two kinds of bicycles, their desired speed distributions are specialized differently in Japanese cases based on a set of empirical free flow speeds from a previous study (Yamamoto et al., 2012).

Other vehicle features include acceleration and deceleration function, following and lateral movement. Cars employ default settings on these features. For bicycles, detailed settings are absent in Japanese studies, thus a research report (COWI, 2013) on cyclist microsimulation in Copenhagen is adopted. To correspond to left-hand traffic in Japan, the desired position, overtaking side, and minimum longitudinal speed are modified. The ratio of e-bikes in all bicycles is set to 20%.

Both cars and bicycles used the car-following model to decide their movement to accelerate or to cruise considering the conditions of their heading vehicles. Depending on the road type and vehicle type, lane-based or non-lane-based vehicle moving rules are applied. In car-only roads, longitudinal and lateral movements are based on fixed lanes. On bicycle-only roads, bicycles use a non-lane-based rule, in which no lanes are specified but only the width of the bikeway area is assigned, thus bicycles can move more freely than lane-based cases and be able to overtake actively without sticking to certain lanes as automobiles. Non-lane-based rule is also applied to both cars and bicycles on mix-use roads. Bicycles basically keep to the left, but in cases where the road is vacant, they also use the middle part of the road to overtake. Cars prefer the middle of the road and can

overtake bicycles on their right.

2.4. Road and Intersection Settings in Microscopic Model

As we plan to evaluate the separate approach when it is applied to a network, it requires the construction of a road network of a wide area. However, building such a large network in the microsimulation software is time-consuming and infeasible for the author. Therefore, we used a "split-assemble" method to split the network into intersections and roads to simulate in microscopic models, and then assemble the output results derived from the model.

Road segment models use the road cross sections introduced in Table 1. Traveling time passing 100m distance is averaged from 50 runs of a period of 4,800 simulation seconds, during which the first 1,200sec are considered to be warming up time for the system thus the results are discarded.

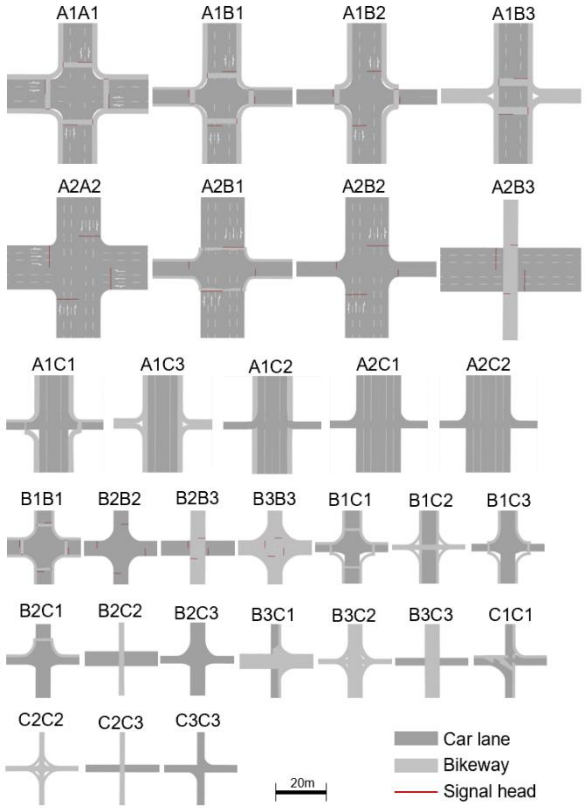

Figure 2. Intersection layouts in microscopic model.

The total size of an intersection, including four connected legs, is 70m * 70m. The layouts of intersections are decided by two crossing roads. Their center parts are shown in Fig.2. Note that at A-C intersections, both straight-forward crossing and right-turn are forbidden, and only left-turns are allowed.

Bicycles and cars use physically separated space before entering junctions in all layouts. When choosing a direction among possible routing decisions, the probability to turn left, to go straight through, and to turn right is 2:6:2. When cars waiting on a two-car-lane road, the ratio of Left-turning: Straight-heading: Right-turning (L: S: R) on the left lane is 2:5:0, on the right lane is 0:1:2. In three-car-lane cases, the L:S: R ratios on the left to right lanes are 2:2:0, 0:4:0, and 0:0:2. Ratios are set assuming that the queues have similar lengths and the time to turn right costs about 2 to 3 times to turn left or to go straight forward.

Bicycles perform hook turns (two-stage turns) to turn right at intersections, except for bicycle-only ones or when crossing one car-lane. To simplify interaction, bicycles travel in one direction when crossing. Cycling behaviors at intersections consist of 4 kinds of behaviors according to (COWI, 2013): (1) cycling in the general lane when keeping left; (2) cyclists in a waiting zone in front of red traffic light; (3) cycling through an intersection; (4) transition from (3) to (1). Cars do not change lanes when approaching intersections. They reduce speed to a maximum of 30km/h at the center of intersections or in a left turn, regardless of the speed limits of the road links connected to the junction.

Conflict areas are locations where vehicle routes overlap and interfere with each other. In general, bicycles take priority over cars. For vehicles heading in different directions, the priority order from high to low is straight-heading, left-turn, and right-turn. In other cases, conflict areas are set to be undetermined, showing no right-of-way specified and vehicles on both sequences watch out for each other and react.

Four signalization types are applied depending on intersection types (Fig. 3). To signalized intersections two-

phase pre-timed signals are applied. In phase 1, vehicles waiting at two opposite legs are released to cross while the vehicles at the other pair of opposite legs are stopped. In phase 2, conditions of the two signal head pairs swap. The compliance rate with signal control is 100%. Intersection passing time is averaged from 50 runs of a period of 4,800 simulation seconds, during which the results from the first 1,200sec are discarded.

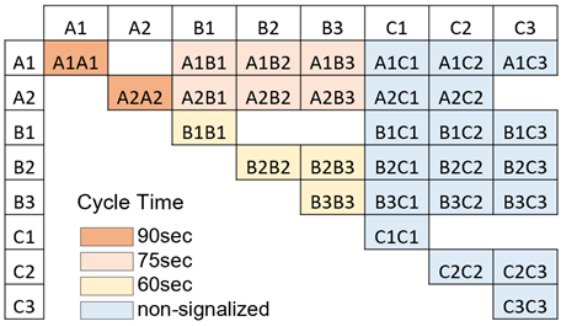

Figure 3. Signal cycles in intersections.

2.5. Efficiency and Cycling Stress Assessment

The "assemble" process to combine results from links and intersections is conducted using software ArcGIS Desktop 10.6.1 and ArcGIS Pro 3.0. In PTV Vissim, passing time through an intersection is collected between the start point on the approaching legs and the end points on the departure legs. These outputs are input into ArcGIS (Fig. 4).

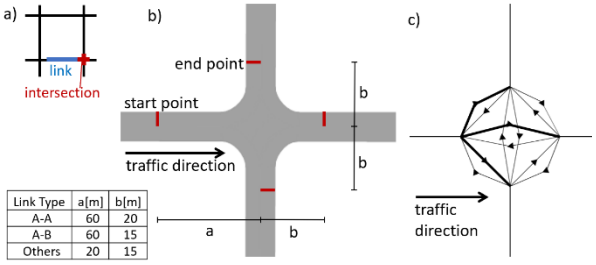

Figure 4. Intersections: a) intersection part split from road link in network, b) start point and end points to collect passing time data in microscopic model, c) intersection line data in ArcGIS.

Note: Thick lines show the lines to which the data is input when traffic direction is as the arrow indicates.

To evaluate transport efficiency in each network scenario, we used the reachable areas in 300sec and 1,800sec. Network models are built in ArcGIS 10.6.1. Each network model contains more than 900 community units to comprise the largest possible reachable area generated by car in 30min from the central area.

Start points are drawn in every block in a community in the central part of the whole network. Block here is defined as a square surrounded by four roads. To simulate departures from all four neighboring streets, four start points are respectively drawn near one of the four roads surrounding the block. Efficiency metric of traffic mode m in scenario k is S_k^m, the average of A_{ki}^m, the largest reachable area from block i in scenario k by mode m, calculated as

$$S_k^m = \overline{A_{ki}^m} \qquad (3)$$

where $A_{ki}^m = \max a_{kij}^m$, and a_{kij}^m is the reachable area from start point j in block i in scenario k by mode m.

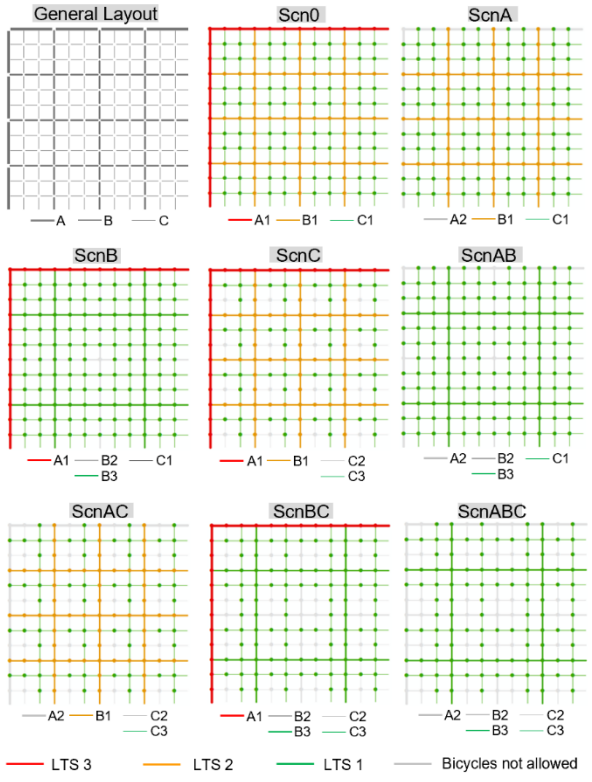

Figure 5. LTS score for intersections and road links.

In communities where bicycle or car cannot start from when no available road for the specified mode, the result A_{ki}^m for it will be the largest reachable area in 525sec or 1725sec from the four Neumann neighborhood blocks, assuming users to walk the distance of a block to their

neighborhood in order to use vehicles. The 75sec subtracted from 600sec and 1800sec is calculated by dividing the length of one side (83.3m) by the walking speed (1.1m/s). The amount of scenarios is summed up to be 144 scenarios (8 network scenarios×3 traffic volume levels×3 bicycle modal share×2 trip length).

To access the cycling environment, Level of Traffic Stress (LTS) scoring system proposed in (Mekuria et al., 2012) is used to compare the scenarios. This scheme classifies cycling traffic stress into four levels 1 to 4, denoting low to high stress the cyclists cognitive. Roads are assessed according to based on road segment features, traffic volume, motor vehicle speed, street width, and traffic mixture. The intersection LTS level is decided by the scores already assigned to the road links to which the intersection connects. The evaluation results are shown in Fig. 5.

To summarize the LTS score in each network scenario, points are assigned to links and intersections that 1 point to Level 1, 2 points to Level 2, and 3 points to Level 3. Scores are weighted and averaged respectively from links and intersections that are covered by the largest reachable areas from every block. The result from road links is weighted by road length and bicycle traffic volume. The result from intersections is weighted by the sum of bicycle traffic from the roads that connect to the intersection. The roads where bicycles are not allowed are considered null in terms of score, thus not included in the average.

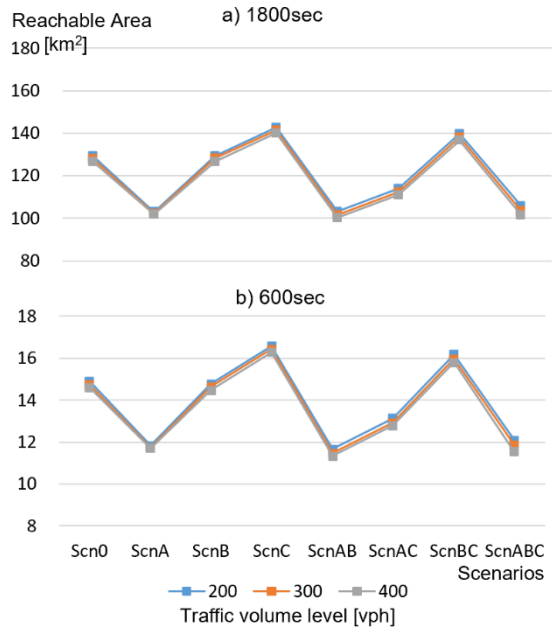

Figure 6. Bicycle efficiency (Bicycle modal share is 20%)

3. Results

3.1 Results from individual indicators

We focus on the results in three individual indicators: efficiency of cars, efficiency of bicycles, and LTS score. When looking at the transportation efficiency of cars, since bicycle modal share does not change the tendency in results significantly, Fig. 6 gives an example when bicycle modal share is 20%.

Compared with scenarios with A1 roads, those with A2 roads perform better as A2 have enlarged car lane for car-dedicated usage. For example, ScnA is better than Scn0, and ScnAB is better than ScnB. While adding a car lane itself does not speed up cars on A-class roads directly, it helps with shortening passing time at intersections and helps with fastening travel on low hierarchies of roads and intersections, functioning by attracting drivers to A-class roads, as the volume distribution method is that that traffic volume proportional to area.

Scenarios that separate bicycles and cars on C-class roads worsen car efficiency. For example, ScnBC is worse than ScnB, and ScnC is worse than Scn0. C-class roads are like capillaries, that although thin, but with non-negligible length and routing alternatives. For example, in scenarios forbidding cars on B-class roads, 4km are affected in one community, but if forbidding on C-class roads, 8km are affected.

When looking at the transportation efficiency of bicycles. Fig. 6 gives an example when bicycle modal share is 20%. The reachable areas are not influenced much by modal share and volume changes. It may suggest that there is sufficient road space that no congestion occurs to hinder cycling. Another reason can be that the speed of bicycles is not as fast as cars, that the slow-down caused by high traffic is not as significant as the latter. While scenarios applying A2, such as ScnA and ScnAB, can

increase car efficiency, forbidding bicycles on A-class roads limits their traversable area.

We assumed that separating bicycles from cars can speed up cycling on single roads. But in the network scenarios, such an effect is of no show. The reason can be that though changing mix-use bikeway to bicycle-only path can expending cycling area, it also attracts more cyclists. Meanwhile, some road space allocation attracts cyclists but cannot provide sufficient width for cycling, which happens in C3 road where bikeway is 1.5m that attracts more cyclists than 1.0m, but since one bicycle needs 1.0m width to ride, it cannot provide better efficiency than 1.0m bikeway.

Intersection is the place where separation makes a difference. When turning through multiple car lanes, bicycles take hook turns for safety when merging with motor traffic rather than turning through the center of the intersection. On bicycle-only streets or one-car-lane roads, hook turns are not required and thus can turn at a higher speed. In the meantime, an intersection generated by a bicycle-only road and a car-only road is a crossing only consisting of straight-ahead routing without a left or right turn, thus simplifying the intersection and speeding vehicles up. Excluding cars also makes cyclists cross intersections smoothly without dodging cars.

Such effects are more apparent when separating on C-class roads than on B-class roads. Since there are more C-class roads thus more intersections. Therefore, ScnBC and ScnC tend to give out the best performance in terms of bicycle efficiency.

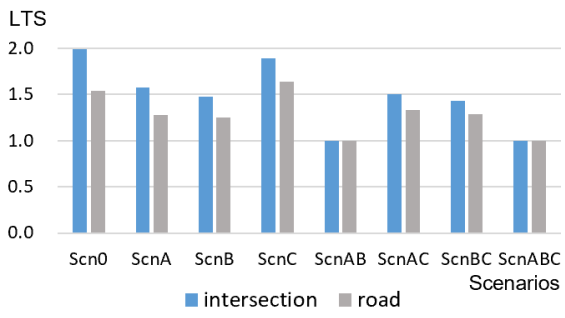

Figure 7. LTS score (Volume at 300vph level, bicycle modal share is 20%, 600sec trips).

Regarding cycling stress evaluation (Fig. 7), all separating scenarios can improve LTS to some extent. For road link, ScnAB, and ABC rank best, as all traversable roads are scored as level 1. Scenario A, B, AC, and BC

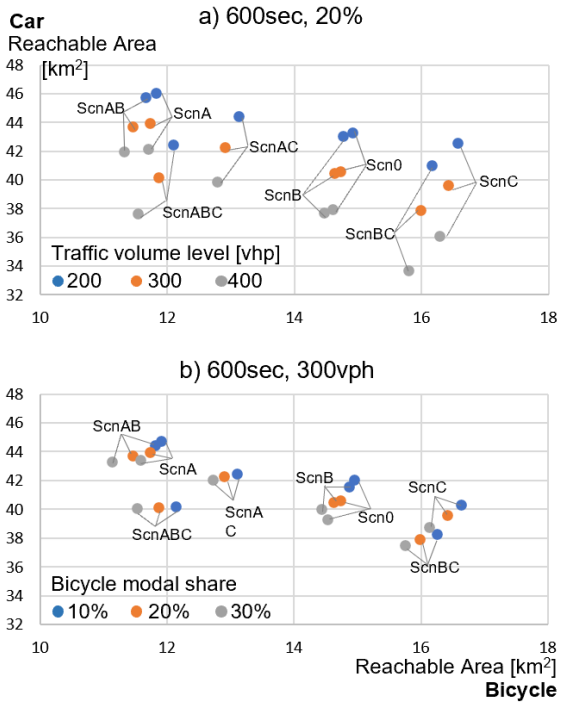

Figure 8. Bicycle vs. car efficiency (600sec trip).

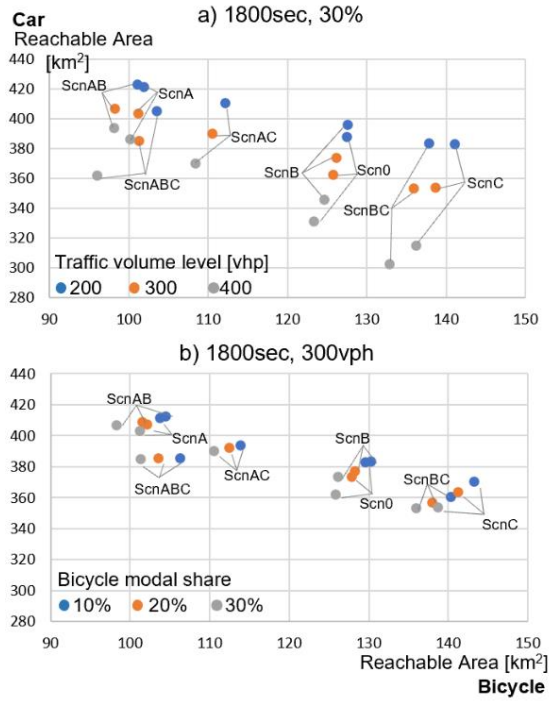

Figure 9. Bicycle vs. car efficiency (1800sec trip).

have similar LTS scores of 1.2~1.3. Following this, Scn0 and C have the worst score among scenarios, above 1.5. For intersections, while ranking groups can be split as intersections as (AB, ABC), (A, B, AC, BC), and (0, C), the difference between scenarios tends to be more apparent than that for road links. The middle group ranges 1.4~1.5, and the worst ranges 1.8~2.0.

3.2. Comprehensive results

When focusing on transportation efficiency (Fig. 8, Fig. 9), cars and bicycles tend to have a trade-off relationship across network scenarios on separated roads, i.e., when compared to the baseline a scenario attractive for drivers usually is unpleasant for cyclists in terms of speed, regardless of its modal share and traffic volume settings. The only scenario that improves both efficiency is the ScnB. Other constraints include bicycle modal share being 20~30%, traffic volume at the level of 300~400vph, and bicycles being cars taking 30min trips. The improvement can be more distinct than otwhen the bicycle modal share is as large as 30%.

Regarding the cycling environment (Fig. 10), ScnBC that separates bicycles from cars on B-class and C-class can upgrade quickness while mitigating stress both at intersections and on roads when compared to baseline Scn0. The scenario not-as-good but fair is ScnC, which provides better speed and comfort on roads but not intersections.

For mitigating conflicts between motorists' calls for speeding and cyclists' requirement for no-stress cycling (Fig. 10), the separating strategy provides a bunch of alternatives including ScnA, ScnB, ScnAC, ScnAB, and ScnABC. Four of these five choices have an approach in common to enlarge A-class roads for car-dedicated use.

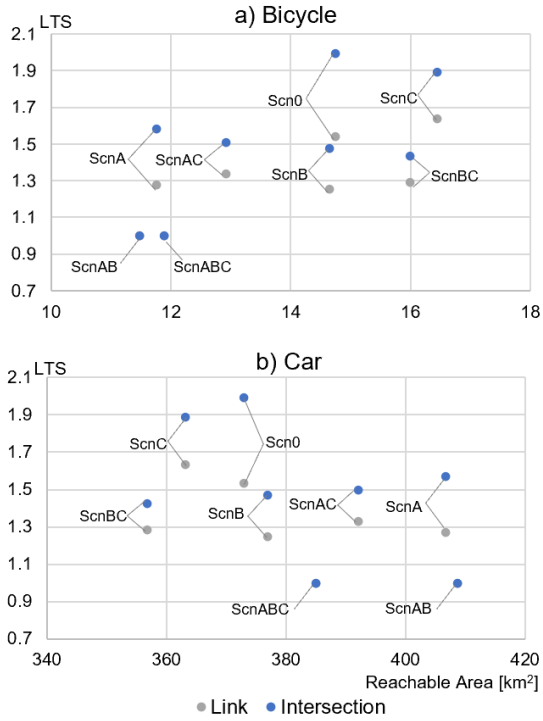

Figure 10. Efficiency vs. LTS score (300vph level, bicycle model share is 20%).
a) Bicycle efficiency (600sec trip) vs. LTS score.
b) Car efficiency (1800sec trip) vs. LTS score.

4. Discussion and Conclusion

The study extends the literature on road allocation methods by exploring an approach where bicycles and cars are separated into different roads at a network scale. Comparing scenarios with variables of traffic volume, modal share, trip length, and hierarchy of separated roads, the study can contribute to providing insights for designing multi-modal transportation systems when considering both the advantages of shared road spaces and of separating.

The main findings are as follows. (1) Cars and bicycles have a trade-off relationship in efficiency across network scenarios on separated roads. The only scenario that improves both is to separate bicycles and cars to different roads at middle-class roads when bicycle modal share is 20~30%, traffic volume at the level of 300~400vph, and bicycles are cars are taking 30min trips.

(2) Regarding the cycling environment, separating

bicycles from cars on different middle-class and local roads can upgrade the overall cycling environment including quickness and comfort on the road and at intersections. The not-as-good but fair scenario is to separate solely on local streets.

(3) To reconcile conflicts between motorized speed and cyclists' comfort, the separating strategy provides a bunch of alternatives. The main idea is to enlarge high-hierarchy roads for car-dedicated use.

Based on the three main findings, we discuss the practical implementation of this separation approach. By the means of efficiency, although (1) shows some potential improvement from the status quo baseline, there is no improvement or it is marginal when bicycle modal share is 10~20%, which is similar to the share in the real world in Japanese cities. While the result suggests an advantage in a 30-minute trip, the network radii (approximately 6km) of derived reachable areas in 30min is longer than 80% of bicycle trips of 5km. Thus, separating bicycles from cars systematically following (1) seems drastic at present.

But efficiency is not all mobility is about. Cycling can be valuable for its fronts of providing a cheap, active, and environmentally friendly alternative for residents. Some pilot projects can test the method in (a), separating middle-class roads in part of the area and even gradually transiting to both middle and minor streets to provide a cozy cycling environment as (2) above suggested, especially in some residential areas.

Note that not only cycling's value but other elements should also be considered in its promotion. For cities with sparsely populated and weak transit systems, cars can be indispensable, and caution is required to promote bicycles as a main task in a city planning vision. In this case, the suggestion in (3) can be useful. The main suggestion in (c) to balance car speed and cycling comfort is excluding bicycles from arterial roads while adding lanes for motorized traffic. It can be a solution to bicycle-car conflicts while bicycle mobility is limited because traversable roads are restricted.

Acknowledgement

The authors wish to acknowledge the support from the Meiji Yasuda Life Foundation of Health and Welfare, and the Epson International Scholarship Foundation. This study was supported in part by JSPS KAKENHI Grant Numbers JP 21H01559.

References

Broach, J., Dill, J. and Gliebe, J. (2012), Where do cyclists ride? A route choice model developed with revealed preference GPS data, *Transportation Research Part A: Policy and Practice*, **46**(10), 1730-1740.

COWI. (2013), *Micro Simulation of Cyclists in Peak Hour Traffic*. Copenhagen: COWI.

del Carmen Almanza Mendoza, A., Aguilar, L.Á.T., Jiménez García, J.A., González, S.H., Esquivas, M.T., Fernández, V.F. and Soto, D.F. (2018), Bikeway system design in the city of Celaya through a micro-simulation approach, *Transportation Research Procedia*, **33**, 371-378.

Kothuri, S., Kading, A., Schrope, A. and White, K. (2018), *Addressing bicycle-vehicle conflicts with alternate signal control strategies. NITC-RR-897*. Portland: Transportation Research and Education Center (TREC)

Mekuria, M.C., Furth, P.G. and Nixon, H. (2012), *Loss-Stress Bicycling and Network Connectivity, MTI Report11-19.CA-MTI-12-1005.* San Jose: Mineta Transportation Institute.

Noland, R.B., Gao, D., Gonzales, E.J. and Brown, C. (2015), Costs and benefits of a road diet conversion, *Case Studies on Transport Policy*, **3** (4), 449-458.

Shinar, D., Valero-Mora, P., van Strijp-Houtenbos, M., Haworth, N., Schramm, A., De Bruyne, G., Cavallo, V., *et al.* (2018), Under-reporting bicycle accidents to police in the COST TU1101 international survey: Cross-country comparisons and associated factors, *Accident Analysis and Prevention*, **110** (December 2016), 177-186.

Stinson, M.A. and Bhat, C.R. (2003), Analysis Using a

Stated Preference Survey, *Transportation Research Record: Journal of the Transportation Research Board*, **1828** (03), 107-115.

Susilo, Y.O. and Cats, O. (2014), Exploring key determinants of travel satisfaction for multi-modal trips by different traveler groups, *Transportation Research Part A: Policy and Practice*, **67**, 366-380.

Winters, M., Teschke, K., Grant, M., Setton, E.M. and Brauer, M. (2010), How far out of the way will we travel? Built environment influences on route selection for bicycle and car travel, *Transportation Research Record*, **2190**(1), 1-10.

Yamamoto, A., Kobayashi, H., Hashimoto, Y., Uesaka, K., Kishida, M. (2012), Proposals for the estimation and use of bicycle travel speeds, *Proceedings of Infrastructure Planning CD-ROM*, **43** (in Japanese).

Regional-Spatial Analysis and Comparison of Social Farming in Japan and the Netherlands by Using GIS

Zile Tian*, Naoko Fujita**, Max Hanssen***, Ding Ma***, Suzu Shimada***

Abstract Approximately 15% of the global population and 9.2% of Japan's population experience disabilities. To facilitate the inclusion of individuals with disabilities into society without physical and social segregation, the concept of "integrating agriculture and care" has gained recognition as a mechanism for enhancing social engagement. Social Farming, the precursor of this integration, is progressively taking diverse shapes in European nations. This study aims to undertake a comparative analysis of social farming initiatives in the Netherlands and Japan, encompassing their subjects, objectives, operational modalities, systems, and regional-spatial dynamics. Drawing insights from advanced instances in the Netherlands, this research endeavors to identify key elements that can foster the advancement of "agriculture and care" integration in Japan.

Keywords: social farming, people with disabilities, combination of agriculture and care, spatial analysis

1. Introduction

According to the UN Enable, approximately 1 billion people worldwide have a disability, which is roughly 15% of the world's population (United Nations Department of Economic and Social Affairs, 2014). According to the 2023 White Paper on Persons with Disabilities in Japan, the number of people with disabilities is 11,602,000, which means that approximately 9.2% of the population has some form of disability (Cabinet Office Japan, 2023). Goals 3, 10, and 16 recommend that people with disabilities live together as members of a society in which physical, social, and psychological barriers are removed. Under these circumstances, this study focuses on "The combination of agriculture and care" as a means of social participation.

“The combination of agriculture and care” is an initiative that links agriculture and welfare and is expected to secure agricultural labor through the participation of people with disabilities in society, maintaining and preserving farmland through the reuse of abandoned farmland, and promoting the revitalization of depopulated rural communities.

In addition, it is expected to help connect the employment needs of people with disabilities with the shortage of labor due to the declining and aging workforce in the agricultural sector, and policymakers are actively promoting the creation of such a system and human resource development (OH Sewoong et al., 2020). There are different terminologies for the combination of agriculture and care, such as green care, care farms, social farming, and farming for health (Hassink and Van Dijk, 2006). In this study, we use the term social farm. Social farms offer day care, assisted workplaces, and/or residential places for clients with various disabilities (Hassink and Van Dijk, 2006). They also promote treatment, rehabilitation, social inclusion, education, and social services by providing farm work and activities that utilize agricultural resources on nature-rich farms. The carrying out of useful activities and an informal and open setting within a green environment turns social farms into

GISA Members
* Student Member; Graduate School of Comprehensive Human Sciences; University of Tsukuba; **s2230508@u.tsukuba.ac.jp**
** Member; Insititude of Art and Design, University of Tsukuba; **fujita.naoko.gf@u.tsukuba.ac.jp**
*** Student Member; Graduate School of Comprehensive Human Sciences; University of Tsukuba

an appealing facility for various client groups (Hassink et al., 2014). Particularly in the Netherlands, social farms have attracted worldwide attention as “a combination of agricultural and care” systems and the number of social farms that provide users of care facilities with agricultural experience as a place for daytime activities has been gradually increasing (Hassink and Van Dijk, 2006).

However, unlike the Netherlands, a leading country in “The combination of agriculture and care” and a solution to the declining and aging farming workforce, Japanese efforts to date in “The combination of agriculture and care” have been aimed at the business interests of the disabled and agriculture, and the positioning of farming by the disabled as a “means” means to realize profits (Tada, 2019). Because of the bias toward “farming,” and the growing willingness of people with disabilities to become farmers, the power of welfare, including the restoration of mental and physical health through agriculture, has been overlooked.

In addition, it is possible that a trend will emerge in Japan in the future to run a farm to realize diversification and the utilization of multiple functions rather than the mass production of agricultural products (Tada, 2019). Therefore, it is necessary to propose the creation of a social farm environment with multifaceted functions to promote the mental and physical health of people with disabilities and revitalize local communities.

2 .Objective

Against this background, this study aims to clarify the actual situation and challenges of social farms and the combination of agriculture and care in Japan and the Netherlands by comparing the target, purpose, and operational forms of social farms and the regional spatial analysis of social farms using ArcGIS. Another purpose of this study is to clarify the actual situation and issues of social farms and agricultural and welfare cooperation in Japan and the Netherlands. Furthermore, based on the actual situation of the combination of agriculture and care in the Netherlands and the efforts of advanced cases, we will try to elucidate the factors that contribute to the promotion of the combination of agriculture and care in Japan.

The first is to clarify the differences in the subjects, purposes, and management forms of social farms in Japan and the Netherlands, and the second is to clarify the regional distribution of social farms in Japan and the Netherlands and the number of social farms in each region.

We believe that this research will form an academic foundation in the field of agriculture and care to realize the creation of social farm environments with multifaceted functions to promote the mental and physical health of various users of social farms, including the disabled and the elderly, and to revitalize local communities in Japan.

3. Method

3.1. Research Subjects

The target sites for this study were social farms in Japan and the Netherlands. In Japan, all social farms engaged in the combination of agriculture and care that are registered with the Ministry of Agriculture, Forestry, and Fisheries or the respective regional agricultural administration offices were included. In the Netherlands, all social farms registered with the Federation of Agriculture and Care were included in the study.

All the combinations of agriculture and care cases in Japan and the Netherlands were included because it would require a huge amount of data to compile a database of the combination of agriculture and care cases and to understand the current status and issues of social farms nationwide.

Geographical data of social farms were included in the study because it was necessary to clarify the regional distribution of social farms in Japan and the Netherlands, regional location trends, and so on. Geographical data on social farms are included in the study.

3.2. Data Collection

We compiled a database of the number and patterns of social farms in Japan and the Netherlands, and investigated the details of the initiatives being undertaken.

Additionally, we conducted a field survey of social farms in Japan and interviewed the people in charge of the details of their initiatives and management systems.

To clarify the geospatial characteristics of social farms, we collected data on the addresses of each case study, as well as data on devastated farmland and underpopulated areas in Japan, from E-stat, Statistics Netherlands, and the Federation of Agriculture and Care in order to identify the geospatial characteristics of social farms.

3.4. Data analysis

Based on data on social farms in Japan and the Netherlands, we compared the targets, purposes, and operational forms of social farms in Japan and the Netherlands and clarified the characteristics of each. In the case of Japan, field surveys and interviews were conducted, while in the case of the Netherlands, literature was used to clarify the structure and management system of the cases studied by establishing items such as the pattern of social farms, size, types of user disabilities, and relationships among stakeholders in the initiatives.

The number and addresses of social farms were ascertained and an Excel list of social farms was created by specifying the degree of history of social farms based on the data. Then, we superimposed the data on underpopulated areas and degraded farmland using ArcGIS software and clarified the regional distribution of social farms and regional location trends.

4. Results

4.1. Overview of Social farms in the Netherlands

The Netherlands is located in northwestern Europe and, as shown in Figure 1, is composed of 12 provinces. Most of the country is a coastal lowland, from which the terrain is flat with reclaimed land and hills to the east (Okhee, 2020). In Netherlands agriculture, land productivity growth was especially high from 1950 to the mid-1970s, while during this period the labor input in agriculture declined from almost 600000 to less than 300000 man-years. This was achieved through large-scale intensification and mechanization. Over the last few decades, there has been a clear change in the role of agriculture in The Netherlands. Agriculture itself has changed: mainstream agriculture is now characterized by the use of large amounts of external inputs, minimal labor efforts per hectare, and high outputs (Meerburg et al., 2009).

According to Statistics Netherlands, 53.8% of the land area of the Netherlands was used for agriculture in 2015. As shown in Figure 2, agricultural land was mainly concentrated in the eastern and central regions of the Netherlands, including the provinces of Drenthe, Overijssel, and Gelderland. While the agricultural industry has been moving toward large-scale production through advanced agricultural production that takes advantage of abundant agricultural resources and advanced technology, traditional small-scale agricultural enterprises with limited competitiveness in agricultural production have been converting to "social farms" as a strategy for promoting disadvantaged agricultural lands in a multifaceted manner (Okayama, A., 2020). Against this background, the spirit of volunteerism has become more prevalent than in the past, and many farm wives have experience working in welfare facilities. These farmers have become more conscious of creating employment through the establishment of social farms. They started hands-on activities on farms as new places for welfare facility users (Bock and Oosting, 2010).

In addition, the Dutch government implemented deregulation and systematic promotion measures to promote disadvantaged farmland in a multifaceted manner through the social support system (WMO), which delegates the right to determine benefits from the national government to local governments through decentralization of the insurance system. Benefits for the disabled and other people who have difficulty working were reduced to a level where shortfalls due to problems, such as ability, were covered by taxes. On Social farms, people with disabilities were not expected to contribute much to production activities as a labor force, and their role as healers through activities in the agricultural space

was strengthened.

Under these circumstances, social farms in the Netherlands have been addressed in various ways. The first is the "multi-faceted effect type," in which agricultural activities are carried out on farmland while also functioning to demonstrate the diverse effects of "agriculture," such as health recovery, motivation for living, and transition to employment. The second type is the "public health type," which does not involve agricultural production on farmland but rather aims to restore people's health through agricultural work. And the last is the "social inclusion type," a pattern in which a portion of an urban park is utilized as a farm and has the function of providing a place to solve social issues specific to drug addicts, criminals, and homeless people (Ueda, 2019).

Figure.1. Administrative division of Netherlands

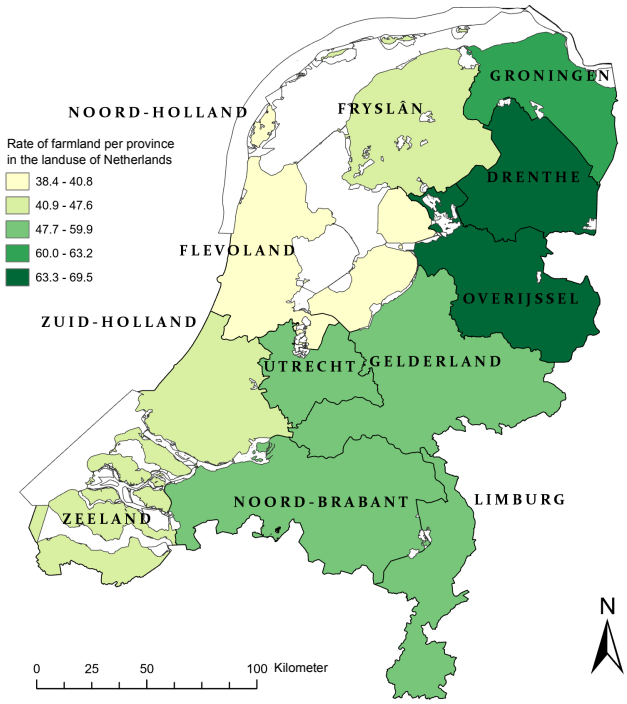

Figure.2. Rate of farmland per province in Netherlands

4.2. Regional distribution of social farms in the Netherlands

The number and regional distribution of social farms in the Netherlands in 2023 (Figure 3) show that social farms are not evenly spread throughout the country, but are concentrated in the central and eastern parts of the Netherlands. Among the 12 provinces in the Netherlands, the provinces with the most social farms are Gelderland (156), Overijssel (113), Noord-Holland (111), and Noord-Brabant (104). Conversely, provinces with fewer social farms are Zeeland (20), Utrecht (23), and Flevoland (30). The regional agricultural land coverage and number and regional distribution of social farms show that social farms are generally distributed in areas with abundant agricultural land resources.

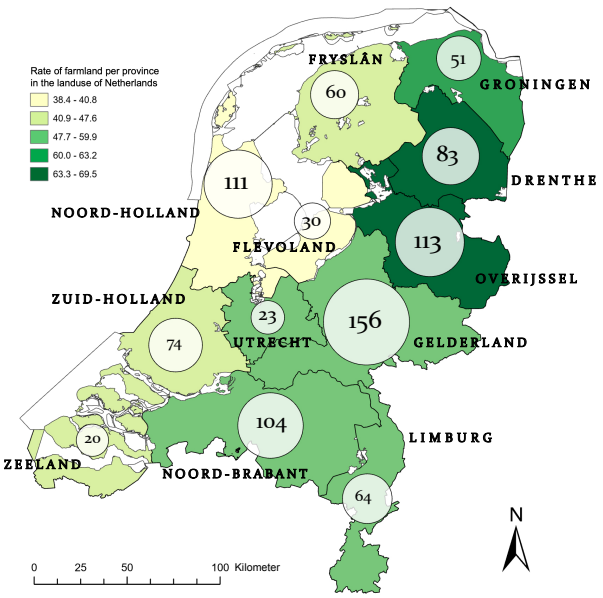

Figure.3. The number and regional distribution of social farms in Netherlands (2023)

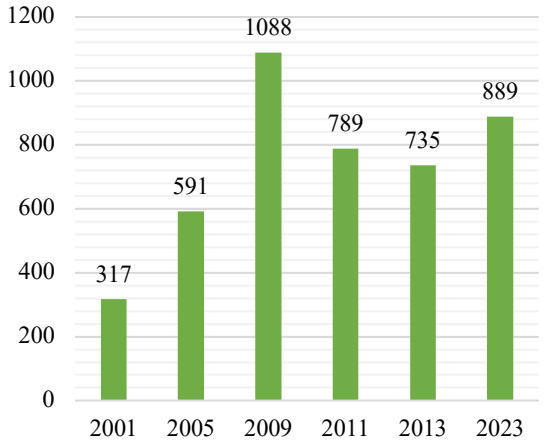

Figure 4. Change in the number of social farms in the Netherlands from 2001 to 2023

Furthermore, data from the Federation of Agriculture and Care revealed the number of social farms by region in the Netherlands from 2001 to 2023 (Figure 4): from 317 in 2001 to 591 in 2005, and then to 1088 in 2009. The number of social farms increased on average by a factor of 1.8 from 2001 to 2023, while the number of social farms decreased from 2009 to 2013. The reason for this is that, since 2011, the number of social farms covered by the Federation of Agriculture and Care has been counted separately; The Federation of Agriculture and Care's unique counting method revealed a systematization of management towards social farms.

4.3. Overview of Social farms in Japan

In Japan, where the population is declining and an aging society is progressing, issues such as the shortage of successors in agriculture and aging of farmers are becoming increasingly serious. As shown in Table 1, the number of core farmers who are mainly engaged in self-employed farming as their usual work has declined in recent years. Therefore, the combination of agriculture and care was established in 2010 in Tottori Prefecture as an initiative on social farms, under the name of "Tottori Initiative! The Combination of Agriculture and Care Project" aiming to integrate agriculture and care. Around the same time, the "Rural Village Revitalization Project Research Team for The combination of agriculture and care" was established at the National Institute of Agriculture, Forestry and Fisheries Policy. Since then, efforts in various forms have spread throughout Japan and the combination of agriculture and care has gained recognition for its significance.

Table.1. Number and Average Age of Core Farmers in Japan

	Core Farmers (10,000)	*Average Age*
2015	175.7	67.1
2016	158.6	66.8
2017	150.7	66.6
2018	145.1	66.6
2019	140.4	66.8
2020	136.3	67.8
2021	130.2	67.9
2022	122.6	68.4

The Ministry of Agriculture, Forestry and Fisheries divides the combination of agriculture and care into three types of social farms: The first is the "Cooperation Type," in which users belonging to welfare facilities work inside the facilities or outside at companies, farmers, etc. The second is the "Direct Employment Type," in which users are directly employed by farmers, and is called "general employment" or "employment for persons with

disabilities." The third is the "welfare-complete" type, in which the welfare office runs the farm itself.

4.4. Regional Distribution of Social Farms in Japan

At present, there are approximately 160 social farms registered in the combination of agriculture and care casebooks of the Ministry of Agriculture, Forestry, and Fisheries of Japan. The country was divided into nine regions: Hokkaido, Tohoku, Hokuriku, Kanto, Tokai, Kinki, Chugoku, Shikoku, Kyushu, and Okinawa. The regions with the largest number of social farms were Kinki (33) and Hokkaido (32). In other regions, the average number of social farms is approximately 15. The social farms in the Kanto and Kinki regions are located in non-populated areas (Figure 5).

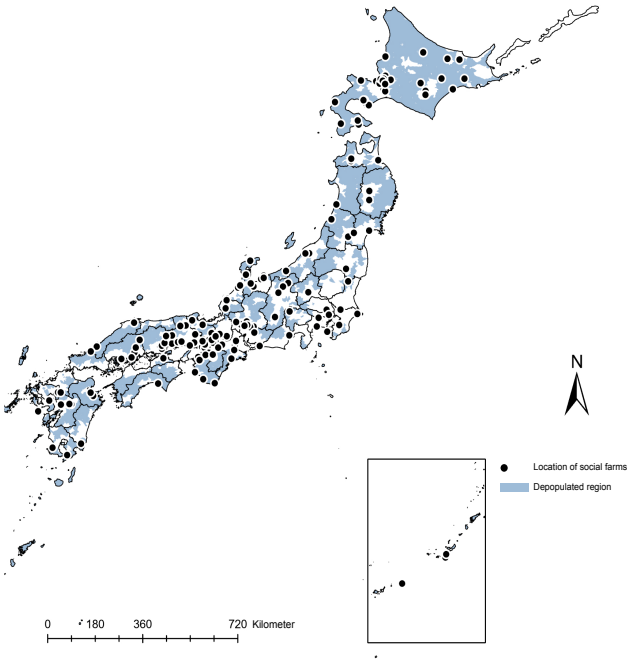

Figure.5. The Relationship Between Depopulated Region and the Distribution of Social Farms

This study analyzed the regional relationship between devastated farmland and social farms in the current situation (Figure 6), where the number of devastated farmlands is increasing owing to the shortage of labor in agriculture and the aging of farm workers.

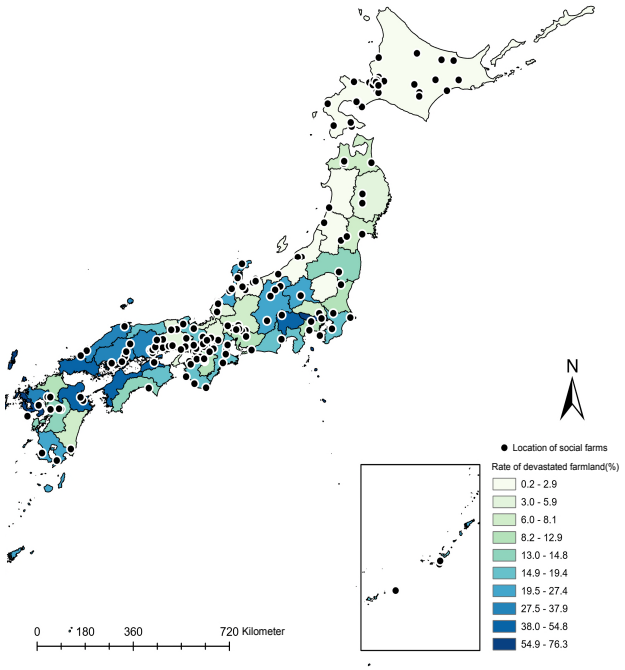

Figure.6 The Relationship between Devastated Farmland and the Distribution of Social Farms

Devastated farmland is defined as farmland that is not currently used for cultivation, has fallen into disrepair due to abandonment of cultivation, and has become objectively impossible to grow using normal farming methods. The rate of degraded farmland (Table 2) was calculated using the following equation:

Rate of Devastated Farmland = Area of Devastated Farmland／(Area of Devastated Farmland＋Area of Operating Cultivated Land)× 100

Kinki (33 farms) and Hokkaido (32 farms), regions with a large number of social farms, have low levels of devastated farmland rates of 9.5% and 0.2%, respectively, below the national average. However, the number of social farms is relatively low in the Chugoku/Shikoku region, Kyushu, and Okinawa, which are regions with a high rate of farmland disrepair. It was clarified that social farms are generally distributed in areas with less devastated farmland, that is, in areas with abundant agricultural resources.

Table.2. The Rate of Devastated Farmlands per region

No.	*Agricultural District*	*Area of Operating Cultivated Land (ha)*	*Area of Devastated Farmland (ha)*	*Rate of Devastated Farmland (%)*
1	Hokkaido	839,358	2,093	0.2%
2	Tohoku	499,842	32,166	6.4%
3	Hokuriku	177,720	8,749	4.9%
4	Kanto	434,949	72,848	16.7%
5	Tokai	136,933	12,933	9.4%
6	Kinki	130,381	12,351	9.5%
7	Chugoku and Shikoku	193,509	66,075	34.1%
8	Kyushu	294,034	71,021	24.2%
9	Okinawa	18,493	3,592	19.4%
10	**Total**	**2,725,219**	**281,828**	**10.3%**

5.Discussion

5.1. Differences between social farms in Japan and the Netherlands

The first difference is the target of social farms. In Japan, the targets of social farms are mainly the disabled and elderly. In the Netherlands, however, social farms are used not only for the disabled and the elderly, but also for various other groups, such as the long-term unemployed, drug addicts, troubled youths, people who have been sentenced to prison, and burnouts.

The second reason is the difference in the purpose of social farms. In Japan, social farms are designed to promote the independence and social participation of people with disabilities and to train them toward general employment by working in institutions, while people with disabilities are expected to become farmers and improve their agricultural production. In the case of the Netherlands, small-scale agricultural enterprises with low competitiveness in agricultural production are converted to "Social farms" and government benefits are used to compensate for shortcomings in terms of ability and other issues, so the disabled are not expected to contribute much to production activities as part of the labor force, and the main objectives are to provide a place to stay, rehabilitation of the disabled, and recovery of health. Its main purpose is to provide a place to stay, rehabilitate, and restore the health of the disabled.

Finally, there is a difference in how social farms operate. Social farms in the Netherlands have more diverse patterns than those in Japan, and they focus on the role of "a place to spend the day in a rich agricultural space" rather than "working. In Japan, the increasing willingness to include people with disabilities in the labor force and the emphasis on connecting the agricultural side with the welfare side have given rise to various forms of operation, but they have not gone beyond the conventional employment support for people with disabilities. We would like to see that Japan seeks to expand its range of users and seek a multifaceted form of operation, as in the Netherlands.

5.2. Comparison of regional spatial characteristics of social farms in Japan and the Netherlands

A comparison of the regional and spatial characteristics of social farms in Japan and the Netherlands is presented in this section.

Regarding the similarities between Japan and the Netherlands, it was found that social farms are not evenly distributed throughout the country in both countries, that there are marked regional differences, and that the characteristics of social farms are more frequently distributed in areas with abundant agricultural resources. In addition, the regions with fewer social farms are almost all recognized as remote areas of the country: Okinawa (three farms) in the case of Japan and Zeeland (20 farms) in the case of the Netherlands.

Regarding the differences in regional spatial characteristics of social farms between Japan and the Netherlands, the number of social farms registered with the Federation of Agriculture and Care in the Netherlands as of 2023 is nearly six times that of Japan (899), which is by far the largest number of social farms in the Netherlands. The density of social farms in the Netherlands is much higher than that in Japan, and the combination of agriculture and care has spread throughout the Netherlands, although the total land area of the Netherlands is only approximately the same as that of Kyushu (41,528 km^2), which is only 1/9 of Japan's land

area (377,975 km²). Social farms in the Netherlands have entered a phase in which quality and professionalism are more important than the number of farms. In Japan, the number of social farms is low nationwide, and the combination of agriculture and care has not progressed sufficiently.

6.Conclusion

This study compares the targets, purposes, and operational forms of social farms in Japan and the Netherlands as well as their regional spatial characteristics to elucidate their actual conditions and challenges. In both Japan and the Netherlands, there are large regional differences in the number of social farms. The fact that many social farms are located in areas with rich agricultural resources suggests that social farms are expected to promote the revitalization of agricultural land in depopulated areas through social farms and that social farms are expected to have a positive effect on regional revitalization.

In the future, we will extract elements that promote the combination of agriculture and care from the case of social farms in the Netherlands and formulate a practical support for the creation of social farms in Japan that have multifaceted functions to promote the mental and physical health of various users of social farms, including the disabled and the elderly, and to revitalize local communities. We will form a practical basis for the creation of a social farm environment with multifaceted functions to improve the physical and mental health of various social farm users, including the disabled and the elderly, and to revitalize communities.

References

1) United Nations Department of Economic and Social Affairs (2014), The World Urbanization Prospects.
2) Cabinet Office Japan (2023) "Annual Report on Government Measures for Persons with Disabilities: *White Paper on Persons with Disabilities 2023*."
3) OH, S., HARADA, J. and YAMANE, K. (2020) "Current Status and Issues of Working Support for Persons with Disabilities through Agriculture-Welfare Collaboration," Journal of the School of regional design Utsunomiya University, (7), pp. 65-76
4) Hassink, J. and Van Dijk, M. (2006) *Farming for health: Green-Care Farming Across Europe and the United States of America*. Springer Science & Business Media.
5) Hassink, J. *et al.* (2007) "Current status and potential of care farms in the Netherlands," *NJAS Wageningen Journal of Life Sciences*, 55(1), pp. 21-36.
6) Hassink, J., Hulsink, W. and Grin, J. (2014) "Farming with care: the evolution of care farming in the Netherlands," *NJAS Wageningen Journal of Life Sciences*, 68(1), pp. 1-11.
7) TADA, M. (2019) "A Study on Possibilities and Problems of Farming for People with Disabilities by Agricultural and Welfare Collaboration," *Josai International University bulletin*, 27(7), pp. 27-39
8) JUNG, O. (2017) "The Operation and the Significance of Care Farms of Mixed Farming Region in the Netherlands," Rikkyo University Bulletin of Studies in Tourism, 19, pp. 66-75.
9) Meerburg, B.G. *et al.* (2009) "The changing role of agriculture in Dutch society," *The Journal of Agricultural Science*, 147(5), pp. 511-521.
10) Okayama, A. (2020) "Cooperation between agriculture and welfare in the Netherlands," Bulletin of Nara Prefecture Agricultural Research and Development Center, (51), pp. 48-56
11) Bock, B.B. and Oosting, S.J. (2010) "A Classification of Green Care Arrangements in Europe," *The Economics of Green Care in Agriculture*, pp. 15-26.
12) UEDA, T. (2021) "The Functions and their Requirement about CareFarm in the Netherland," Japanese Journal of Farm Management, 58(4), pp. 15-20

Accessibility of Third Places around a University Campus
- A Spatial Analysis on Travel Times and Usage Patterns -

Max Hanssen*, Fujita Naoko**, Ding Ma***, Suzu Shimada***, Zile Tian***, Linda Gadhoum***, Joris Zandbergen****, André Jacob Lodewijks****, SeungHee Lee*****

Abstract This study examines "third places" within a university campus and their potential for fostering social engagement among students and staff. Utilizing Geographic Information Systems (GIS), this research analyzes the distribution and accessibility of "first places" (residences), "second places" (university buildings), and "third places" (social gathering spots). Through spatial and cluster analyses, and transportation mode comparison, this study categorizes third places into ten types: Baths, Co-Working Spaces, Dog Care, Eateries, Entertainment, Gyms, Libraries, Nature, Parks, and Shops. The findings show a positive correlation between travel and stay times, with most third places being accessible by walking or cycling. This informs campus planning of improved spatial layouts that enhance social interaction, place attachment, and community well-being.

Keywords: public space, communal interaction, urban planning, user experience

1. Introduction

1.1 Third Places in University Campuses

In the dynamic landscape of university campuses, the interactions between various environments play a significant role in shaping the community and promoting social engagement. At the heart of this intricate web of interactions lies the concept of "third places" – distinct gathering spots that go beyond the conventional realms of residence and academia (Oldenburg and Brissett, 1982). Renowned for its potential to strengthen community cohesion, third places have garnered scholarly attention (Mehta and Bosson, 2010). Within the context of a university campus, where students and faculty navigate between living quarters and academic buildings, the significance of these third places becomes even more pronounced (Lee, 2022).

1.2 Research Objective

The purpose of this research is to reveal the spatial dynamics of "third places" within a university campus area and their different usages and significance as hubs for social engagement among university students and staff. Through the integration of Geographic Information Systems (GIS) mapping and spatial analysis, this study seeks to clarify the distribution, interrelationships, and accessibility patterns among "first places" (residential areas), "second places" (university buildings), and the identified "third places" (social gathering spots), ultimately contributing to a deeper understanding of the role played by third places in facilitating social interactions and community cohesion.

The findings obtained from this study will contribute to the long-term aim of addressing differences in the roles of third places between people in different life stages. Specifically, this research aims to reveal how third places play a pivotal role in aiding the transition from formative student years to working years, and ultimately into the unstructured expanse of retirement.

1.3 Review and Clear Indication of Relevancy

Research across various contexts has emphasized the significance of third places in fostering social interactions

* Student Member (GISA); Graduate School of Comprehensive Human Science, University of Tsukuba; 1-1-1 Tennodai, Tsukuba, Ibaraki, Japan; S2330515@u.tsukuba.ac.jp
** Member (GISA), Institute of Art and Design, University of Tsukuba, Email: fujita.naoko.gf@u.tsukuba.ac.jp
*** Student Member (GISA), Graduate School of Comprehensive Human Science, University of Tsukuba
**** Master Industrial Design, University of Technology Eindhoven
***** Institute of Art and Design, University of Tsukuba

and enhancing well-being. A recent study that explored the relationship between perceptions of accessible third places and quality of life underscored the importance of third-place accessibility within communities (Jeffres *et al.*, 2009). This finding highlights the need for accessible tertiary places. However, while third places are recognized as hosts of quality interactions among the general population, their social impact on individuals of different ages and living circumstances remains unexplored. To address this gap, another study examined how social space design can stimulate utilization in Continuing Care Retirement Communities (CCRCs) (Campbell, 2014). This investigation found that spaces characterized by third-place attributes were more favored and used, indicating their potential contribution to healthier residents' social lives. Moreover, a recent study explored the connection between the existence of third places and self-esteem among Japanese adolescents (Fujiwara *et al.*, 2020). This study revealed that the lack of a third place was significantly associated with lower self-esteem among adolescents, highlighting the importance of third places in preventing low self-esteem.

While past research has explored and established the positive impacts of third-place characteristics on well-being, a crucial gap remains regarding how these preferred characteristics and contributions might differ among individuals in various life stages. This gap is particularly evident in the context of university students and staff, where research in third places remains underexplored. Nevertheless, related works have touched on topics related to third places within university campuses. O'Rourke and Baldwin (2016) investigated student engagement through placemaking at an Australian university campus. Chow and Healey (2008) examined the elements influencing place attachment and identity during the transition from home to university. Additionally, Lukita and Xenia (2017) conducted a case study on the significance of a Starbucks Café in the central area of Universitas Indonesia, Depok. Although these studies touch on place attachment and university campuses, they do not explicitly reference the term 'third place, creating a gap between the existing literature and third place concepts.

Notably, although the accessibility of third places has been acknowledged as pivotal (Jeffres *et al.*, 2009), this aspect remains underexplored, both within the realm of third places and university campuses. Consequently, this research targets the vicinity of the University of Tsukuba Campus in Japan. The aim was to comprehensively identify the accessibility and usage of third places among university students and staff, ultimately bridging the gap in the existing literature.

1.4 Research Significance

This research has significant implications for the domain of social engagement in university campuses. By delving into the interactions among "first places," "second places," and the critical "third places," this study advances our understanding of the specific role these spaces play within the context of a university campus. While earlier research has recognized the influence of third places on diverse aspects of well-being, socialization, and identity, this study takes a novel approach by investigating the distinct preferences and contributions of third places for university students and staff— a territory that has remained largely unexplored until now. By harnessing the power of Geographic Information Systems (GIS) mapping and spatial analysis techniques, this research not only advances the comprehension of spatial relationships and travel dynamics among these different types of spaces, but also bridges the divide between existing literature and the conceptual framework of "third places" within the university campus context. Consequently, this study lays a crucial foundation for informed campus planning and design strategies that optimize spatial layouts to promote social interactions, foster place attachment, and enhance community well-being. By enriching the academic experience of all members of the university community, these strategies facilitate a more vibrant and cohesive academic environment.

2. Methodology

2.1 Research Subjects

This study was conducted within the city of Tsukuba, situated in the Ibaraki Prefecture of Japan, encompassing an area spanning 283.72 km² and home to a population of 253,559 residents (Tsukuba City, 2023). The focal point was the University of Tsukuba campus, which extends across 2.58 km² and hosts 16,507 students (Tsukuba 2019). The university is celebrated for its academic prominence and ranking among the largest campus areas in Japan, making it a suitable research site.

Participants were recruited using convenience sampling, specifically targeting voluntary participation from both students and staff affiliated with the University of Tsukuba. To ensure a well-rounded sample population, efforts were undertaken to gather an equitable representation spanning diverse demographics, varying academic disciplines, and perspectives of both genders.

2.2 Data Collection

Semi-structured interviews were employed to delve into the spatial dynamics and behaviors associated with third places in the vicinity of the University of Tsukuba campus. These interviews offered a qualitative approach to capture participants' perspectives and experiences.

The interview process began with an explanation of the research, followed by the collection of informed consent authorizing participation and publication of results. Demographic information was gathered, including the participants' profession, years living in Tsukuba, age, and hobbies. Using GIS, participants collaboratively identified and mapped their personal "first places," "second places," and "third places," while also indicating preferred modes of transportation between these spaces.

The heart of each interview revolved around an in-depth exploration of third place. Participants elaborated on the purpose, travel time, duration of stay, co-attendees, frequency of visits, and when they started visiting each third place. The semi-structured nature of the interviews allowed for qualitative insights and anecdotes, contributing to an understanding of the usage patterns.

2.3 Data Analysis

GIS data from semi-structured interviews were subjected to multifaceted spatial relationship analysis. Utilizing (1) spatial analysis, (2) cluster analysis, and (3) travel pattern analysis, this study aimed to unveil spatial connections, travel patterns, visit frequencies, and communal networks at the University of Tsukuba Campus (Figure 1). Geographic Information Systems (GIS) are integral to comprehending spatial dynamics. GIS facilitated the creation of detailed maps showcasing participants' third place distributions. Overlaying these maps revealed spatial clusters, aiding the recognition of relationships. Additionally, similar third places were grouped to highlight the most popular types. Cluster analysis examined the travel time-stay time link,

plotting participants' third places as data points using Python 3.0 to reveal diverse user segments. The goal was to cluster outcomes, illustrating the categories of third places in each cluster, to uncover usage patterns between third place types, travel time, and stay duration. Travel behaviors were also explored to identify patterns among the participants. GIS analyzes distinctive travel behaviors that shape dynamics between place types by dissecting preferred modes: walking, cycling, and motorized vehicles.

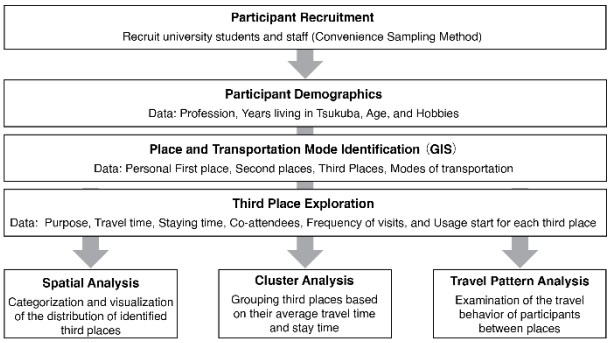

Figure 1 Study flow

Table 1 Third place categories and participants' average traveling and staying time

Third-Place Category	Identified Third-Places	Average Travel Time	Average Stay Time	Frequency (Per Participant)	Time Per Week (Per Participant)
Bath	3	00:35	02:20	0.2x per week	00:23
Co-Working Space	7	00:10	02:30	0.7x per week	01:48
Dog Care	2	00:20	03:15	0.2x per week	00:30
Eatery	14	00:12	02:53	0.5x per week	01:28
Entertainment	8	00:38	03:34	0.3x per week	01:05
Gym	8	00:13	02:00	0.7x per week	01:28
Library	7	00:07	02:32	0.4x per week	01:07
Nature	11	02:16	02:00	0.3x per week	00:34
Park	12	00:08	00:33	0.6x per week	00:20
Shop	25	00:14	01:14	2.0x per week	02:29

3. Results

3.1 Third Place Categorization and Mapping

22 participants, either students or professors, were recruited and participated in semi-structured interviews. Consequently, 97 third places were identified. The third place was divided into ten different categories, as shown in Table 1. The first category 'Bath' includes places such as Japanese hot springs or public baths. 'Co-working space,' includes places destined for people to do remote work such as university study rooms or public resting areas. 'Dog Care' includes third places aimed for recreational activities for dogs and their owners. 'Eatery' refers to cafes, restaurants, or bars. 'Entertainment' includes third places that aim to entertain customers, ranging from gaming centers to museums. 'Gym' includes fitness gyms and particular-sporting places such as tennis courts, swimming pools, or dance studios. 'Library' includes places that are considered libraries. 'Nature' includes places that mainly do not hold any commercial value but are rather visited for their nature, such as seas, forests, or mountains. 'Park' includes any third places that is generally considered a park. Finally, 'Shop' includes any third place with the main purpose of selling products or services, ranging from groceries to clothing stores.

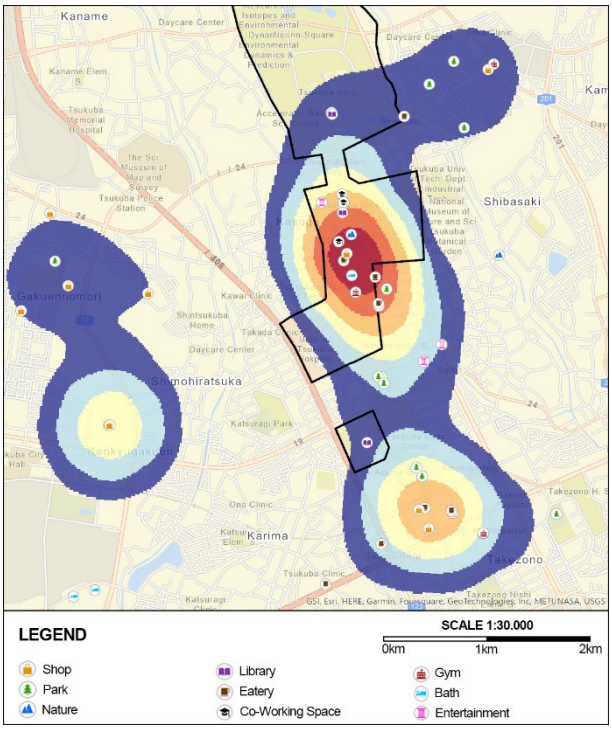

Figure 2 Density of the identified third-places

A kernel density plot was constructed to visualize the location of the identified third places for all categories. Figure 2 shows the third place within an area of 3 km from the university campus. The most identified third places were centered within the University of Tsukuba campus area. However, two clusters were also found 1 to 3km from the campus area, which mostly include third places classified in the category 'Shop' or 'Eatery.'

3.2 The Relation between Travel Time and Stay Time

Participants also mentioned the approximate travel time and stay time for each third place. Table 1 also lists the average travel time and staying time. Moreover, the average frequency and time spent by each participant in each third-place category were calculated. As a result,

Table 1 shows that third places in the category 'Shop' were the most popular, as each participant spent about 2:29 hours per week, on average, twice a week. Moreover, participants also spend more than 1 h per week in third places of the categories 'Eatery,' 'Co-Working Space,' 'Entertainment,' 'Gym,' and 'Library' on average.

A scatter plot was plotted to visualize the relationship between the staying and traveling times, as shown in Figure 3. Outliers with a travel time of more than 20.000 seconds (333 min) were excluded from the scatter plot.

K-means clustering was conducted to identify clusters in the scatter plot. Cluster 0's center point is at a travel time of 12 minutes and stay time of 60 minutes, and therefore labeled with 'Short Travel Short Stay.' Cluster 1's center point is at a travel time of 85 minutes and stay time of 265 minutes, and therefore labeled with 'Short Travel Long Stay.' Cluster 2's center point is at a travel time of 14 minutes and stay time of 214 minutes and therefore labeled with 'Long Travel Long Stay.'

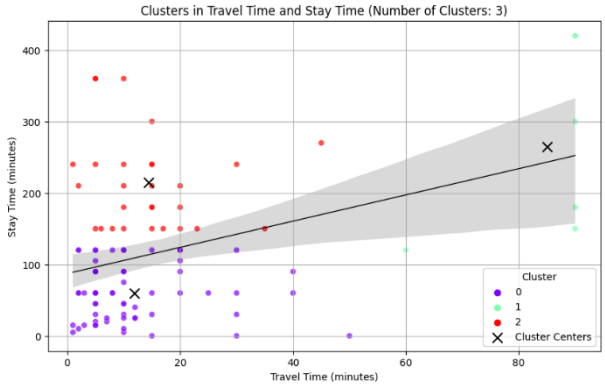

Figure 3 Scatter plot for travel and stay time

Moreover, a trend line was added to the scatter plot, represented by the black line in Figure 3, to show the general direction of the data points and to verify whether there was a linear relationship. The trend line indicates a positive correlation between the travel time and stay time. This suggests that as the travel time to a location increases, visitors tend to stay longer, on average. This relationship is further supported by the positive slope of the trend line, indicating that the longer the travel time, the greater the corresponding increase in stay time.

Finally, the number of third-place categories in each cluster is summarized in Table 2. Shops, parks, nature, and gyms, which act as third places, mainly belong to cluster 0, while dog care and libraries mainly belong to cluster 2. Co-working spaces, baths, entertainment, and eateries were equally divided among multiple clusters.

Table 2 Identified third-place categories among clusters

Third-Place Category	**Cluster 0** Short Travel Short Stay	**Cluster 1** Short Travel Long Stay	**Cluster 2** Long Travel Long Stay
Shop	21	1	3
Park	12	0	0
Nature	5	1	2
Library	2	0	5
Eatery	6	0	8
Dog Care	0	0	2
Gym	7	0	1
Bath	1	1	1
Entertainment	3	3	2
Co-working	3	0	4

3.3 Travel Behavior Analysis

Three different kernel density plots were made for third places accessed by (1) walking, (2) cycling, and (3) driving to visualize the differences between travel behaviors.

3.3.1 Travel Behavior: Walking

As a result of the density-based clustering for third places accessed by walking, five different clusters of 2–12 third

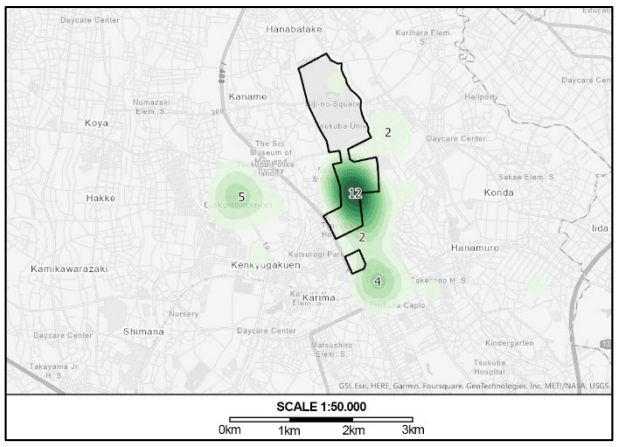

Figure 4 Third-places accessed by walk

places were found, as shown in Figure 4. Therefore, 25 out of the 30 third places accessed by the walking were recognized in clusters around the University of Tsukuba campus. The kernel-density plot further showed that most clusters were within 1 km of the campus area, with only one cluster of five third places located approximately 2 km from campus.

3.3.2 Travel Behavior: Cycling

As a result of the density-based clustering for the third places accessed by bicycle, the presence of five clusters of three to fifteen third places were found, as shown in Figure 5. Therefore, 39 of the 44 third places accessed were recognized in clusters around the University of Tsukuba campus. The locations of these clusters are similar to the location of the clusters found for third places accessed by foot. The kernel-density plot further showed that most clusters were within 1 km of the campus area, with only one cluster of four third places located approximately 2 km from campus.

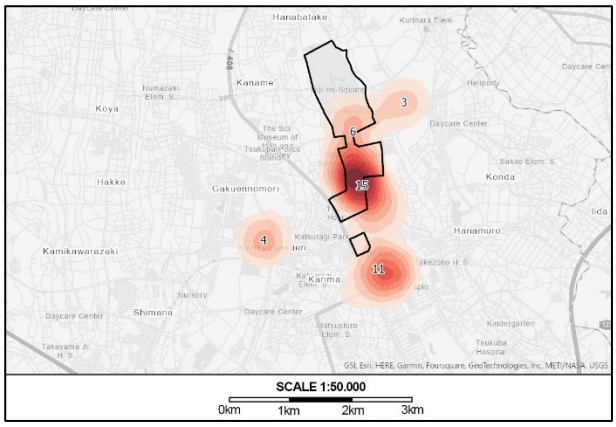

Figure 5 Third-places accessed by bicycle

3.3.3 Travel Behavior: Driving

The density-based clustering for third places around the campus showed four clusters of two to seven third places accessed by motorized vehicles, as shown in Figure 6. Therefore, 15 of the 23 third accessed places were recognized in the clusters. The kernel-density plot shows that the three clusters were in similar locations to the previous clusters for cycling and walking. However, one new cluster was located approximately 5 km North from campus.

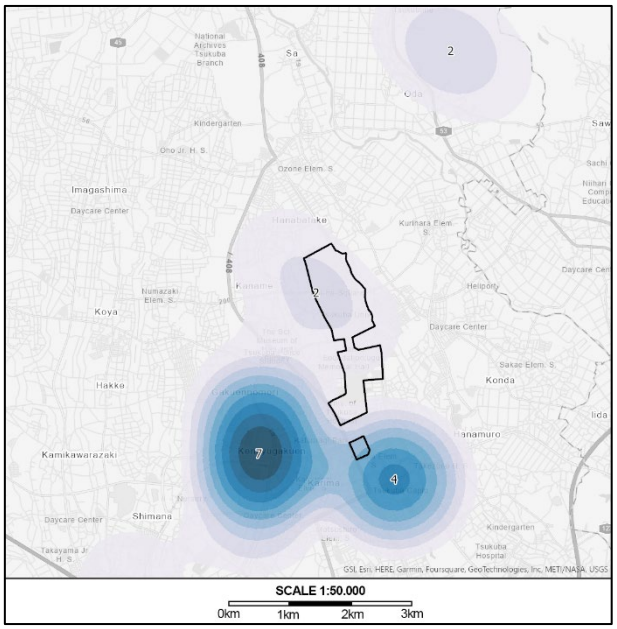

Figure 6 Third-places accessed by motorized vehicle

4. Discussion

The GIS analyses and interview results clarified the clear differences in travel behaviors and usage patterns, specifically regarding travel and staying time in third places. The insights have implications for urban planning, tourism management, and facility design, where optimizing the balance between travel time and expected stay duration can lead to enhanced visitor satisfaction.

Based on the research results so far, this study explored how the distribution and usage patterns of third places around a university campus differ based on accessibility and third place categories. From the answers of the semi-structured interviews, it was found that participants' third places could be classified across ten categories: bath, co-working space, dog care, eatery entertainment, gym, library, nature, park, and shop. Moreover, K-means clustering showed that travel and stay times differ per category, with shops being mostly accessed with short traveling and staying times, while libraries are usually accessed with long traveling and staying times. Additionally, travel behavior analysis

showed that most third places in the campus area are accessed by either bicycle or foot, while people with motorized vehicles often have third places further away from the campus. The results suggest that university students and staff prioritize shops, co-working spaces, eateries, and gyms. This indicates the possibility that these types of third places with good accessibility for pedestrians and cyclists could enhance people's staying time in university campuses and contribute to students' academic performance and overall well-being.

Past research has studied topics such as place attachment in the context of university campuses (Chow & Healey, 2008). However, none of these mentioned or recognized the term third places. Only one recent study examined the psychological benefits of third places in university campuses and revealed their significance on the mental health of students in America by serving as places of leisure (Lee, 2022). However, this study also mentioned the need for further analysis on population groups outside America. Moreover, this study mentioned the limitations of using only a photo-based survey to identify the potential psychological benefits of third places. These only reflect certain types and designs of third places, leaving the full range of third places still underexplored. Therefore, compared with related works, the results of this research provide new insights by directly asking university students and staff what places are their third place and further analyzing how different categories, travel times, and staying times change accessibility and usage patterns.

However, this study had several limitations. First, while this research aims to reveal the spatial dynamics of third places within a university campus area and their different usage and significance among university students and staff, it currently only holds a sample size of 22 participants. Although 97 third places were identified from the semi-structured interviews, the small sample size still left a bias in the data. Therefore, this study recognizes the requirement for further studies with a larger sample size. Second, the third places were identified together with participants during the semi-structured interviews by directly asking participants to mention the third places they used in their daily lives. Hence, the results solely depended on the participants' memory, which leaves the chance that certain third places were forgotten. Moreover, usage of third places may change over short periods of time, depending on the season and weather. The interviews in this study were conducted during Summer in Japan, which increases the possibility that third places used during other seasons remain unidentified.

To compensate for the limitations of this study, future studies should verify the results obtained in this study by increasing the sample size. To that end, an online questionnaire could be created to increase the study's reach, which mainly asked participants to mention their third place's location, preferred mode of transportation, travel time, and stay time. Moreover, questionnaires should be distributed in the other three seasons in Japan to further verify whether there are any statistical differences in the mentioned third place across all seasons.

5. Conclusion

This study aims to elucidate the distribution, interrelationships, and accessibility patterns among residential areas, university buildings, and third places on a university campus. By doing so, it aims to provide a comprehensive understanding of the significance of third places in promoting community cohesion among university students and staff. The ultimate goal was to contribute to the broader objective of addressing the variations in the roles of third places across individuals at different life stages. Using semi-structured interviews and spatial analyses, the study identified ten distinct categories of third places preferred by university students and staff, with shops emerging as the most popular choice. Cluster analysis further revealed a direct relationship between travel time and duration of stay in third places. Additionally, the findings underscored that the majority of university students and staff access nearby third places, predominantly by walking or cycling.

Against the backdrop of the growing

acknowledgment of the positive impact of third places on well-being (Lee, 2022) and the increasing interest in enhancing university campus design (Chow and Healey, 2008), this research underscores the pivotal role of accessibility in shaping third place experiences. Consequently, this study lays a solid foundation for the formulation of campus planning and design strategies aimed at optimizing spatial configurations to foster meaningful social interactions. By delving deeper into the diverse patterns of third-place usage across various environments and among individuals at different life stages, this research aims to offer strategies to cultivate more vibrant and cohesive campus environments.

Acknowledgement

This work was supported by JST SPRING, Grant Number JPMJSP2124.

References

Campbell, N.M. (2015) Third place characteristics in planned retirement community social spaces. *Journal of Architectural and Planning Research*, pp.55-67.

Chow, K. and Healey, M. (2008) Place attachment and place identity: First-year undergraduates making the transition from home to university. *Journal of Environmental psychology*, **28**, pp.362-372.

Fujiwara, T., Doi, S., Isumi, A. and Ochi, M. (2020) Association of existence of third places and role model on suicide risk among adolescent in japan: results from A-CHILD study. *Frontiers in psychiatry*, **11**, p.529818.

Jeffres, L.W., Bracken, C.C., Jian, G. and Casey, M.F. (2009) The impact of third places on community quality of life. *Applied research in quality of life*, **4**, pp.333-345.

Lee, N. (2022). Third place and psychological well-being: The psychological benefits of eating and drinking places for university students in Southern California, USA. *Cities*, **131**, p.104049.

Lukito, Y.N. and Xenia, A.P. (2017) December. Café as third place and the creation of a unique space of interaction in UI Campus. In *IOP Conference Series: Earth and environmental science* (Vol. 99, No. 1, p. 012028). IOP Publishing.

Mehta, V. and Bosson, J.K. (2010) Third places and the social life of streets. *Environment and behavior*, **42**, pp.779-805.

Oldenburg, R. and Brissett, D. (1982) The third place. *Qualitative sociology*, **5**, pp.265-284.

O'Rourke, V. and Baldwin, C. (2016) Student engagement in placemaking at an Australian university campus. *Australian Planner*, **53**, pp.103-116.

Tsukuba City (2023) *Municipal Data (Tsukuba City)*. https://www.pref.ibaraki.jp/kikaku/tokei/fukyu/tokei/sugata/local/tsukuba.html (Accessed: 9 May 2023).

University of Tsukuba (2019) *The University of Tsukuba in Maps and Data*. https://www.tsukuba.ac.jp/images/ut-leaflet-2019.pdf (Accessed: 9 May 2023).